NOVEL ANTIMICROBIAL DEVELOPMENT BY TARGETING THE FIRST TWO COMMITTED ENZYMES IN THE METHYL ERYTHRITOL PHOSPHATE PATHWAY, DXP REDUCTOISOMERASE AND MEP CYTIDYLYLTRANSFERASE

by

Amanda Haymond

A Dissertation
Submitted to the
Graduate Faculty
of
George Mason University
in Partial Fulfillment of
The Requirements for the Degree
of
Doctor of Philosophy
Biochemistry

Committee:

_____	Dr. Robin Couch, Dissertation Director
_____	Dr. Cynthia Dowd, Committee Member
_____	Dr. Schroeder Noble, Committee Member
_____	Dr. Virginia Espina, Committee Member
_____	Dr. Barney Bishop, Committee Member
_____	Dr. Gerald Weatherspoon, Department Chairperson
_____	Dr. Donna M. Fox, Associate Dean, Office of Student Affairs & Special Programs, College of Science
_____	Dr. Peggy Agouris, Dean, College of Science
Date: _____	Spring Semester 2017 George Mason University Fairfax, VA

Novel Antimicrobial Development by Targeting the First Two Committed Enzymes in the Methyl Erythritol Phosphate Pathway, DXP Reductoisomerase and MEP Cytidylyltransferase

A Dissertation submitted in partial fulfillment of the requirements for the degree of Doctor of Philosophy at George Mason University

by

Amanda Haymond
Bachelor of Science
George Mason University, 2013

Director: Robin Couch, Professor
Department of Chemistry and Biochemistry

Spring Semester 2017
George Mason University
Fairfax, VA

Copyright 2017 Amanda Haymond
All Rights Reserved

DEDICATION

To my parents, for supporting me and encouraging me no matter how many times I called home in angst. To my best friend Kelly, for reminding me that school doesn't last forever, even though it feels like it will. To my fiancé Will, for being willing to rearrange weekend plans to let me check my "bugs"… and for spending date nights listening to me rant about my dissertation. To my siblings Matthew and Megan, for giving me two reasons to set a good example and inspiring me to work harder. To God, for giving me the grace to make it through one day at a time.

ACKNOWLEDGEMENTS

This dissertation could never have been completed without the help of a myriad of friends and family. To the Couch lab graduate students and technicians, especially Justin, Allyson, and Chinchu, thank you for the support, encouragement, and help on all of my projects over the years. To Dr. Couch, thank you for being a wonderful mentor and for pushing me to improve in everything I do. To my committee members, thank you for investing your time in me and offering your perspectives and your support. And to coffee, thanks for compensating for my weaknesses and pulling me over the finish line.

TABLE OF CONTENTS

LIST OF TABLES

LIST OF FIGURES

LIST OF ABBREVIATIONS

1-Deoxy-D-xylulose 5-phosphate ..... DXP
2-C-Methyl-D-erythritol 4-phosphate ..... MEP
3-hydroxy-3-methyl-glutaryl-coenzyme A ..... HMG-CoA
4-(cytidine 5'-diphospho)-2-C-methyl-D-erythritol ..... CDP-ME
Aminoglycoside acetyltransferases ..... AAC
Aminoglycoside nucleotidyltransferase ..... ANT
Aminoglycoside phosphotransferase ..... APH
ATP-binding cassette family ..... ABC
Center for Disease Control ..... CDC
Chloramphenicol acetyltransferases ..... CAT
Cytidine monophosphate ..... CMP
Cytidine triphosphate ..... CTP
Deoxyribonucleic acid ..... DNA
Difference between ..... Δ
Dihydrofolate reductase ..... DHFR
Dihydropteroate synthetase ..... DHPS
Dimethylallyl pyrophosphate ..... DMAPP
Dipivaloyloxymethyl ..... POM
DXP reductoisomerase ..... IspC
Escherichia coli ..... Ec
Francisella tularensis ..... Ft
Geranyl Pyrophosphate ..... GPP
High-throughput screen ..... HTS
Inhibition constant ..... K_I
Isopentenyl pyrophosphate ..... IPP
Library of Pharmacologically Active Compounds ..... LOPAC^{1280}
Lipopolysaccharide ..... LPS
Liquid Chromatography Qualitative Time of Flight ..... LC-QToF
Liquid chromatography, tandem mass spectrometry ..... LC-MS/MS
Major facilitator superfamily ..... MFS
MEP cytidylyltransfease ..... IspD
Methicillin resistant staphylococcus aureus ..... MRSA
Methyl-2,4-pentanediol ..... MPD
Mevalonic acid ..... MVA
Michaelis constant ..... K_M
Minimum inhibitory concentration ..... MIC

Multidrug and toxic compound extrusion family ..... MATE
Mycobacterium tuberculosis ..... Mtb
N-acetylglucosamine ..... GlcNAc
N-acetylmuramic acid ..... MurNAc
Nicotinamide adenine dinucleotide phosphate ..... NADPH
Para-aminobenzoic acid ..... PABA
Penicillin binding protein ..... PBP
Peptidyl transferase center ..... PTC
Resistance –nodulation-division ..... RND
Ribosomal ribonucleic acid ..... rRNA
Small multidrug resistance family ..... SMR
Standard operating procedure ..... SOP
Structure activity relationship ..... SAR
Transfer ribonucleic acid ..... tRNA
Uridine diphosphate ..... UDP
World Health Organization ..... WHO
Yersinia pestis ..... Yp

ABSTRACT

NOVEL ANTIMICROBIAL DEVELOPMENT BY TARGETING THE FIRST TWO COMMITTED ENZYMES IN THE METHYL ERYTHRITOL PHOSPHATE PATHWAY, DXP REDUCTOISOMERASE AND MEP CYTIDYLYLTRANSFERASE

Amanda Haymond, Ph.D.

George Mason University, 2017

Dissertation Director: Dr. Robin Couch

The threat of both natural and engineered acquisition of antibiotic resistance by microbes necessitates development of novel antimicrobial compounds. The methyl erythritol phosphate (MEP) pathway presents a unique opportunity for such development, as it is both essential in bacteria in which it is found, as well as absent in mammalian cells. The MEP pathway produces two five-carbon lipid precursors isopentenyl pyrophosphate (IPP) and dimethylallyl pyrophosphate (DMAPP), essential cellular building blocks that condense to produce a host of vital downstream isoprenoids. The first two committed enzymes in the pathway, DXP reductoisomerase (IspC) and MEP cytidylyltransferase (IspD), are both promising targets for antimicrobial development. Herein we describe three approaches to identifying and developing novel inhibitors (rational, structure-based drug design; high-throughput screening of a commercial compound library; and high-throughput screening of a natural product library) conducted with both IspC and IspD in order to explore the chemical space for inhibition of these enzymes. To aid in screening a

large commercially purchased compound library, we also describe the validation of a high-throughput screening protocol with respect to both IspC and IspD, with appropriate control assays to identify false positive compounds. Based on these library screens, we report promising lead compounds with respect to both enzymes, and propose models for their mechanism of action.

INTRODUCTION

"The future of humanity and microbes likely will unfold as episodes of a suspense thriller that could be titled *Our Wits versus Their Genes*."
-Dr. Joshua Lederberg, Nobel Laureate [1]

Humans and bacteria have coexisted for as long as humans have walked the planet; indeed, the symbiotic relationships that developed between humans and certain bacteria are essential for our well being. From synthesizing essential nutrients such as Vitamin K and assorted B-Vitamins[2] to breaking down food products such as complex carbohydrates[3] to supporting the innate immune system[4], the human microbiome is responsible for influencing human health in profound ways. However, not all human-microbial interactions are this beneficial or peaceful. While humans provide an isolated ecological niche that microorganisms can adapt to live within, some of these microorganisms adapt in ways that are deleterious to the human host.

Bacterial pathogenesis acquired through point mutations, genetic rearrangements, or horizontal gene transfer[5] can provide some selective advantage to a microorganism that conflicts with human health, leading to the emergence of bacterial diseases. Throughout history, bacteria have been the causative agents of some of the deadliest diseases on record. Tuberculosis, caused by the bacterium *Mycobacterium tuberculosis*, is the leading cause of death of HIV-positive individuals and was responsible for 1.5 million deaths in 2014 alone[6]. The Black Death, an outbreak of the

plague caused by *Yersinia pestis*, was estimated to have wiped out over 1/3 of Europe's population during the Dark Ages[7]. *Vibrio cholerae*, responsible for cholera, still causes an estimated 2.8 million cases annually, killing an estimated 91,000 people despite advances in sanitation[8]. Typhoid fever affects 21.5 million people each year, resulting in over 200,000 deaths primarily in the developing world, and is caused by the bacterium *Salmonella typhi*[9]. It is true that through vaccination, the commercialization of antibiotics, and improvements in sanitation, the death toll in the United States from infectious disease has fallen dramatically since the 1950s[10]. However, despite these noted improvements, bacterial disease remains a huge problem in the developing world. Additionally, as microbes evolve new resistance mechanisms to overcome first-line medicines, it is rapidly becoming apparent that humans need additional techniques to manage the spread of bacterial pathogens.

History of Antibiotics and their Key Targets

Management of bacterial disease occurs through both preventative and reactive measures. Preventative measures, including improving sanitation, increasing access to healthcare and information, and vaccinating when such treatments are available decreases the number of cases of bacterial disease. However, once a patient is infected with a bacterial pathogen, the primary reactive treatment is a course of antibiotics. Antibiotics are compounds that either kill (bactericidal) or stop the growth (bacteriostatic) of bacterial cells, without harming mammalian cells. The field of antibiotic development was initially borne more of luck than of strategy. Alexander Fleming first famously discovered penicillin, one of the first commercialized

antibiotics, in the bacteria-killing fungus contaminating his cultures[11]. Since that time, we have learned much about the structure and mechanism of penicillin, and have used that information to develop of host of antibiotics that share its mechanism. Investigation into the secondary metabolites of soil bacteria, particularly *Streptomyces* species[12], lead to the discovery of additional antibacterial compounds with new modes of action. As the field of antibiotic discovery grew, it went through a rapid growth phase during 1950s and 1960s, often referred to as the "golden age of antibiotics", during which time over half of the most commonly used antibiotics today were discovered[13]. Table 1 lists the name, date of discovery, and target of some of the most significant antibiotic classes developed in the past 100 years[13, 14, 15, 16].

Table 1. Target and Introduction Date of Major Antibiotic Classes

Class	Year Introduced	Target
Sulfonamides, "sulfa drugs"	1935	Folic acid metabolism
Penicillins (β-lactams)	1940	Cell wall synthesis
Aminoglycosides	1944	Protein synthesis
Polymyxins	1947	Cell wall integrity
Chloramphenicol	1949	Protein synthesis
Tetracyclines	1950	Protein synthesis
Macrolides	1952	Protein synthesis
Cephalosporins (β-lactams)	1953	Cell wall synthesis
Glycopeptides	1956	Cell wall synthesis
Rifamycins	1957	RNA polymerase
Quinolones	1962	DNA gyrase
Trimethoprim	1968	Folic acid metabolism
Carbapenems (β-lactams)	1976	Cell wall synthesis
Monobactams (β-lactams)	1982	Cell wall synthesis
Oxazolidinones	2000	Protein Synthesis
Lipopeptides	2003	Cell wall integrity

It is noteworthy that roughly 75% of the antibiotic classes currently available target one of two major cellular processes: cell wall synthesis and protein synthesis. These processes, and the way key antibiotics inhibit these processes, are described in brief below and allow understanding of how antimicrobial resistance is able to develop.

Cell Wall Synthesis

Cell wall synthesis is a complex process involving a large number of enzymes, but can be broken down into three keys steps, each taking place in a different part of the cell: synthesis of monomers in the cytoplasm; linking of monomers, branching, and translocation at the cell membrane, and transglycosylation and transpeptidation at the cell wall[17]. These three steps are shown below in Figure 1.

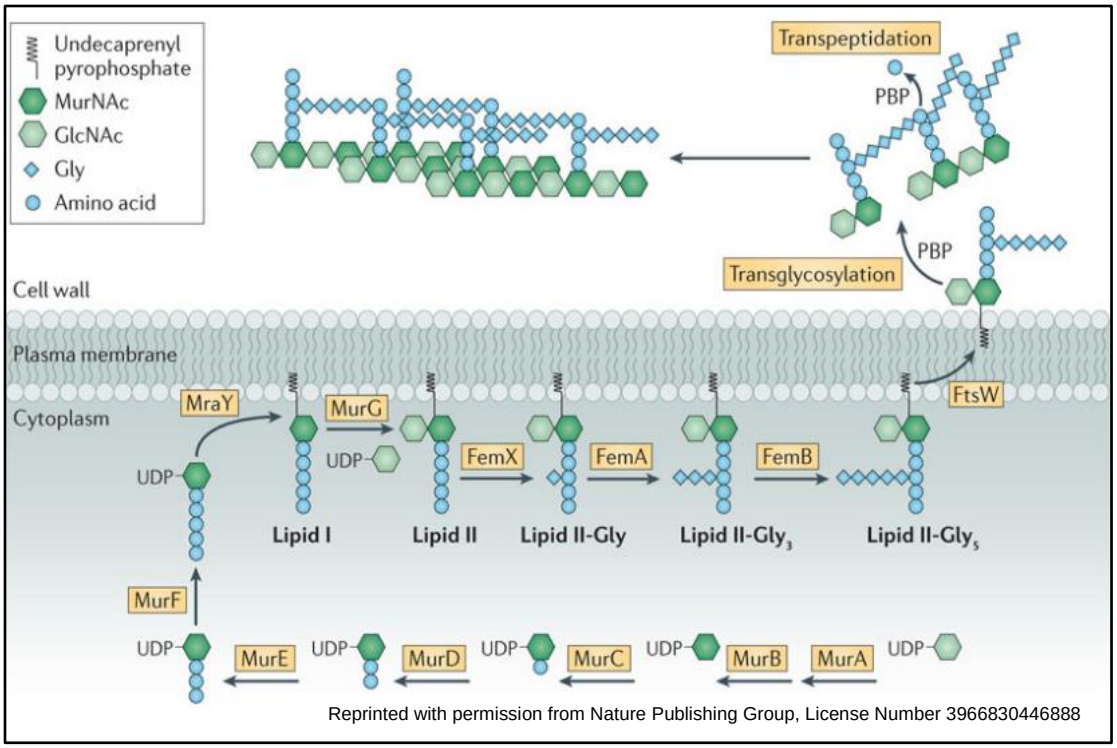

Figure 1. Mechanism of Cell Wall Synthesis[17]. Synthesis of peptidoglycan, the major constituent of the bacterial cell wall, takes place in three stages that occur at three different locations in the cell (see the figure). The process begins in the cytoplasm, where the nucleotide sugar-linked precursors UDP-*N*-acetylmuramyl (UDP-MurNAc)-pentapeptide and UDP-*N*-acetylglucosamine (UDP-GlcNAc) are synthesized. The second stage takes place at the cytoplasmic membrane, where the UDP-MurNAc-pentapeptide precursor is linked to the transport lipid (undecaprenyl pyrophosphate), resulting in the formation of lipid I. The subsequent addition of GlcNAc from UDP-GlcNAc produces lipid II. A peptide crossbridge (in the case of *Staphylcoccus aureus*, five glycine residues, as shown) is added at the third amino acid in species in which peptidoglycan is not directly crosslinked. Lipid II is then flipped to the external side of the cell membrane (most probably by FtsW proteins), where it is incorporated into nascent peptidoglycan by penicillin-binding proteins (PBPs). During the third stage, PBPs catalyse transglycosylation and transpeptidation reactions, resulting in the respective polymerization and crosslinking of the glycan strands via flexible peptides. PBPs are often divided into high-molecular-mass (HMM) and low-molecular-mass (LMM) PBPs[18]. HMM PBPs can be further classified as class A or class B PBPs according to their functional domains[18] . Class A PBPs are bifunctional, having both transglycosylase and transpeptidase activities, whereas class B PBPs have only transpeptidase activity. LMM PBPs have a penicillin-binding domain and are usually D,D-peptidases[19], although some, such as *S. aureus* PBP4, have transpeptidase activity [20].

Uridine diphosphate (UDP) acts as a carrier for the aminosugars N-acetylmuramic acid (MurNAc) and N-acetylglucosamine (GlcNAc) in the cytoplasm. Through the action of a host of enzymes, the UDP-MurNAc precursor is modified with five amino acids

forming the "pentapeptide linker", or the amino acid bridge that will be used for later cross-linking[17]. The final two amino acids in this pentapeptide linker are D-Alanine, and are important for subsequent recognition of the pentapeptide linker by downstream enzymes[21]. Upon localization on the inner plasma membrane through the addition of an undecaprenyl tail, UDP-GlcNAc donates its amino sugar to create the disaccharide monomer, while another host of enzymes add an additional branch of glycine residues for use in later crosslinking[17]. Upon translocation to the cell wall, penicillin-binding proteins (PBPs) first facilitate the linking of the disaccharide monomers through transglycosylation, and second facilitate crosslinking of the monomers by attaching the glycine chain to the terminal end of the pentapeptide linker of the adjacent monomer[17]. The completed, crosslinked amino-sugar wall is called peptidoglycan, and its presence both protects the bacterial cell from harsh environments, as well as provides a target for antibacterial compounds. The lack of a peptidoglycan layer in mammalian cells limits the amount of side effects that a compound targeting bacterial cell wall synthesis might have on a host cell.

Compounds targeting bacterial synthesis of the cell wall are classified as either β-lactam antibiotics or as glycopeptide antibiotics. β-lactam antibiotics are so named due to a conserved structural β-lactam ring that is essential for function. Figure 2 shows the structures of 4 major classes of β-lactam antibiotics, alongside the D-alanyl-D-alanine terminus of the pentapeptide linker.

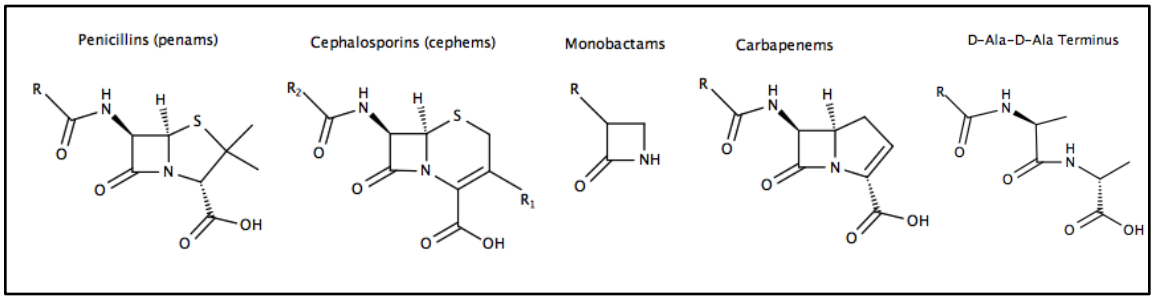

Figure 2. Structures of the major classes of β-lactam antibiotics as compared to the D-Ala-D-Ala terminus

β-lactam antibiotics function by inhibiting cross-linking between nascent strands of peptidoglycan that form the bacterial cell wall. Cross-links formed from the pentapeptide linker regions are bound by the enzyme transpeptidase, a PBP[22]. Structural similarity between the β-lactam ring and the D-alanyl-D-alanine moiety allows β-lactam antibiotics to bind transpeptidase and inhibit proper peptidoglycan crosslinking[22].

While glycopeptides also target the process of cell wall synthesis, they do not inhibit transpeptidase directly. Instead, glycopeptides interact with the D-alanyl-D-alanine moiety of the pentapeptide crosslinker, forming a complex that prevents binding of transpeptidase[23]. The interaction between the glycopeptide vancomycin and D-alanyl-D-alanine is shown below in Figure 3[24].

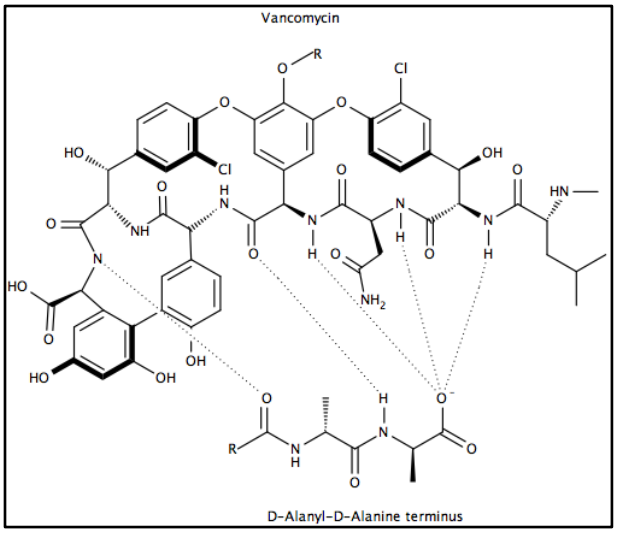

Figure 3. Vancomycin's interaction with the D-Alanyl-D-Alanine terminus of the pentapeptide linker

Both the glycopeptides and the β-lactams tend to be significantly more effective against Gram positive microrganisms due to the fact that the antibiotics can interact directly with the cell wall. Gram negative organisms have a lipopolysaccharide (LPS) layer and an outer plasma membrane protecting against direct access to the peptidoglycan cell wall, making most compounds in these classes significantly less effective against Gram negative organisms.

Protein Synthesis

The second largest target of antibiotics is bacterial protein synthesis, proceeding in the ribosome. The ribosome is composed of two rRNA-protein subunits, the 50S subunit and the 30S subunit, that come together to complete the complex around the transcript, forming 3 distinct tRNA binding sites referred to as the A (aminoacyl) site, the P (peptidyl) site, and the E (exit) site[25]. While initiation of translation is gated by a host of initiation factors, and the translation process requires significant levels of

regulation, the multitude of steps required provides an opportunity to interrupt protein synthesis at many different points. Specificity of antibiotics for the bacterial ribosome versus the eukaryotic ribosome is achieved due to subtle structural differences between the eukaryotic and prokaryotic ribosomes.

Figure 4[26] shows the binding locations of 25 antibiotics on the bacterial ribosome. The aminoglycosides, one of the earliest classes of antibiotics shown to target bacterial protein synthesis, function by binding to various sites on the 16S rRNA, the segment of RNA in the 30S ribosomal subunit that forms the A site[27]. Binding of the aminoglycosides to the A site prevents proper codon-anticodon interaction and facilitates either incorrect tRNA binding or prevents tRNA from progressing to the P site[27]. Neomycin, unlike the other aminoglycosides shown in Figure 4, has a second binding site on the 50S subunit and branches across the two subunits, affecting the ribosome's ability to separate and recycle after protein translation is complete[26]. The tetracyclines also bind to the 30S subunit, preventing binding of the aminoacyl-tRNA to the A site[28].

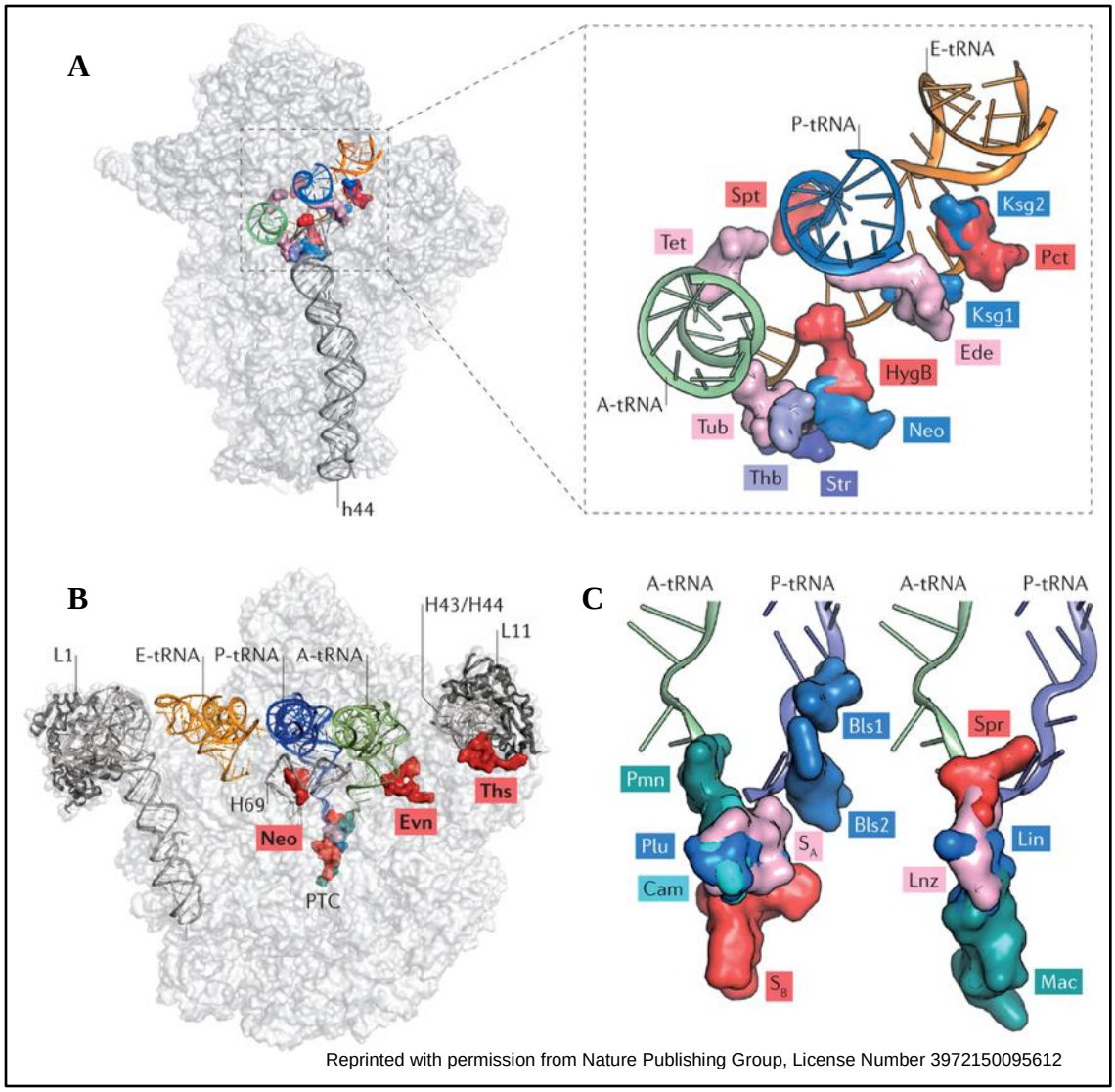

Reprinted with permission from Nature Publishing Group, License Number 3972150095612

Figure 4. Antibiotics targeting the ribosome[26]. A) Overview and enlargement of antibiotic binding sites along the mRNA binding channel of the 30S subunit, including tetracycline (Tet; Protein Data Bank (PDB) accession 4G5K–N)[29] spectinomycin (Spt; PDB accession 2QOU–X)[30] kasugamycin (Ksg1 and Ksg2; PDB accession 2HHH)[31] pactamycin (Pct; PDB accession 1HNX)[32], edeine (Ede; PDB accession 1I95)[33], hygromycin B (HygB; PDB accession 3DF1–4)[34], neomycin (Neo; PDB accession 4GAQ/R/S/U)[35], streptomycin (Str; PDB accession 1FJG)[36], thermorubin (Thb; PDB accession 3UXQ–T)[37] and tuberactinomycins (Tub; PDB accession 3KNH–K)[38]. The A-site tRNA (green), P-site tRNA (blue), E-site tRNA (orange) and h44 are highlighted for reference. B) Overview of the binding sites of neomycin (Neo; PDB accession 4GAQ/R/S/U)[35], evernimicin (Evn)[39] and thiostrepton (Ths; PDB accession 3CF5)[40] on the 50S subunit. The A-site tRNA (green), P-site tRNA (blue), E-site tRNA (orange), H43/H44, H69, peptidyl-transferase centre (PTC) and the L1 and L11 stalks are highlighted for reference. C) Enlargement of the binding sites of blasticidin S (Bls1 and Bls2; PDB accession 1KC8)[41], sparsomycin (Spr; PDB accession 1M90)[42], lincomycin (Lin; PDB accession 3OFX/Y/Z/0)[43], linezolid (Lnz; PDB accession 3DLL)[44], macrolides (Mac; PDB accession 1K9M)[45], puromycin (Pmn; PDB accession 1M90)[42], pleuromutilins (Plu; PDB accession 1XBP)[46], chloramphenicol (Cam; PDB accession 3OFA–D)[43] and streptogramins A and B (SA and SB; PDB accession 1SM1)[47] relative to the A-site and P-site tRNAs.

The 50S subunit of the ribosome contains the peptidyl-transferase center (PTC), or the region where peptide bond formation occurs and the growing peptide chain is transferred to the next tRNA. While some compounds associating with the 50S subunit bind outside this region, such as the oligosaccharide antibiotic evernimicin or peptide antibiotic thiostrepton, the PTC is the predominant site of antibiotic binding to the 50S subunit. Major antibiotic classes including chloramphenicol, the lincosamides, the oxazolidonones, the macrolides, the pleuromutilins, and the streptogramins all bind in similar regions of the PTC. Also binding in the PTC are the nucleoside antibiotics, which are a class of compounds that inhibit protein translation in both eukaryotes and prokaryotes (Figure 4). Because they mimic the structure of the nucleosides, they bind most closely to the tRNA in the A and P sites, and thus do not distinguish between eukaryotic and prokaryotic ribosomes.

Other Pathways

Other major pathways targeted by clinically relevant antibiotics include folic acid synthesis, DNA/RNA replication, and cell membrane integrity. The first antibiotics clinically available, the sulfonamides ("sulfa drugs") target folic acid synthesis by competitively inhibiting the enzyme dihydropteroate synthetase (DHPS), which utilizes the natural substrate para-aminobenzoic acid (PABA) as a building block of folic acid[48]. Additionally, trimethoprim also targets this pathway by inhibiting the conversion of dihydrofolate to tetrahydrofolate, the active form of folic acid, by dihydrofolate reductase (DHFR)[49]. Shown in Figure 5 is an abbreviated schematic of

the bacterial folate metabolism pathway, with the targets and structures of the sulfonamides and trimethoprim labeled.

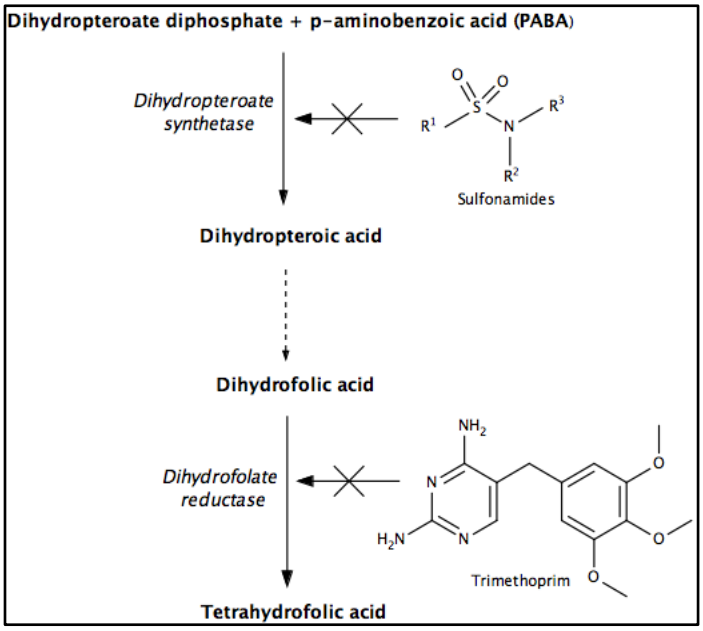

Figure 5. Antibiotics targeting folic acid metabolism

DNA/RNA replication is primarily targeted by the rifamycins and quinolones. Rifamycins are bactericidal compounds targeting the DNA-dependent RNA polymerase; they bind in the β-subunit RNA-channel, blocking the path of elongating RNA after the transcript reaches 2 to 3 nucleotides in length[50]. The rifamycins are particularly active against mycobacterial species and are standard of care when treating tuberculosis, although high rates of resistance often necessitate that rifamycins be administered in conjunction with other antibacterial compounds[51]. The quinolones target DNA replication by binding to DNA gyrase, which is responsible for relieving

torsional strain during replication by creating strand breaks in the DNA and partially unwinding the strands before ligating. Quinolones intercalate into the DNA after cleavage, preventing ligation of the double stranded DNA and leaving the DNA strand broken[52]. In this way, quinolones turn DNA gyrase into a toxic protein that fragments bacterial DNA[52]. The structures of rifamycin B, a representative rifamycin, and ciprofloxin, a representative quinolone, are shown in Figure 6.

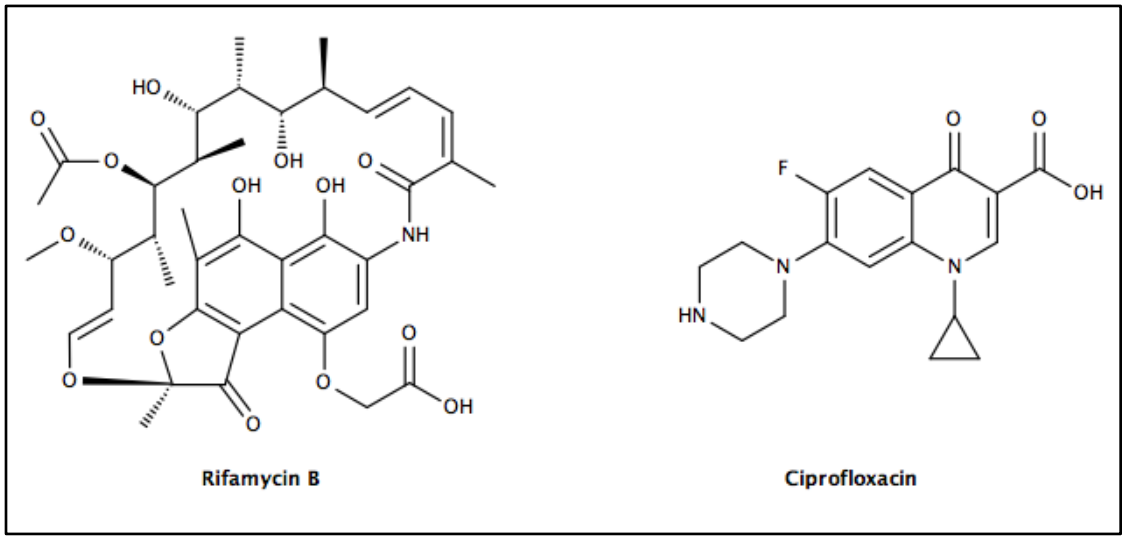

Figure 6. Representative structures of the rifamycins (left, rifamycin B) and the quinolones (right, ciprofloxacin)

One last major target of antibiotics is cell wall integrity. Antibiotics such as the polymyxins and lipopeptides are both non-ribosomal synthesized cyclic peptides with hydrophobic tails. Polymyxins, identified in 1947, are fermentation products of various *Paenibacillus polymyxa* species containing a heavily positively charged heptapeptide ring with an attached tail of three hydrophobic amino acids and a fatty acid[53]. The positively charged ring interacts with the negatively charged lipopolysaccharide (LPS)

layer of Gram negative bacteria, binding to the outer cellular membrane. This disrupts the membrane permeability, leading to leaking cell contents and ultimately cell death[53]. The lipopeptides, brought to market roughly 50 years after the polymyxins, consist of a decapeptide macrolactone ring with an attached tail of three hydrophobic amino acids and a fatty acid. Lipopeptides are not heavily positively charged and do not target LPS[54]. The longer hydrophobic tail is thought to drive insertion into the bacterial membrane, leading to membrane destabilization, leaking of cellular contents, and ultimately cell death. Unlike the polymyxins, the lipopeptides are primarily active against Gram positive bacteria. Representative structures of the polymyxins and lipopeptides are shown in Figure 7.

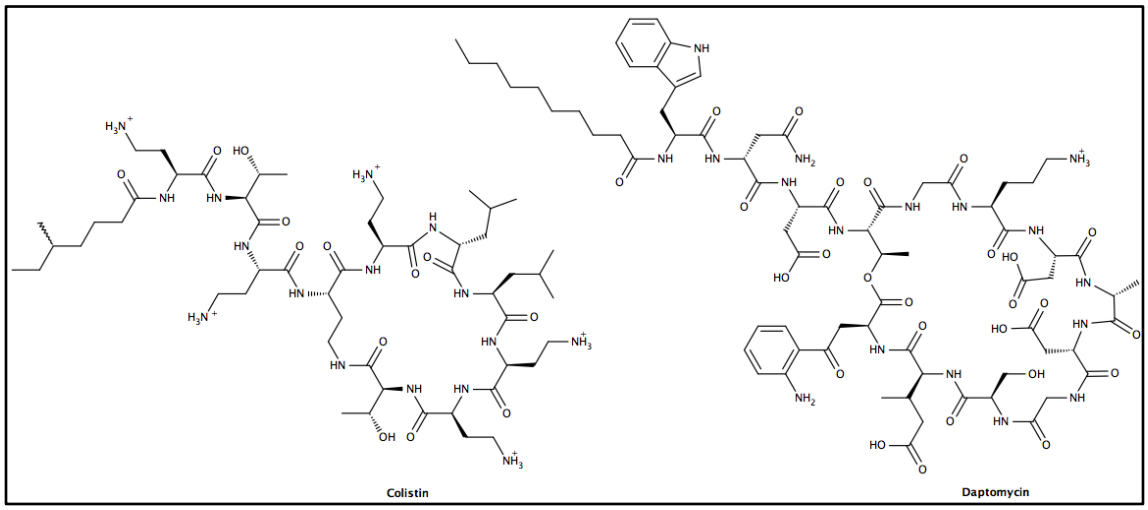

Figure 7. Representative structures of the polymyxins (left, collistin) and the lipopeptides (right, daptomycin)

Antibiotic Resistance

While the classes of compounds above have saved countless lives since they were developed, many are losing their efficacy due to rapidly spreading antimicrobial resistance. Antimicrobial resistance is defined by the World Health Organization (WHO) as the following:

> "Antimicrobial resistance is resistance of a microorganism to an antimicrobial drug that was originally effective for treatment of infections caused by it… The evolution of resistant strains is a natural phenomenon that occurs when microorganisms replicate themselves erroneously or when resistant traits are exchanged between them. The use and misuse of antimicrobial drugs accelerates the emergence of drug-resistant strains."[55]

The species of bacteria developing or acquiring resistance include disease-causing agents from many diverse sectors: from nosocomial infections (such as MRSA) to sexually-transmitted infections (such as gonorrhea) to infections prominent in the third world (such as tuberculosis) to infections prominent in American elementary schools (such as pneumococcus, responsible for childhood ear infections) [56]. Additionally, microorganisms exposed to antimicrobial compounds, whether pathogenic or not, may develop resistance that can be passed to other pathogenic species through gene transfer. Resistant microbes cross age, gender, culture, and lifestyle boundaries to become a threat to almost every human population. The Center for Disease Control released a report in 2013 stating that in the United States alone, at least 2 million people have suffered from infections that developed resistance to at least one frontline antibiotic for that disease, resulting in at least 23,000 deaths directly from these resistant bacterial species[56]. WHO published a global report in May 2014 stating that the problem of

antimicrobial resistance is

> "…a problem so serious that it threatens the achievements of modern medicine. A post-antibiotic era—in which common infections and minor injuries can kill—far from being an apocalyptic fantasy, is instead a very real possibility for the 21st century."[57]

There are many mechanisms of antibiotic resistance, but the most prevalent mechanisms include compound inactivation, target modification, and efflux[58]. Through one or all of these three mechanisms, resistance has been documented to every class of antibiotics listed in Table 1. The most clinically relevant resistance mechanisms for each class of antibiotics is presented in Table 2, although it should be noted that most classes are now known to have multiple diverse mechanisms of resistance.

Table 2: Primary Bacterial Resistance Mechanism to Major Classes of Antibiotics

Class	Resistance Mechanism	Reference
Sulfonamides, "sulfa drugs"	Target Modification	59
Penicillins (β-lactams)	Compound Inactivation and Target Modification	60
Aminoglycosides	Compound Inactivation	27
Polymyxins	Target Modification	61
Chloramphenicol	Compound Inactivation	62
Tetracyclines	Efflux	28
Macrolides	Target Modification	63
Cephalosporins (β-lactams)	Compound Inactivation and Target Modification	60
Glycopeptides	Target Modification	64
Rifamycins	Target Modification	51
Quinolones	Target Modification	52
Trimethoprim	Target Modification	49
Carbapenems (β-lactams)	Compound Inactivation and Target Modification	60
Monobactams (β-lactams)	Compound Inactivation and Target Modification	60
Oxazolidinones	Target Modification	65
Lipopeptides	Target Modification	66

Of the three major mechanisms of resistance, the most common is target modification, followed by compound (drug) inactivation, then efflux. Each mechanism is discussed in brief, along with examples from the list of major antibiotic classes above.

Target Modification

Antibiotics target bacterial proteins that are essential to either bacterial growth or survival, making these targets indispensable for the microorganism. However, despite their necessity, most bacterial proteins can be modified slightly to decrease affinity for the antibiotic while still carrying out their cellular function, resulting in resistant strains. Spontaneous mutations in the coding region for bacterial targets conferring resistance can be selected for under pressure with the antibiotic, leaving behind primarily resistant species.

There are many clinical examples of target modification mutations. Methicillin resistant *staphylococcus aureus*, or MRSA, is resistant to most β-lactam antibiotics by the acquisition of a mutated mecA gene, encoding the transpeptidase PBP2a[67]. When a β-lactam antibiotic binds to a PBP, an active site nucleophilic serine attacks the β-lactam ring, hydrolyzing the ring and acylating the serine. This forms a stable covalent complex, inactivating the PBP[68]. PBP2a has a 3-4 fold lower rate constant for the acylation of serine than does the wild-type PBP, conferring significant resistance to β-lactams[67]. MRSA is only one of many species whose acquisition of altered PBPs confers resistance; altered PBPs have been documented in isolates of *S. pneumoniae, N. gonorrhoeae, N. meningitides, E. faecalis, E. faecium, H. influenzae, H. pylori, P. mirablis, A. baumanii, P. aeruginosa, S. pyogenes,* and *L. monocytogenes*, representing

multiple mutations in PBP genes[67].

Compound (Drug) Inactivation

While the most common antibiotic resistance mechanism is spontaneous mutations to decrease affinity for an antibiotic, in some cases bacteria are able to repurpose genes to break down or modify antibiotic compounds to eliminate their activity. As discussed by Wright et. al,

> "….in several cases, the antibiotics or their action actually genetically regulate the expression of resistance genes. Therefore, bacterial cells expend a considerable amount of energy and genetic space to actively resist antibiotics." [69]

Perhaps the best characterized example of compound inactivation relates to the β-lactamases. Unlike Gram-positive organisms, whose primary resistance to β-lactams is through modification of PBPs as mentioned above, Gram-negative organisms originally sensitive to β-lactams primarily resist through the production of β-lactamases[64]. β-lactamases cleave the β-lactam ring through one of two mechanisms, either the use of an active site serine in a manner similar to the original cleavage of the β-lactam ring in PBPs (Ser-β-lactamases), or through an active site water activated by a Zn^{2+} center (metallo-β-lactamases)[69]. With over 200 known β-lactamases, efforts have been made to directly inhibit β-lactamases in hopes of restoring activity of the original antibiotic. The most successful has been the introduction of clavulanic acid, a compound with a β-lactam ring that functions to covalently inactivate β-lactamases in a similar manner to the covalent inactivation of PBPs by β-lactam antibiotics[70].

Other examples of compound inactivation include resistance mechanisms to the aminoglycosides and chloramphenicol. Bacterial additions/modifications to the core structure of the aminoglycoside antibiotics effectively inhibit their binding to the ribosome. Aminoglycoside resistant strains utilizing this mechanism express one of three classes of resistance enzymes, including aminoglycoside phosphotransferases (APHs), aminoglycoside nucleotidyltransferases (ANTs), or aminoglycoside acetyltransferases (AACs)[27]. Addition of phosphoryl, nucleotidyl, or acetyl groups to any key hydroxyl group of an aminoglycoside severely reduces its binding affinity. Chloramphenicol likewise can be inactivated by group-transfer enzymes, primarily through chloramphenicol acetyltransferases (CATs).

Efflux

Efflux mechanisms involve specific membrane bound proteins that pump antibiotics out of the bacterial cell. While more regularly found in Gram-negative species, efflux pumps have been recognized as clinically significant in Gram-positive species as well[71]. Efflux pumps can be generally categorized in five different groups based on their structures and mechanism of transport: the major facilitator superfamily (MFS), the ATP-binding cassette family (ABC), the resistance–nodulation-division family (RND), the small multidrug resistance family (SMR), and the multidrug and toxic compound extrusion family (MATE)[72]. Efflux pumps are rarely the primary mechanism of resistance to specific antibiotics as they are often not specific for single antimicrobials, but instead have broad substrate specificity[71]. However, there are some well characterized examples including the first-discovered antibacterial efflux pump

TetA, conferring resistance to tetracycline in *E.coli*[72]. There are now at least 20 known tetracycline-specific efflux pumps, all belonging to the major facilitator superfamily (MFS)[72].

Conclusions on Antimicrobial Resistance

In light of the concerns of widespread antibiotic resistance developing in pathogenic bacteria, one would anticipate a robust antibiotic pipeline bringing novel compounds to market. However, relatively few new antibiotics have been approved since the golden age of antibiotics in the 1940s-1960s, and the few new compounds emerging are heavily focused on the same cellular targets[73]. Additionally, the time from introduction of a novel antibiotic into the clinical setting to documented resistance is generally 10 years or less, giving most new antibiotics an "expiration date", further underscoring the need to develop additional novel antibiotics[74]. The issue is such that the Obama administration released *The National Action Plan for Combating Antibiotic Resistant Bacteria* in 2015, citing five goals of slowing the emergence and spread of resistant bacteria, strengthening national surveillance efforts, advancing development and use of rapid diagnostic tests for resistant species, accelerating basic and applied research towards development of novel treatments, and improving international collaboration for resistance prevention[75].

Given the relative paucity of bacterial proteins currently targeted by approved antibiotics, one way to progress towards the President's fourth goal of additional novel antibacterials is to identify novel bacterial proteins to target. Any new bacterial target must not only be essential for bacterial growth and survival, but must also be specific to

bacterial species to avoid mammalian cell toxicity. The methyl erythritol phosphate (MEP) pathway, present primarily in Gram negative eubacteria[76], is one pathway that may prove a significant source of novel antibacterial targets.

Introduction to the MEP Pathway

The methyl erythritol phosphate pathway, shown in Figure 8, is comprised of seven enzymes that convert glycolytic metabolites pyruvate (Compound **a**) and glyceraldehyde 3-phosphate (Compound **b**) to isopentenyl pyrophosphate (IPP, Compound **j**) and dimethylallyl pyrophosphate (DMAPP, Compound **k**). Each of these five-carbon lipid building blocks are used to synthesize isoprenoids (also known as terpenoids), the largest class of natural products with over 25,000 individual metabolites currently identified[77]. Because all isoprenoids are derived from condensation of IPP and DMAPP, inhibition of the MEP pathway can have deleterious effects on a cell. Electron transport, for example, is dependent on a class of electron carrier molecules collectively known as prenylquinones, such as Coenzyme Q (ubiquinone)[78]. These compounds utilize an isoprenoid tail to anchor the prenylquinone in the lipid bilayer, such that inhibition of the MEP pathway thereby interferes with microbial electron transfer by preventing proper localization of prenylquinones. Membrane fluidity in bacteria is also modulated by isoprenoid metabolites called hopanoids[79], compounds that are structurally related to the mammalian isoprenoid product cholesterol and function in a similar manner. Additionally, as illustrated in Figure 1, cell wall biosynthesis requires the isoprenoid undecaprenyl pyrophosphate to anchor the growing cell wall monomers to the cell membrane prior to translocation to

the peptidoglycan structure[17]. These key cellular functions of isoprenoid metabolites are underscored by the fact that knockout of MEP pathway genes proves lethal in numerous bacteria, including *Mycobacterium tuberculosis* [80], *Francisella tularensis* [81], *Escherichia coli* [82], and *Vibrio cholera* [83].

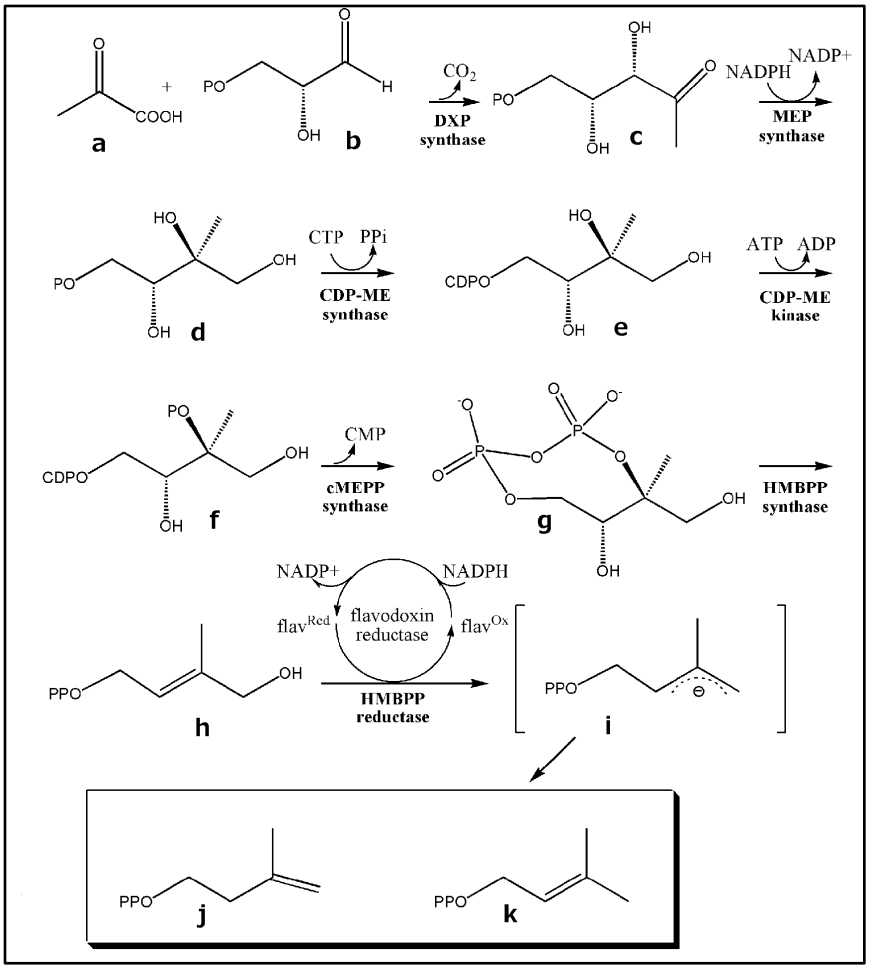

Figure 8. Schematic of the MEP pathway. The MEP pathway is used by higher plants, the plastids of algae, apicomplexan protozoa, and many eubacteria, including numerous human pathogens. Pyruvate (**a**) is condensed with glyceraldehyde 3-phosphate (**b**) to yield 1-deoxy-D-xylulose 5-phosphate (DXP; (**c**)) [84], a branch point intermediate with a role in E. coli vitamin B1 and B6 biosynthesis [85 86 87 88] as well as isoprene biosynthesis. In the first committed step of the E. coli MEP pathway, 1-Deoxy-D-xylulose 5-phosphate reductoisomerase (also called MEP synthase, Dxr or IspC) catalyzes the reduction and rearrangement of **c** to yield MEP (**d**) [89]. CDP-ME synthase then converts MEP into 4-(cytidine 5'-diphospho)-2-C-methyl-D-erythritol (CDP-ME; (**e**)). CDP-ME kinase phosphorylates CDP-ME to **f**, which is subsequently cyclized (coupled with the loss of CMP) by cMEPP synthase to yield 2-C-methyl-D-erythritol 2,4-cyclodiphosphate (**g**) [90 91 92 93 94]. A reductive ring opening of **g** produces 1-

hydroxy-2-methyl-2-butenyl diphosphate (HMBPP; (**h**)) [95 96 97 98 99], which is then reduced to both IPP (**i**) and DMAPP (**j**) in a ~5:1 ratio [100 101 102 103 104 105 106].

Relative to drug development, in addition to being essential in bacteria, MEP pathway enzymes are not present in mammalian cells. Mammals synthesize isoprenoids via the separate mevalonic acid (MVA) pathway, which does not share any enzymes or intermediates in common with the MEP pathway. The MVA pathway is utilized exclusively by most other eukaryotes as well; exceptions include plants, which use the MEP pathway for isoprenoid production in the chloroplast[107], and certain protists containing plastid-like organelles, such as apicomplexans[76]. The apicomplexan malarial parasite *Plasmodium falciparum,* for example, exclusively uses the MEP pathway for isoprenoid production[108]. The essentiality of the MEP pathway in numerous pathogenic bacteria and apicomplexans, coupled with its absence in mammalian cells, make the MEP pathway an attractive target for the development of novel antimicrobials.

The focus of this investigation is on the first two enzymes of the MEP pathway, namely DXP reductoisomerase (IspC, also known as MEP Synthase or DXR) and MEP cytidylyltransferase (aka IspD).

DXP Reductoisomerase (IspC)

The first committed step in the MEP pathway is catalyzed by the enzyme IspC, in which 1-deoxy-D-xylulose 5-phosphate (DXP) is isomerized and reduced into MEP, as shown in Figure 9.

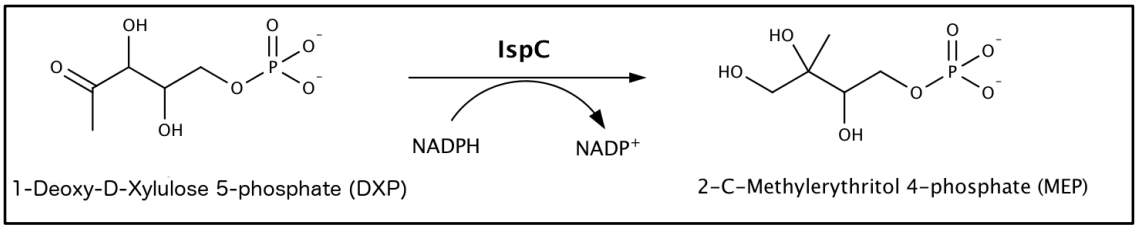

Figure 9. Reaction catalyzed by IspC

The binding order and catalytic mechanism of the enzyme have been established. Binding of cofactor and substrate proceeds via a sequential ordered mechanism, with NADPH binding first, followed by DXP[109]. Conversion of DXP to 2-C-methyl-D-erythritol 4-phosphate (MEP) proceeds through a retroaldol-aldol mechanism, as shown in Figure 10, which despite some originally conflicting evidence[110] is generally accepted based upon the strong experimental support[111,112]. Upon NADPH and subsequent DXP binding (coordinated by an active site divalent cation such as magnesium[113]), the enzyme deprotonates the C4 hydroxyl group of DXP, leading to the generation of the retroaldol intermediates. These two intermediates are formed from cleavage of the C3-C4 bond. Subsequent deprotonation of the C3 carbon facilitates re-formation of a single molecule via an aldol condensation and subsequent re-protonation of the C4 carbon. Attack by the donated hydride of NADPH reduces the C3 carbonyl to the alcohol, such that the product MEP is formed and both MEP and $NADP^+$ leave the active site.

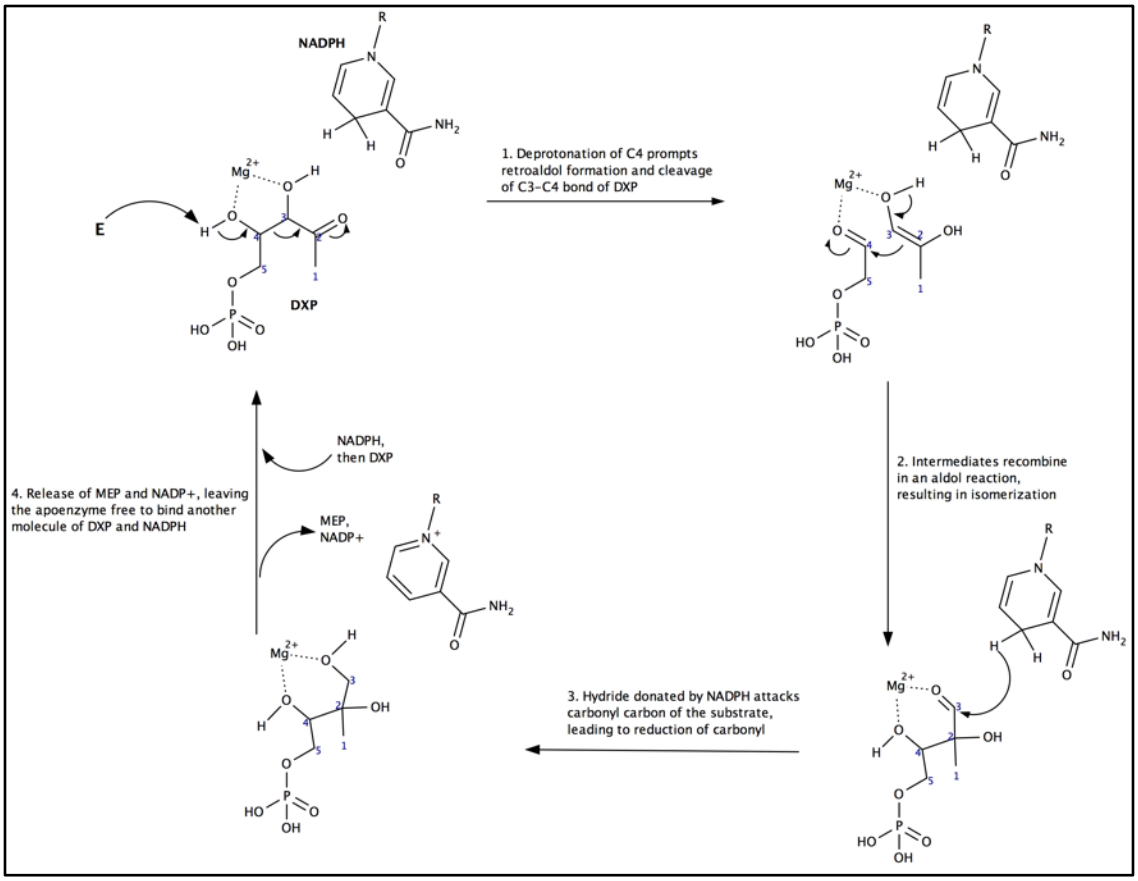

Figure 10. Mechanism of IspC

Crystal structures of the *M. tuberculosis* IspC were the first to reveal conformation changes in the protein coinciding with the binding of each of the substrates[114, 115, 113]. The enzyme first binds NADPH, with the resulting protein conformational change forming the DXP site. DXP then binds to the enzyme, which prompts a disordered "flap region" of the protein to become ordered and close over the substrate binding cleft, protecting the enzyme active site[116]. In the first crystal structures of apo *E.coli* IspC, a single asymmetric unit in the crystal contained three protein molecules, each with the flap region in a different conformation, emphasizing the flexibility of this flap region

prior to substrate binding[117]. Figure 11 shows the conformation change upon substrate binding, using Trp 212 to follow the movement of the flap region. The flap region, and in particular Trp 212, seem to have a role in substrate recognition or orientation[118].

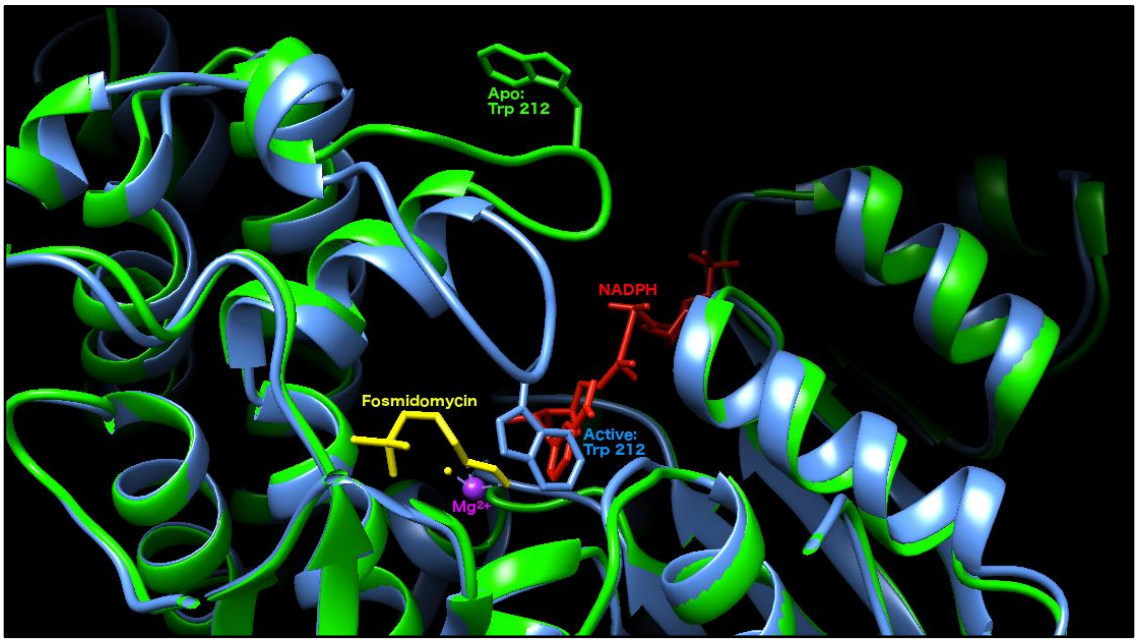

Figure 11. The *Ec*IspC active conformation (PDB 2EGH, colored blue) and an *Ec* apo structure (PDB 1K5H, colored green). The two conformations show significant differences in the loop region, as followed by Trp 212. In the apo conformation, the flap region is open and situated above the active site. In the active conformation, the flap region closes down over the substrate binding site and prevents solvent access. A magnesium cation (purple), NADPH (red), and DXP-analog fosmidomycin (yellow) are shown bound in the active conformation of IspC.

The DXP-analogs known as fosmidomycin[119] and FR900098 (the acetyl derivative of fosmidomycin; Figure 12)[120] are streptomycete natural product inhibitors of IspC. These inhibitors binds to the enzyme after NADPH is bound, inducing the conformational change in the flap region[121].

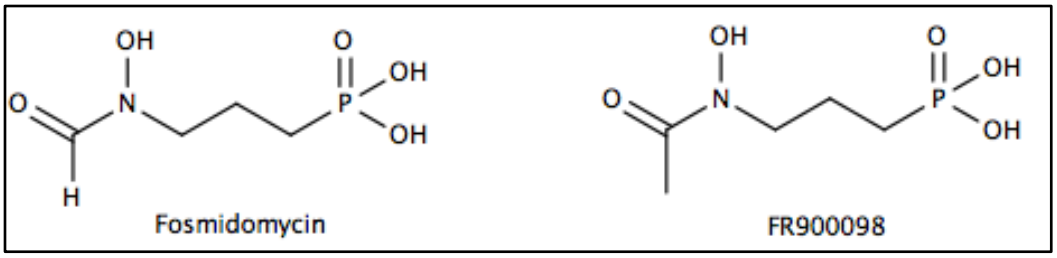

Figure 12. Streptomycete natural product inhibitors of IspC, fosmidomycin (left) and FR900098 (right)

Both FR900098 and fosmidomycin are slow, tight-binding inhibitors of IspC, with nanomolar K_i values[109]. Additionally, initial clinical trials showed that fosmidomycin, when used alone, was safe and partially effective in clearing uncomplicated malaria in patients infected with *Plasmodium falciparum*, with a monotherapy cure rate of 22%[122]. However, the high rates of recrudescent infections eliminate the possibility of using fosmidomycin as a monotherapy for malaria[123]. As a combination therapy with clindamycin, fosmidomycin treatment showed a 100% cure rate, as compared to the previously mentioned 22% cure rate in the control group treated with fosmidomycin alone[122]. A second randomized clinical trial of fosmidomycin-clindamycin combination therapy versus standard treatment sulfadoxine-primethamine showed equivalent cure rates of 94% between the two treatments[124]. Further clinical trials verified that lower dosing, with fosmidomycin-clindamycin treatment at 900 and 300-600 mg respectively every 6 hours for 5 days would lead to the lowest possible dose with a 95% cure rate[125].

While these clinical trials showed that fosmidomycin is safe and effective when used in combination with other drugs, its lack of efficacy and high rate of recrudescene when used as a monotherapy pose problems. Due to rapidly spreading drug resistance

among other approved antimicrobial compounds, novel compounds that can only be used with existing compounds do not represent ideal candidates for combating drug resistant infections. The primary reason for fosmidomycin's lack of efficacy as a monotherapy has been hypothesized to be its low bioavailability of 20-30%, with a serum half-life of 1.5-2 h[126]. This low bioavailability is attributed to fosmidomycin's hydrophilicity, making efforts to increase the lipophilicity of the compound an attractive drug design strategy.

The vast majority of rationally designed inhibitors for IspC are based on a fosmidomycin scaffolding, incorporating substituents, often aromatic, to the carbon linker region or to the retrohydroxamate nitrogen or oxygen. These substituents can be designed to occupy different sites, such as the nicotinamide pocket of the NADPH site, displacing NADPH, as described in this work[127]. Additionally, the Trp 212 of the flap region (see Figure 11) can be utilized for pi-stacking interactions to accept aryl additions, or can be displaced by aryl additions to disrupt formation of the active complex, as given in several crystal structures, and described in part in this work[128, 114].

MEP Cytidylyltransferase (IspD)

The second committed step in the MEP pathway, catalyzed by IspD, involves the transfer of a cytidine monophosphate [CMP] group from cytidine triphosphate [CTP] to MEP, yielding 4-disphosphocytidyl-2-C-methylerythritol [CDP-ME] (Figure 13).

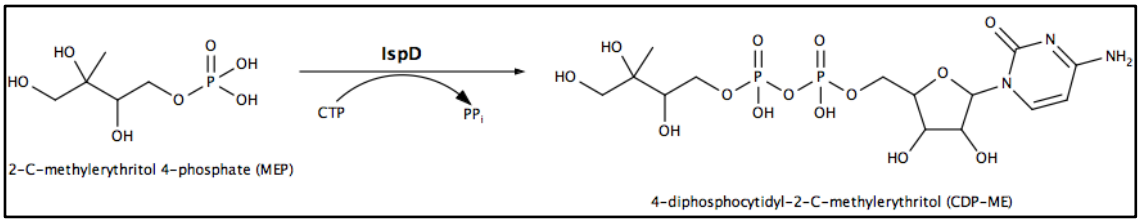

Figure 13. Reaction catalyzed by IspD

Initial kinetic and crystallographic work from the Cane and Noel groups[129,130] has elucidated the catalytic mechanism of IspD. As shown in Figure 14, IspD catalyzes a CMP transfer through a proximity effect in which a nucleophilic oxygen of MEP's phosphoryl group is positioned next to the alpha-phosphorous of CTP, allowing nucleophilic attack on CTP with inorganic pyrophosphatase eliminated as a leaving group[129].

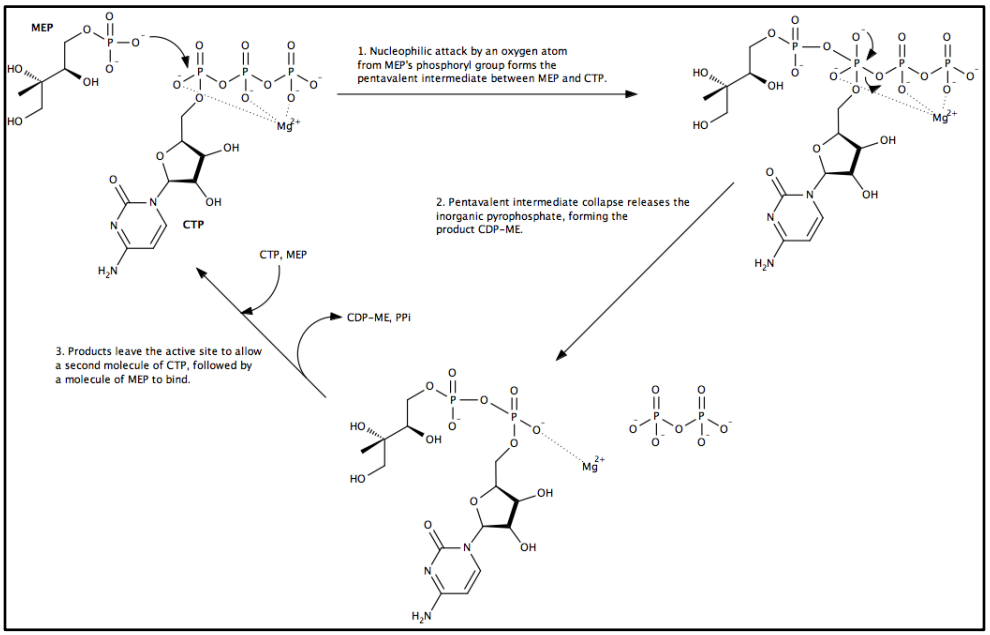

Figure 14. Mechanism of IspD

Kinetic analysis indicates the reaction follows an ordered sequential mechanism in which CTP binding is required prior to MEP binding[130]. Like IspC, IspD also requires a divalent cation for activity. While there are fewer crystal structures reported for IspD than IspC, structures are available for species such as *E. coli*, *F. tularensis*, *M. tuberculosis*, and *A. thaliana*. It is worth noting that *Pf*IspD has a more widely divergent amino acid sequence as compared to bacterial homologs, being much larger and containing a roughly 60 residue hydrophilic chain region not seen in other species[131]. It was suggested that this chain, found in the middle of the protein, could link IspD domains, explaining the larger size of the protein. Unfortunately, no crystal structures of *Pf*IspD are available. In some species, including several pathogenic bacteria such as *H. pylori*, *C. jejuni*, and *T. pallidum*, the genes for IspD and downstream MEP pathway protein IspF are fused, generating a bifunctional IspDF protein[132]. The only bifunctional IspDF protein crystallized is the homolog from *C. jejuni*, which forms a hexameric structure (in contrast to the typical homodimeric IspD and homotrimeric IspF)[133]. It has been suggested that the bifunctionality of IspDF, as well as evidence of association between *E. coli* proteins IspD, IspE, and IspF, are supportive of the formation of a metabolon *in-vivo* to facilitate substrate channeling in all or part of the MEP pathway[133].

In silico analysis reveals that the active site of IspD is the least lipophilic of all of the enzymes in the MEP pathway[134], which taken along with the rather solvent-exposed binding site of CTP, render the enzyme challenging for drug design. An allosteric site on IspD could prove a better target for design of inhibitors with structures

that are “drug-like” enough to move forward to clinical use. Current reports of an allosteric pocket on IspD provide this opportunity. Discovered during a high-throughput screening (HTS) campaign for novel herbicides targeting IspD, compounds binding in this allosteric site were both potent (the best compound had an IC_{50} against *Arabidopsis thaliana* IspD of 140 nM) and lipophilic[135]. As shown in Figure 15, the amino acids in this binding site are partially conserved in several bacterial homologs, suggesting that they could have an allosteric pocket similar to that observed in AtIspD.

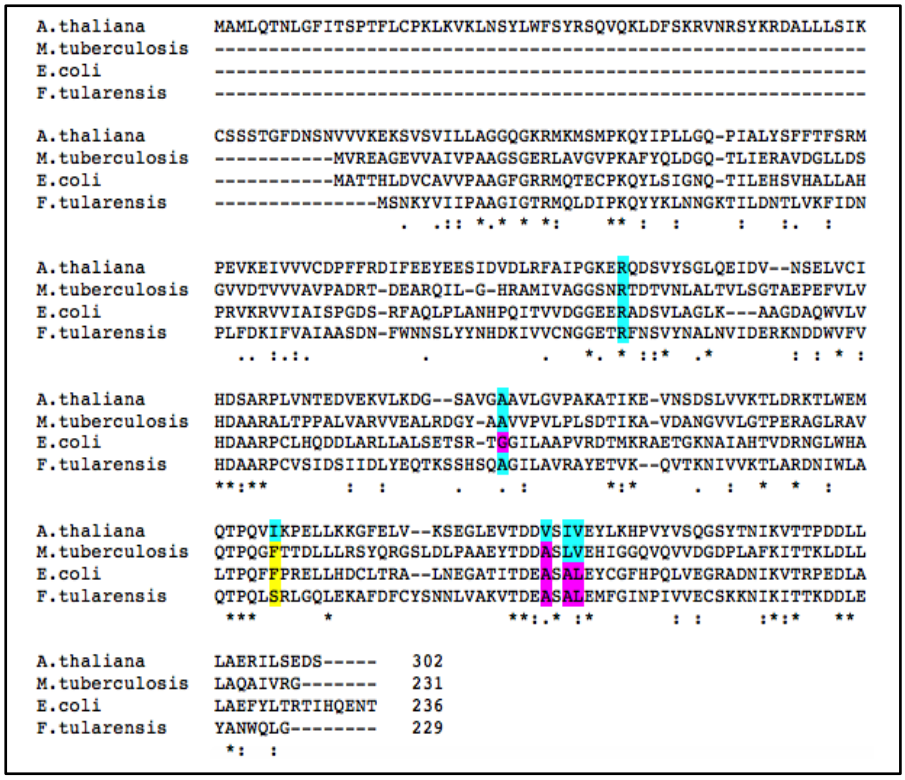

Figure 15. Sequence alignment of *Arabidopis thaliana* IspD with several bacterial homologs. Shown in blue are those residues identified as part of the allosteric pocket found in AtIspD and conserved in the selected bacterial homologs, while pink indicates similar residues to those found in the AtIspD allosteric site and yellow indicates residues that are not similar to the residue found in the AtIspD allosteric site.

Figure 16 details the structural changes that occur upon inhibitor binding to the allosteric site on AtIspD, showing how a small lipophilic compound can inhibit the activity of IspD, despite the enzyme's generally hydrophilic active site[134]. Upon binding the small molecule, the active site is constricted. While the evidence of an allosteric site on the *Arabidopsis* homolog was first being published in 2011, and the list of compounds binding in the site expanded in 2014[136] , there has not been significant work published indicating the presence of a lipophilic, allosteric site on any bacterial homologs.

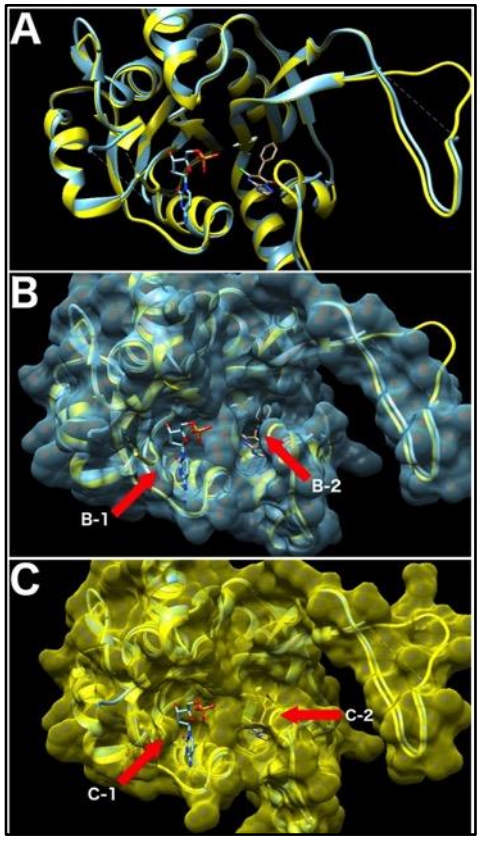

Figure 16. Changes in conformation upon binding the allosteric inhibitor. A) Blue: CMP-bound *A.thaliana* IspD, 1W77 Yellow: Inhibitor-bound *A.thaliana* IspD, 2YC3. Inhibitor bound AtIspD does not show a significantly different tertiary structure from the CMP bound structure. Inhibitor activity is due to subtle changes near the active

site. B) Space filling model of CMP-bound AtIspD (blue). This structure shows a clear CTP binding pocket (B-1), while the pocket where the inhibitor binds is slightly occluded (B-2). C) Space filling model of inhibitor-bound AtIspD. Upon inhibitor binding to the allosteric site (C-2), the CTP pocket is constricted (C-1), which prevents CTP binding.

Overall, while there have been very few inhibitors of bacterial IspD homologs published, the plasmodial IspD homolog has proven to be a clinically relevant target with potent inhibitors identified. The publically available Malaria Box, a collection of 400 chemotypes with known antimalarial activity[137], includes a compound MMV008138 with a previously unknown target. After the collection was made available, it was revealed that MMV008138 was a potent and specific inhibitor of *Plasmodium falciparum* IspD, binding competitively with CTP[138]. Additionally, a series of benzoisothiazolones have recently been shown to be potent inhibitors of PfIspD *in vitro*. Potency against PfIspD correlated to antimalarial activity, suggesting some level of specificity for IspD *in vivo*[139]

Conclusions

Given the growing problem of antimicrobial resistance, and the relative lack of new antimicrobial compounds being introduced to the clinic, there is a desperate need for novel targets and novel compounds. The MEP pathway provides a very attractive target for novel antibiotics, as it is present in a number of clinically relevant pathogens, lacks homologs in mammalian cells, and is essential for microbial growth and survival. The first two committed steps in the pathway, IspC and IspD, both provide opportunities and challenges for drug development. This thesis presents research utilizing rational and random chemical libraries to identify novel scaffolds for inhibitors

of IspC and IspD. Lead compounds from both libraries are compared and contrasted in terms of their potency, binding mode, and antimicrobial activity.

SPECIFIC AIMS AND DISSERTATION OVERVIEW

The primary purpose of this research is to screen both IspC and IspD with multiple types of chemically-diverse libraries (rational and random in design), determining mechanism of enzyme inhibition and relative antimicrobial activity of select hit compounds, in order to bring new chemical classes forward for antimicrobial therapeutic development. To attain this goal, we proposed and performed the following four specific aims:

Specific Aims

Specific Aim 1: Rational Compound Screen with IspC and IspD

In this Aim, both IspC and IspD are used in structure–activity relationship (SAR) assays, guiding the development of rationally-designed inhibitors. The IspC inhibitors, provided by our collaborator Dr. Cynthia Dowd, consist of synthetic, rationally-designed compounds (based on the scaffolding of the known competitive inhibitor fosmidomycin) designed to interact with either the substrate binding pocket or to bridge the substrate binding pocket and the cofactor binding site (a "bisubstrate" approach). Recombinant IspC homologs from *Yersinia pestis*, *Mycobacterium tuberculosis*, *Plasmodium falciparum*, and *Escherichia coli* were expressed, purified, and selectively utilized in this SAR effort. We hypothesize that compounds with aryl additions to the fosmidomycin scaffold will result in more potent inhibitors of IspC

than will compounds with cycloalkyl additions, as the aryl addition will bind in the nicotinamide binding pocket for NAPDH, based upon docking studies. Furthermore, we hypothesize that compounds with substituents to fosmidomycin's formyl group ("amide-linked") will be more potent than compounds with substituents to the hydroxyl group of the retrohydroxamate ("O-linked"), since the latter participates in chelation of the enzyme bound divalent cation[140].

The IspD inhibitors, provided by collaborators at Walter Reed Army Institute of Research, contain rationally designed compounds docked into active site of the *F. tularensis* crystal structure, with the compounds designed to occupy a site bridging the substrate and cofactor binding sites. As such, we hypothesize that these inhibitors will be competitive with respect to both MEP and CTP binding. For Specific Aim 1, we used recombinant *F. tularensis* IspD in the screening.

Overall, in performing Specific Aim 1, numerous molecules were evaluated as potential inhibitors of IspC or IspD, and several of these were further examined by determining their IC_{50} value, mechanism of enzyme inhibition, and antimicrobial activity, to contribute towards an iterative SAR process.

Specific Aim 2: LOPAC^{1280} Library Screen with IspC and IspD

In Specific Aim 2, IspC and IspD were individually assayed with compounds present in the commercially available LOPAC^{1280} library, containing 1280 molecules, many of which are FDA-approved pharmaceuticals. This high-throughput screen (HTS) was conducted with *Yersinia pestis* IspC and *Francisella tularensis* IspD, utilizing a 96-well plate-based assay developed in house. All hits are coupled to a secondary screen

using an appropriate homolog (*Mycobacterium tuberculosis* IspC or *Escherichia coli* IspD) to test for broad spectrum activity. Furthermore, a tertiary screen was employed to control for false-positives, using an IspC-IspD coupled assay for IspC hits, and a pyrophosphatase assay for IspD hits. Select hit compounds were subsequently evaluated for IC_{50} value, mechanism of enzyme inhibition, and antimicrobial activity. Given a typical HTS hit rate of 0.1-0.5%[143], we hypothesized that a library of at least 1000 compounds was sufficient to generate at least one hit molecule for each enzyme assayed.

Specific Aim 3: Natural Product Library Screen with IspC and IspD

In this Specific Aim, *Yersinia pestis* IspC and *Francisella tularensis* IspD were individually assayed with our in-house, proprietary collection of natural product extracts, obtained from various plants and fungi. Given the diversity of compounds produced by plants and fungi, we hypothesized that an inhibitor of YpIspC and/or FtIspD will be identified and serve as a novel scaffold for the development of a new class of MEP pathway inhibitors. After screening the library for inhibitory activity, hit-extracts were assessed for IC_{50} activity, mechanism of enzyme inhibition, and antimicrobial activity, and where appropriate the active inhibitor/molecule was identified using an affinity purification technique coupled with LC-MS/MS.

Specific Aim 4: Crystallographic Structure Determination of IspC and/or IspD

To aid in the rational design and development of inhibitors, in Specific Aim 4 protein crystal structures of IspC and IspD were sought, using purified recombinant enzymes cloned from *Yersinia pestis* and *Francisella tularensis*. Using conditions

established for the crystallization of the apo form of both YpIspC and FtIspD, we hypothesized that modifications to the buffer conditions, protein concentration, and temperature will yield high resolution structures of IspC/IspD with and without bound inhibitor. Where suitable, co-crystallization studies were explored using promising library compounds (hits/leads) identified in Specific Aims 1-3.

Dissertation Overview

A Note to My Thesis Committee:

A significant amount of the work described herein has already been published in peer-reviewed journals[127, 144, 128, 145], with myself as primary author for one of these papers and as a co-author for the other four. For clarity, in this thesis I have subdivided Specific Aim 1 into two distinct parts; the first involving rational compound screens with purified recombinant IspC, and the second part involving rational compound screens with purified recombinant IspD. The published material is the work reported in Part 1. As such, in Part I of Specific Aim 1, I present in the thesis each of the 5 papers with a brief synopsis, and include sequentially embedded images of each peer-reviewed publication in Appendix I (per Mason guidelines, the embedded papers must be placed in the Appendix of the thesis; all figures and text from these references were reproduced with permission from the respective journals). The rest of the thesis material is currently unpublished and is sequentially presented in detail herein.

SPECIFIC AIM 1, PART 1 — RATIONAL COMPOUND SCREENS WITH ISPC

In Part 1 of Specific Aim 1, IspC was used in structure–activity relationship (SAR) assays, guiding the development of rationally-designed inhibitors. The IspC inhibitors, provided by our collaborator Dr. Cynthia Dowd, consist of synthetic, rationally-designed compounds (based on the scaffolding of the known competitive inhibitor FR900098) designed to interact with either the substrate binding pocket or to bridge the substrate binding pocket and the cofactor binding site (a "bisubstrate" approach). Recombinant IspC homologs from *Yersinia pestis*, *Mycobacterium tuberculosis*, *Plasmodium falciparum*, and *Escherichia coli* were expressed, purified, and selectively utilized in the SAR effort. Select inhibitors of IspC were evaluated for IC_{50} value, mechanism of enzyme inhibition, and antimicrobial activity, to facilitate the iterative SAR process.

Specific Aim 1, Part 1 covers the rational compound screens with IspC and is comprised of five peer-reviewed publications, referenced below as Papers I-V. All five papers are presented in "Appendix 1 – Published Work" in their final published format.

Paper I: Design of Potential Bisubstrate Inhibitors against Mycobacterium tuberculosis (Mtb) 1-Deoxy-D-Xylulose 5-Phosphate Reductoisomerase (Dxr)- Evidence of a Novel Binding Mode

San Jose G, Jackson ER, Uh E, Johny C, Haymond A, Lundberg L, et al. *MedChemComm.* 2013; 4: 1099–1104. doi:10.1039/C3MD00085K

Synopsis

Due to poor cellular uptake of natural products fosmidomycin and FR900098 by *Mycobacterium tuberculosis*, lipophilic analogs based on the fosmidomycin core structure were generated to improve cellular penetration. These analogs were designed using docking studies with the MtbIspC crystal structure to bind to both the DXP and NADPH binding sites. The most potent compound inhibited both IspC activity and *Mycobacterium tuberculosis* growth, and binds to the enzyme with a non-bisubstrate binding mode.

Attributions and Contributions

Reproduced with permission from the Royal Society of Chemistry. All supplementary information as referenced in the text can be found in Appendix 2. The author was responsible for the generation of the enzyme kinetics data reported in Table 1 and the information presented in Figure 4.

Published Text

Please refer to "Paper I: Design of Potential Bisubstrate Inhibitors against Mycobacterium tuberculosis (Mtb) 1-Deoxy-D-Xylulose 5-Phosphate Reductoisomerase (Dxr)- Evidence of a Novel Binding Mode" given in Appendix 1, page 167 for the full text of the paper as it appears in print.

Paper II: Kinetic Characterization and Allosteric Inhibition of the Yersinia pestis 1-Deoxy-D-Xylulose 5-Phosphate Reductoisomerase (MEP Synthase)

Haymond A, Johny C, Dowdy T, Schweibenz B, Villarroel K, Young R, et al. *PLoS ONE*. 2014; 9: e106243. doi:10.1371/journal.pone.0106243

Synopsis

IspC from *Yersinia pestis* was cloned, expressed, purified, and characterized. Determination of K_i values for FR900098 and fosmidomycin revealed a preference for FR90098 over fosmidomycin, in contrast to MtbIspC. Initial screens with a rationally-designed bisubstrate library and a natural product library produced one rationally-designed hit with an apparent bisubstrate mechanism, and one natural product extract with an apparent allosteric mechanism.

Attributions and Contributions

Reproduced with permission from the Public Library of Science. All supplementary information as referenced in the text can be found in Appendix 2. The author was responsible for performing the experiments, writing the text of the paper, as well as the generation of Figure 3, Figures 8-14, and Figure 17.

Published Text

Please refer to "Paper II: Kinetic Characterization and Allosteric Inhibition of the Yersinia pestis 1-Deoxy-D-Xylulose 5-Phosphate Reductoisomerase (MEP Synthase)" given in Appendix 1, page 174 for the full text of the paper as it appears in print.

Paper III: The effect of chain length and unsaturation on Mtb Dxr inhibition and antitubercular killing activity of FR900098 analogs

Jackson ER, San Jose G, Brothers RC, Edelstein EK, Sheldon Z, Haymond A, et al. *Bioorg Med Chem Lett.* 2014; 24: 649–653. doi:10.1016/j.bmcl.2013.11.067

Synopsis

A series of analogs of FR900098 and fosmidomycin were generated to determine the optimal carbon linker length and tolerance of unsaturation between the retrohydroxamate and phosphonate moieties of the parent compounds. While optimal chain length was determined to be 3 carbon units, both propyl and propenyl linkers were tolerated. Ethyl and pivaloyl esters of these compounds displayed anti-tubercular activity, with the pivaloyl ester of compound **22** (propenyl analog of FR900098) showing greater activity than the pivaloyl ester of the saturated parent compound.

Attributions and Contributions

Reproduced with permission from Elsevier. The author was responsible for the generation of the kinetic data in Tables 1 and 3.

Published Text

Please refer to "Paper III: The effect of chain length and unsaturation on Mtb Dxr inhibition and antitubercular killing activity of FR900098 analogs" given in Appendix 1, page 191 for the full text of the paper as it appears in print.

Paper IV: Synthesis and bioactivity of β-substituted fosmidomycin analogues targeting 1-deoxy-D-xylulose-5-phosphate reductoisomerase

Chofor R, Sooriyaarachchi S, Risseeuw MDP, Bergfors T, Pouyez J, Johny C, et al. *J Med Chem.* 2015;58: 2988–3001. doi:10.1021/jm5014264

Synopsis

Analogs of FR900098 containing either aryl or alkylaryl additions to the β-position of the parent compound were assayed with IspC from *P. falciparum*, *E.coli*, and *M. tuberculosis.* In general, these compounds were more potent against PfIspC than against Ec or MtbIspC; when assayed against whole cells, five compounds had nanomolar EC_{50} values against *Plasmodium falciparum* K1. Crystal structures of the most potent compounds indicate that the aryl substituents disrupt a key tryptophan residue in the flap region of IspC, leading to an aberrant flap structure.

Attributions and Contributions

Reproduced with permission from the American Chemical Society. Copyright 2015 American Chemical Society. All supplementary information as referenced in the text can be found in Appendix 2. The author was responsible for the generation of the MtbIspC kinetic data in Figure 4 and Table 1.

Published Text

Please refer to "Paper IV: Synthesis and bioactivity of β-substituted fosmidomycin analogues targeting 1-deoxy-D-xylulose-5-phosphate reductoisomerase" given in Appendix 1, page 197 for the full text of the paper as it appears in print.

Paper V: Structure-Activity Relationships of the MEPicides: N-Acyl and O-linked Analogs of FR900098 as Inhibitors of Dxr from Mycobacterium tuberculosis and Yersinia pestis

San Jose G, Jackson ER, Haymond A, Johny C, Edwards RL, Wang X, et al.
ACS Infect Dis. 2016; doi:10.1021/acsinfecdis.6b00125

Synopsis

Fosmidomycin analogs functionalized with aryl moieties on the formyl group (the N-acyl series) or on the hydroxyl group of the retrohydroxamate (the O-linked series) were assayed with MtbIspC and YpIspC. In general, compounds from both classes were more potent against YpIspC than MtbIspC. The most potent compound against both homologs had nanomolar IC_{50}s, a bisubstrate mechanism, and its dipivaloyloxymethyl ester analog had notable anti-tubercular activity.

Attributions and Contributions

Reproduced with permission from the American Chemical Society. Copyright 2016 American Chemical Society. All supplementary information as referenced in the text can be found in Appendix 2. The author was responsible for the generation of kinetic data in Figure 3 and Table 1, and Figures 4 and 5.

Published Text

Please refer to "Paper V: Structure-Activity Relationships of the MEPicides: N-Acyl and O-linked Analogs of FR900098 as Inhibitors of Dxr from Mycobacterium tuberculosis and Yersinia pestis" given in Appendix 1, page 213 for the full text of the paper as it appears in print.

SPECIFIC AIM 1, PART 2 — RATIONAL COMPOUND SCREEN WITH ISPD

In Part 2 of Specific Aim 1, the second enzyme of the MEP pathway (IspD) was used in structure–activity relationship (SAR) assays, guiding the development of rationally-designed inhibitors. The compounds to be screened were provided by collaborators at Walter Reed Army Institute of Research, and consist of rationally designed compounds docked into active site of the *F. tularensis* crystal structure, with the compounds designed to occupy a site bridging the substrate and cofactor binding sites. For Specific Aim 1, we used recombinant *F. tularensis* IspD in the screening.

Recombinant *F. tularensis* IspD was used as the target enzyme, and after an initial assessment of relative potency, select inhibitors of IspD were further evaluated for IC_{50} value, mechanism of enzyme inhibition, and antimicrobial activity. This material is currently unpublished work, and as such, is fully detailed below.

Introduction

Identified during a HTS campaign for novel herbicides, compounds binding to an allosteric site on *Arabidopsis thaliana* IspD were discovered and found to be both potent (the best compound had an IC_{50} against AtIspD of 140 nM) and lipophilic[135]. As discussed in the MEP Cytidylyltransferase (IspD) introduction, the amino acids in this binding site are partially conserved across several bacterial homologs (refer to Figure 15), suggesting that they too may have an allosteric pocket similar to that observed in AtIspD. However, the active site of IspD may also be able to accommodate lipophilic inhibitors if they bind in a more bisubstrate manner. Hence, we set out to identify novel inhibitors of the bacterial IspD by screening a small, lipophilic molecular library with cloned, expressed, and purified *F. tularensis* IspD. In collaboration with WRAIR, the hit molecules were used to guide the synthesis of a targeted library of compounds, which were subsequently evaluated for activity against FtIspD. Overall, this study reveals three lipophilic compounds with activity against IspD, and two with activity against whole-cell *F. tularensis* subsp. *novicida* and *Y. pestis* subsp. A1122.

Initial Design Considerations and Preliminary Results

In order to facilitate the rational screening effort, structurally diverse compounds from the National Cancer Institute's Developmental Therapeutics Program compound database[146] were docked with the *F. tularensis* crystal structure (PDB ID: 4MYB, Noble, S.M., Tsang, A.K., Couch R.D.). Thirty-five lipophilic compounds found to bind in the active site were obtained and were screened at 100 μM against FtIspD. While none of the compounds showed appreciable inhibitory activity when

assayed after the addition of CTP to the assay mixture (data not shown), two compounds displayed inhibitory activity when preincubated with the enzyme prior to the addition of CTP. As shown in Figure 17, these two compounds are known as NSC 110039 and NSC 401145. The structure of each compound is presented in Figure 18.

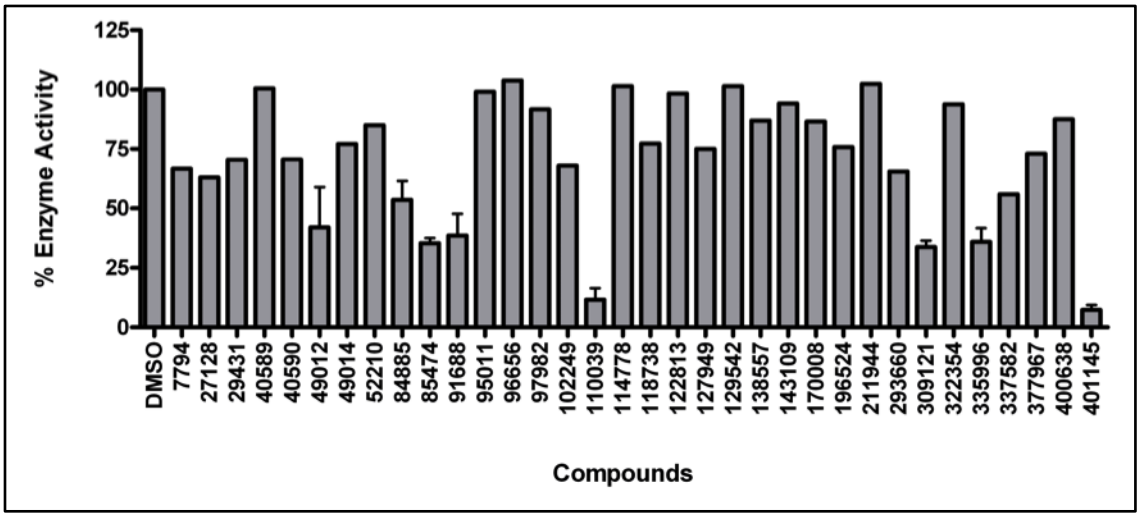

Figure 17. Pilot-scale library screened with FtIspD. Each compound was assayed at 100 µM and preincubated with FtIspD prior to the addition of CTP. Of these 35 compounds, 2 showed appreciable activity, NSC 110039 and NSC 401145. Error bars are calculated as the deviation from the mean of two independent measurements.

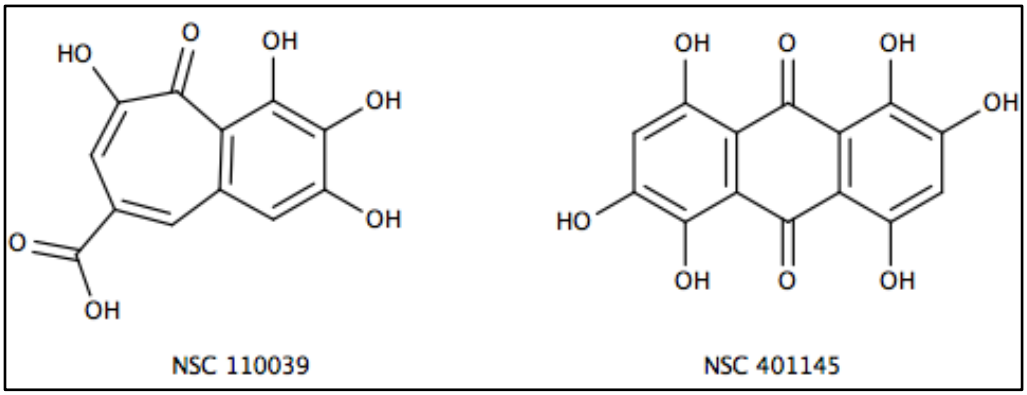

Figure 18. Structures of IspD hit compounds NSC 110039 and NSC 401145

Since each of the two compounds reduced the catalytic activity of the enzyme by more than 80% (Figure 17), the dose-response plot for each was determined. As shown in Figure 19, each compound was found to have an IC_{50} value in the low micromolar range.

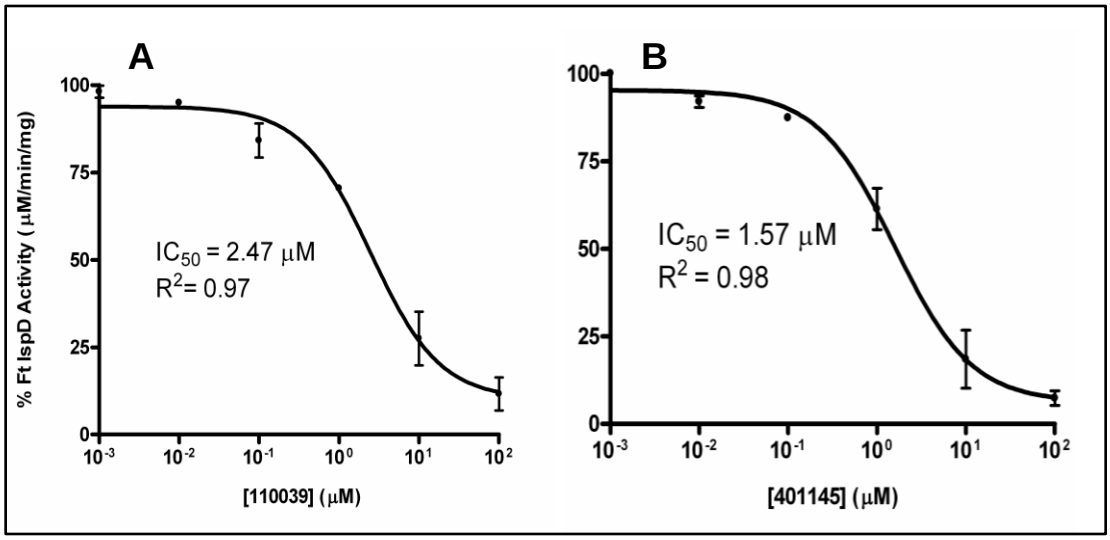

Figure 19. IC_{50} determination for hit IspD compounds A) NSC 110039 and B) NSC 401145

When examining each compound for activity in bacterial growth-inhibition assays, NSC 401145 had only very mild antibacterial activity, partially attributed to poor solubility in the growth media. However, NSC 110039 showed significant antibacterial activity at 100 μM against *Y. pestis* subsp. A1122 (Figure 20). This activity is comparable to kanamycin at 100 μM, and as such, full dose-response curves for NSC 110039 were warranted to determine potency.

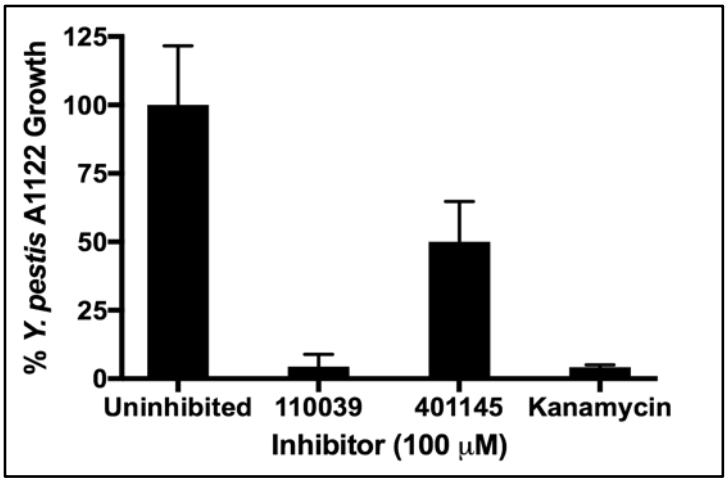

Figure 20. *Y.pestis* subsp. A1122 growth in the presence of NSC 110039 and NSC 401145. While 401145 showed only very mild antibacterial activity, 110039 showed antibacterial activity of the same magnitude as known antibiotic kanamycin at 100 μM. Error bars are calculated as the deviation from the mean of two independent measurements.

As seen in Figure 21, the dose-response curves reveal that NSC 110039 has activity with respect to both *Y. pestis* subsp. A1122 and *F. tularensis* subsp. *novicida*, demonstrating a high micromolar EC_{50} value with both bacteria. It was less potent than the reference inhibitor kanamycin with respect to *F. tularensis* subsp. novicida, with an EC_{50} of 69.24 μM (18.29 μg/mL) versus kanamycin's EC_{50} of 5.077 (2.46 μg/mL; data shown in Figure 22). However, NSC 110039 had a similar potency to kanamycin with respect to *Yersinia pestis* subsp. A1122, with an EC_{50} of 49.97 μM (13.2 μg/mL) as compared to kanamycin's EC_{50} of 33.4 μM (16.2 μg/mL; data shown in Figure 22). Interestingly, both dose-response curves for *F. tularensis* subsp. novicida and *Y. pestis* subsp. A1122 had very steep slopes, with Hill coefficients of 8.5 and 4.1 respectively, as compared to a standard 1.0 in a curve following normal Hill kinetics. While the biological implications of such deviation is an area of current research, the kinetics of

drug uptake have been shown to be one factor influencing Hill coefficients[147]. Investigation into uptake and efflux of NSC 110039 would be warranted during further development of these compounds to better understand the unusual dose-response curves.

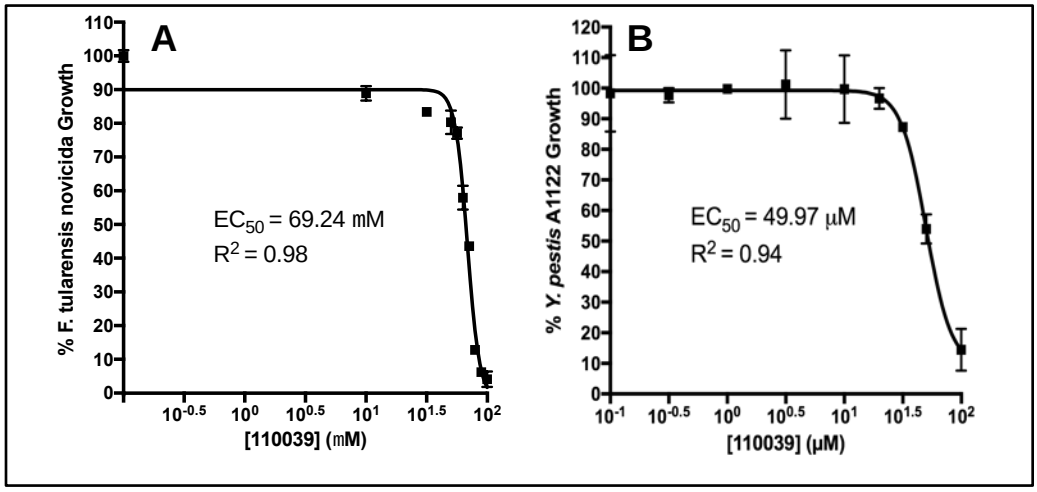

Figure 21. EC_{50} of NSC 110039 with respect to A) *F. tularensis* subsp. *novicida* and B) *Y. pestis* subsp. A1122. Error bars are calculated as the deviation from the mean of two independent measurements.

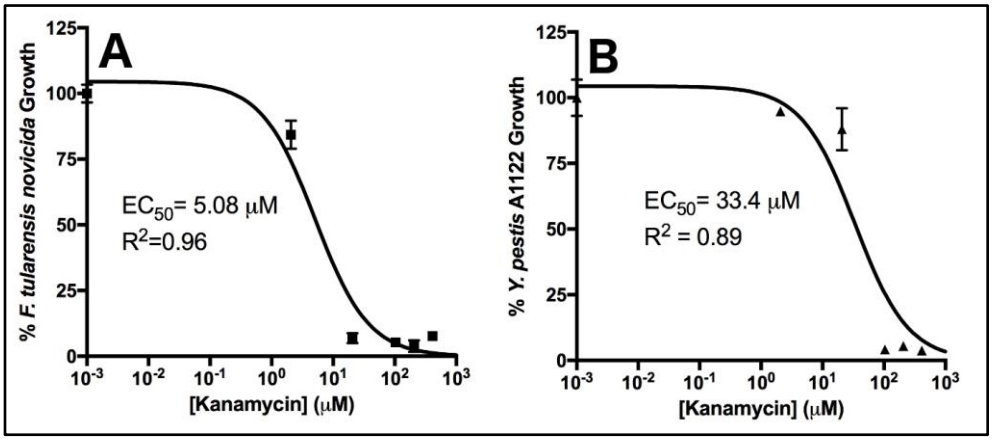

Figure 22. EC_{50} of kanamycin with respect to A) *F. tularensis* subsp. *novicida* and B) *Y. pestis* subsp. A1122. Error bars are calculated as the deviation from the mean of two independent measurements.

Mechanism of Enzyme Inhibition

Given the low IC_{50} values of the above compounds (refer to Figure 19), and in particular the antibacterial activity of NSC 110039, information about the potential binding site of both NSC 110039 and NSC 401145 was desired. Classical Lineweaver-Burk plots were generated to determine mechanism of inhibition of each compound with respect to CTP and MEP. NSC 110039 proved to bind competitively to IspD with respect to both CTP and MEP (Figure 23). This mechanism of action data can be interpreted to support two different proposed binding modes: in the first binding model, the inhibitor could be binding in the active site itself, such that it interferes directly with CTP and MEP binding. In the second, the inhibitor could be binding in an allosteric pocket, such that inhibitor binding induces changes in the topology of the active site such that neither CTP nor MEP can bind. In this second proposed binding mode, the competitive mechanism of action plots are obtained because inhibitor and substrate binding are mutually exclusive, even though the substrate and inhibitor do not bind in the same pocket. It is worth commenting that while all noncompetitive inhibitors are allosteric, not all allosteric inhibitors are noncompetitive[148]. Thus the competitive profile with respect to both MEP and CTP does not preclude the possibility of an allosteric binding site for NSC 110039.

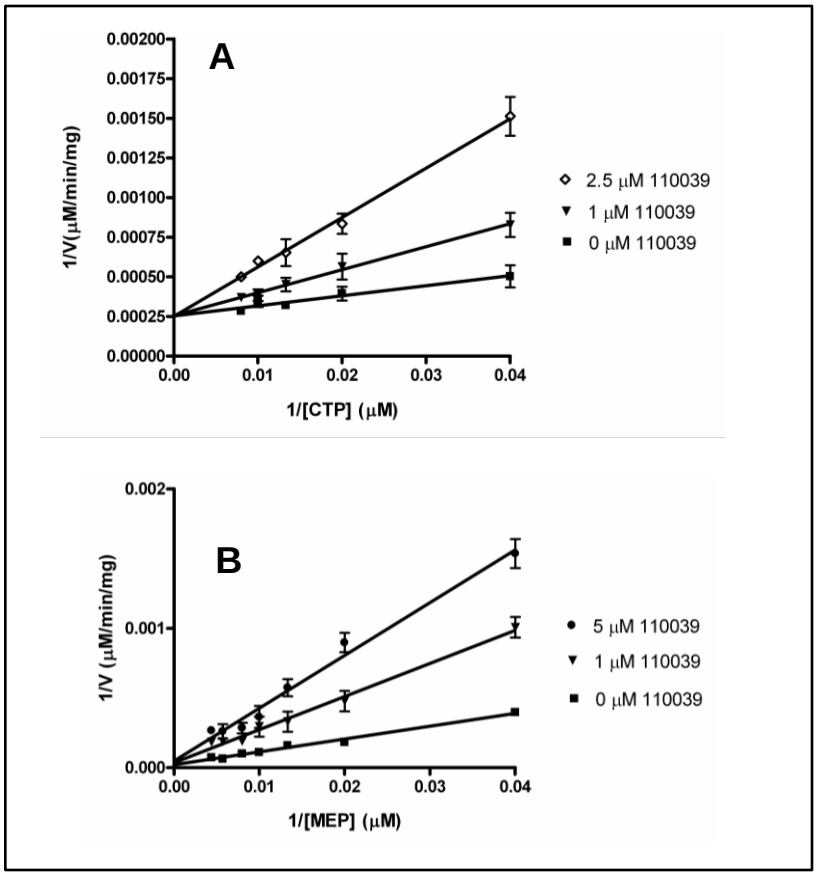

Figure 23. Mechanism of action plots for NSC 110039 assayed with FtIspD with respect to A) CTP and B) MEP. NSC 110039 shows a competitive profile with respect to both the substrates. Error bars are calculated as the deviation from the mean of two independent measurements.

Given the structure of the compound (Figure 18) and the hydrophilicity of the active site of the enzyme to accommodate CTP and MEP, it is not certain that the inhibitor is binding in the active site; however, docking studies demonstrate binding at the intersection of the CTP and MEP sites. Figure 24 shows the active site of EcIspD with CTP bound for reference, and shows the location of the active site with respect to the entire enzyme structure, emphasizing its solvent exposure. The lack of a large lipophilic pockets found at the active site underscores the difficulty of assuming the

active site as the binding pocket for NSC 110039, given other lipophilic pockets on FtIspD are present.

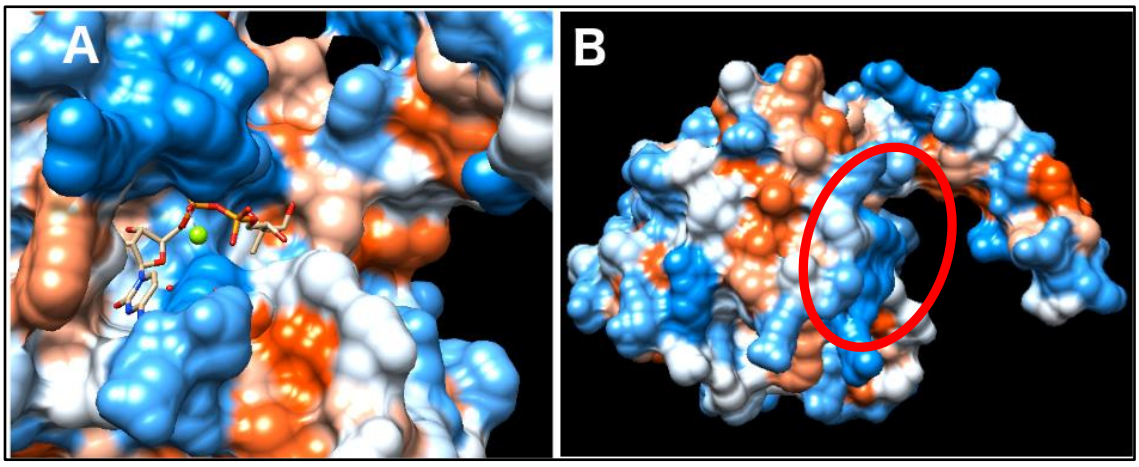

Figure 24. Hydrophilicity of active site of EcIspD, PDB 1I52. A) Active site of EcIspD shown with bound with CTP. Hydrophobicity of residues is indicated according to the Kyle Doolite scale, with blue being the most hydrophilic and orange being the most hydrophobic. **B)** Monomer of EcIspD, with active site circled in red. The active site is particularly solvent exposed.

However, given the competitive profile of NSC 110039 with respect to both substrates, any proposed binding pocket for NSC 110039 must influence the active site when the inhibitor is bound in a way that directly prohibits the binding of both substrates. This kind of binding is illustrated in the case study of AtIspD. Figure 25 illustrates the constriction of the active site in the presence of the lipophilic inhibitor, which binds in a location in close proximity to the active site in Figure 25A. When the inhibitor is absent (Figure 25A), the CTP and MEP pockets are unobstructed. When the inhibitor binds to this site, the conformation of the protein changes to that shown in Figure 25B. In this conformation, the CTP binding site is constricted by the movement

of the backbone carbon of Gly 87 into the CTP binding pocket, labeled and shown in red. This tightening of the CTP pocket indicates how an inhibitor binding at a remote location could prevent CTP binding, thus giving a competitive profile with respect to CTP. Additionally, the side chain of Asp 262 twists from facing outside the protein in the apo structure to branching over the inhibitor and into the MEP binding site, labeled and shown in red in Figure 25B. This intrusion into the MEP binding site indicates how binding of the inhibitor could prevent MEP binding, thus giving a competitive profile with respect to MEP.

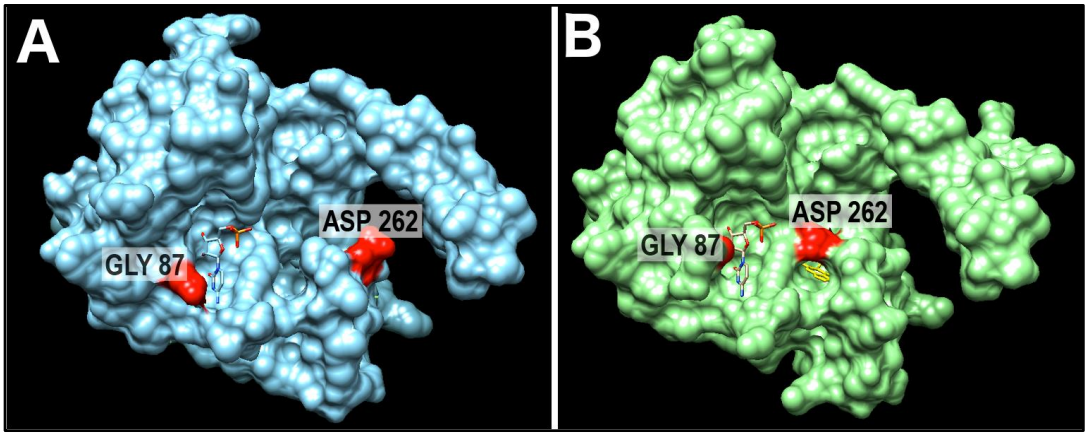

Figure 25. Conformational changes upon inhibitor binding in AtIspD model. A) AtIspD structure with CMP bound shown in blue (1W77). Both Gly 87 and Asp 262 are clear of active site binding pockets. B) Lipophilic inhibitor, shown in yellow, bound to AtIspD, shown in green (2YC3). Intrusion into the CTP site by Gly 87 (red) and into the MEP site by Asp 262 (red) restricts the size of the active site.

In light of the AtIspD inhibitor-bound crystal structure, NSC 110039 could potentially binding to FtIspD at an allosteric site in a similar fashion as seen with AtIspD[135]. Because allostery refers to the location of inhibitor binding (i.e. a site other than the active site) rather than the manner of binding with respect to a substrate,

allosteric inhibitors can have competitive, noncompetitive, or uncompetitive mechanism of inhibition profiles with respect to a substrate[148]. Given the AtIspD model, it is unclear if NSC 110039 is binding in the active site or at a lipophilic site elsewhere. Further crystallographic evidence will be required to clarify the binding mode of NSC 110039.

Lineweaver-Burk plots were also completed for NSC 401145, despite the poorer antimicrobial activity. As shown in Figure 26, NSC 401145 was also found to be competitive with respect to both CTP and MEP.

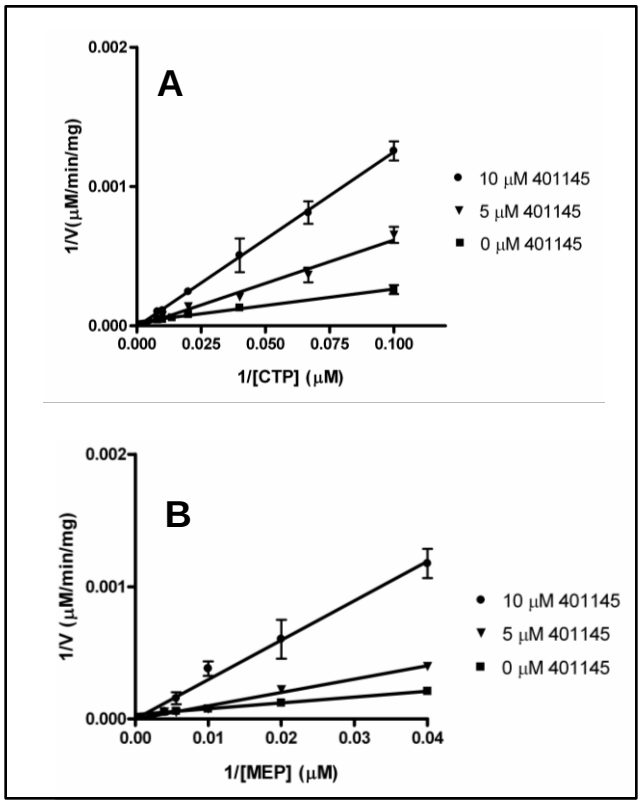

Figure 26. Mechanism of action plots for NSC 401145 assayed with FtIspD with respect to A) CTP and B) MEP. NSC 401145 shows a competitive profile with respect to both the substrates. Error bars are calculated as the deviation from the mean of two independent measurements.

Given the differences in the structures of NSC 110039 and NSC 401145 (Figure 18), it is unknown whether they could bind in a similar allosteric pocket or in the same site in the active site. The identified allosteric pocket on AtIspD was shown to be quite flexible, accommodating both an azolopyrimidine as well as a halogenated pseudilin[136]. Further crystallographic studies to identify the binding pocket of NSC 110039 and NSC 401145 on FtIspD are essential to understanding the inhibitory mechanism of these compounds.

Second Generation of Inhibitors

Based on the hit compounds NSC 401145 and NSC 110039, seven additional lipophilic compounds were synthesized at WRAIR in order to see if modifications to the inhibitor structures could increase potency against the enzyme and/or microbes. As shown in Figure 27, of the seven new compounds, only one showed significant activity against FtIspD at 100 µM (compound WR016773-3).

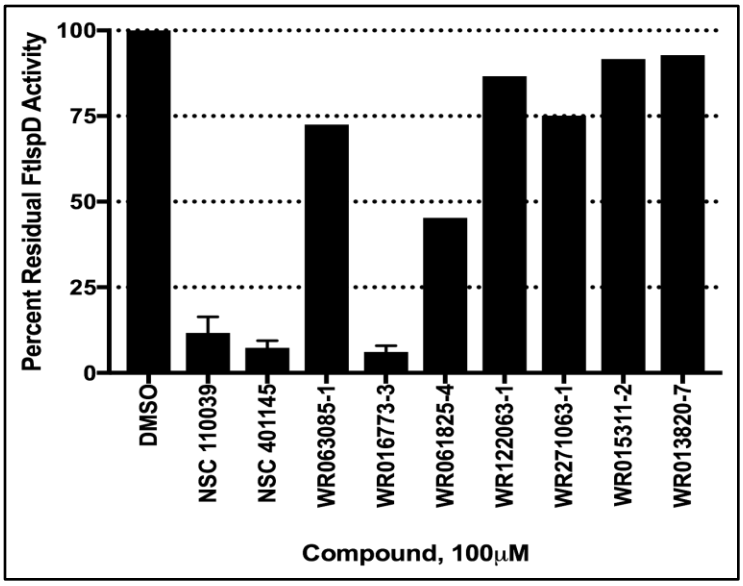

Figure 27. Second generation library screened with FtIspD. Each compound was assayed at 100 μM and was preincubated with FtIspD prior to the addition of CTP. The activity of FtIspD with compounds NCS 110039 and NSC 401145 are shown for comparison. Of the 7 new compounds, WR016773-3 is the only compound with appreciable activity. Error bars are calculated as the deviation from the mean of two independent measurements.

Given the activity of WR016773-3, the IC_{50} value was next determined. Like NSC 401145 and NSC 110039, WR016773-3 is a micromolar inhibitor of FtIspD, although with slightly reduced potency relative to the two original compounds (Figure 28).

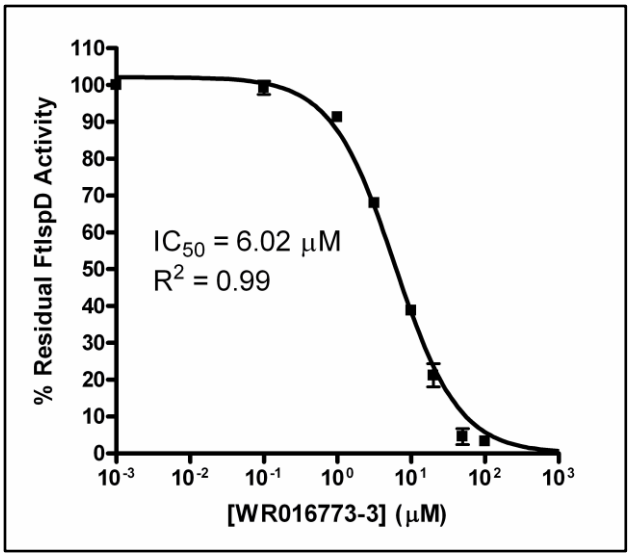

Figure 28. IC_{50} determination for hit IspD compound WR016773-3 . Error bars are calculated as the deviation from the mean of two independent measurements.

Despite the slightly larger IC_{50} value, improvement was observed in antibacterial assays with WR016773-3 and either *F. tularensis* subsp. *novicida* or *Y. pestis* subsp. A1122 (Figure 29), relative to NSC 110039 (Figure 21). In fact, EC_{50} values for WR016773-3 with respect to *F. tularensis* susbsp. novicida and *Y.pestis* subsp. A1122 are comparable to the EC_{50} values for each species with kanamycin (the EC_{50} with respect to *F.tularensis* is 7.64 μM (1.95 μg/mL) versus 5.077 μM (2.46 μg/mL) for kanamycin, and the EC_{50} with respect to *Y. pestis* is 24.09 μM (6.17 μg/mL) versus 33.5 μM (16.20 μg/mL) for kanamycin). This improvement in antibacterial activity could potentially be due to improvements in cellular penetration or reductions in efflux. Hill coefficients were less steep than found with NSC 110039, at 2.9 for *F. tularensis* subsp. novicida, and 1.3 for *Y. pestis* subsp. A1122.

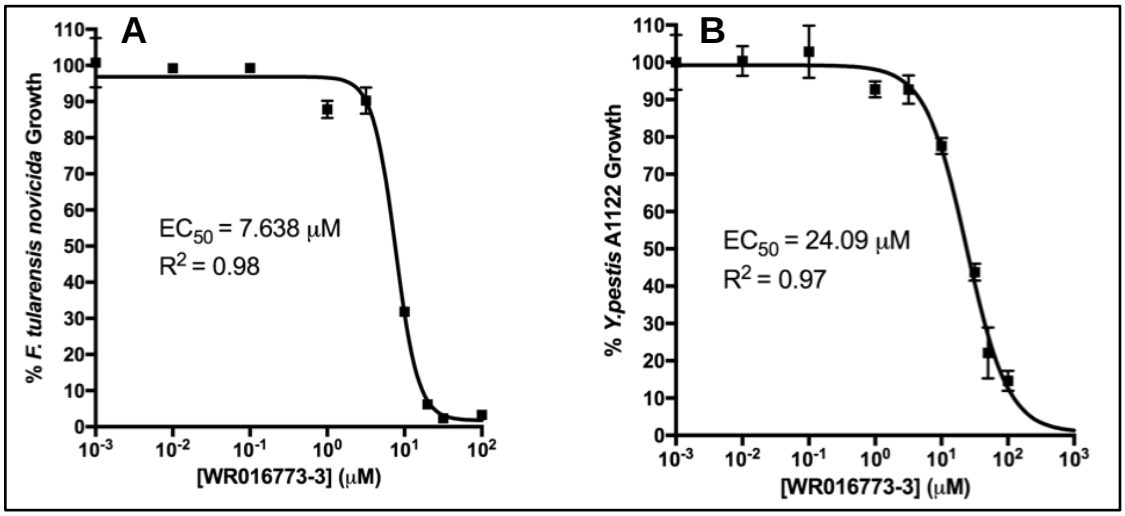

Figure 29. EC_{50} of WR016773-3 with respect to A) *F. tularensis* subsp. *novicida* and B) *Y.pestis* subsp. A1122. Error bars are calculated as the deviation from the mean of two independent measurements.

Conclusions

Based on the above kinetic evidence, bacterial homologs of IspD are inhibited by aromatic, lipophilic compounds as previously shown for the AtIspD species. While the precise binding site on FtIspD is currently unknown, mechanism of inhibition plots in conjunction with the resolved crystal structure of inhibitor-bound AtIspD suggest that these inhibitors potentially bind at an allosteric site, altering active site topology such that neither CTP nor MEP are able to bind to the inhibitor-bound enzyme. Crystallographic studies are currently being conducted to identify the precise binding site of these inhibitors for further rational design.

SPECIFIC AIM 2 — LOPAC^{1280} LIBRARY SCREEN WITH ISPC AND ISPD

In this Specific Aim, IspC and IspD were individually assayed with compounds present in the commercially available LOPAC^{1280} library, containing 1280 different molecules, many of which are FDA approved pharmaceuticals. These high-throughput screens (HTS) were conducted with *Yersinia pestis* IspC and *Francisella tularensis* IspD, each utilizing a 96-well plate-based assay developed in house. All hits are coupled to a secondary screen using an appropriate homolog (*Mycobacterium tuberculosis* IspC or *Escherichia coli* IspD) to test for broad spectrum activity. Furthermore, a tertiary screen was employed to control for false-positives, using an IspC-IspD coupled assay for IspC hits, and a pyrophosphatase assay for IspD hits.

A Note to My Thesis Committee:

An overview of the screening paradigm for this Specific Aim is presented below, and the results of screening the LOPAC library then follow within this section of the thesis. However, since the screening of both the LOPAC library (Specific Aim 2) and our natural product extract library (Specific Aim 3) converge on the same downstream steps following the screen, we elected to include a section of the thesis called "Specific Aim 2 and 3 — Hit Characterization", wherein we detail the characterization of the hits obtained from these two screens. As you will see, this makes

particular sense given our finding that the hit molecules likely share a common mechanism by which they inhibit the enzyme.

Overview of the Approach to High-Throughput Screening

In separate high-throughput screens, the LOPAC^{1280} library from Sigma Aldrich (containing 1280 purified pharmaceutically active compounds) was screened for inhibitory activity against purified recombinant IspC and IspD. In order to identify hit compounds from the LOPAC^{1280} library, a stepwise screen was performed in the manner illustrated in Figure 30.

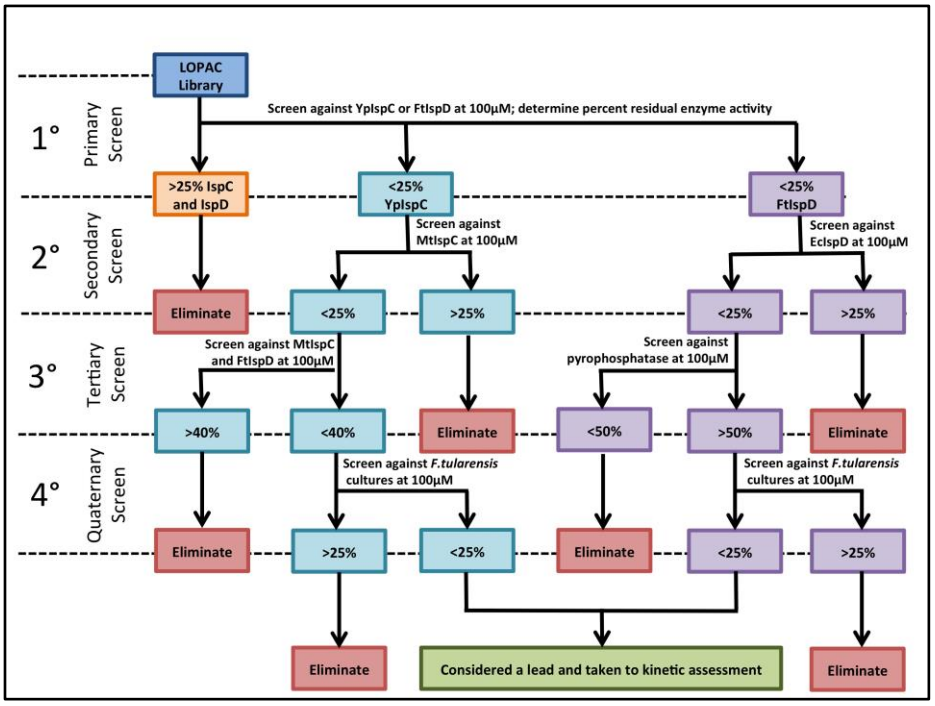

Figure 30. Tiered screening procedure utilized with the LOPAC^{1280} library screen. Compounds were passed through 4 tiers of screening for both IspC (teal) and IspD (purple). For IspC, these included a primary screen with YpIspC, a secondary screen with MtbIspC, a tertiary screen with MtbIspC coupled with FtIspD, and a quaternary antibacterial assay. For IspD, these included a primary screen with FtIspD, a secondary screen with EcIspD, a tertiary screen with pyrophosphatase, and a quaternary antibacterial screen. Cut-off values for each screen are indicated (% residual enzyme activity or % residual growth). Compounds retained through the quaternary screen for both IspC and IspD were considered lead compounds and were examined for mechanism of inhibition.

For the IspC screens (shown in teal in Figure 29), initial inhibitory activity was assayed in a primary screen using *Yersinia pestis* IspC (YpIspC), then compounds demonstrating ≥75% inhibition of native enzyme activity were taken into a secondary screen performed with the *Mycobacterium tuberculosis* IspC (MtbIspC). Compounds with ≥75% inhibition in the secondary screen were subsequently evaluated in a tertiary screen involving a coupled IspC-IspD assay. This tertiary screen was designed to identify and eliminate library molecules harboring chromophores with absorbance at 340 nm (which would appear as false hits in the primary and secondary screens). Compounds retained from the tertiary screen were evaluated for antimicrobial activity in a quaternary screen with *F. tularensis* subsp. *novicida*, and were considered leads for further characterization if the compound reduced microbial growth by 75% or greater at 100 μM.

For the IspD screens (shown in purple in Figure 30), initial inhibitory activity was assayed in a primary screen using *Francisella tularensis* IspD (FtIspD), then compounds demonstrating ≥75% inhibition of native enzyme activity were taken into a secondary screen performed with *Escherichia coli* IspD (EcIspD). Compounds with ≥75% inhibition in the secondary screen were subsequently evaluated in a tertiary screen investigating inhibition of pyrophosphatase, a component of the IspD assay. This tertiary screen was designed to identify and eliminate library molecules which inhibited pyrophosphatase activity rather than IspD activity in the primary and secondary screens. As for the inhibitors identified with IspC, compounds retained from the tertiary screen with pyrophosphatase were evaluated in a quaternary screen with *F. tularensis*

subsp. *novicida* to determine antimicrobial activity. Compounds reducing microbial growth by 75% or greater were retained and subsequently further characterized.

The Screening of the LOPAC^{1280} Library — IspC

In the primary screen with IspC, all 1280 compounds were evaluated at 100 µM, using a fixed-time 96-well plate assay with YpIspC. The large dynamic range of the assay with YpIspC gives it a Z-score value of 0.9, making it highly suitable for high-throughput screening[141]. Known IspC inhibitor FR900098 was used as a positive control for inhibition. Percent residual enzyme activity values are calculated from the ratio of ΔA_{340} with the test compound over the ΔA_{340} of an uninhibited assay (containing DMSO), and are reported for all 1280 compounds in Appendix 2, Table 19. To minimize the consumption of library compounds, the multi-well assay is designed such that the inhibitory activity of each library compound is calculated relative to an inhibitor-free reference well (rather than a substrate-free assay blank containing each inhibitor). Consequently, negative residual activity values are a reflection of library compounds that absorb at 340 nm (and hence may or may not be false hits, which is resolved via the secondary and tertiary screens). Compounds resulting in less than 25% residual enzyme activity in the primary screen were deemed worthy of further investigation (a total of 232 compounds) and were moved forward into the secondary screen.

A secondary screen utilizing purified recombinant MtbIspC was used to evaluate the specificity of the 232 compounds highlighted in the primary screen. Assays were performed in a manner similar to the primary screen, with each compound tested

at 100 µM. However, to minimize the effect of A_{340} interference from the library compounds, the activity of each inhibitor was determined relative to its own assay blank (devoid of the substrate, DXP, but containing the library compound). A total of 18 compounds were identified which result in less than 25% residual enzyme activity (Figure 31A). These 18 compounds (Figure 31B) were carried forward into the tertiary screen.

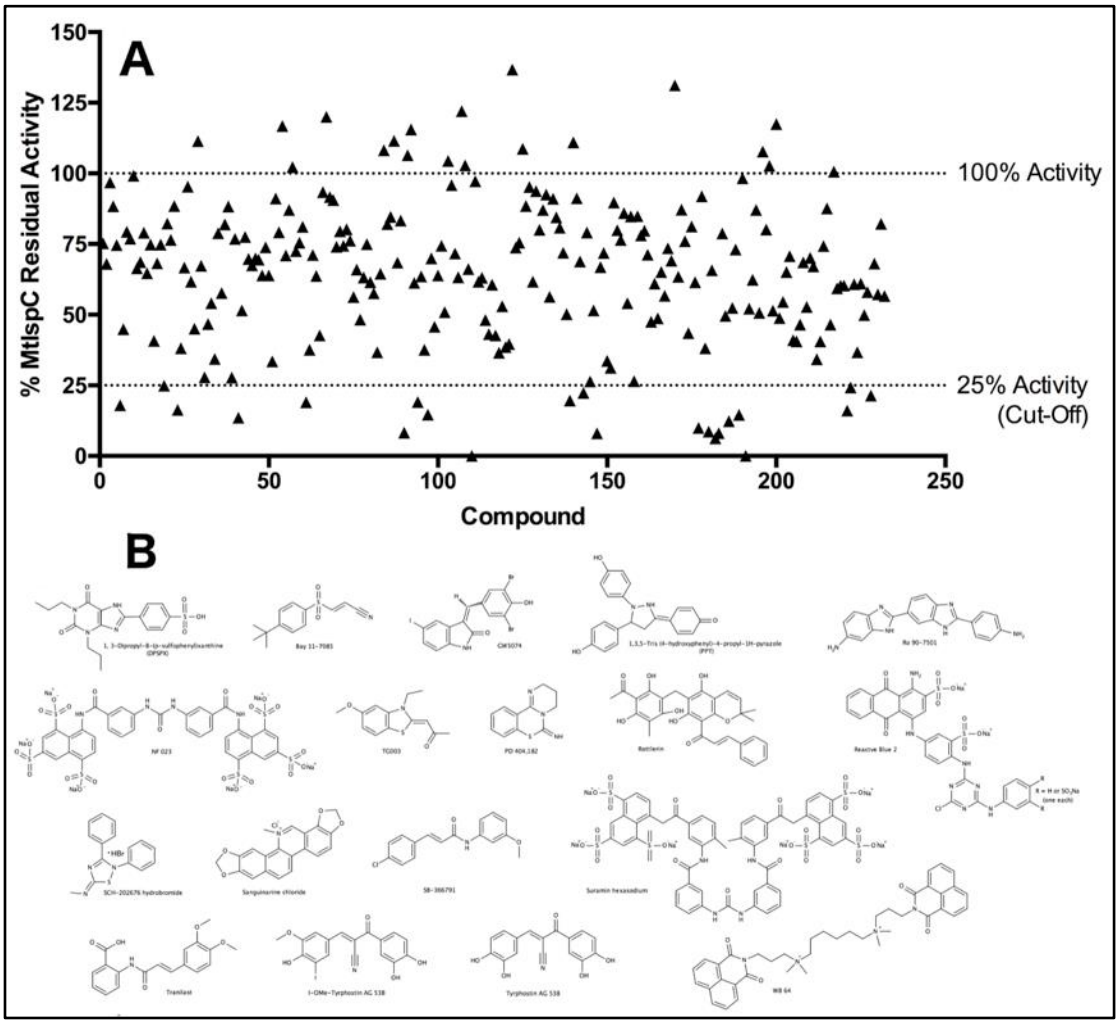

Figure 31. Secondary screening of the LOPAC^{1280} library primary screen hits against MtbIspC. A) Residual activity of MtbIspC when assayed in the presence of 100 µM of each of the LOPAC^{1280} library compounds identified

in the primary screen. For clarity, each library molecule was assigned a numeric designation, ranging from 1-232 (the association of number, compound name, and residual enzyme activity is tabulated in Appendix 2, **Table 20**). Residual activity exceeding 100% reflects additional oxidation of NADPH over a well containing vehicle only. Library compounds demonstrating 75% or greater reduction in MtbIspC activity were selected for the tertiary screen. B) Structures of each compound reducing MtbIspC activity below 25% in the secondary screen. Each of these compounds was retained for tertiary screening.

To again address the fact that several of the LOPAC^{1280} library compounds demonstrate innate absorbance at 340 nm, and thus potentially appear as false inhibitors in the primary and secondary screens, a coupled MtbIspC/*F.tularensis* IspD assay was developed in which the product of MtbIspC (i.e. MEP) is successively used as substrate by FtIspD, which is also present in the assay mixture. This combined assay also incorporates pyrophosphatase and a malachite green solution to quantify inorganic phosphate production as a result of FtIspD activity, as previously described[149]. Hence, inhibitors of IspC are revealed by suppressed IspD activity, as spectrophotometrically measured at 660 nm. Residual enzyme activity is calculated as the ratio of ΔA_{660} in the presence of the test compound to the ΔA_{660} of an uninhibited assay. As with the primary and secondary screens, the known IspC inhibitor FR900098 was used as a control in the tertiary screen. It is notable that the residual activity of MtbIspC in the presence of 100 µM FR900098 is nearly 15% greater when measured using the IspC-IspD coupled assay than when measured with IspC alone. As a consequence, a cut-off value of 40% or lower residual enzyme activity was deemed significant in the tertiary screen. As shown in Figure 32, a total of 7 compounds were identified which reduce the catalytic activity of MtbIspC by at least 60%.

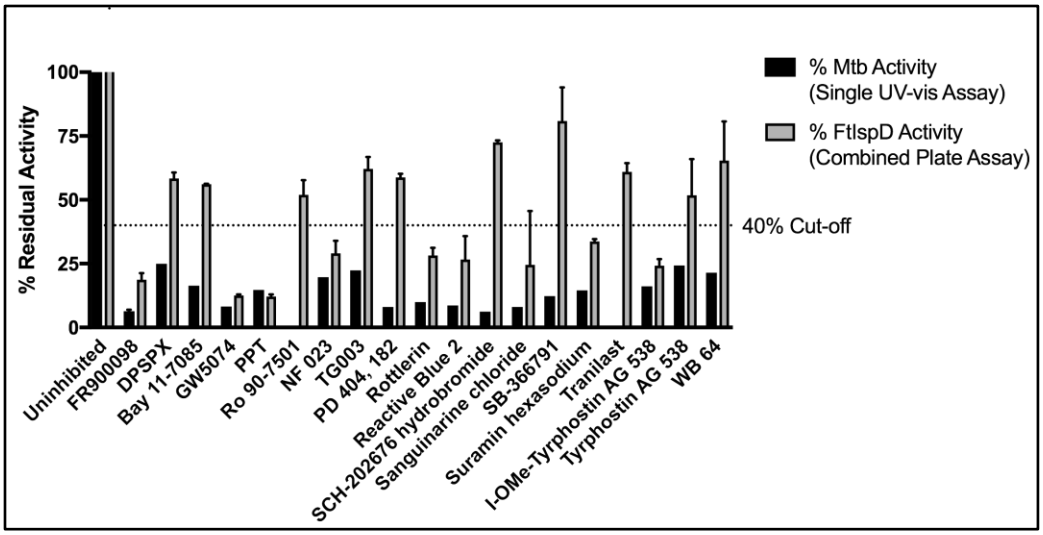

Figure 32. Tertiary screening of the LOPAC^{1280} library secondary screen hits via MtbIspC-FtIspD coupled assay. The residual activity of MtbIspC was measured with a coupled assay utilizing *M. tuberculosis* IspC and *F. tularensis* IspD (grey), and compared to the secondary screen values measuring MtbIspC activity using the A_{340} (black). Those compounds with less than 40% residual activity in the coupled assay were retained for quaternary antibacterial screening. Error bars are calculated as the deviation from the mean of two independent measurements.

From the primary through tertiary screens with IspC, a total of seven compounds were identified as potential lead molecules and moved forward to a quaternary screen for antibacterial activity. The antibacterial activity of the seven highlighted library compounds was evaluated using a growth-inhibition assay with *Francisella tularensis* subsp. *novicida* Utah 112. All compounds were screened in duplicate at 100 µM. As shown in Figure 33, four of the compounds significantly inhibit bacterial growth (full chemical names and structures of the compounds are provided in Table 3).These compounds were thus considered lead molecules as inhibitors of IspC.

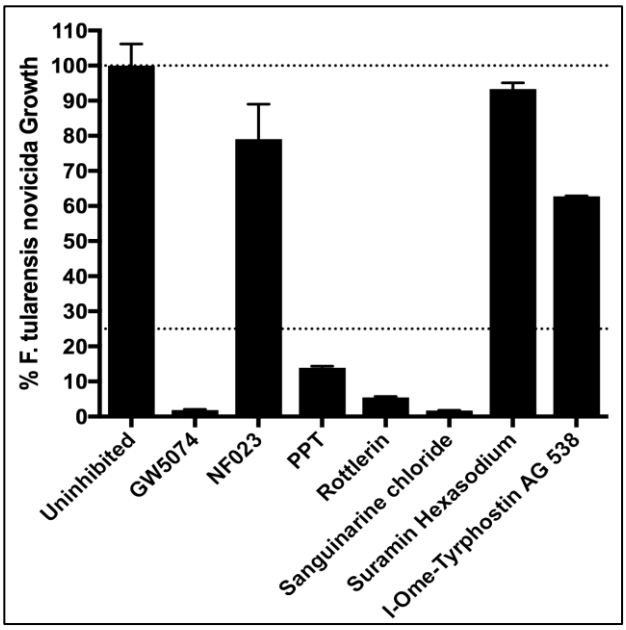

Figure 33. Quaternary screening of the LOPAC^{1280} tertiary screen hits for IspC against *F. tularensis novicida.* Antibacterial activity of LOPAC^{1280} inhibitors against *F. tularensis* subsp. *novicida* Utah 112 was measured in duplicate at 100 µM; compounds with less than 25% fractional bacterial growth were selected for EC_{50} determination. Fractional growth is calculated as the ratio of cell density (OD_{600}) in the presence of 100 µM inhibitor to cell density in the presence of vehicle only. Error bars are calculated as the deviation from the mean of two independent measurements.

Table 3. LOPAC^{1280} library inhibitors of IspC demonstrating antibacterial activity against *F. tularensis novicida*.

Compound	Chemical Name	Structure
GW5074	3-(3, 5-Dibromo-4-hydroxybenzylidine-5-iodo-1,3-dihydro-indol-2-one)	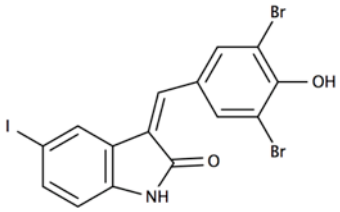
PPT	1,3,5-tris(4-hydroxyphenyl)-4-propyl-1H-pyrazole	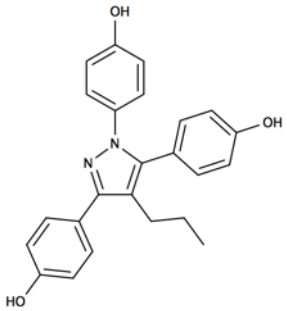

Rottlerin	3'-[(8-Cinnamoyl-5,7-dihy droxy-2,2-dimethyl-2H-1-benzopyran-6-yl)methyl]-2',4',6'-trihydroxy-5'-methylacetophenone	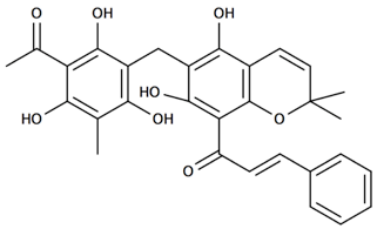
Sanguinarine chloride	13-Methyl-[1,3]benzodioxolo[5,6-c]-1,3-dioxolo[4,5-i] phenanthridinium chloride	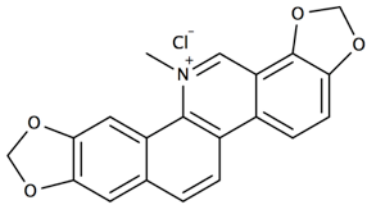

To quantify the potency of each of these molecules, EC_{50} values were derived from additional growth-inhibition assays performed with either *F. tularensis* subsp. *novicida* Utah 112 or *Yersinia pestis* subsp. A1122 (the EC_{50} values are reported in Table 4.; the dose-response plots for *F. tularensis* are presented in Figure 34 and for *Y. pestis* are presented in Figure 35).

Table 4. Antibacterial potency of LOPAC[1280] library inhibitors of IspC.

Compound	EC_{50} against *F. tularensis* subsp. *novicida* U112 (μM)	EC_{50} against *Yersinia pestis* subsp. A1122 (μM)
GW5074	2.84	4.44
PPT	8.16	12.16
Rottlerin	1.90	4.03
Sanguinarine chloride	2.19	15.66

As each of the four select compounds demonstrate low micromolar growth-inhibitory activity against *F. tularensis* and *Y. pestis*, we elected to further characterize

each in follow-on enzyme assays performed with YpIspC and FtIspD (detailed following Specific Aim 3, in the section titled "Specific Aim 2 and 3 — Hit Characterization").

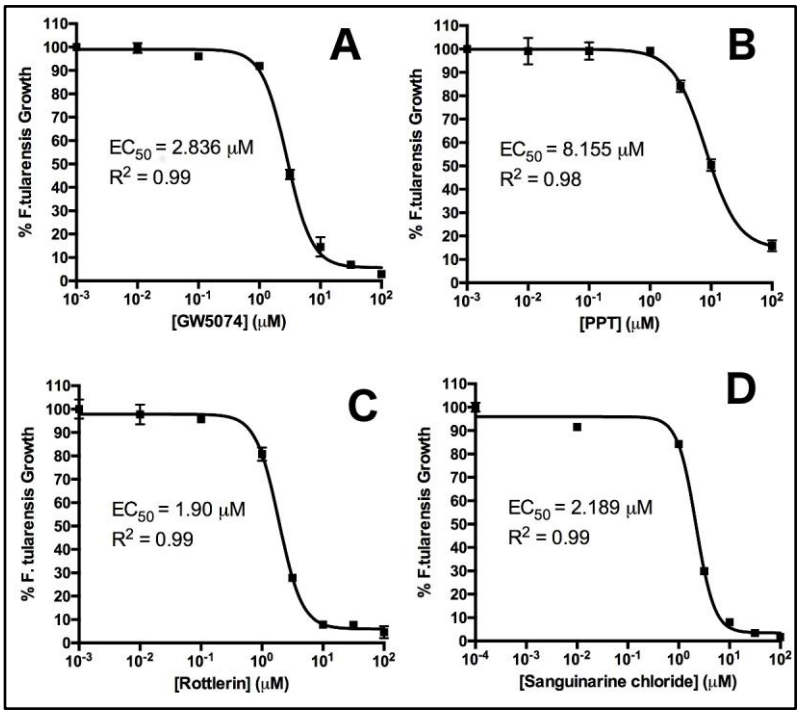

Figure 34. Half-maximal effective concentration of LOPAC^{1280} IspC hit compounds against *F. tularensis* subsp *novicida* Utah 112. Percent residual growth is calculated as the ratio of cell density (OD_{600}) in the presence of inhibitor to cell density in the presence of vehicle (DMSO) only for inhibitors A) GW5074, B) PPT, C) Rottlerin, and D) Sanguinarine. The EC_{50} values and R^2 values for each plot are indicated. Error bars are calculated as the deviation from the mean of two independent measurements.

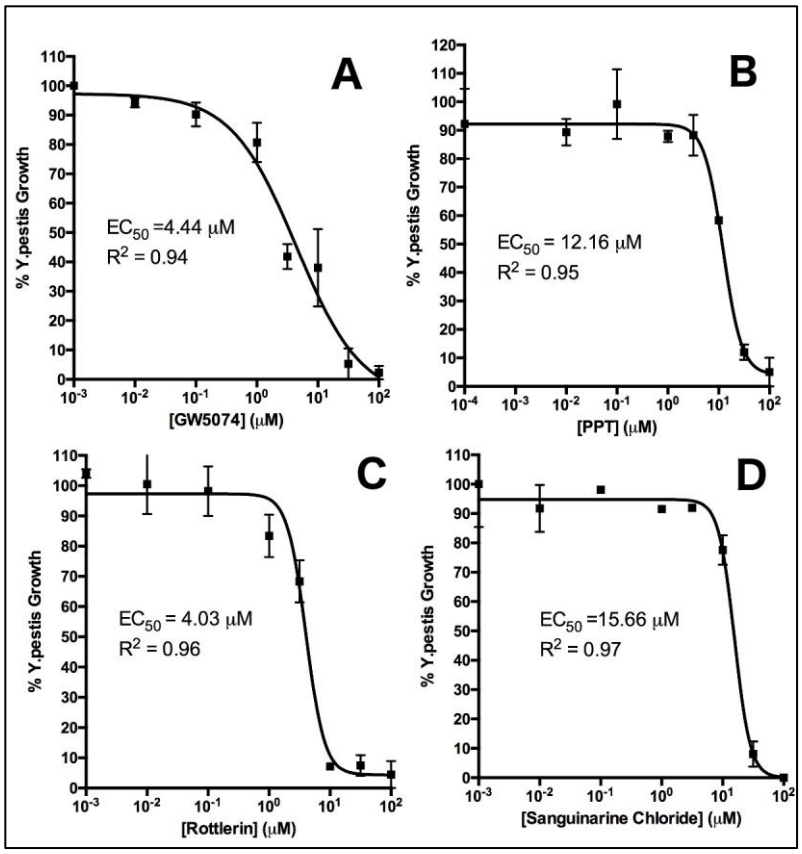

Figure 35. Half-maximal effective concentration of LOPAC^{1280} IspC hit compounds against *Y. pestis* subsp A1122. Percent residual growth is calculated as the ratio of cell density (OD_{600}) in the presence of inhibitor to cell density in the presence of vehicle (DMSO) only for inhibitors A) GW5074, B) PPT, C) Rottlerin, and D) Sanguinarine. The EC_{50} values and R^2 values for each plot are indicated. Error bars are calculated as the deviation from the mean of two independent measurements.

At the conclusion of primary through quaternary screening of the LOPAC^{1280} library with IspC, the 4 identified hit compounds from the initial library of 1280 gives a hit rate of 0.31%.

The Screening of the LOPAC^{1280} Library — IspD

In the primary screen with IspD, all 1280 compounds were evaluated at 100 µM using a fixed time 96-well plate assay with FtIspD. Like YpIspC, FtIspD has a large dynamic range for this assay and is highly suitable for high-throughput screening, with a Z-score value of 0.8[148]. Percent residual enzyme activity is calculated from the ratio of ΔA_{660} with the test compound over the ΔA_{660} of an uninhibited assay (containing DMSO), and are reported in Appendix 2, Table 19 for all 1280 library compounds. As with the IspC primary screen, compounds resulting in less than 25% residual enzyme activity in the primary screen were deemed worthy of further investigation (a total of 33 compounds). Due to measurement at 660 nm rather than 340 nm, fewer false positives due to intrinsic compound absorption were expected. As such, significantly fewer compounds were identified in the primary screen of FtIspD than in the primary screen with YpIspC.

A secondary screen utilizing EcIspD was then used to evaluate the specificity of the 33 compounds identified in the primary screen. The activity of each inhibitor in the secondary screen was determined relative to its own assay blank (in the presence of inhibitor but absence of substrate). At 100 µM concentration, a total of 7 compounds result in residual EcIspD activity less than 25% of the uninhibited enzyme (the 7 compounds are shown in Figure 36).

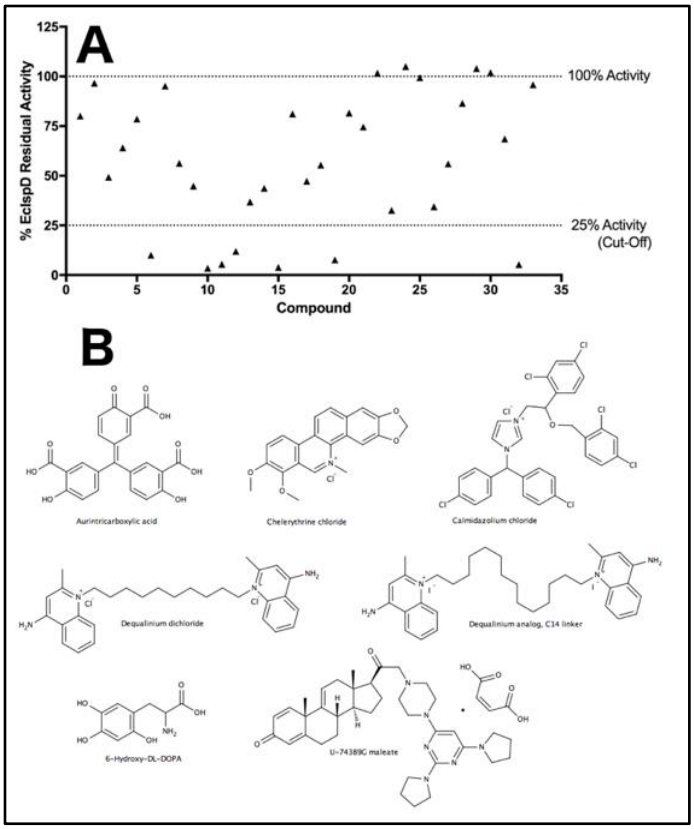

Figure 36. Secondary screening of the LOPAC^{1280} library primary screen hits against EcIspD. A) Residual activity of EcIspD when assayed in the presence of 100 µM of each of the LOPAC^{1280} library compounds identified in the primary screen. For clarity, each library molecule was assigned a numeric designation, ranging from 1-33 (the association of number, compound name, and residual enzyme activity is tabulated in Appendix 2, **Table 21**. Library compounds demonstrating 75% or greater reduction in EcIspD activity were selected for the tertiary screen. B) Structures of each compound reducing EcIspD activity below 25% in the secondary screen.

Three compounds (Aurintricarboxylic acid; Dequalinium analog, C-14 linker; and 6-Hydroxy-DL-DOPA) with activity in the secondary screen of IspD were also hits in the secondary screen of IspC (Figure 31). As IspD inhibitors would interfere with the tertiary screen for IspC, which utilizes IspD to allow quantification via A_{660}, these compounds were culled from the list of IspC inhibitors after identification in the secondary screen for IspD, prior to completing the tertiary screen for IspC. However, these compounds were retained in the tertiary screen for IspD.

In the assay used for the primary and secondary screens, the activity of IspD is coupled to the activity of pyrophosphatase, which cleaves the pyrophosphate released by IspD, resulting in two molecules of inorganic phosphate that form a complex with a malachite green dye solution added to the assay mixture. To address the fact that apparent suppressed IspD activity could in fact be suppressed pyrophosphatase activity, each of the 7 compounds identified in the IspD secondary screen were subsequently assayed with pyrophosphatase in a tertiary screen. Because the pyrophosphatase is used in excess in the IspD assay, compounds that did not reduce pyrophosphatase activity more than 50% were considered to be significant IspD inhibitors. As seen in Figure 37, five compounds inhibited IspD activity without significantly inhibiting the pyrophosphatase activity.

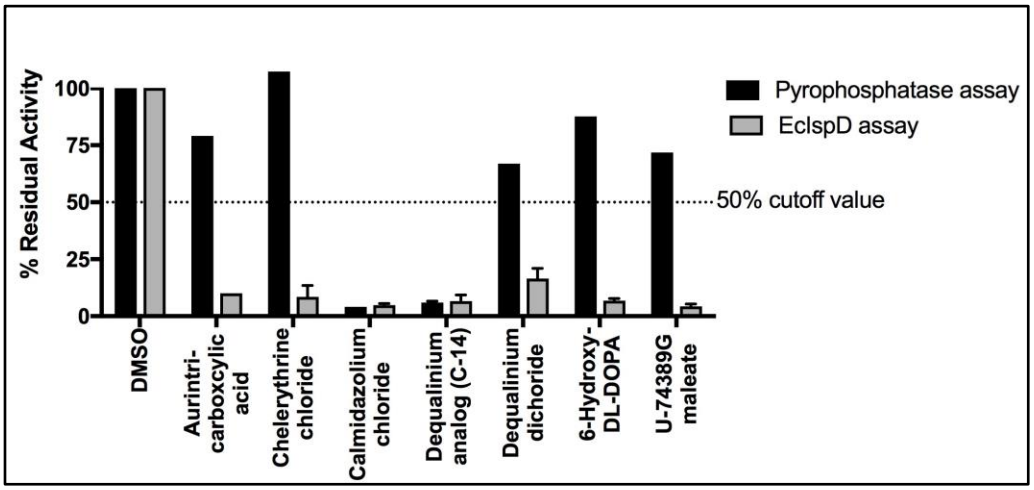

Figure 37. Tertiary screening of the LOPAC^{1280} secondary screen hits against pyrophosphatase. Shown in black is the residual activity of pyrophosphatase versus the residual activity of EcIspD shown in grey in the presence of 100 µM inhibitor. Those compounds with greater than 50% residual activity in the pyrophosphatase assay were retained for quaternary antibacterial screening. Error bars are calculated as the deviation from the mean of two independent measurements.

A total of five compounds were identified as potential lead molecules for IspD and were moved forward to a quaternary screen. As with IspC, the quaternary screen measured antibacterial activity of each of the potential lead molecules, evaluated using a growth-inhibition assay with *Francisella tularensis* subsp. *novicida* Utah 112. All compounds were screened in duplicate against the microbe at 100 µM as previously done. Shown in Figure 38, two of the compounds significantly inhibit bacterial growth (full chemical names and structures of the compounds are provided in Table 5). These compounds were thus considered lead molecules as inhibitors of IspD.

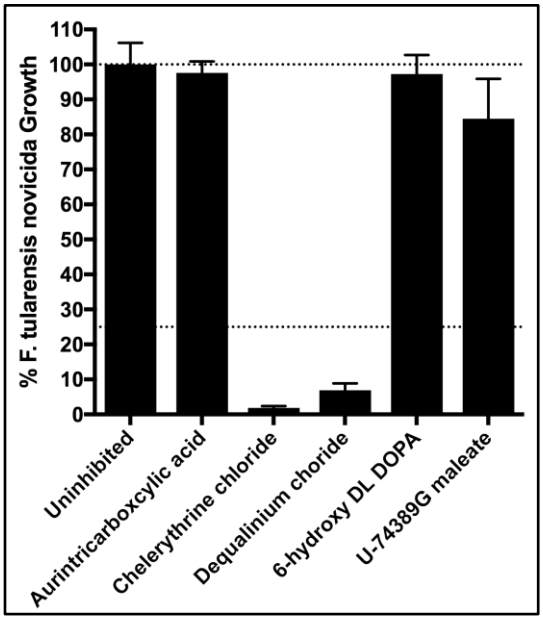

Figure 38. Quaternary screening of the LOPAC^{1280} tertiary screen hits for IspD against F. tularensis novicida. Antibacterial activity of LOPAC^{1280} inhibitors against *F. tularensis* subsp. *novicida* Utah 112 was measured in duplicate at 100 µM; compounds with less than 25% fractional bacterial growth were selected for EC_{50} determination. Fractional growth is calculated as the ratio of cell density (OD_{600}) in the presence of 100 µM inhibitor to cell density in the presence of vehicle only. Error bars are calculated as the deviation from the mean of two independent measurements.

Table 5. LOPAC[1280] library inhibitors of IspD demonstrating antibacterial activity against *F. tularensis novicida*.

Compound	Chemical Name	Structure
Chelerythrine chloride	1,2-Dimethoxy-N-methyl(1,3) benzodioxolo(5,6-c)phenanthridinium chloride	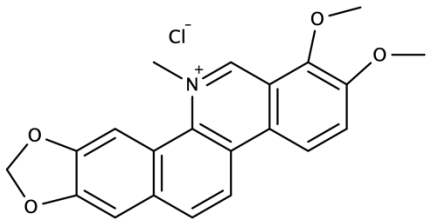
Dequalinium chloride	1,1′-Decamethylenebis(4-aminoquinaldinium) dichloride hydrate	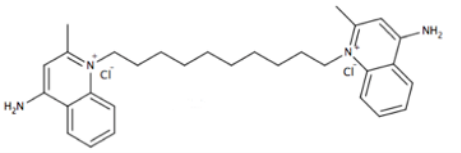

For the two lead compounds, EC_{50} values were determined from additional growth-inhibition assays performed with either *F. tularensis* subsp. *novicida* Utah 112 or *Yersinia pestis* subsp. A1122 (the EC_{50} values are reported in Table 6; the dose-response plots for *F. tularensis* are presented in Figure 39). Both compounds demonstrate low micromolar growth-inhibitory activity against *F. tularensis*, but neither is active against *Y. pestis*. In fact, both compounds showed no reduction in *Y. pestis* growth up to 100 µM. Given that the compounds were effective against *F. tularensis*, we elected to further characterize each in follow-on enzyme assays performed with YpIspC and FtIspD (detailed following Specific Aim 3, in the section titled "Specific Aim 2 and 3 — Hit Characterization").

Table 6. Antibacterial potency of LOPAC^{1280} library inhibitors of IspD. EC_{50} values were not determined for *Y.pestis* given the lack of growth reduction by either compound up to 100 µM.

Compound	EC_{50} against *F. tularensis* subsp. *novicida* U112 (µM)	EC_{50} against *Yersinia pestis* subsp. A1122 (µM)
Chelerythrine chloride	5.31	n.d.
Dequalinium dichloride	0.76	n.d.

n.d. = not determined

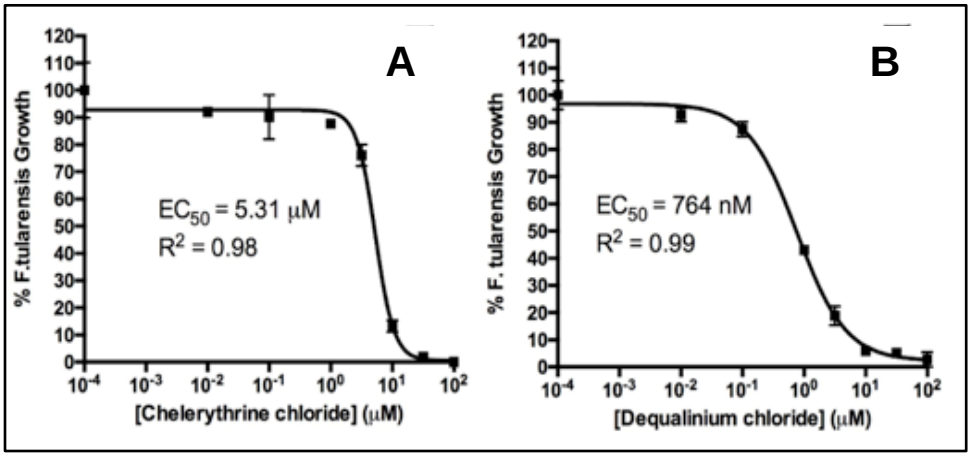

Figure 39. Half-maximal effective concentration of LOPAC^{1280} IspD hit compounds against *F. tularensis* subsp *novicida* Utah 112. Fractional growth is calculated as the ratio of cell density (OD_{600}) in the presence of inhibitor to cell density in the presence of vehicle (DMSO) only for inhibitors A) Chelerythrine chloride and B) Dequalinium chloride. The EC_{50} values and R^2 values for each plot are indicated. Error bars are calculated as the deviation from the mean of two independent measurements.

At the conclusion of primary through quaternary screening of the LOPAC^{1280} library with IspD, the 4 identified hit compounds from the initial library of 1280 gives a hit rate of 0.15%.

SPECIFIC AIM 3 — NATURAL PRODUCT LIBRARY SCREEN WITH ISPC AND ISPD

In this Specific Aim, IspC (*Yersinia pestis*) and IspD (*Francisella tularensis*) were individually assayed with compounds present in our in-house, proprietary collection of natural product extracts, obtained from various plants and fungi. After screening, select extracts demonstrating inhibitory activity were assessed for IC_{50} activity, mechanism of enzyme inhibition, and antimicrobial activity, and the active inhibitor/molecule was identified using an affinity purification technique coupled with LC-MS/MS.

A Note to My Thesis Committee:

The screening of our natural product library and the subsequent identification of top active components are reported within this section of the thesis. However, as the downstream characterization of the hit compounds from this natural product library follows the same protocol/approach as the characterization of hits from the screening of the LOPAC library, characterization of hits from both libraries are grouped and discussed together in the section of the thesis called "Specific Aim 2 and 3 — Hit Characterization". As you will see, this makes particular sense given our finding that the hit molecules likely share a common mechanism by which they inhibit the enzyme.

Overview of the Approach to Natural Product Screening

In separate screens, a proprietary natural product library prepared in house (containing 155 individual natural product extracts) was screened for inhibitory activity against purified recombinant IspC and IspD. In order to identify hit compounds from the natural product library, a stepwise screen was performed in the manner illustrated in Figure 40.

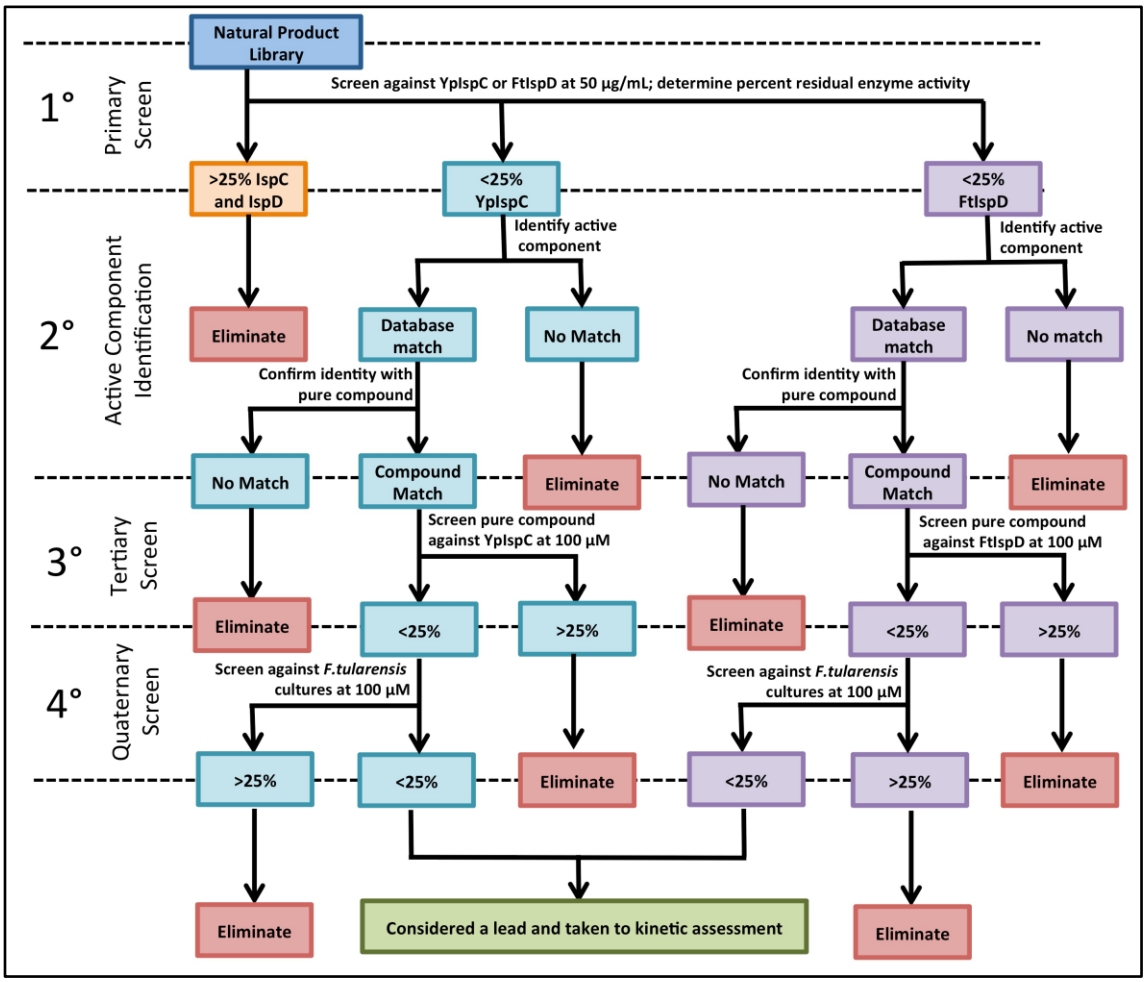

Figure 40. Tiered screening procedure utilized with the natural product library screen. Compounds were passed through 4 tiers of screening for both IspC (teal) and IspD (purple). For both enzymes, these included a primary screen with the appropriate enzyme (YpIspC for IspC screen, and FtIspD for IspD screen), a secondary assessment to determine the active component in the extract, a tertiary screen to confirm the compound identification, and a quaternary screen for antibacterial activity. Cut-off values for each screen are indicated (%

residual enzyme activity in primary and tertiary screens or % residual growth for quaternary antibacterial screen). Compounds retained through the quaternary screen for both IspC and IspD were considered lead compounds and were examined for mechanism of inhibition.

For the IspC screens (shown in blue in Figure 40) and the IspD screens (shown in purple in Figure 40), initial inhibitory activity was assessed in a primary screen with either YpIspC or FtIspD, respectively. Compounds demonstrating ≥75% inhibition of native enzyme activity were considered suitable compounds for active component identification, and select compounds were pursued based on percent inhibition of the enzyme and abundance of the starting material (the extract). Active components were identified using an affinity extraction method utilizing the enzyme as bait and subsequent matching of an MS/MS spectrum of the isolated compound to that of a standard in the Metlin metabolite database. Once a compound was initially identified using database matching, the pure compound was purchased and its MS/MS spectrum was derived then compared to the MS/MS spectrum of the compound isolated from the extract. If matched, then the compound was moved forward to a tertiary screen with the purified enzyme (YpIspC for the IspC screen or FtIspD for the IspD screen). Residual enzyme activity under 25% justified moving the compound to quaternary antibacterial screen with *F. tularensis* subsp. *novicida*. Compounds reducing microbial growth by at least 75% at 100 μM were retained for EC_{50} determination and subsequent further characterization.

The Screening of a Natural Product Extract Library

Run separate from the LOPAC^{1280} library screen, a natural product library was also evaluated for inhibitory activity utilizing purified recombinant YpIspC and FtIspD. This library was produced in-house and comprises 155 individual ethyl acetate extracts, derived from a wide variety of regional plants and fungi, each extract containing a diverse mixture of metabolites. The extracts were individually evaluated in the assay at 50 µg/mL final concentration, while 100 µM fosmidomycin and FR900098 were each used as positive controls for inhibition of IspC, and 100 µM anthracene blue was used as the positive control for IspD. Overall, nine different extracts were found to inhibit YpIspC activity by 75% or greater, and 11 different extracts were found to inhibit FtIspD activity by 75% or greater (Figure 41).

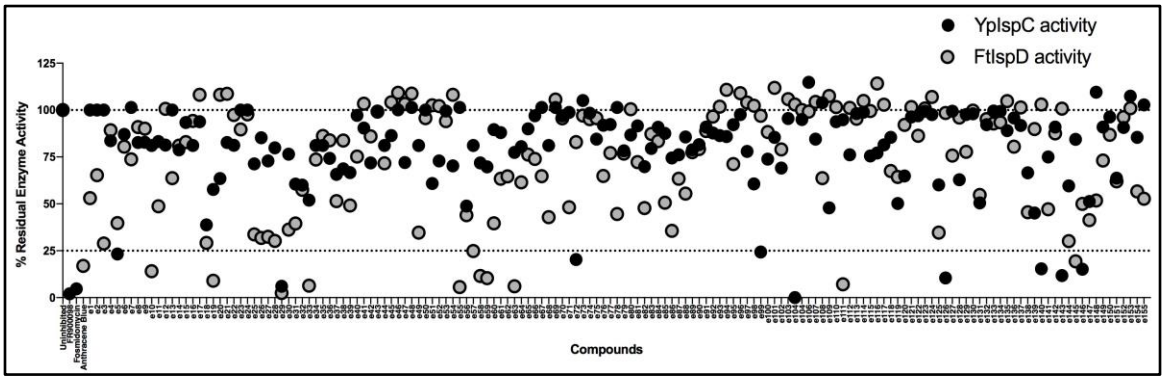

Figure 41. Primary natural product library screen for inhibitors of IspC or IspD. Each natural product extract is alphanumerically identified as e1 through e155. FR900098 and fosmidomycin (100 µM) serve as positive inhibition controls with YpIspC. Anthracene blue (100 µM) serves as a positive control for FtIspD. The residual enzyme activity for YpIspC is indicated in black, whereas the residual enzyme activity of FtIspD is indicated in grey. All residual activity values were calculated using an uninhibited assay with vehicle (DMSO) only.

Most interestingly, e29 was found to inhibit the activity of both YpIspC and FtIspD by greater than 95%. In light of this, e29 was prioritized for subsequent active component identification.

The e29 extract was obtained from the plant *Rumex crispus*, commonly known as Curly Dock (Figure 42), an invasive weed species found throughout North America[150].

Figure 42. *Rumex crispus*, commonly known as Curly Dock. This invasive weed species is part of the dock family and distinguished by its curly leaves.[150]

Although e29 inhibited both YpIspC and FtIspD, YpIspC was chosen first for active component identification via the use of YpIspC as an affinity bait. After

incubation of the extract with the enzyme, the enzyme-inhibitor complex was separated from the extract by centrifugation through a 30 kDa ultrafiltration concentrator (the enzyme-inhibitor complex remains in the retentate). Subsequent heat denaturation of the enzyme-inhibitor complex releases the associated inhibitor, which was immediately recovered by centrifugation through a second 30kDa ultrafiltration concentrator (the enzyme remains in the retentate whereas the inhibitor is now in the filtrate). The filtrate is then directly analyzed using an LC-QToF (LC-MS/MS). Mass spectra comparison of the inhibitor to the METLIN Metabolite and Tandem MS Database identified the molecule quercetin as the putative IspC inhibitor. Figure 43 shows a comparison of the MS/MS spectrum of the isolate from e29 and the MS/MS spectrum of a purchased quercetin standard analyzed on our LC-QToF at collison energies of 10, 20, and 40 V.

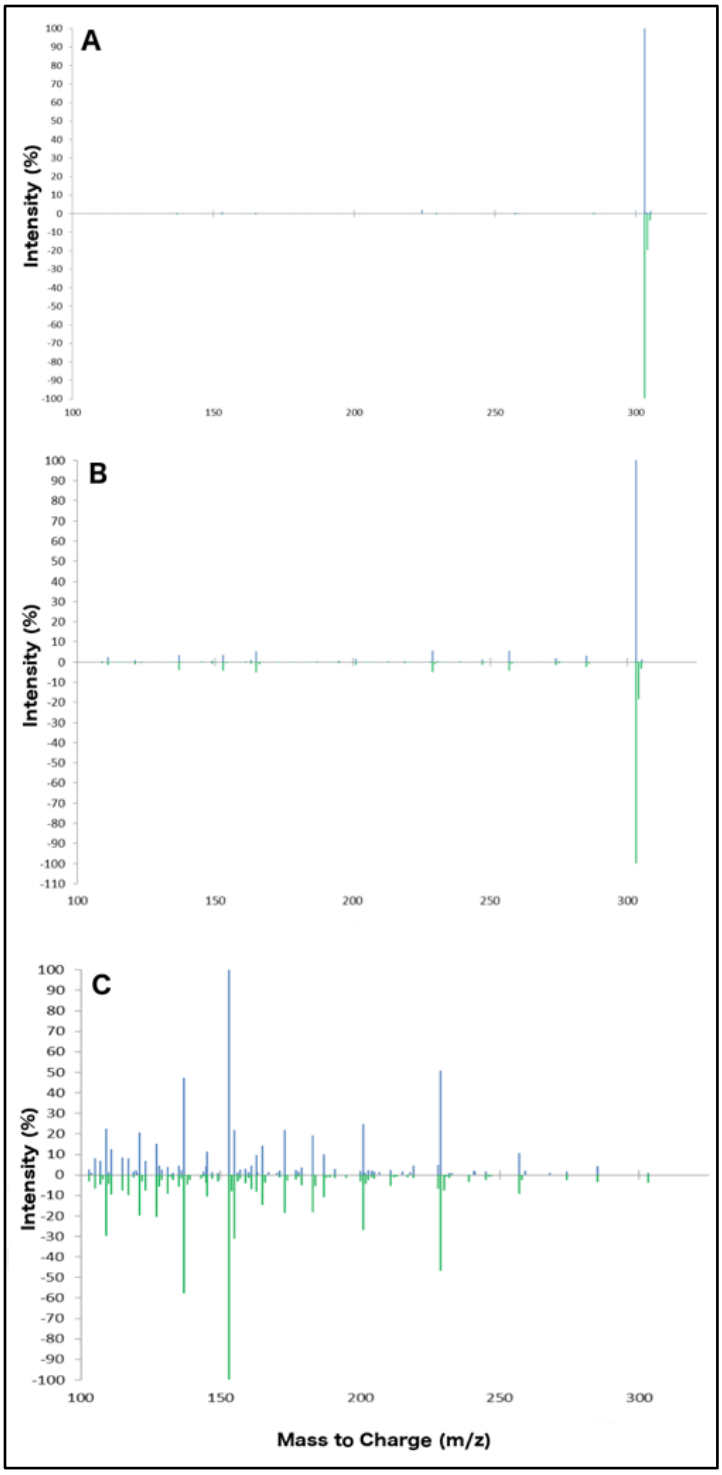

Figure 43. Secondary IspC screen for active compound identification of e29. Comparison of MS/MS spectrum of e29 active component with respect to YpIspC (blue) with an MS/MS spectrum of a pure quercetin standard run in-house (green). Comparison of spectra shown at collision energies of A) 10 V, B) 20 V, and C) 40 V. Peaks at 302 m/z indicate the precursor ion.

To validate the inhibitory activity of quercetin, it and a small series of related flavonoids, including common glycosylated forms of quercetin and the structurally similar catechins, were purchased and screened at 100 µM against YpIspC in a tertiary screen. As reported in Table 7, quercetin effectively inhibits over 95% of the catalytic activity of YpIspC, while none of the glycosylated forms of quercetin nor the catechins showed any significant inhibitory activity.

Table 7. Tertiary IspC Screen for inhibitory activity of commercially purchased quercetin and additional structurally related flavonoids when assayed with YpIspC.

Compound	Structure	% Residual Activity
Quercetin	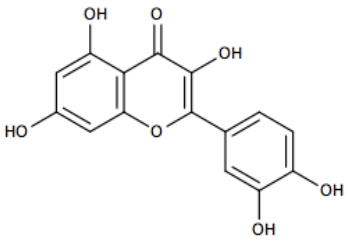	4.83
Quercitrin	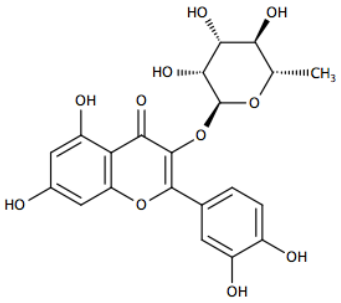	78.21
Quercetin 3-β-D-glucoside	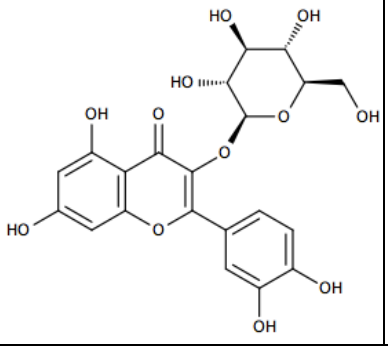	76.25

Quercetin 3-D-Galactoside	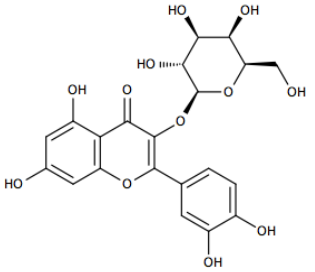	76.779
Catechin	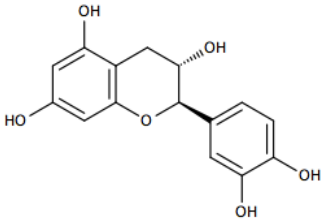	96.65
Epicatechin	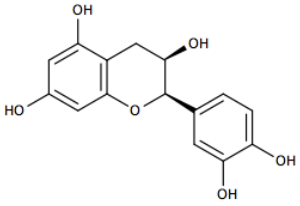	97.50

Quaternary bacterial growth-inhibition assays performed with quercetin and *Francisella tularensis* subsp. *novicida* Utah 112 at 100 µM showed less than 25% residual growth (Figure 44), justifying subsequent EC_{50} determination.

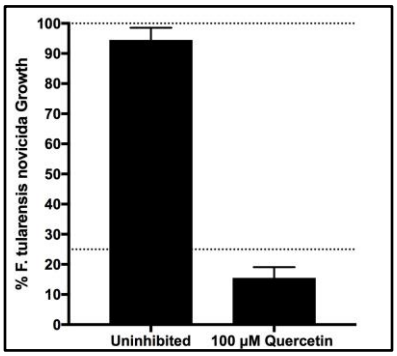

Figure 44. Quaternary screening of the natural product tertiary screen hit quercetin for IspC against F. tularensis novicida. Antibacterial activity of quercetin against *F. tularensis* subsp. *novicida* Utah 112 was measured

in duplicate at 100 μM; quercetin inhibited bacterial growth by greater than 75% and was selected for EC_{50} determination. Percent residual growth is calculated as the ratio of cell density (OD_{600}) in the presence of 100 μM inhibitor to cell density in the presence of vehicle only. Error bars are calculated as the deviation from the mean of two independent measurements.

Significant inhibitory activity associated with quercetin is observed against both *Yersinia pestis* subsp. A1122 and *Francisella tularensis* subsp. *novicida* Utah 112 (Figure 45), with EC_{50} values under 50 μM for both microbes. Notably, the EC_{50} values with quercetin are comparable to those obtained in growth inhibition assays performed with FR900098 (*Francisella tularensis*: 36 μM with quercetin, 23 μM with FR900098[151]; *Yersinia pestis*: 29 μM with quercetin, 29 μM with FR900098[141]).

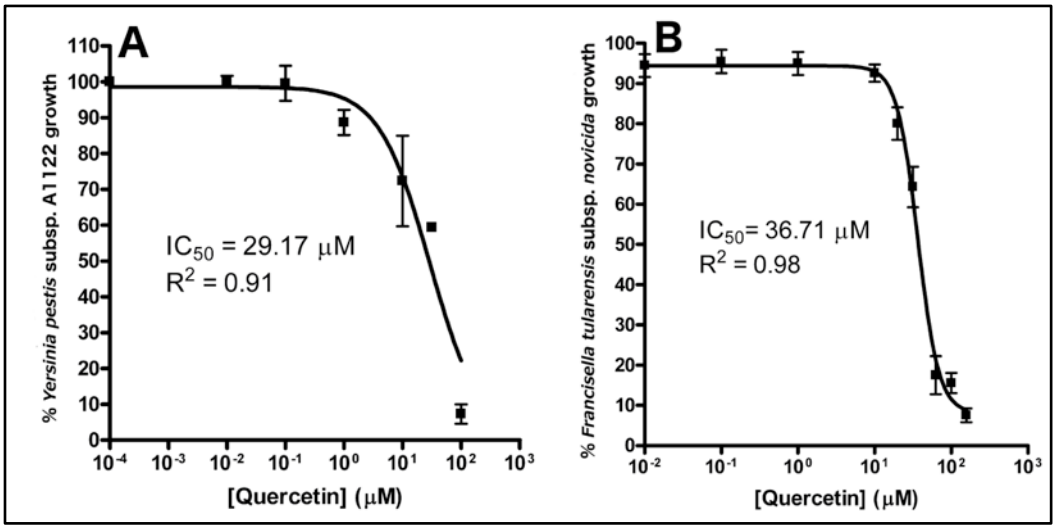

Figure 45. Half-maximal effective concentration of quercetin against liquid cultures of A) *Y. pestis* subsp. A1122 and B) *F. tularensis* subsp. *novicida* Utah 112. Percent residual growth is calculated as the ratio of culture cell density (OD_{600}) in the presence of quercetin to culture cell density in the presence of vehicle (DMSO) alone. The potency (EC_{50}) and R^2 values for each plot are indicated. Error bars are calculated as the deviation from the mean of two independent measurements.

Next, to identify the inhibitor of IspD present in e29, we used the same affinity bait approach described with YpIspC. As shown in Figure 46, LC-MS/MS reveals the active inhibitor of IspD to also be quercetin. To validate this discovery, we assayed the activity of FtIspD in the presence of 100 µM commercially purchased quercetin. As reported in Table 8, the FtIspD activity is reduced to 4% of the uninhibited control, confirming that quercetin is indeed an inhibitor of IspD. Given the known antibacterial activity of quercetin against both *F. tularensis* and *Y.pestis* (as determined in the quaternary natural product screen for IspC inhibitors; see Figure 45), quercetin was retained as a lead molecule for inhibition of IspD. We next elected to further characterize quercetin, along with the 6 top hits obtained from the LOPAC^{1280} library screen. This characterization is fully described in the subsequent section, "Specific Aim 2 and 3 — Hit Characterization".

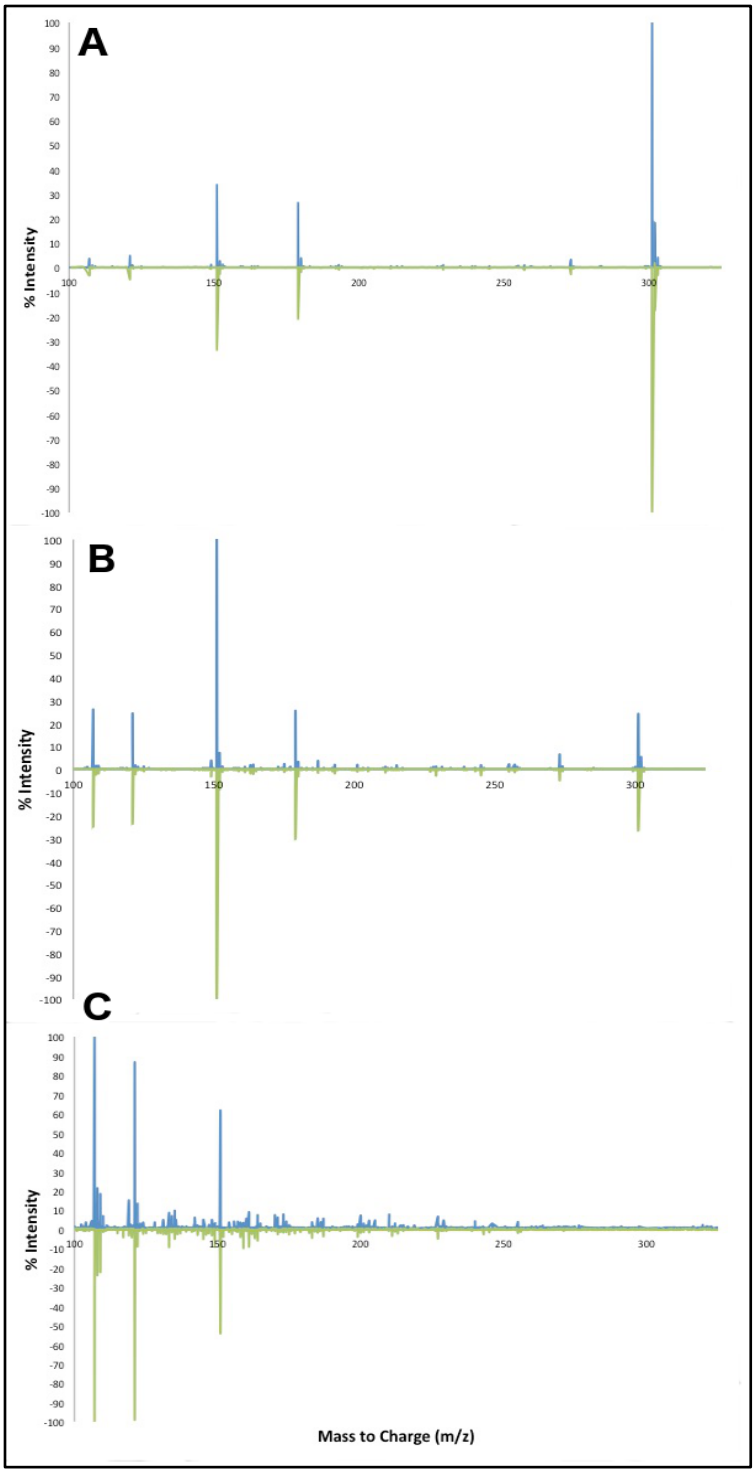

Figure 46. Secondary IspD screen for active compound identification of e29. Comparison of MS/MS spectrum of e29 active component with respect to FtIspD (blue) with an MS/MS spectrum of a pure quercetin standard run in-house (green). Comparison of spectra shown at collision energies of A) 10 V, B) 20 V, and C) 40 V. Peaks at 302 m/z indicate the precursor ion.

Table 8. Tertiary IspD Screen for inhibitory activity of commercially purchased quercetin at 100 µM.

Compound	Structure	% Residual Activity
Quercetin	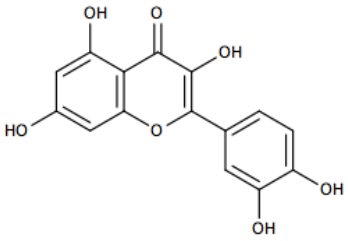	4.01

SPECIFIC AIM 2 AND 3 — HIT CHARACTERIZATION

To determine relative potency of the hit compounds from both the LOPAC^{1280} and natural product libraries, inhibitory dose-response curves for quercetin and each of the 6 LOPAC^{1280} hit compounds were determined using the enzyme assay with YpIspC or FtIspD, as appropriate. Many of the derived half maximal inhibitory activities (IC_{50}) were considerably greater than those observed in the bacterial growth-inhibition assays (see Table 6 versus Figure 47), raising questions as to whether IspC or IspD is the primary intracellular target for these inhibitors. Additionally, as seen in Figure 47, the steep dose-response curves produced with compounds GW5074, PPT, and sanguinarine chloride against YpIspC hinted to the possibility of an aggregation inhibition mechanism[152], in which planar, dye-like molecules form aggregates that inhibit proteins [153].

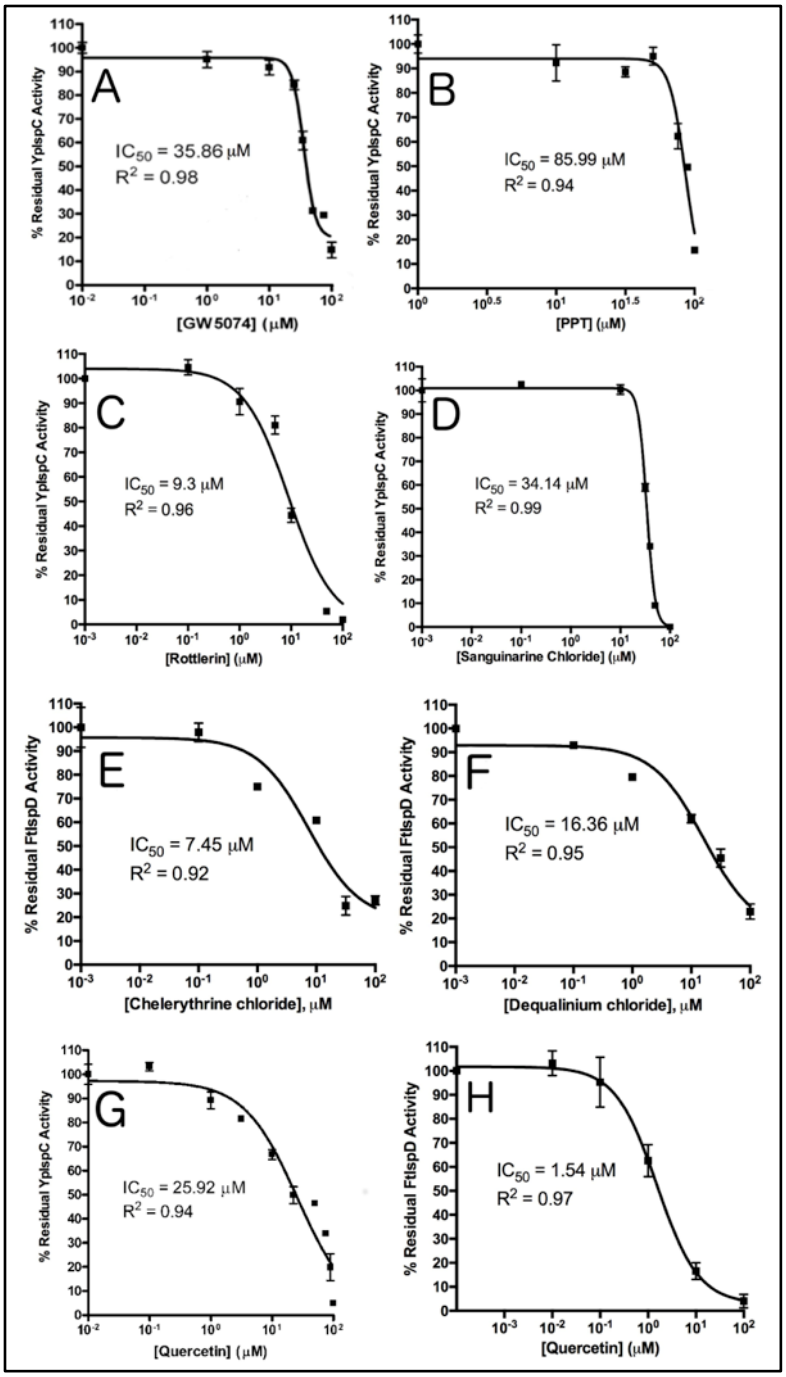

Figure 47. Dose-response plots of select inhibitors of YpIspC or FtIspD. Assays were performed with each enzyme with various concentrations of inhibitors including A) GW5074 with YpIspC, B) PPT with YpIspC, C) Rottlerin with YpIspC, D) Sanguinarine with YpIspC, E) Chelerythrine chloride with FtIspD, F) Dequalinium chloride with FtIspD, G) Quercetin with YpIspC and H) Quercetin with FtIspD For each assay, after a ten minute incubation of the enzyme with inhibitor and cofactor, the substrate was added to initiate the reaction. The IC_{50} and goodness-of-fit (R^2) value for each plot is indicated. The enzymatic activity is relative to an uninhibited control using vehicle (DMSO) alone. All assays were performed in duplicate. Error bars are calculated as the deviation from the mean of two independent measurements.

Of the evaluated compounds, both rottlerin and quercetin showed more classical dose-response curves with respect to IspC. Lineweaver -Burk plots presented in Figure 48 indicate that rottlerin has an uncompetitive profile with respect to NADPH, and a noncompetitive (mixed) profile with respect to DXP. This suggests that rottlerin selectively binds to the IspC-NADPH complex, but does not bind at the DXP site. This profile could be indicative of an allosteric inhibitor, or it could also be indicative of aggregation inhibition[153].

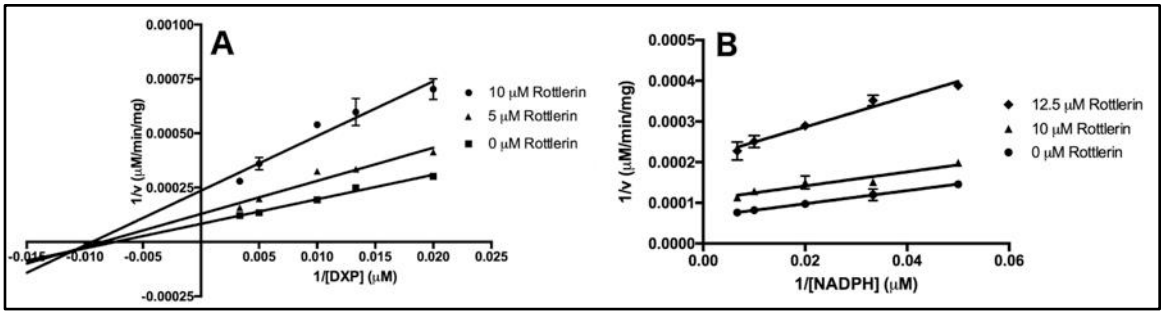

Figure 48. Mechanism of inhibition by rottlerin. The Lineweaver–Burk plots indicate that rottlerin is noncompetitive with respect to A) DXP and uncompetitive with respect to B) NADPH. All assays were performed in duplicate using purified YpIspC. Error bars are calculated as the deviation from the mean of two independent measurements.

When quercetin was examined for mechanism of inhibition with YpIspC (Figure 49), it too showed an uncompetitive profile with respect to NADPH and a noncompetitive (mixed) profile with respect to DXP, suggestive of an allosteric binding site[141]. However, the possibility of aggregation inhibition also exists, as flavonoids such as quercetin have been shown to aggregate in solution[154]. Hence, quercetin along with

the 6 identified LOPAC[1280] inhibitors were subsequently investigated to evaluate the possibility of an aggregation-inhibition mechanism.

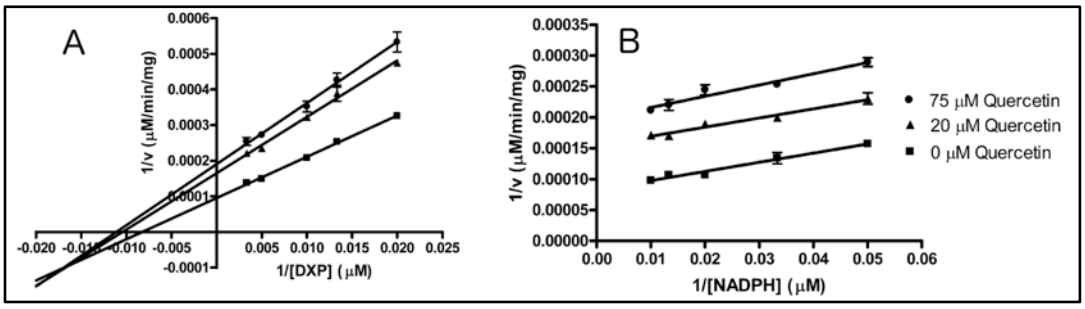

Figure 49. Mechanism of inhibition by quercetin. The Lineweaver–Burk plots indicate that quercetin is noncompetitive with respect to A) DXP and uncompetitive with respect to B) NADPH. All assays were performed in duplicate using purified YpIspC. Error bars are calculated as the deviation from the mean of two independent measurements.

Aggregation Inhibition

Aggregation inhibition is a phenomena in which, above a critical solution concentration, a small molecule self-associates in solution, forming large particle aggregates that can nonspecifically adsorb proteins onto the particle's surface, sequestering and partially denaturing the protein[153]. The concentration at which aggregates begin to form is called the critical aggregation concentration[155], similar to a critical micelle concentration, and can lead to dose response curves with steep Hill slopes[152]. There is currently no single test that can perfectly identify an aggregation inhibitor, however a flowchart has been developed to guide the identification of an aggregation inhibitor (summarized in Table 9[153]). When a compound fails a number of these, it may potentially behave as an aggregation inhibitor. Of all of the tests listed in

Table 9, screening with Triton X-100 is simple and is typically regarded as the most predictive test to identify an aggregation inhibitor[156].

Table 9. Recommended Experiments for the Identification of Aggregating Compounds. This table is published in Shoichet,' 2006[153].

Assessment of a Compound for Aggregating Behavior
1. Is inhibition significantly attenuated by small amounts of non-ionic detergent? i. If so, the compound is very likely acting through aggregation. ii. In cases where you cannot use detergent, e.g. cell-based assays, it may be possible to use high (1 mg/mL) concentrations of serum albumin instead/
2. Is inhibition significantly attenuated by increasing enzyme concentration? i. If so, the compound is very likely an aggregator. Except for when the enzyme concentration to Ki ratio is high, increasing enzyme concentration should not affect percent inhibition.
3. Is inhibition competitive? If so, the compound is unlikely to be an aggregator.
4. Does the inhibitor retain activity after spinning for several minutes in a microfuge? If not, particle formation is likely (see point 5).
5. Can you directly observe particles in the 50-1000 nm size range, as identified by dynamic light scattering? Formation of particles does not guarantee promiscuous inhibition, but it is a worrying sign.
6. Is the dose-response curve unusually steep? There are classical reasons for these curves, but they too are a worrying sign.

In order to evaluate if one or more of the hit compounds from the library screens are acting through an aggregation-inhibition mechanism, each compound was re-assayed at 100 μM, but in the presence of 0.01% Triton X-100. The presence of a non-ionic detergent such as Triton X-100 is thought to break up small-molecule aggregates by interfering with their self-association, leading to severe reductions in inhibition of an enzyme if the mechanism of inhibition is based upon aggregation-inhibition[153]. Figure 50 shows each inhibitor assayed in the absence (open bars) and presence of 0.01% Triton X-100 (hatched bars), using either YpIspC (white bars) or FtIspD (grey bars).

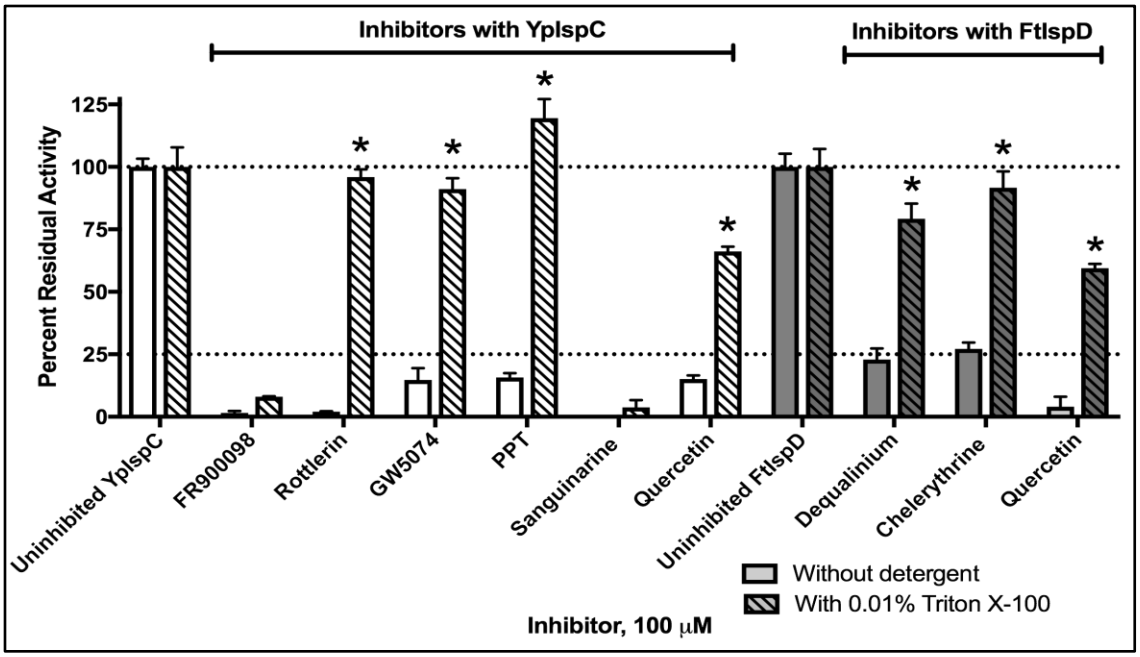

Figure 50. Residual activity of YpIspC (white) or FtIspD (grey) in the absence (open bars) and presence (hatched bars) of 0.01% Triton X-100. All samples are standardized to an uninhibited control containing the vehicle (DMSO) and 0.01% Triton X-100 if necessary. FR900098 was used as a positive control for inhibition, and its inhibitory activity is not significantly influenced by the addition of Triton X-100. In contrast, with the exception of sanguinarine, the activity of the other evaluated inhibitors is significantly attenuated in the presence of Triton X-100. The cut-off for significant attenuation of inhibition was set as 25% or greater increase in residual enzyme activity; compounds with significantly attenuated activity in the presence of Triton X-100 are indicated with a star. Error bars are calculated as the deviation from the mean of two independent measurements.

The cut-off value for significant attenuation of inhibition is not straightforward to establish and there are a variety of cut-off values used in literature.[158] We chose to set the cut-off for significant attenuation of inhibition as a 25% increase in residual enzyme activity or greater in the presence of non-ionic detergent. All of the selected inhibitors reduced residual activity of the enzyme to 25% or less of an uninhibited sample in the absence of Triton X-100; an increase in residual activity by greater than 25% indicates at least a fold change increase in activity of the enzyme in the presence of non-ionic detergent.

Given a 25% increase in residual enzyme activity in the presence of 0.01% Triton X-100 as a cut-off for significance, Figure 50 implicates GW5074, PPT, rottlerin, and quercetin as compounds with a potential aggregation-inhibition based mechanism with respect to IspC, as inhibition is significantly attenuated in the presence of the non-ionic detergent. The known specific inhibitor of IspC, FR900098, was used as a positive control and did not show significant reduction in potency with the addition of 0.01% Triton X-100. Only sanguinarine retained its activity in the presence of detergent. Similarly, each IspD inhibitor was found to lose potency in the presence of 0.01% Triton X-100, with greater than 25% increases in FtIspD activity.

A literature search reveals reports of rottlerin and quercetin forming aggregates in solution, demonstrating aggregation-inhibition activity[159, 154]. More recently, quercetin was identified in a screen with EcIspC and found to inhibit via aggregation inhibition[160]. Collectively, given the attenuation of inhibition by Triton X-100, the literature reports of aggregation-inhibition associated with quercetin and rottlerin, and the non-competitive profile of each of these two compounds, we hypothesize that both quercetin and rottlerin are acting as aggregating inhibitors of IspC. Further, given the activity of quercetin against both IspC and IspD, we hypothesize that quercetin is also acting as an aggregation inhibitor of IspD.

Unlike rottlerin and quercetin, there have been no literature reports of aggregation-inhibition by PPT or GW5074. However, both of these compounds have unusually steep dose response curves (Hill Slope = 7.5 for PPT, 4.6 for GW5074), which could be indicative of reaching critical aggregation concentration at roughly 50

μM for PPT and 10 μM for GW5076, at which point enzyme activity drops dramatically (see Figure 47). Coupled with the attenuation of inhibition in the presence of Triton X-100, we hypothesize that PPT and GW5074 are also acting as aggregating inhibitors of IspC.

The activity of dequalinium and chelerythrine, both identified as inhibitors of IspD, was attenuated in the presence of Triton X-100. A literature search reveals that dequalinium has been shown to form micelle-like aggregates in aqueous solution[161]. Cholesterol, which is structurally similar to chelerythrine, has also been known to aggregate in aqueous solutions[162, 163]. Based on the attenuation of inhibition by the addition of Triton X-100, and the literature reports of aggregation by the same or similar compounds, we hypothesize that dequalinium and chelerythrine are also aggregating inhibitors of IspD.

Because sanguinarine inhibition was not attenuated by Triton X-100, further investigation was performed to determine if sanguinarine might be acting as an aggregation-inhibitor. The steep dose-response curve (Hill Slope = 5.2) could be due to the presence of cooperativity between multiple binding sites, and alone could not be used to hypothesize aggregation.

Mechanism of inhibition plots shown in Figure 51 indicate that sanguinarine acts noncompetitively with respect to both NADPH and DXP. Unless sanguinarine is binding in an allosteric site on YpIspC, these noncompetitive plots suggest an aggregation mechanism.

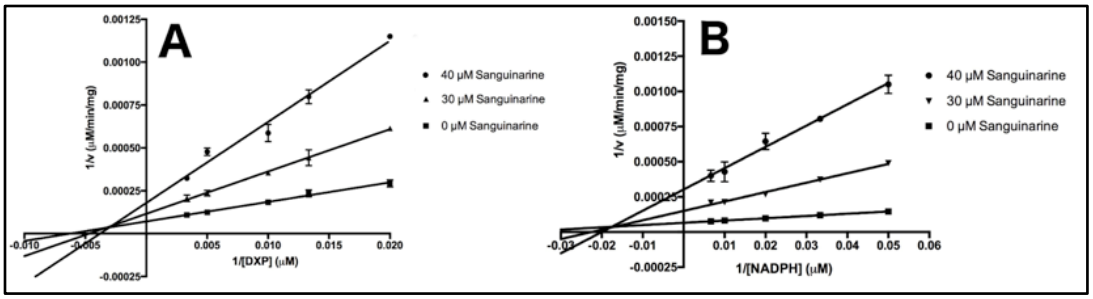

Figure 51. Mode of inhibition by sanguinarine. The Lineweaver–Burk plots indicate that sanguinarine is noncompetitive with respect to A) DXP and noncompetitive with respect to B) NADPH. All assays were performed in duplicate using purified YpIspC. Error bars are calculated as the deviation from the mean of two independent measurements.

Based on Table 9, a second critical experiment to identify aggregating inhibitors is to investigate the dependence of activity on enzyme concentration[153]. Unless the ratio of the enzyme concentration to K_i is high (i.e. a tight-binding scenario), the activity of an inhibitor should be independent of enzyme concentration.

Sanguinarine was assayed against YpIspC at decreasing enzyme concentrations, as shown in Figure 52, leading to a linear decrease in IC_{50} against YpIspC.

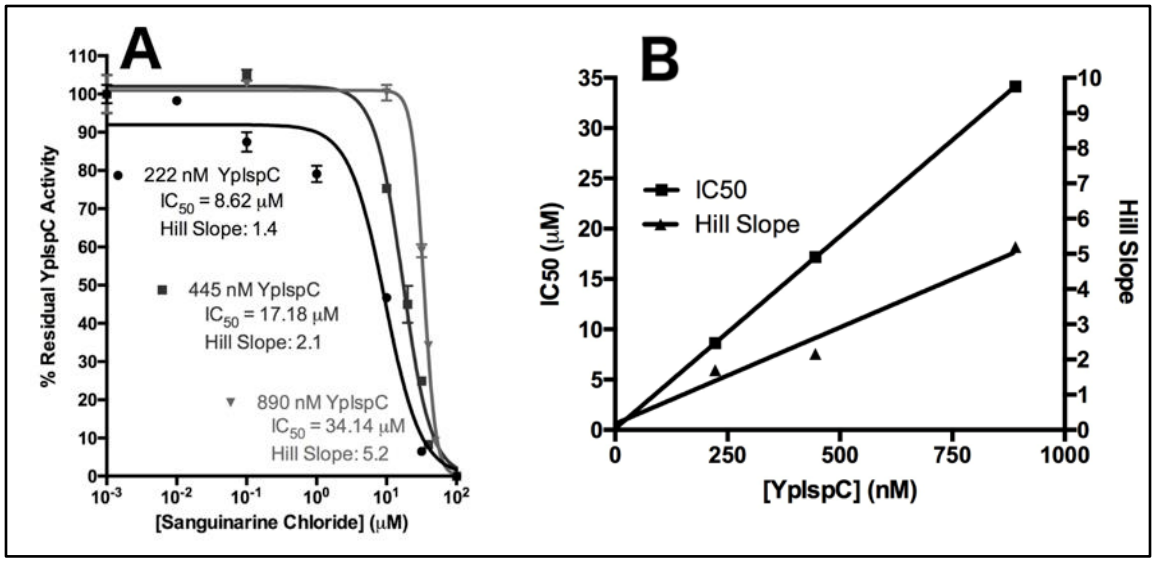

Figure 52. Dependence of IC_{50} with sanguinarine on enzyme concentration. A) IC_{50} with sanguinarine decreases with a decrease in YpIspC concentration. Concentrations of YpIspC, IC_{50}, and Hill slope are indicated. Error bars are calculated as the deviation from the mean of two independent measurements. B) The dependence of IC_{50} value and Hill slope of each IC_{50} plot decreased linearly with decrease in YpIspC concentration.

As indicated, this dependence of IC_{50} on enzyme concentration could indicate either aggregation or tight-binding phenomena (high enzyme to K_i ratio). When the IC_{50} concentration of sanguinarine is compared to the enzyme concentration (34 μM IC_{50} of sanguinarine versus 890 nM YpIspC), a tight binding mechanism would indicate not a 1 to 1 ratio of inhibitor to enzyme, but a roughly 60 to 1 ratio of inhibitor to enzyme. This ratio does not suggest that sanguinarine is a tight binding inhibitor. Additionally, the Hill slope of each IC_{50} plot decreased linearly with enzyme concentration, as has been shown for aggregating inhibitors[152]. Based on the steep-dose response curves, the dependence of IC_{50} on enzyme concentration, and the high IC_{50} versus enzyme concentration that rules out tight-binding phenomena, sanguinarine is also hypothesized to inhibit IspC via aggregation.

Specific Inhibitors of IspC and IspD

Given the lack of suspected specific lead compounds identified in the LOPAC^{1280} and natural product screen, further investigation was considered for LOPAC^{1280} compounds that passed primary, secondary and tertiary screening, but did not show antibacterial activity. Both *Francisella tularensis* and *Yersinia pestis* are Gram negative microbes that may be limiting antimicrobial activity through reduced cell well penetration or efflux pumps. Therefore, it was hypothesized that select other compounds that were identified in the LOPAC^{1280} screening campaign still may function as novel scaffolds for IspC or IspD inhibitor development, albeit that these scaffolds would likely need to be optimized to improve cellular penetration. There were three inhibitors of IspC and of IspD identified in tertiary screening that failed to show significant antimicrobial activity in the quaternary screen (Figure 33 and Figure 38): NF023, Suramin Hexasodium, and I-OMe-Tyrphostin AG 538 with respect to IspC, and Aurintricarboxylic acid, 6-hydroxy-DL-DOPA, and U-74389G maleate with respect to IspD. These compounds were subsequently examined for their inhibition in the presence and absence of Triton X-100 to determine if any of these compounds were also functioning as aggregators. Shown in Figure 53, addition of 0.01% Triton X-100 did not attenuate inhibition for suramin hexasodium, an identified IspC inhibitor, or 6-hydroxy-DL-DOPA, an identified IspD inhibitor. Because neither of these compounds were as likely to be aggregating inhibitors given the insensitivity to detergent, both were investigated for potency and mechanism of action.

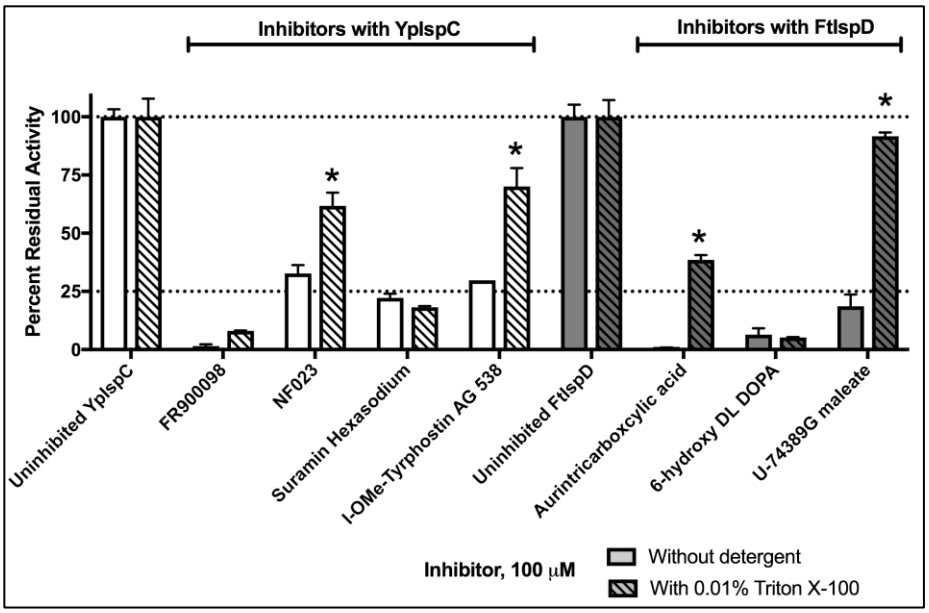

Figure 53. Residual activity of YpIspC (white) or FtIspD (dark grey) in the absence (open bars) and presence (hatched bars) of 0.01% Triton X-100. All samples are standardized to an uninhibited control containing the vehicle (DMSO) and 0.01% Triton X-100 if necessary. FR900098 was used as a positive control for specific inhibition. Inhibition is attenuated in the presence of Triton X-100 for all inhibitors except suramin hexasodium, an inhibitor of IspC, and 6-hydroxy DL DOPA, an inhibitor of IspD. The cut-off for significant attenuation of inhibition was set as 25% or greater increase in residual enzyme activity; compounds with significantly attenuated activity in the presence of Triton X-100 are indicated with a star. Error bars are calculated as the deviation from the mean of two independent measurements.

The IC_{50} of suramin with respect to YpIspC was determined to be 34.6 μM, shown in Figure 54. The IC_{50} also was not dependent on enzyme concentration, suggesting that suramin was not an aggregating inhibitor. The structure of suramin is shown in in Figure 54.

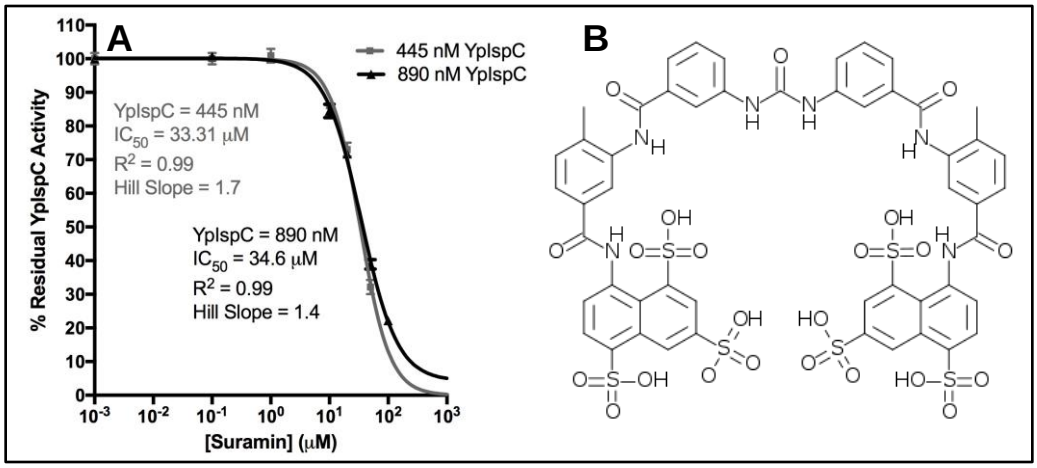

Figure 54. Dependence of IC_{50} with suramin on enzyme concentration. A) The IC_{50} with suramin does not significantly decreases with a decrease in YpIspC concentration, nor does the Hill slope decrease. Error bars are calculated as the deviation from the mean of two independent measurements. B) Structure of suramin

Based on its potential specificity, suramin was examined for its mechanism of action with respect to YpIspC. Lineweaver Burk plots shown in Figure 55 suggest that suramin is not competing with either NADPH or DXP binding, as anticipated based on its structure.

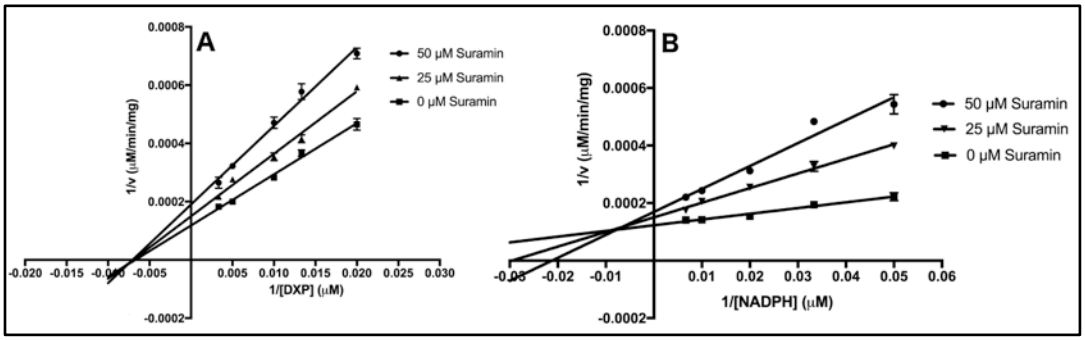

Figure 55. Mode of inhibition by suramin. The Lineweaver–Burk plots indicate that suramin is noncompetitive with respect to A) DXP and noncompetitive with respect to B) NADPH. All assays were performed in duplicate using purified YpIspC. Error bars are calculated as the deviation from the mean of two independent measurements.

Suramin is used commercially as an antiparasitic drug for African sleeping sickness as well as river blindness in children and adults; it is noted to have a high number of side effects[164]. A literature search identified a plethora of other protein targets of suramin outside of parasites[165, 166, 167, 168], and suramin is known to require high dosing to overcome significant protein binding in plasma[169]. Based on this eveidence, it may be that suramin has a high affinity for many proteins, and may not be specific for IspC *in vivo*. Further studies to deduce suramin's precise interaction with IspC could shed light on whether this compound has the potential to be pursued for development of a novel antibiotic.

For specific inhibitors of IspD, 6-hydroxy-DL-DOPA is a small molecule analog of L-DOPA, a compound that is not known to aggregate. Its structure and IC_{50} determination (IC_{50} = 6.8 μM) are shown in Figure 56.

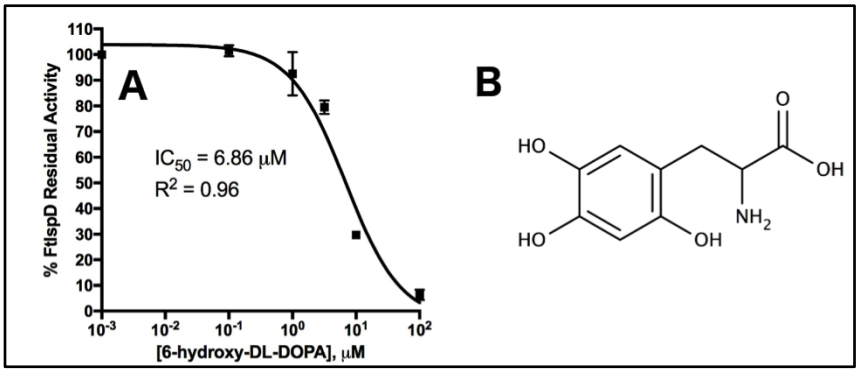

Figure 56. IC_{50} of 6-hydroxy-DL-DOPA. A) IC_{50} of 6-hydroxy-DL-DOPA with FtIspD, and B) Structure of 6-hydroxy-DL-DOPA. Error bars are calculated as the deviation from the mean of two independent measurements.

Investigation into 6-hydroxy-DL-DOPA's mechanism of action revealed that it is competitive with CTP, binding exclusively in the CTP site without interfering with MEP binding, as indicated by the noncompetitive (mixed) profile with respect to MEP (Figure 57).

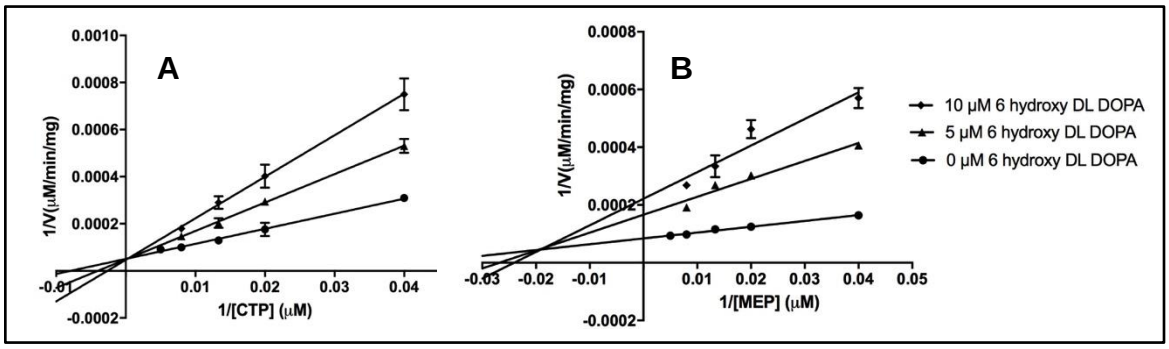

Figure 57. Mode of inhibition by 6-hydroxy-DL-DOPA. The Lineweaver–Burk plots indicate that 6-hydroxy-DL-DOPA is competitive with respect to A) CTP and noncompetitive with respect to B) MEP. All assays were performed in duplicate using purified FtIspD. Error bars are calculated as the deviation from the mean of two independent measurements.

A competitive profile with respect to CTP poses new challenges in that drugs binding in the CTP pocket may be toxic, lacking specificity for the IspD enzyme over other mammalian enzymes requiring CTP. Additionally, 6-hydroxy-DL-DOPA is a known neurotoxin, acting as an excitotoxic agonist of AMPA receptors[170]. Oxidation of 6-hydroxy-DL-DOPA occurs spontaneously in aerobic conditions at biological pH[171], leading to a variety of quinone oxidation products that may also be exerting some effect on FtIspD. Taken together, the potential cytotoxicity via CTP-dependent enzyme inhibition, the known neurotoxicity, and the sensitivity in solution to oxidative

degradation indicate that 6-hydroxy-DL-DOPA would certainly be a challenging lead molecule for the development of IspD inhibitors.

Conclusions

Each of the initial hits compounds identified from the LOPAC^{1280} and natural product libraries displaying antimicrobial activity showed evidence of aggregation, either through sensitivity of inhibition to detergent, or sensitivity of inhibition to enzyme concentration. Given the percentage of hits identified as aggregators in HTS campaigns, both in this work and others[172], not including such analysis of hits increases the likelihood of pursuing compounds that do not inhibit the expected target in a specific manner.

Given aggregating inhibitors would be expected to inhibit diverse enzymes if assay conditions are similar, further investigation into the specificity of each cohort of LOPAC^{1280} inhibitors is warranted. For the aggregating inhibitors of IspD, investigation into the IspC primary and secondary screens reveals that both chelerythrine and dequalinium were identified as inhibitors of IspC in the primary screen with YpIspC. They were subsequently both eliminated following the secondary screen with MtbIspC, with chelerythrine reducing the residual activity of MtbIspC to 27%, only 2% over the set 25% cut-off for the secondary screen. It is likely that the identified aggregating inhibitors of IspD function as aggregating inhibitors of IspC, with decreases in potency just great enough to avoid being brought forward past the secondary screen of IspC.

In the same way, investigation of the aggregating IspC inhibitors reveals that all showed some activity against IspD in the primary screen, with rottlerin being the least

potent at 52% residual FtIspD activity in the primary screen. Sanguinarine reduced FtIspD residual activity to 27%, just missing the primary screen cut-off. Both GW5074 and PPT were identified as inhibitors of FtIspD in the primary screen, and were eliminated with 47% and 55% residual activity of EcIspD in the secondary screen, respectively. It is known that aggregating inhibitors are exceptionally sensitive to changes in protein concentration, as shown in Figure 52. Because the IspD assays were performed with roughly twice the concentration of enzyme as the IspC assays (1.8 μM versus 0.89 μM), in addition to the pyrophosphatase, it is perhaps unsurprising that aggregating inhibitors in the IspC assays were in general less potent when examined in the IspD assays.

The discovery that the LOPAC^{1280} library contains a wealth of compounds both with unhelpful aggregating properties or known instability at recommended storage conditions (6-hydroxy DL-DOPA) requires a closer evaluation of the compounds selected for the LOPAC^{1280} library itself. Aurintricarboxcylic acid, for example, was a hit according to our cut-off values in both the IspC and IspD screening campaigns, and was investigated as an IspD inhibitor. Further experimentation (Figure 53) suggests it could be an aggregating inhibitor. Literature reports that aurintricarboxcylic acid spontaneously polymerizes in aqueous solution, forming a high molecular weight, free-radical species[173]. This polymerization may explain why Triton X-100 could only partially rather than fully alleviate inhibition. Aurintricarboxycylic acid is therefore a poor scaffold for aqueous, *in vitro* enzyme screening given its suspected aggregation and autopolymerization properties. Future users of this library should be aware of the

multitude of interference compounds present, and perhaps use the LOPAC^{1280} library primarily in searching for *in vivo* biological effects rather than *in vitro* inhibition of enzyme targets. One can speculate that the high biological activity, a requirement for a compound's inclusion in this library, may have therefore biased the collection towards such nonspecific or promiscuous compounds, as these compounds would be reported to have effects in a wide variety of screening campaigns.

With regards to those identified inhibitors without antimicrobial activity, both suramin and 6-hydroxy-DL-DOPA were determined to be challenging lead molecules. While suramin's lack of antimicrobial activity, probable lack of specificity, and large molecular weight leading to difficult analog production are challenging, the knowledge that there exists some interaction with IspC may be worth investigating. If suramin does interact with a pocket such that activity is attenuated, other compounds designed for this pocket could be engineered for higher specificity and cellular penetration. Similarly, while 6-hydroxy-DL-DOPA's lack of antimicrobial activity, neurotoxicity, and instability in aqueous buffer make it unlikely to move forward as an antibiotic, additional substituents appended to its structure for the purpose of branching into the MEP site could increase specificity. Both compounds, suramin and 6- hydroxy-DL-DOPA, represent new approaches to targeting both IspC and IspD.

Finally, the HTS protocol delineated provides a rational start to probing IspC and IspD for additional sites to expand the chemical space for inhibitors of this enzyme. Further HTS against IspC or IspD may aid not only in developing novel antibacterials, but also in helping to elucidate the regulatory mechanisms of this pathway. Use of this

HTS protocol for IspC and IspD with additional molecular libraries, including the appropriate control assays and investigation for aggregation, may unveil further compounds suitable as novel antibiotics.

SPECIFIC AIM 4 — CRYSTALLOGRAPHIC STRUCTURE DETERMINATION OF ISPC AND/OR ISPD

To aid in the rational design and development of inhibitors, in Specific Aim 4 protein crystal structures of IspC and IspD were sought, using purified recombinant enzymes cloned from *Yersinia pestis* and *Francisella tularensis*. Where suitable, co-crystallization studies were explored using promising library compounds (hits/leads) identified in Specific Aims 1-3.

Specific Aim 4 is comprised of currently unpublished work. This section details crystallization experiments with both YpIspC and FtIspD, and proposes the most promising way forward to obtain crystal structures of each, based on the trials run to date. Consideration is given to whether project goals would be best met by utilizing alterative homologs of IspC and IspD.

Crystallization of IspC from *Yersinia pestis*

Phosphate Conditions

Initial screening of YpIspC with multiple crystallization screens resulted in an initial hit in Condition 35 from the Crystal Screen Cryo screen from Hampton Research[174]. Because YpIspC is suspected to be a very conformational flexible protein due to its sequence similarity and modeled structural similarity to EcIspC[141, 145], it was anticipated that YpIspC may be difficult to crystalize. Condition 35, which contained 0.075 M HEPES pH 7.5, 600 mM sodium phosphate monobasic, 600 mM potassium phosphate monobasic, and 25% glycerol, could potentially be stabilizing the protein through phosphate binding. The active site of IspC contains four phosphate binding pockets (three pockets to accommodate the three phosphate groups of NADPH, and one pocket to accommodate the phosphate group of DXP). The high concentration of phosphate salts in Condition 35 could lead to packing of the active site cleft and subsequent stabilization of a very flexible protein. Additionally, the favorable pH range for this hit suggested that conditions based on this hit would likely be an appropriate pH range to facilitate ligand binding, making it an attractive hit condition to optimize. A crystal harvested from the original optimization of these conditions yielded diffraction data used to determine the structure of YpIspC to 3.3 Å. However, it is worth noting that some diffraction patterns from the collected data set were atypical, with some missing reflections. While a sufficient quantity of data without missing reflections was available for structure determination, further optimization of these conditions was desired to improve the resolution and quality of diffraction patterns.

When screened in a hanging drop tray with 8 mg/mL YpIspC at a 2:2 drop ratio, original phosphate conditions promoted the growth of many small plate crystals, as shown in Figure 58.

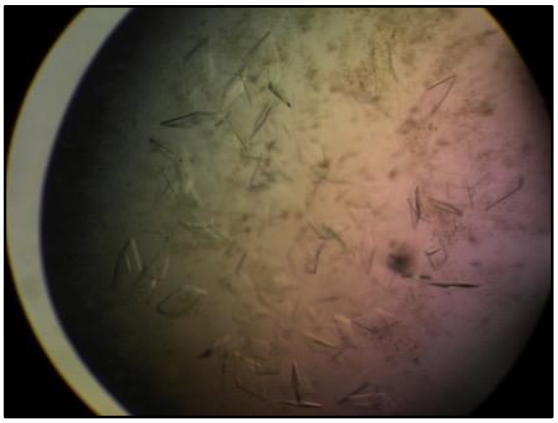

Figure 58. YpIspC crystals set 10/01/2014. Conditions: 8 mg/mL YpIspC, 22°C, 2:2 drop ratio, hanging drop tray, 75 mM HEPES pH 7.5, 700 mM NaH_2PO_4, 700 mM KH_2PO_4, 30% glycerol.

Initial optimization of phosphate concentrations and glycerol concentrations were focused on increasing crystal size and improving crystal morphology from the plate-like crystals first identified. No significant difference was noted between using protein that had been prepared same-day versus protein that had been snap frozen, echoing our kinetics findings that flash-frozen YpIspC is still very catalytically active. The initial optimization screens were conducted in hanging drop trays at both 22°C and 16°C, with crystals appearing more frequently and regularly at 22°C. As shown in Figure 58, plate-like structures were common in most optimization screens initially conducted in the hanging drop trays. Early results showed that glycerol conditions between 20-30% were well tolerated, and that crystallization was more sensitive to

phosphate salt concentrations. Crystals were infrequent but large in conditions with 500 mM sodium phosphate monobasic and 500 mM potassium phosphate monobasic. As the concentrations of each phosphate salt were increased by 100 mM, crystals became both more consistently reproducible, but smaller and more plate like.

Crystallization was then compared in sitting drop trays versus hanging drop trays, to see if the larger, less plate like crystals observed in 500 mM phosphate salt conditions were more reproducible in the sitting drop trays. While the crystals tended to be mildly larger in the hanging drop trays, sitting drop trays also yielded crystals of good quality, with less tendency to form plates. For this reason, further optimization was conducted in sitting drop trays. Covering sitting drops with oil seemed to improve the crystallization of YpIspC in the 500 mM conditions, leading to more reproducible single crystals. Silicon oil, parafin oil, and each with the addition of beta-mercaptoethanol (BME) were tested. Using silicon oil alone as a covering, crystals diffracted to 3.9 Å (2/20/2015, 75 mM HEPES pH 7.5, 500 mM NaH_2PO_4/KH_2PO_4, 25% glycerol, no cryoprotection). Crystals covered with paraffin oil and BME diffracted better than did crystals grown under silicon oil, with paraffin oil covered crystals diffracting to 3.4 Å (01/28/15, 75 mM HEPES pH 7.5, 400 mM NaH_2PO_4/KH_2PO_4, 22.5% glycerol, no cryoprotection).

The Hampton Additive Screen[175] was used to determine if larger crystals could be grown in the presence of some other additive. Of those additives tested, Additive 34, glycine, improved crystal size. However, when glycine addition was coupled to paraffin oil covering and addition of BME, the average diffraction of crystals did not improve.

The best diffraction observed was 3.7 Å (2/20/15, 75 mM HEPES pH 7.5, 500 mM NaH_2PO_4/KH_2PO_4, 22.5% glycerol, no cryoprotection). Based on these results, glycine addition was abandoned as it did not improve diffraction.

Due to the known flexibility of EcIspC and the suspected similarity YpIspC[141, 145], it was anticipated that the addition of inhibitors such the bisubstrate inhibitors may improve crystal quality by decreasing protein flexibility. Crystals were only obtained using co-crystalization with **8**e and **16**j (as described in Paper V: Structure-Activity Relationships of the MEPicides: N-Acyl and O-linked Analogs of FR900098 as Inhibitors of Dxr from Mycobacterium tuberculosis and Yersinia pestis), however these conditions were not reproducible. Crystals could be regularly obtained with the addition of NADPH or FR900098, but are almost always plate-like and unsuitable for diffraction, and grow best at 16°C. So far, addition of inhibitors in this screen does not increase crystal size or quality, but in fact decreases crystal reproducibility and quality. It could be hypothesized that the high phosphate salt concentrations stabilize the very conformationally flexible protein by filling the active site (which has four phosphate binding pockets), and that this high phosphate concentration disrupts interactions between the protein and the inhibitor.

Given the seemingly local minima of diffraction at roughly 3.5 Å in the 22°C YpIspC crystallization conditions explored to this point, temperature screening and pH screening was employed to search for related conditions that may improve diffraction. At 16°C, crystals are fairly reproducible at 500 mM concentrations of phosphate salts,

though higher concentration of salt yield crystals that are highly unpredictable. Shown in Figure 59 is a single crystal grown at 16°C with 500 mM NaH_2PO_4/KH_2PO_4.

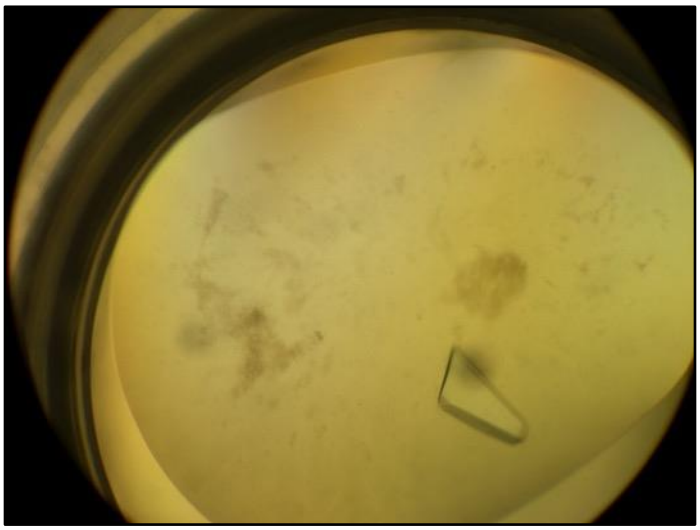

Figure 59. YpIspC crystals set 3/13/15. Conditions: 8 mg/mL YpIspC, 16°C, 2:2 drop ratio, sitting drop tray, 75 mM HEPES pH 7.5, 500 mM NaH_2PO_4/KH_2PO_4, 25% glycerol

A pH screen was conducted screening Tris pH 8.0, Tris pH 8.5, and bicine pH 9.0. While no crystals were observed in the pH 8.5 or pH 9.0 conditions, crystals were obtained with 75 mM Tris pH 8.0. Shown in Figure 60 is a crystal grown at 16°C at pH 8. For comparison, a crystal grown with 75 mM HEPES pH 7.5 in the otherwise same conditions is shown for comparison in Figure 61. The crystals are of roughly the same shape and size, leading to no significant improvement at higher pH.

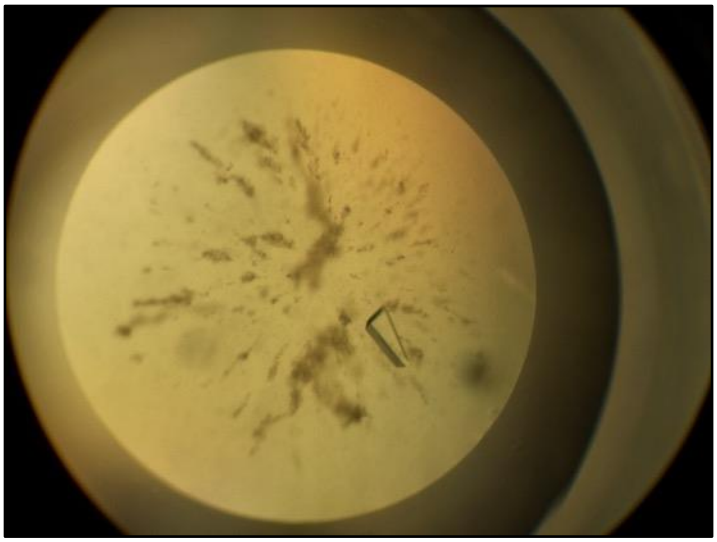

Figure 60. YpIspC crystals set 9/23/15. Conditions: 8 mg/mL YpIspC, 16°C, 2:2 drop ratio, sitting drop tray, 75 mM Tris pH 8.0, 500 mM NaH_2PO_4/KH_2PO_4, 30% glycerol

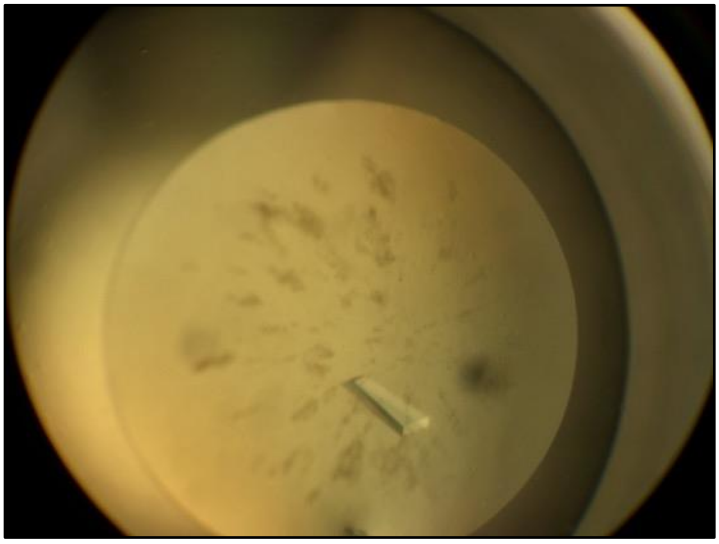

Figure 61. YpIspC crystals set 9/23/15. Conditions: 8 mg/mL YpIspC, 16°C, 2:2 drop ratio, sitting drop tray, 75 mM HEPES pH 7.5, 500 mM NaH_2PO_4/KH_2PO_4, 30% glycerol

Additional protein concentration screening at 16°C at 10 mg/mL, 12.5 mg/mL, and 15 mg/mL showed that both 10 mg/mL and 12.5 mg/mL yielded crystals, while 15 mg/mL was over-nucleated. The 12.5 mg/mL YpIspC conditions gave the best

diffracting crystal of the higher protein concentration screen at 4.09 Å (01/08/2016, 12.5 mg/mL YpIspC, 75 mM HEPES pH 7.5, 500 mM NaH_2PO_4/KH_2PO_4, 22.5% glycerol, no cryoprotection) but had a few more plate-like crystals, common in higher concentrations of YpIspC, than did the 10 mg/mL. Shown below in Figure 62 is a crystal at 10 mg/mL.

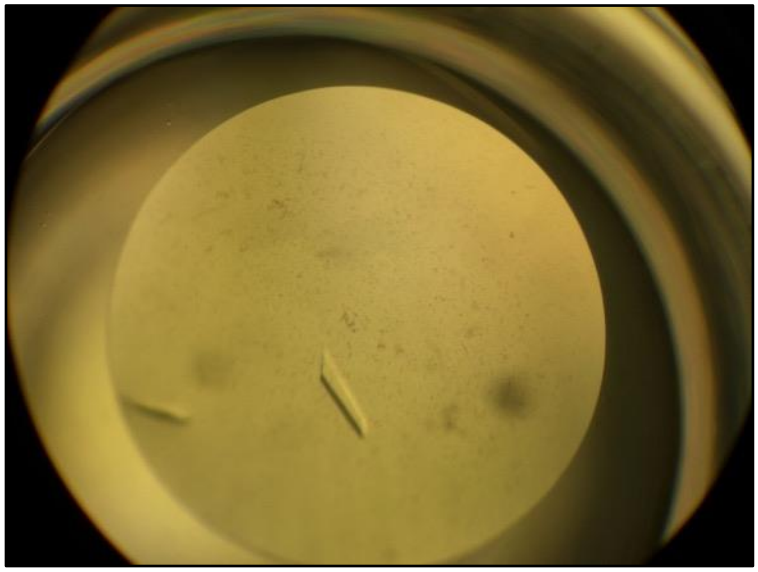

Figure 62. YpIspC crystals set 10/09/15. Conditions: 10 mg/mL YpIspC, 16C, 2:2 drop ratio, sitting drop tray, 75mM Tris pH 7.5, 500mM NaH_2PO_4/KH_2PO_4, 35% glycerol.

Given the lack of improvement in diffraction, additional broad screens were conducted to identify alternative conditions for the crystallization of YpIspC.

Cation Conditions

Screening of the Index crystallization screen from Hampton Research[176] yielded hits in conditions 82-85 and 92-93, given in Table 10 below.

Table 10. Index Hit conditions with 8 mg/mL YpIspC, 1:1 drop ratio, hanging drop

Index Condition Number	Conditions
82	100 mM Bis-Tris pH 5.5, 200 mM magnesium chloride hexahydrate, 25% PEG 3350
83	100 mM Bis-Tris pH 6.5, 200 mM magnesium chloride hexahydrate, 25% PEG 3350
84	100 mM HEPES pH 7.5, 200 mM magnesium chloride hexahydrate, 25% PEG 3350
85	100 mM Tris pH 8.5, 200 mM magnesium chloride hexahydrate, 25% PEG 3350
92	0.1 M magnesium formate dehydrate 15% PEG 3350
93	0.05 M Zinc acetate dehydrate 20% PEG 3350

While crystals were obtained in each of the above conditions, conditions 82 and 83 produced primarily needles, while conditions 84 and 85 produced small single crystals, with the largest crystals in condition 84. Therefore, further optimization was conducted with conditions 84, 92, and 93. It is worth noting that there is currently one structure for *Yersinia pestis* IspC in the PDB (5DUL) that was deposited by the Seattle Structural Genomics Group. Full methods for crystallization have not been published, but the crystallization conditions given were 100 mM HEPES pH 7.5, 200 mM sodium chloride, 25% PEG 3350, and 10 mM NADPH, with crystals grown in sitting drop trays at 16°C. While we were unable to reproduce their results, it is notable that the published conditions do show significant similarity to Index 84, with only a change in the salt used. For this reason, it was decided that a cation screen with the above conditions would be conducted.

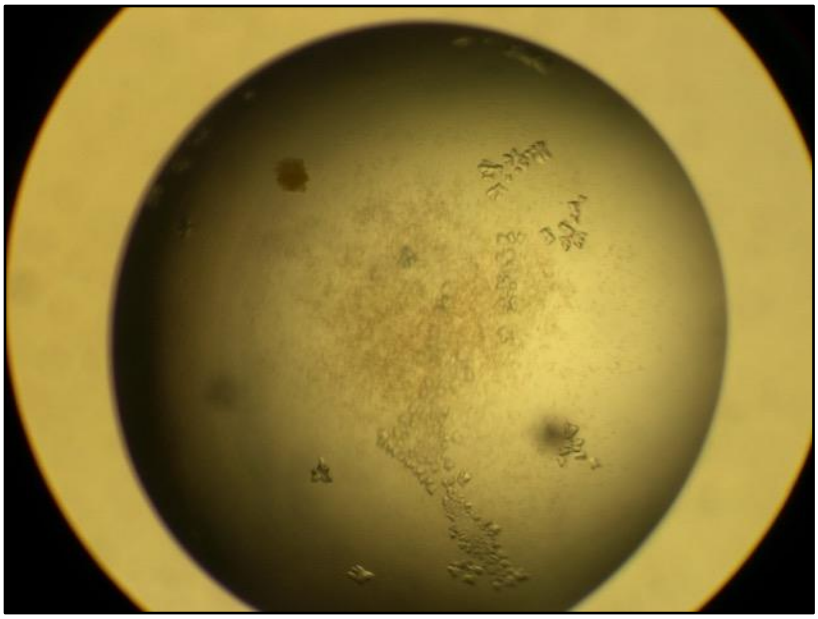

Figure 63. YpIspC crystals set 4/15/16. Conditions: 8 mg/mL YpIspC, 22°C, 1:1 drop ratio, hanging drop tray, 100mM HEPES pH 7.5, 200 mM magnesium chloride hexahydrate, 30% PEG 3350

Early optimization based on conditions 92 and 93 yielded crystals that were exceedingly small and of poor quality. However, conditions based on condition 84 were very reproducible, although the crystals obtained from these screens were very small, as shown in Figure 63. Further optimization with the magnesium chloride conditions was conducted, starting with an optimization of protein concentration. When screened with 5, 8, and 12 mg/mL YpIspC, the largest crystals were obtained at 8 mg/mL, the initial screening concentration. The crystals were also mildly larger at higher concentrations of PEG 3350 than the initial hit, although the crystals were still very small, and have a clustered morphology. Drop ratios of 1:1 and 3:3 showed that crystals were larger in the 3:3 drops. The largest crystals are shown below in Figure 64.

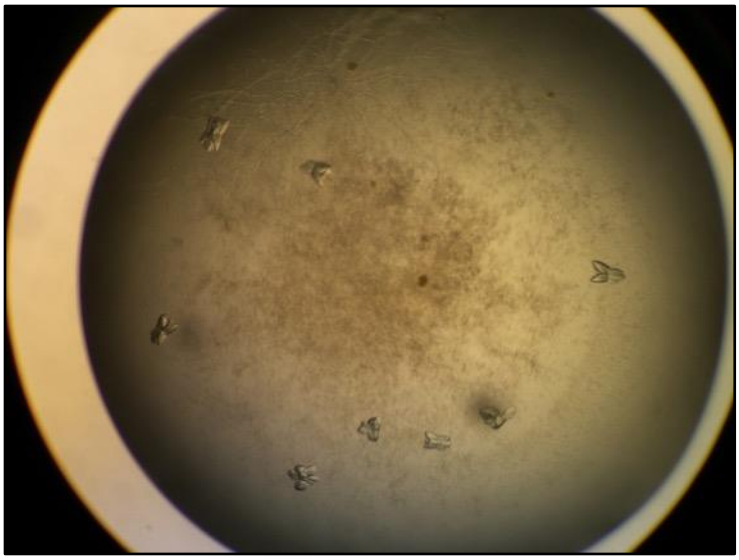

Figure 64. YpIspC crystals set 4/29/16. Conditions: 8 mg/mL YpIspC, 22°C, 3:3 drop ratio, hanging drop tray, 100 mM HEPES pH 7.5, 250 mM magnesium chloride hexahydrate, 32.5% PEG 3350.

While 16°C did not lead to any discernable difference in crystal size or quality with hanging drop trays, temperature did have a more significant effect on crystals grown in sitting drop trays. When sitting drop trays were compared at 22°C and 16°C, it was observed that those crystals grown at 16°C in sitting drop trays (Figure 65) were larger than those grown at 22°C (Figure 66).

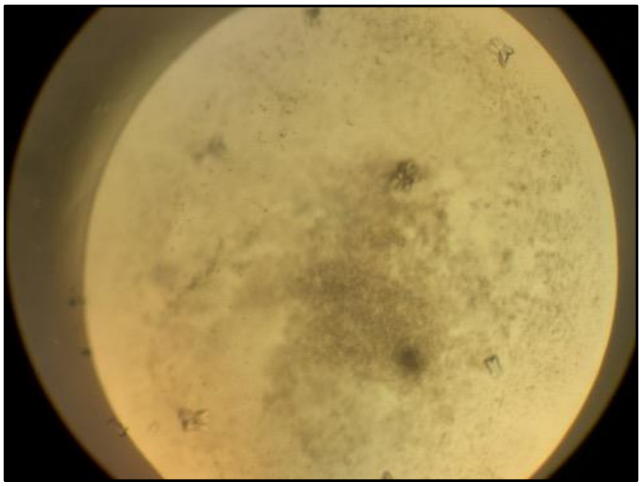

Figure 65. YpIspC crystals set 5/13/16. Conditions: 8 mg/mL YpIspC, 16°C, 2:2 drop ratio, sitting drop tray, 100 mM HEPES pH 7.5, 250 mM magnesium chloride hexahydrate, 30% PEG 3350

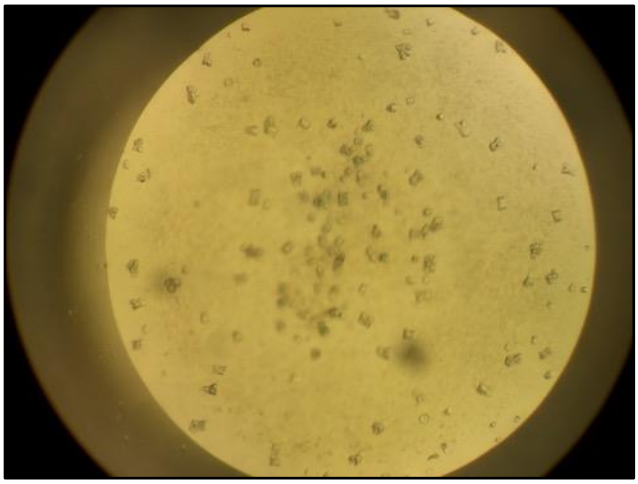

Figure 66. YpIspC crystals set 5/13/16. Conditions: 8 mg/mL YpIspC, 16°C, 2:2 drop ratio, sitting drop tray, 100 mM HEPES pH 7.5, 250 mM magnesium chloride hexahydrate, 37.5% PEG 3350

It was not clear whether the crystals grown in the hanging drop trays at 22°C (Figure 64) or those grown in the sitting drop trays at 16°C (Figure 65) were larger. As the crystals were still too small to screen, their size needed to be improved.

Future Directions

Despite intense efforts using the conditions described in Phosphate Conditions, crystals were never obtained of appropriate in-house diffraction levels in the presence of inhibitors to determine inhibitor binding. The more recently investigated Cation Conditions need further development in order to produce crystals suitable for inhibitor binding and screening. It is also worth noting that the primary purpose of these crystallization experiments was to validate the binding mode of the bisubstrate inhibitors described in Paper V: Structure-Activity Relationships of the MEPicides: N-Acyl and O-linked Analogs of FR900098 as Inhibitors of Dxr from Mycobacterium tuberculosis and Yersinia pestis **.** For that reason, the homolog used to determine binding mode is flexible; compound **16j** has been kinetically shown to be a bisubstrate inhibitor with respect to MtbIspC as well. MtbIspC has known crystallization conditions, and it would be beneficial to begin screening with this homolog. The crystallization conditions for EcIspC are known as well, and if the bisubstrate inhibitors can be kinetically shown to act via a bisubstrate mechanism against EcIspC, this homolog could too be investigated. Screening additional IspC homologs could maximize the probability of obtaining a suitable IspC-inhibitor crystal for binding mode determination.

Crystallization of IspD from *Francisella tularensis*

Crystal Structure of FtIspD

The crystal structure of FtIspD has been solved to 2.4 Å (4MYB) and is shown in Figure 67. Like other IspD species[129], FtIspD assembles as a dimer with a β-sheet "arm" region that extends to interact with the homodimer partner.

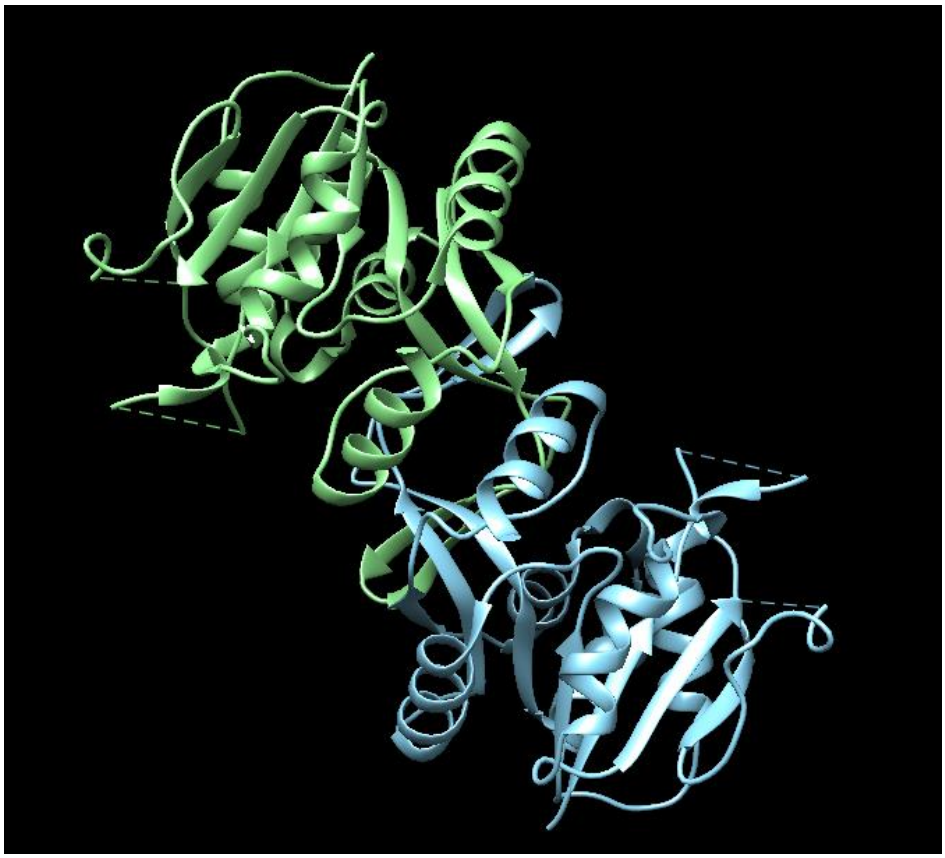

Figure 67. Biological Assembly of FtIspD as a homodimer. Chain A, shown in green, and Chain B, shown in blue, are linked via a β-sheet "arm" region.

As seen in the EcIspD structure (1INJ[129]), the FtIspD active site is comprised of residues from both IspD monomers, with Thr 141 and Arg 156 on the β-sheet "arm" region from one chain forming part of the active site in the second chain. This architecture is shown in Figure 68, with Thr 141 and Arg 156 numbered for clarity.

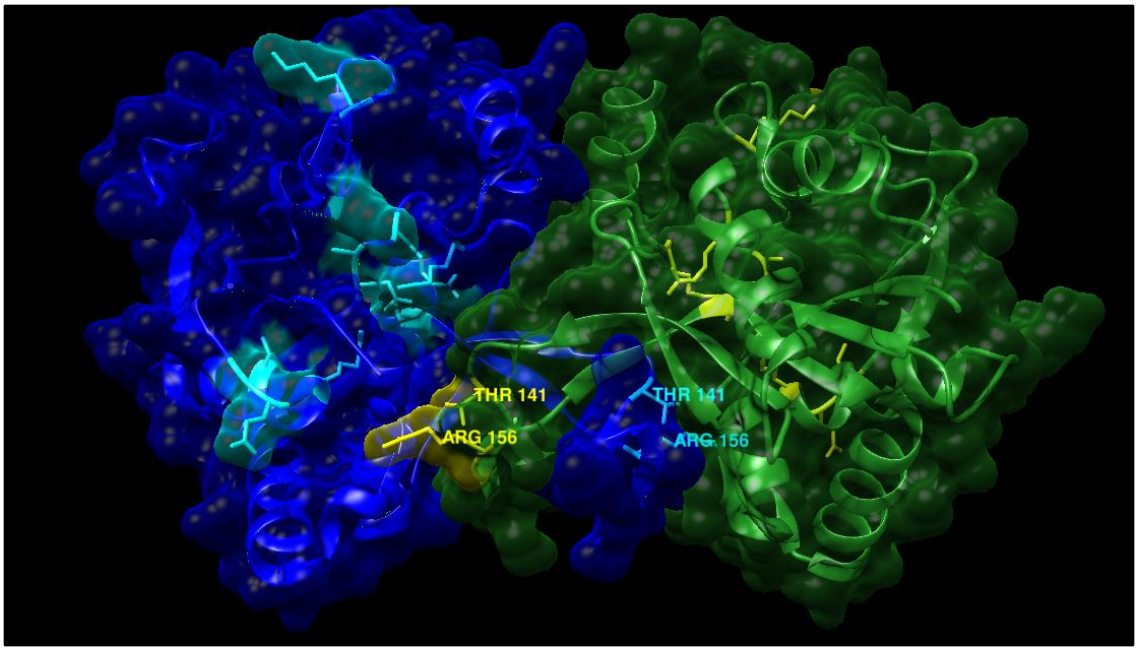

Figure 68. FtIspD homodimer showing active site residues. Chain A (dark blue ribbon structure, surface shown at 70% transparency) has active site residues shown in light blue. Chain B (green ribbon structure, surface shown at 70% transparency) has active site residues shown in yellow. Residues Thr 141 and Arg 156 from one chain contribute to the architecture of the active site of its homodimer partner. Active site residues were identified via homology to EcIspD active site residues[129] and are strictly conserved between the two species.

The sequence of FtIspD shows 30% or greater identity to several other IspD sequences for which there are crystal structures available. Table 11 gives the sequence identity of FtIspD to six other IspD homologs and a representative crystal structure of each. The first IspD crystal structure solved was that of *E. coli (*1INJ [129]); this structure was used to solve the FtIspD 4MYB structure via molecular replacement.

Table 11. Sequence Homology of FtIspD to homologs for which crystal structures are available

Homolog	Sequence Identity to FtIspD	Representative Crystal Structure
E. coli IspD	36%	1INJ
M. tuberculosis IspD	30%	2XWN
A. thaliana IspD	34%	1W77
N. gonorrhoeae IspD	35%	1VGZ
B. subtilis IspD	37%	5DDT
B.thailandensis IspD	34%	4YS8

A comparison of the FtIspD and EcIspD structures shows some differences near the active site, particularly in the position of the β-sheet "arm" region of each monomer, as depicted in Figure 69.

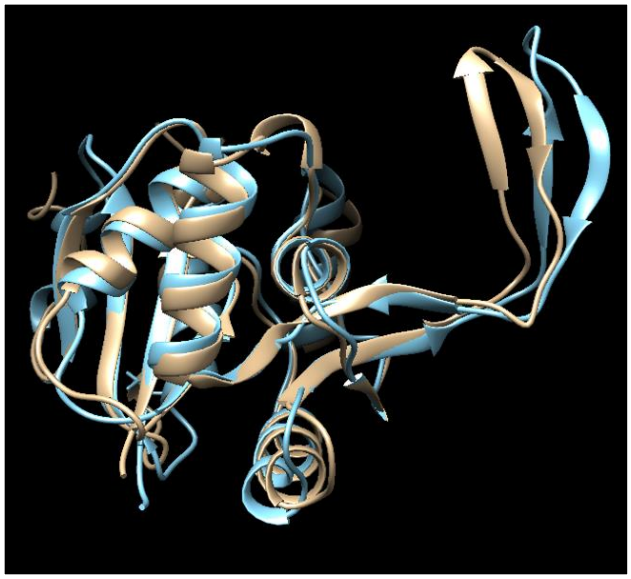

Figure 69. Crystal structure of EcIspD (brown, 1INJ) and FtIspD (blue, 4MYB). Structures aligned using the Matchmaker tool of UCSF Chimera v. 1.8.1 on default alignment settings. Aligned structures show the greatest difference in the β-sheet "arm" region of the protein.

The differences in β "arm" orientation are not unique to FtIspD and EcIspD; indeed the β "arm" region has been shown to have some flexibility between structures. A close-pair structural alignment of 11 IspD structures performed by Bjorkelid, et.al[131] shows changes in the position of the β "arm", indicated as βb and βc in Figure 70.

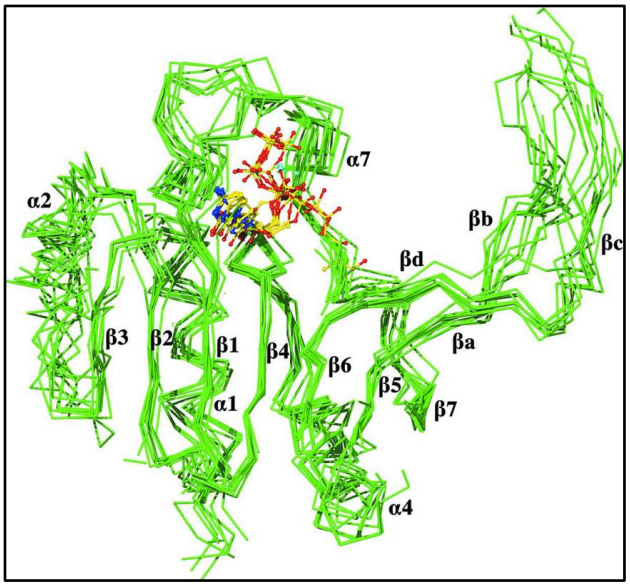

Figure 70. Alignment of 11 IspD structures indicating structural differences in the β "arm" region. The view was chosen to highlight variation in the β "arm" region; front plane clipping was used to simplify the image. Image reproduced from [131] with permission; copyright International Union of Crystallography.

These structural differences, along with the noted differences in alpha helical regions α2 and α4, indicate there may be species-specific variations between structures including in the active site. Additionally, Bjorkelid, et.al[131] also found that the positioning of the twofold axis in each dimer of the 11 species aligned above in Figure 70 varied, such that there was no tight clustering of the dimeric structures. These kinds

of structural differences could provide avenues for the design of species-specific drugs; further crystal structures with bound compounds are needed to evaluate this possibility.

Citric Acid Conditions

The crystal structure of FtIspD was solved in crystallization conditions for the apo structure of 100 mM citric acid pH 4.5, 0.5 M lithium chloride, and 7% PEG6000. These conditions were the starting point for optimization for a ligand-bound structure. Initial screening conditions with 200 µM of inhibitors NSC 110039 and NSC 401145 gave large crystals, with one shown in Figure 71. The best crystal diffracted to 2.9 Å (05/08/2015, 12.1 mg/mL FtIspD, 100 mM citric acid pH 4.5, 500 mM LiCl , 9% PEG6000, 200 µM 110039, cryoprotection = 30% ethylene glycol, 70% well solution), with the diffraction pattern shown in Figure 72. However, upon examining the data collected on this crystal, there was no additional density due to an inhibitor. It was supposed that the inhibitor concentration must be raised significantly.

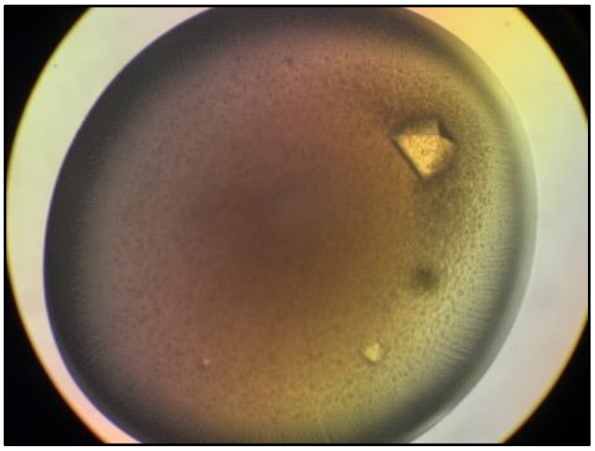

Figure 71. FtIspD crystals set 4/25/15. Conditions: 12.1 mg/mL FtIspD, 22°C, 3:3 drop ratio, hanging drop tray, 100 mM citric acid pH 4.5, 1 M LiCl, 8% PEG6000, 200 µM 401145.

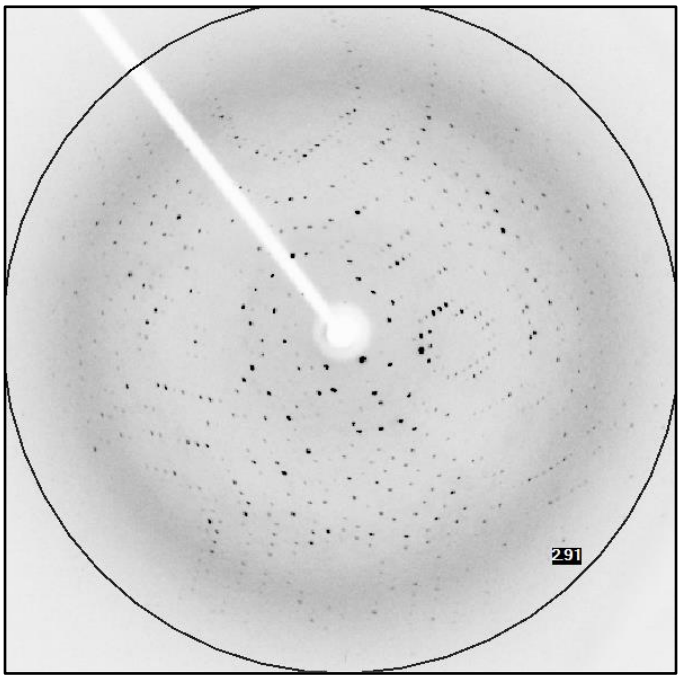

Figure 72. Diffraction pattern of FtIspD crystal to 2.9 Å on 05/08/15. Crystal grown in 100 mM citric acid pH 4.5, 500 mM LiCl , 9% PEG6000, 200 µM 110039 and cryoprotected with 30% ethylene glycol, 70% well solution.

An additional crystal then was selected from the 200 µM NSC 110039 tray, and subject to repeated soaking with NSC 110039 over 3 days, with an additional 0.1 µL of NSC 110039 from a 50 mM stock added to the drop each day. The crystal did not dissolve and was an orange/brown color (the color of NSC 110039) following soaking, with a final concentration of roughly 2.5 mM NSC 110039. Initial diffraction of this crystal was 3.17 Å (06/11/15, 12.1 mg/mL FtIspD, 100mM citric acid, 1M LiCl, 8% PEG600, 2.5 mM NSC 110039), but again upon data collection, there was no presence of the inhibitor.

Co-crystallization was conducted with higher concentrations of inhibitor. Varying the inhibitor concentration between 200 µM, 1 mM, and 5 mM showed crystal growth at every inhibitor concentration except 5 mM NSC 110039. By increasing the concentration of protein to 17.9 mg/mL, crystals could even be obtained in the presence of 5 mM 110039. One such crystal from this tray is shown in Figure 73, where the crystal is clearly an orange color, suggesting incorporation of the inhibitor.

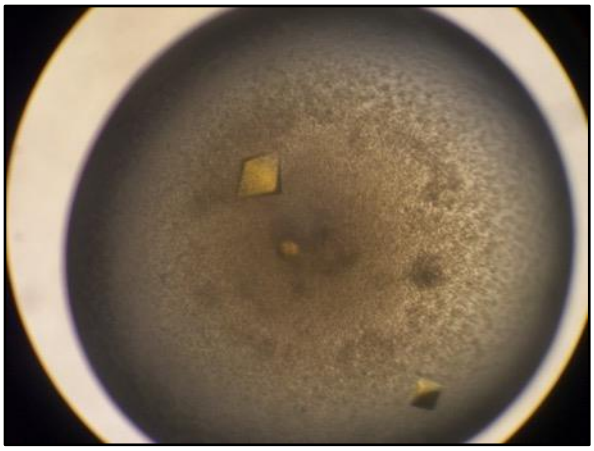

Figure 73. FtIspD crystals set 8/07/15. Conditions: 17.9 mg/mL FtIspD, 22C, 3:3 drop ratio, hanging drop tray, 100 mM citric acid pH 4.5, 0.5 M LiCl, 10% PEG6000, 5 mM 110039.

Data collected on a crystal from this tray (08/21/15, 17.9 mg/mL FtIspD, 100 mM citric acid, 1 M LiCl, 11% PEG600, 5 mM final concentration 110039), like all other crystals tested, did not show any bound inhibitor.

Considering the lack of inhibitor in any of the screened crystals, it was determined that new crystal conditions would be necessary to get a ligand-bound structure of FtIspD. The main hypothesis of the failure of the LiCl conditions was the low pH of the crystallization solution. The amino acids necessary for the catalytic activity of IspD are the following (*E. coli* numbering): Gly82, Asp83, Arg85, Ser88, Ala107, Lys27, Lys213, Asp106, Arg109, Thr165, Thr140', Arg157' (where ' indicates residues from the homodimer partner in creating the active site) [130]. Any changes in protonation in key residues could modify the structure enough to impact inhibitor binding. For these reasons, any new conditions for FtIspD crystallization were desired to be in a more physiologically relevant pH. Due to the low solubility of the lipophilic

NSC 110039 and NSC 401145 in the aqueous buffer, precipitation of the inhibitor out of solution could have caused it to settle on the growing crystals, giving the appearance of color that suggested inhibitor incorporation. If possible, it was desired to find conditions that improved the solubility of the inhibitor in the crystal drops.

Methyl-2,4-pentanediol (MPD) Conditions

Screening of the Hampton Crystal Screen 1[177] and Crystal Screen 2[178] from Hampton Research as well as pH Clear I[179] and pH Clear II[180] from Qiagen revealed three classes of hits. Hampton Screen 2 had two hits, condition 35 and condition 40. The pH Clear screen had two hits including conditions 82 and 87, in addition to condition 37 which was based on the known citric acid/LiCl conditions and was discarded. The pH Clear II screen had six hits, conditions 40, 45, 46, 47, and 48, in addition to condition 7, which was also based on the known citric acid/LiCl conditions already discarded. Table 12 below details the hits from these four screens, showing three classes of conditions based on the inclusion of a volatile organic compound of tert-butanol, methyl-2,4-pentanediol (MPD), or isopropanol.

Table 12. FtIspD Hit Conditions from Hampton Crystal Screen 1, 2 and pH Clear I, II, with 13.5 mg/mL FtIspD, 3:3 drop ratio, 22C, hanging drop trays

Screen	Number	Conditions
Hampton Crystal Screen 2	35	0.1 M HEPES pH 7.5, 70% v/v (+/-) methyl-2,4-pentanediol
	40	0.1 M Tris pH 8.5, 25% v/v tert-butanol
pH Clear I	82	0.1 M HEPES pH 7.0, 20% (v/v) methyl-2,4-pentanediol
	87	0.1 M MES pH 6.0, 40% (v/v) methyl-2,4-pentanediol
pH Clear II	39	0.1 M MES, pH 6.0, 20%(v/v) isopropanol
	40	0.1 M HEPES, pH 7.0, 20%(v/v) isopropanol
	45	0.1 M MES, pH 6.0, 30% (v/v) isopropanol
	46	0.1 M HEPES, pH 7.0, 30% (v/v) isopropanol
	47	0.1 M Tris, pH 8.0, 30% (v/v) isopropanol
	48	0.1 M Bicine, pH 9.0, 30% (v/v) isopropanol

Based on the hits obtained with MPD, the pH range was in a biologically relevant range, and crystals were obtained over a wide range of MPD conditions. Optimization of these conditions lead to very large crystals, but all of these crystals diffracted very poorly. Shown in Figure 74 is a sample of the MPD crystals, none of which had sharp edges.. It is hypothesized that high incorporation of solvent in these crystals could lead to poor diffraction and soft edges. The best diffraction obtained with crystals grown in the presence of MPD was 7.2 Å (11/06/15, 13.5 mg/mL FtIspD, 100 mM HEPES pH 7.0, 45% MPD, cryoprotectant = 30% ethylene glycol, 70% well solution). Based on the poor diffraction seen in these conditions, the MPD conditions were discarded for more favorable hits.

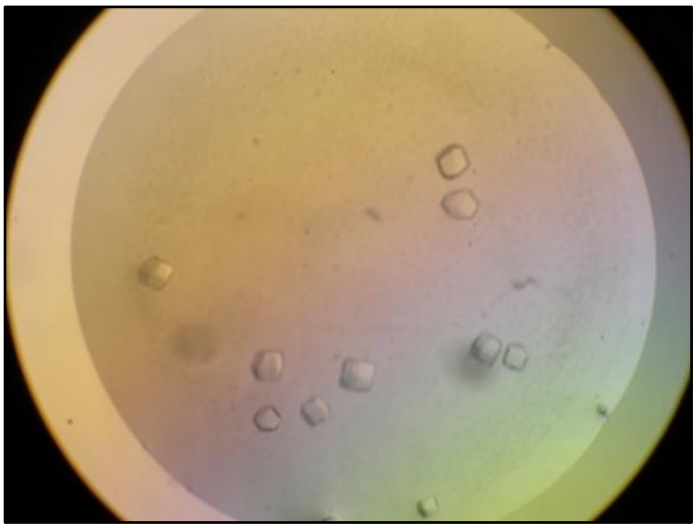

Figure 74. FtIspD crystals set 10/23/15. Conditions: 13.5 mg/mL FtIspD, 22°C, 3:3 drop ratio, hanging drop tray, 100 mM HEPES pH 7.0, 43% MPD.

Tert-butanol Conditions

Hampton Screen 2, Condition 40 (Table 12) was subsequently investigated. Early optimization produced crystals that were highly clustered, but very short and stubby. Early screening of crystals from these conditions produced one crystal that diffracted to 3.7 Å (08/12/16, 15 mg/mL FtIspD, 100 mM Tris pH 8.0, 24% t-BuOH, cryoprotectant = 30% ethylene glycol, 70% well solution). However, a crystal grown in similar conditions with 5 mM WR016773-3 only diffracted to 7.0 Å (08/12/16, 15 mg/mL FtIspD, 100 mM Tris pH 8.0, 26% t-BuOH, 5 mM WR016773-3, cryoprotectant = 30% ethylene glycol, 70% well solution). Further screening of trays under similar conditions at 22°C were able to bring the diffraction of a co-crystal with WR016773-3 down to 3.8 Å (08/26/16, 15 mg/mL FtIspD, 100 mM Tris pH 7.8, 26% t-BuOH, 5mM WRAIR #16, cryoprotectant = 30% ethylene glycol, 70% well solution), but not to a resolution that the crystal could be examined for incorporated inhibitor. As the likely limit on diffraction was crystal size, the concentration of FtIspD was raised and the temperature was increased to room temperature (roughly 25°C in the lab). Shown in Figure 75, the morphology was similar to that seen before, with highly clustered crystals, but the actual crystal rods were larger than those observed at 22°C. Screening of a rod from this drop gave a diffraction of 4.0 Å (10/14/16, 23 mg/mL FtIspD, 100 mM Tris pH 8.0, 25% t-BuOH, cryoprotectant = 30% ethylene glycol, 70% well solution).

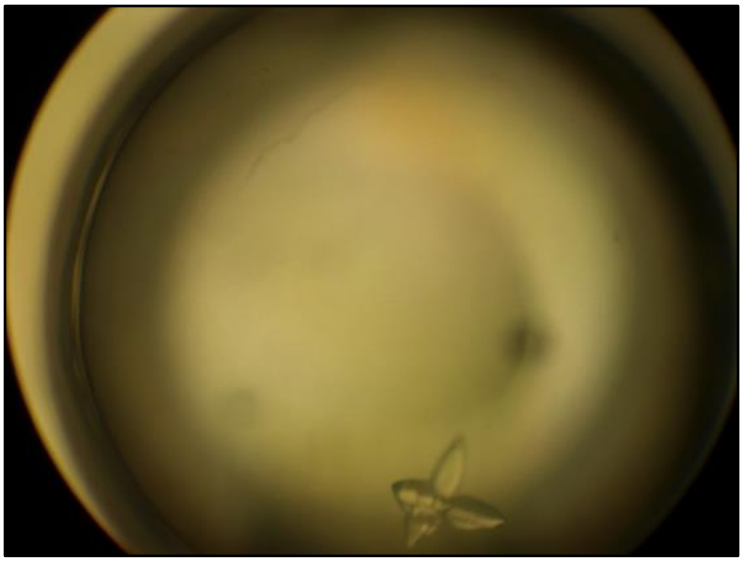

Figure 75. FtIspD crystals set 9/30/16. Conditions: 23 mg/mL FtIspD, 25°C, 3:3 drop ratio, sitting drop tray, 100 mM Tris pH 8.0, 25% t-BuOH.

Crystals from these higher FtIspD concentration, higher temperature conditions were examined after cocrystalization with 5mM WR016773-3 (shown Figure 76) as well as soaking with WR016773-3 for 2 hours (shown Figure 77, both before and after soaking.) Neither crystal diffracted. It is worth noting that WR016773-3, like NSC 110039 and NSC 401145, is poorly soluble in the crystallization solutions, as is apparent in the Figures due to the precipitation of the inhibitor. Given that the inhibitors are typically dissolved in 100% DMSO, which can only be added in small concentration to avoid dissolving crystals and thus does not significantly aid in inhibitor solubility in the drop, further investigation into alternative solvents was conducted.

Figure 76. FtIspD crystals set 9/30/16. Conditions: 23 mg/mL FtIspD, 25°C, 3:3 drop ratio, sitting drop tray, 100 mM Tris pH 8.0, 25% t-BuOH, 5 mM WR016773-3.

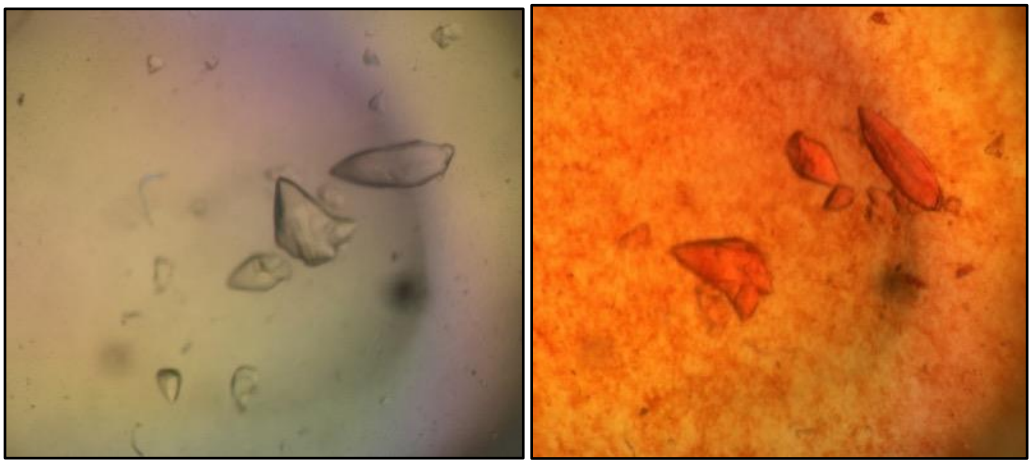

Figure 77. FtIspD crystals set 9/30/16. Conditions: 23 mg/mL FtIspD, 25°C, 3:3 drop ratio, sitting drop tray, 100 mM Tris pH 8.0, 25% t-BuOH, shown left prior to soaking and shown right, after 2 hours of soaking with WR016773-3 to a final concentration of ~4 mM in the drop.

After running a solubility screening test, 5 mM WR016773-3 was soluble from 100%-40% tert-butanol, mostly soluble in 30% tert-butanol, and insoluble below 30% tert-butanol. In order to keep the inhibitor in solution in crystallization screens, crystals grown in the original lower tert-butanol conditions were soaked with WR016773-3

dissolved in 50% tert-butanol, to bring the final concentration in the crystal drop to 30%. Crystals soaked in this manner were stable for 2 hours, with no visible softening. However, crystals soaked in this way only diffracted to 8 Å (12/09/16, 20 mg/mL FtIspD, 100 mM Tris pH 7.8, 25% t-BuOH, cryoprotectant = 30% ethylene glycol, 70% modified well solution with WR016773-3). Crystals from the same conditions without the soaking diffracted to 4.5 Å (12/09/16, 20 mg/mL FtIspD, 100 mM Tris pH 7.8, 25% t-BuOH, cryoprotectant = 30% ethylene glycol, 70% well solution). Based on the relatively poor diffraction of the apo crystals (average of about 4 Å), coupled with a general loss of diffraction when co-crystallized or soaked with inhibitor, these conditions were not pursued further.

Isopropanol Conditions

Based on the pH Clear II hit conditions 39, 40, 45, 46, 47, and 48 (detailed in Table 12), FtIspD conditions utilizing isopropanol as the precipitant were investigated. Initial optimized screens sharp, bunched rod crystals as shown in Figure 78, both before and after the crystal cluster was disturbed.

Figure 78. FtIspD crystals set 10/20/15. Conditions: 13.5 mg/mL FtIspD, 22°C, 3:3 drop ratio, hanging drop tray, 100mM Tris pH 8.8, 22% i-PrOH

Crystals in these conditions diffracted to 3.9 Å (11/06/15, 13.5 mg/mL FtIspD, 100 mM Tris pH 8.8, 22% i-PrOH, cryoprotectant = 22.5% ethylene glycol, 77.5% well solution), with the diffraction pattern shown in Figure 79.

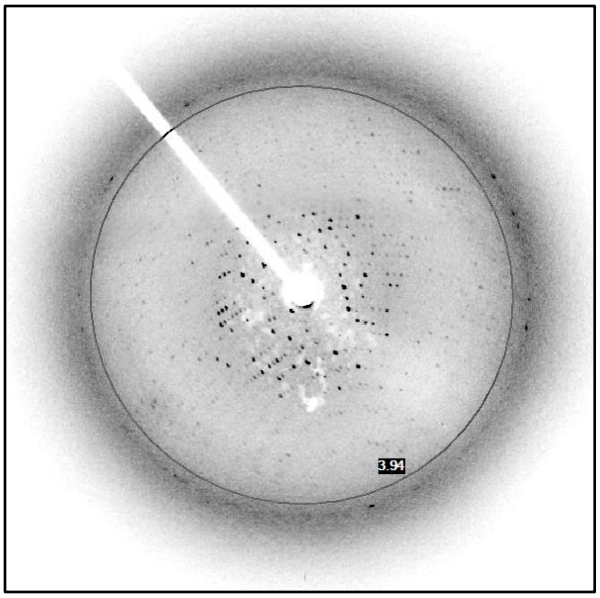

Figure 79. Diffraction pattern of FtIspD crystal to 3.9 Å on 11/06/15. Crystal grown in 100 mM Tris pH 8.8, 22% i-PrOH and cryoprotected with 22.5% ethylene glycol, 77.5% well solution

Soaking of these crystals with WR016773-3 for 2 hours showed no visible signs of softening, and diffracted to 4.0 Å (11/13/15, 13.5 mg/mL FtIspD, 100 mM Tris pH 8.8, 22% i-PrOH, cryoprotectant = 25% ethylene glycol, 75% well solution). Given little resolution was lost on soaking, these conditions were promising, if the crystal size can be increased in size to improve resolution. Unfortunately, these crystals also dissolved within 3 months of being set, so further optimization was needed to stabilize these crystals.

The first attempts at crystal stabilization involved growing crystals in sitting drop trays rather than hanging drop trays. While this switch did prevent the crystals from dissolving in 3 months, it also prevented them from forming for about 3 months.

The crystals that formed were stable, but even thinner than those seen in the hanging drop trays, as shown in Figure 80.

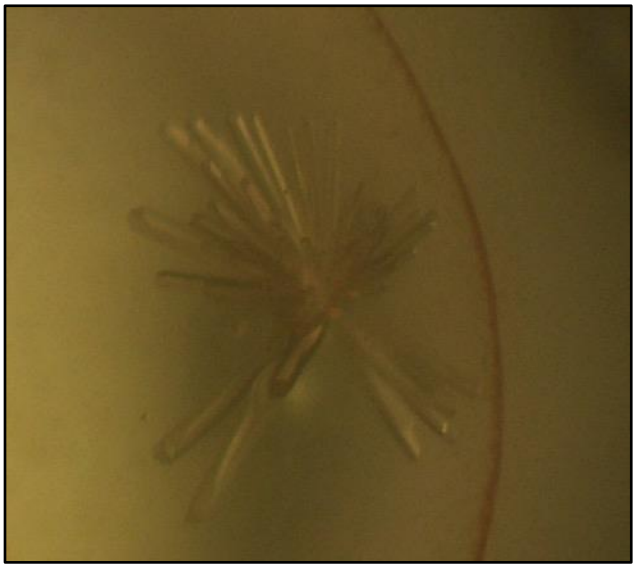

Figure 80. FtIspD crystals set 12/04/15. Conditions: 15 mg/mL FtIspD, 22°C, 3:3 drop ratio, sitting drop tray, 100mM Tris pH 8.8, 21% i-PrOH, 5mM WR016773-3

In order to speed up crystallization in the sitting drop trays, microseeding was conducted using crystals from the sitting drop trays. Crystals grown by microseeding grew within 1 week, but were very small and had unusual bunched morphology, rather than the long sharp needles previously observed in the sitting drop trays. These seeded crystals are shown in Figure 81.

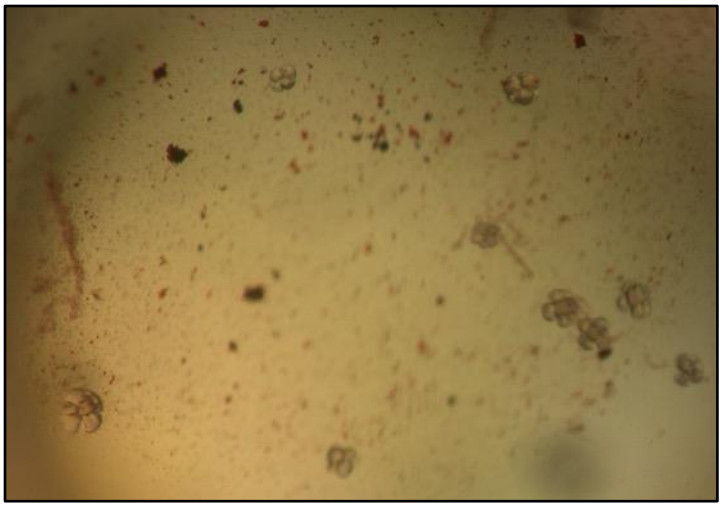

Figure 81. FtIspD crystals set 4/01/16. Conditions: 15 mg/mL FtIspD, 22C, 2:2 drop ratio, sitting drop tray, 100mM Tris pH 8.8, 20% i-PrOH, 5mM WR016773-3, seeded with 0.2 µL of a 1/500 seed solution

The effect of reservoir volume and drop ratio on the length of time for crystal formation was also investigated. The drop ratio was lowered to 1:1, and the reservoir volume of each well was set at 250 µL, 500 µL, and 1000 µL. No crystals were obtained in any of these conditions, indicating that a 1:1 drop ratio, regardless of reservoir volume, is not suitable for crystal formation. Because the iPrOH is volatile, the drop ratio could play a significant factor in how quickly the drop is concentrated. Changes to the protein concentration and temperature did not improve crystallization time; crystals still took months to form when set at 16°C and when set at 10 or 18 mg/mL FtIspD. Crystallization speed was finally improved to 1 week by lowering the pH to 7.0 in the sitting drop trays at 22°C. However, the crystals were still exceedingly thin, with the best crystal diffracting to 8.0 Å (8/12/16, 15 mg/mL FtIspD, 100 mM Tris pH 7.8, 23% i-PrOH, cryoprotectant = 25% ethylene glycol, 75% well solution). Based

on these optimizations, none of the sitting drop isopropanol tray variations were superior to the hanging drop trays set under the isopropanol conditions originally.

Future Directions

Given the reasonable diffraction and morphology of crystals grown under the isopropanol conditions in hanging drop trays, coupled with the maintenance of resolution upon soaking, these conditions should be further optimized. Other stabilization efforts, including setting trays at 22°C then transferring to 4°C should be considered. Current crystal conditions yield crystals diffracting to an average of 4 Å; improvements of about a half angstrom or so in these conditions may allow us to determine if the inhibitor is bound, and justify a synchrotron trip to obtain a high resolution structure.

CONCLUSIONS

Inhibition of IspC

Active Site Inhibition

Rationally-designed inhibitors of IspC, based on a fosmidomycin scaffolding, remain a promising area of IspC inhibition. A bi-substrate approach, with substitutions to either the N-hydroxy oxygen atom ("O-linked") or to the amide carbonyl group of the retrohydroxamate ("amide-linked") both proved to be valid strategies to designing IspC inhibitors. However, as a class, the O-linked compounds were more potent against both homologs of IspC tested, YpIspC and MtbIspC. This outcome was particularly surprising, given that the O-linked class of compounds lacked the hydroxyl group thought to be necessary for metal ion coordination via deprotonation. Our results indicate that coordination of the metal ion by the inhibitor is not necessary for potent inhibition. Indeed, the highest performing O-linked compound, compound **16j**, displayed a nanomolar IC_{50} and a competitive profile against both substrates NADPH and DXP with YpIspC[141]. This activity was mirrored with MtbIspC, giving a low micromolar IC_{50} and a competitive profile against both substrates[145]. In addition to potent *in vitro* inhibition of IspC, compound **16j** showed good growth inhibition of *Mycobacterium tuberculosis* cultures when functionalized with additional lipophilic tails (dipivaloyloxymethyl (POM) additions masking phosphonate charge) to improve

cellular penetration[145]. Several related O-linked compounds, when functionalized with POM groups, also showed excellent activity against *M. tuberculosis* cultures[145]. While there remains room for improvement in the antibacterial activity of these compounds against Gram negative species such as *E. coli* or *Y. pestis*, it is hypothesized that efflux prevents significant accumulation of compound inside the bacterial cells, leading to low potency. Indeed, knockout of a major efflux pump in *E. coli* increases the antimicrobial activity of these compounds, further supporting the efflux hypothesis[145]. Additionally, it is known that inhibitors fosmidomycin and FR900098 depend on the transporter GlpT for uptake[151]; it is possible that decreased potency of these inhibitors is due to the possibility that the inhibitors are no longer substrates for GlpT but are dependent on passive diffusion for entry into the cell.

Introducing unsaturation in the main carbon chain of FR900098 of these inhibitors was tolerated by the enzyme, with the α/β unsaturated, POM-functionalized analog of FR900098 (**26**[144]) showing improvement over the parent compound, POM-functionalized FR900098 (**29**[144]) in *Mycobacterium tuberculosis* whole cell assays. However, the POM-functionalized analog of **16j** (**20**[145]) had higher potency than both compounds **26** and **29** against *Mycobacterium tuberculosis* whole cells in GAST-Fe media. Three other POM-functionalized "O-linked" compounds (**17**, **18**, and **19**[145]) also showed lower MIC values than **26** or **29** in GAST-Fe media. For this reason, unsaturation in the main chain may be advantageous to increase antitubercular activity if introduced into some of the saturated O-linked compounds described in Paper V[145].

However, a head-to-head comparison shows unsaturation to be inferior to O-linkages in improving the antitubercular activity of POM-functionalized FR900098.

When considering non-bisubstrate analogs, such as the β-substituted compound series[128], it was noted that none of the synthesized compounds showed any significant activity against whole cell *M.smegmatis*, a surrogate for *M. tuberculosis*, and their activity *in vitro* against MtbIspC was generally poor. It is worth noting that none of these compounds were POM-functionalized, indicating that the low activity in whole cell assays may be largely due to a lack of cellular penetration However, the *in vitro* enzyme assays alone indicate that at least with respect to MtbIspC, the most potent bi-substrate compounds[145] are more active that the most potent β-substituted compounds[128]. What is particularly notable is the potency of these β-substituted compounds against *P. falciparum* cultures and PfIspC in comparison to their relative lack of activity against *M. smegmatis* and MtbIspC. Two compounds, **8c** and **8d**, had nanomolar IC_{50} values against not only the PfIspC enzyme itself, but also against *P.falciparum* K1 cultures, improving on the reported IC_{50} of both FR900098 and fosmidomycin[128]. Crystal structures of **8c** and **8d** with PfIspC indicate that the β-substitutions interfere with the flap-region of IspC, preventing it from closing properly over the active site in the catalytic conformation. The aryl moieties of the β-substituent in **8c** and **8d** actually displace the flap region tryptophan residue[145], indicating that potency could be partially conferred by the β-substitution taking advantage of an aryl hotspot that normally stabilizes the tryptophan in the closed flap confirmation. It is

currently not clear what differences in the flap region or active site of MtbIspC prohibit this binding mode of **8c** and **8d** that is favored in PfIspC.

Due to the stark differences in activity between the PfIspC enzyme and the bacterial IspC homologs with the β-substituted compounds[128], it would be informative to examine some of the bisubstrate compounds[145] with PfIspC. Further understanding of differences between the plasmodial and bacterial IspC homologs would allow more precise tailoring of compounds to target one homolog of IspC over others. What is evident is that even for homologous proteins, there remain subtle structural differences that allow for vastly different responses to series of compounds tested; what remains elusive is a series of compounds with higher potency against MtbIspC than against other IspC homologs. Continued investigation into the SAR of these compound classes, with a priority on screening a larger panel of IspC homologs to identify differences in activity between species, may yet reveal structural elements that favor MtbIspC over others.

Allosteric Inhibition

In order to regulate flux through a biological pathway, many organisms employ feedback inhibition mechanisms, in which a downstream product of the metabolic pathway will selectively inhibit an earlier step, allowing for overabundance of pathway metabolites to limit further production. Given the lack of information about MEP pathway regulation, it is unknown if any of the enzymes in the pathway might be regulated in this way, or which downstream metabolites could be effecting pathway flux. Given the lipophilic nature of the metabolite products of this pathway, it is

possible that a binding site for a downstream MEP pathway metabolite could be targeted by compounds with favorable drug-like properties. Identifying an allosteric site of regulation could open the doors to a broader subset of chemical scaffoldings that could be pursued as MEP pathway inhibitors. For IspC in particular, the fosmidomycin scaffolding has proven useful in the design of potent enzyme inhibitors, but compounds based on this scaffolding have not yet made it to the clinic.

The possibility of allosteric regulation of IspC has been raised throughout many of the experiments discussed here, but has yet to be fully realized. Early compounds postulated to be allosteric inhibitors, such as quercetin or sanguinarine, appear to be aggregating compounds. There does remain the possibility that suramin may be allosterically modulating the activity of IspC. It certainly does not appear to be acting as an aggregator, as its activity was not only unaffected by detergent but was also insensitive to changes in enzyme concentration. However, suramin's plethora of reported additional targets beyond those in the parasites it is prescribed to treat, as well as its high concentration of protein binding in serum suggest that suramin has an affinity for a large number of proteins. While the interaction with IspC may be specific, suramin is unlikely to be selective *in vivo*. Suramin's lack of selectivity coupled with the lack of antibacterial activity indicates that suramin may be a very challenging lead. However, further investigation into the binding site on IspC may yield a site that proves more amenable to targeting with other compounds. It remains to be seen if the elusive proposed IspC allosteric site can be authenticated.

Inhibition of IspD

Substrate Analogs

Given the known polarity of the IspD active site[134], it is perhaps unsurprising that there is little reported research into designing substrate analogs specifically for the IspD active site. However, our research did reveal 6-hydroxy-DL-DOPA as a competitive inhibitor with respect to CTP. While alone, a CTP-competitive compound may run the risk of cytotoxicity, using 6-hydroxy-DL-DOPA as a scaffold could allow further specificity to be conferred through additional chemical substituents. In a manner similar to the bi-substrate approach taken with IspC inhibition[141, 145], CTP could be functionalized with a group that could occupy the MEP binding site, allowing for further specificity. That specificity would likely come at a cost, however; MEP is hydrophilic, and any substituents binding in that site may decrease the overall drug-like qualities of the inhibitor. While inhibition by a bisubstrate approach is intriguing, it may be more promising to pursue the WRAIR compounds identified in Specific Aim 1, part 2, which were designed to be bisubstrate inhibitors yet retain a more lipophilic structure.

WRAIR Compounds

The rationally designed inhibitors of IspD from Walter Reed discussed here represent the most promising future direction in terms of IspD inhibition. Even a potent IspD inhibitor binding only in the CTP or MEP pocket will likely be very hydrophilic, conferring poor pharmacokinetic properties as in the case of fosmidomycin. The more drug-like lipophilic compounds identified with FtIspD would likely have better

pharmacokinetic profiles. Compounds NSC 110039 and WR016773-3 both have low micromolar IC_{50} values and antimicrobial activity. Compounds NSC 110039 and NSC 401145 were both hypothesized to bind to an either an allosteric site in close proximity to the active site, as observed for other lipophilic compounds with AtIspD[135], or directly in the active site itself, in neither the CTP not MEP pocket exclusively, but a pocket branching into both sites. Additional rational design of these compounds to increase potency and antibacterial activity is desired.

High-Throughput Library Screening

In order to expand the number of compounds screened against IspC and IspD, and to diversify the chemical space of the compounds screened, a high-throughput screen for both IspC and IspD with appropriate control assays was developed. This HTS platform was used to screen the LOPAC[1280] library, revealing a host of false positive compounds that were flagged as aggregators in follow-on control assays. Additionally, an in-house natural product library was also screened, yielding an extract with high potency against IspC and IspD. The active component of the extract with respect to both compounds was determined to be quercetin, a natural flavonoid with known aggregation properties. While it was anticipated that the chemical diversity of the library compounds could afford enough structural coverage for at least one compound with respect to either IspC or IspD that might serve as a lead molecule for further development, very few compounds were actually identified. Those compounds that may function as specific inhibitors of IspC or IspD certainly had challenges associated with their continued development. The high number of aggregators in the

LOPAC[1280] library itself should cause question in the suitability of this library for *in vitro* enzyme screening. The criteria for inclusion in the library, known pharmacological activity, could predispose compounds that naturally interact with many proteins, yielding diverse biological effects and thus high bioactivity. For example, quercetin was included in the LOPAC[1280], despite known aggregating properties and poor bioavailability. This inclusion was ostensibly due to the incredibly large number diverse biological activities it is reported to have[181]. However, the diversity of reported effects itself should raise attention. A multitude of biological effects does not necessarily preclude a compound from clinical use; aspirin for example is a very important clinical compound with a host of reported non-anti-inflammatory activities, including antifungal and antibacterial activities[182] as well as protective effects with respect to cancer[183]. However, it should be a concern if a compound is noted to have a wide variety of unrelated biological effects *in vitro* while also being known to have a low bioavailability, indicating the potential for effects that are irrelevant on a clinical scale. In the future, care should be taken to examine the proposed library, the types of compounds it includes, and its suitability for *in vitro* enzyme screening.

Challenges and Changes

Based on the results of the experimentation in Specific Aims 1 through 4, there are still challenges to be surmounted in ongoing research, as well as changes to experimentation that could be implemented to reduce problems encountered in future research. For investigation into the IspC bisubstrate inhibitors (Specific Aim 1, Part 1), improvements in potency of the tested compounds will require changes to the SOP used

to evaluate them. As described here, compounds with appreciable activity in a 100 μM screen are evaluated for their IC_{50}, and if sufficiently potent, evaluated for mechanism of enzyme inhibition. As the IC_{50} of many of these compounds approach the nanomolar range, further assays to elucidate tight-binding effects will be required, most specifically IC_{50} variation as a function of enzyme concentration. If the IC_{50} is dependent on the quantity of IspC, tight binding can be inferred. There are alterative methods for determination of mechanism of inhibition of tight binding compounds, and they will have to be used for the more potent compounds anticipated in the future. Additionally, care will have to be given to the issue of preincubation of compounds in these series. While it was shown that preincubation improves the potency of the bi-substrate inhibitors[141], compounds that bind after NADPH may not benefit from such preincubation. The β-substituted compounds are thought to belong to this category. Going forward, preincubation may need to be tested individually by class to determine the most appropriate method for conducting IspC assays.

With regards to the WRAIR inhibitors developed for IspD (Specific Aim 1, Part 2 and Specific Aim 4), perhaps the most significant unanswered question is the precise location of the inhibitor binding site. Crystallization experiments conducted herein have not revealed the location of this pocket. With continued exploration of crystallization conditions, it is anticipated that a high resolution co-crystal structure of IspD with one of the lead lipophilic inhibitors will be resolved. Additionally, crystallographic identification of this site may also prove valuable to increasing our knowledge on MEP pathway regulation (via allosteric control of enzyme activity). IspC and IspD assays

performed in the presence of 100 μM IPP, DMAPP, or GPP did not show a reduction of activity for either enzyme, suggesting that feedback inhibition of the MEP pathway does not occur with accumulation of these metabolites. The precise location and topology of an allosteric site on either of these enzymes remains intriguing unanswered questions.

With regards to the LOPAC^{1280} library screen (Specific Aim 2), there are several changes to the HTS protocol itself that may reduce the amount of time spent correcting for false positives in future HTS applications (with IspC or IspD). First, a modification the primary screen might eliminate false positive aggregators. While the primary screen was conducted at 100 μM, and cut-off for inhibition was set at 25% residual enzyme activity, a lower concentration of inhibitor but higher cut-off may alleviate some of the aggregation effects observed. As aggregation is a highly concentration-dependent phenomena, as evidenced by the steep IC_{50} dose-response plots, lowering the concentration of inhibitor drastically reduces the inferred potency as compared to a noncovalently bound reversible inhibitor. While a reversible and an aggregating inhibitor may each have similar residual activities at 100 μM, many aggregator's steep dose response will lead to lower than anticipated potencies at lower concentrations. As seen in Figure 47, a screen with a cut-off value at 50% residual activity with 10 μM compound would have retained only rottlerin as an inhibitor with respect to IspC, and only quercetin as an inhibitor with respect to IspD. This lower concentration, higher cut-off may afford some protection against false-positive aggregators. One argument for the higher concentration, lower cut-off value paradigm

taken in this study is that it increases the dynamic range between an uninhibited sample and a positive hit. However, using a sufficiently active enzyme in the primary screen, such as YpIspC and FtIspD, should allow significant resolution to separate hit compounds. Given the availability of high activity homologs for both IspC and IspD (YpIspC, EcIspC, FtIspD, and EcIspD all have maximum velocities over 10,000 μM/min/mg), the 50% cut-off for residual enzyme activity is a feasible end point for the primary assay.

In addition, a second improvement to the HTS protocol is to include detergent in the assays earlier on, at least during the secondary screen (but preferably during the primary screen, cost permitting). This simple addition will reduce the number of aggregating inhibitor hits obtained in the HTS campaign.

Finally, antibacterial activity was used herein as an assessment for selecting and identifying top hit compounds. However, by adjusting the primary screen endpoints and including detergent earlier in the SOP, as discussed above, it may be advantageous to pursue an enzyme inhibitor hit, independent of the magnitude of its antibacterial activity. Given that antibacterial activity is heavily dependent on cellular penetration, resistance to modification, and lack of efflux from the cell, an antibacterial screen may not be the best way to distinguish the most promising compounds. As evidenced by the LOPAC^{1280} screen, where the only specific hits for IspC and IspD were those without significant antimicrobial activity, the antimicrobial activity of a compound should not be a prioritizing factor in selecting compounds to pursue further

.

Significance

The threat of antibiotic resistance is certainly one of the more worrying health crisis of our time, and deserves significant attention. Drug discovery must be complemented by more judicious antibiotic use and better diagnostic tools to identify resistances in patients. However, the fact that this resistance is often times naturally occurring underscores the idea that the fight against resistance will be an ongoing drug discovery battle. As discussed in this dissertation, there remain promising angles for MEP pathway inhibition to continue to be explored in the hopes of developing new compounds for the clinic. Despite noted challenges, the MEP pathway is an attractive target for further antibiotic study, and despite recent attention, still holds many underexplored yet promising areas for scientists to investigate.

MATERIALS AND METHODS

Specific Aim 1, Part 2 — Rational Compound Screen with IspD

Rational Compound Screen with IspD

Enzyme Assays

IspD activity was monitored colorimetrically by quantifying production of inorganic phosphate using pyrophosphatase and malachite green dye as described previously[149]. Enzymatic activity was monitored using 250 µL assay solutions containing 100 mM Tris pH 8.2, 1 mM $MgCl_2$, 1 mM DTT, 200 µM CTP, 100 mU/mL pyrophosphatase, 1.8 µM FtIspD, and 100 µM of inhibitor. Assay solutions were incubated at 37ºC for 10 minutes to allow CTP and the inhibitor to associate with the enzyme. The addition of 200 µM MEP was used to initiate the reaction. Every 30 seconds, 40 µL aliquots were removed from the assay mixture and combined with 40 µL of the acidic malachite green assay solution and 120 µL water. The A_{660} of each solution was measured on an Agilent 8453 spectrophotometer equipped with a multi-cuvette holder. Where appropriate, half maximal inhibitory activity (IC_{50}) was determined by assaying FtIspD in the presence of varying concentrations of inhibitor, ranging from 1 nM to 100 µM, then plotting fractional enzyme activity as a function of inhibitor concentration. GraphPad Prism (La Jolla, CA) was used for nonlinear curve fitting the assay results to a sigmoidal dose response curve. Mechanism of action plots

were generated by varying either MEP at fixed CTP concentration (200 μM), or by varying CTP at fixed MEP concentration (200 μM).

Antibacterial Assays

The following reagents were obtained through the NIH Biodefense and Emerging Infections Research Resources Repository, NIAID, NIH: *Yersinia pestis* subsp. A1122 and *Francisella tularensis* subsp. *novicida* strain Utah 112. Both species were cultured at 37°C in Tryptic Soy Broth with 0.1% cysteine (TSB-C) and constantly shaken at 250 rpm. For dose response curves generated with NSC 401145 and NSC 110039, *Francisella tularensis* subsp. *novicida* strain Utah 112 was grown in Chamberlin's Modified Minimal Media[81]. 1.5% wt/vol agar was added to prepare solid media. An overnight culture of *Y. pestis* subsp. A1122 or *F. tularensis* subsp. novicida was diluted to OD_{600} of 0.2. Aliquots of the culture (40 μL) were then dispensed into foam-capped 1.5 mL microcentrifuge tubes containing 360 μL of fresh TSB and the appropriate concentration of inhibitor. Bacterial growth was monitored until $OD_{600} >$ 1.5 for uninhibited samples; approximately 22 hours for *Y. pestis* and 7 hours for *F. tularensis*. Each condition was evaluated in duplicate. Nonlinear regression fitting the resulting dose-response plot was achieved using GraphPad Prism version 4.00 for Windows (GraphPad software Inc, San Diego, CA) and the equation $F = 1/(1+[I]/IC_{50})$ where F = fractional growth and [I] = inhibitor concentration.

Specific Aims 2 and 3

Expression and Purification of Enzymes

Recombinant Y. pestis IspC (YpIspC), M. tuberculosis IspC (MtbIspC), F. tularensis IspD (FtIspD), and E.coli IspD (EcIspD) were expressed and purified essentially as described in detail previously[141], [148]. In general, a 10 mL overnight culture of E.coli BL21 Codon Plus (DE3)-RIL containing the protein-encoding plasmid was used to inoculate 1 L of Luria-Bertani media in a 2800 mL Fernbach shake flask. Protein expression was induced with 0.5 mM isopropyl β-D-thiogalactopyranoside (IPTG) upon shake flask cultures reaching an OD_{600} of 1.2. Cells were harvested 18 hours later by centrifugation at 4°C and 5000 rpm and stored at -80°C. Cell pellets were thawed and lysed with Lysis Buffer A, containing 100 mM Tris pH 8, 0.032% lysozyme at 3 mL per g cell pellet, then Lysis Buffer B, containing 0.1 M $MgCl_2$, 0.1 M $CaCl_2$, 0.020% DNase at 0.3 mL per g cell pellet. Total concentration of NaCl was brought to 0.1 M and clarified cell lysate was obtained by centrifugation (48,000 x g, 20 min, 4°C). His-tagged proteins were purified on a TALON metal affinity chromatography column (Clontech Laboratories, Mountain View, CA) by washing with 20 column volumes of 1X equilibrium buffer (50 mM HEPES pH 7.5, 300 mM NaCl), 10 column volumes of 1X wash buffer (50 mM HEPES pH 7.5, 300 mM NaCl, 10 mM imidazole), and 15 column volumes of 2X wash buffer (100 mM HEPES pH 7.5, 600 mM NaCl, 20 mM imidazole). The protein was then eluted with 5 column volumes of 1X elution buffer (150 mM imidazole pH 7.0, 300 mM NaCl). Buffer was exchanged with 0.1 M Tris pH 7.8, 1 mM NaCl, 5 mM DTT during concentration by

ultrafiltration. Protein concentration was determined using Advanced Protein Assay Reagent (Cytoskeleton, Denver CO) with γ-globulins (Sigma-Aldrich) as the standard. Purified protein was visualized via Coomassie-stained SDS-PAGE.

IspC Enzyme Assays

IspC activity was assayed by spectrophotometrically monitoring the enzyme-catalyzed oxidation of NADPH, as described previously[184] The screening of a commercially available chemical library was conducted in three stages with the Library of Pharmacologically Active Compounds (LOPAC^{1280}) purchased from Sigma-Aldrich [185]. The primary screen of the LOPAC^{1280} library consisted of 96-well plate based assays, with 0.5 µL of DMSO (for the uninhibited control) or the appropriate inhibitor (dissolved in DMSO) first added directly to the plate, to give a final inhibitor concentration of 100 µM in a total assay volume of 50 µL. Subsequently, 45 µL of assay master mix, containing 100 mM Tris pH 7.8, 25 mM $MgCl_2$, 150 µM NADPH, and 0.89 µM YpIspC was added to each well and the plate was allowed to incubate at room temperature for 10 minutes to facilitate inhibitor binding. The reaction was initiated with the addition of the K_m value of DXP (225 µM[141]), and was subsequently quenched after 1 minute with the addition of EDTA to a final concentration of 100 mM. Decrease in A_{340} as compared to wells without DXP was measured using a Beckman Coulter DTX800 plate reader.

The secondary screen consisted of cuvette-based assays with MtbIspC. Enzymatic activity was monitored using 120 µL assay solutions containing 100 mM Tris pH 7.8, 25 mM $MgCl_2$, 150 µM NADPH, 0.89 µM MtbIspC, and 100 µM

inhibitor. Assay solutions were incubated at 37ºC for 10 minutes to allow NADPH and the inhibitor to associate with the enzyme. Addition of the K_m value of DXP (47 µM[186]) was then used to initiate the reaction. The enzymatic consumption of NADPH was continuously monitored (A_{340}) using an Agilent 8453 spectrophotometer equipped with a multi-cuvette holder.

The tertiary screen consisted of a YpIspC-FtIspD coupled assay, where the 96-well plate assay used for the primary screen was adapted to assay IspD activity, as detailed elsewhere[149]. The assay master mix of the primary screen was modified to additionally contain 1.8 µM FtIspD, 200 µM CTP, and 100 mU/mL pyrophosphatase. The assay was quenched after 1 minute by the addition of 40 µL of an acidic malachite green assay solution (2.4 M sulfuric acid containing 1.5% ammonium molybdate, 1.6% Tween 20, and 9.5% malachite green) and 120 µL water. Sodium citrate was added to 3.4% after 10 minutes, and an increase in A_{660} as compared to wells without DXP was read using a Beckman Coulter DTX800 plate reader.

To screen the inhibitory activity of the natural product extracts, the YpIspC activity was monitored using 120 µL assay solutions containing 100 mM Tris pH 7.8, 25 mM $MgCl_2$, 150 µM NADPH, 0.89 µM YpIspC, and 50 µg/mL natural product extract. Assay solutions were incubated at 37ºC for 10 minutes to allow NADPH and the inhibitor to associate with the enzyme. Addition of 225 µM DXP was used to initiate the reaction. The enzymatic consumption of NADPH was then continuously monitored (A_{340}) using an Agilent 8453 spectrophotometer equipped with a multi-cuvette holder.

Where appropriate, half maximal inhibitory activity (IC_{50}) was determined by assaying YpIspC in the presence of varying concentrations of inhibitor, ranging from 1 nM to 100 µM, then plotting fractional enzyme activity as a function of inhibitor concentration. GraphPad Prism (La Jolla, CA) was used for nonlinear curve fitting the assay results to a sigmoidal dose response curve.

Lineweaver Burk plots were used to determine the mechanism of enzyme inhibition. Accordingly, 120 µL assay solutions contained 100mM Tris pH 7.8, 25 mM $MgCl_2$, 0.89 µM YpIspC, and variable concentrations of an inhibitor. Each assay solution was incubated for 10 min at 37°C to facilitate inhibitor binding. NADPH was subsequently added, at 150 µM for DXP-dependent plots, and at variable concentrations for the NADPH-dependent plots (ranging from 20 to 100 µM), and the assays were incubated an additional 10 minutes to allow NADPH binding. Enzymatic reactions were then initiated with addition of 225 µM DXP for NADPH dependent plots, and at variable concentrations (from 50 to 300 µM) for the DXP-dependent plots. Lineweaver-Burk plots were fit by linear regression using GraphPad Prism.

IspD Enzyme Assays

IspD activity was monitored colorimetrically by quantifying production of inorganic phosphate using pyrophosphatase and malachite green dye as described previously[149]. The screening of a commercially available chemical library was conducted in three stages with the Library of Pharmacologically Active Compounds (LOPAC^{1280}) purchased from Sigma-Aldrich[185]. The primary screen of the LOPAC^{1280} library consisted of 96-well plate based assays, with 0.5 µL of DMSO (for the

uninhibited control) or the appropriate inhibitor (dissolved in DMSO) first added directly to the plate, to give a final inhibitor concentration of 100 µM in a total assay volume of 50 µL. Subsequently, 45 µL of assay master mix, containing 100 mM Tris pH 8.2, 1 mM $MgCl_2$, 1mM DTT, 200 µM CTP, 100 mU/mL pyrophosphatase, and 1.8 µM FtIspD was added to each well and the plate was allowed to incubate at room temperature for 10 minutes to facilitate inhibitor binding. The assay was initiated with the addition of 200 µM MEP. The assay was quenched after 1 minute by the addition of 40 µL of an acidic malachite green assay solution (2.4 M sulfuric acid containing 1.5% ammonium molybdate, 1.6% Tween 20, and 9.5% malachite green) and 120 µL water. Sodium citrate was added to 3.4% after 10 minutes, and an increase in A_{660} as compared to wells without DXP was read using a Beckman Coulter DTX800 plate reader.

The secondary screen consisted of cuvette-based assays with EcIspD. Enzymatic activity was monitored using 250 µL assay solutions containing 100 mM Tris pH 8.2, 1 mM $MgCl_2$, 1mM DTT, 200 µM CTP, 100 mU/mL pyrophosphatase, 1.8 µM EcIspC, and 100 µM inhibitor. Assay solutions were incubated at 37^{o}C for 10 minutes to allow CTP and the inhibitor to associate with the enzyme. The addition of 200 µM MEP was used to initiate the reaction. Every 30 seconds, 40 µL aliquots were removed from the assay mixture and combined with 40 µL of the acidic malachite green assay solution and 120 µL water. The A_{660} of each solution was measured on an Agilent 8453 spectrophotometer equipped with a multi-cuvette holder.

The tertiary screen consisted of a pyrophosphatase assay. Enzymatic activity was monitored using 250 uL assay solutions containing 100mM Tris pH8.2, 1mM $MgCl_2$, 1mM DTT, 100mU/mL pyrophosphatase, and 100µM inhibitor. Assay solutions were incubated for 10 minutes to allow the inhibitor to bind, then enzymatic activity was initiated with the addition of 20 µM pyrophosphate. Every 30 seconds, 40 µL aliquots were removed from the assay mixture and combined with 40 µL of the acidic malachite green assay solution and 120 µL water. The A_{660} of each solution was measured on an Agilent 8453 spectrophotometer.

To screen the inhibitory activity of the natural product extracts, FtIspD activity was monitored using 250 µL assay solutions containing 100 mM Tris pH 8.2, 1 mM $MgCl_2$, 1mM DTT, 200 µM CTP, 100mU/mL pyrophosphatase, 1.8 µM FtIspD, and 50 µg/mL natural product extract. Assays were conducted as described above in the secondary IspD screen for the LOPAC library.

Where appropriate, half maximal inhibitory activity (IC_{50}) was determined by assaying FtIspD in the presence of varying concentrations of inhibitor, ranging from 1 nM to 100 µM, then plotting fractional enzyme activity as a function of inhibitor concentration. GraphPad Prism (La Jolla, CA) was used for nonlinear curve fitting the assay results to a sigmoidal dose response curve.

Preparation of Natural Product Extracts

A natural product extract library was curated in house using specimens of plants and fungi indigenous to the northern Virginia area. One gram of each specimen was frozen with liquid nitrogen, ground with a mortar and pestle, and mixed with 15 mL of

ethyl acetate. The mixture was vacuum-filtered using a Büchner funnel and subsequently collected and transferred into a round bottom flask. The flask was placed on a rotovaporator with a 44°C water bath to remove the solvent. Samples were then resuspended to 1.0 mL in ethyl acetate, transfered into a tared 1.5 mL microcentrifuge tube, then evaporated to dryness in a SpeedVac. Each residue was weighed and stored at 4°C. Working solutions were prepared by resuspending the dry extracts in DMSO to a concentration of 10 mg/mL.

Selective Binding and Isolation of the Active Inhibitor from the Natural Product Extract

IspC solutions (1.5 mL) were prepared with 50 mM Tris pH 7.8, 25 mM $MgCl_2$, 150 µM NADPH, 1.8 µM YpIspC, and 3.3% wt/vol of either DMSO (negative control) or the natural product extract (e29). Samples were incubated at 37°C for 15 min, then transferred to a centrifugal filter concentrator with 30 kDa cutoff (Amicon Millipore). Additional wash buffer (500 µL) was added to each sample (50 mM Tris-HCL pH.7.8, 25 mM MgCl) before centrifugation at 35°C and 4000 x g to a final sample volume of 200 µL. The sample retentate was removed and combined with 200 µL of wash buffer in a microcentrifuge tube. The microfuge tube was placed at 65°C for 20 minutes to denature the protein (and release of the active inhibitor from the enzyme), then the denatured sample was transferred to a 10 kDa concentrator and centrifuged at 30°C, 4000 x g, for 1 hr. The filtrate containing the inhibitor was retained at -80ºC for LC-QToF analysis.

IspD solutions (1.5 mL) were prepared with 100 mM Tris pH 8.2, 1 mM $MgCl_2$, 200 µM CTP, 1.8 µM FtIspD, 1 mM DTT and 3.3% wt/vol of either DMSO (negative

control) or the natural product extract (e29). The inhibitor was extracted essentially as above, using a wash buffer of 100 mM Tris pH 8.2, 1 mM $MgCl_2$, 1 mM DTT.

LC-QToF Analysis

Filtrate samples containing the active inhibitor were removed from the -80ºC freezer, diluted 1:1 with LC-MS Grade acetonitrile (Fisher Scientific), filtered using a Supelco (54145-U) Iso-disc, N-4-2 nylon, 4 mm x 0.2 µm filter (Sigma-Aldrich), and transferred to high recovery amber vials (Agilent Technologies, Inc., Santa Clara, CA). Reverse-phase liquid chromatography was performed on the purified analyte using an Agilent 1290 Infinity Ultra High-Performance Liquid Chromatography system (UHPLC) coupled with an Agilent 6530 Quadrupole Time of Flight (QToF) detector. Mobile phase was delivered by a binary pump at a flow rate of 0.4 mL/min. Solvent A was composed of LCMS Grade water + 0.1% v/v formic acid (Proteochem, Loves Park, IL) and solvent B was composed of LCMS Grade acetonitrile + 0.1% v/v formic acid (Proteochem). The chromatography gradient used is as follows: 0-1 min, 5% solvent B; 10 min, 30% B; 15 min, 70% B; 22 min, 90% B; 24-25 min, 100% B; 27 min, 2% B; 30 min, 5% B. The autosampler was set with an injection volume of 5 µL. Flush port was set to clean the injection needle for 30 s intervals. A ZORBAX Rapid Resolution High-throughput (RRHT), 2.1 x 50 mm, 1.8 µm C18 column (Agilent Technologies, Inc.) was used for the chromatography. The column was maintained at an isothermal temperature of 38ºC. The QToF was equipped with an electrospray ionization (ESI) source, and was set for detection of ions within a mass-to-charge ratio (m/z) ranging from 100 to 1000. A dedicated isocratic pump continuously infused reference standards

of purine (Agilent Technologies, Inc.) and hexakis-H, 1H, 3H-tetrafluoropropoxy-phosphazine, or HP-921 (Agilent Technologies, Inc.) at flow rate of 0.5 mL/min to achieve accurate mass correction. The nebulizer pressure was set at 35 psig with a surrounding sheath gas temperature of 350^{o}C and gas flow rate of 11 L/min. Drying gas temperature was set at 300^{o}C with a flow rate of 10 L/min. Default settings were used to set voltage gradient for nozzle at 1000 V, skimmer at 65 V, capillary (VCap) at 3500 V, and fragmentor at 175 V. Each cycle of acquisition was performed at a constant collision energy that varied between 0 V, 10 V, 20 V, and 40 V for subsequent tandem MS analysis. Agilent MassHunter Acquisition SW Version, 6200 series TOF/6500 series Q-TOF B.05.01 (B5125.1) was used to record LCMS data. Agilent MassHunter Qualitative Analysis B.06.00 was used to analyze data and to generate the total ion chromatogram (TIC), extracted compound chromatogram (ECC) and mass spectra for analyte compounds. Tandem mass spectra were processed using the Find Compound by MS/MS function to envelope product ions and related features (adducts, isotopes, and fragment ions that elute at the same retention time). Mass spectra of analytes were processed using the Find Compound by Options function set to consider factors including sodium (Na^+) and hydrogen (H^+) adducts and neutral loses of water (H_2O) while utilizing METLIN Metabolite Personal Compound Database add-in for Agilent MassHunter Qualitative Analysis B.06.00. The initial step in the identification of metabolites relied on the METLIN Metabolite PCD match-scoring criteria filters that evaluated m/z, potential adducts, potential neutral loses, accurate mass and isotope effect to calculate and propose chemical formula matches for precursor ions[187]. Follow-

on manual comparative analysis of raw tandem MS data was performed with online MS/MS spectra library references.

Antibacterial Assays

The following reagents were obtained through the NIH Biodefense and Emerging Infections Research Resources Repository, NIAID, NIH: Yersinia pestis subsp. A1122 and Francisella tularensis subsp. novicida strain Utah 112. Both species were cultured at 37°C in Tryptic Soy Broth with 0.1% cysteine (TSB-C) and constantly shaken at 250 rpm. Agar (1.5% wt/vol) was added to prepare solid media. For whole cell assays, dose-response plot of cell growth (OD_{600}) was measured as a function of inhibitor concentration. An overnight culture of *Y. pestis* subsp. A1122 or *F. tularensis* subsp. *novicida* was grown in TSB-C and diluted to OD_{600} of 0.2. Aliquots of the culture (40µL) were then dispensed into foam-capped 1.5 mL microcentrifuge tubes containing 360 µL of fresh TSB and the appropriate concentration of inhibitor. Bacterial growth was monitored until $OD_{600} > 1.5$ for uninhibited samples; approximately 22 hours for Y. pestis and 7 hours for F. tularensis. Each condition was evaluated in duplicate. Nonlinear regression fitting the resulting dose-response plot was achieved using GraphPad Prism version 4.00 for Windows (GraphPad software Inc, San Diego, CA) and the equation $F = 1/(1+[I]/IC_{50})$ where F = fractional growth and [I] = inhibitor concentration.

Specific Aim 4

Preparation of Enzyme Solutions

Recombinant Y. pestis IspC (YpIspC), and F. tularensis IspD (FtIspD), and were expressed and purified essentially as described in detail previously[141, 148]. In general, a 10 mL overnight culture of E.coli BL21 Codon Plus (DE3)-RIL containing the protein-encoding plasmid was used to inoculate 1 L of Luria-Bertani media in a 2800 mL Fernbach shake flask. Protein expression was induced with 0.5 mM isopropyl B-D-thiogalactopyranoside (IPTG) upon shake flask cultures reaching an OD_{600} of 1.2. Cells were harvested 18 hours later by centrifugation at 4°C and 5000 rpm and stored at -80°C. Cell pellets were thawed and lysed with Lysis Buffer A, containing 100 mM Tris pH 8, 0.032% lysozyme at 3 mL per g cell pellet, then Lysis Buffer B, containing 0.1 M $MgCl_2$, 0.1 M $CaCl_2$, 0.020% DNase at 0.3 mL per g cell pellet. Total concentration of NaCl was brought to 0.1 M and clarified cell lysate was obtained by centrifugation (48,000 x g, 20 min, 4°C). His-tagged proteins were purified on a TALON metal affinity chromatography column (Clontech Laboratories, Mountain View, CA) by washing with 20 column volumes of 1X equilibrium buffer (50 mM HEPES pH 7.5, 300 mM NaCl), 10 column volumes of 1X wash buffer (50 mM HEPES pH 7.5, 300 mM NaCl, 10 mM imidazole), and 15 column volumes of 2X wash buffer (100 mM HEPES pH 7.5, 600 mM NaCl, 20 mM imidazole). The protein was then eluted with 5 column volumes of 1X elution buffer (150 mM imidazole pH 7.0, 300 mM NaCl). Buffer was exchanged with 0.1 M Tris pH 7.8, 1 mM NaCl, during concentration by ultrafiltration. No DTT was added to the buffer. Protein concentration

was determined using A_{280}, with an extinction coefficient of 36900 M^{-1} cm^{-1} and a molecular weight of 25909.5 Da for FtIspD and an extinction coefficient of 22900 M^{-1} cm^{-1} and a molecular weight of 43100 Da for YpIspC. Extinction coefficients were calculated using the ExPasy ProtParam calculation tool[188].

Preparation of Crystallization Trays

All aqueous crystallization stock solutions were filter sterilized using a 0.2 µm filter prior to use. Unless otherwise noted, reservoir volumes for each well in sitting drop and hanging drop trays were 500 µL. Hanging drop trays with screw-on lids were purchased from Qiagen (EasyXtal 15-Well Tool). Sitting drop trays were purchased from Hampton Research (CrysChem Plate, 24 Well) and sealed with tape.

Crystal Screening

All crystals were screened manually in house on a Bruker Microstar X-ray Generator (copper anode, $\lambda = 1.5418$) with a Platinum 135 CCD Detector. Soaked crystals were allowed to sit in inhibitor solution for 2 hours prior to screening. Crystals were looped directly from the drop and submerged into cryoprotectant solution if required, then plunged into a liquid nitrogen stream for snap freezing.

APPENDIX 1 – PUBLISHED WORK

Specific Aim 1, Part 1 — Rational Compound Screen with IspC

Paper I: Design of Potential Bisubstrate Inhibitors against Mycobacterium tuberculosis (Mtb) 1-Deoxy-D-Xylulose 5-Phosphate Reductoisomerase (Dxr)- Evidence of a Novel Binding Mode

San Jose G, Jackson ER, Uh E, Johny C, Haymond A, Lundberg L, et al. *MedChemComm.* 2013;4: 1099–1104. doi:10.1039/C3MD00085K

Attributions and Contributions

Reproduced with permission from the Royal Society of Chemistry. All supplementary information as referenced in the text can be found in Appendix 2. The author was responsible for the generation of the data in Table 1 and Figure 4.

MedChemComm

RSC Publishing

CONCISE ARTICLE

View Article Online
View Journal | View Issue

Published on 29 May 2013. Downloaded by George Mason University on 12/11/2013 02:15:22.

Cite this: *Med. Chem. Commun.*, 2013, **4**, 1099

Design of potential bisubstrate inhibitors against *Mycobacterium tuberculosis* (Mtb) 1-deoxy-D-xylulose 5-phosphate reductoisomerase (Dxr)—evidence of a novel binding mode†

Géraldine San Jose,[a] Emily R. Jackson,[a] Eugene Uh,[a] Chinchu Johny,[bc] Amanda Haymond,[bc] Lindsay Lundberg,[c] Chelsea Pinkham,[c] Kylene Kehn-Hall,[c] Helena I. Boshoff,[d] Robin D. Couch[bc] and Cynthia S. Dowd*[a]

Received 14th March 2013
Accepted 28th May 2013

DOI: 10.1039/c3md00085k

www.rsc.org/medchemcomm

In most bacteria, the nonmevalonate pathway is used to synthesize isoprene units. Dxr, the second step in the pathway, catalyzes the NADPH-dependent reductive isomerization of 1-deoxy-D-xylulose-5-phosphate (DXP) to 2-C-methyl-D-erythritol-4-phosphate (MEP). Dxr is inhibited by natural products fosmidomycin and FR900098, which bind in the DXP binding site. These compounds, while potent inhibitors of Dxr, lack whole cell activity against *Mycobacterium tuberculosis* (Mtb) due to their polarity. Our goal was to use the Mtb Dxr-fosmidomycin co-crystal structure to design bisubstrate ligands to bind to both the DXP and NADPH sites. Such compounds would be expected to demonstrate improved whole cell activity due to increased lipophilicity. Two series of compounds were designed and synthesized. Compounds from both series inhibited Mtb Dxr. The most potent compound (**8**) has an IC_{50} of 17.8 μM. Analysis shows **8** binds to Mtb Dxr *via* a novel, non-bisubstrate mechanism. Further, the diethyl ester of **8** inhibits Mtb growth making this class of compounds interesting lead molecules in the search for new antitubercular agents.

Tuberculosis (TB) remains a significant threat to global public health.[1] TB is caused by the bacillus *Mycobacterium tuberculosis* (Mtb). According to the World Health Organization (WHO),[2] one-third of the world's population is currently infected with Mtb, which is responsible for nearly 2 million deaths each year. Current treatment of uncomplicated TB requires a combination of four drugs (isoniazid, rifampin, pyrazinamide, ethambutol) over a 6–9 months period.[3] Emergence of drug-resistant Mtb strains is a serious threat to TB control and treatment.[4–6] Further, co-infection of TB and HIV has fueled the epidemic. Therefore, there remains an urgent need for the discovery and development of novel antitubercular agents.

As in most bacteria, Mtb synthesizes five-carbon isoprenoids *via* the nonmevalonate pathway (NMP). These metabolites are needed for bacterial cell wall biosynthesis and other essential processes. Humans use the alternate (mevalonate) pathway to biosynthesize the same isoprenoid units. Thus, there are no human homologs for the enzymes of the NMP. Targeting the bacterial enzymes for antibiotic development should not interfere with human isoprene biosynthesis,[7] making the NMP an attractive pathway in the search for novel drugs.

The second step of the NMP is mediated by the enzyme 1-deoxy-D-xylulose 5-phosphate reductoisomerase (Dxr, Fig. 1).[1,8] Dxr is essential for Mtb survival[9] and catalyzes the isomerization and reduction of 1-deoxy-D-xylulose-5-phosphate (DXP) to 2-C-methyl-D-erythritol-4-phosphate (MEP). In the reaction, NADPH is a hydride donor and a metal cation (Mg^{2+} or Mn^{2+}) is a required enzyme cofactor. Current anti-TB drugs do not target the NMP, thus, Dxr inhibition would be a new

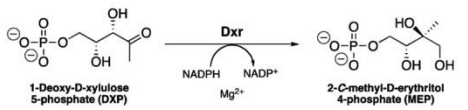

Fig. 1 Dxr catalyzes the reduction and isomerization of DXP to form MEP.

[a]*Department of Chemistry, George Washington University, Washington, DC 20052, USA. E-mail: cdowd@gwu.edu; Fax: +1 202 994 5873; Tel: +1 202 994 8405*

[b]*Department of Chemistry and Biochemistry, George Mason University, Manassas, VA 20110, USA. E-mail: rcouch@gmu.edu; Fax: +1 703 993 8430; Tel: +1 703 993 4770*

[c]*National Center for Biodefense and Infectious Diseases, George Mason University, Manassas, VA 20110, USA. E-mail: kkhall@gmu.edu; Fax: +1 703 993 4280; Tel: +1 703 993 8869*

[d]*Tuberculosis Research Section, Laboratory of Clinical Infectious Diseases, National Institute of Allergy and Infectious Diseases, NIH, Bethesda, MD 20892, USA. E-mail: hboshoff@niaid.nih.gov; Fax: +1 301 480 5705; Tel: +1 301 451 9438*

† Electronic supplementary information (ESI) available: Full experimental details and spectral information for intermediates *N*-(benzyloxy)acetamide, **10–13a-d**, **17–18a,b**, and ligand **9**, as well as biochemical and Mtb assay methods and full results. See DOI: 10.1039/c3md00085k

This journal is © The Royal Society of Chemistry 2013

Published on 29 May 2013. Downloaded by George Mason University on 12/11/2013 02:15:22.

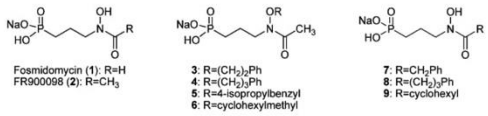

Fig. 2 Structures of fosmidomycin (**1**), FR900098 (**2**) and amide- or *O*-linked analogs (**3–9**).

mechanism of action, and Dxr inhibitors would be expected to be effective against drug-resistant strains of Mtb.

Fosmidomycin (**1**) and its acetyl derivative FR900098 (**2**) are natural products isolated from *Streptomyces lavendulae* (Fig. 2).[10] These secondary metabolites are both known inhibitors of Dxr,[11] and fosmidomycin is currently under clinical investigation due to its activity against a variety of Gram-negative and Gram-positive bacteria, as well as malaria parasites.[12–14] In these pathogens, fosmidomycin is actively transported into cells *via* a glycerol-3-phosphate transporter, GlpT.[15] Mtb, however, does not have GlpT. This, combined with both the hydrophilic nature of fosmidomycin and the highly hydrophobic Mtb cell wall, renders fosmidomycin inactive against Mtb.[9,16] However, we have shown that lipophilic prodrugs of FR900098 demonstrate effective antitubercular activity[17] and act in a GlpT-independent manner.[18] Additionally, a range of synthetic fosmidomycin and FR900098 analogs have been described, designed to compete with DXP at the substrate-binding site.[19–27] While demonstrating potent inhibition of the purified enzyme, none of these analogs, to our knowledge, is active against intact mycobacteria. Our goal was to expand on this work designing Dxr inhibitors with a novel binding mechanism and sufficient lipophilicity to gain whole cell antimycobacterial activity.

Several crystal structures of Dxr have been reported, facilitating the rational design of novel inhibitors.[28,29] The structure of Mtb Dxr in complex with the competitive inhibitor fosmidomycin has led to the identification of binding sites in the enzyme and is an excellent template for protein-ligand docking.[28] In particular, the crystal structure has revealed chelation between the retrohydroxamate moiety of fosmidomycin and a metal cation, the phosphonate binding site, and the close binding proximity of fosmidomycin and NADPH. The nicotinamide ring of NADPH binds approximately 3.5 Å from the formyl carbon atom of fosmidomycin (Fig. 3A). Hence, our approach toward Dxr inhibitor development was based on the design of fosmidomycin/FR900098 analogs that target the two major binding sites in Dxr: the fosmidomycin/DXP site and the NADPH site. Our goal was to bridge these adjacent binding sites to yield a high affinity, bisubstrate ligand, while considering the need for increased lipophilicity compared with fosmidomycin/FR900098. We report here the design, synthesis, and evaluation of two series of compounds with either amide- or *O*-linked substituents appended to the retrohydroxamate moiety of FR900098 (Fig. 2) and evidence of a novel, non-bisubstrate mode of binding.

Results

Modeling of amide- and *O*-linked ligands

Several studies describe the *in silico* evaluation of inhibitors against Dxr.[20,30–35] These reports highlight the challenges of modeling a protein that undergoes significant conformational change upon cofactor binding. We sought to use docking to discern whether bisubstrate inhibition of Mtb Dxr with amide or *O*-linked compounds was feasible.

200 Compounds with the general structures shown in Fig. 2 were docked into the Mtb Dxr structure.[28] NADPH and fosmidomycin were removed from the active site, while Mn^{2+} was kept in place. The analogs retained the phosphonate and backbone of the parent compounds, designed to ensure affinity to the DXP binding site in the enzyme. The analogs were appended with (un)substituted aromatic, alkylaryl, or (cyclo)alkyl substituents to the *N*-hydroxy oxygen atom or the amide carbonyl group of the retrohydroxamate. These structural features were designed to increase affinity to the NADPH binding site. Specifically, we were interested in testing aromatic substituents as mimics of the nicotinamide ring of NADPH, aiming to increase affinity to that pocket. Cycloalkyl groups were used to examine the importance of an aryl substituent.

The docking results predicted that our ligands would adopt a bisubstrate binding mode and bridge the two adjacent binding sites. Representative docking images are shown in Fig. 3B and C. In general, the amide-linked compounds were expected to bind with greater affinity compared with the *O*-linked

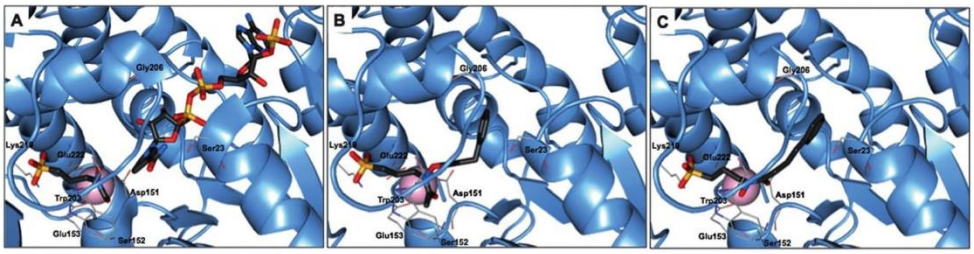

Fig. 3 Mtb Dxr active site and docking results. (A) Active site of Mtb Dxr with fosmidomycin (left ligand) and NADPH (right ligand) bound (pdb 2JCZ).[18] Ligands are separated by ~3.5 Å. (B) Docked *O*-linked ligand **4**. (C) Docked amide ligand **8**. Protein chain A is shown as cartoon (blue), Mn^{2+} as a sphere (pink), ligands are shown as sticks colored by atom type, protein residues as lines colored by atom type. Hydrogen atoms have been hidden for clarity.

This journal is © The Royal Society of Chemistry 2013

Published on 29 May 2013. Downloaded by George Mason University on 12/11/2013 02:15:22.

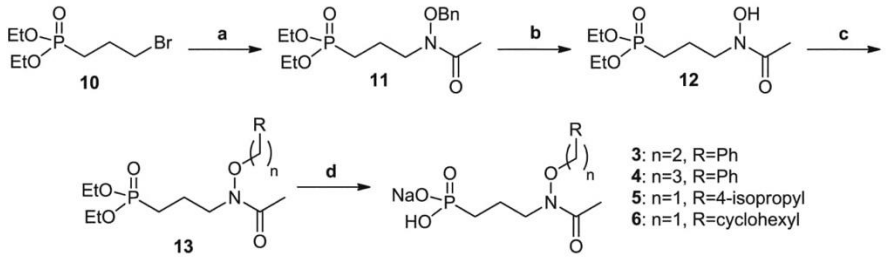

Scheme 1 Synthesis of *O*-linked compounds **3–6**. *Conditions*: (a) BnONHAc, NaH, NaI, THF, 70 °C, 75%; (b) H_2, Pd/C, MeOH, 76%; (c) $R(CH_2)_nBr$, NaH, THF, 70 °C, 27–81%; (d) (i): TMSBr, CH_2Cl_2, (ii): H_2O, (iii): NaOHaq., 61%-quant.

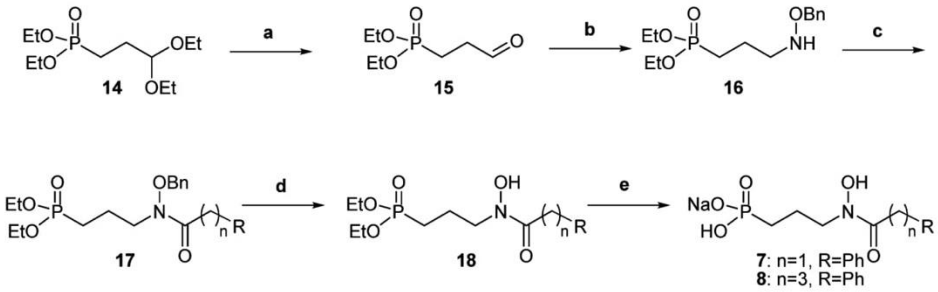

Scheme 2 Synthesis of amide ligands **7** and **8**. *Conditions*: (a) 2N HCl, 84%; (b) $BnONH_2$, MeOH, 40 °C, then $NaBH_3CN$, HCl, MeOH, 79%; (c) $R(CH_2)_nCOCl$, Et_3N, CH_2Cl_2, 50–75%; (d) H_2, Pd/C, MeOH, 56–59%; (e) (i): TMSBr, CH_2Cl_2, (ii): H_2O, (iii): NaOHaq., quant.

compounds. This was anticipated due to differences between the two series in binding the divalent cation. Prior work has shown that the unsubstituted hydroxyl oxygen of the retrohydroxamate is required for tight coordination of the metal.[36] The aryl groups from each series docked in the NADPH binding site (Fig. 3B and C). Collectively, the docking results indicated that the two series might work well as bisubstrate inhibitors of Mtb Dxr and, as such, bind in a manner distinct from fosmidomycin and FR900098.

Synthesis

The preparation of these compounds is shown in Schemes 1 and 2 and in ESI.† A new synthetic route was developed for the synthesis of the *O*-linked compounds **3–6**, using straightforward reactions allowing fast access to small, structurally modified molecules in good yield (Scheme 1).

3-Bromopropylphosphonate **10** was prepared from triethyl phosphite and 1,3-dibromopropane, using the Arbuzov reaction under microwave irradiation.[37] Compound **10** and *N*-(benzyloxy) acetamide were then combined under basic conditions to give **11**, which yielded hydroxylamine **12** after hydrogenation. *O*-linked compounds **13a–d** were obtained by alkylation of intermediate **12** using sodium hydride and the corresponding aryl or alkyl bromide. The four desired monosodium salts **3–6** were obtained after removal of the diethyl ester using bromotrimethylsilane, hydrolysis of the resulting silylester with water, and treatment with 1 equivalent of sodium hydroxide.

Amide ligands **7** and **8** were prepared using the synthetic route shown in Scheme 2. Aldehyde **15** was synthesized from commercially available acetal **14** in acidic conditions. Compound **15** was combined with *O*-benzylhydroxylamine. Reduction with sodium cyanoborohydride and hydrochloric acid gave diethyl ester **16**.[38] Alkylation of **16** using triethylamine and the corresponding acyl chloride gave amide intermediates **17**. Monosodium salts **7** and **8** were afforded after deprotection of both the retrohydroxamate and the phosphonate ester. Amide **9** was prepared using a similar path shown in the ESI.†

As has been seen with related compounds, most of the monosodium salts were isolated and evaluated as a mixture of two conformers.[39] Indeed, Zinglé *et al.* showed that *N*-substituted or *N*- and *O*-substituted hydroxamic acids were usually present as a mixture of *Z* and *E* conformers because of the restricted rotation around the C–N bond.[39] Moreover, the ratio was dependent on the substituent and the nature of the solvent.

Biochemical and antitubercular evaluation

To evaluate the inhibitory activity of compounds **3–9**, enzyme assays were performed with purified Mtb Dxr using a reported spectrophotometric assay monitoring NADPH consumption.[28,40,41] The half maximal inhibitory activity (IC_{50}) of the

Published on 29 May 2013. Downloaded by George Mason University on 12/11/2013 02:15:22.

Table 1 Mtb Dxr IC_{50} values of amide and *O*-linked ligands

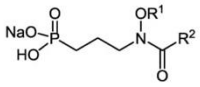

compd	R^1	R^2	IC_{50} (μM)
1	H	H	0.31[16]
2	H	CH_3	2.39
3	$(CH_2)_2Ph$	CH_3	(81.5)[a]
4	$(CH_2)_3Ph$	CH_3	(77.5)[a]
5	4-Ipr-benzyl	CH_3	48.4
6	CH_2cyclohexyl	CH_3	(83.5)[a]
7	H	CH_2Ph	26.9
8	H	$(CH_2)_3Ph$	17.8
9	H	Cyclohexyl	(80.0)[a]

[a] Values in parentheses are percent remaining enzyme activity at 100 μM.

compounds is shown in Table 1 (see also ESI,† Fig. 1). Among the *O*-linked ligands (compounds **3**–**6**), compound **5** demonstrated the greatest inhibition, with an IC_{50} of 48.4 μM. The activity of the *O*-linked ligands is surprising and challenges the notion that chelation of the metal cation by the retrohydroxamate is required for binding to the enzyme. For the *O*-linked compounds, binding of the aryl substituent could compensate for diminished coordination of the cation.

Table 1 shows that amide ligands **7** and **8** are more potent inhibitors of the enzyme with values of 26.9 and 17.8 μM, respectively. This result may arise from more efficient coordination of the metal cation by the amide *versus* *O*-linked analogs. In the amide series, a slightly longer chain length between the retrohydroxamate and the aryl group may be preferable, as compound **8** gave slightly better inhibition than compound **7**. Weaker inhibition by compounds **6** and **9**, both with a nonaromatic ring, highlight the importance of having an aromatic group in the inhibitor.

Since we designed our inhibitors to occupy both the DXP and NADPH binding sites, compound **8** was further examined to discern its mechanism of inhibition. Catalysis by Mtb Dxr undergoes an ordered bi bi reaction mechanism, wherein NADPH must bind to the enzyme before DXP can bind.[42] This process is reflective of a protein conformational change that occurs upon NADPH binding, resulting in the formation of the DXP binding site. Fosmidomycin and FR900098 are competitive inhibitors with respect to DXP and uncompetitive relative to NADPH[42] (see also ESI Fig. 1†). Hence, NADPH must bind to Dxr before either of these inhibitors can occupy the Dxr binding site. With this mechanism in mind, we used classical competition experiments to assess the mode of binding of ligand **8**.

As illustrated in Fig. 4, the double reciprocal plots indicate that ligand **8** is competitive with respect to DXP, but noncompetitive relative to NADPH. Thus, in stark contrast to fosmidomycin and FR900098, the binding mechanism of compound **8** does not require the initial binding of NADPH. Since inhibitor **8** does not directly compete with the binding of NADPH, the phenylpropyl

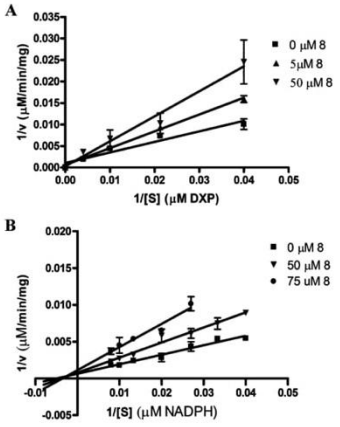

Fig. 4 Mode of inhibition by ligand **8**. The Lineweaver–Burk plots indicate that **8** is competitive with respect to DXP (A), but noncompetitive with respect to NADPH (B).

Table 2 Antitubercular activity of ligands and their diethyl esters

Compd	H37Rv Mtb MIC (μg mL^{-1})
Fosmidomycin (**1**)	>500
FR900098 (**2**)	>500
Diethyl-**1**	250
8	>200
Diethyl-**8** (**18b**)	200

substituent of **8** is likely binding in an alternate location. Interestingly, this site is likely distinct from the NADPH site, but may promote the same structural change that gives rise to DXP binding. Studies are underway to further elucidate the nature and kinetics of this novel mode of inhibitor binding to Dxr.

To complement the characterization of compound **8** against purified Mtb Dxr, we assayed the efficacy of **8** and its lipophilic diethyl phosphonate ester (diethyl-**8**, **18b**) against whole cell Mtb (H37Rv, Table 2). While the hydrophilic fosmidomycin, FR900098, and compound **8** do not inhibit Mtb, the diethyl phosphonate ester of fosmidomycin[17] and **18b** display measurable antitubercular activity (Table 2). Collectively, the enzyme and growth inhibition assays highlight the novel antitubercular activity of the amide-linked series of Dxr inhibitors, identifying compound **8** as a prototypical lead molecule for the further development of a new class of novel antimycobacterial agents.

Conclusions

There is an urgent need for the development of new, highly active, and less toxic anti-TB drugs. Dxr is an attractive target since humans do not have the enzyme or a homolog. Dxr inhibitors should be effective against drug-resistant Mtb

This journal is © The Royal Society of Chemistry 2013

Published on 29 May 2013. Downloaded by George Mason University on 12/11/2013 02:15:22.

strains, and, due to NMP's importance in early points of bacterial metabolism, may be effective against both active and latent Mtb. Aided by an available co-crystal structure, our docking studies suggested that analogs of FR900098 with amide- or *O*-linked aryl substituents on the retrohydroxamate could be novel and potent inhibitors of Mtb Dxr. The inhibition data from our initial set of ligands (**3–9**), while not more active than the parent compounds, show promising results, with our best compound (**8**) having an IC_{50} of 17.8 μM. Indeed, our inhibition results align with prior reports of similar *N*-acyl analogs against *E. coli* and *P. falciparum* Dxr.[26,33,35]

Compound **8** displays a new mode of binding to Mtb Dxr not previously seen with parent compounds fosmidomycin and FR900098 or other known Dxr inhibitors. Prior modeling studies on similar *N*-acyl analogs indicated possible binding in a non-NADPH site.[26] Ligand **8** could be using this alternate binding site and current studies are aimed at elucidating this. While this binding mode was not part of our original bisubstrate design *per se*, demonstration of a novel binding mode is both interesting and significant.

The MIC of the simple diethyl ester of **8** is comparable to the corresponding fosmidomycin ester and represents a new class of antitubercular compounds. As the MIC reflects both the lipophilicity and enzyme inhibition of **8**, we expect it to improve as inhibitors with optimized potencies against Dxr are developed. Work is currently underway to explore an expanded set of analogs, reveal a comprehensive SAR, prove an on-target mechanism, and discern details of this new binding mode. Taken together, our data suggests new possibilities in the design and development of novel, antimycobacterial Dxr inhibitors.

Acknowledgements

This work was supported by the Intramural Research Program of NIAID/NIH, the George Washington University Department of Chemistry, the GWU University Facilitating Fund, and NIH (AI086453 to CSD). RDC was supported by George Mason University's Department of Chemistry and Biochemistry and the U.S. Army Medical Research and Materiel Command W23RYX1291N601.

Notes and references

1 C. Dye, P. Glaziou, K. Floyd and M. Raviglione, *Annu. Rev. Public Health*, 2013, **34**, 271–286.
2 *Global Tuberculosis Control 2009: Epidemiology, Strategy, Financing*, WHO Press, Geneva, Switzerland, 2009.
3 WHO, *Treatment of Tuberculosis: Guideline for National Programmes*, Geneva, Switzerland, 2003.
4 A. Wright, *MMWR Morb. Mortal. Wkly. Rep.*, 2006, **55**, 301–305.
5 *Emergency Update, 2008: Guidelines for the programmatic management of drug-resistant tuberculosis*, WHO Press, Geneva, Switzerland, 2008.
6 Z. F. Udwadia, R. A. Amale, K. K. Ajbani and C. Rodrigues, *Clin. Infect. Dis.*, 2012, **54**, 579–581.
7 C. A. Testa and M. J. Brown, *Curr. Pharm. Biotechnol.*, 2003, **4**, 248–259.
8 P. J. Proteau, *Bioorg. Chem.*, 2004, **32**, 483–493.
9 A. C. Brown and T. Parish, *BMC Microbiol.*, 2008, **8**, 78.
10 M. Okuhara, Y. Kuroda, T. Goto, M. Okamoto, H. Terano, M. Kohsaka, H. Aoki and H. Imanaka, *J. Antibiot.*, 1980, **33**, 13–17.
11 T. Kuzuyama, T. Shimizu, S. Takahashi and H. Seto, *Tetrahedron Lett.*, 1998, **39**, 7913–7916.
12 H. Jomaa, J. Wiesner, S. Sanderbrand, B. Altincicek, C. Weidemeyer, M. Hintz, I. Turbachova, M. Eberl, J. Zeidler, H. K. Lichtenthaler, D. Soldati and E. Beck, *Science*, 1999, **285**, 1573–1576.
13 N. Singh, G. Cheve, M. A. Avery and C. R. McCurdy, *Curr. Pharm. Des.*, 2007, **13**, 1161–1177.
14 Y. Nolan, D. Martin, V. A. Campbell and M. A. Lynch, *J. Neuroimmunol.*, 2004, **151**, 12–23.
15 Y. Sakamoto, S. Furukawa, H. Ogihara and M. Yamasaki, *Biosci., Biotechnol., Biochem.*, 2003, **67**, 2030–2033.
16 R. K. Dhiman, M. L. Schaeffer, A. M. Bailey, C. A. Testa, H. Scherman and D. C. Crick, *J. Bacteriol.*, 2005, **187**, 8395–8402.
17 E. Uh, E. R. Jackson, G. San Jose, M. Maddox, R. E. Lee, R. E. Lee, H. I. Boshoff and C. S. Dowd, *Bioorg. Med. Chem. Lett.*, 2011, **21**, 6973–6976.
18 E. S. McKenney, M. Sargent, H. Khan, E. Uh, E. R. Jackson, G. San Jose, R. D. Couch, C. S. Dowd and M. L. van Hoek, *PLoS One*, 2012, **7**, e38167.
19 M. Andaloussi, L. M. Henriksson, A. Wieckowska, M. Lindh, C. Bjorkelid, A. M. Larsson, S. Suresh, H. Iyer, B. R. Srinivasa, T. Bergfors, T. Unge, S. L. Mowbray, M. Larhed, T. A. Jones and A. Karlen, *J. Med. Chem.*, 2011, **54**, 4964–4976.
20 L. Deng, J. Diao, P. Chen, V. Pujari, Y. Yao, G. Cheng, D. C. Crick, B. V. Prasad and Y. Song, *J. Med. Chem.*, 2011, **54**, 4721–4734.
21 V. Devreux, J. Wiesner, H. Jomaa, J. Rozenski, J. Van der Eycken and S. Van Calenbergh, *J. Org. Chem.*, 2007, **72**, 3783–3789.
22 V. Devreux, J. Wiesner, H. Jomaa, J. Van der Eycken and S. Van Calenbergh, *Bioorg. Med. Chem. Lett.*, 2007, **17**, 4920–4923.
23 T. Haemers, J. Wiesner, S. Van Poecke, J. Goeman, D. Henschker, E. Beck, H. Jomaa and S. Van Calenbergh, *Bioorg. Med. Chem. Lett.*, 2006, **16**, 1888–1891.
24 T. Kurz, C. Behrendt, M. Pein, U. Kaula, B. Bergmann and R. D. Walter, *Arch. Pharm.*, 2007, **340**, 661–666.
25 T. Kurz, K. Schluter, M. Pein, C. Behrendt, B. Bergmann and R. D. Walter, *Arch. Pharm.*, 2007, **340**, 339–344.
26 R. Ortmann, J. Wiesner, K. Silber, G. Klebe, H. Jomaa and M. Schlitzer, *Arch. Pharm.*, 2007, **340**, 483–490.
27 T. Verbrugghen, P. Cos, L. Maes and S. Van Calenbergh, *J. Med. Chem.*, 2010, **53**, 5342–5346.
28 L. M. Henriksson, T. Unge, J. Carlsson, J. Aqvist, S. L. Mowbray and T. A. Jones, *J. Biol. Chem.*, 2007, **282**, 19905–19916.
29 A. Mac Sweeney, R. Lange, R. P. Fernandes, H. Schulz, G. E. Dale, A. Douangamath, P. J. Proteau and C. Oefner, *J. Mol. Biol.*, 2005, **345**, 115–127.

Published on 29 May 2013. Downloaded by George Mason University on 12/11/2013 02:15:22.

30 M. Andaloussi, M. Lindh, C. Bjorkelid, S. Suresh, A. Wieckowska, H. Iyer, A. Karlen and M. Larhed, *Bioorg. Med. Chem. Lett.*, 2011, **21**, 5403–5407.
31 T. Bodill, A. C. Conibear, G. L. Blatch, K. A. Lobb and P. T. Kaye, *Bioorg. Med. Chem. Lett.*, 2011, **19**, 1321–1327.
32 L. Deng, S. Sundriyal, V. Rubio, Z. Z. Shi and Y. Song, *J. Med. Chem.*, 2009, **52**, 6539–6542.
33 D. Giessmann, P. Heidler, T. Haemers, S. Van Calenbergh, A. Reichenberg, H. Jomaa, C. Weidemeyer, S. Sanderbrand, J. Wiesner and A. Link, *Chem. Biodiversity*, 2008, **5**, 643–656.
34 A. K. Patel, *Int. J. Pharma Bio Sci.*, 2012, **3**, 72–91.
35 K. Silber, P. Heidler, T. Kurz and G. Klebe, *J. Med. Chem.*, 2005, **48**, 3547–3563.
36 C. J. Marmion, D. Griffith and K. B. Nolan, *Eur. J. Inorg. Chem.*, 2004, **15**, 3003–3016.
37 D. Villemin, F. Simeon, H. Decreus and P.-A. Jaffres, *Phosphorus, Sulfur Silicon Relat. Elem.*, 1998, **133**, 209–213.
38 P. D. M. Puyau and J. J. Perie, *Phosphorus, Sulfur Silicon Relat. Elem.*, 1996, **112**, 71–90.
39 C. Zingle, L. Kuntz, D. Tritsch, C. Grosdemange-Billiard and M. Rohmer, *J. Org. Chem.*, 2010, **75**, 3203–3207.
40 S. Jawaid, H. Seidle, W. Zhou, H. Abdirahman, M. Abadeer, J. H. Hix, M. L. van Hoek and R. D. Couch, *PLoS One*, 2009, **4**, e8288.
41 A. Tsang, H. Seidle, S. Jawaid, W. Zhou, C. Smith and R. D. Couch, *PLoS One*, 2011, **6**, e20884.
42 A. T. Koppisch, D. T. Fox, B. S. Blagg and C. D. Poulter, *Biochemistry*, 2002, **41**, 236–243.

 This journal is © The Royal Society of Chemistry 2013

Paper II: Kinetic Characterization and Allosteric Inhibition of the Yersinia pestis 1-Deoxy-D-Xylulose 5-Phosphate Reductoisomerase (MEP Synthase)

Haymond A, Johny C, Dowdy T, Schweibenz B, Villarroel K, Young R, et al. *PLoS ONE*. 2014; 9: e106243. doi:10.1371/journal.pone.0106243

Attributions and Contributions

Reproduced with permission from the Public Library of Science. All supplementary information as referenced in the text can be found in Appendix 2. The author was responsible for performing the experiments, writing the text of the paper, as well as the generation of Figure 3, Figures 8-14, and Figure 17.

OPEN ACCESS Freely available online

PLOS ONE

Kinetic Characterization and Allosteric Inhibition of the *Yersinia pestis* 1-Deoxy-D-Xylulose 5-Phosphate Reductoisomerase (MEP Synthase)

Amanda Haymond[1], Chinchu Johny[1], Tyrone Dowdy[1], Brandon Schweibenz[1], Karen Villarroel[1], Richard Young[1], Clark J. Mantooth[1], Trishal Patel[1], Jessica Bases[1], Geraldine San Jose[2], Emily R. Jackson[2], Cynthia S. Dowd[2], Robin D. Couch[1]*

1 Department of Chemistry and Biochemistry, George Mason University, Manassas, Virginia, United States of America, **2** Department of Chemistry, George Washington University, Washington DC, United States of America

Abstract

The methylerythritol phosphate (MEP) pathway found in many bacteria governs the synthesis of isoprenoids, which are crucial lipid precursors for vital cell components such as ubiquinone. Because mammals synthesize isoprenoids via an alternate pathway, the bacterial MEP pathway is an attractive target for novel antibiotic development, necessitated by emerging antibiotic resistance as well as biodefense concerns. The first committed step in the MEP pathway is the reduction and isomerization of 1-deoxy-D-xylulose-5-phosphate (DXP) to methylerythritol phosphate (MEP), catalyzed by MEP synthase. To facilitate drug development, we cloned, expressed, purified, and characterized MEP synthase from *Yersinia pestis*. Enzyme assays indicate apparent kinetic constants of $K_M^{DXP} = 252\ \mu M$ and $K_M^{NADPH} = 13\ \mu M$, IC_{50} values for fosmidomycin and FR900098 of 710 nM and 231 nM respectively, and K_i values for fosmidomycin and FR900098 of 251 nM and 101 nM respectively. To ascertain if the *Y. pestis* MEP synthase was amenable to a high-throughput screening campaign, the Z-factor was determined (0.9) then the purified enzyme was screened against a pilot scale library containing rationally designed fosmidomycin analogs and natural product extracts. Several hit molecules were obtained, most notably a natural product allosteric affector of MEP synthase and a rationally designed bisubstrate derivative of FR900098 (able to associate with both the NADPH and DXP binding sites in MEP synthase). It is particularly noteworthy that allosteric regulation of MEP synthase has not been described previously. Thus, our discovery implicates an alternative site (and new chemical space) for rational drug development.

Citation: Haymond A, Johny C, Dowdy T, Schweibenz B, Villarroel K, et al. (2014) Kinetic Characterization and Allosteric Inhibition of the *Yersinia pestis* 1-Deoxy-D-Xylulose 5-Phosphate Reductoisomerase (MEP Synthase). PLoS ONE 9(8): e106243. doi:10.1371/journal.pone.0106243

Editor: Fatah Kashanchi, George Mason University, United States of America

Received March 19, 2014; **Accepted** July 29, 2014; **Published** August 29, 2014

Copyright: © 2014 Haymond et al. This is an open-access article distributed under the terms of the Creative Commons Attribution License, which permits unrestricted use, distribution, and reproduction in any medium, provided the original author and source are credited.

Data Availability: The authors confirm that all data underlying the findings are fully available without restriction. All relevant data are within the paper and its Supporting Information files.

Funding: This study was supported by George Mason University's Department of Chemistry and Biochemistry and the U.S. Army Medical Research and Materiel Command W23RYX1291N601. The funders had no role in study design, data collection and analysis, decision to publish, or preparation of the manuscript.

Competing Interests: The authors have declared that no competing interests exist.

* Email: rcouch@gmu.edu

Introduction

Referred to as "The Great Mortality" by contemporaries, Black Death irrevocably changed the social and economic structure of 14th century Europe, killing one-third of the Western European population [1]. Black Death, an outbreak of the plague, was caused by the Gram negative bacterium *Yersinia pestis* [1], [2]. In light of its high morbidity/mortality rate, ease of dissemination, associated emergency response procedures, and significant social impact, *Y. pestis* is now categorized by the US Centers for Disease Control and Prevention (CDC) as a Category A biological threat agent (i.e. an agent of greatest concern). Our vulnerability to outbreaks of infectious disease is further underscored by the 2009 H1N1 swine flu pandemic, the 2003 SARS outbreak, the 2001 anthrax letter attacks, and the 1984 Rajneeshee Salmonella attacks, stressing the necessity of effective vaccines and antimicrobial/antiviral therapeutics. The ease by which antibiotic resistance can be deliberately engineered into bacteria, and the increasing prevalence of antibiotic resistant strains, also emphasizes the need for continued development of novel antibiotics against new bacterial targets.

Isoprenoids are a crucial family of molecules that includes compounds such as quinones and cholesterol and are involved in a number of cellular processes, from electron transport to signal transduction to the regulation of membrane fluidity. Each member of this diverse family of molecules is derived from two common building blocks; isopentenyl pyrophosphate (IPP) and its isomer dimethylallyl pyrophosphate (DMAPP), synthesized via the mevalonic acid (MVA) or methyl erythritol phosphate (MEP) pathways (Figure 1). Because the MEP pathway is exclusively utilized by many human pathogens, and knockout of MEP pathway genes has proven lethal in bacteria such as *Mycobacterium tuberculosis* [3], *Francisella tularensis* [4], *Escherichia coli* [5], and *Vibrio cholerae* [6], the MEP pathway enzymes have received considerable attention as promising targets for the development of novel antibiotics (reviewed in [7] [8] [9]).

The drug discovery process typically involves five distinguishable phases; target identification, target validation, lead molecule identification, lead optimization, and preclinical and clinical trials. The identification of lead molecules often involves the screening of a molecular library. In general, molecular libraries typically contain synthetic compounds, either rational or random in design, and/or natural products extracted from a wide variety of plant, bacteria, or fungal sources. While natural products underwent a period of reduced attention (a consequence of several factors including the substantial effort required to isolate the active component from a complex mixture, the effort required to elucidate the chemical structure of the active component, significant advances in protein structure determination by crystallography and NMR, improvements to *in silico* rational drug design using the protein structure, and the combinatorial chemistry approach to rapidly populating synthetic chemical libraries), natural product libraries are coming back in vogue, as the number of new chemical entities entering into clinical trials continues to decline. Nearly one-third of the pharmaceuticals worldwide are natural products or their derivatives. In fact, most antibacterial drugs originate from natural products, including the β-lactams, tetracyclines, aminoglycosides, chloramphenicol, cephalosporins, macrolides, lincosamides, rifamycins, streptogramins, the glycopeptides, and the lipopeptides. The blockbuster anticholesterol drug Mevacor (lovastatin), a natural product produced by the fungus *Aspergillus terreus*, inhibits HMG-CoA reductase, thereby blocking the rate limiting enzyme in the MVA isoprene biosynthetic pathway (Fig. 1) [10] [11].

Several groups have demonstrated an interest in developing small molecule inhibitors of the MEP pathway enzymes, including those that target DXP synthase [12], [13], MEP synthase (reviewed in [14]), CDP-ME synthase [15], [16], CDP-ME kinase [17], [18], cMEPP synthase [19], [20], HMB-PP synthase [21], [22], and HMB-PP reductase [23], [24]. While each of these MEP pathway enzymes is a viable target for drug development [25] the focus of this report is on MEP synthase. Herein we describe the cloning, expression, and kinetic characterization of purified *Y. pestis* MEP synthase, the first committed enzyme of the MEP isoprene biosynthetic pathway. Using known MEP synthase inhibitors, we demonstrate the effectiveness of inhibiting both the purified enzyme and liquid cultures of *Y. pestis*. We also report the outcome of an in-house high-throughput screen of both a

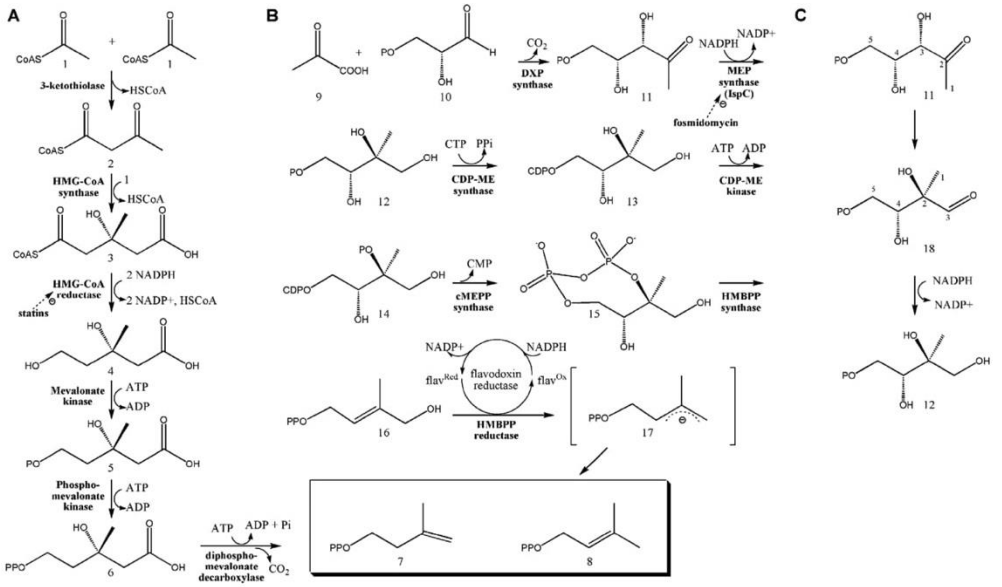

Figure 1. The MVA and MEP biosynthetic pathways. A) The MVA pathway is utilized by humans and other eukaryotes, archaebacteria, and certain eubacteria to produce IPP and DMAPP, the building blocks of isoprenoids. The pathway is initiated by the enzymatic condensation of 3 molecules of acetyl-CoA (1) to form 3-hydroxy-3-methylglutaryl CoA (HMG-CoA) (3), which is then reduced to MVA by HMG-CoA reductase (4) [54] [55] Subsequent phosphorylation and decarboxylation yield IPP (7) [56] [57] [58] which is converted to DMAPP (8) by an isomerase [59]. B) The MEP pathway is used by higher plants, the plastids of algae, apicomplexan protozoa, and many eubacteria, including numerous human pathogens. Pyruvate (9) is condensed with glyceraldehyde 3-phosphate (10) to yield 1-deoxy-D-xylulose 5-phosphate (DXP; (11)) [60], a branch point intermediate with a role in *E. coli* vitamin B1 and B6 biosynthesis [61] [62] [63] [64] as well as isoprene biosynthesis. In the first committed step of the *E. coli* MEP pathway, 1-Deoxy-D-xylulose 5-phosphate reductoisomerase (also called MEP synthase, Dxr or IspC) catalyzes the reduction and rearrangement of 11 to yield MEP (12) [28]. CDP-ME synthase then converts MEP into 4-(cytidine 5′-diphospho)-2-C-methyl-D-erythritol (CDP-ME; (13)). CDP-ME kinase phosphorylates CDP-ME, which is subsequently cyclized (coupled with the loss of CMP) by cMEPP synthase to yield 2-C-methyl-D-erythritol 2,4-cyclodiphosphate (15) [65] [66] [67] [68] [69]. A reductive ring opening of 15 produces 1-hydroxy-2-methyl-2-butenyl diphosphate (HMBPP; (16)) [70] [71] [72] [73] [74], which is then reduced to both IPP and DMAPP in a ~5:1 ratio [8] [75] [76] [77] [78] [79] [80]. C) The reaction catalyzed by MEP synthase. The intermediate 2-C-methyl-D-erythrose 4-phosphate (18), produced by isomerization via cleavage of the bond between C3 and C4 and formation of a new bond between C2 and C4 [81] [82], is subsequently reduced to yield MEP (12).
doi:10.1371/journal.pone.0106243.g001

rationally designed synthetic compound library and a natural product library, resulting in the identification of several inhibitor hits, including a completely novel class of MEP synthase inhibitors that functions via an allosteric mechanism.

Materials and Methods

Bacterial strains and growth conditions

The following reagent was obtained through the NIH Biodefense and Emerging Infections Research Resources Repository, NIAID, NIH: *Yersinia pestis* subsp. A1122, cultured at 37°C in Tryptic Soy Broth with 0.1% cysteine (TSB). Recombinant proteins were expressed in *Escherichia coli* BL21 CodonPlus (DE3)-RIL cells from Stratagene, La Jolla, CA that were grown at 37°C in Luria-Bertani (LB) media supplemented with 100 μg/mL ampicillin and 50 μg/ml chloramphenicol. All liquid cultures were constantly shaken at 250 rpm. Agar (1.5% wt/vol) was added to prepare solid media.

Growth inhibition assays

The half-maximal inhibitory concentration (IC_{50}) for FR900098, a known MEP synthase inhibitor [7], was determined via a dose-response plot of cell growth (OD_{600}) as a function of inhibitor concentration. An overnight culture of *Y. pestis* subsp. A1122 was grown in TSB and harvested by centrifugation (15 min, 2450×g, 25°C). The resulting cell pellet was washed twice with 1 mL of TSB then diluted to an OD_{600} of 0.2. Aliquots of the culture were then dispensed into 10×1 cm foam-capped test tubes containing 2 mL of fresh TSB and FR900098 added to the tubes at the indicated concentrations. Bacterial growth was monitored over 24 hrs. Each condition was evaluated in duplicate. Nonlinear regression fitting the resulting dose-response plot was achieved using GraphPad Prism version 4.00 for Windows (GraphPad software Inc, San Diego, CA) and the equation $F = 1/(1+[I]/IC_{50})$ where F = fractional growth and [I] = inhibitor concentration. For growth inhibition assays run with rationally designed compounds, a small volume protocol was used in which a diluted overnight culture was used to inoculate 400 μL of TSB containing the appropriate concentration of inhibitor. Cultures were grown in foam-capped, 1.5 mL microcentrifuge tubes and monitored over 24 hours. For the small volume protocol, each condition was evaluated in triplicate.

The cloning, expression, and purification of *Y. pestis* MEP synthase

The *Y. pestis* CO92 MEP synthase gene (*ispC*) was identified in the complete genome sequence using primary sequence homology with orthologs from other organisms. Sequence alignment was accomplished using Clustal Omega, with the following reference sequence numbers and protein sequence numbers obtained from the National Center for Biotechnology Information (NCBI): *Y. pestis* (NC_003143.1, YP_002346091.1), *E. coli* (U00096.2, AAC73284.1), *M. tuberculosis* (NC_000962.3, NP_217386.2), *F. tularensis* (AJ749949.2, CAG46207.1), *V. cholerae* (NC_002505.1, NP_231885.1), *B. anthracis* (AE016879.1, AAP27179.1), *M. leprae* (NC_002677.1, NP_302094.1), and *T. pallidum* (NC_000919.1, NP_219039.1) The *Y. pestis ispC* gene was synthesized (GenScript USA Inc, Piscataway, NJ) and cloned into a pET101/D-TOPO vector, facilitating the expression of a C-terminal His-tagged protein. Restriction mapping and DNA sequencing were used to confirm the construction of the plasmid (pYpIspC). The plasmid was transformed into chemically competent *E. coli* BL21 CodonPlus (DE3)-RIL cells (Stratagene, La Jolla, CA) for protein expression.

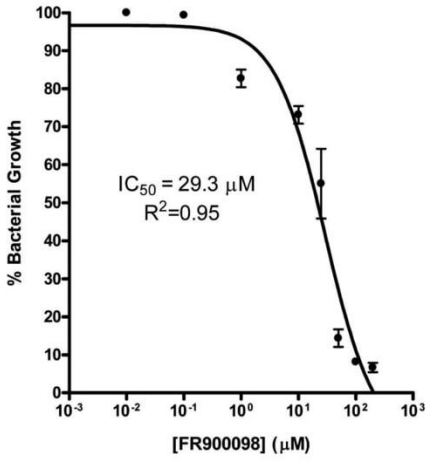

Figure 2. Dose-response plot of *Y. pestis* growth as a function of FR900098 concentration. Fractional growth is calculated as the ratio of cell density (OD_{600}) in the presence of inhibitor to cell density in the absence of inhibitor. Nonlinear regression fitting was performed, resulting in an IC_{50} of 29 μM (6.4 μg/mL). The goodness-of-fit (R^2) value is indicated. For comparison, the IC_{50} of ampicillin is 10.8 μM (3.8 μg/mL; see Figure S1).
doi:10.1371/journal.pone.0106243.g002

A 10 mL overnight seed culture of *E. coli* BL21 CodonPlus (DE3)-RIL+pYpIspC was added to 1 L of LB media and incubated with shaking at 37°C and 250 rpm. Once an OD_{600} of 1.8 was achieved, protein expression was induced using 0.5 mM isopropyl β-D-thiogalactopyranoside (IPTG) and the culture was allowed to incubate for an additional 18 hours. Cells were harvested via centrifugation (4650×g, 20 min) and stored at −80°C. Protein was isolated and purified from the cells via chemical lysis and affinity chromatography. Cell lysis was achieved using Lysis Buffer A (100 mM Tris pH 8, 0.032% lysozyme, 3 mL per mg cell pellet), followed by Lysis Buffer B (0.1 M $CaCl_2$, 0.1 M $MgCl_2$, 0.1 M NaCl, 0.020% DNase, 0.3 mL per mg cell pellet). Centrifugation (48,000×g, 20 min) yielded the clarified cell lysate that was passed through a TALON immobilized metal affinity column (Clontech Laboratories, Mountain View, CA). The column was washed with 20 column volumes of 1× equilibrium buffer (50 mM HEPES pH 7.5, 300 mM NaCl), 10 column volumes of 1× wash buffer (50 mM HEPES pH 7.5, 300 mM NaCl, 10 mM imidazole), and 15 column volumes of 2× wash buffer (100 mM HEPES pH 7.5, 600 mM NaCl, 20 mM imidazole). The protein was then eluted with 5 column volumes of 1× elution buffer (150 mM imidazole pH 7.0, 300 mM NaCl). Buffer was exchanged with 0.1 M Tris pH 7.5, 1 mM NaCl, 5 mM DTT during concentration by ultrafiltration. Protein concentration was determined using Advanced Protein Assay Reagent (Cytoskeleton, Denver CO) with γ-globulins (Sigma-Aldrich) as the standard. Purified protein was visualized via Coomassie stained SDS-PAGE. The yield of YpIspC averaged 30 mg per 1 L shake flask. *M. tuberculosis* and *F. tularensis* MEP synthase [26] were cloned, expressed, and purified essentially as described above.

Figure 3. Purification of recombinant *Y. pestis* MEP synthase. A Coomassie stained SDS-PAGE shows two lanes of purified His-tagged MEP synthase alongside a molecular weight marker (MW). His-tagged MEP synthase has a predicted molecular weight of 46.7 kDa. The typical yield of purified protein averaged 30 mg per 1 L shake flask.
doi:10.1371/journal.pone.0106243.g003

Enzyme Assays

MEP synthase activity was assayed at 37°C by spectrophotometrically monitoring the enzyme catalyzed oxidation of NADPH (Fig. 1C), as previously described [27]. All assays were performed in duplicate. To determine the apparent K_M for 1 deoxy-D-xylulose 5-phosphate (DXP), 120 µL assay solutions contained 100 mM Tris pH 7.8, 25 mM $MgCl_2$, 150 µM NADPH, 0.89 µM MEP synthase, and variable concentrations of DXP (Echelon Biosciences, Salt Lake City, UT). The assay solution was incubated at 37°C for 10 minutes to allow NADPH to associate with the enzyme prior to the addition of DXP. To determine the apparent K_M for NADPH, assays were performed with fixed DXP concentration (0.4 mM) and a variable concentration of NADPH. Nonlinear regression to the Michaelis-Menton equation enabled the determination of kinetic constants. To determine cation specificity, assays were performed with 25 mM $MgCl_2$, $CaCl_2$, $CoCl_2$, $CuCl_2$, $MnCl_2$, or $NiCl_2$. Assays performed with isopentenyl pyrophosphate, dimethylallyl pyrophosphate, and geranyl pyrophosphate (Echelon Biosciences, Salt Lake City, Utah) included a 10 minute preincubation with the enzyme (37°C) before addition of NADPH. The half-maximal inhibition (IC_{50}) by fosmidomycin and FR900098 were determined by using a plot of enzyme fractional activity as a function of inhibitor concentration. As they are slow, tight binding inhibitors [28], fosmidomycin and FR900098 were pre-incubated with the enzyme for 10 minutes prior to the addition of the substrate. Molecular library screening for inhibitors also included this pre-incubation step.

Molecular Modeling

The *Y. pestis* MEP synthase was homology-modeled using I-TASSER (http://zhanglab.ccmb.med.umich.edu/I-TASSER/) [29] [30] [31]. Templates were selected by I-TASSER's threading alignment algorithm which considers predicted secondary structure features in the sequence and identifies analogous and homologous protein templates. The optimized model was then evaluated with ProQ2 (http://www.bioinfo.ifm.liu.se/ProQ2/) [32], which uses features such as atom-atom contacts, residue-residue contacts, solvent accessibility, and secondary structure information to assign an accuracy score from 0 (unreliable) to 1 (reliable). Swiss- PdbViewer 4.0 (http://spdbv.vital-it.ch/) was used to visualize and annotate the model.

Library Screening

A rationally designed, small molecule library was compiled using compounds synthesized as described [33]. Each compound was designed from resolved crystal structures of *M. tuberculosis* MEP synthase in complex with fosmidomycin [33] [34] and contains an amide-linked or O-linked functional group.

A natural product library was compiled in house using extracts obtained from 80 different biological sources. After solvent extraction, the extracts were dried under vacuum, dispensed by mass, and resuspended in dimethyl sulfoxide (DMSO) for use in

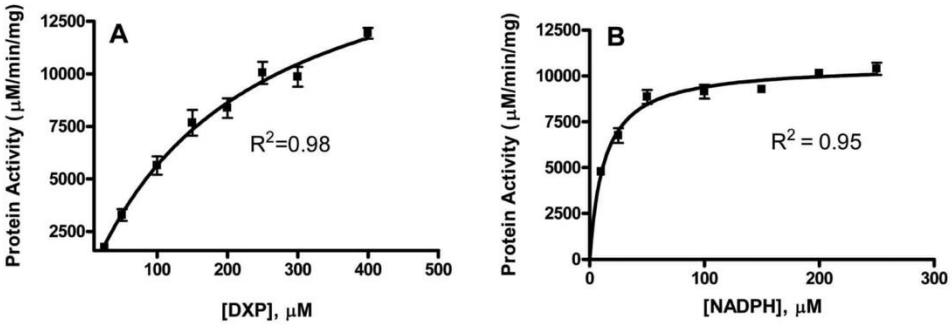

Figure 4. The substrate dependent catalytic activity of *Y. pestis* MEP synthase. Shown are the Michaelis-Menten plots of reaction velocity as a function of A) DXP concentration and B) NADPH concentration. Least-squares best fit of the data to the Michaelis-Menten equation produces the kinetic parameters listed in Table 1. The R^2 value for each plot is indicated. All assays were performed in duplicate.
doi:10.1371/journal.pone.0106243.g004

Table 1. MEP synthase Apparent Kinetic Parameters.

MEP Synthase	K_m^{DXP} (μM)	K_m^{NADPH} (μM)	K_{cat}^{DXP} (s^{-1})	K_{cat}^{NADPH} (s^{-1})	K_{cat}^{DXP}/K_m^{DXP} (M^{-1} min^{-1})	IC_{50}^{fos} (nM)	K_i^{fos} (nM)	$IC_{50}^{FR900098}$ (nM)	$K_i^{FR900098}$ (nM)	Ref.
Y.pestis	221.5±34.3	12.7±1.5	1.7	1.0	4.6×10^5	710	968	231	170±7.10	This study
F.tularensis	103.7±12.1	13.3±1.5	2.0±0.09	1.3±0.04	$1.2 \times 10^6 \pm 9 \times 10^4$	247	98.9±4.5	230	–	[26]PM, [39]PM
E.coli	81–250	0.5–18	33	–	2.4×10^7	35	21–215	35	–	[45]PM, [83]PM, [35]PM, [84]PM
M.tuberculosis	47	29.7	1.2	–	1.5×10^6	80	–	160	–	[46]PM, [48]PM
Synechocytis sp PCC6803	170	3.5	17	–	6×10^6	–	4	–	2	[85]PM, [86]PM

doi:10.1371/journal.pone.0106243.t001

Figure 5. Cation specificity of *Y. pestis* MEP synthase. Enzyme assays were performed with fixed NADPH (150 μM), DXP (400 μM), and divalent cation (25 mM) concentration. *Y. pestis* MEP synthase has comparable activity with either Mg^{2+} or Mn^{2+}. Assays were performed in duplicate.
doi:10.1371/journal.pone.0106243.g005

the screen. For dose-response and mechanism of inhibition plots, inhibitor concentrations are dilutions relative to the original stock solution.

Results and Discussion

Validating the *Y. pestis* MEP pathway as an antimicrobial target

The streptomycete natural products known as fosmidomycin [35] and FR900098 [36] belong to the phosphonate class of molecules and are well characterized inhibitors of MEP synthase, the enzyme responsible for catalyzing the first committed step in the MEP pathway (Fig. 1). Fosmidomycin is currently undergoing clinical trials due to its demonstrated inhibitory activity against a variety of Gram-negative and Gram-positive bacteria, as well as malaria parasites [37], [7]. The phosphonate inhibitors are actively transported into cells via a glycerol-3-phosphate transporter (GlpT, [38]), although lipophilic phosphonate prodrugs have proven highly effective MEP pathway inhibitors against pathogens lacking the GlpT protein (e.g. *Mycobacterium tuberculosis* [39] [40]). A BLAST search with the *E. coli* GlpT sequence (accession P08194) identifies a homologous transport protein in the *Y. pestis* CO92 proteome (YP_002347496; 18% identity/33% homology to the *E. coli* GlpT sequence). To evaluate the effectiveness of MEP pathway inhibition in *Y. pestis*, a growth inhibition assay was performed using FR900098. As depicted in Figure 2, FR900098 clearly inhibits *Y. pestis* proliferation in a dose-dependent manner, with half maximal inhibition (IC_{50}) at 29 μM (6.4 μg/mL), comparable to the potency observed with ampicillin (Figure S1) and to the activity of fosmidomycin with *F. tularensis* (12.1 μM; [26]). Hence, MEP pathway inhibition appears to be a valid and effective means of inhibiting the propagation of *Y. pestis*. Thus, to facilitate the development of novel MEP synthase inhibitors, we next cloned and characterized the *Y. pestis* enzyme.

Characterization of the *Y. pestis* MEP synthase

The 1197 bp MEP synthase gene (*ispC*; Gene ID: 1173888) was identified in the fully virulent *Y. pestis* subsp. *orientalis* str. CO92 genome sequence (NC_003143.1) through its homology with other known *ispC* gene sequences. The predicted amino acid sequence of the CO92 MEP synthase is identical to those predicted from the

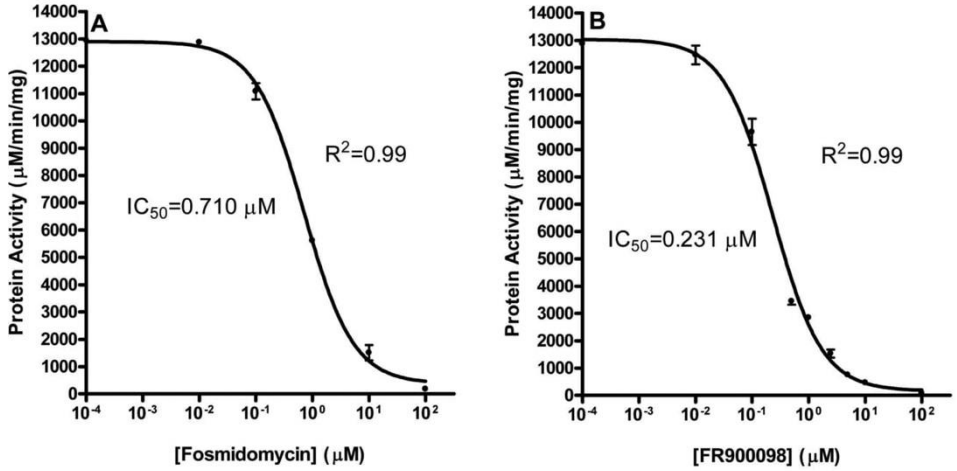

Figure 6. Dose-dependent inhibition of the *Y. pestis* MEP synthase. IC_{50} values were determined using A) fosmidomycin or B) FR900098. The R^2 value for each plot is indicated. Assays were performed in duplicate.
doi:10.1371/journal.pone.0106243.g006

genomes of the virulent KIM 10+ and avirulent A1122 *Y. pestis* strains (NC_004088.1 and NC_017168.1, respectively), encoding a projected 43.1 kDa protein. Figure S2 displays a primary sequence alignment of the *Y. pestis* MEP synthase with several bacterial homologs, highlighting the conservation among the family of enzymes. In particular, active site catalytic residues are strictly conserved across the enzymes, as is the serine residue identified previously as a potential site of phosphoregulation [26]. Figure S3 presents a predicted tertiary structure of the *Y. pestis* MEP synthase, homology-modeled using I-TASSER. Overall, the predicted topology of the enzyme active site is highly conserved with those seen in the structurally resolved MEP synthases [41], [42]. However, subtle but notable differences are observed. Most significantly, the positioning of histidine 209, an active site residue known to coordinate the phosphonate moiety of fosmidomycin in the *M. tuberculosis* MEP synthase [43], is more akin to that

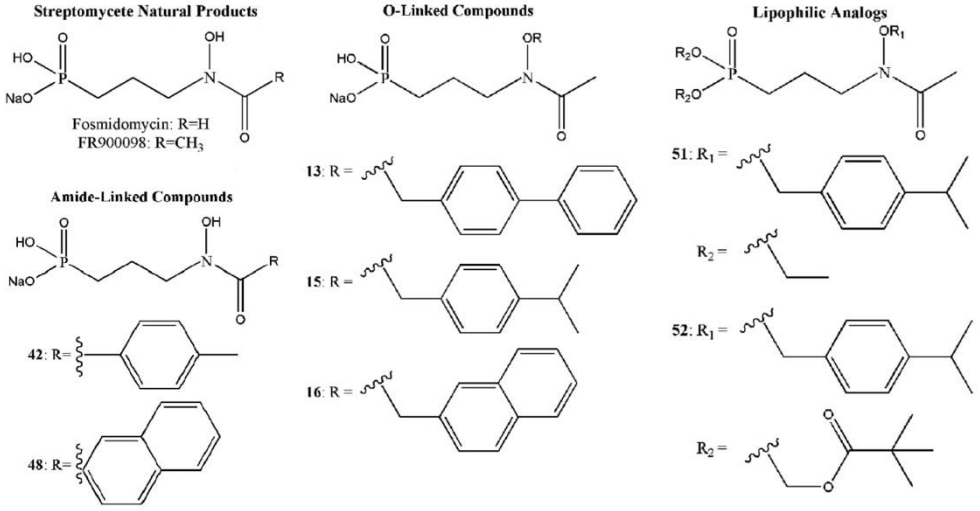

Figure 7. MEP synthase inhibitors. The structures of fosmidomycin, FR900098, and select rationally designed amide-linked and O-linked inhibitors are shown, including lipophilic prodrug analogs of compound **15**.
doi:10.1371/journal.pone.0106243.g007

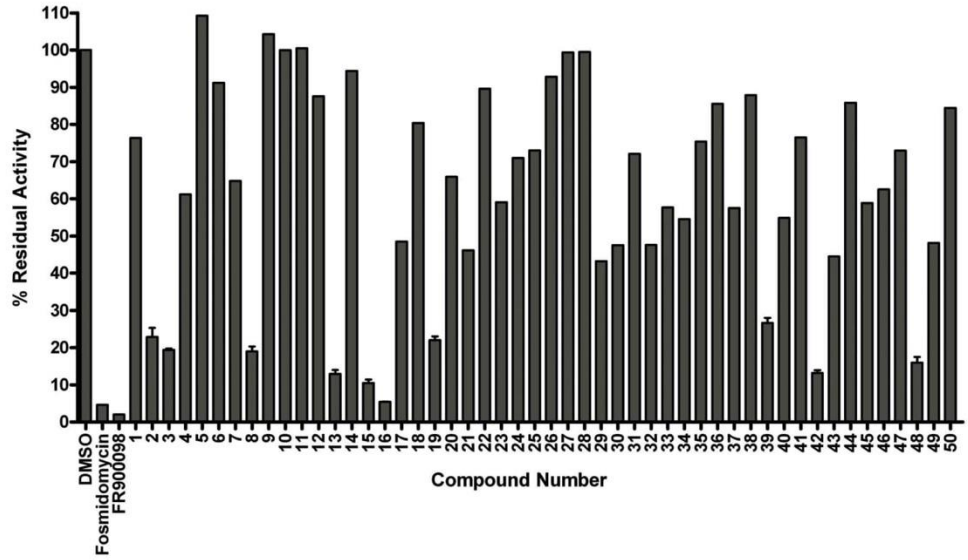

Figure 8. Screening a rationally designed molecular library. The *Y. pestis* MEP synthase was assayed in the presence of 100 μM of the indicated inhibitor. Residual activity is relative to the assay performed with vehicle alone (DMSO). All assays were performed in duplicate. Of those compounds tested, five inhibit the enzymatic activity by >75%, including compounds **13**, **15**, **16**, **42**, and **48**.
doi:10.1371/journal.pone.0106243.g008

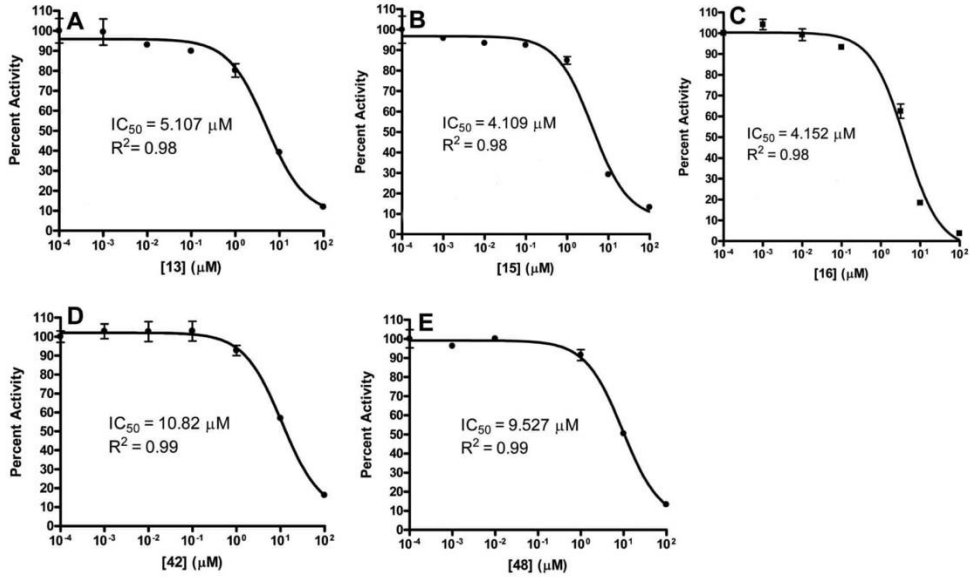

Figure 9. Dose-response plot of *Y. pestis* MEP synthase with the top five rationally designed inhibitors; compounds A) 13, B) 15, C) 16, D) 42 and E) 48. Assays were performed by combining the enzyme with 150 μM NADPH, followed by addition of the inhibitor. After five minute incubation at 37°C, substrate was added to initiate the reaction. The R^2 value for each plot is indicated. The enzymatic activity is relative to an uninhibited control. All assays were performed in duplicate.
doi:10.1371/journal.pone.0106243.g009

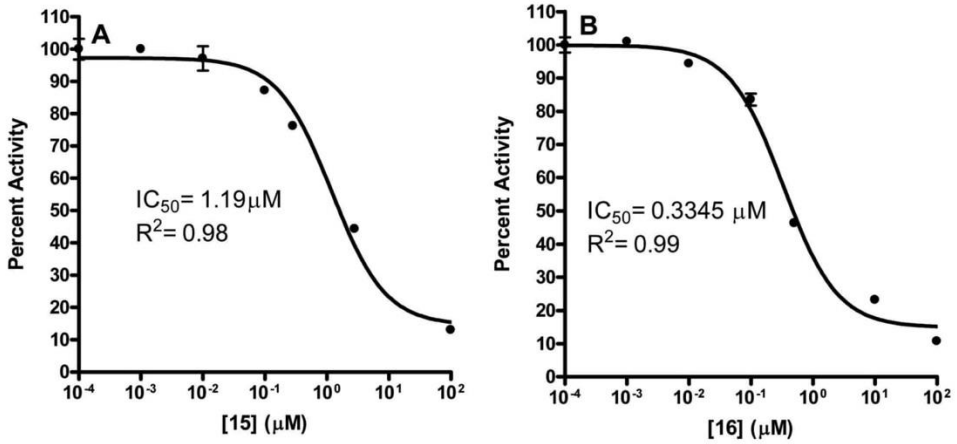

Figure 10. Dose-response plot of the *Y. pestis* MEP synthase when preincubated with the inhibitor. Assays were performed by combining the enzyme with either A) compound **15** or B) compound **16** and preincubating at 37°C for 10 min before addition of NADPH and DXP. All assays were performed in duplicate. Activity of the enzyme is relative to an uninhibited control.
doi:10.1371/journal.pone.0106243.g010

observed in the *E. coli* homolog, wherein this histidine does not specifically associate with the phosphonate [44]. While the predicted structural differences may simply be a consequence of computational modeling, the slight alterations in active site topology might account for differences observed among the derived kinetic constants and the relative potency of inhibitors with the various homologs of MEP synthase (as described below).

To enable the enzymatic characterization of the *Y. pestis* MEP synthase, the CO92 *ispC* gene was cloned into the pET101/D expression vector, transformed into *E. coli* BL21(DE3) codon plus RIL cells, and the resulting recombinant protein was affinity

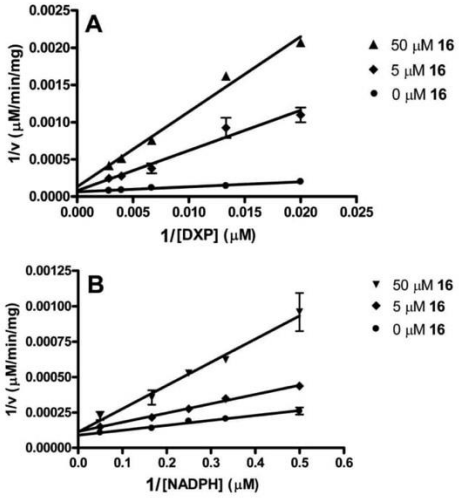

Figure 11. Mode of inhibition by compound 16. The Lineweaver–Burk plots indicate that compound **16** is competitive with respect to DXP (A) and competitive with respect to NADPH (B). All assays were performed in duplicate using purified *Y. pestis* MEP synthase. The enzyme was not preincubated with compound **16**, in contrast to Figure 12.
doi:10.1371/journal.pone.0106243.g011

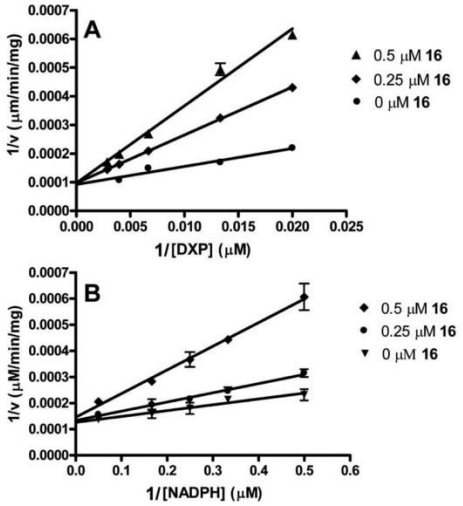

Figure 12. Mode of inhibition with preincubation. When the *Y. pestis* MEP synthase is preincubated with compound **16** (37°C, 10 min) prior to the addition of NADPH and DXP, the Lineweaver–Burk plots still indicate that compound **16** is competitive with respect to DXP (A) and NADPH (B). All assays were performed in duplicate.
doi:10.1371/journal.pone.0106243.g012

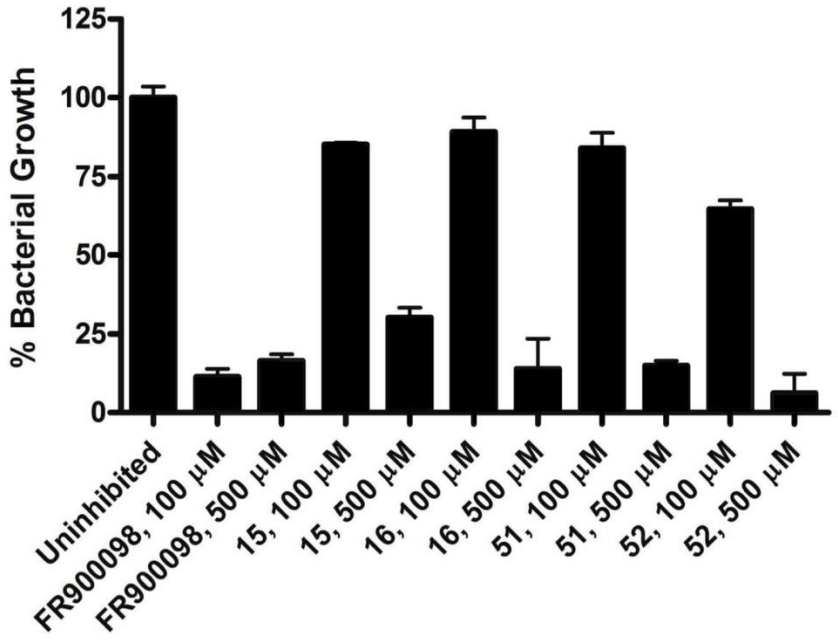

Figure 13. Growth inhibition assay with liquid cultures of *Y. pestis*. *Y. pestis* A1122 was cultured in the presence of either 100 µM or 500 µM of the indicated inhibitor. Bacterial growth is relative to an uninhibited culture. All assays were performed in triplicate. At 500 µM, compounds **15**, **16**, **51**, and **52** have inhibitory activity comparable to FR900098, however relatively poor inhibitory activity is observed at 100 µM. See text for further discussion.
doi:10.1371/journal.pone.0106243.g013

purified to near homogeneity via a C-terminal histidine tag (Figure 3). The catalytic activity of the purified recombinant enzyme was determined by a spectrophotometric assay monitoring the substrate dependent oxidation of NADPH (Fig. 1C). Nonlinear regression fitting of enzyme velocity versus substrate concentration was used to determine the apparent kinetic constants (Figure 4 and Table 1). The K_M^{app} for 1-deoxy-D-xylulose 5-phosphate (DXP) was obtained using assays performed with a saturating concentration of NADPH (150 µM), whereas the K_M^{app} for NADPH was determined using assays with 400 µM DXP. In general, the recombinant *Y. pestis* MEP synthase has $K_M^{app,DXP}$ *and* $K_M^{app,NADPH}$ values that are comparable to those reported for homologous enzymes from other organisms (Table 1). The apparent specificity constant (K_{cat}^{DXP}/K_M^{DXP}) is also similar to the *Francisella*, *Mycobacterium*, and *Synechocystis* enzymes, although it is nearly 50 fold lower than that reported for the *E. coli* enzyme, predominantly due to the difference in K_{cat}^{DXP}. An evaluation of various divalent cations reveals that recombinant *Y. pestis* MEP synthase can equally use Mg^{2+} or Mn^{2+} (Figure 5), in contrast to the *F. tularensis* enzyme, which demonstrates a clear preference for Mg^{2+} [26], and the *E. coli* enzyme which can utilize Mg^{2+}, Mn^{2+}, or Co^{2+} [45]. The *M. tuberculosis* enzyme, initially thought to be strictly dependent upon Mg^{2+} [46], was also shown to utilize Mn^{2+} ([47], [43]).

We next determined the susceptibility of the *Y. pestis* MEP synthase to the phosphonate inhibitors fosmidomycin and FR900098. The resolved crystal structures of *M. tuberculosis* MEP synthase co-crystalized with either fosmidomycin [43] or FR900098 [34] reveal a slight steric clash among an active site tryptophan residue and the ketone methyl group of FR900098, which is reflected in the corresponding half maximal inhibitory concentration (IC_{50}) of fosmidomycin (80 nM) and FR900098 (160 nM) [48]. However, this phenomenon appears unique to the *M. tuberculosis* enzyme, as FR900098 is more potent than fosmidomycin when assayed with the MEP synthase from *F. tularensis* [26], *P. falciparum* [49], and Synechocytis sp. PCC6803 [50] and is comparable in potency to fosmidomycin with the MEP synthase from *E. coli* [49] and *P. aeruginosa* [51]. In agreement with this consensus, as depicted in Figure 6, while the efficacy (E_{max}) of the two inhibitors are nearly identical, FR900098 demonstrates greater potency with the *Y. pestis* MEP synthase than does fosmidomycin, with IC_{50} values of 231 nM and 710 nM, respectively. Furthermore, this preference is further apparent in comparison of the measured inhibition constants, with a K_i^{fos} of 968 nM and $K_i^{FR900098}$ of 170 nM (Table 1 and Figure S4). Hence, while there appear to be subtle nuances in the active site topology of the *M. tuberculosis* MEP synthase that confers specificity for fosmidomycin, the *Y. pestis* MEP synthase demonstrates a clear preference for FR900098, as is also observed with the other aforementioned orthologs.

Molecular Library Screening

We next sought to evaluate the amenability of the *Y. pestis* MEP synthase in a high throughput screening format. The quality and

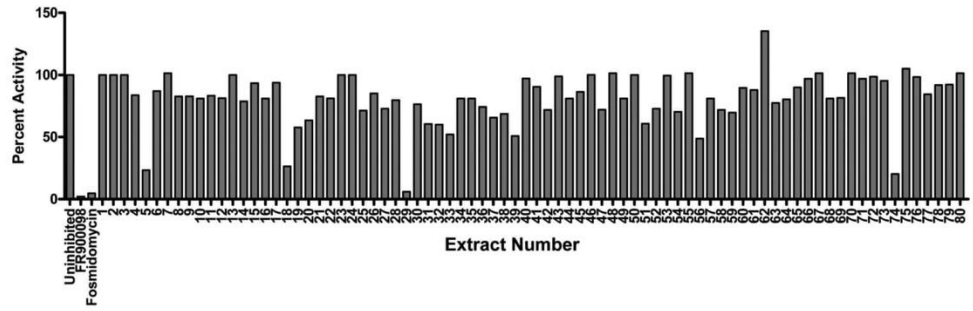

Figure 14. Screening of a natural product library. The *Y. pestis* MEP synthase was assayed in the presence of ca. 75 μg/mL of the indicated extract. Residual activity is relative to the assay performed with vehicle alone (DMSO). Assays with fosmidomycin and FR900098 were performed with 100 μM inhibitor. All assays were performed in duplicate. Of those compounds tested, four inhibit the enzymatic activity by >75%, including e5, e18, e29, and e74. The activity of e29 is comparable to that of fosmidomycin.
doi:10.1371/journal.pone.0106243.g014

robustness of an enzyme assay are important considerations for the reliable screening of a molecular library, and are typically described in terms of the Z-factor [52]. Ideally, an assay should have a large dynamic range (the difference between the uninhibited and inhibited signals) and small standard deviation across replicates, which corresponds to a Z-factor score near a value of 1 (an assay with a Z-factor score between 0.5 and 1.0 is considered excellent for screening). To determine the Z-factor for the spectrophotometric assay using the *Y. pestis* MEP synthase, we fixed the DXP concentration to the K_M, used a saturating concentration of NADPH (150 mM), and evaluated three separate lots of purified enzyme in a series of assays performed over three consecutive days. FR900098 was used as a positive control for inhibition. The Z-factor was determined to be 0.9, indicative of an assay well suited for library screening.

Rational Library Screening

To further assess the *Y. pestis* MEP synthase in a screening platform, we screened two pilot scale molecular libraries for inhibitory activity. The first library consists of 50 rationally designed synthetic compounds, primarily modeled on the structures of the *M. tuberculosis* MEP synthase in complex with fosmidomycin or FR900098 ([43], [34]). As introduced elsewhere [33], the strategy for the synthesis of this library was to create novel compounds with either amide- or O-linked substituents appended to the retrohydroxamate moiety of fosmidomycin/FR900098, thereby targeting the two major binding sites in MEP synthase; the fosmidomycin/DXP site and the NADPH site, bridging these adjacent sites to yield a highly specific ligand. Select structures of the inhibitors are shown in Figure 7. As anticipated, when screening this rational library against the purified *Y. pestis* MEP synthase, several of the compounds were found to demonstrate significant inhibitory activity (>75% inhibition), as illustrated in Figure 8. The top five inhibitors were subsequently evaluated in dose-response assays (Figure 9), with compounds **15** and **16** demonstrating the greatest potency. Due to the potential for competitive bisubstrate inhibition, we also evaluated **15** and **16** by preincubating the enzyme with inhibitor prior to the addition of NADPH or DXP (in contrast to the assays depicted in Figure 9, wherein the enzyme was concomitantly exposed to NADPH and the inhibitor). As shown in Figure 10, the resulting IC_{50} values for compounds **15** and **16** improve approximately 3- and 12-fold, respectively, supportive of competitive inhibition relative to both NADPH and DXP. It is particularly noteworthy that the IC_{50} for compound **16** (0.3345 μM) approximates one half of the MEP synthase concentration used in the assay, indicative of a tight-binding inhibitor.

To further explore if compound **16** inhibits by occupying both the DXP and NADPH binding sites, we next performed inhibitor modality assays with the purified *Y. pestis* MEP synthase. Catalysis by MEP synthase involves an ordered bi bi reaction mechanism, wherein NADPH must bind to the enzyme before DXP [45]. This mechanism is indicative of an underlying conformation change accompanying the binding of NADPH, thereby resulting in the formation of the DXP binding site. Accordingly, relative to DXP, fosmidomycin and FR900098 are competitive inhibitors of MEP synthase, while they are uncompetitive with respect to the binding of NADPH [45] [33] (Figure S5). Hence, NADPH must first bind to the enzyme before fosmidomycin/FR900098 can compete with DXP for its binding site.

In light of the fosmidomycin and FR900098 mechanism of inhibition, and given the anticipated mechanism for the bisubstrate inhibitor **16**, we performed mode of inhibition assays in each of two ways; the first with **16** added after preincubating the enzyme with NADPH (Figure 11) and the second with compound **16** preincubated with the enzyme prior to the addition of any other substrates (Figure 12). As illustrated in Figures 11 and 12, compound **16** is competitive with respect to DXP and competitive with respect to NADPH, under either of the two assay conditions. Thus, in contrast to fosmidomycin and FR900098, compound **16** does not require the initial binding of NADPH to the enzyme. In fact, as it competes with NADPH for a binding site, its activity is more potent when preincubated with MEP synthase in the absence of NADPH (contrast the concentrations of **16** used in the plots shown in Figures 11 and 12). Due to its ability to bind to the NADPH site, compound **16** appears capable of promoting the same structural change in the enzyme as does NADPH, causing the ensuing formation of the DXP binding site. Consequently, compound **16** behaves as a tightly bound inhibitor, binding to the NADPH site and causing a conformation change that subsequently "locks" the inhibitor into the DXP site. Further exploration of this mechanism is currently underway.

Satisfied that the *Y. pestis* MEP synthase performed well in the pilot scale high throughput screen, we next sought to complete our evaluation of the rational library by determining if compounds **15** and **16** would make good lead molecules for subsequent drug

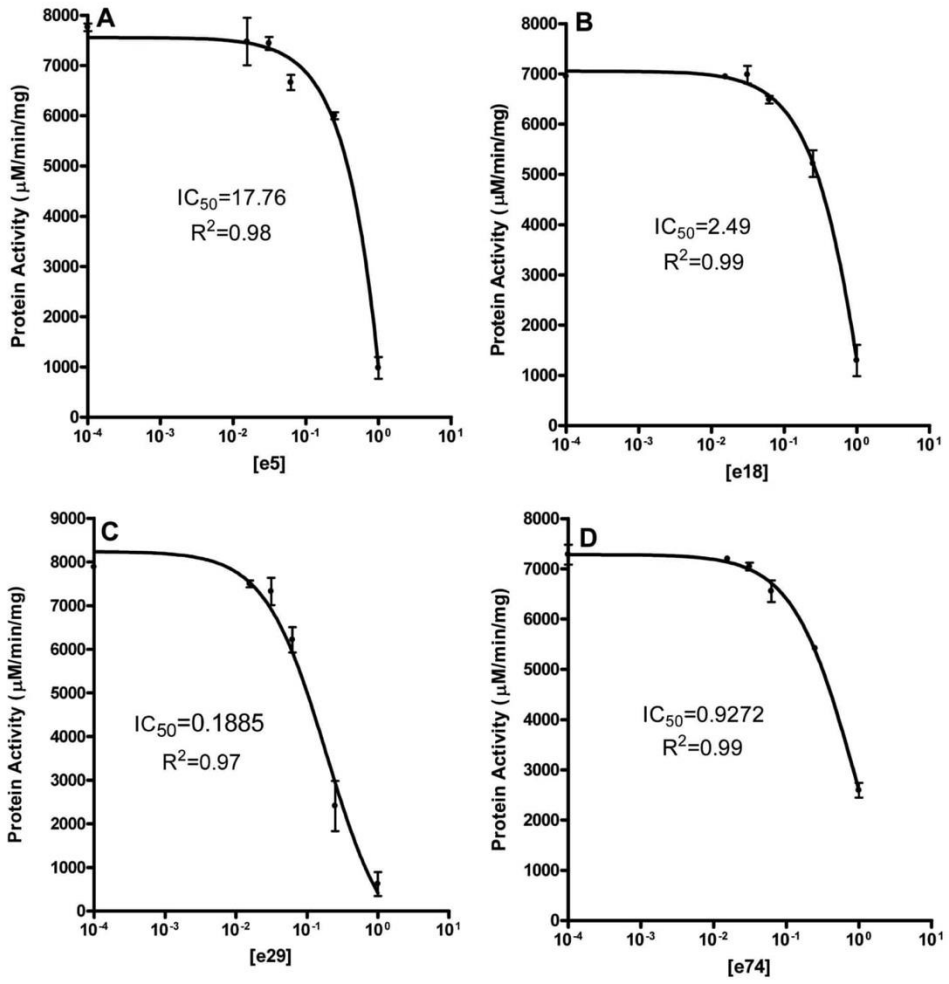

Figure 15. Dose-response plots of the *Y. pestis* MEP synthase with the top four natural product extracts. The enzyme was assayed with various concentrations of A) e5, B) e18, C) e29, or D) e74 and the resulting activity plotted as a function of extract concentration. The concentration of each extract stock solution, ca. 15 mg/mL, is defined as 1 and serial dilutions from these stocks were then used for the analysis. R^2 and IC_{50} values are indicated. All assays were performed in duplicate.
doi:10.1371/journal.pone.0106243.g015

development. Secondary to the enzyme assays, compounds **15** and **16** were next evaluated in a growth inhibition assay with liquid cultures of *Y. pestis* A1122. As shown in Figure 13, relative to FR900098, compounds **15** and **16** demonstrate measurable but modest inhibitory activity towards *Y. pestis*. Given the potent activity of these compounds towards the isolated enzyme, we speculated that the relatively poor activity towards whole cells might reflect cell permeability limitations. However, as seen in Fig. 13, inhibitory activity is not dramatically improved with lipophilic ester derivatives of compound **15** (compounds **51** and **52**), suggesting that compound efflux and/or intracellular instability may impact the effective concentration of the inhibitor. While further investigation is required to deduce the specific details pertaining to the activity of compounds **15** and **16**, our pilot scale screening of a rational library demonstrates the amenability of the *Y. pestis* MEP synthase to high throughput screening (and underscores the importance of the secondary screen in lead molecule selection).

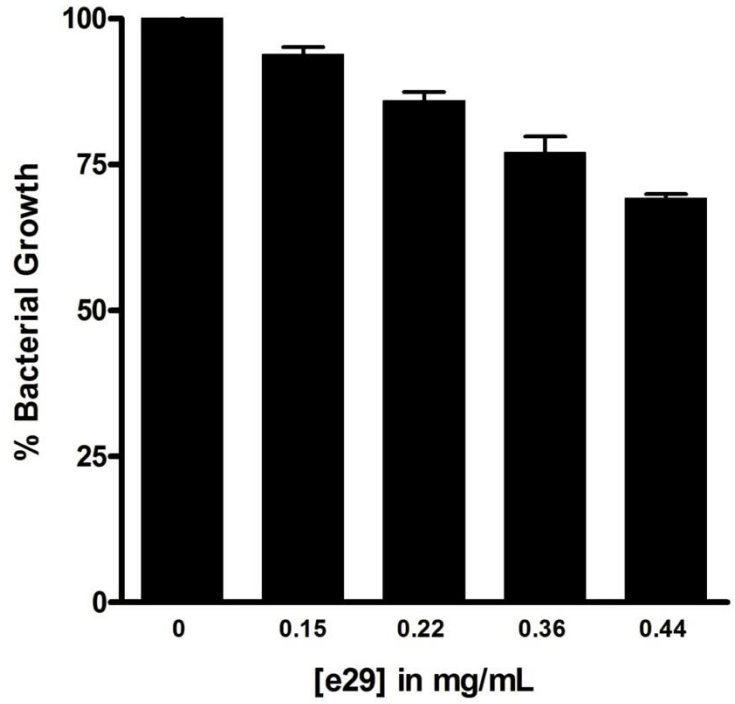

Figure 16. *Yersinia pestis* **growth inhibition assay with extract 29.** *Y. pestis* A1122 was cultured in the presence of e29 at the indicated concentrations. Bacterial growth is relative to an uninhibited culture. All assays were performed in duplicate. The extract inhibits bacterial growth in a dose-dependent fashion.
doi:10.1371/journal.pone.0106243.g016

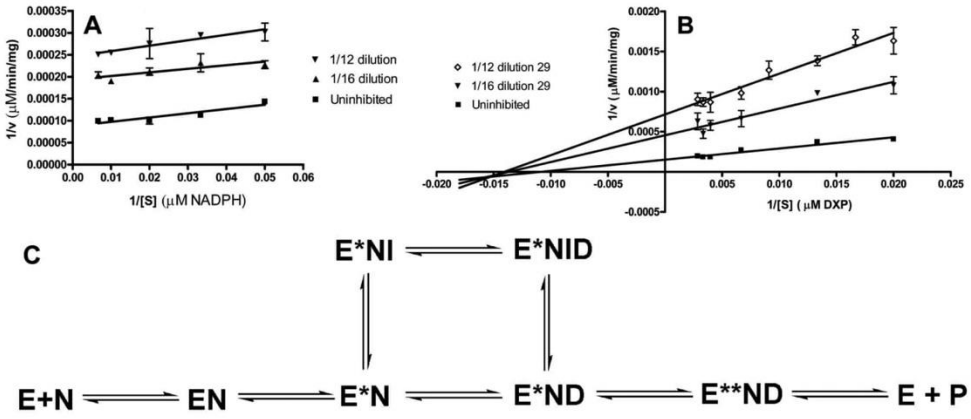

Figure 17. Mechanism of inhibition by e29. A) Relative to NADPH, e29 is an uncompetitive inhibitor of the purified *Y. pestis* MEP synthase. B) Relative to DXP, e29 is a noncompetitive inhibitor. C) A model of e29 inhibition. MEP synthase (E) undergoes a conformational change (E*) upon binding of NADPH (N), exposing an allosteric site to which the inhibitor (I) binds. As the inhibitor is noncompetitive with respect to DXP (D), I may bind the E*N or E*ND complex, thereby inhibiting the enzyme.
doi:10.1371/journal.pone.0106243.g017

Natural Product Library Screening

In addition to screening a rationally designed molecular library, we also screened our proprietary natural product library for inhibitory activity against the purified *Y. pestis* MEP synthase. This library contains 80 different extracts obtained from widely diverse biological sources. Each individual extract consists of a complex mixture of metabolites (a metabolome) isolated via a non-targeted organic extraction. As shown in Figure 14, four of the 80 extracts demonstrate significant inhibitory activity (>75% inhibition). Subsequent dose-response assays confirm this inhibitory activity and identify extract 29 (e29) as the most potent inhibitor among the four (Figure 15). A follow-on *Y. pestis* growth inhibition assay demonstrates the dose-dependent activity of e29 (Figure 16).

In light of its inhibitory activity, we next determined the e29 mechanism of action using the purified *Y. pestis* MEP synthase (Figure 17). While FR900098 is uncompetitive with respect to NADPH and competitive with respect to DXP (Figure S5), the binding of e29 is uncompetitive with respect to NADPH but noncompetitive with respect to DXP. As this represents an entirely new class of MEP synthase inhibitor, we performed additional, confirmatory assays with purified recombinant *F. tularensis* and *M. tuberculosis* MEP synthase, the results of which corroborate this discovery (Figure S6). Hence, e29 contains an active compound that serves as an allosteric inhibitor of MEP synthase (Figure 17C). To date, no such inhibitors of MEP synthase have been reported, making the inhibitory compound in e29 a novel class of inhibitor, and suggesting a new binding site on MEP synthase amenable to rational drug design. As MEP synthase regulates metabolic flux through the MEP pathway [53], we speculated that isopentenyl pyrophosphate (IPP), dimethylallyl pyrophosphate (DMAPP), and/or geranyl pyrophosphate (GPP) might serve as feedback inhibitors of the enzyme. Hence, we assayed the *Y. pestis* MEP synthase in the presence of each of these individual compounds at concentrations of 100, 500, and 1000 μM. No enzyme inhibition was observed under any of the assay conditions (data not shown). Thus, the active component of e29 is not likely to be any of these three isoprenoids. Effort is currently underway to isolate and identify the active component in e29.

Concluding Remarks

In response to the urgent need for novel antibiotics, MEP synthase has received considerable attention as a target for drug development. The *Y. pestis* MEP synthase demonstrates significant sequence conservation with its orthologous counterparts, therefore leading to a predicted tertiary structure that is comparable to crystallographic-defined structures of MEP synthase. However, structural comparison identifies subtle differences among the MEP synthase family, particularly within the active site of the *M. tuberculosis* homolog, thereby rationalizing the observed differences in measured inhibitor activity. These structural differences warrant further consideration when developing rationally designed broad spectrum antibiotics.

The screening of a rationally designed, synthetic, bisubstrate molecular library, developed from crystal structures of the *M. tuberculosis* MEP synthase, demonstrated the amenability of the *Y. pestis* MEP synthase to a screening campaign and identified several effective inhibitors of the purified enzyme. Subsequent mechanistic assays reveal that the most effective inhibitor (compound **16**) binds to both the NADPH and DXP sites, acting as a potent tight binding inhibitor of the enzyme. However, a growth inhibition secondary screen reveals that the whole-cell inhibitory activity of compound **16** is relatively poor, indicating the need for additional structure−activity relationship studies to elucidate the underlying etiology.

By screening a library of natural product extracts, we identified four biological mélanges containing an inhibitor of MEP synthase. The most potent extract, e29, reduced MEP synthase enzymatic activity by roughly 90% and demonstrated a dose-dependent inhibition of *Y. pestis* growth *in vitro*. While all previously reported MEP synthase inhibitors bind in the active site of the enzyme, the active component in e29 is the founding member of a new class of desirable allosteric inhibitors of the enzyme. Unlike competitive inhibitors of an enzyme, which lose potency as the substrate pools accumulate, an allosteric inhibitor maintains effectiveness while metabolic flux through the pathway is impeded.

Supporting Information

Figure S1 Dose-response plot of *Y. pestis* growth as a function of ampicillin concentration. Fractional growth is calculated as the ratio of cell density (OD_{600}) in the presence of inhibitor to cell density in the absence of inhibitor. Ampicillin is an FDA approved inhibitor of bacterial transpeptidase, resulting in the disruption of cell wall biosynthesis. Nonlinear regression fitting was performed, resulting in an IC_{50} of 10.8 μM (3.8 μg/mL). The goodness-of-fit (R^2) value is indicated.
(TIF)

Figure S2 Sequence alignment of various MEP synthase homologs using Clustal Omega, where identical residues are denoted by an asterisk (*) and chemically similar residues are denoted by a colon (:). Each residue involved in catalysis [43] is colored based on the substrate or cofactor with which it primarily interacts, with residues in pink associating with NADPH, residues in blue associating with DXP, and residues in yellow coordinating the divalent cation. The serine residue boxed in red was identified in [26] as a possible phosphorylation site used for regulation of the enzyme.
(TIF)

Figure S3 Structural features of the *Y. pestis* MEP synthase. A) Predicted structure of the *Y. pestis* MEP synthase, homology modeled using templates selected by I-TASSER's threading alignment algorithm. A cartoon representation of the tertiary structure is shown, with alpha helices colored pink, beta sheets colored yellow, and coiled regions colored white. Residues comprising the substrate binding site (colored dark blue with backbone and sidechain residues shown) were identified via primary sequence alignment and the resolved structure of *M. tuberculosis* MEP synthase [43]. B) Overlay of the predicted *Y. pestis* MEP synthase (shown as a cartoon representation) and the resolved crystal structure of the *E. coli* MEP synthase (PBD 2EGH; shown as a purple ribbon). The two structures are highly similar, with a TM-score of 0.996 and a RMSD of 0.46. C) ProQ2 was used to evaluate the quality of the *Y. pestis* MEP synthase model, providing scores ranging from 0 (unreliable) to 1 (reliable). Regions of the model scoring <0.5 are colored light blue in the structure shown in A), and are comprised of residues 1, 301, 303, 397, and 398.
(TIFF)

Figure S4 Graphical determination of the inhibition constant. Because fosmidomycin and FR900098 are slow, tight binding inhibitors, the *Y. pestis* MEP synthase was preincubated with the inhibitor for 10 minutes prior to addition of substrate. The absolute value of the X intercept of the line produced from linear regression fitting the plot of $K_M^{app,DXP}$ as a function of inhibitor concentration defined the K_i as 968 nM and 170 nM for

fosmidomycin and FR900098, respectively. The R^2 values are indicated.
(TIF)

Figure S5 Mode of inhibition by FR900098. The Lineweaver–Burk plots indicate that FR900098 is uncompetitive with respect to NADPH (A), but competitive with respect to DXP (B). All assays were performed in duplicate using purified *Y. pestis* MEP synthase.
(TIF)

Figure S6 Mode of inhibition by e29. The Lineweaver–Burk plots generated from assays with purified *F. tularensis* MEP synthase (A and B) or purified *M. tuberculosis* MEP synthase (C and D) indicate that e29 is uncompetitive with respect to NADPH and noncompetitive with respect to DXP.
(TIFF)

Author Contributions

Conceived and designed the experiments: RC CD. Performed the experiments: AH CJ TD BS KV RY CJM TP JB GSJ ERJ. Analyzed the data: AH CJ TD RC CD GSJ ERJ. Contributed reagents/materials/analysis tools: RC CD. Contributed to the writing of the manuscript: RC AH CD.

References

1. Raoult D, Aboudharam G, Crubézy E, Larrouy G, Ludes B, et al. (2000) Molecular identification by "suicide PCR" of Yersinia pestis as the agent of Medieval Black Death. Proc Natl Acad Sci 97: 12800–12803. doi:10.1073/pnas.220225197.
2. Haensch S, Bianucci R, Signoli M, Rajerison M, Schultz M, et al. (2010) Distinct Clones of Yersinia pestis Caused the Black Death. PLoS Pathog 6: e1001134. doi:10.1371/journal.ppat.1001134.
3. Brown AC, Parish T (2008) Dxr is essential in Mycobacterium tuberculosis and fosmidomycin resistance is due to a lack of uptake. BMC Microbiol 8: 78. doi:10.1186/1471-2180-8-78.
4. Gallagher LA, Ramage E, Jacobs MA, Kaul R, Brittnacher M, et al. (2007) A comprehensive transposon mutant library of Francisella novicida, a bioweapon surrogate. Proc Natl Acad Sci 104: 1009–1014. doi:10.1073/pnas.0606713104.
5. Baba T, Ara T, Hasegawa M, Takai Y, Okumura Y, et al. (2006) Construction of Escherichia coli K-12 in-frame, single-gene knockout mutants: the Keio collection. Mol Syst Biol 2: 2006.0008. doi:10.1038/msb4100050.
6. Cameron DE, Urbach JM, Mekalanos JJ (2008) A defined transposon mutant library and its use in identifying motility genes in Vibrio cholerae. Proc Natl Acad Sci 105: 8736–8741. doi:10.1073/pnas.0803281105.
7. Singh N, Chevé G, Avery MA, McCurdy CR (2007) Targeting the methyl erythritol phosphate (MEP) pathway for novel antimalarial, antibacterial and herbicidal drug discovery: inhibition of 1-deoxy-D-xylulose-5-phosphate reductoisomerase (DXR) enzyme. Curr Pharm Des 13: 1161–1177.
8. Rohdich F, Bacher A, Eisenreich W (2005) Isoprenoid biosynthetic pathways as anti-infective drug targets. Biochem Soc Trans 33: 785. doi:10.1042/BST0330785.
9. Rohmer M (2008) From molecular fossils of bacterial hopanoids to the formation of isoprene units: discovery and elucidation of the methylerythritol phosphate pathway. Lipids 43: 1095–1107. doi:10.1007/s11745-008-3261-7.
10. Moore RN, Bigam G, Chan JK, Hogg AM, Nakashima TT, et al. (1985) Biosynthesis of the hypocholesterolemic agent mevinolin by Aspergillus terreus. Determination of the origin of carbon, hydrogen, and oxygen atoms by carbon-13 NMR and mass spectrometry. J Am Chem Soc 107: 3694–3701. doi:10.1021/ja00298a046.
11. Alberts AW (1988) Discovery, biochemistry and biology of lovastatin. Am J Cardiol 62: J10–J15. doi:10.1016/0002-9149(88)90002-1.
12. Smith JM, Warrington NV, Vierling RJ, Kuhn ML, Anderson WF, et al. (2014) Targeting DXP synthase in human pathogens: enzyme inhibition and antimicrobial activity of butylacetylphosphonate. J Antibiot (Tokyo) 67: 77–83. doi:10.1038/ja.2013.105.
13. Matsue Y, Mizuno H, Tomita T, Asami T, Nishiyama M, et al. (2010) The herbicide ketoclomazone inhibits 1-deoxy-D-xylulose 5-phosphate synthase in the 2-C-methyl-D-erythritol 4-phosphate pathway and shows antibacterial activity against Haemophilus influenzae. J Antibiot (Tokyo) 63: 583–588. doi:10.1038/ja.2010.100.
14. Jackson ER, Dowd CS (2012) Inhibition of 1-deoxy-D-xylulose-5-phosphate reductoisomerase (Dxr): a review of the synthesis and biological evaluation of recent inhibitors. Curr Top Med Chem 12: 706–728.
15. Kunfermann A, Witschel M, Illarionov B, Martin R, Rottmann M, et al. (2014) Pseudilins: halogenated, allosteric inhibitors of the non-mevalonate pathway enzyme IspD. Angew Chem Int Ed Engl 53: 2235–2239. doi:10.1002/anie.201309557.
16. Witschel MC, Höffken HW, Seet M, Parra L, Mietzner T, et al. (2011) Inhibitors of the herbicidal target IspD: allosteric site binding. Angew Chem Int Ed Engl 50: 7931–7935. doi:10.1002/anie.201102281.
17. Tidten-Luksch N, Grimaldi R, Torrie LS, Frearson JA, Hunter WN, et al. (2012) IspE Inhibitors Identified by a Combination of In Silico and In Vitro High-Throughput Screening. PLoS ONE 7: e35792. doi:10.1371/journal.pone.0035792.
18. Tang M, Odejinmi SI, Allette YM, Vankayalapati H, Lai K (2011) Identification of novel small molecule inhibitors of 4-diphosphocytidyl-2-C-methyl-D-erythritol (CDP-ME) kinase of Gram-negative bacteria. Bioorg Med Chem 19: 5886–5895. doi:10.1016/j.bmc.2011.08.012.
19. Ramsden NL, Buetow L, Dawson A, Kemp LA, Ulaganathan V, et al. (2009) A structure-based approach to ligand discovery for 2C-methyl-D-erythritol-2,4-cyclodiphosphate synthase: a target for antimicrobial therapy. J Med Chem 52: 2531–2542. doi:10.1021/jm801475n.
20. Zhang Z, Jakkaraju S, Blain J, Gogol K, Zhao L, et al. (2013) Cytidine derivatives as IspF inhibitors of Burkolderia pseudomallei. Bioorg Med Chem Lett 23: 6860–6863. doi:10.1016/j.bmcl.2013.09.101.
21. Nakagawa K, Takada K, Imamura N (2013) Probable novel MEP pathway inhibitor and its binding protein, IspG. Biosci Biotechnol Biochem 77: 1449–1454.
22. Wang W, Oldfield E (2014) Bioorganometallic chemistry with IspG and IspH: structure, function, and inhibition of the [Fe(4)S(4)] proteins involved in isoprenoid biosynthesis. Angew Chem Int Ed Engl 53: 4294–4310. doi:10.1002/anie.201306712.
23. Span I, Wang K, Eisenreich W, Bacher A, Zhang Y, et al. (2014) Insights into the Binding of Pyridines to the Iron-Sulfur Enzyme IspH. J Am Chem Soc. doi:10.1021/ja501127j.
24. Janthawornpong K, Krasutsky S, Chaignon P, Rohmer M, Poulter CD, et al. (2013) Inhibition of IspH, a [4Fe-4S]2+ enzyme involved in the biosynthesis of isoprenoids via the methylerythritol phosphate pathway. J Am Chem Soc 135: 1816–1822. doi:10.1021/ja309557s.
25. Gräwert T, Groll M, Rohdich F, Bacher A, Eisenreich W (2011) Biochemistry of the non-mevalonate isoprenoid pathway. Cell Mol Life Sci CMLS 68: 3797–3814. doi:10.1007/s00018-011-0753-z.
26. Jawaid S, Seidle H, Zhou W, Abdirahman H, Abadeer M, et al. (2009) Kinetic characterization and phosphoregulation of the Francisella tularensis 1-deoxy-D-xylulose 5-phosphate reductoisomerase (MEP synthase). PloS One 4: e8288. doi:10.1371/journal.pone.0008288.
27. Takahashi S, Kuzuyama T, Watanabe H, Seto H (1998) A 1-deoxy-d-xylulose 5-phosphate reductoisomerase catalyzing the formation of 2-C-methyl-d-erythritol 4-phosphate in an alternative nonmevalonate pathway for terpenoid biosynthesis. Proc Natl Acad Sci 95: 9879–9884. doi:10.1073/pnas.95.17.9879.
28. Andrew T Koppisch DTF (2002) E. coli MEP synthase: steady-state kinetic analysis and substrate binding. Biochemistry (Mosc) 41: 236–243.
29. Roy A, Kucukural A, Zhang Y (2010) I-TASSER: a unified platform for automated protein structure and function prediction. Nat Protoc 5: 725–738. doi:10.1038/nprot.2010.5.
30. Roy A, Yang J, Zhang Y (2012) COFACTOR: an accurate comparative algorithm for structure-based protein function annotation. Nucleic Acids Res 40: W471–W477. doi:10.1093/nar/gks372.
31. Zhang Y (2008) I-TASSER server for protein 3D structure prediction. BMC Bioinformatics 9: 40. doi:10.1186/1471-2105-9-40.
32. Ray A, Lindahl E, Wallner B (2012) Improved model quality assessment using ProQ2. BMC Bioinformatics 13: 224. doi:10.1186/1471-2105-13-224.
33. San Jose G, Jackson ER, Uh E, Johny C, Haymond A, et al. (2013) Design of Potential Bisubstrate Inhibitors against Mycobacterium tuberculosis (Mtb) 1-Deoxy-D-Xylulose 5-Phosphate Reductoisomerase (Dxr)-Evidence of a Novel Binding Mode. MedChemComm 4: 1099–1104. doi:10.1039/C3MD00085K.
34. Björkelid C, Bergfors T, Unge T, Mowbray SL, Jones TA (2012) Structural studies on Mycobacterium tuberculosis DXR in complex with the antibiotic FR-900098. Acta Crystallogr Sect D 68: 134–143. doi:10.1107/S0907444911052231.
35. Kuzuyama T, Shimizu T, Takahashi S, Seto H (1998) Fosmidomycin, a specific inhibitor of 1-deoxy-d-xylulose 5-phosphate reductoisomerase in the nonmevalonate pathway for terpenoid biosynthesis. Tetrahedron Lett 39: 7913–7916. doi:10.1016/S0040-4039(98)01755-9.
36. Okuhara M, Kuroda Y, Goto T, Okamoto M, Terano H, et al. (1980) Studies on new phosphonic acid antibiotics. I. FR-900098, isolation and characterization. J Antibiot (Tokyo) 33: 13–17.
37. Jomaa H, Wiesner J, Sanderbrand S, Altincicek B, Weidemeyer C, et al. (1999) Inhibitors of the nonmevalonate pathway of isoprenoid biosynthesis as antimalarial drugs. Science 285: 1573–1576.
38. Sakamoto Y, Furukawa S, Ogihara H, Yamasaki M (2003) Fosmidomycin resistance in adenylate cyclase deficient (cya) mutants of Escherichia coli. Biosci Biotechnol Biochem 67: 2030–2033.
39. Uh E, Jackson ER, San Jose G, Maddox M, Lee RE, et al. (2011) Antibacterial and antitubercular activity of fosmidomycin, FR900098, and their lipophilic

analogs. Bioorg Med Chem Lett 21: 6973–6976. doi:10.1016/j.bmcl.2011.09.123.
40. McKenney ES, Sargent M, Khan H, Uh E, Jackson ER, et al. (2012) Lipophilic prodrugs of FR900098 are antimicrobial against Francisella novicida in vivo and in vitro and show GlpT independent efficacy. PloS One 7: e38167. doi:10.1371/journal.pone.0038167.
41. Yajima S, Hara K, Iino D, Sasaki Y, Kuzuyama T, et al. (2007) Structure of 1-deoxy-D-xylulose 5-phosphate reductoisomerase in a quaternary complex with a magnesium ion, NADPH and the antimalarial drug fosmidomycin. Acta Crystallograph Sect F Struct Biol Cryst Commun 63: 466–470. doi:10.1107/S1744309107024475.
42. Umeda T, Tanaka N, Kusakabe Y, Nakanishi M, Kitade Y, et al. (2011) Molecular basis of fosmidomycin's action on the human malaria parasite Plasmodium falciparum. Sci Rep 1: 9. doi:10.1038/srep00009.
43. Henriksson LM, Unge T, Carlsson J, Aqvist J, Mowbray SL, et al. (2007) Structures of Mycobacterium tuberculosis 1-deoxy-D-xylulose-5-phosphate reductoisomerase provide new insights into catalysis. J Biol Chem 282: 19905–19916. doi:10.1074/jbc.M701935200.
44. Mac Sweeney A, Lange R, Fernandes RPM, Schulz H, Dale GE, et al. (2005) The crystal structure of E.coli 1-deoxy-D-xylulose-5-phosphate reductoisomerase in a ternary complex with the antimalarial compound fosmidomycin and NADPH reveals a tight-binding closed enzyme conformation. J Mol Biol 345: 115–127. doi:10.1016/j.jmb.2004.10.030.
45. Koppisch AT, Fox DT, Blagg BSJ, Poulter CD (2002) E. coli MEP synthase: steady-state kinetic analysis and substrate binding. Biochemistry (Mosc) 41: 236–243.
46. Dhiman RK, Schaeffer ML, Bailey AM, Testa CA, Scherman H, et al. (2005) 1-Deoxy-d-Xylulose 5-Phosphate Reductoisomerase (IspC) from Mycobacterium tuberculosis: towards Understanding Mycobacterial Resistance to Fosmidomycin. J Bacteriol 187: 8395–8402. doi:10.1128/JB.187.24.8395-8402.2005.
47. Humnabadkar V, Jha RK, Ghatnekar N, Sousa SMD (2011) A High-Throughput Screening Assay for Simultaneous Selection of Inhibitors of Mycobacterium tuberculosis 1-Deoxy-D-Xylulose-5-Phosphate Synthase (Dxs) or 1-Deoxy-D-Xylulose 5-Phosphate Reductoisomerase (Dxr). J Biomol Screen 16: 303–312. doi:10.1177/1087057110394845.
48. Andaloussi M, Henriksson LM, Wieckowska A, Lindh M, Björkelid C, et al. (2011) Design, synthesis, and X-ray crystallographic studies of α-aryl substituted fosmidomycin analogues as inhibitors of Mycobacterium tuberculosis 1-deoxy-D-xylulose 5-phosphate reductoisomerase. J Med Chem 54: 4964–4976. doi:10.1021/jm2000085.
49. Haemers T, Wiesner J, Poecke SV, Goeman J, Henschker D, et al. (2006) Synthesis of α-substituted fosmidomycin analogues as highly potent Plasmodium falciparum growth inhibitors. Bioorg Med Chem Lett 16: 1888–1891. doi:10.1016/j.bmcl.2005.12.082.
50. Woo Y-H, Fernandes RPM, Proteau PJ (2006) Evaluation of fosmidomycin analogs as inhibitors of the Synechocystis sp. PCC6803 1-dcoxy-D-xylulose 5-phosphate reductoisomerase. Bioorg Med Chem 14: 2375–2385. doi:10.1016/j.bmc.2005.11.012.
51. Altincicek B, Hintz M, Sanderbrand S, Wiesner J, Beck E, et al. (2000) Tools for discovery of inhibitors of the 1-deoxy-D-xylulose 5-phosphate (DXP) synthase and DXP reductoisomerase: an approach with enzymes from the pathogenic bacterium Pseudomonas aeruginosa. FEMS Microbiol Lett 190: 329–333. doi:10.1111/j.1574-6968.2000.tb09307.x.
52. Zhang Chung, Oldenburg (1999) A Simple Statistical Parameter for Use in Evaluation and Validation of High Throughput Screening Assays. J Biomol Screen 4: 67–73.
53. Carretero-Paulet L, Cairó A, Botella-Pavía P, Besumbes O, Campos N, et al. (2006) Enhanced flux through the methylerythritol 4-phosphate pathway in Arabidopsis plants overexpressing deoxyxylulose 5-phosphate reductoisomerase. Plant Mol Biol 62: 683–695. doi:10.1007/s11103-006-9051-9.
54. M JP, N GP (1983) Mechanism of action of beta-oxoacyl-CoA thiolase from rat liver cytosol. Direct evidence for the order of addition of the two acetyl-CoA molecules during the formation of acetoacetyl-CoA. Available: http://www.biochemj.org/bj/213/bj2130153.htm Accessed 15 August 2013.
55. Miziorko HM, Lane MD (1977) 3-Hydroxy-3-methylglutaryl-CoA synthase. Participation of acetyl-S-enzyme and enzyme-S-hydroxymethylglutaryl-SCoA intermediates in the reaction. J Biol Chem 252: 1414–1420.
56. Amdur BH, Rilling H, Bloch K (1957) The Enzymatic Conversion of Mevalonic Acid to Squalene. J Am Chem Soc 79: 2646–2647. doi:10.1021/ja01567a077.
57. BLOCH K, CHAYKIN S, PHILLIPS AH, DE WAARD A (1959) Mevalonic acid pyrophosphate and isopentenylpyrophosphate. J Biol Chem 234: 2595–2604.
58. Dhe-Paganon S, Magrath J, Abeles RH (1994) Mechanism of Mevalonate Pyrophosphate Decarboxylase: Evidence for a Carbocationic Transition State. Biochemistry (Mosc) 33: 13355–13362. doi:10.1021/bi00249a023.
59. Agranoff BW, Eggerer H, Henning U, Lynen F (1959) Isopentenol Pyrophosphate Isomerase. J Am Chem Soc 81: 1254–1255. doi:10.1021/ja01514a059.
60. Lange BM, Wildung MR, McCaskill D, Croteau R (1998) A family of transketolases that directs isoprenoid biosynthesis via a mevalonate-independent pathway. Proc Natl Acad Sci U S A 95: 2100–2104.
61. Julliard JH, Douce R (1991) Biosynthesis of the thiazole moiety of thiamin (vitamin B1) in higher plant chloroplasts. Proc Natl Acad Sci 88: 2042–2045. doi:10.1073/pnas.88.6.2042.
62. Julliard J-H (1992) Biosynthesis of the pyridoxal ring (vitamin B6) in higher plant chloroplasts and its relationship with the biosynthesis of the thiazole ring (vitamin B1). Comptes Rendus Académie Sci Sér 3 Sci Vie 314: 285–290.
63. Hill RE, Sayer BG, Spenser ID (1989) Biosynthesis of vitamin B6: incorporation of D-1-deoxyxylulose. J Am Chem Soc 111: 1916–1917. doi:10.1021/ja00187a076.
64. Hill RE, Himmeldirk K, Kennedy IA, Pauloski RM, Sayer BG, et al. (1996) The Biogenetic Anatomy of Vitamin B6 A 13C NMR Investigation of the Biosynthesis of Pyridoxol in Escherichia Coli. J Biol Chem 271: 30426–30435. doi:10.1074/jbc.271.48.30426.
65. Rohdich F, Wungsintaweekul J, Fellermeier M, Sagner S, Herz S, et al. (1999) Cytidine 5′-triphosphate-dependent biosynthesis of isoprenoids: YgbP protein of Escherichia coli catalyzes the formation of 4-diphosphocytidyl-2-C-methylerythritol. Proc Natl Acad Sci U S A 96: 11758–11763.
66. Kuzuyama T, Takagi† M, Kaneda K, Dairi T, Seto H (2000) Formation of 4-(cytidine 5′-diphospho)-2-C-methyl-d-erythritol from 2-C-methyl-d-erythritol 4-phosphate by 2-C-methyl-d-erythritol 4-phosphate cytidylyltransferase, a new enzyme in the nonmevalonate pathway. Tetrahedron Lett 41: 703–706. doi:10.1016/S0040-4039(99)02143-7.
67. Kuzuyama T, Takagi † M, Kaneda K, Watanabe H, Dairi T, et al. (2000) Studies on the nonmevalonate pathway: conversion of 4-(cytidine 5′-diphospho)-2-C-methyl-d-erythritol to its 2-phospho derivative by 4-(cytidine 5′-diphospho)-2-C-methyl-d-erythritol kinase. Tetrahedron Lett 41: 2925–2928. doi:10.1016/S0040-4039(00)00295-1.
68. Lüttgen H, Rohdich F, Herz S, Wungsintaweekul J, Hecht S, et al. (2000) Biosynthesis of terpenoids: YchB protein of Escherichia coli phosphorylates the 2-hydroxy group of 4-diphosphocytidyl-2C-methyl-d-erythritol. Proc Natl Acad Sci 97: 1062–1067. doi:10.1073/pnas.97.3.1062.
69. Herz S, Wungsintaweekul J, Schuhr CA, Hecht S, Lüttgen H, et al. (2000) Biosynthesis of terpenoids: YgbB protein converts 4-diphosphocytidyl-2C-methyl-d-erythritol 2-phosphate to 2C-methyl-d-erythritol 2,4-cyclodiphosphate. Proc Natl Acad Sci 97: 2486–2490. doi:10.1073/pnas.040554697.
70. Altincicek B, Kollas A-K, Eberl M, Wiesner J, Sanderbrand S, et al. (2001) LytB, a novel gene of the 2-C-methyl-D-erythritol 4-phosphate pathway of isoprenoid biosynthesis in Escherichia coli. FEBS Lett 499: 37–40. doi:10.1016/S0014-5793(01)02516-9.
71. Campos N, Rodríguez-Concepción M, Seemann M, Rohmer M, Boronat A (2001) Identification of gcpE as a novel gene of the 2-C-methyl-D-erythritol 4-phosphate pathway for isoprenoid biosynthesis in Escherichia coli. FEBS Lett 488: 170–173. doi:10.1016/S0014-5793(00)02420-0.
72. Hecht S, Eisenreich W, Adam P, Amslinger S, Kis K, et al. (2001) Studies on the nonmevalonate pathway to terpenes: The role of the GcpE (IspG) protein. Proc Natl Acad Sci 98: 14837–14842. doi:10.1073/pnas.201399298.
73. Kollas A-K, Duin EC, Eberl M, Altincicek B, Hintz M, et al. (2002) Functional characterization of GcpE, an essential enzyme of the non-mevalonate pathway of isoprenoid biosynthesis. FEBS Lett 532: 432–436. doi:10.1016/S0014-5793(02)03725-0.
74. Rohdich F, Zepeck F, Adam P, Hecht S, Kaiser J, et al. (2003) The deoxyxylulose phosphate pathway of isoprenoid biosynthesis: Studies on the mechanisms of the reactions catalyzed by IspG and IspH protein. Proc Natl Acad Sci 100: 1586–1591. doi:10.1073/pnas.0337742100.
75. Altincicek B, Kollas A-K, Sanderbrand S, Wiesner J, Hintz M, et al. (2001) GcpE Is Involved in the 2-C-Methyl-d-Erythritol 4-Phosphate Pathway of Isoprenoid Biosynthesis in Escherichia coli. J Bacteriol 183: 2411–2416. doi:10.1128/JB.183.8.2411–2416.2001.
76. Cunningham FX, Lafond TP, Gantt E (2000) Evidence of a Role for LytB in the Nonmevalonate Pathway of Isoprenoid Biosynthesis. J Bacteriol 182: 5841–5848. doi:10.1128/JB.182.20.5841-5848.2000.
77. Altincicek B, Duin EC, Reichenberg A, Hedderich R, Kollas A-K, et al. (2002) LytB protein catalyzes the terminal step of the 2-C-methyl-D-erythritol-4-phosphate pathway of isoprenoid biosynthesis. FEBS Lett 532: 437–440. doi:10.1016/S0014-5793(02)03726-2.
78. McAteer S, Coulson A, McLennan N, Masters M (2001) The lytB Gene of Escherichia coli Is Essential and Specifies a Product Needed for Isoprenoid Biosynthesis. J Bacteriol 183: 7403–7407. doi:10.1128/JB.183.24.7403-7407.2001.
79. Rohdich F, Hecht S, Gärtner K, Adam P, Krieger C, et al. (2002) Studies on the nonmevalonate terpene biosynthetic pathway: Metabolic role of IspH (LytB) protein. Proc Natl Acad Sci 99: 1158–1163. doi:10.1073/pnas.032658999.
80. Adam P, Hecht S, Eisenreich W, Kaiser J, Gräwert T, et al. (2002) Biosynthesis of terpenes: Studies on 1-hydroxy-2-methyl-2-(E)-butenyl 4-diphosphate reductase. Proc Natl Acad Sci 99: 12108–12113. doi:10.1073/pnas.182412599.
81. Arigoni D, Sagner S, Latzel C, Eisenreich W, Bacher A, et al. (1997) Terpenoid biosynthesis from 1-deoxy-d-xylulose in higher plants by intramolecular skeletal rearrangement. Proc Natl Acad Sci 94: 10600–10605. doi:10.1073/pnas.94.20.10600.
82. Putra SR, Lois LM, Campos N, Boronat A, Rohmer M (1998) Incorporation of [2,3-13C2]- and [2,4-13C2]-d-1-Deoxyxylulose into Ubiquinone of Escherichia coli via the Mevalonate-Independent Pathway for Isoprenoid Biosynthesis. Tetrahedron Lett 39: 23–26. doi:10.1016/S0040-4039(97)10458-0.
83. Kuzuyama T, Takahashi S, Takagi M, Seto H (2000) Characterization of 1-Deoxy-d-xylulose 5-Phosphate Reductoisomerase, an Enzyme Involved in Isopentenyl Diphosphate Biosynthesis, and Identification of Its Catalytic Amino Acid Residues. J Biol Chem 275: 19928–19932. doi:10.1074/jbc.M001820200.

84. Walker JR, Poulter CD (2005) Synthesis and evaluation of 1-deoxy-D-xylulose 5-phosphate analogues as chelation-based inhibitors of methylerythritol phosphate synthase. J Org Chem 70: 9955–9959. doi:10.1021/jo0516786.
85. Woo Y-H, Fernandes RPM, Proteau PJ (2006) Evaluation of fosmidomycin analogs as inhibitors of the Synechocystis sp. PCC6803 1-deoxy-d-xylulose 5-phosphate reductoisomerase. Bioorg Med Chem 14: 2375–2385. doi:10.1016/j.bmc.2005.11.012.
86. Yin X, Proteau PJ (2003) Characterization of native and histidine-tagged deoxyxylulose 5-phosphate reductoisomerase from the cyanobacterium Synechocystis sp. PCC6803. Biochim Biophys Acta 1652: 75–81.

Paper III: The effect of chain length and unsaturation on Mtb Dxr inhibition and antitubercular killing activity of FR900098 analogs

Jackson ER, San Jose G, Brothers RC, Edelstein EK, Sheldon Z, Haymond A, et al. *Bioorg Med Chem Lett.* 2014;24: 649–653. doi:10.1016/j.bmcl.2013.11.067

Attributions and Contributions

Reproduced with permission from Elsevier. The author was responsible for the generation of the kinetic data in Tables 1 and 3.

ARTICLE IN PRESS

Bioorganic & Medicinal Chemistry Letters xxx (2013) xxx–xxx

Contents lists available at ScienceDirect

Bioorganic & Medicinal Chemistry Letters

journal homepage: www.elsevier.com/locate/bmcl

The effect of chain length and unsaturation on Mtb Dxr inhibition and antitubercular killing activity of FR900098 analogs

Emily R. Jackson [a], Géraldine San Jose [a], Robert C. Brothers [a], Emma K. Edelstein [a], Zachary Sheldon [a], Amanda Haymond [b], Chinchu Johny [b], Helena I. Boshoff [c], Robin D. Couch [b], Cynthia S. Dowd [a,*]

[a] Department of Chemistry, George Washington University, 725 21st Street NW, Corcoran 107, Washington, DC 20052, United States
[b] Department of Chemistry and Biochemistry and the National Center for Biodefense and Infectious Diseases, George Mason University, Manassas, VA 20110, United States
[c] Tuberculosis Research Section, Laboratory of Clinical Infectious Diseases, National Institute of Allergy and Infectious Diseases, NIH, Bethesda, MD 20892, United States

ARTICLE INFO

Article history:
Received 21 October 2013
Revised 20 November 2013
Accepted 25 November 2013
Available online xxxx

Keywords:
Mycobacterium tuberculosis
Nonmevalonate pathway
Dxr
Antibiotic

ABSTRACT

Inhibition of the nonmevalonate pathway (NMP) of isoprene biosynthesis has been examined as a source of new antibiotics with novel mechanisms of action. Dxr is the best studied of the NMP enzymes and several reports have described potent Dxr inhibitors. Many of these compounds are structurally related to natural products fosmidomycin and FR900098, each bearing retrohydroxamate and phosphonate groups. We synthesized a series of compounds with two to five methylene units separating these groups to examine what linker length was optimal and tested for inhibition against Mtb Dxr. We synthesized ethyl and pivaloyl esters of these compounds to increase lipophilicity and improve inhibition of Mtb growth. Our results show that propyl or propenyl linker chains are optimal. Propenyl analog **22** has an IC_{50} of 1.07 μM against Mtb Dxr. The pivaloyl ester of **22**, compound **26**, has an MIC of 9.4 μg/mL, representing a significant improvement in antitubercular potency in this class of compounds.

© 2013 Elsevier Ltd. All rights reserved.

Tuberculosis (TB), caused by *Mycobacterium tuberculosis* (Mtb), remains one of the world's deadliest infectious diseases.[1] Emergence of multi-drug (MDR) and extensively-drug (XDR) resistant strains, as well as co-infection with HIV, has made TB both difficult and expensive to treat.[2] New TB therapies are needed to shorten treatment, be effective against all strains and metabolic states of the organism, and work well with HIV drugs. Thus, there remains a significant need for new and improved strategies against Mtb. The nonmevalonate pathway (NMP) of isoprene biosynthesis (Fig. 1) is essential for Mtb survival and, as it is not present in humans, is an attractive set of targets for novel drug development.[3–5] The NMP synthesizes 5-carbon building blocks from pyruvate and glyceraldehyde-3-phosphate. These building blocks are the starting materials for many complex cellular metabolites. 1-Deoxy-D-xylulose-5-phosphate reductoisomerase (Dxr), is the first committed step in the NMP and is responsible for conversion of 1-deoxy-D-xylulose-5-phosphate (DXP) to 2-*C*-methyl-D-erythritol 4-phosphate (MEP).[6] Dxr catalyzes both a reduction and isomerization using NADPH as a cofactor.

Natural products fosmidomycin (**1**) and FR900098 (**2**) inhibit Mtb Dxr by mimicking DXP's polar character and kill many non-mycobacterial organisms reliant on this enzyme (Fig. 2).[7–9] Our early work in this area showed that lipophilic analogs of **1** and **2** more effectively kill a range of bacterial strains, including Mtb.[10–12] Since that time, we and others have reported Dxr inhibitors belonging to several structural families,[11,13–16] but very few of these have displayed potent antitubercular activity. Many of these inhibitors retain key structural features found in the parent compounds **1** and **2**: a retrohydroxamic acid, a phosphonate, and an *n*-propyl carbon chain linking the nitrogen and phosphorus atoms. In the 1980s, a series of *Streptomyces*-derived and inspired products exchanging the *n*-propyl chain for ethylene and propenyl chains were described.[17,18] Among these, the propenyl compound was found to be comparable to the propyl analogs **1** and **2** and showed potent antibacterial activity against *Bacillus subtilis* and *Escherichia coli*.[18] As this work came before the discovery of Dxr as the cellular target of these inhibitors, the inhibitory activity of these carbon chain-modified analogs against the purified enzyme is largely unknown. To fill this gap and expand on the set of analogs examined, we synthesized analogs of **1** and **2**, varying the length of the carbon linker from 2 to 5 methylene groups. We also prepared the propenyl analog to examine the influence of unsaturation within the propyl chain. As our interest is the development of antitubercular agents working through Dxr inhibition, we evaluated these analogs as inhibitors of Mtb Dxr. To study the effects of these structural changes on antitubercular activity, the ethyl and selected pivaloyl esters were prepared. The compounds synthesized and evaluated are shown in Figure 2.

* Corresponding author. Tel.: +1 202 994 8405; fax: +1 202 994 5873.
E-mail address: cdowd@gwu.edu (C.S. Dowd).

0960-894X/$ - see front matter © 2013 Elsevier Ltd. All rights reserved.
http://dx.doi.org/10.1016/j.bmcl.2013.11.067

Please cite this article in press as: Jackson, E. R.; et al. *Bioorg. Med. Chem. Lett.* (2013), http://dx.doi.org/10.1016/j.bmcl.2013.11.067

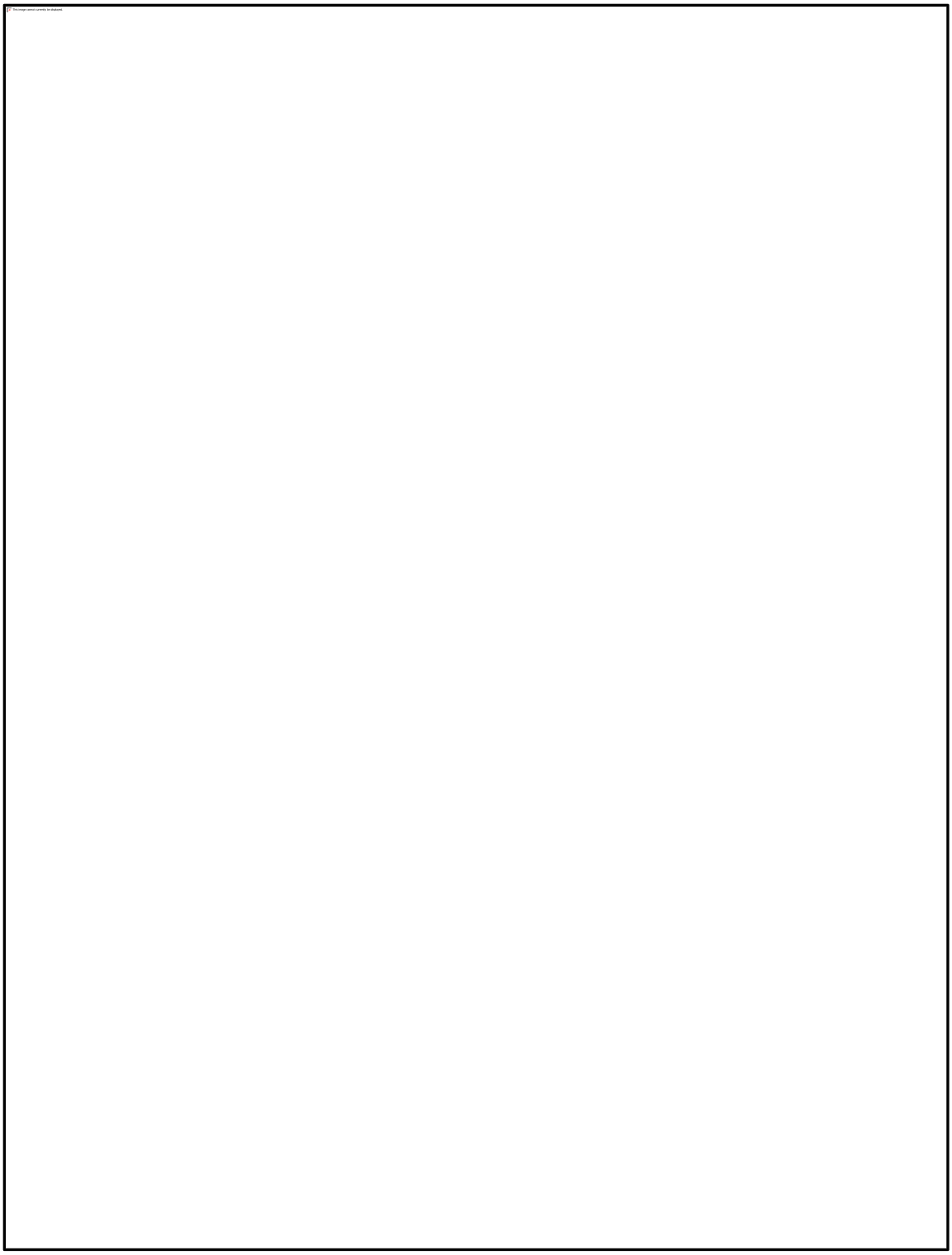

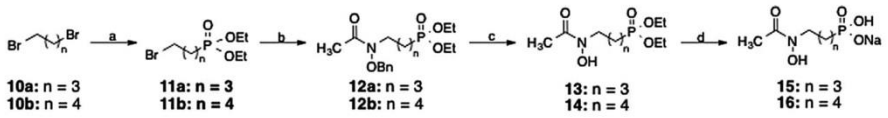

Scheme 2. Reagents and conditions: (a) $P(OEt)_3$, microwave 20%, 10–15 min; (b) BnONHAc, NaH, NaI, THF, reflux, 18 h; (c) H_2 10% Pd/C, MeOH, rt, 18 h;(d) (i) TMSBr, CH_2Cl_2, 0 °C to rt, 18 h, (ii) H_2O, rt, 18 h, (iii) NaOH aq, rt, 18 h.

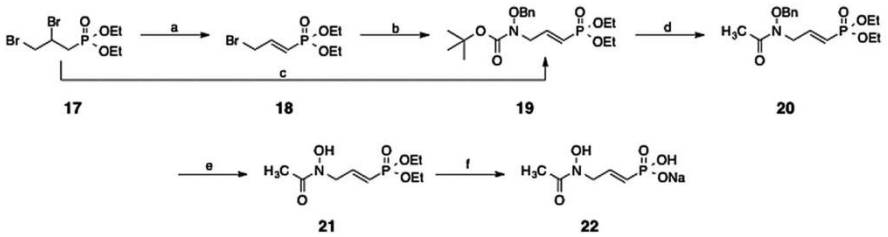

Scheme 3. Reagents and conditions: (a) NaH, THF, 60 °C, 18 h; (b) BocNHOBn, NaH, THF, rt, 18 h; (c) BocNHOBn, NaH, NaI, THF, rt, 18 h; (d) (i) AcCl, MeOH, CH_2Cl_2, rt, 30 min, (ii) AcCl, Na_2CO_3, CH_2Cl_2, rt, 3 h, (e) BCl_3, CH_2Cl_2, −50 °C, 2 h; (f) (i) TMSBr BSTFA, CH_2Cl_2, 0 °C to rt, 18 h, (ii) H_2O, rt, 18 h, (iii) NaOH aq, rt, 18 h.

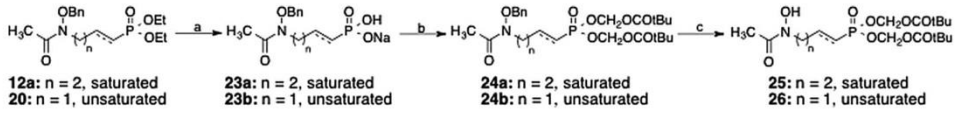

Scheme 4. Reagents and conditions: (a) (i) TMSBr, CH_2Cl_2, 0 °C to rt, 18 h, (ii) H_2O, rt, 18 h for **23a** or H_2O, NaOH, rt, 18 h for **23b**; (b) chloromethylpivalate, 60 °C TEA/DMF/6–16 h; (c) H_2 10% Pd/C, THF, rt, 18 h for **25** or BCl_3, CH_2Cl_2, −70 °C, 10 h for **26**.

in a microwave-assisted Michaelis–Arbuzov reaction to form **11a** (61%) and **11b** (64%).[22] Acetylated *O*-benzylhydroxylamine[23,24] was treated with sodium hydride and compounds **11a** and **11b** to form intermediates **12a** (79%) and **12b** (37%). Compounds **12a** and **12b** underwent hydrogenation to form compounds **13** (34%) and **14** (49%). Deprotection of the ethyl esters gave compounds **15** and **16** in quantitative yield.

Synthesis of unsaturated FR900098 analog **22** is shown in Scheme 3. Dibromo compound **17**[25] was treated with sodium hydride to effect elimination, yielding compound **18** (41%). Boc-protected *O*-benzylhydroxylamine[26] was reacted with sodium hydride and then compound **18** to form substituted product **19** (84%). Alternately, compound **19** was prepared directly from **17** in one step using a single treatment of NaH and the amine in 41% yield. Removal of the BOC protecting group in situ and subsequent acetylation yielded compound **20** (70%).[27] To preserve the double bond, BCl_3 was used to remove the benzyl group of **20**, affording compound **21** (52%).[28] Deprotection with bromotrimethylsilane gave α/β-unsaturated phosphonic acid **22** (quantitative).[29]

To assist penetration of compounds across the mycobacterial cell wall[10,30], pivaloyl esters were prepared from two phosphonic acids (Scheme 4). Diethyl protected intermediates **12a** and **20** were treated with bromotrimethylsilane yielding compounds **23a** (87%) and **23b**[31] (quantitative). Subsequent reaction with chloromethylpivalate gave esters compounds **24a** (6%) and **24b**[32] (40%). Catalytic hydrogenation removed the benzyl group in saturated analog **24a**, yielding compound **25** (85%). Treatment with BCl_3 deprotected unsaturated analog **24b** to yield compound **26** (13%).[33]

Table 1
Effect of chain length on Mtb Dxr inhibition and Mtb MIC

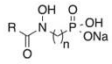

Compound	R	*n*	Mtb Dxr IC_{50} (μM) (% inh at 100 μM)	MIC (μg/mL) 7H9 (GAST)
Fosmidomycin (**1**)	H	3	0.44	>500
FR900098 (**2**)	CH_3	3	2.39	>500
9	CH_3	2	(74%)	>200 (150)
15	CH_3	4	(80%)	>200 (>200)
16	CH_3	5	(86%)	>200 (>200)

Mtb = *Mycobacterium tuberculosis*; IC_{50} = inhibitory concentration at 50%; inh = inhibition; MIC = minimum inhibitory concentration; 7H9 = rich media; GAST = minimal media.

Please cite this article in press as: Jackson, E. R.; et al. *Bioorg. Med. Chem. Lett.* (2013), http://dx.doi.org/10.1016/j.bmcl.2013.11.067

Table 2
Effect of esterification on Mtb MIC

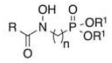

Compound	R	R^1	*n*	MIC (μg/mL) 7H9 (GAST)
27	H	CH_2CH_3	3	400
7	H	CH_2CH_3	2	>500
8	CH_3	CH_2CH_3	2	>500
28	CH_3	CH_2CH_3	3	200–400
29	CH_3	$CH_2OCOtBu$	3	50–100
13	CH_3	CH_2CH_3	4	>200 (75)
25	CH_3	$CH_2OCOtBu$	4	⩾200 (150)
14	CH_3	CH_2CH_3	5	>200 (200)

Table 3
Effect of unsaturation on Mtb Dxr inhibition and Mtb MIC

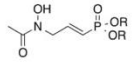

Compound	R	Mtb Dxr IC_{50} (μM)	MIC (μg/mL) 7H9 (GAST)
22	H/Na	1.07	>200 (150)
21	CH_2CH_3	ND[a]	>200 (150)
26	$CH_2OCOtBu$	ND	9.4 (12.5)

[a] ND = not determined.

The analogs were evaluated for inhibition of Mtb Dxr and growth of Mtb (Tables 1–3). All of the saturated compounds, with chain lengths between two and five methylene groups, inhibited Mtb Dxr to some extent (Table 1). Among these acids, compounds with three methylene groups separating the nitrogen and phosphorus atoms (that is, compounds **1** and **2**) were the most active. Not surprisingly, these compounds did not inhibit mycobacterial growth in nutrient-rich media (>200 μg/mL in 7H9), although **9** had a very slight effect when minimal media was used (150 μg/mL in GAST). The polarity of these compounds diminishes penetration of the lipophilic mycobacterial cell wall.[10,30]

Diethyl and dipivaloyl esterification of these compounds improved antimycobacterial activity (Table 2). As previously shown, diethyl esters of **1** and **2** (**27** and **28**, respectively) are weakly potent inhibitors of Mtb growth with MIC values of 200–400 μg/mL.[10] Pivaloyl ester **29** showed improved potency with an MIC of 50–100 μg/mL, and this compound was the most potent in the saturated series. Taken together, these data show that linker chains of two, four or five methylene units are not advantageous for Mtb Dxr inhibition or inhibition of Mtb cell growth.

The compounds listed in Table 3 were synthesized to examine the effect of unsaturation on Mtb Dxr inhibition and cell growth. Interestingly, α/β-unsaturated compound **22** is a potent inhibitor of Mtb Dxr with an IC_{50} of 1.07 μM. Indeed, **22** is more active than parent compound **2**. While **21** and **22** do not inhibit Mtb, the more lipophilic pivaloyl ester of **22** (compound **26**) is a potent inhibitor of mycobacterial growth with an MIC of 9.4 μg/mL in rich media and 12.5 μg/mL in minimal media. To our knowledge, compound **26** displays the most potent antitubercular activity of all compounds that work through a Dxr-mediated mechanism.

Overall, the results collectively indicate that a carbon propyl or propenyl chain between the nitrogen and phosphorus atoms of fosmidomycin/FR900098 analogs yields the highest potency. Lipophilic esters of these compounds improve their antitubercular activity. α/β-Unsaturated compound **22** and its lipophilic pivaloyl ester **26** show higher potency than the parent compound FR900098 (**2**) on Mtb Dxr inhibition and antitubercular activity. These data improve our understanding of the Mtb Dxr active site and its tolerance to length variation between the phosphonate and retrohydroxamate groups. These results are significant for aiding the rational design of Mtb Dxr inhibitors using the phosphonate/retrohydroxamate scaffold and guide the development of Dxr inhibitors as antitubercular agents.

Acknowledgments

This work was supported by the Intramural Research Program of NIAID/NIH, the George Washington University Department of Chemistry, the GWU University Facilitating Fund, and NIH (AI086453 to C.S.D.). R.D.C. was supported by George Mason University's Department of Chemistry and Biochemistry and the U.S. Army Medical Research and Materiel Command W23RYX1291N601.

References and notes

1. Dye, C.; Glaziou, P.; Floyd, K.; Raviglione, M. *Annu. Rev. Public Health* **2013**, *34*, 271.
2. WHO, 'Global Tuberculosis Report', 2012.
3. Rohmer, M. *Lipids* **2008**, *43*, 1095.
4. Perez-Gil, J.; Rodriguez-Concepcion, M. *Biochem. J.* **2013**, *452*, 19.
5. Grawert, T.; Groll, M.; Rohdich, F.; Bacher, A.; Eisenreich, W. *Cell. Mol. Life Sci.* **2011**, *68*, 3797.
6. Jackson, E. R.; Dowd, C. S. *Curr. Top. Med. Chem.* **2012**, *12*, 706.
7. Mine, Y.; Kamimura, T.; Nonoyama, S.; Nishida, M.; Goto, S.; Kuwahara, S. *J. Antibiot.* **1980**, *33*, 36.
8. Kuroda, Y.; Okuhara, M.; Goto, T.; Okamoto, M.; Terano, H.; Kohsaka, M.; Aoki, H.; Imanaka, H. *J. Antibiot.* **1980**, *33*, 29.
9. Iguchi, E.; Okuhara, M.; Kohsaka, M.; Aoki, H.; Imanaka, H. *J. Antibiot.* **1980**, *33*, 19.
10. Uh, E.; Jackson, E. R.; San Jose, G.; Maddox, M.; Lee, R. E.; Boshoff, H. I.; Dowd, C. S. *Bioorg. Med. Chem. Lett.* **2011**, *21*, 6973.
11. San Jose, G.; Jackson, E. R.; Uh, E.; Johny, C.; Haymond, A.; Lundberg, L.; Pinkham, C.; Kehn-Hall, K.; Boshoff, H. I.; Couch, R. D.; Dowd, C. S. *MedChemComm* **2013**, *4*, 1099.
12. McKenney, E. S.; Sargent, M.; Khan, H.; Uh, E.; Jackson, E. R.; San Jose, G.; Couch, R. D.; Dowd, C. S.; van Hoek, M. L. *PLoS One* **2012**, *7*, e38167.
13. Andaloussi, M.; Henriksson, L. M.; Wieckowska, A.; Lindh, M.; Bjorkelid, C.; Larsson, A. M.; Suresh, S.; Iyer, H.; Srinivasa, B. R.; Bergfors, T.; Unge, T.; Mowbray, S. L.; Larhed, M.; Jones, T. A.; Karlen, A. *J. Med. Chem.* **2011**, *54*, 4964.
14. Deng, L.; Diao, J.; Chen, P.; Pujari, V.; Yao, Y.; Cheng, G.; Crick, D. C.; Prasad, B. V.; Song, Y. *J. Med. Chem.* **2011**, *54*, 4721.
15. Jansson, A. M.; Wieckowska, A.; Bjorkelid, C.; Yahiaoui, S.; Sooriyaarachchi, S.; Lindh, M.; Bergfors, T.; Dharavath, S.; Desroses, M.; Suresh, S.; Andaloussi, M.; Nikhil, R.; Sreevalli, S.; Srinivasa, B. R.; Larhed, M.; Jones, T. A.; Karlen, A.; Mowbray, S. L. *J. Med. Chem.* **2013**, *56*, 6190.
16. Verbrugghen, T.; Vandurm, P.; Pouyez, J.; Maes, L.; Wouters, J.; Van Calenbergh, S. *J. Med. Chem.* **2013**, *56*, 376.
17. Hashimoto, M.; Hemmi, K.; Takeno, H.; Kamiya, T. *Tetrahedron Lett.* **1980**, *21*, 99.
18. Hemmi, K.; Takeno, H.; Hashimoto, M.; Kamiya, T. *Chem. Pharm. Bull.* **1982**, *30*, 111.
19. Balczewski, P.; Pietrzykowski, W. M. *Tetrahedron* **1996**, *52*, 13681.
20. Zwierzak, A.; Osowska, K. *Synthesis* **1984**, *3*, 223.
21. Blazewska, K.; Gajda, T. *Tetrahedron* **2003**, *59*, 10249.
22. Villemin, D.; Simeon, F.; Decreus, H.; Jaffres, P.-A. *Phosphorus, Sulfur Silicon Relat. Elem.* **1998**, *133*, 209.
23. Ortmann, R.; Wiesner, J.; Reichenberg, A.; Henschker, D.; Beck, E.; Jomaa, H.; Schlitzer, M. *Arch. Pharm.* **2005**, *338*, 305.
24. Reichenberg, A.; Wiesner, J.; Weidemeyer, C.; Dreiseidler, E.; Sanderbrand, S.; Altincicek, B.; Beck, E.; Schlitzer, M.; Jomaa, H. *Bioorg. Med. Chem. Lett.* **2001**, *11*, 833.
25. Laureyn, I.; Stevens, C. V.; Soroka, M.; Malysa, P. *Arkivoc* **2003**, *iv*, 102.
26. Kadi, N.; Oves-Costales, D.; Barona-Gomez, F.; Challis, G. L. *Nat. Chem. Biol.* **2007**, *3*, 652.
27. *Compound **20***. Acetyl chloride (1.8 mL, 25.0 mmol) and dry MeOH (0.5 mL) were added dropwise to **19** (0.19 g, 2.5 mmol) in dry CH_2Cl_2 (6 mL) under N_2. The reaction mixture was allowed to stir at rt for 30 min. Dry Na_2CO_3 (0.5 g, 5.0 mmol) and additional acetyl chloride (0.7 mL, 9.8 mmol) were added, and the reaction mixture was allowed to stir at rt for 3 h. The reaction mixture was filtered over celite, and the solvent was removed under reduced pressure. The crude oil was purified by column chromatography using silica gel (CH_2Cl_2/MeOH, 49:1) to yield **20** (0.13 g, 0.36 mmol, 77%) as a clear, colorless oil. ^1H NMR ($CDCl_3$, 200 MHz), δ (ppm): 7.37 (s, 5H), 6.82–6.57 (m, 1H), 5.90–5.72 (m,

1H), 4.83 (s, 2H), 4.34 (br s, 2H), 4.13–3.99 (m, 4H), 2.13 (s, 3H), 1.34–1.27 (m, 6H). LCMS (ESI) *m/z*: 705.1 (2 M+Na).

28. *Compound* ***21***. A solution of **20** (0.117 g, 0.34 mmol) in dry CH_2Cl_2 (6.0 mL) was cooled to −50 °C and BCl_3 (1.4 mL, 1 M in CH_2Cl_2) was added dropwise, and the reaction mixture was allowed to stir for 2 h. The reaction was quenched with saturated $NaHCO_3$ (aq, 9.0 mL) and allowed to warm to rt. The aqueous solution was extracted with CH_2Cl_2. The organic fractions were combined, dried over $MgSO_4$, filtered and the solvent was removed under reduced pressure. The resulting crude residue was purified using an Isolera Flash Chromatography system and a silica column (EtOAc/MeOH, 49:1) to yield **21** (45 mg, 0.18 mmol, 52%) as a light yellow oil. ^{1}H NMR (200 MHz, $CDCl_3$) δ (ppm): 1.28 (t, 6H), 2.15 (s, 3H), 4.02 (q, 4H),4.43–4.25 (m, 2H), 5.84 (t, J = 18.8 Hz, 1H), 6.83–6.52 (m, 1H), 9.88 (br s, 1H). ^{13}C NMR (50 MHz, $CDCl_3$) δ (ppm): 16.30, 20.36, 50.47 (d, J = 27.2 Hz), 62.37 (d, J = 7.1 Hz), 120.02, 147.62, 172.66. LCMS (ESI) *m/z* 252.1 (M+H).
29. *Compound* ***22***. *N,O*-Bis(trimethylsilyl)trifluoroacetamide (0.18 mL, 0.67 mmol) was added to **21** (0.03 g, 0.12 mmol) in CH_2Cl_2 (0.60 mL) under N_2. The reaction mixture was allowed to stir at rt for 20 min. The reaction mixture was cooled to 0 °C, and bromotrimethylsilane (0.18 mL, 1.34 mmol) was added dropwise. The reaction was allowed to warm to rt and was stirred overnight under N_2. Ethyl bromide and excess silylating agent were removed under reduced pressure, and the residue was dissolved in aqueous NaOH (0.68 mL, 7.8 mg/mL) and stirred overnight. The mixture was extracted between H_2O and CH_2Cl_2. The aqueous portions were combined, and the solvent was removed by lyophilization to give **22** (0.03 g, 0.12 mmol, quant.) as a yellow solid. ^{1}H NMR (400 MHz, D_2O) δ (ppm): 2.36 (s, 3H), 4.61–4.46 (m, 2H), 6.19–6.06 (m, 1H), 6.56–6.43 (m, 1H). ^{13}C NMR (101 MHz, D_2O) δ (ppm): 19.34, 50.81 (d, J = 23.7 Hz), 126.91, 137.79, 174.18. HRMS (ESI) *m/z* calcd for $C_{10}H_{18}N_2NaO_{10}P_2$ (2 M+Na]): 411.0328, found: 411.0334.
30. Brown, A. C.; Parish, T. *BMC Microbiol.* **2008**, *8*, 78.
31. *Compound* ***23b***. Trimethylsilylbromide (1.75 mL, 11.7 mmol) was added dropwise to a stirring solution of **20** (0.5 g, 1.5 mmol) in dry CH_2Cl_2 (20 mL) under N_2 at 0 °C. The reaction mixture was allowed to warm to room temperature. After 3.5 h, the mixture was evaporated to dryness, dissolved in dry CH_2Cl_2, and evaporated to dryness again (3×). The resulting residue was stirred overnight in water (3 mL) and NaOH (5.5 mL, 3 mmol, aq). After 20 h, the aqueous mixture was washed with CH_2Cl_2. The organic portion was separated, and the water was removed by lyophilization to give **23b** (0.53 g, quant.) as white crystals. ^{1}H NMR ($CDCl_3$, 400 MHz), δ (ppm): 2.28 (s, 3H), 4.53 (s, 2H), 5.17 (s, 2H), 6.07–6.15 (m, 1H), 6.30–6.40 (m, 1H), 7.65–7.68 (m, 5H). LCMS (ESI) *m/z*: 286 (M_{acid}+H), 571 ($2M_{acid}$+H), 856 ($3M_{acid}$+H).
32. *Compound* ***24b***. Chloromethylpivalate (2.15 mL, 15 mmol) was added to a stirred solution of **23b** (0.49 g, 1.5 mmol) and triethylamine (0.45 mL, 3 mmol) in DMF (40 mL). The reaction mixture was heated to 60 °C for 16 h. Water (50 mL) was added, and the aqueous layer was extracted with CH_2Cl_2. The organic layer was washed with brine, dried over $MgSO_4$, and the solvent was removed under reduced pressure. The crude oil was purified by column chromatography using silica gel and CH_2Cl_2/EtOAc to yield **24b** (0.22 g, 28%). ^{1}H NMR ($CDCl_3$, 400 MHz), δ (ppm): 1.20 (s, 18H), 2.12 (s, 3H), 4.33 (br s, 2H), 4.82 (s, 2H), 5.65 (d, J = 12.8 Hz, 4H), 5.80–5.89 (m, 1H), 6.70–6.81 (m, 1H), 7.35–7.38 (m, 5H). LCMS (ESI) *m/z*: 536 (M+Na).
33. *Compound* ***26***. BCl_3 (1 M in CH_2Cl_2, 0.88 mL) was added dropwise to a stirred solution of **24b** (190 mg, 0.37 mmol) in dry CH_2Cl_2 (5 mL) under N_2 at −78 °C. After 10 h, the reaction mixture was poured into satd. $NaHCO_3$ (aq) and was extracted with CH_2Cl_2. The organic layers were combined and washed with brine, dried over $MgSO_4$, and the solvent was removed under reduced pressure. The crude oil was purified by column chromatography using EtOAc, CH_2Cl_2, and MeOH. The oil was further purified over a silica plug, washed with hexanes and CH_2Cl_2, and then eluted with EtOAc to give **26** as a pale yellow oil (21 mg, 13.4%). ^{1}H NMR ($CDCl_3$, 400 MHz), δ (ppm): 1.22 (s, 18H), 2.19 (s, 3H), 4.41 (s, 2H), 5.61–5.69 (m, 4H), 5.87–5.97 (m, 1H), 6.71–6.84 (m, 1H), 8.61 (s, 1H). ^{13}C NMR ($CDCl_3$, 100 MHz), δ (ppm): 20.47, 26.93, 38.88, 50.30 (d, J = 26.5 Hz), 81.70 (d, J = 5.3 Hz), 117.95 (d, J = 188.2 Hz), 148.50, 172.87, 177.30. LCMS (ESI) *m/z*: 446 (M+Na), 847 (2 M+H), 869 (2 M+Na).

Please cite this article in press as: Jackson, E. R.; et al. *Bioorg. Med. Chem. Lett.* (2013), http://dx.doi.org/10.1016/j.bmcl.2013.11.067

Paper IV: Synthesis and bioactivity of β-substituted fosmidomycin analogues targeting 1-deoxy-D-xylulose-5-phosphate reductoisomerase

Chofor R, Sooriyaarachchi S, Risseeuw MDP, Bergfors T, Pouyez J, Johny C, et al. *J Med Chem.* 2015; 58: 2988–3001. doi:10.1021/jm5014264 [128]

Attributions and Contributions

Reproduced with permission from the American Chemical Society. Copyright 2015 American Chemical Society. All supplementary information as referenced in the text can be found in Appendix 2. The author was responsible for the generation of MtbIspC kinetic data in Figure 4 and Table 1.

Journal of Medicinal Chemistry

Article

pubs.acs.org/jmc

Synthesis and Bioactivity of β-Substituted Fosmidomycin Analogues Targeting 1-Deoxy-D-xylulose-5-phosphate Reductoisomerase

René Chofor,[†] Sanjeewani Sooriyaarachchi,[‡] Martijn D. P. Risseeuw,[†] Terese Bergfors,[‡] Jenny Pouyez,[§] Chinchu Johny,[∥] Amanda Haymond,[∥] Annelien Everaert,[⊥] Cynthia S. Dowd,[#] Louis Maes,[¶] Tom Coenye,[⊥] Alexander Alex,[▽] Robin D. Couch,[∥] T. Alwyn Jones,[‡] Johan Wouters,[§] Sherry L. Mowbray,*[,‡] and Serge Van Calenbergh*[,†]

[†]Laboratory for Medicinal Chemistry (FFW), Universiteit Gent, Ottergemsesteenweg 460, B-9000 Gent, Belgium

[‡]Department of Cell and Molecular Biology, Science for Life Laboratory, Uppsala University, Biomedical Center, Box 596, SE-751 24 Uppsala, Sweden

[§]Department of Chemistry, University of Namur, Rue de Bruxelles 61, B-5000 Namur, Belgium

[∥]Department of Chemistry and Biochemistry, George Mason University, Manassas, Virginia 20110, United States

[⊥]Laboratory of Pharmaceutical Microbiology, Ghent University, Ottergemsesteenweg 460, 9000 Ghent, Belgium

[#]Department of Chemistry, George Washington University, Washington, D.C. 20052, United States

[¶]Laboratory for Microbiology, Parasitology and Hygiene (LMPH), Faculty of Pharmaceutical, Biomedical and Veterinary Sciences, University of Antwerp, Universiteitsplein 1, B-2610 Antwerp, Belgium

[▽]Evenor Consulting Ltd., The New Barn, Mill Lane, Eastry, Kent CT13 0JW, United Kingdom

Supporting Information

ABSTRACT: Blocking the 2-C-methyl-D-erythrithol-4-phosphate (MEP) pathway for isoprenoid biosynthesis offers interesting prospects for inhibiting *Plasmodium* or *Mycobacterium* spp. growth. Fosmidomycin (**1**) and its homologue FR900098 (**2**) potently inhibit 1-deoxy-D-xylulose-5-phosphate reductoisomerase (Dxr), a key enzyme in this pathway. Here we introduced aryl or aralkyl substituents at the β-position of the hydroxamate analogue of **2**. While direct addition of a β-aryl moiety resulted in poor inhibition, longer linkers between the carbon backbone and the phenyl ring were generally associated with better binding to the enzymes. X-ray structures of the parasite Dxr−inhibitor complexes show that the "longer" compounds generate a substantially different flap structure, in which a key tryptophan residue is displaced, and the aromatic group of the ligand lies between the tryptophan and the hydroxamate's methyl group. Although the most promising new Dxr inhibitors lack activity against *Escherichia coli* and *Mycobacterium smegmatis*, they proved to be highly potent inhibitors of *Plasmodium falciparum in vitro* growth.

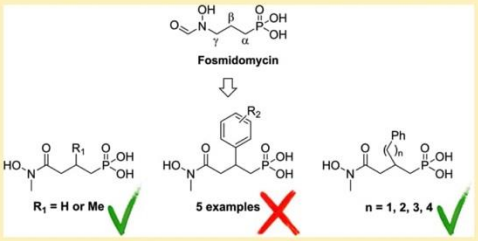

INTRODUCTION

Malaria and tuberculosis feature on the World Health Organization's work plan as infectious diseases requiring urgent attention. *Plasmodium falciparum* is responsible for the most severe malaria cases,[1] while human tuberculosis (TB) results mainly from infection with *Mycobacterium tuberculosis* (Mtb). Global statistics reveal that between 2000 and 2012, scale-up of interventions helped to reduce malaria incidence rates by 29%. However, an estimated 1300 children under the age of five years died from malaria every day in 2012, and the annual number of fatalities due to malaria was close to 1 million.[2] That same year, 8.6 million people developed TB and 1.3 million died from the disease, many of whom were HIV-positive.[3] Even though malaria and tuberculosis are preventable and usually treatable, the high incidence of both diseases and evolving resistance to many drugs compel us to continue efforts toward the discovery of novel therapeutics.

A common denominator for both pathogens is their dependence on the 2-C-methyl-D-erythrithol-4-phosphate (MEP) pathway for the biosynthesis of the isoprenoid precursors, isopentenyl diphosphate (IPP) and dimethylallyl diphosphate (DMAPP).[4,5] Humans obtain these vital building blocks via an alternate route, known as the mevalonate pathway.[6] Since the two pathways utilize nonhomologous enzymes, the MEP pathway has several interesting targets for

Received: September 17, 2014
Published: March 17, 2015

ACS Publications © 2015 American Chemical Society

DOI: 10.1021/jm5014264
J. Med. Chem. 2015, 58, 2988−3001

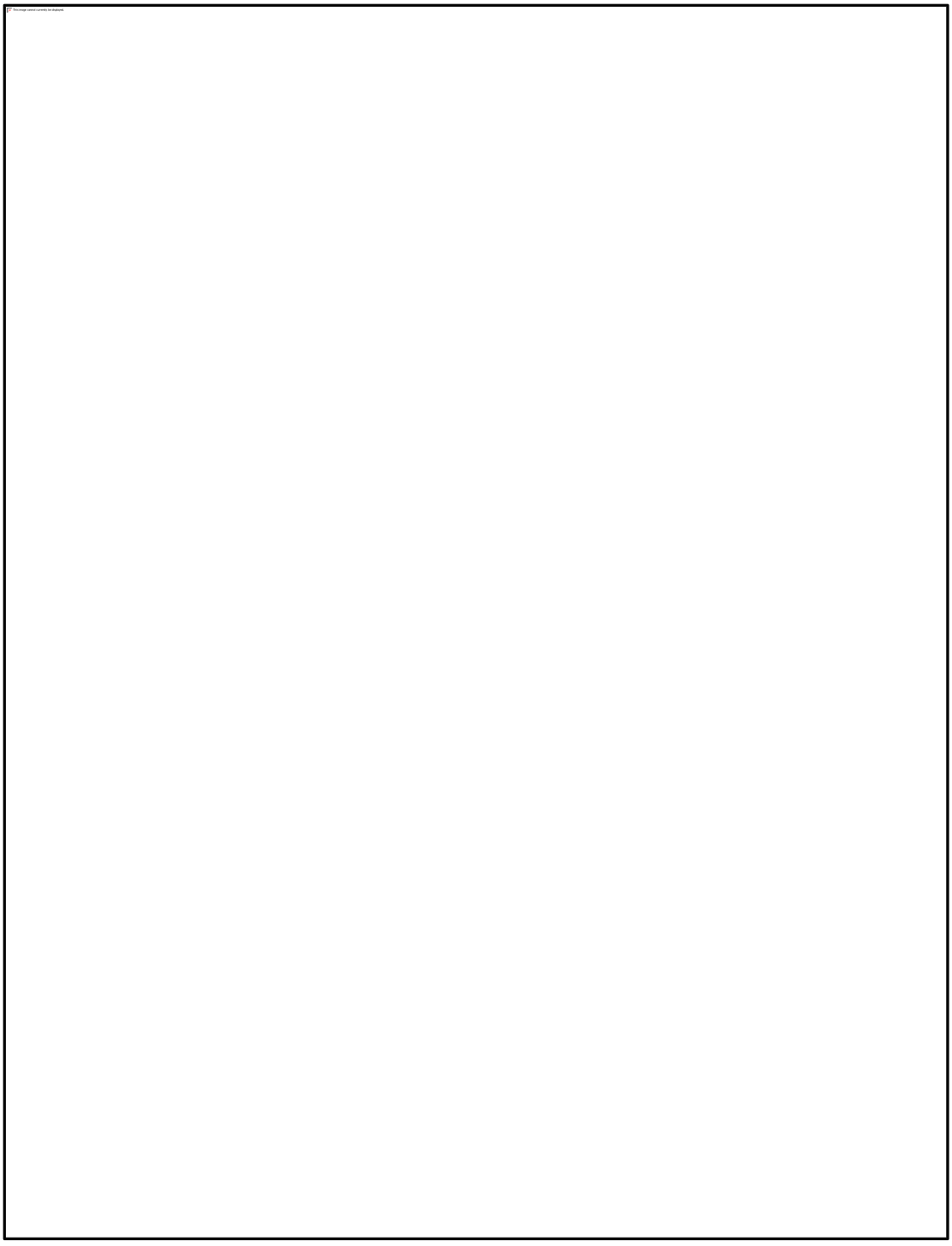

derivative was almost equipotent to **2**,[41] Brucher et al. demonstrated that β-oxa modifications combined with α-aryl substituents may afford potent PfDxr inhibitors (e.g., **6a**), with promising *in vitro* antiplasmodial activity.[42] The Kurz group showed that replacement of the β-methylene group with a sulfur atom in **6b** resulted in lower IC_{50} values for *E. coli* and MtbDxr compared with the oxa ligand **6a**.[43] Furthermore, they demonstrated that the PfDxr inhibitory activity of the *S*-(+)-enantiomers was clearly superior to that of the *R*-(−) distomers (e.g., *S*-(+)-**6c** IC_{50} = 9.4 nM, *R*-(−)-**6c** IC_{50} = 12 μM), in agreement with results from crystallographic studies on the Dxr binding of **3a** and related analogues carried out by Andaloussi et al.[30] and Jansson et al.[31]

The objective of this work was to assess the effect of introducing aromatic moieties in the β-position of the propyl backbone of **4b** on Dxr inhibition (Figure 3). First, we decided

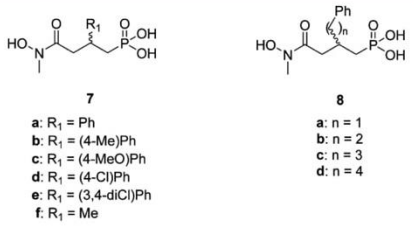

Figure 3. β-Substituted fosmidomycin analogues.

to introduce aryl groups (**7a**−**e**) based on Topliss' scheme,[44] an operational decision tree that suggests the optimum substitution pattern on a phenyl ring for attaining drug potency. Additionally, an analog of compound **4b** bearing a methyl group in the β-position (**7f**) was prepared. Although the latter compound has not been reported before, its retro-hydroxamate formyl and acetyl counterparts appear in a patent[45] and have been studied *in silico*.[46,47] The known **4b**[39] was resynthesized to serve as a positive control for evaluation. Compounds **8a**−**d** were synthesized to assess the optimal linker length between the propyl backbone of fosmidomycin and the phenyl ring.

RESULTS AND DISCUSSION

Synthesis. Scheme 1 shows the synthetic route followed to prepare compounds **7a**−**f**. The commercially available cinnamic acids **10a**−**e** were esterified by treatment with di-*tert*-butyl dicarbonate in *tert*-butanol.[48] The resulting *tert*-butyl cinnamates **11a**−**c** and the purchased *tert*-butyl crotonate **11f** served as Michael acceptors in a reaction with dibenzyl methylphosphonate to furnish predominantly the desired 1,4-addition adducts **12a**−**c**,**f** as described by Yamaguchi and co-workers.[49] Previously encountered complications during catalytic hydrogenation of related compounds bearing a chlorinated phenyl ring led to the use of diethyl methylphosphonate as a Michael donor for addition to **11d** and **11e** to yield **14d** and **14e**, respectively. Hydrolysis of the *tert*-butyl ester group of **12a**−**c**,**f** and **14d**,**e** with 20% TFA in CH_2Cl_2 and subsequent EDC-mediated coupling of the resulting carboxylic acids with *O*-benzyl-*N*-methyl-hydroxylamine yielded the protected *N*-methylhydroxamates **13a**−**c**,**f** and **15d**,**e**. Compounds **13a**−**c** and **13f** were deprotected by catalytic hydrogenolysis to access target phosphonates **7a**−**c** and **7f**. The hydroxamate group of **15d** and **15e** was unmasked with BCl_3. Bromotrimethyl silane (TMSBr) mediated deprotection of phosphonate esters **16d** and **16e** and basic workup yielded **7d**−**e** as bisammonium salts.

The synthesis of target compounds **8a**−**d** is outlined in Scheme 2. The preparation of the appropriate Michael acceptors **19a**−**d** commenced with a Dess−Martin oxidation of commercially available alcohols **17a**−**d** to afford aldehydes

Scheme 1. Synthesis of β-Aryl Analogues of 4b[a]

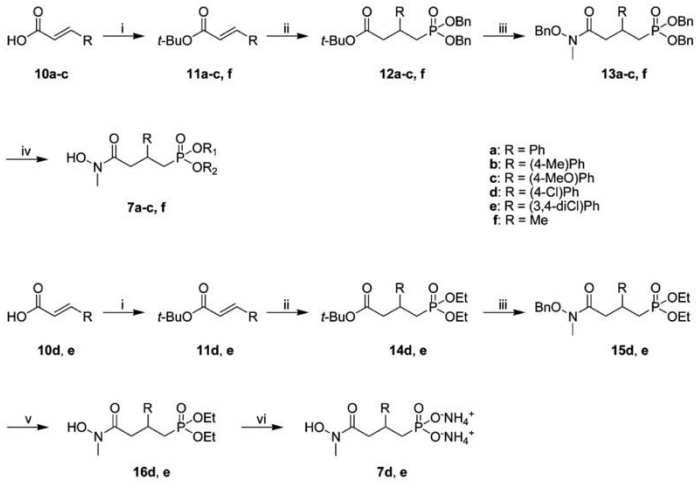

[a]Reagents and conditions: (i) Boc_2O, DMAP, *tert*-BuOH, rt, overnight; (ii) $(BnO)_2OPMe$ (for **12a**−**c**, **f**), $(EtO)_2OPMe$ (for **14d** and **14e**), *n*-BuLi, THF, −78 °C, 2.5 h; (iii) (a) TFA, CH_2Cl_2, 45 min, 0 °C to rt; (b) MeNH(OBn), EDC, DMAP, CH_2Cl_2, rt, overnight; (iv) H_2, Pd/C, MeOH, NaOH(aq), 25 °C, 10−15 min; (v) BCl_3, CH_2Cl_2, −78 °C, 1 h; (vi) (a) TMSBr, BSTFA, CH_2Cl_2, 0 °C to rt, 22 h; (b) H_2O, NH_4OH(aq).

DOI: 10.1021/jm5014264
J. Med. Chem. 2015, 58, 2988−3001

Scheme 2. Synthesis of β-Phenylalkyl Homologues of 4b[a]

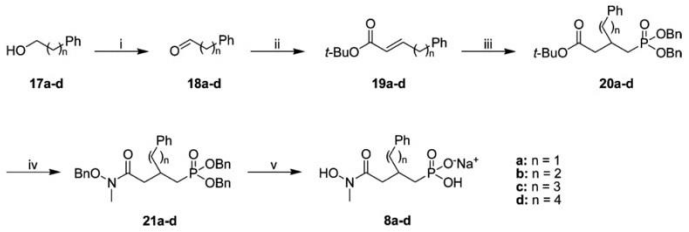

[a]Reagents and conditions: (i) Dess–Martin periodinane, CH_2Cl_2; (ii) $Ph_3P{=}CHCOO$*tert*-Bu, toluene, 120 °C; (iii) $(BnO)_2OPMe$, *n*-BuLi, THF, −78 °C, 2.5 h; (iv) (a) TFA, CH_2Cl_2, 45 min, 0 °C to rt; (b) MeNH(OBn), EDC, DMAP, CH_2Cl_2, rt; (v) H_2, Pd/C, MeOH, NaOH(aq), 25 °C, 10–15 min.

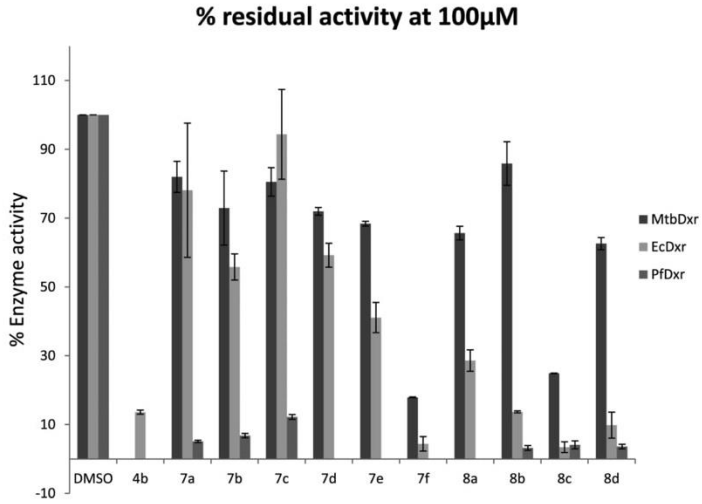

Figure 4. Residual Dxr activity upon treatment with 100 μM of the indicated compounds. The enzyme assays for EcDxr and MtbDxr were performed at 37 °C with a saturating concentration of NADPH (150 μM), a DOXP concentration fixed at its K_M (47 μM for MtbDxr and 100 μM for EcDxr), and 100 μM of the indicated inhibitor. For MtbDxr, the results were identical whether the enzyme was preincubated with the inhibitor for 10 min prior to the addition of NADPH or the enzyme was preincubated with NADPH prior to the addition of the inhibitor. For EcDxr, the enzyme was preincubated with the inhibitor and the cofactor for 5 min at 37 °C. Enzyme activity was initiated by adding the substrate DOXP. Details specific to the assay for PfDxr are given in the Supporting Information. Enzyme activity was spectrophotometrically monitored immediately following the addition of DOXP at 340 nm. Residual enzyme activity is relative to an assay performed with vehicle alone (DMSO). All assays were performed in duplicate for MtbDxr and in triplicate for EcDxr, and bars indicate standard deviation.

18a–d, which were swiftly transformed to the corresponding *tert*-butyl esters **19a–d** via Wittig olefination. Michael addition of dibenzyl methylphosphonate to **19a–d** predominantly afforded 1,4-addition adducts **20a–d** due to steric hindrance of the *tert*-butyl group. Compounds **20a–d** were converted to the desired phosphonates **8a–d** as before. ^{35}P NMR spectra of **7a–f** and **8a** indicate that these appear as rotameric mixtures, a known[50,51] phenomenon that was further validated by variable-temperature ^{31}P NMR studies.

Biological Evaluation. Final compounds were tested for inhibition of recombinant enzymes using a spectrophotometric assay monitoring the substrate-dependent oxidation of NADPH associated with the Dxr-catalyzed reaction.[11] Initially, Dxr inhibition was studied at a compound concentration of 100 μM (Figure 4). At this point, differences among the enzymes and compounds were already evident.

As anticipated, the known hydroxamate **4b**[39] was highly effective at inhibiting MtbDxr. A lipophilic prodrug of this compound has recently been shown to effectively inhibit *M. smegmatis* growth in Kirby–Bauer disk diffusion assays.[52] In contrast, compounds **7a–e** had only modest activity on MtbDxr and EcDxr. Interestingly, compound **7f**, characterized by the presence of a β-methyl substituent rather than the bulkier aromatic group, retained good inhibitory activity. Other noteworthy trends were the fact that **8a–d** were more potent on EcDxr than the **7**-series compounds and that PfDxr was more effectively inhibited than the other two enzymes.

DOI: 10.1021/jm5014264
J. Med. Chem. 2015, 58, 2988–3001

Table 1. IC_{50} (±sd) Values for Recombinant Dxrs from *E. coli*, *M. tuberculosis*, and *P. falciparum*

compound	EcDxr IC_{50} (μM)	MtbDxr IC_{50} (μM)	PfDxr IC_{50} (μM)
fosmidomycin	0.030 ± 0.008[28]	0.438 ± 0.09	0.036 ± 0.006
4b	0.159 ± 0.018	1.15 ± 0.21	*a*
7a	*a*	*a*	3.3 ± 0.17
7b	*a*	*a*	9.3 ± 0.75
7c	*a*	*a*	18.8 ± 4.2
7f	0.205 ± 0.052	7.13 ± 1.2	*a*
8a	*a*	*a*	*a*
8b	31.39 ± 21.61	*a*	1.36 ± 0.02
8c	0.843 ± 0.163	10.35 ± 1.3	0.117 ± 0.012
8d	6.67 ± 1.48	273.2 ± 54.6	0.069 ± 0.005

[a]Not determined.

Table 2. MIC_{50} Values against *in Vitro* Growth of *E. coli* and *M. smegmatis* and IC_{50} Values against the *P. falciparum* K1 Strain

compound	*E. coli* ATCC 8739 MIC_{50} (μM)	*E. coli* ATCC 25922 MIC_{50} (μM)	*E. coli* K-12 MIC_{50} (μM)	*M. smegmatis* ATCC 607 MIC. (μM)	*M. smegmatis* ATCC 700084 MIC_{50} (μM)	*P. falciparum-K1* IC_{50} (μM)
fosmidomycin (**1**)	0.98	250	7.8	>250	>250	1.73 ± 0.89[58]
2	7.8	62.5	15.6	>250	>250	0.42 ± 0.17[58]
4b	31.25	15.6	31.25	>250	>250	0.26 ± 0.02
7a	>250	>250	>250	>250	>250	>64
7b	>250	>250	>250	>250	>250	>64
7c	>250	>250	>250	>250	>250	>64
7d	>250	>250	>250	>250	>250	>64
7e	>250	>250	>250	>250	>250	>64
7f	*a*	*a*	*a*	*a*	*a*	0.74 ± 0.13
8a	*a*	*a*	*a*	*a*	*a*	≥56.8 ± 10.1
8b	>250	>250	>250	>250	>250	35.4 ± 8.7
8c	>250	>250	>250	>250	>250	0.43 ± 0.09
8d	>250	>250	>250	>250	>250	<0.25 ± 0.00

[a]Not determined.

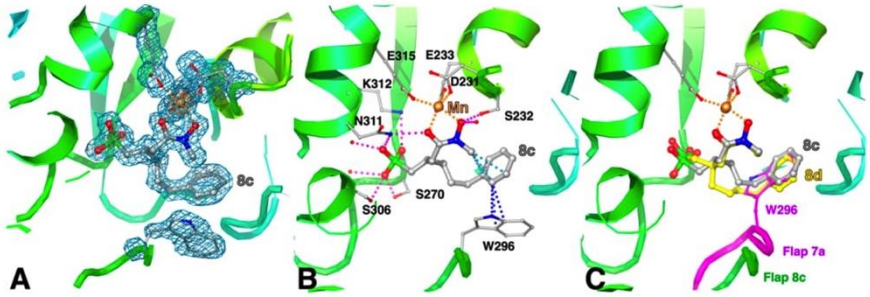

Figure 5. Active site of PfDxr bound to **8c** and **8d**. The background cartoon was created with a red-to-blue rainbow coloring for one chain. Water molecules are shown as small red spheres, and the Mn^{2+} ion is gold. (A) Electron density for the inhibitor **8c** and selected nearby residues is contoured at the rms value of the σ-weighted $(2m|F_o| - D|F_c|)$ electron-density map[57] (0.33 e/Å^3) in light blue, as well as at 2.5 e/Å^3 (gold) to show the higher electron density near the metal ion. (B) Magenta colored dots show hydrogen-bond interactions between **8c** and protein or solvent, while gold ones show metal coordination; blue and cyan dots indicate close contacts (<3.7 Å) between the phenyl group of **8c** and the indole ring of Trp296 from the flap or within the inhibitor, respectively. (C) The structures of bound **8c** and **8d** are superimposed. The flap in the complex with **7a** is shown in magenta for comparison.

IC_{50} values of the most promising compounds (determined as described in the Supporting Information) are reported in Table 1. Again, differences between the various enzymes were apparent. PfDxr was most easily inhibited (followed by EcDxr), and for this enzyme, the **8**-series compounds were more potent than **7a**−**c**. For the homologue series **8a**−**d**, the activity against EcDxr was most dependent on the linker length, although all enzymes were sensitive to this parameter to some degree. In general, a three-carbon linker appeared to be best for EcDxr and MtbDxr, but both three- and four-carbon linkers showed very good activity on PfDxr.

Table 2 summarizes the antibacterial/antiparasitic activity of these compounds. Of the compounds evaluated against *E. coli*, only **4b** showed moderate activity (MIC_{50} 15.6−31.25 μM,

DOI: 10.1021/jm5014264
J. Med. Chem. 2015, 58, 2988−3001

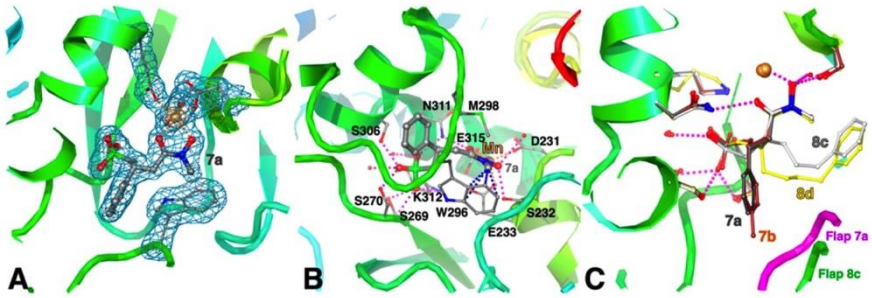

Figure 6. Active site of PfDxr bound to **7a** and **7b**. The cartoon is presented as described for Figure 5. (A) Electron density for **7a** and selected nearby residues is contoured at the rms of the map (0.28 e/Å^3) in light blue, as well as at 2.5 e/Å^3 (gold) to show the higher electron density near the metal ion. (B) Magenta-colored dots show hydrogen-bond interactions between **7a** and protein or solvent, while gold ones show metal coordination; blue dots indicate close contacts (<3.7 Å) between the methyl group of **7a** and the indole ring of Trp296 from the flap. (C) The structures of bound **7a**, **7b**, **8c**, and **8d** are superimposed. The flap in the complex with **7a** is shown in magenta for comparison with that of **8c**. Dots indicate the hydrogen bond interactions of **8c** with the enzyme and solvent.

generally comparable to those of fosmidomycin and **2**). The most promising MtbDxr inhibitors, **4b** and **8c**, were also tested against intact *M. smegmatis* cells. *M. smegmatis* was used as a model for Mtb due to its nonpathogenicity and shorter doubling time.[53] However, as for the other compounds tested (Table 2), they showed no activity (MIC_{50} > 250 μM). Overall, the lack of correlation between activity against purified enzymes and activity against whole bacteria suggests a lack of uptake or active efflux of these molecules.

All analogues were also evaluated *in vitro* for schizontocidal activity against the *P. falciparum* K1 strain. This activity correlated surprisingly well with the PfDxr inhibitory activity summarized in Table 1. Compounds **7a**−**e** were not active against blood stage *P. falciparum*. Compound **4b**, the congener of **2** with a hydroxamate group, showed potent antiplasmodial activity (IC_{50} < 0.26 μM). Introduction of a β-methyl group (**7f**) was well tolerated (IC_{50} = 0.74 μM). The activity trend in the homologue series **8b**−**d** was similar to that observed for PfDxr enzyme inhibition and indicates that a linker of three or four carbons is optimal in this case. Comparison of the *P. falciparum* K1 growth inhibition assay with the enzyme activity results suggests that there is an improved interaction with the *Plasmodium* enzyme with longer linker lengths, but there could also be a positive influence on cell permeability.

X-ray Structures of PfDxr in Complex with Four Inhibitors. As described in more detail in the Supporting Information, the structures of PfDxr in complex with four of the new β-substituted inhibitors (**7a**, **7b**, **8c**, and **8d**) have been solved at resolutions of 1.9, 2.1, 1.6, and 1.9 Å, respectively. These structures were refined to crystallographic *R*-factors of 18.7%, 21.7%, 17.7%, and 16.5% and free *R*-factors of 21.8%, 25.2%, 20.6%, and 19.6%. Each structure includes a dimer in the asymmetric unit, with a manganese ion and inhibitor in both active sites. The overall electron density is of high quality, and complete models of the enzyme are deposited at the PDB for residues 77−486 in each chain. Although the compounds were synthesized as racemic mixtures, the high resolution of the study (Figures 5 and 6 and Supporting Information, Figure S1) allowed us to identify the favored enantiomer for each ligand. Tests of both enantiomers in the refinement strongly suggested that all compounds were bound primarily as the *R*-enantiomer, although chemical rules of priority mean that the actual arrangement of the β-substituent at the chiral carbon is different for **7a** and **7b** compared with **8c** and **8d**.

The protein in the complexes with **7a** and **7b** is for the most part identical, with an rms distance of only 0.2 Å when the subunits are compared. The largest difference is at Pro294 of the active-site flap, where the Cα position differs by approximately 1 Å in the two structures; there is well-ordered electron density for all residues in the respective flaps. This movement is directly linked to the addition of the methyl group in **7b** and correlates well with the observation that IC_{50} increases as larger groups are added at this position. Interactions with the hydroxamate and phosphonate are essentially the same. The methyl group of the hydroxamic acid in each case makes close interactions with the indole ring of Trp296 (Figure 6B). Both of these protein structures are quite similar to the complexes with fosmidomycin and **2**, with the caveat that His293, Met298, and Ile302 must adjust somewhat to accommodate the new β-substituent.

More substantial differences are observed for the complexes with **8c** and **8d**. As can be seen in Figure 6C, the β-substituents are placed in a very different way in the two series of compounds. Again, most of the protein is very similar, but the active-site flaps are pushed further away as the β-substituent of **8c** and **8d** displaces Trp296. In the **8c** complex, density is weak between 293 and 295 of both chains. Only the flap of the A molecule of the **8d** complex has continuous density at the RMS of the map; in the B-site, there is a break between residues 292 and 296. In each complex, the methylene linker of the inhibitor is found in a depression described in numerous Cα-aryl complexes, wedged between three ordered and one often-disordered loop (containing PfDxr residues 272, 338, 358, and 296, respectively). As shown in Figures 5C and 6C, the flexibility of the linker means it can take on a boomerang shape that allows the phenyl group of each inhibitor to interact with its methyl group (Figure 5B). The phenyl ring occupies the place normally assumed by the indole ring of the conserved tryptophan of the flap (Figure 5C), resulting in acyl-group-to-ring interactions similar to those seen in the **7a** and **7b** complexes (Figure 6B and Supporting Information, Figure S1), as well as **2** ternary complexes.[36] In three of the four active sites where we are able to observe Trp296, the face of the indole ring stacks on the edge of the phenyl ring of the inhibitor (Figure

DOI: 10.1021/jm5014264
J. Med. Chem. 2015, 58, 2988−3001

5B). These favorable interactions are achieved in the **8c** complex with the same ligand backbone conformation normally observed in antibiotic/NADPH ternary complexes. In the **8d** complex, fitting in the extra methylene group while conserving the position of the phenyl group requires a rearrangement of the fosmidomycin backbone (Figures 5C and 6C). While the position of the hydroxamate remains unchanged, there are small but significant changes in the orientation of the phosphonate. These changes do not cause a ripple of differences in protein side chains involved in phosphonate binding, but instead there is a rearrangement of which phosphonate oxygen interacts with which hydrogen-bond donor. Figure 6C shows a superposition of the hydrogen-bond donors that interact with **7a**, **7b**, **8c**, or **8d**. Clearly, they are structurally highly conserved, while the phosphonate groups are not so tightly clustered. Table S3, Supporting Information, highlights the various sets of interactions and shows that only one phosphonate oxygen has the full set of three interacting groups in all complexes, a second oxygen has two interacting groups, and the third has either two or three interacting groups. Only oxygen 1 has the same interacting groups in all four complexes, and only five groups interact in the same site in all complexes, while one group (Lys312-NZ) interacts in all complexes but with two different oxygens. The rearrangement of the fosmidomycin backbone in **8c** would produce a close contact with the usual conformation seen for Lys312, and so a small conformational change is needed to relieve this clash while maintaining an interaction with the phosphonate (Figure 6C). The side chain of His293 does not contribute to phosphonate binding in any of the complexes, in contrast to observations in antibiotic/NADPH ternary complexes.

In all active sites, in all complexes, the hydroxamic acid group adopts a synperiplanar conformation (O═C−N—O angle is 0°), in which both oxygen atoms coordinate to the manganese, as does a single carboxyl oxygen atom from each of the highly conserved acidic residues, Asp231, Asp233, and Glu315. The differences from the usual set of interactions observed in the antibiotic/NADPH ternary complexes are merely a consequence of the hydroxamate group in the new structures. Figures 5C and 6B show that the hydrogen bonding interactions are conserved, and the *N*-formyl oxygen now accepts a hydrogen bond from Asn311-ND2, while the *N*-hydroxyl oxygen interacts with Ser232-OG and a conserved water molecule.

Molecular Modeling on MtbDxr. At present, it is not clear why such large differences are observed for the inhibition of the different enzymes. Modeling experiments were therefore performed in an attempt to gain insights into how the new inhibitors might interact with MtbDxr. Specifically, we were interested in understanding how the phenylpropyl substituent of **8c** might be interacting with the Trp-containing loop of Dxr. In the X-ray structure of MtbDxr in complex with **2** (PDB code 4A03),[54] a loop containing Trp203 closes over the bound ligand, while this loop is disordered in the reported X-ray structures of Dxr cocomplexes with α-phenyl-substituted analogues, which are all less potent inhibitors of the enzyme.

When comparing the predicted binding of **7f** and the aromatic analogues **8a−d** to the measured binding of fosmidomycin, one makes an interesting observation with respect to Ser213. In the cocrystal structure with fosmidomycin bound, Ser213 is hydrogen bonded to the phosphate of the ligand. This same orientation is predicted when **7f** is bound. For the aromatic analogues, however, Ser213 is reoriented and points instead toward His200. It appears that the hydrogen bonding between Ser213 and the phosphate is disrupted upon binding of the aromatic analogues. His203 appears to bind to Ser213 in order to compensate for the loss of interaction with the phosphate. This might explain the loss of activity of aromatic analogues **8a−d** relative to fosmidomycin.

The modeled structure of **8c** (white carbons) compared with the X-ray structure of the protein with fosmidomycin bound (green carbons) is shown in Figure 7.

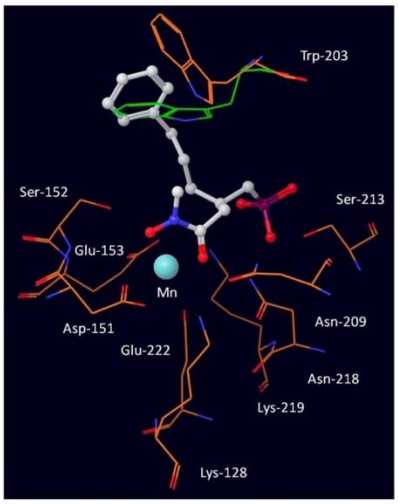

Figure 7. Optimized geometry of **8c** in the minimized protein structure PDB entry 4A03 (MtbDxr). Only relevant residues close to the ligand are shown for clarity and labeled according to their residue numbers in the 4A03 structure. The position of Trp203 in 4A03 is shown with green carbon atoms. The carbon atoms of the optimized protein residues are shown in orange, while the ligand carbon atoms are shown in white. The position of the Trp203 indole ring overlaps with the position of the phenyl ring in **8c**. In the optimized structure, Trp203 forms a T-stacking interaction with the phenyl ring of **8c**.

In the minimized structure of **8c**, the aromatic ring occupies almost exactly the same position as the phenyl portion of Trp203 in the complex with fosmidomycin. Since the aromatic ring of Trp203 occupies what is presumably a stable position in the folded protein, it could be assumed that this position would also be favorable for a ligand to occupy when the loop needs to be displaced for steric reasons. This could be described as an aromatic "hotspot". Therefore, it could be that this results in favorable van der Waals and lipophilic interactions of the phenyl ring in this position, which accounts for the better activity of **8c** compared with the shorter **8b**, which may not reach the hotspot, and **8d**, where the carbon chain is too long for the phenyl to occupy the same position. In addition, Trp203 in the loop of the minimized structure with **8c** makes an edge-to-face interaction with the phenyl ring of the ligand, potentially stabilizing the *loop and ligand* in this position.

■ CONCLUSIONS

We present here the first systematic study on β-substituted analogues of fosmidomycin. A series of analogues with different aromatic moieties connected directly to the β-carbon (**7a−e**)

DOI: 10.1021/jm5014264
J. Med. Chem. 2015, 58, 2988−3001

failed to inhibit EcDxr and MtbDxr and proved moderately active against PfDxr. None of these compounds was capable of inhibiting the growth of *E. coli*, *M. smegmatis*, or *P. falciparum* strain K-1. Exploration of alkyl linkers of different lengths between the β-carbon and a phenyl ring resulted in establishment of a three-carbon linker (**8c**) as optimal for *E. coli* and *M. tuberculosis* Dxr inhibition and a four-carbon linker (**8d**) for inhibition of *P. falciparum* Dxr. While compounds **8a**−**d** also lacked activity against *E. coli* and *M. smegmatis*, **8c** and **8d** showed submicromolar schizontocidal activity against the *P. falciparum* K1 strain, where essentially the same SAR was observed as for PfDxr inhibition. Interestingly, the activity of **8c** and **8d** surpassed that of **7f**, indicating a favorable contribution of the phenylpropyl and phenylbutyl substituents to antiplasmodial growth inhibition.

Crystallographic studies on four of the compounds most active on PfDXR (**7a**, **7b**, **8c**, and **8d**) show two different, novel modes of binding to the enzyme. The compounds showing the best enzyme inhibition and best *in vitro* activity against the parasite mimic the favorable interactions between the indole ring of the conserved tryptophan in the flap with the fosmidomycin backbone that have been seen in a number of antibiotic-bound ternary complexes. However, this mimicry is achieved by intramolecular interactions within each inhibitor (**8c**, **8d**), such that the phenyl ring common to this series spatially overlaps the usual position of the indole ring. Rearrangement of the flap results in favorable interactions between the phenyl ring of the inhibitors and the tryptophan. The improved activity of **8d** compared with **8c** is likely a consequence of this set of interactions.

■ EXPERIMENTAL SECTION

General. All reactions described were performed under an argon atmosphere and at ambient temperature unless stated otherwise. All reagents and solvents were purchased from Sigma-Aldrich (Diegem, Belgium), Acros Organics (Geel, Belgium), or TCI Europe (Zwijndrecht, Belgium) and used as received (except THF). THF was dried over sodium/benzophenone. NMR solvents were purchased from Eurisotop (Saint-Aubin, France). Reactions were monitored by TLC analysis using TLC aluminum sheets (Macherey-Nagel, Alugram Sil G/UV_{254}). Detection was achieved by spraying with a solution of $(NH_4)_6Mo_7O_{24}{\cdot}4H_2O$ (25 g/L) and $(NH_4)_4Ce(SO_4)_4{\cdot}2H_2O$ (10 g/L) in H_2SO_4 (10%) followed by charring or immersion in an aqueous solution of $KMnO_7$ (20 g/L) and K_2CO_3 (10 g/L) or an ethanolic solution of ninhydrin (2 g/L) and acetic acid (1% v/v) followed by charring. Silica gel column chromatography was performed manually using Grace Davisil 60 Å silica gel (40−63 μm) or automated using a Grace Reveleris X2 system and the corresponding flash cartridges. High-resolution spectra were recorded with a Waters LCT Premier XE Mass spectrometer. ^{1}H and ^{13}C NMR spectra were recorded with a Varian Mercury-300BB (300/75 MHz) spectrometer. Chemical shifts are given in ppm (δ) relative to tetramethylsilane (^{1}H NMR) or the NMR solvent (^{13}C NMR) as an internal standard. In ^{31}P NMR, signals are referenced to the $CDCl_3$ or D_2O lock resonance frequency according to IUPAC referencing, with H_3PO_4 set to 0.00 ppm. Coupling constants are given in hertz. Preparative HPLC purifications were carried out using a Laprep preparative HPLC system equipped with an Xbridge Prep C18 column (19 mm × 250 mm, 5 μm) using a water/acetonitrile/formic acid gradient solvent system. All synthesized compounds were ≥95% pure as verified by LCMS. NMR analysis showed a rotameric mixture for some of the prepared compounds. At high temperature (80 °C), the phosphorus signals of the two rotameric forms of a representative compound (**7b**) merged into a single peak.

General Procedure I: Synthesis of *tert*-Butyl Cinnamates 11a−e. To a 0.1 M solution of the appropriate cinnamic acid (40−45 mmol, 1 equiv) in *tert*-butanol at 35 °C was added di-*tert*-butyl dicarbonate (2.0 equiv) and 4-dimethylaminopyridine (0.3 equiv). The mixture was heated to 35 °C overnight and then poured into water and extracted three times with dichloromethane. The organic fractions were pooled, washed once with brine, and dried over $NaSO_4$. Filtration, *in vacuo* concentration, and subsequent silica gel column chromatography gave the respective *tert*-butyl cinnamates. Characterization was in agreement with reported data.[55,56]

General Procedure II: Dess−Martin Oxidation and Concomitant Wittig Olefination. A 0.05 M solution of the starting material in CH_2Cl_2 and a nitrogen atmosphere was cooled to 0 °C. Solid Dess−Martin periodinane (2.0 equiv) was added, and the temperature was allowed to rise to RT. Upon completion of the reaction (TLC monitoring; typically 3 h), the mixture was washed with a mixture (5:1 v/v) of $NaHCO_3$ (sat. aq) and $Na_2S_2O_3$ (aq, 2.0 M). The formed water layer was then extracted three times with diethyl ether. The organic fractions were combined, washed with HCl (0.1 M, once) and brine (once), and dried over anhydrous Na_2SO_4 before *in vacuo* concentration. The resulting crude aldehyde was dissolved in toluene under a nitrogen atmosphere, and 3.0 equiv of *tert*-butyl (triphenylphosphoranylidene)acetate was added. The mixture was refluxed at 120 °C overnight. It was allowed to cool to RT and concentrated *in vacuo*. The crude mixture was adsorbed onto Celite and purified by silica gel chromatography.

General Procedure III: Michael Addition of Methylphosphonatediesters to α,β-Unsaturated *tert*-Butyl Esters. To a 1.0 M solution of dibenzylmethyl- or diethylmethyl-phosphonate (2.0 equiv) in THF was added *n*-BuLi (1.6 M solution in hexanes, 2.0 equiv) at −78 °C under a N_2 atmosphere. After 30 min, a 0.5 M solution of the α,β-unsaturated ester (1.0 equiv) in THF was added dropwise. When the reaction was complete (typically 3 h), the reaction was quenched with sat. aq NH_4Cl and transferred to a separatory funnel. The aqueous solution was extracted three times with EtOAc. The organic fractions were combined, washed once with brine, dried (Na_2SO_4), filtered, and concentrated. Column chromatography of the residue yielded the Michael adduct.

General Procedure IV: Acidic Cleavage of the *tert*-Butyl Ester and Protected Hydroxamate Formation. A 0.1 M solution of the *tert*-butyl ester (1.0 equiv) in CH_2Cl_2/TFA (80:20) at 0 °C, was stirred for 2 h, after which an excess of toluene was added to the reaction mixture and concentrated *in vacuo*. The crude acid was redissolved in CH_2Cl_2 (0.1 M), followed by addition of EDC (1.2 equiv), DMAP (1.2 equiv) and DiPEA (2.0 equiv). *O*-Benzyl-*N*-methylhydroxylamine TFA salt (1.2 equiv) was added as a 0.2 M solution in CH_2Cl_2, and the ensemble was allowed to stir overnight at room temperature. The mixture was quenched with sat. aq $NaHCO_3$, extracted three times with CH_2Cl_2, washed with brine, and dried over Na_2SO_4. Column chromatography produced the protected hydroxamic acids.

General Procedure V: Catalytic Hydrogenolysis of Benzyl Protective Groups. The benzyl protected compound was dissolved in MeOH (10 mg/mL) under a nitrogen atmosphere, and a catalytic amount of Pd/C (10%) was added. The resulting mixture was then stirred under a hydrogen atmosphere for 10 min. Upon completion of the reaction (confirmed by MS), the mixture was filtered and neutralized with 1.0 equiv of NaOH (aq, 1.0 M). It was then concentrated *in vacuo*, redissolved in a mixture of water and *tert*-butanol (1:1 v/v, 1.0 mL/10 mg starting material), frozen, and lyophilized affording the desired phosphonic acid monosodium salts in quantitative yield.

General Procedure VI: Boron Trichloride Mediated Selective Debenzylation of the Hydroxamate. A 0.1 M solution of the benzylated hydroxamate in dichloromethane was cooled to −75 °C. BCl_3 (1 M solution in CH_2Cl_2, 3.0 equiv) was added dropwise, and the mixture allowed to stir at this temperature for 45 min. Next, the reaction mixture was poured into aqueous $NaHCO_3$ and extracted 4 times with CH_2Cl_2. The organic fractions were combined, washed with brine, dried (Na_2SO_4), filtered, and concentrated *in vacuo*. The residue was purified by silica gel column chromatography to obtain the free hydroxamate.

DOI: 10.1021/jm5014264
J. Med. Chem. 2015, 58, 2988−3001

failed to inhibit EcDxr and MtbDxr and proved moderately active against PfDxr. None of these compounds was capable of inhibiting the growth of *E. coli*, *M. smegmatis*, or *P. falciparum* strain K-1. Exploration of alkyl linkers of different lengths between the β-carbon and a phenyl ring resulted in establishment of a three-carbon linker (**8c**) as optimal for *E. coli* and *M. tuberculosis* Dxr inhibition and a four-carbon linker (**8d**) for inhibition of *P. falciparum* Dxr. While compounds **8a**−**d** also lacked activity against *E. coli* and *M. smegmatis*, **8c** and **8d** showed submicromolar schizontocidal activity against the *P. falciparum* K1 strain, where essentially the same SAR was observed as for PfDxr inhibition. Interestingly, the activity of **8c** and **8d** surpassed that of **7f**, indicating a favorable contribution of the phenylpropyl and phenylbutyl substituents to antiplasmodial growth inhibition.

Crystallographic studies on four of the compounds most active on PfDXR (**7a**, **7b**, **8c**, and **8d**) show two different, novel modes of binding to the enzyme. The compounds showing the best enzyme inhibition and best *in vitro* activity against the parasite mimic the favorable interactions between the indole ring of the conserved tryptophan in the flap with the fosmidomycin backbone that have been seen in a number of antibiotic-bound ternary complexes. However, this mimicry is achieved by intramolecular interactions within each inhibitor (**8c**, **8d**), such that the phenyl ring common to this series spatially overlaps the usual position of the indole ring. Rearrangement of the flap results in favorable interactions between the phenyl ring of the inhibitors and the tryptophan. The improved activity of **8d** compared with **8c** is likely a consequence of this set of interactions.

■ EXPERIMENTAL SECTION

General. All reactions described were performed under an argon atmosphere and at ambient temperature unless stated otherwise. All reagents and solvents were purchased from Sigma-Aldrich (Diegem, Belgium), Acros Organics (Geel, Belgium), or TCI Europe (Zwijndrecht, Belgium) and used as received (except THF). THF was dried over sodium/benzophenone. NMR solvents were purchased from Eurisotop (Saint-Aubin, France). Reactions were monitored by TLC analysis using TLC aluminum sheets (Macherey-Nagel, Alugram Sil G/UV_{254}). Detection was achieved by spraying with a solution of $(NH_4)_6Mo_7O_{24}{\cdot}4H_2O$ (25 g/L) and $(NH_4)_4Ce(SO_4)_4{\cdot}2H_2O$ (10 g/L) in H_2SO_4 (10%) followed by charring or immersion in an aqueous solution of $KMnO_7$ (20 g/L) and K_2CO_3 (10 g/L) or an ethanolic solution of ninhydrin (2 g/L) and acetic acid (1% v/v) followed by charring. Silica gel column chromatography was performed manually using Grace Davisil 60 Å silica gel (40−63 μm) or automated using a Grace Reveleris X2 system and the corresponding flash cartridges. High-resolution spectra were recorded with a Waters LCT Premier XE Mass spectrometer. ^{1}H and ^{13}C NMR spectra were recorded with a Varian Mercury-300BB (300/75 MHz) spectrometer. Chemical shifts are given in ppm (δ) relative to tetramethylsilane (^{1}H NMR) or the NMR solvent (^{13}C NMR) as an internal standard. In ^{31}P NMR, signals are referenced to the $CDCl_3$ or D_2O lock resonance frequency according to IUPAC referencing, with H_3PO_4 set to 0.00 ppm. Coupling constants are given in hertz. Preparative HPLC purifications were carried out using a Laprep preparative HPLC system equipped with an Xbridge Prep C18 column (19 mm × 250 mm, 5 μm) using a water/acetonitrile/formic acid gradient solvent system. All synthesized compounds were ≥95% pure as verified by LCMS. NMR analysis showed a rotameric mixture for some of the prepared compounds. At high temperature (80 °C), the phosphorus signals of the two rotameric forms of a representative compound (**7b**) merged into a single peak.

General Procedure I: Synthesis of *tert*-Butyl Cinnamates 11a−e. To a 0.1 M solution of the appropriate cinnamic acid (40−45 mmol, 1 equiv) in *tert*-butanol at 35 °C was added di-*tert*-butyl dicarbonate (2.0 equiv) and 4-dimethylaminopyridine (0.3 equiv). The mixture was heated to 35 °C overnight and then poured into water and extracted three times with dichloromethane. The organic fractions were pooled, washed once with brine, and dried over $NaSO_4$. Filtration, *in vacuo* concentration, and subsequent silica gel column chromatography gave the respective *tert*-butyl cinnamates. Characterization was in agreement with reported data.[55,56]

General Procedure II: Dess−Martin Oxidation and Concomitant Wittig Olefination. A 0.05 M solution of the starting material in CH_2Cl_2 and a nitrogen atmosphere was cooled to 0 °C. Solid Dess−Martin periodinane (2.0 equiv) was added, and the temperature was allowed to rise to RT. Upon completion of the reaction (TLC monitoring; typically 3 h), the mixture was washed with a mixture (5:1 v/v) of $NaHCO_3$ (sat. aq) and $Na_2S_2O_3$ (aq, 2.0 M). The formed water layer was then extracted three times with diethyl ether. The organic fractions were combined, washed with HCl (0.1 M, once) and brine (once), and dried over anhydrous Na_2SO_4 before *in vacuo* concentration. The resulting crude aldehyde was dissolved in toluene under a nitrogen atmosphere, and 3.0 equiv of *tert*-butyl (triphenylphosphoranylidene)acetate was added. The mixture was refluxed at 120 °C overnight. It was allowed to cool to RT and concentrated *in vacuo*. The crude mixture was adsorbed onto Celite and purified by silica gel chromatography.

General Procedure III: Michael Addition of Methylphosphonatediesters to α,β-Unsaturated *tert*-Butyl Esters. To a 1.0 M solution of dibenzylmethyl- or diethylmethyl-phosphonate (2.0 equiv) in THF was added *n*-BuLi (1.6 M solution in hexanes, 2.0 equiv) at −78 °C under a N_2 atmosphere. After 30 min, a 0.5 M solution of the α,β-unsaturated ester (1.0 equiv) in THF was added dropwise. When the reaction was complete (typically 3 h), the reaction was quenched with sat. aq NH_4Cl and transferred to a separatory funnel. The aqueous solution was extracted three times with EtOAc. The organic fractions were combined, washed once with brine, dried (Na_2SO_4), filtered, and concentrated. Column chromatography of the residue yielded the Michael adduct.

General Procedure IV: Acidic Cleavage of the *tert*-Butyl Ester and Protected Hydroxamate Formation. A 0.1 M solution of the *tert*-butyl ester (1.0 equiv) in CH_2Cl_2/TFA (80:20) at 0 °C, was stirred for 2 h, after which an excess of toluene was added to the reaction mixture and concentrated *in vacuo*. The crude acid was redissolved in CH_2Cl_2 (0.1 M), followed by addition of EDC (1.2 equiv), DMAP (1.2 equiv) and DiPEA (2.0 equiv). *O*-Benzyl-*N*-methylhydroxylamine TFA salt (1.2 equiv) was added as a 0.2 M solution in CH_2Cl_2, and the ensemble was allowed to stir overnight at room temperature. The mixture was quenched with sat. aq $NaHCO_3$, extracted three times with CH_2Cl_2, washed with brine, and dried over Na_2SO_4. Column chromatography produced the protected hydroxamic acids.

General Procedure V: Catalytic Hydrogenolysis of Benzyl Protective Groups. The benzyl protected compound was dissolved in MeOH (10 mg/mL) under a nitrogen atmosphere, and a catalytic amount of Pd/C (10%) was added. The resulting mixture was then stirred under a hydrogen atmosphere for 10 min. Upon completion of the reaction (confirmed by MS), the mixture was filtered and neutralized with 1.0 equiv of NaOH (aq, 1.0 M). It was then concentrated *in vacuo,* redissolved in a mixture of water and *tert*-butanol (1:1 v/v, 1.0 mL/10 mg starting material), frozen, and lyophilized affording the desired phosphonic acid monosodium salts in quantitative yield.

General Procedure VI: Boron Trichloride Mediated Selective Debenzylation of the Hydroxamate. A 0.1 M solution of the benzylated hydroxamate in dichloromethane was cooled to −75 °C. BCl_3 (1 M solution in CH_2Cl_2, 3.0 equiv) was added dropwise, and the mixture allowed to stir at this temperature for 45 min. Next, the reaction mixture was poured into aqueous $NaHCO_3$ and extracted 4 times with CH_2Cl_2. The organic fractions were combined, washed with brine, dried (Na_2SO_4), filtered, and concentrated *in vacuo*. The residue was purified by silica gel column chromatography to obtain the free hydroxamate.

DOI: 10.1021/jm5014264
J. Med. Chem. 2015, 58, 2988−3001

General Procedure VII: Trimethylbromosilane Mediated Deprotection of Diethyl Phosphonates. To a 0.1 M solution of starting material in dichloromethane was added BSTFA (4.0 equiv). The mixture was allowed to stir at room temperature for 15 min before an ice bath was installed, and TMSBr (10.0 equiv) was added. The ice bath was removed after 10 min, and the reaction allowed to stir until phosphorus NMR confirmed complete deprotection. All volatiles were removed *in vacuo*, and the resultant oil was redissolved in acetonitrile. Concentrated ammonia was added, and the mixture was allowed to stir at room temperature for 20 min. Evaporation of volatiles and subsequent lyophilization from a mixture of *tert*-butanol and water afforded the compound in quantitative yield.

*Dibenzyl 2-Phenyl-3-(tert-butoxycarbonyl)propylphosphonate (**12a**).* Prepared from compound **11a** (715 mg, 3.50 mmol) according to general procedure III. Colorless oil; purification 1.5:1 Hex/EtOAc v/v; yield 72%. ^{1}H NMR (300 MHz, $CDCl_3$) δ_H ppm 1.25 (br, 9H, *t*-Bu), 2.17 (dd, J = 3.5 Hz, 18.6 Hz, 1H, P−CH_2−), 2.19 (dd, J = 2.8 Hz, 18.6 Hz, 1H, P−CH_2−), 2.52 (ddd, J = 1.3 Hz, J = 9.3 Hz, 15.2 Hz, 1H, −CH_2−CO), 2.78 (dd, J = 6.2 Hz, 15.2 Hz, 1H, −CH_2−CO), 3.44−3.62 (m, 1H, −C<u>H</u>−), 4.66−4.87 (m, 4H, −CH_2Ph), 7.17−7.36 (m, 15H, Ar−H). ^{13}C NMR (75 MHz, $CDCl_3$) δ_C ppm 27.8, 32.8 (d, $^1J_{C-P}$ = 139.2 Hz), 36.9, (d, $^2J_{C-P}$ = 3.1 Hz), 43.1 (d, $^3J_{C-P}$ = 12.9 Hz), 66.8 (d, $^2J_{C-P}$ = 6.5 Hz), 67.1 (d, $^2J_{C-P}$ = 6.4 Hz), 80.5, 126.9, 127.5, 127.8, 127.9, 128.3, 128.4, 136.2 (d, $^3J_{C-P}$ = 6.2 Hz), 136.3 (d, $^3J_{C-P}$ = 6.1 Hz), 142.9 (d, $^3J_{C-P}$ = 8.9 Hz), 170.5. ^{31}P NMR (121.5 MHz, $CDCl_3$): δ_P ppm = 32.9. HRMS (ESI): calculated for $C_{28}H_{34}O_3P$ [(M + H)$^+$] 481.2138; found 481.2148.

*Dibenzyl 2-(p-Methylphenyl)-3-(tert-butoxycarbonyl)-propylphosphonate (**12b**).* Prepared from compound **11b** (680 mg, 3.11 mmol) according to general procedure III. Colorless oil; purification 2:1 Hex/EtOAc v/v; yield 73%. ^{1}H NMR (300 MHz, $CDCl_3$) δ_H ppm 1.27 (br, 9H, *t*-Bu), 2.11−2.23 (m, 2H, P−CH_2−), 2.28 (s, 3H, −Ph−CH_3), 2.50 (ddd, J = 1.5 Hz, 9.2 Hz, 15.2 Hz, 1H, −CH_2−CO), 2.75 (dd, J = 6.4 Hz, 15.2 Hz, 1H, −CH_2−CO), 3.40−3.57 (m, 1H, −C<u>H</u>−), 4.68−4.88 (m, 4H, −C<u>H_2</u>−Ph), 7.01−7.11 (m, 4H, Ar−H), 7.18−7.36 (m, 10H, Ar−H). ^{13}C NMR (75 MHz, $CDCl_3$) δ_C ppm 21.0, 27.9, 32.8 (d, $^1J_{C-P}$ = 139.6 Hz), 36.5 (d, $^2J_{C-P}$ = 3.2 Hz), 43.3 (d, $^3J_{C-P}$ = 12.8 Hz), 66.8 (d, $^2J_{C-P}$ = 6.4 Hz), 67.0 (d, $^2J_{C-P}$ = 6.6 Hz), 80.4, 127.3, 127.8, 127.8, 128.2, 128.5, 129.1, 136.3 (d, $^2J_{C-P}$ = 6.1 Hz), 136.4 (d, $^2J_{C-P}$ = 6.0 Hz), 139.9 (d, $^3J_{C-P}$ = 8.8 Hz), 170.7. ^{31}P NMR (121.5 MHz, $CDCl_3$): δ_P ppm = 31.4. HRMS (ESI): calculated for $C_{29}H_{36}O_3P$ [(M + H)$^+$] 495.2295; found 495.2315.

*Dibenzyl 2-(p-Methoxyphenyl)-3-(tert-butoxycarbonyl)-propylphosphonate (**12c**).* Prepared from compound **11c** (700 mg, 2.99 mmol) according to general procedure III. White crystal; purification 1:1 Hex/EtOAc v/v; yield 69%. ^{1}H NMR (300 MHz, $CDCl_3$) δ_H ppm 1.27 (br, 9H, *t*-Bu), 2.04−2.27 (m, 2H, P−CH_2−), 2.48 (ddd, J = 1.4 Hz, 9.3 Hz, 15.2 Hz, 1H, −CH_2−CO), 2.73 (dd, J = 6.3 Hz, 15.2 Hz, 1H, −CH_2−CO), 3.40−3.57 (m, 1H, −CH−), 3.74 (s, 3H, −Ph−O−CH_3), 4.68−4.91 (m, 4H, −CH_2Ph), 6.78 (d, J = 8.5 Hz, 2H, Ar−H), 7.11 (d, J = 8.5 Hz, 2H, Ar−H), 7.18−7.37 (m, 10H, Ar−H). ^{13}C NMR (75 MHz, $CDCl_3$) δ_C ppm 27.8, 32.9 (d, $^1J_{C-P}$ = 137.7 Hz), 36.2 (d, $^2J_{C-P}$ = 3.5 Hz), 43.4 (d, $^3J_{C-P}$ = 12.2 Hz), 55.1, 66.8 (d, $^2J_{C-P}$ = 5.8 Hz), 67.0 (d, $^2J_{C-P}$ = 5.8 Hz), 80.4, 113.7, 127.8, 127.8, 128.2, 128.4, 134.9 (d, $^3J_{C-P}$ = 8.5 Hz), 136.2 (d, $^3J_{C-P}$ = 5.9 Hz), 136.3 (d, $^3J_{C-P}$ = 5.3 Hz), 158.4, 170.5. ^{31}P NMR (121.5 MHz, $CDCl_3$): δ_P ppm = 30.25 HRMS (ESI): calculated for $C_{29}H_{36}O_6P$ [(M + H)$^+$] 511.2244; found 511.2260.

*Dibenzyl 2-Methyl-3-(tert-butoxycarbonyl)propylphosphonate (**12f**).* Prepared from compound *tert*-butylcrotonate (890 mg, 6.26 mmol) according to general procedure III. Colorless oil; purification 1.5:1 Hex/EtOAc v/v; yield 62%. ^{1}H NMR (300 MHz, $CDCl_3$) δ_H ppm 1.08 (d, J = 6.5 Hz, 3H, −CH(CH_3)−), 1.42 (br, 9H, *t*-Bu), 1.61−1.79 (m, 2H, P−CH_2−), 1.83−2.00 (m, 1H, −CH_2−CO), 2.06−2.20 (m, 1H, −CH−), 2.28−2.47 (m, 2H, −CH_2−CO), 4.90−5.10 (m, 4H, −C<u>H_2</u>−Ph), 7.27−7.41 (m, 10H, Ar−H). ^{13}C NMR (75 MHz, $CDCl_3$) δ_C ppm 21.7 ($^3J_{C-P}$ = 8.6 Hz), 25.1 ($^2J_{C-P}$ = 5.2 Hz), 27.8, 32.4 ($^1J_{C-P}$ = 139.5 Hz), 39.7 ($^3J_{C-P}$ = 12.0 Hz), 67.01 ($^2J_{C-P}$ = 6.5 Hz), 67.03 ($^2J_{C-P}$ = 6.5 Hz), 76.2, 127.9, 127.9, 129.2, 134.5, 136.17 ($^3J_{C-P}$ = 5.9 Hz), 173.3. ^{31}P NMR (121.5 MHz, $CDCl_3$): δ_P ppm = 32.87. HRMS (ESI): calculated for $C_{23}H_{32}O_3P$ [(M + H)$^+$] 419.1982; found 419.1904.

*Dibenzyl 3-(N-(Benzyloxy)-N-methylcarbamoyl)-2-phenylpropyl-phosphonate (**13a**).* Prepared from compound **12a** (1.0 g, 2.08 mmol) according to general procedure IV. Colorless oil; purification 97:3 CH_2Cl_2/MeOH v/v; yield 51%. ^{1}H NMR (300 MHz, $CDCl_3$) δ_H ppm 2.04−2.39 (m, 2H, P−CH_2−), 2.69−2.90 (m, 2H, −CH_2−CON−), 3.07 (s, 3H, N−CH_3), 3.56−3.75 (m, 1H, −C<u>H</u>(Ph)−), 4.63 (s, 2H, NOC<u>H_2</u>Ph) 4.67−4.91 (m, 4H, POC<u>H_2</u>Ph), 7.13−7.41 (m, 20H, Ar−H). ^{13}C NMR (75 MHz, $CDCl_3$) δ_C ppm 32.2 (d, $^1J_{C-P}$ = 137.6 Hz), 36.1 (d, $^2J_{C-P}$ = 3.4 Hz), 39.8 (d, $^3J_{C-P}$ = 12.6 Hz), 66.8 (d, $^2J_{C-P}$ = 6.4 Hz), 67.1 (d, $^2J_{C-P}$ = 6.4 Hz), 76.1, 126.8, 127.5, 127.8, 127.9, 128.1, 128.2, 128.5, 128.7, 128.9, 129.2, 134.5, 136.3, (d, $^3J_{C-P}$ = 6.6 Hz), 136.4 (d, $^3J_{C-P}$ = 6.4 Hz), 143.6 (d, $^3J_{C-P}$ = 8.4 Hz), 172.9. ^{31}P NMR (121.5 MHz, $CDCl_3$): δ_P ppm = 33.16. HRMS (ESI): calculated for $C_{32}H_{35}NO_5P$ [(M + H)$^+$] 544.2247; found 544.2318.

*Dibenzyl 3-(N-(Benzyloxy)-N-methylcarbamoyl)-2-p-tolylpropyl-phosphonate (**13b**).* Prepared from compound **12b** (980 mg, 1.98 mmol) according to general procedure IV. Colorless oil; purification 97:3 CH_2Cl_2/MeOH v/v; yield 56%. ^{1}H NMR (300 MHz, $CDCl_3$) δ_H ppm 2.04−2.37 (m, 5H, P−CH_2−, Ph−CH_3), 2.69−2.90 (m, 2H, −CH_2CO), 3.08 (s, 3H, N−CH_3), 3.54−3.71 (m, 1H, −CH−), 4.64 (s, 2H, −NOC<u>H_2</u>Ph), 4.70−4.89 (m, 4H, POC<u>H_2</u>Ph), 7.05 (m, 4H, Ar−H), 7.15−7.40 (m, 15H, Ar−H). ^{13}C NMR (75 MHz, $CDCl_3$) δ_C ppm 20.9, 32.2 (d, $^1J_{C-P}$ = 139.6 Hz), 35.5, 39.7 (d, $^3J_{C-P}$ = 11.8 Hz), 66.6 (d, $^2J_{C-P}$ = 5.7 Hz), 66.8 (d, $^3J_{C-P}$ = 6.4 Hz), 66.4, 127.2, 127.6, 127.7, 128.0, 128.3, 128.5, 128.7, 130.0, 129.1, 134.4, 136.0, 136.2 (d, $^3J_{C-P}$ = 6.9 Hz), 136.3 (d, $^3J_{C-P}$ = 6.3 Hz), 140.4 (d, $^3J_{C-P}$ = 8.3 Hz), 172.7. ^{31}P NMR (121.5 MHz, $CDCl_3$): δ_P ppm = 31.67. HRMS (ESI): calculated for $C_{33}H_{37}NO_5P$ [(M + H)$^+$] 558.2404; found 558.2408.

*Dibenzyl 3-(N-(Benzyloxy)-N-methylcarbamoyl)-2-(4-methoxyphenyl)propylphosphonate (**13c**).* Prepared from compound **12c** (850 mg, 1.67 mmol) according to general procedure IV. Colorless oil; purification gradient 0−5% MeOH in CH_2Cl_2; yield 47%. ^{1}H NMR (300 MHz, $CDCl_3$) δ_H ppm 2.01−2.37 (m, 2H, P−CH_2−), 2.66−2.88 (m, 2H, −C<u>H_2</u>−CO), 3.07 (s, 3H, N−CH_3), 3.53−3.70 (m, 1H, −CH−), 3.72 (s, 3H, Ph−O−CH_3), 4.64 (s, 2H, NOC<u>H_2</u>Ph), 4.70−4.90 (m, 4H, −C<u>H_2</u>−Ph), 6.76 (d, J = 8.8 Hz, 2H, Ar−H), 7.08 (d, J = 8.8 Hz, 2H, Ar−H), 7.14−7.39 (m, 15H, Ar−H). ^{13}C NMR (75 MHz, $CDCl_3$) δ_C ppm 32.3 ($^1J_{C-P}$ = 138.72 Hz), 35.2 ($^3J_{C-P}$ = 3.99 Hz), 39.9 ($^3J_{C-P}$ = 13.1 Hz), 55.0, 66.6 ($^2J_{C-P}$ = 7.1 Hz), 66.8 ($^2J_{C-P}$ = 7.0 Hz), 75.9, 113.7, 127.6, 127.8, 128.1, 128.1, 128.3, 128.3, 128.6, 128.8, 129.1, 134.4, 135.5 ($^3J_{C-P}$ = 9.0 Hz), 136.2 ($^3J_{C-P}$ = 7.1 Hz), 136.33 ($^3J_{C-P}$ = 7.1 Hz), 158.2. ^{31}P NMR (121.5 MHz, $CDCl_3$): δ_P ppm = 30.59. HRMS (ESI): calculated for $C_{33}H_{37}NO_6P$ [(M + H)$^+$] 574.2353; found 574.2306.

*Dibenzyl 3-(N-(Benzyloxy)-N-methylcarbamoyl)-2-methylpropyl-phosphonate (**13f**).* Prepared from compound **12f** (1.0 g, 2.39 mmol) according to general procedure IV. Colorless oil; purification gradient 0−5% MeOH in CH_2Cl_2; yield 62%. ^{1}H NMR (300 MHz, $CDCl_3$) δ_H ppm 1.06 (d, J = 6.5 Hz, 3H, −CH(C<u>H_3</u>)−CH_2−), 1.61−1.73 (m, 1H, P−CH_2−), 1.88−2.05 (m, 1H, P−CH_2−), 2.26−2.60 (m, 3H, −C<u>H</u>(CH_3)−, −C<u>H_2</u>−CO), 3.15 (s, 1H, N−CH_3), 4.75 (s, NOC<u>H_2</u>Ph), 4.89−5.09 (m, 4H, −C<u>H_2</u>−Ph), 7.27−7.42 (m, 15H, Ar−H). ^{13}C NMR (75 MHz, $CDCl_3$) δ_C ppm 21.4 ($^3J_{C-P}$ = 8.6 Hz), 25.2 ($^2J_{C-P}$ = 5.2 Hz), 32.3 ($^1J_{C-P}$ = 138.5 Hz), 39.7 ($^3J_{C-P}$ = 12.9 Hz), 67.0 ($^2J_{C-P}$ = 6.5 Hz), 67.0 ($^2J_{C-P}$ = 6.5 Hz), 76.2, 127.9, 127.9, 128.3, 128.5, 128.7, 128.9, 129.3, 134.5, 136.5 ($^3J_{C-P}$ = 6.1 Hz), 173.7. ^{31}P NMR (121.5 MHz, $CDCl_3$): δ_P ppm = 33.16. HRMS (ESI): calculated for $C_{27}H_{33}NO_5P$ [(M + H)$^+$] 482.2091; found 482.2086.

*Diethyl 2-(p-Chlorophenyl)-3-(tert-butoxycarbonyl)-propylphosphonate (**14d**).* Prepared from compound **11d** (784 mg, 3.28 mmol) according to general procedure III. Pale yellow oil; purification 1.5:1 Hex/Me_2CO v/v; yield 71%. ^{1}H NMR (300 MHz, $CDCl_3$) δ_H ppm 1.17−1.34 (m, 6H, P−CH_2C<u>H_3</u>), 1.29 (br, 9H, *t*-Bu), 1.96−2.22 (m, 2H, −CH_2−), 2.52 (dd, J = 9.5 Hz, 15.8 Hz, 1H, −CH_2−CO), 2.80 (dd, J = 6.3 Hz, 15.8 Hz, 1H, −CH_2−CO), 3.40−3.58 (m, 1H, −CH−), 3.86−4.05 (m, 4H, P−C<u>H_2</u>CH_3), 7.18 (d, J = 8.4 Hz, 2H, Ar−H), 7.27 (d, J = 8.4 Hz, 2H, Ar−H). ^{13}C NMR (75 MHz, $CDCl_3$) δ_C ppm 16.1 (d, $^3J_{C-P}$ = 16.1 Hz), 16.1 (d, $^3J_{C-P}$ = 6.3

DOI: 10.1021/jm5014264
J. Med. Chem. 2015, 58, 2988−3001

Hz), 27.7, 32.2 (d, $^{1}J_{C-P}$ = 140.8 Hz), 36.3 (d, $^{2}J_{C-P}$ = 3.5 Hz), 42.8 (d, $^{3}J_{C-P}$ = 12.7 Hz), 61.2 (d, $^{2}J_{C-P}$ = 6.9 Hz), 61.4 (d, $^{2}J_{C-P}$ = 6.9 Hz), 80.5, 128.3, 128.8, 132.3, 141.5 (d, $^{3}J_{C-P}$ = 9.6 Hz), 170.2. ^{31}P NMR (121.5 MHz, $CDCl_3$): δ_P ppm 28.47. HRMS (ESI): calculated for $C_{18}H_{29}ClO_5P$ [$(M + H)^+$] 391.1436; found 391.1610.

*Diethyl 2-(3,4-Dichlorophenyl)-3-(tert-butoxycarbonyl)-propylphosphonate (**14e**).* Prepared from compound **11e** (656 mg, 2.40 mmol) according to general procedure III. Pale yellow oil; purification 1:1 Hex/Me_2CO v/v; yield 73%. ^{1}H NMR (300 MHz, $CDCl_3$) δ_H ppm 1.22 (t, J = 7.1 Hz, 3H, $-OCH_2\underline{CH_3}$), 1.23 (t, J = 7.2 Hz, 3H, $-OCH_2\underline{CH_3}$), 1.32 (br, 9H, *t*-Bu), 1.95−2.21 (m, 2H, P−CH_2−), 2.52 (ddd, J = 1.2 Hz, 9.3 Hz, 15.8 Hz, 1H, $-CH_2-CO$), 2.80 (dd, J = 6.1 Hz, 15.8 Hz, 1H, $-CH_2-CO$), 3.40−3.55 (m, 1H, −CH−), 3.88−4.07 (m, 4H, $OC\underline{H_2}CH_3$), 7.10 (dd, J = 2.1 Hz, 8.4 Hz, 1H, Ar−H), 7.34 (d, J = 2.1 Hz, 1H, Ar−H), 7.37 (d, J = 8.4 Hz, 1H, Ar−H). ^{13}C NMR (75 MHz, $CDCl_3$) δ_C ppm 16.2 (d, $^{3}J_{C-P}$ = 2.9 Hz), 16.3 (d, $^{3}J_{C-P}$ = 2.4 Hz), 27.9, 32.1 (d, $^{1}J_{C-P}$ = 140.7 Hz), 36.3 (d, $^{2}J_{C-P}$ = 3.9 Hz), 42.7 (d, $^{3}J_{C-P}$ = 12.1 Hz), 61.5 (d, $^{2}J_{C-P}$ = 7.8 Hz), 61.6 (d, $^{2}J_{C-P}$ = 7.3 Hz), 80.9, 126.9, 129.6, 130.2, 130.6, 132.2, 143.4 (d, $^{3}J_{C-P}$ = 9.0 Hz), 170.1. ^{31}P NMR (121.5 MHz, $CDCl_3$): δ_P ppm = 27.96. HRMS (ESI): calculated for $C_{18}H_{28}Cl_2O_5P$ [$(M + H)^+$] 425.1046; found 425.1029.

*Diethyl 3-(N-(Benzyloxy)-N-methylcarbamoyl)-2-(4-chlorophenyl)propylphosphonate (**15d**).* Prepared from compound **14d** (870 mg, 2.23 mmol) according to general procedure IV. Colorless oil; purification 97:3 CH_2Cl_2/MeOH v/v; yield 46%. ^{1}H NMR (300 MHz, $CDCl_3$) δ_H ppm 1.16 (app. t, J = 7.1 Hz, 3H, P−$CH_2\underline{CH_3}$), 1.21 (app. t, J = 7.1 Hz, 3H, P−$CH_2\underline{CH_3}$), 1.91−2.26 (m, 2H, P−CH_2−), 2.67−2.89 (m, 2H, $-CH_2-CO-$), 3.10 (s, 3H, N−CH_3), 3.50−3.66 (m, 1H, −CH−), 3.86−4.03 (m, 4H, $POC\underline{H_2}Ph$), 4.72 (app. d., J = 3.3 Hz, 2H, $NOC\underline{H_2}Ph$), 7.02−7.15 (m, 2H, Ar−H), 7.21−7.27 (m, 2H Ar−H), 7.30−7.42 (m, 5H, Ar−H). ^{13}C NMR (75 MHz, $CDCl_3$) δ_C ppm 16.11−6.39 (m), 31.88 (d, $^{1}J_{C-P}$ = 140.2 Hz), 35.50 (d, $^{2}J_{C-P}$ = 3.2 Hz), 39.60 (d, $^{3}J_{C-P}$ = 12.5 Hz), 61.33 (d, $^{2}J_{C-P}$ = 6.4 Hz), 61.55 (d, $^{2}J_{C-P}$ = 6.6 Hz), 76.2, 128.4, 128.7, 128.9, 129.0, 129.3, 132.3, 134.4, 140.4, 142.3 (d, $^{3}J_{C-P}$ = 8.3 Hz), 167.1. ^{31}P NMR (121.5 MHz, $CDCl_3$): δ_P ppm 29.87. HRMS (ESI): calculated for $C_{22}H_{30}ClNO_5P$ [$(M + H)^+$] 454.1545; found 454.0736.

*Diethyl 3-(N-(Benzyloxy)-N-methylcarbamoyl)-2-(3,4-dichlorophenyl)propylphosphonate (**15e**).* Prepared from compound **14e** (700 mg, 1.65 mmol) according to general procedure IV. Colorless oil; purification 95:5 CH_2Cl_2/MeOH v/v; yield 49%. ^{1}H NMR (300 MHz, $CDCl_3$) δ_H ppm 1.18 (app. t, J = 7.1 Hz, 3H, P−$CH_2\underline{CH_3}$), 1.22 (app. t, J = 7.2 Hz, 3H, P−$CH_2\underline{CH_3}$), 1.86−2.24 (m, 2H, P−CH_2−), 2.61−2.85 (m, 2H, $-CH_2-CO-$), 3.12 (s, 3H, N−CH_3), 3.44−3.62 (m, 1H, −CH−), 3.82−4.05 (m, 4H, $POC\underline{H_2}CH_3$), 4.75 (s, 2H, $NOC\underline{H_2}Ph$), 7.02 (dd, J = 2.2 Hz, 8.34 Hz, 1H, Ar−H), 7.23−7.44 (m, 7H, Ar−H). ^{13}C NMR (75 MHz, $CDCl_3$) δ_C ppm 16.2 (d, $^{3}J_{C-P}$ = 6.8 Hz), 16.3 (d, $^{3}J_{C-P}$ = 6.6 Hz), 31.7 (d, $^{1}J_{C-P}$ = 140.4 Hz), 33.4, 35.3 (d, $^{2}J_{C-P}$ = 3.3 Hz), 39.3 (d, $^{3}J_{C-P}$ = 13.1 Hz), 61.4 (d, $^{2}J_{C-P}$ = 6.7 Hz), 61.6 (d, $^{2}J_{C-P}$ = 6.6 Hz), 76.1, 127.1, 128.7, 129.0, 129.3, 129.5, 130.2, 130.4, 132.1, 134.3, 144.1 (d, $^{3}J_{C-P}$ = 7.9 Hz), 172.3. ^{31}P NMR (121.5 MHz, $CDCl_3$): δ_P ppm 28.22. HRMS (ESI): calculated for $C_{22}H_{29}Cl_2NO_5P$ [$(M + H)^+$] 488.1155; found 488.1144.

*Diethyl 3-(N-Hydroxy-N-methylcarbamoyl)-2-(4-chlorophenyl)-propylphosphonate (**16d**).* Prepared from compound **15d** (400 mg, 0.88 mmol) according to general procedure VI. Colorless oil; purification gradient 0−10% MeOH in CH_2Cl_2, 1% triethylamine; yield 79%. ^{1}H NMR (300 MHz, $CDCl_3$) δ_H ppm 1.18 (app. t, J = 7.1 Hz, 3H, P−$CH_2\underline{CH_3}$), 1.26 (app. t, J = 7.0 Hz, 3H, P−$CH_2\underline{CH_3}$), 1.90−2.37 (m, 2H, P−CH_2−), 2.66−2.80 (m, 1H of $-CH_2-CO-$), 3.11−3.29 (m, 3H, N−CH_3, 1H of $-CH_2-CO-$), 3.51−3.74 (m, 1H, −CH−), 3.82−3.05 (m, 4H, $POC\underline{H_2}Ph$), 7.15−7.33 (m, 4H, Ar−H), 9.46 (s, 1H, N−OH). ^{13}C NMR (75 MHz, $CDCl_3$) δ_C ppm 16.0−16.5 (m), 31.5 (d, $^{1}J_{C-P}$ = 139.2 Hz), 33.2, 35.8 (d, $^{3}J_{C-P}$ = 8.7 Hz), 37.7 (d, $^{2}J_{C-P}$ = 7.0 Hz), 61.9 (d, $^{2}J_{C-P}$ = 7.2 Hz), 62.2 (d, $^{2}J_{C-P}$ = 6.5 Hz), 128.6, 128.7, 132.5, 142.7 (d, $^{3}J_{C-P}$ = 11.1 Hz), 171.7. ^{31}P NMR (121.5 MHz, $CDCl_3$): rotamers at δ_P ppm 29.46, 30.85. HRMS (ESI): calculated for $C_{15}H_{24}ClNO_5P$ [$(M + H)^+$] 364.1075; found 364.0480.

*Diethyl 3-(N-Hydroxy-N-methylcarbamoyl)-2-(3,4-dichlorophenyl)propylphosphonate (**16e**).* Prepared from compound **15e** (350 mg, 0.72 mmol) according to general procedure VI. Colorless oil; purification gradient 0−10% MeOH in CH_2Cl_2, 1% triethylamine; yield 74%. ^{1}H NMR (300 MHz, $CDCl_3$) δ_H ppm 1.21 (app. t, J = 7.2 Hz, 3H, P−$CH_2\underline{CH_3}$), 1.27 (app. t, J = 7.1 Hz, 3H, P−$CH_2\underline{CH_3}$), 2.00−2.27 (m, 2H, P−CH_2−), 2.74 (dd, J = 6.5 Hz, 15.17 Hz, 1H, $-CH_2CO$), 3.19 (dd, J = 8.1 Hz, 15.2 Hz, 1H, $-CH_2CO$), 3.22 (s, 3H, N−CH_3), 3.52−3.72 (m, 1H, −CH−), 3.87−4.07 (m, 4H, -$POC\underline{H_2}CH_3$), 7.14 (d, J = 8.1 Hz, 1H, Ar−H), 7.32−7.45 (m, 2H, Ar−H), 9.44 (s, 1H, N−OH). ^{13}C NMR (75 MHz, $CDCl_3$) δ_C ppm 16.2 (d, $^{3}J_{C-P}$ = 6.7 Hz), 16.3 (d, $^{3}J_{C-P}$ = 6.4 Hz), 31.3 (d, $^{1}J_{C-P}$ = 141.7 Hz), 35.6 (d, $^{2}J_{C-P}$ = 3.3 Hz), 35.9, 37.6 (d, $^{3}J_{C-P}$ = 7.5 Hz), 62.0 (d, $^{2}J_{C-P}$ = 6.9 Hz), 62.3 (d, $^{2}J_{C-P}$ = 7.8 Hz), 126.9, 129.3, 130.4, 132.4, 130.7, 144.5 (d, $^{3}J_{C-P}$ = 12.2 Hz), 171.4. ^{31}P NMR (121.5 MHz, $CDCl_3$): rotamers at δ_P ppm 29.01, 30.45. HRMS (ESI): calculated for $C_{15}H_{23}Cl_2NO_5P$ [$(M + H)^+$] 398.0685; found 398.0705.

*(E)-tert-Butyl 4-Phenylbut-2-enoate (**19a**).* Prepared from compound **17a** (1.0 g, 8.19 mmol) according to general procedure II. Yellow oil; purification 97:3 Hex/Et_2O v/v; yield 80% over two steps. ^{1}H NMR (300 MHz, $CDCl_3$) δ_H ppm 1.46 (br, 9H, *t*-Bu), 3.46 (dd, J = 1.6 Hz, 6.7 Hz, 2H $-CH_2-$), 5.73 (dt, J = 1.7 Hz, 15.6 Hz, 1H, −CH=C<u>H</u>−CO−), 6.99 (dt, J = 6.7 Hz, 15.5 Hz, 1H, −C<u>H</u>=CH−CO−), 7.14−7.34 (m, 5H, Ar−H). ^{13}C NMR (75 MHz, $CDCl_3$) δ_C ppm 28.1, 38.1, 80.2, 124.1, 126.5, 128.6, 128.8, 137.9, 145.9, 165.8.

*(E)-tert-Butyl 5-Phenylpent-2-enoate (**19b**).* Prepared from compound **17b** (1.0 g, 7.34 mmol) according to general procedure II. Colorless oil; purification 97:3 Hex/Et_2O v/v; yield 84% over two steps. ^{1}H NMR (300 MHz, $CDCl_3$) δ_H ppm 1.48 (br, 9H, *t*-Bu), 2.43−2.54 (m, 2H, $-CH_2C$=CH−), 2.78 (t, J = 7.4 Hz, 2H, Ph−CH_2−), 5.78 (dt, J = 1.8 Hz, 15.5 Hz, 1H, −CH=C<u>H</u>−CO−), 6.90 (dt, J = 6.7 Hz, 15.5 Hz, 1H, −C<u>H</u>=CH−CO−), 7.13−7.43 (m, 5H, Ar−H). ^{13}C NMR (75 MHz, $CDCl_3$) δ_C ppm 28.2, 33.8, 34.5, 80.1, 123.4, 126.1, 128.3, 128.5, 141.1, 147.0, 166.0.

*(E)-tert-Butyl 6-Phenylhex-2-enoate (**19c**).* Prepared from compound **17c** (1.5 g, 9.99 mmol) according to general procedure II. Colorless oil; purification 98:2 Hex/Et_2O v/v; yield 79% over two steps. ^{1}H NMR (300 MHz, $CDCl_3$) δ_H ppm 1.48 (br, 9H, *t*-Bu), 1.78 (app. quin, 2H, $-CH_2-$), 2.15−2.25 (m, 2H, $-C\underline{H_2}CH$=CH−), 2.64 (t, J = 7.6 Hz, 2H, Ph−CH_2−), 5.75 (dt, J = 1.6 Hz, 15.6 Hz, 1H, CH=C<u>H</u>−CO−), 6.87 (dt, J = 6.8 Hz, 15.6 Hz, 1H, −CH=C<u>H</u>−CO−), 7.13−7.33 (m, 5H, Ar−H). ^{13}C NMR (75 MHz, $CDCl_3$) δ_C ppm 28.2, 29.8, 31.5, 35.3, 80.1, 123.3, 125.9, 128.4, 128.4, 141.8, 147.5, 166.1. HRMS (ESI): calculated for $C_{16}H_{23}O_2$ [$(M + H)^+$] 247.1693; found 247.1630.

*(E)-tert-Butyl 7-Phenylhept-2-enoate (**19d**).* Prepared from compound **17d** (1.0 g, 6.09 mmol) according to general procedure II. Colorless oil; purification 98:2 Hex/Et_2O v/v; yield 87% over two steps. ^{1}H NMR (300 MHz, $CDCl_3$) δ_H ppm 1.44−1.55 (m, 9H, *t*-Bu, 2H, $-CH_2-$), 1.58−1.71 (m, 2H, $-CH_2-$), 2.14−2.24 (m, 2H, $-CH_2-$), 2.61 (t, J = 7.5 Hz, 2H, Ph−C<u>H</u>$_2$-), 5.7 (dt, J = 1.6 Hz, 15.6 Hz, 1H, −CH=C<u>H</u>−CO−), 6.84 (dt, J = 6.9 Hz, 15.6 Hz, 1H, −C<u>H</u>=CH−CO−), 7.13−7.32 (m, 5H, Ar−H). ^{13}C NMR (75 MHz, $CDCl_3$) δ_C ppm 27.7, 28.2, 30.9, 31.9, 35.7, 80.0, 123.1, 125.7, 123.3, 128.4, 142.3, 147.7, 166.1. HRMS (ESI): calculated for $C_{17}H_{25}O_2$ [$(M + H)^+$] 261.1849; found 261.1865.

*Dibenzyl 2-((tert-Butoxycarbonyl)methyl)-3-phenylpropyl-phosphonate (**20a**).* Prepared from compound **19a** (1.2 g, 5.50 mmol) according to general procedure III. Colorless oil; purification 5:1 Hex/Me_2CO v/v; yield 66%. ^{1}H NMR (300 MHz, $CDCl_3$) δ_H ppm 1.41 (br, 9H, *t*-Bu), 1.624−2.03 (m, 2H, P−CH_2−), 2.32−2 0.40 (m, 2H, $-CH_2-CO$), 2.38−2.56 (m, 3H, $-C\underline{H}(C\underline{H_2}-Ph)-$), 4.81−5.18 (m, 4H, $O-C\underline{H_2}-Ph$), 7.01−7.41 (m, 15H, Ar−H). ^{13}C NMR (75 MHz, $CDCl_3$) δ_C ppm 28.0, 29.4 (d, $^{1}J_{C-P}$ = 138.9 Hz), 30.5 (d, $^{2}J_{C-P}$ = 4.5 Hz), 32.2, 37.1 (d, $^{3}J_{C-P}$ = 11.1 Hz), 41.2 (d, $^{3}J_{C-P}$ = 9.1 Hz), 67.12 (d, $^{2}J_{C-P}$ = 6.1 Hz), 67.13 (d, $^{2}J_{C-P}$ = 6.50 Hz), 80.40, 127.30, 127.32 127.9, 128.4, 139.81 (d, $^{3}J_{C-P}$ = 6.06 Hz), 139.84 (d, $^{3}J_{C-P}$ = 6.1 Hz), 141.1, 173.3. ^{31}P NMR (121.5 MHz, $CDCl_3$): δ_P ppm = 33.0. HRMS (ESI): calculated for $C_{29}H_{36}O_5P$ [$(M + H)^+$] 495.2295; found 495.2321.

DOI: 10.1021/jm5014264
J. Med. Chem. 2015, 58, 2988−3001

*Dibenzyl 2-((tert-Butoxycarbonyl)methyl)-4-phenylbutylphosphonate (**20b**).* Prepared from compound **19b** (1.0 g, 4.30 mmol) according to general procedure III. Colorless oil; purification 5:1 Hex/Me_2CO v/v; yield 63%. ^1H NMR (300 MHz, $CDCl_3$) δ_H ppm 1.41 (br, 9H, *t*-Bu), 1.62−2.00 (m, 4H, $-CH_2-$), 2.22−2 0.39 (m, 2H, $-CH_2-$), 2.43−2.52 (m, 1H, −CH−), 2.56 (t, *J* = 8.4 Hz, 2H, $-CH_2-$), 4.89−5.09 (m, 4H, $-CH_2-$Ph), 7.07−7.26 (m, 5H, Ar−H), 7.30−7.37 (m, 10H, Ar−H). ^{13}C NMR (75 MHz, $CDCl_3$) δ_C ppm 28.1, 29.8 (d, $^1J_{C-P}$ = 138.8 Hz), 30.1 (d, $^2J_{C-P}$ = 4.7 Hz), 32.7, 36.33 (d, $^3J_{C-P}$ = 10.1 Hz), 40.1 (d, $^3J_{C-P}$ = 9.4 Hz), 67.0 (d, $^2J_{C-P}$ = 6.4 Hz), 67.1 (d, $^2J_{C-P}$ = 6.5 Hz), 80.4, 125.7, 127.9, 128.3, 128.5, 136.3 (d, $^3J_{C-P}$ = 6.1 Hz), 136.4 (d, $^3J_{C-P}$ = 6.1 Hz), 141.7, 171.5. ^{31}P NMR (121.5 MHz, $CDCl_3$): δ_P ppm = 33.04. HRMS (ESI): calculated for $C_{30}H_{38}O_5P$ [(M + H)$^+$] 509.2451; found 509.2466.

*Dibenzyl 2-((tert-Butoxycarbonyl)methyl)-5-phenylpentylphosphonate (**20c**).* Prepared from compound **19c** (1.35 g, 5.48 mmol) according to general procedure III. Colorless oil; purification 6:1 Hex/Me_2CO v/v; yield 71%. ^1H NMR (300 MHz, $CDCl_3$) δ_H ppm 1.41 (br, 9H, *t*-Bu), 1.42−1.63 (m, 4H, $-CH_2-$), 1.72−2.03 (m, 2H, $-CH_2-$), 2.16−2.56 (m, 4H, $-CH_2-$, 1H, −CH−), 4.86−5.09 (m, 4H, $-CH_2-$Ph), 7.03−7.47 (m, 15H, Ar−H). ^{13}C NMR (75 MHz, $CDCl_3$) δ_C ppm 28.0, 28.3, 29.8 (d, $^1J_{C-P}$ = 139.4 Hz), 30.3 (d, $^2J_{C-P}$ = 4.1 Hz), 34.2 (d, $^3J_{C-P}$ = 10.4 Hz), 35.8, 40.2 (d, $^3J_{C-P}$ = 9.6 Hz), 66.9 (d, $^2J_{C-P}$ = 6.2 Hz), 67.1 (d, $^2J_{C-P}$ = 6.3 Hz), 80.3, 125.6, 127.9, 128.2, 128.3, 128.49, 129.4, 136.4 (d, $^3J_{C-P}$ = 6.1 Hz), 136.4 (d, $^3J_{C-P}$ = 6.1 Hz), 142.2, 171.6. ^{31}P NMR (121.5 MHz, $CDCl_3$): δ_P ppm 33.16. HRMS (ESI): calculated for $C_{31}H_{40}O_5P$ [(M + H)$^+$] 523.2608; found 523.2411.

*Dibenzyl 2-((tert-Butoxycarbonyl)methyl)-6-phenylhexylphosphonate (**20d**).* Prepared from compound **19d** (1.0 g, 3.84 mmol) according to general procedure III. Colorless oil; purification 6:1 Hex/Me_2CO v/v; yield 68%. ^1H NMR (300 MHz, $CDCl_3$) δ_H ppm 1.20−1.35 (m, 2H, $-CH_2-$), 1.41 (br, 9H, *t*-Bu), 1.43−1.61 (m, 4H, $-CH_2-$), 1.77−1.92 (m, 2H, $-CH_2-$), 2.16−2.32 (m, 3H, $-CH_2-$, −CH−), 2.55 (t, *J* = 7.6 Hz, 2H, $-CH_2-$), 4.90−5.08 (m, 4H, $-CH_2-$Ph), 7.10−7.37 (m, 15H, Ar−H). ^{13}C NMR (75 MHz, $CDCl_3$) δ_C ppm 26.0, 28.1, 29.9 (d, $^1J_{C-P}$ = 138.4 Hz), 30.3 (d, $^2J_{C-P}$ = 3.9 Hz), 31.3, 34.4 (d, $^3J_{C-P}$ = 10.2 Hz), 35.7, 40.2 (d, $^3J_{C-P}$ = 9.7 Hz), 67.0 (d, $^2J_{C-P}$ = 6.6 Hz), 67.1 (d, $^2J_{C-P}$ = 6.7.1 Hz), 80.3, 125.6, 127.9, 128.2, 128.3, 128.3, 128.5, 136.4 (d, $^3J_{C-P}$ = 6.3 Hz), 136.4 (d, $^3J_{C-P}$ = 6.3 Hz), 142.5, 171.7. ^{31}P NMR (121.5 MHz, $CDCl_3$): δ_P ppm = 33.32. HRMS (ESI): calculated for $C_{32}H_{42}O_5P$ [(M + H)$^+$] 537.2764; found 537.2784.

*Dibenzyl 2-((N-(Benzyloxy)-N-methylcarbamoyl)methyl)-3-phenylpropylphosphonate (**21a**).* Prepared from compound **20a** (1.0 g, 2.02 mmol) according to general procedure IV. Colorless oil; purification gradient 0−5% MeOH in CH_2Cl_2; yield 43%. ^1H NMR (300 MHz, $CDCl_3$) δ_H ppm 1.77−2.07 (m, 2H, $P-CH_2-$), 2.40−2.83 (m, 5H, $-CH_2-$CO-, −CH−CH_2−Ph), 3.11 (s, 3H, $N-CH_3$), 4.63 (s, 2H, NOCH_2Ph), 4.86−5.05 (m, 4H, POCH_2Ph), 7.07−7.42 (m, 20H, Ar−H). ^{13}C NMR (75 MHz, $CDCl_3$) δ_C ppm 29.0 (d, $^1J_{C-P}$ = 138.7 Hz), 31.6 (d, $^2J_{C-P}$ = 3.1 Hz), 35.9 (d, $^3J_{C-P}$ = 9.6 Hz), 40.9 (d, $^3J_{C-P}$ = 11.4 Hz), 67.2 (d, $^2J_{C-P}$ = 6.6 Hz), 67.3 (d, $^2J_{C-P}$ = 6.7 Hz), 76.1, 126.2, 127.9, 127.9, 128.3, 128.3, 128.5, 128.6, 128.8, 129.2, 129.4, 134.5, 136.6 (d, $^3J_{C-P}$ = 6.8 Hz), 136.7 (d, $^3J_{C-P}$ = 6.4 Hz), 139.6, 165.7. ^{31}P NMR (121.5 MHz, $CDCl_3$): δ_P ppm 33.28. HRMS (ESI): calculated for $C_{33}H_{37}NO_5P$ [(M + H)$^+$] 558.2404; found 558.2431.

*Dibenzyl 2-((N-(Benzyloxy)-N-methylcarbamoyl)methyl)-4-phenylbutylphosphonate (**21b**).* Prepared from compound **20b** (1.0 g, 1.97 mmol) according to general procedure IV. Colorless oil; purification gradient 0−5% MeOH in CH_2Cl_2; yield 60%. ^1H NMR (300 MHz, $CDCl_3$) δ_H ppm 1.64−2.09 (m, 4H, $-CH_2-$), 2.31−2.58 (m, 3H, $-CH_2-$, 1H, −CH−), 2.65 (dd, *J* = 7.1 Hz, *J* = 16.5 Hz, 1H, $-CH_2-$), 3.14 (s, 3H, $N-CH_3$), 4.73 (br. s, 2H, NOCH_2Ph), 4.87−5.08 (m, 4H, $-CH_2-$Ph), 7.04−7.26 (m, 5H, Ar−H), 7.27−7.39 (m, 15H, Ar−H). ^{13}C NMR (75 MHz, $CDCl_3$) δ_C ppm 29.6 (d, $^2J_{C-P}$ = 4.0 Hz), 29.6 (d, $^1J_{P-C}$ = 138.2 Hz), 32.9, 33.5, 36.5 ($^3J_{C-P}$ = 9.6 Hz), 36.6 ($^3J_{C-P}$ = 6.7 Hz), 67.0 ($^2J_{C-P}$ = 6.5 Hz), 76.1, 125.7, 127.9, 127.9, 128.3, 128.3, 128.5, 128.6, 128.9, 129.3, 134.6, 136.4 ($^3J_{C-P}$ = 6.3 Hz), 173.7. ^{31}P NMR (121.5 MHz, $CDCl_3$): δ_P ppm = 32.26. HRMS (ESI): calculated for $C_{34}H_{39}NO_5P$ [(M + H)$^+$] 572.2560; found 572.2585.

*Dibenzyl 2-((N-(Benzyloxy)-N-methylcarbamoyl)methyl)-5-phenylpentylphosphonate (**21c**).* Prepared from compound **20c** (1.5 g, 2.87 mmol) according to general procedure IV. Colorless oil; purification gradient 0−5% MeOH in CH_2Cl_2; yield 68%. ^1H NMR (300 MHz, $CDCl_3$) δ_H ppm 1.36−1.63 (m, 4H, $-CH_2-$), 1.72−2.03 (m, 2H, $-CH_2-$), 2.26−2.66 (m, 5H, $-CH_2-$, −CH−), 3.12 (s, 3H, $N-CH_3$), 4.72 (s, 2H, NOCH_2Ph), 4.82−5.06 (m, 4H, POCH_2Ph), 7.03−7.43 (m, 20H, Ar−H). ^{13}C NMR (75 MHz, $CDCl_3$) δ_C ppm 28.2, 28.6, 29.7 (d, $^2J_{C-P}$ = 3.2 Hz), 29.7 (d, $^1J_{C-P}$ = 138.6 Hz), 34.6 (d, $^3J_{C-P}$ = 9.3 Hz), 35.8, 36.7 (d, $^3J_{C-P}$ = 8.3 Hz), 66.8−67.2 (m), 76.1, 125.7, 127.9, 128.2, 128.3, 128.4, 128.51, 128.53, 128.7, 128.9, 129.3, 136.5 (d, $^3J_{C-P}$ = 7.0 Hz), 142.4, 172.1. ^{31}P NMR (121.5 MHz, $CDCl_3$): δ_P ppm 33.40. HRMS (ESI): calculated for $C_{35}H_{41}NO_5P$ [(M + H)$^+$] 586.2717; found 586.2709.

*Dibenzyl 2-((N-(Benzyloxy)-N-methylcarbamoyl)methyl)-6-phenylhexylphosphonate (**21d**).* Prepared from compound **20d** (1.28 g, 2.39 mmol) according to general procedure IV. Colorless oil; purification gradient 0−15% MeOH in CH_2Cl_2; yield 74%. ^1H NMR (300 MHz, $CDCl_3$) δ_H ppm 1.12−1.31 (m, 2H, $-CH_2-$), 1.34−1.56 (m, 4H, $-CH_2-$), 1.71−2.02 (m, 2H, $-CH_2-$), 2.22−2.63 (m, 4H, $-CH_2-$, 1H, −CH−), 3.11 (s, 3H, $N-CH_3$), 4.69 (s, 2H, −NOCH_2Ph), 4.88−5.06 (m, 4H, POCH_2Ph), 7.07−7.42 (m, 20H, Ar−H). ^{13}C NMR (75 MHz, $CDCl_3$) δ_C ppm 25.9, 27.9, 29.4 (d, $^2J_{C-P}$ = 3.9 Hz), 29.5 (d, $^1J_{C-P}$ = 137.7 Hz), 31.1, 34.4 (d, $^3J_{C-P}$ = 9.4 Hz), 35.5, 36.5 (d, $^3J_{C-P}$ = 9.4 Hz), 66.6−66.8 (m), 75.8, 125.4, 127.7, 128.0, 128.1, 128.2, 128.3, 128.4, 128.6, 129.1, 134.4, 136.2−136.3 (m), 142.3, 173.6. ^{31}P NMR (121.5 MHz, $CDCl_3$): δ_P ppm = 32.52. HRMS (ESI): calculated for $C_{36}H_{43}NO_5P$ [(M + H)$^+$] 600.2873; found 600.2814.

*Sodium Hydrogen 3-(N-Hydroxy-N-methylcarbamoyl)-2-phenylpropylphosphonate (**7a**).* Prepared from compound **13a** (150 mg, 0.28 mmol) according to general procedure V. White powder. ^1H NMR (300 MHz, D_2O) δ_H ppm 1.69−1.96 (m, 2H, $P-CH_2-$), 2.89−3.14 (m, 5H, $-CH_2-$, $N-CH_3$), 3.23−3.50 (m, 1H, −CH−) 7.16−7.41 (m, 5H, Ar−H). ^{13}C NMR (75 MHz, D_2O) δ_C ppm 29.4, 36.1 (d, $^1J_{C-P}$ = 127.7 Hz), 38.1 (d, $^2J_{C-P}$ = 2.8 Hz), 38.5 (d, $^3J_{C-P}$ = 5.3 Hz), 126.3, 127.3, 128.4, 146.1 (d, $^3J_{C-P}$ = 12.1 Hz), 174.0. ^{31}P NMR (121.5 MHz, D_2O): rotamers at δ_P ppm 19.64, 19.87. HRMS (ESI): calculated for $C_{11}H_{15}NO_5P$ [(M − H)$^-$] 272.0693; found 272.0622.

*Sodium Hydrogen 3-(N-Hydroxy-N-methylcarbamoyl)-2-p-tolylpropylphosphonate (**7b**).* Prepared from compound **13b** (150 mg, 0.27 mmol) according to general procedure V. White powder. ^1H NMR (300 MHz, D_2O) δ_H ppm 1.73−1.97 (m, 2H, $P-CH_2-$), 2.26 (s, 3H, Ph−CH_3), 2.86−3.09 (m, 5H, $-CH_2-$CO, $N-CH_3$), 3.20−3.46 (m, 1H, −CH−), 7.10−7.25 (m, 4H, Ar−H). ^{13}C NMR (75 MHz, D_2O) δ_C ppm 20.2, 35.9, 36.1 (d, $^1J_{C-P}$ = 130.5 Hz), 37.7 (d, $^2J_{C-P}$ = 2.8 Hz), 38.9 (d, $^3J_{C-P}$ = 6.7 Hz), 127.5, 129.2, 136.5, 142.8 (d, $^3J_{C-P}$ = 13.1 Hz), 174.4. ^{31}P NMR (121.5 MHz, D_2O): rotamers at δ_P ppm 24.34, 24.65. HRMS (ESI): calculated for $C_{12}H_{17}NO_5P$ [(M − H)$^-$] 286.0849; found 286.0816.

*Sodium Hydrogen 3-(N-Hydroxy-N-methylcarbamoyl)-2-(4-methoxyphenyl)propylphosphonate (**7c**).* Prepared from compound **13c** (200 mg, 0.35 mmol) according to general procedure V. White powder. ^1H NMR (300 MHz, D_2O) δ_H ppm 1.55−1.81 (m, 2H, $P-CH_2-$), 2.72−2.98 (m, 5H, $-CH_2-$CO, $N-CH_3$), 3.11−3.37 (m, 1H, −CH−), 3.71 (s, 3H, Ph−O−CH_3), 6.84 (d, *J* = 7.4 Hz, 2H, Ar−H), 7.18 (d, *J* = 7.4 Hz, 2H, Ar−H). ^{13}C NMR (75 MHz, D_2O) δ_C ppm 36.8, 37.1 (d, $^1J_{C-P}$ = 132.9 Hz), 40.3 (d, $^3J_{C-P}$ = 8.3 Hz), 45.6 (d, $^2J_{C-P}$ = 5.8 Hz), 55.4, 113.6, 128.6, 139.5 (d, $^3J_{C-P}$ = 11.7 Hz), 156.7, 167.8. ^{31}P NMR (121.5 MHz, D_2O): δ_P ppm = 20.79, 20.83. HRMS (ESI): calculated for $C_{12}H_{17}NO_6P$ [(M − H)$^-$] 302.0799; found 302.0926.

*3-(N-Hydroxy-N-methylcarbamoyl)-2-(p-chlorophenyl)-propylphosphonic Acid, Bisammonium Salt (**7d**).* Prepared from compound **16d** (200 mg, 0.55 mmol) according to general procedure VII. Brown powder. ^1H NMR (300 MHz, D_2O) δ_H ppm 1.87−2.09 (m, 2H, $P-CH_2-$), 2.81−2 0.97 (m, 2H, $-CH_2-$CO−), 3.04 (s, 5/6 of $N-CH_3$), 3.11 (s, 1/6 of $N-CH_3$), 3.24−3.51 (m, 1H, −CH−),

DOI: 10.1021/jm5014264
J. Med. Chem. 2015, 58, 2988−3001

7.20−7.38 (m, 4H, Ar−H). ^{13}C NMR (75 MHz, D_2O) δ_C ppm 34.8 (d, $^1J_{C-P}$ = 131.6 Hz), 35.6, 37.0 (d, $^2J_{C-P}$ = 2.5 Hz), 39.4 (d, $^3J_{C-P}$ = 10.8 Hz), 128.3, 128.8, 131.5, 142.7 (d, $^3J_{C-P}$ = 9.5 Hz), 173.6. ^{31}P NMR (121.5 MHz, D_2O): rotamers at δ_P ppm 23.25, 23.52. HRMS (ESI): calculated for $C_{11}H_{14}ClNO_5P$ [(M − H)$^-$] 306.0304; found 306.0306.

*3-(N-Hydroxy-N-methylcarbamoyl)-2-(3,4-dichlorophenyl)-propylphosphonic Acid, Bisammonium Salt (**7e**).* Prepared from compound **16e** (150 mg, 0.38 mmol) according to general procedure VII. Brown powder. ^{1}H NMR (300 MHz, D_2O) δ_H ppm 1.84−2.08 (m, 2H, P−CH_2−), 2.57−3.02 (m, 2H, −CH_2−CO), 3.06 (s, 5/6 of N−CH_3), 3.16 (s, 1/6 of N−CH_3), 3.24−3.50 (m, 1H, −CH−), 7.18 (dd, J = 2.18 Hz, 8.50 Hz, 1H, Ar−H), 7.40−7.50 (m, 2H, Ar−H). ^{13}C NMR (75 MHz, D_2O) δ_C ppm 34.8 (d, $^1J_{C-P}$ = 131.5 Hz), 35.9, 37.2 (d, $^2J_{C-P}$ = 2.7 Hz), 39.5 (d, $^3J_{C-P}$ = 11.3 Hz), 127.51, 129.53, 129.8, 130.4, 131.6, 144.9 (d, $^3J_{C-P}$ = 9.4 Hz), 173.6. ^{31}P NMR (121.5 MHz, D_2O): rotamers at δ_P ppm 22.47, 22.72. HRMS (ESI): calculated for $C_{11}H_{13}Cl_2NO_5P$ [(M − H)$^-$] 339.9914; found 340.0130.

*Sodium Hydrogen 3-(N-Hydroxy-N-methylcarbamoyl)-2-methyl-propylphosphonate (**7f**).* Prepared from compound **13f** (125 mg, 0.26 mmol) according to general procedure V. Colorless oil. ^{1}H NMR (300 MHz, D_2O) δ_H ppm 1.01 (d, J = 8.40 Hz, 3H, −CH(CH_3)−), 1.41−172 (m, 2H, P−CH_2−), 2.06−2.34 (m, 1H, −CH−), 2.36−2.49 (m, 1H, −CH_2−CO), 2.59 (dd, J = 6.3 Hz, 14.02 Hz), 3.20 (s, 5/6 of N−CH_3), 3.38 (s, 1/6 of N−CH_3). ^{13}C NMR (75 MHz, D_2O) δ_C ppm 20.6 (d, $^3J_{C-P}$ = 8.0 Hz), 28.6 (d, $^2J_{C-P}$ = 3.4 Hz), 35.0 (d, $^3J_{C-P}$ = 132.1 Hz), 36.1, 40.2 (d, $^3J_{C-P}$ = 13.3 Hz), 175.2. ^{31}P NMR (121.5 MHz, D_2O): rotamers at δ_P ppm 25.03, 25.42. HRMS (ESI): calculated for $C_6H_{13}NO_5P$ [(M − H)$^-$] 210.0537; found 210.1632.

*Sodium Hydrogen 2-((N-Hydroxy-N-methylcarbamoyl)methyl)-3-phenylpropylphosphonate (**8a**).* Prepared from compound **21a** (200 mg, 0.36 mmol) according to general procedure V. White powder. ^{1}H NMR (300 MHz, D_2O) δ_H ppm 1.46−1.79 (m, 2H, P−CH_2−), 2.34−2.66 (m, 4H, −CH_2−), 2.80−2.9 (m, 1H, −CH−), 3.08 (s, 5/6 of N−CH_3), 3.18 (s, 1/6 of N−CH_3), 7.13−7.39 (m, 5H, Ar−H). ^{13}C NMR (75 MHz, D_2O) δ_C ppm 32.2 (d, $^1J_{C-P}$ = 132.3 Hz), 32.7 (d, $^2J_{C-P}$ = 3.8 Hz), 35.8, 36.6, 41.0 (d, $^3J_{C-P}$ = 9.2 Hz), 126.2, 128.4, 129.4, 140.4, 174.6. ^{31}P NMR (121.5 MHz, D_2O): rotamers at δ_P ppm 24.68, 25.01. HRMS (ESI): calculated for $C_{12}H_{17}NO_5P$ [(M − H)$^-$] 286.0850; found 286.0821.

*Sodium Hydrogen 2-((N-Hydroxy-N-methylcarbamoyl)methyl)-4-phenylbutylphosphonate (**8b**).* White powder. Prepared from compound **21b** (130 mg, 0.23 mmol) according to general procedure V. ^{1}H NMR (300 MHz, D_2O) δ_H ppm 1.34−1.84 (m, 4H, −CH_2−), 2.08−2.27 (m, 1H, −CH−), 2.54−2.77 (m, 4H, −CH_2−), 3.20 (s, 5/6 of N−CH_3), 3.35 (s, 1/6 of N−CH_3), 7.17−7.40 (m, 5H, Ar−H). ^{13}C NMR (75 MHz, D_2O) δ_C ppm 32.0 (d, $^1J_{C-P}$ = 3.7 Hz), 32.5, 33.0 (d, $^1J_{C-P}$ = 129.9 Hz), 36.1, 36.3 (d, $^3J_{C-P}$ = 6.4 Hz), 37.7 (d, $^3J_{C-P}$ = 10.6 Hz), 126.0, 128.7, 128.8, 143.5, 175.0. ^{31}P NMR (121.5 MHz, D_2O): δ_P ppm 22.47. HRMS (ESI): calculated for $C_{13}H_{19}NO_5P$ [(M − H)$^-$] 300.1006; found 300.1204.

*Sodium Hydrogen 2-((N-Hydroxy-N-methylcarbamoyl)methyl)-5-phenylpentylphosphonate (**8c**).* Prepared from compound **21c** (175 mg, 0.30 mmol) according to general procedure V. White powder. ^{1}H NMR (300 MHz, D_2O) δ_H ppm 1.28−1.70 (m, 6H, −CH_2−), 2.05−2.26 (m, 1H, −CH−), 2.50−2.72 (m, 4H, P−CH2-, CH_2−CON-), 3.18 (s, 5/6 of N−CH_3), 3.35 (s, 1/6 of N−CH_3), 7.18−7.36 (m, 5H, Ar−H). ^{13}C NMR (75 MHz, D_2O) δ_C ppm 28.2, 31.8 (d, $^2J_{C-P}$ = 3.6 Hz), 33.0 (d, $^1J_{C-P}$ = 130.1 Hz), 35.0 (d, $^3J_{C-P}$ = 10.3 Hz), 35.3, 36.1, 36.6 (d, $^3J_{C-P}$ = 6.2 Hz), 126.0, 128.7, 128.8, 143.7, 175.2. ^{31}P NMR (121.5 MHz, D_2O): δ_P ppm = 23.18. HRMS (ESI): calculated for $C_{14}H_{21}NO_5P$ [(M − H)$^-$] 314.1163; found 314.1101.

*Sodium Hydrogen 2-((N-Hydroxy-N-methylcarbamoyl)methyl)-6-phenylhexylphosphonate (**8d**).* Prepared from compound **21d** (175 mg, 0.29 mmol) according to general procedure V. White powder. ^{1}H NMR (300 MHz, D_2O) δ_H ppm 1.20−1.66 (m, 8H, −CH_2−), 2.11 (m, 1H, −CH−), 2.46−2.68 (m, 4H, −CH_2−), 3.18 (s, 5/6 of N−CH_3), 3.34 (s, 1/6 of N−CH_3), 7.15−7.38 (m, 5H, Ar−H). ^{13}C NMR (75 MHz, D_2O) δ_C ppm 25.6, 31.2, 31.9 (d, $^2J_{C-P}$ = 3.8 Hz), 33.1 (d, $^1J_{C-P}$ = 130.2 Hz), 35.1, 35.3 (d, $^3J_{C-P}$ = 10.0 Hz), 36.1, 36.6 (d, $^3J_{C-P}$ = 7.0 Hz), 125.9, 128.7, 128.8, 143.7, 175.3. ^{31}P NMR (121.5 MHz, D_2O): δ_P ppm = 23.20. HRMS (ESI): calculated for $C_{15}H_{23}NO_5P$ [(M − H)$^-$] 328.1319; found 328.1340.

■ ASSOCIATED CONTENT

Supporting Information

Additional information concerning cloning, expression, protein purification, enzyme assays, pathogen testing, and crystallographic work, as well as ^{1}H, ^{13}C, and ^{31}P NMR spectra of compound **7a−f** and **8a−d**. This material is available free of charge via the Internet at http://pubs.acs.org.

Accession Codes

Coordinates and structure factor data have been deposited at the PDB with entry codes 4Y6R, 4Y6S, 4Y67, and 4Y6P for complexes with **7a**, **7b**, **8c**, and **8d**, respectively.

■ AUTHOR INFORMATION

Corresponding Authors

*Dr. Sherry Mowbray. E-mail: mowbray@xray.bmc.uu.se. Phone: +46 18 471 49 90.

*Dr. Serge Van Calenbergh. E-mail: serge.vancalenbergh@ugent.be. Phone: +32 9 264 81 24. Fax: + 32 9 264 81 46.

Notes

The authors declare no competing financial interest.

■ ACKNOWLEDGMENTS

T.C. and S.V.C. received support of the FWO Flanders. R.C. received a doctoral scholarship of the Special Research Fund of the UGent. T.A.J. and S.L.M. have been supported by the Swedish Research Council (VR), FORMAS, and Uppsala University. We thank An Matheeussen for running the *in vitro* antiplasmodial evaluation and Izet Karalic for the technical assistance. Anna Jansson assisted with the construction of the expression plasmid for PfDxr.

■ ABBREVIATIONS USED

BSTFA, *N*,*O*-bis(trimethylsilyl)trifluoroacetamide; DiPEA, *N*,*N*-diisopropylethylamine; DMAP, 4-dimethylaminopyridine; DOXP, 1-deoxy-D-xylulose-5-phosphate; Dxr, 1-deoxy-D-xylulose-5-phosphate reductoisomerase; Ec, *Escherichia coli*; EDC, 1-ethyl-3-(3-dimethylaminopropyl)carbodiimide; MEP, 2-*C*-methyl-D-erythritol-3-phosphate; Mtb, *Mycobacterium tuberculosis*; Pf, *Plasmodium falciparum*; SAR, structure−activity relationship; TB, tuberculosis; TMSBr, bromotrimethylsilane

■ REFERENCES

(1) Snow, R. W.; Guerra, C. A.; Noor, A. M.; Myint, H. Y.; Hay, S. I. The global distribution of clinical episodes of *Plasmodium falciparum* malaria. *Nature* **2005**, *434*, 214−217.

(2) World Health Organization. World malaria report 2014. http://www.who.int/malaria/publications/world_malaria_report_2014/en/.

(3) World Health Organization. Global tuberculosis report 2014. http://www.who.int/tb/publications/global_report/en/.

(4) Jomaa, H.; Wiesner, J.; Sanderbrand, S.; Altincicek, B.; Weidemeyer, C.; Hintz, M.; Turbachova, I.; Eberl, M.; Zeidler, J.; Lichtenthaler, H. K.; Soldati, D.; Beck, E. Inhibitors of the non mevalonate pathway of isoprenoid biosynthesis as antimalarial drugs. *Science* **1999**, *285*, 1573−1576.

(5) Brown, A. C.; Parish, T. Dxr is essential in *Mycobacterium tuberculosis* and fosmidomycin resistance is due to lack of uptake. *BMC Microbiol.* **2008**, *8*, No. 78.

(6) Rohmer, M. Diversity in isoprene unit biosynthesis: The methylerythritol phosphate pathway in bacteria and plastids. *Pure Appl. Chem.* **2007**, *79*, 739−751.

DOI: 10.1021/jm5014264
J. Med. Chem. 2015, 58, 2988−3001

(7) Sauret-Gueto, S.; Ramos-Valdivia, A.; Ibanez, E.; Boronat, A.; Rodriguez-Concepcion, M. Identification of lethal mutations in *Escherichia coli* genes encoding enzymes of the methylerythritol phosphate pathway. *Biochem. Biophys. Res. Commun.* **2003**, *307*, 408−415.
(8) Rohmer, M. The discovery of a mevalonate-independent pathway for isoprenoid biosynthesis in bacteria, algae and higher plants. *Nat. Prod. Rep.* **1999**, *16*, 565−574.
(9) Masini, T.; Hirsch, A. K. H. Development of inhibitors of the 2*C*-Methyl-D-erythritol 4-phosphate (MEP) pathway enzymes as potential anti-infective agents. *J. Med. Chem.* **2014**, *57*, 9740−9763.
(10) Takahashi, S.; Kuzuyama, T.; Watanabe, H.; Seto, H. A 1-deoxy-D-xylulose 5-phosphate reductoisomerase catalyzing the formation of 2-C-methyl-D-elythritol 4-phosphate in an alternative nonmevalonate pathway for terpenoid biosynthesis. *Proc. Natl. Acad. Sci. U.S.A.* **1998**, *95*, 9879−9884.
(11) Kuzuyama, T.; Shimizu, T.; Takahashi, S.; Seto, H. Fosmidomycin, a specific inhibitor of 1-deoxy-D-xylulose 5-phosphate reductoisomerase in the nonmevalonate pathway for terpenoid biosynthesis. *Tetrahedron Lett.* **1998**, *39*, 7913−7916.
(12) van der Meer, J. Y.; Hirsch, A. K. The isoprenoid-precursor dependence of Plasmodium spp. *Nat. Prod. Rep.* **2012**, *29* (7), 721−728.
(13) Wiesner, J.; Henschker, D.; Hutchinson, D. B.; Beck, E.; Jomaa, H. *In vitro* and *in vivo* synergy of fosmidomycin, a novel antimalarial drug, with clindamycin. *Antimicrob. Agents Chemother.* **2002**, *46*, 2889−2894.
(14) Borrmann, S.; Adegnika, A. A.; Matsiegui, P. B.; Issifou, S.; Schindler, A.; Mawili-Mboumba, D. P.; Baranek, T.; Wiesner, J.; Jomaa, H.; Kremsner, P. G. Fosmidomycin-clindamycin for *Plasmodium falciparum* infections in African children. *J. Infect. Dis.* **2004**, *189*, 901−908.
(15) Borrmann, S.; Lundgren, I.; Oyakhirome, S.; Impouma, B.; Matsiegui, P. B.; Adegnika, A. A.; Issifou, S.; Kun, J. F. J.; Hutchinson, D.; Wiesner, J.; Jomaa, H.; Kremsner, P. G. Fosmidomycin plus clindamycin for treatment of pediatric patients aged 1 to 14 years with *Plasmodium falciparum* malaria. *Antimicrob. Agents Chemother.* **2006**, *50*, 2713−2718.
(16) Lanaspa, M.; Moraleda, C.; Machevo, S.; González, R.; Serrano, B.; Macete, E.; Cisteró, P.; Mayor, A.; Hutchinson, D.; Kremsner, P. G.; Alonso, P.; Menéndez, C.; Bassata, Q. Inadequate efficacy of a new formulation of fosmidomycin-clindamycin combination in Mozambican children less than three years old with uncomplicated *Plasmodium falciparum* malaria. *Antimicrob. Agents Chemother.* **2012**, *56*, 2923−2928.
(17) Murakawa, T.; Sakamoto, H.; Fukada, S.; Konishi, T.; Nishida, M. Pharmacokinetics of Fosmidomycin, a new phosphonic acid antibiotic. *Antimicrob. Agents Chemother.* **1982**, *21*, 224−230.
(18) Kuemmerle, H. P.; Murakawa, T.; De Santis, F. Pharmacokinetic evaluation of fosmidomycin, a new phosphonic acid antibiotic. *Chemioterapia* **1987**, *6*, 113−119.
(19) Lell, B.; Ruangweerayut, R.; Wiesner, J.; Missinou, M. A.; Schindler, A.; Baranek, T.; Hintz, M.; Hutchinson, D.; Jomaa, H.; Kremsner, P. G. Fosmidomycin, a novel chemotherapeutic agent for malaria. *Antimicrob. Agents Chemother.* **2003**, *47*, 735−738.
(20) Dhiman, R. K.; Schaeffer, M. L.; Bailey, A. M.; Testa, C. A.; Scherman, H.; Crick, D. C. 1-Deoxy-D-xylulose 5-phosphate reductoisomerase (IspC) from *Mycobacterium tuberculosis*: Towards understanding mycobacterial resistance to fosmidomycin. *J. Bacteriol.* **2005**, *187*, 8395−8402.
(21) Sakamoto, Y.; Furukawa, S.; Ogihara, H.; Yamasaki, M. Fosmidomycin resistance in adenylate cyclase deficient (cya) mutants of Escherichia coli. *Biosci. Biotechnol. Biochem.* **2003**, *67*, 2030−2033.
(22) Nair, S. C.; Brooks, C. F.; Goodman, C. D.; Strurm, A.; McFadden, G. I.; Sundriyal, S.; Anglin, J. L.; Song, Y.; Moreno, S. N. J.; Striepen, B. Apicoplast isoprenoid precursor synthesis and the molecular basis of fosmidomycin resistance in *Toxoplasma gondii*. *J. Exp. Med.* **2011**, *208*, 1547−1559.
(23) Hemmi, K.; Takeno, H.; Hashimoto, M.; Kamiya, T. Studies on phosphonic acid antibiotics. IV. Synthesis and antibacterial activity of analogs of 3-(N-acetyl-N-hydroxyamino)-propylphosphonic acid (FR-900098). *Chem. Pharm. Bull.* **1982**, *30*, 111−118.
(24) Woo, Y.; Fernandes, R.; Proteau, P. Evaluation of fosmidomycin analogs as inhibitors of the Synechocystis sp PCC6803 1-deoxy-D-xylulose 5-phosphate reductoisomerase. *Bioorg. Med. Chem.* **2006**, *14*, 2375−2385.
(25) Chofor, R.; Risseeuw, M. D. P.; Pouyez, J.; Johny, C.; Wouters, J.; Dowd, C. S.; Couch, R. D.; Van Calenbergh, S. Synthetic fosmidomycin analogues with altered chelating moieties do not inhibit 1-deoxy-D-xylulose 5-phosphate reductoisomerase or *Plasmodium falciparum* growth in vitro. *Molecules* **2014**, *19*, 2571−2587.
(26) Zingle, C.; Kuntz, L.; Tritsch, D.; Grosdemange-Billiard, C.; Rohmer, M. Isoprenoid biosynthesis via the methylerythritol phosphate pathway: structural variations around phosphonate anchor and spacer of fosmidomycin, a potent inhibitor of deoxyxylulose phosphate reductoisomerase. *J. Org. Chem.* **2010**, *75*, 3203−3207.
(27) Jackson, E. R.; San Jose, G. S.; Brothers, R. C.; Edelstein, E. K.; Sheldon, Z.; Haymond, A.; Johny, C.; Boshoff, H. I.; Couch, R. D.; Dowd, C. S. The effect of chain length and unsaturation on Mtb Dxr inhibition and antitubercular killing activity of FR900098 analogs. *Bioorg. Med. Chem. Lett.* **2014**, *24*, 649−653.
(28) Haemers, T.; Wiesner, J.; Van Poecke, S.; Goeman, J.; Henschker, D.; Beck, E.; Jomaa, H.; Van Calenbergh, S. Synthesis of α-substituted fosmidomycin analogues as highly potent *Plasmodium falciparum* growth inhibitors. *Bioorg. Med. Chem. Lett.* **2006**, *16*, 1888−1891.
(29) Behrendt, C. T.; Kunfermann, A.; Illarionova, V.; Matheeussen, A.; Pein, M. K.; Grawert, T.; Kaiser, J.; Bacher, A.; Eisenreich, W.; Illarionov, B.; Fischer, M.; Maes, L.; Groll, M.; Kurz, T. Reverse fosmidomycin derivatives against the antimalarial drug target IspC (Dxr). *J. Med. Chem.* **2011**, *54*, 6796−802.
(30) Andaloussi, M.; Henriksson, L. M.; Wieckowska, A.; Lindh, M.; Bjorkelid, C.; Larsson, A. M.; Suresh, S.; Iyer, H.; Srinivasa, B. R.; Bergfors, T.; Unge, T.; Mowbray, S. L.; Larhed, M.; Jones, T. A.; Karlen, A. Design, synthesis, and X-ray crystallographic studies of α-aryl substituted fosmidomycin analogues as inhibitors of *Mycobacterium tuberculosis* 1-deoxy-D-xylulose 5-phosphate reductoisomerase. *J. Med. Chem.* **2011**, *54*, 4964−4976.
(31) Jansson, A. M.; Wieckowska, A.; Bjorkelid, C.; Yahiaoui, S.; Sooriyaarachchi, S.; Lindh, M.; Bergfors, T.; Dharavath, S.; Desroses, M.; Suresh, S.; Andaloussi, M.; Nikhil, R.; Sreevalli, S.; Srinivasa, B. R.; Larhed, M.; Jones, T. A.; Karlén, A.; Mowbray, S. L. DXR inhibition by potent mono- and disubstituted fosmidomycin analogues. *J. Med. Chem.* **2013**, *56*, 6190−6199.
(32) Deng, L.; Diao, J.; Chen, P.; Pujari, V.; Yao, Y.; Cheng, G.; Crick, D. C.; Prasad, B. V.; Song, Y. Inhibition of 1-deoxy-D-xylulose-5-phosphate reductoisomerase by lipophilic phosphonates: SAR, QSAR, and crystallographic studies. *J. Med. Chem.* **2011**, *54*, 4721−4734.
(33) Xue, J.; Diao, J.; Cai, G.; Deng, L.; Zheng, B.; Yao, Y.; Song, Y. Antimalarial and structural studies of pyridine-containing inhibitors of 1-deoxyxylulose-5-phosphate reductoisomerase. *ACS Med. Chem. Lett.* **2013**, *4*, 278−282.
(34) Henriksson, L. M.; Unge, T.; Carlsson, J.; Aqvist, J.; Mowbray, S. L.; Jones, T. A. Structures of *Mycobacterium tuberculosis* 1-deoxy-D-xylulose-5-phosphate reductoisomerase provide new insights into catalysis. *J. Biol. Chem.* **2007**, *282*, 19905−19916.
(35) Umeda, T.; Tanaka, N.; Kusakabe, Y.; Nakanishi, M.; Kitade, Y.; Nakamura, K. T. Molecular basis of fosmidomycin's action on the human malaria parasite *Plasmodium falciparum*. *Sci. Rep.* **2011**, *1*, No. 9.
(36) Björkelid, C.; Bergfors, T.; Unge, T.; Mowbray, S. L.; Jones, T. A. Structural studies on *Mycobacterium tuberculosis* DXR in complex with the antibiotic FR-900098. *Acta Crystallogr., Sect. D: Biol. Crystallogr.* **2012**, *68*, 134−143.
(37) Kunfermann, A.; Lienau, C.; Illarionov, B.; Held, J.; Gräwert, T.; Behrendt, C. T.; Werner, P.; Hähn, S.; Eisenreich, W.; Riederer, U.;

DOI: 10.1021/jm5014264
J. Med. Chem. 2015, 58, 2988−3001

Mordmüller, B.; Bacher, A.; Fischer, M.; Groll, M.; Kurz, T. IspC as target for antiinfective drug discovery: Synthesis, enantiomeric separation, and structural biology of fosmidomycin thia isosters. *J. Med. Chem.* **2013**, *56*, 8151−8162.
(38) Konzuch, S.; Umeda, T.; Held, J.; Hähn, S.; Brücher, K.; Lienau, C.; Behrendt, C. T.; Gräwert, T.; Bacher, A.; Illarionov, B.; Fischer, M.; Mordmüller, B.; Tanaka, N.; Kurz, T. Binding modes of reverse fosmidomycin analogs toward the antimalarial target IspC. *J. Med. Chem.* **2014**, *57*, 8827−38.
(39) Kuntz, L.; Tritsch, D.; Grosdemange-Billiard, C.; Hemmerlin, A.; Willem, A.; Bacht, T.; Rohmer, M. Isoprenoid biosynthesis as a target for antibacterial and antiparasitic drugs: Phosphonohydroxamic acids as inhibitors of deoxyxylulose phosphate reducto-isomerase. *Biochem. J.* **2005**, *386*, 127−135.
(40) Kurz, T.; Schluter, K.; Kaula, U.; Bergmann, B.; Walter, R. D.; Geffken, D. Synthesis and antimalarial activity of chain substituted pivaloyloxymethyl ester analogues of Fosmidomycin and FR900098. *Bioorg. Med. Chem.* **2006**, *14*, 5121−5135.
(41) Haemers, T.; Wiesner, J.; Gießmann, D.; Verbrugghen, T.; Hillaert, U.; Ortmann, R.; Jomaa, H.; Link, A.; Schlitzer, M.; Van Calenbergh, S. Synthesis of β- and γ-oxa isosteres of fosmidomycin and FR900098 as antimalarial candidates. *Bioorg. Med. Chem.* **2008**, *16*, 3361−3371.
(42) Brucher, K.; Illarionov, B.; Held, J.; Tschan, S.; Kunfermann, A.; Pein, M. K.; Bacher, A.; Gräwert, T.; Maes, L.; Mordmüller, B.; Fischer, M.; Kurz, T. α-Substituted β-oxa isosteres of fosmidomycin: synthesis and biological evaluation. *J. Med. Chem.* **2012**, *55*, 6566−6575.
(43) Kunfermann, A.; Lienau, C.; Illarionov, B.; Held, J.; Gräwert, T.; Behrendt, C. T.; Werner, P.; Hähn, S.; Eisenreich, W.; Riederer, U.; Mordmüller, B.; Bacher, A.; Fischer, M.; Groll, M.; Kurz, T. IspC as target for antiinfective drug discovery: Synthesis, enantiomeric Separation, and structural biology of fosmidomycin thia isosters. *J. Med. Chem.* **2013**, *56*, 8151−8162.
(44) Topliss, J. G. A manual method for applying the Hansch approach to drug design. *J. Med. Chem.* **1977**, *20*, 463−469.
(45) Kamiya, T. S.; Hashimoto, M. T.; Hemmi, K. K.; Takeno, H. N. Hydroxyaminohydrocarbonphosphonic acids. US Patent 4,206,156, June 3, 1980.
(46) Silber, K.; Heidler, P.; Kurz, T.; Klebe, G. AFMoC enhances predictivity of 3D QSAR: A case study with DOXP-reductoisomerase. *J. Med. Chem.* **2005**, *48*, 3547−3563.
(47) Goble, J. L.; Adendorff, M. R.; De Beer, T. A. P.; Stephens, L. L.; Blatch, G. L. The malaria drug target *Plasmodium falciparum* 1-deoxy-D-xylulose-5-phosphate reductoisomerase (PfDxr): development of a 3-D model for identification of novel, structural and functional features and for inhibitor screening. *Protein Pept. Lett.* **2010**, *17*, 109−120.
(48) Kazuyoshi, T.; Akira, A.; Hiroko, N.; So-ichi, T.; Yoshihisa, M.; Hiroaki, T.; Yoshihiro, H. Dicarbonates: Convenient 4-dimethylaminopyridine catalyzed esterification reagents. *Synthesis* **1994**, 1063−1066.
(49) Yamaguchi, M.; Tsukamoto, Y.; Hayashi, A.; Minami, T. A stereoselective Michael addition of α-lithiated phosphonates to α,β-unsaturated esters. *Tetrahedron Lett.* **1990**, *31*, 2423−2424.
(50) Nair, S. C.; Brooks, C. F.; Goodman, C. D.; Strurm, A.; McFadden, G. I.; Sundriyal, S.; Anglin, J. L.; Song, Y.; Moreno, S. N. J.; Striepen, B. Apicoplast isoprenoid precursor synthesis and the molecular basis of fosmidomycin resistance in *Toxoplasma gondii*. *J. Exp. Med.* **2011**, *208*, 1547−1559.
(51) Zinglé, C.; Kuntz, L.; Tritsch, D.; Grosdemange, C. B.; Rohmer, M. Modifications around the hydroxamic acid chelating group of fosmidomycin, an inhibitor of the metalloenzyme 1-deoxyxylulose 5-phosphate reductoisomerase (DXR). *Bioorg. Med. Chem. Lett.* **2012**, *22*, 6563−6567.
(52) Ponaire, S.; Zinglé, C.; Tritsch, D.; Grosdemange-Billiard, C.; Rohmer, M. Growth inhibition of *Mycobacterium smegmatis* by prodrugs of deoxyxylulose phosphate reducto-isomerase inhibitors, promising anti-mycobacterial agents. *Eur. J. Med. Chem.* **2012**, *51*, 227−285.
(53) Shiloh, M. U.; Champion, P. A. To catch a killer. What can mycobacterial models teach us about Mycobacterium tuberculosis pathogenesis? *Curr. Opin Microbiol.* **2010**, 86−92.
(54) Bjorkelid, C.; Bergfors, T.; Unge, T.; Mowbray, S. L.; Jones, T. A. Structural studies on *Mycobacterium tuberculosis* DXR in complex with the antibiotic FR-900098. *Acta Crystallogr., Sect. D: Biol. Crystallogr.* **2012**, *68*, 134−143.
(55) Ming-Kui, Z.; Jun-Feng, Z.; Teck-Peng, L. Palladium-catalyzed C−C bond formation of arylhydrazines with olefins via carbon-nitrogen bond cleavage. *Org. Lett.* **2011**, *13*, 6308−6311.
(56) Wei-Ting, W.; Jiann-Yih, Y.; Ting-Shen, K.; Hsyueh-Liang, W. Highly enantioselective rhodium-catalyzed asymmetric 1,4-addition reactions of arylboronic acids to acyclic α,β-unsaturated compounds: the formal synthesis of (−)-indatraline. *Chem.—Eur. J.* **2011**, *17*, 11405−11409.
(57) Read, R. J. Improved Fourier coefficients for maps using phases from partial structures with errors. *Acta Crystallogr., Sect. A* **1986**, *42*, 140−149.
(58) Verbrugghen, T.; Cos, P.; Maes, L.; Van Calenbergh, S. Synthesis and evaluation of β-halogenated analogues of 3-(acetylhydroxyamino)propylphosphonic acid (FR900098) as antimalarials. *J. Med. Chem.* **2010**, *53*, 5342−5346.

DOI: 10.1021/jm5014264
J. Med. Chem. 2015, 58, 2988−3001

Paper V: Structure-Activity Relationships of the MEPicides: N-Acyl and O-linked Analogs of FR900098 as Inhibitors of Dxr from Mycobacterium tuberculosis and Yersinia pestis

San Jose G, Jackson ER, Haymond A, Johny C, Edwards RL, Wang X, et al. *ACS Infect Dis.* 2016; doi:10.1021/acsinfecdis.6b00125 [145]

Attributions and Contributions

Reproduced with permission from the American Chemical Society. Copyright 2016 American Chemical Society. All supplementary information as referenced in the text can be found in Appendix 2. The author was responsible for the generation of kinetic data in Figure 3 and Table 1, and Figures 4 and 5.

ACS Infectious Diseases

Article

pubs.acs.org/journal/aidcbc

Structure–Activity Relationships of the MEPicides: *N*-Acyl and *O*-Linked Analogs of FR900098 as Inhibitors of Dxr from *Mycobacterium tuberculosis* and *Yersinia pestis*

Géraldine San Jose,[†,#] Emily R. Jackson,[†,#] Amanda Haymond,[‡] Chinchu Johny,[‡] Rachel L. Edwards,[§] Xu Wang,[†] R. Carl Brothers,[†] Emma K. Edelstein,[†] Audrey R. Odom,[§] Helena I. Boshoff,[⊥] Robin D. Couch,[‡] and Cynthia S. Dowd*[,†]

[†]Department of Chemistry, George Washington University, 800 22nd Street NW, Washington D.C. 20052, United States

[‡]Department of Chemistry and Biochemistry, George Mason University, 10900 University Boulevard, Manassas, Virginia 20110, United States

[§]Department of Pediatrics, Washington University School of Medicine, 660 S Euclid Avenue, St. Louis, Missouri 63110, United States

[⊥]Tuberculosis Research Section, LCID, NIAID/NIH, 9000 Rockville Pike, Bethesda, Maryland 20892, United States

Supporting Information

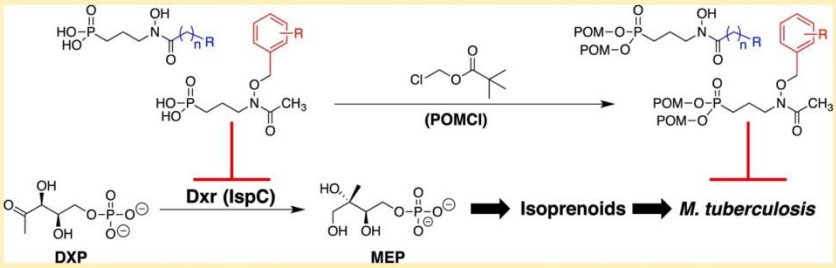

ABSTRACT: Despite continued research efforts, the threat of drug resistance from a variety of bacteria continues to plague clinical communities. Discovery and validation of novel biochemical targets will facilitate development of new drugs to combat these organisms. The methylerythritol phosphate (MEP) pathway to make isoprene units is a biosynthetic pathway essential to many bacteria. We and others have explored inhibitors of the MEP pathway as novel antibacterial agents. *Mycobacterium tuberculosis*, the causative agent of tuberculosis, and *Yersinia pestis*, resulting in the plague or "black death", both rely on the MEP pathway for isoprene production. 1-Deoxy-D-xylulose 5-phosphate reductoisomerase (Dxr) catalyzes the first committed step in the MEP pathway. We examined two series of Dxr inhibitors based on the parent structure of the retrohydroxamate natural product FR900098. The compounds contain either an extended *N*-acyl or *O*-linked alkyl/aryl group and are designed to act as bisubstrate inhibitors of the enzyme. While nearly all of the compounds inhibited both Mtb and Yp Dxr to some extent, compounds generally displayed more potent inhibition against the Yp homologue, with the best analogs displaying nanomolar IC_{50} values. In bacterial growth inhibition assays, the phosphonic acids generally resulted in poor antibacterial activity, likely a reflection of inadequate permeability. Accordingly, diethyl and dipivaloyloxymethyl (POM) prodrug esters of these compounds were made. While the added lipophilicity did not enhance *Yersinia* activity, the compounds showed significantly improved antitubercular activities. The most potent compounds have Mtb MIC values of 3–12 μg/mL. Taken together, we have uncovered two series of analogs that potently inhibit Dxr homologues from Mtb and Yp. These inhibitors of the MEP pathway, termed MEPicides, serve as leads for future analog development.

KEYWORDS: *MEP pathway, antibiotic, phosphonate prodrug, Mycobacterium tuberculosis, Yersinia pestis*

Despite a recent surge in the search for novel antibiotics, there continues to be a significant and pressing need for additional therapies in our clinical arsenal combatting bacterial pathogens.[1−3] Disease due to drug-resistant strains of bacteria worsens public health and highlights the lack of novel chemical entities in the drug discovery pipeline.[1,4,5] Resistance to first- and second-line treatments has increased over the last several years, resulting in bacterial strains with very limited therapeutic options. It is therefore imperative that new drugs target biochemical

Received: July 6, 2016
Published: September 27, 2016

ACS Publications © 2016 American Chemical Society

DOI: 10.1021/acsinfecdis.6b00125
ACS Infect. Dis. 2016, 2, 923−935

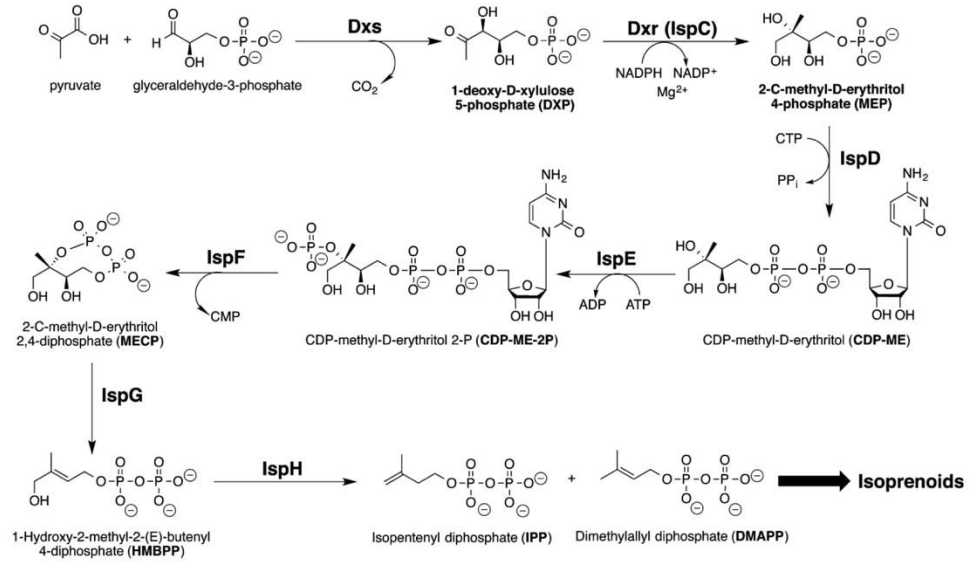

Figure 1. Methylerythritol phosphate (MEP) pathway of isoprenoid biosynthesis.

pathways not currently used by existing antibiotics. These novel mechanisms-of-action must be validated to pave the way for successful drug candidates.

The goal of our work is to design small molecule inhibitors of specific biochemical pathways, which can then serve as chemical tools to validate these new drug targets. Pathways found in common across several microbial pathogens, but not in humans, are particularly attractive for drug discovery. Although pathogens may share the same rate-limiting enzyme, known structural variations within the active sites can be considered when developing specific inhibitors. Alternatively, exploring inhibition across species is an efficient and economical way to develop a broad-spectrum agent. The paucity of novel antibiotics argues strongly that both approaches should be employed.

Our work has recently focused on two organisms, *Mycobacterium tuberculosis* (Mtb), causing tuberculosis (TB), and *Yersinia pestis* (Yp), causing plague (or black death).[6−10] TB is still responsible for nearly 2 million deaths each year and threatens public health in both developed and developing countries.[11−13] Gram-negative *Yersinia pestis*, a bacterial cousin of Mtb, continues to infect individuals worldwide.[14] Drug resistant strains of both organisms have been well characterized and pose significant threats to public health.[15]

The methylerythritol phosphate (MEP, or nonmevalonate) pathway of isoprene synthesis is common to most bacteria, including Mtb and Yp. First identified in plants and bacteria,[16,17] this pathway catalyzes the synthesis of five-carbon isopentenyl (IPP) and dimethylallyl (DMAPP) pyrophosphate units from pyruvate and glyceraldehyde-3-phosphate (Figure 1). IPP and DMAPP are essential building blocks of larger, more complex molecules required for several pathways including respiration, cell wall biosynthesis, and cell signaling. While humans also require the production of IPP and DMAPP, these molecules are synthesized via the mevalonate pathway, distinct from the MEP pathway. There are no human homologues of the MEP enzymes. As such, we and others have explored this pathway as a source of novel targets for antibacterial drug discovery.

1-Deoxy-D-xylulose 5-phosphate reductoisomerase (Dxr, IspC) catalyzes the first-committed step of the MEP pathway and has been widely explored as a novel antibiotic target.[18−21] Catalyzing both the reduction and isomerization of DXP to MEP, Dxr has been shown essential in several organisms including *Plasmodium falciparum* (causing malaria), Mtb, and *Escherichia coli*.[22−26] Natural products fosmidomycin (**1**) and FR900098 (**2**) (Figure 2)

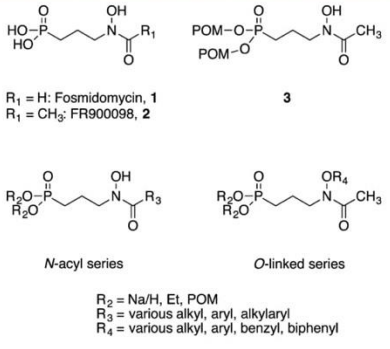

Figure 2. Natural products fosmidomycin and FR900098 and their lipophilic esters (such as **3**) are known Dxr inhibitors with antibacterial activity. *N*-Acyl and *O*-linked analogs show potent Dxr inhibition and are the focus of this work.

potently inhibit Dxr;[27−30] however their polar nature prevents cellular penetration in organisms such as Mtb that have a cell wall rich in mycolic acids.[22] Accordingly, we have demonstrated that increasing the lipophilic character of these Dxr inhibitors

DOI: 10.1021/acsinfecdis.6b00125
ACS Infect. Dis. 2016, 2, 923−935

Scheme 1[a]

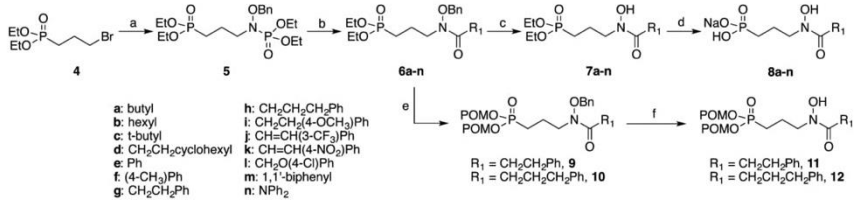

[a]Reagents and conditions: (a) NaH, $NH(OBn)PO(OEt)_2$, TBABr, NaI; (b) (i) 2 N HCl; (ii) $R(CH_2)_nCOCl$, Et_3N; (c) H_2, Pd/C or BCl_3; (d) (i) TMSBr, BSTFA; (ii) NaOH; (e) (i) TMSBr; (ii) NaOH; (iii) POMCl, Et_3N; (f) H_2, Pd/C or BCl_3.

Scheme 2[a]

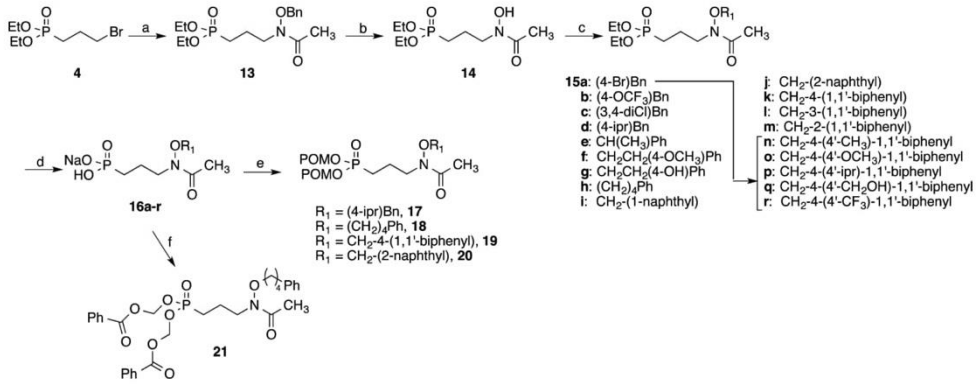

[a]Reagents and conditions: (a) NaH, NH(OBn)Ac, NaI; (b) H_2, Pd/C; (c) NaH, NaI, $Ar(CH_2)_nBr$; (d) (i) TMSBr; (ii) NaOH; (e) POMCl, Et_3N; (f) $PhCO_2CH_2Cl$, Et_3N (16 h).

using a phosphonate ester prodrug strategy significantly improves their antitubercular activity.[6] Compound **3**, for example, has an MIC of 50−100 μg/mL against Mtb where FR900098 is essentially inactive. Notably, these prodrugs also demonstrate inhibitory activity toward Gram-negative bacteria harboring a mutation of the bacterial glycerol-3-phosphate transporter (Glp-T; a fosmidomycin/FR900098 influx protein), known to confer resistance to fosmidomycin/FR900098 treatment.[7] While a specific mechanism has not been reported, cleavage of the prodrug moiety is thought to occur via nonspecific esterases inside the cell.[31]

We and others have examined the SAR of fosmidomycin and FR900098 as it relates to Dxr inhibition and antimicrobial effects. Unsaturation within the propyl chain is tolerated, while changing the chain length is not.[10] Substitution at the α position (relative to the phosphorus atom) enhances inhibitor potency.[32−34] Recently, we explored a bisubstrate approach where compounds were designed to occupy both the DXP and NADPH binding sites.[8] These compounds stem from two structure classes: an *N*-acyl series includes extensions of fosmidomycin's formyl group, and an *O*-linked series explores substitution of the hydroxyl group of the retrohydroxamate (Figure 2). Early modeling efforts suggested that compounds from both series would act as Dxr ligands.[8] We refer to these compounds collectively as MEPicides (inhibitors of the MEP pathway displaying antimicrobial activity). While a small set of compounds from these series has been reported,[8,9,34] we describe here an expanded set of compounds from both chemical classes, SAR of these compounds against Dxr from Mtb and Yp, and antibacterial activities of these compounds against Mtb, Yp, and *E. coli*.

Our prior work indicated that *N*-acyl and *O*-linked compounds could act as bisubstrate inhibitors of Dxr, binding to both the DXP and NADPH binding sites.[8] An interesting conclusion from this work pertained to the importance of the retrohydroxamate in Dxr inhibition. The retrohydroxamate, found in fosmidomycin, FR900098, and most Dxr inhibitors reported to date, is expected to coordinate a divalent cation resident between the DXP and NADPH binding sites. The cation is necessary for catalysis and a prominent feature of Dxr crystal structures.[19] For retrohydroxamate inhibitors, deprotonation of the hydroxyl group proton is thought to occur, leaving the anion able to bind the metal cation.[35] This putative mode of binding is reasonable for the *N*-acyl analogs. The *O*-linked compounds, with a substituted hydroxyl group, are unable to form the corresponding anion and, thus, are not expected to interact with the cation in the same way. One prediction might be that the *O*-linked compounds would be significantly less active compared with the *N*-acyl analogs, as a result. Here, we describe the synthesis and evaluation of a larger series of *N*-acyl and *O*-linked compounds designed to test this hypothesis. Our results indicate that an anion to strongly coordinate the metal cation is not necessary for potent Dxr inhibition.

DOI: 10.1021/acsinfecdis.6b00125
ACS Infect. Dis. 2016, 2, 923−935

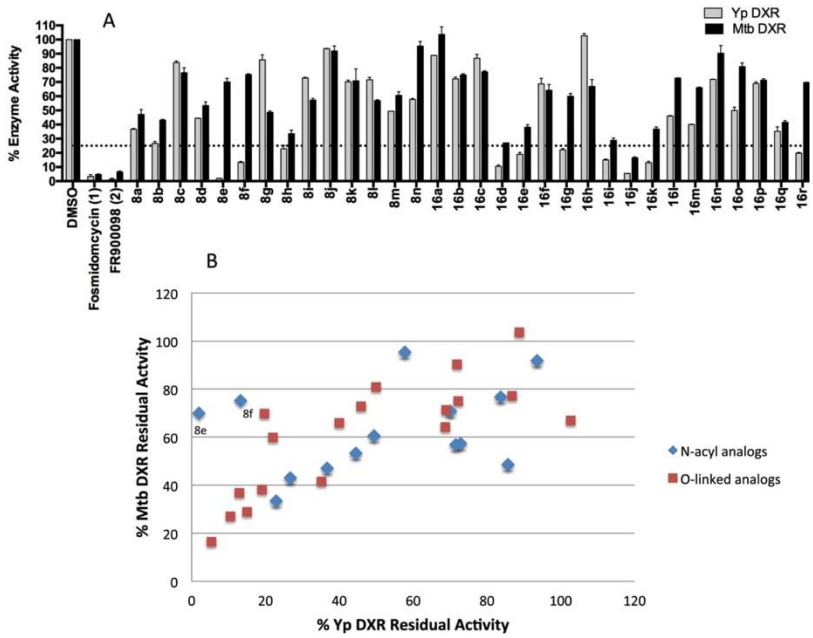

Figure 3. Inhibition of Mtb and Yp Dxr by *N*-acyl and *O*-linked MEPicides. (A) Percent residual activity of Yp Dxr (gray) and Mtb Dxr (black) when treated with 100 μM of inhibitor, compared to an uninhibited sample (DMSO). Fosmidomycin (**1**) and FR900098 (**2**) are positive controls. (B) Inhibition of homologous Dxr enzymes by *N*-acyl (diamonds) and *O*-linked MEPicides (squares) were correlated, especially when outlier *N*-acyl analogs **8e** and **8f** were ignored. Pearson coefficients: 0.76 (*O*-linked), 0.37 (all *N*-acyl analogs), and 0.71 (*N*-acyl analogs leaving **8e** and **8f** out).

RESULTS AND DISCUSSION

Synthesis. The synthetic routes used to prepare the *N*-acyl and *O*-linked compounds are shown in Schemes 1 and 2, respectively. Scheme 1 shows the synthetic route used to prepare the phosphonate salts (**8a**–**n**) and esters (**7a**–**n**, **11**, and **12**) of the *N*-acyl series. Benzyl-protected diethyl phosphoramidate[36] was deprotonated using sodium hydride and combined with diethyl phosphonate ester **4** to yield substituted phosphoramidate **5**.[6,36] Compound **5** was hydrolyzed under acidic conditions[36] and then acylated[10] with a series of acid chlorides to give *N*-acyl analogs **6a**–**n**. Removal of the benzyl group using either hydrogenolysis or BCl_3[10,37] yielded diethyl esters **7a**–**n**. Treatment of these esters with trimethylsilyl bromide[38] and BSTFA,[10,39] followed by sodium hydroxide gave monosodium salts **8a**–**n**. To obtain the dipivaloyloxymethyl (POM) esters (**9** and **10**), compounds **6g** and **6h** were treated with TMSBr/BSTFA and reprotected using POM chloride and triethylamine.[6] Removal of the benzyl group using either catalytic hydrogenation or BCl_3 gave POM-protected *N*-acyl analogs **11** and **12**.

A related synthetic pathway was used to prepare the phosphonate salts (**16a**–**r**) and esters (**15a**–**r** and **17**–**21**) of the *O*-linked series (Scheme 2). Compound **4** was treated with sodium hydride and acetylated *O*-benzylhydroxylamine[40,41] to give compound **13**. Hydrogenolysis removed the benzyl group, affording compound **14**.[10] Ether formation using sodium hydride and a series of alkyl/aryl halides gave the diethyl ester compounds **15a**–**m**. Suzuki coupling using the benzyl analog (**15a**), and a series of boronic acids gave ethers **15n**–**r**. Treatment with TMSBr and sodium hydroxide converted the diethyl esters to their sodium salts **16a**–**r**. Dipivaloyloxymethyl esters (**17**–**20**) were obtained by treating the acids of **16d**, **16h**, **16k**, and **16j**, respectively, with POM chloride and triethylamine. Alternate ester **21** was similarly obtained by treating **16h** with chloromethyl benzoate[42] and triethylamine.

Biological Evaluation. The target compounds were examined for biological activity in two ways. First, all phosphonic acids (**8a**–**n** and **16a**–**r**) were examined as inhibitors of Dxr from both Mtb and Yp at 100 μM (Figure 3A). This data yielded information about the intrinsic activity of each compound, as well as trends seen across compound classes and homologous enzymes (Figure 3B). Full inhibition curves were generated, and IC_{50} values were determined for compounds displaying >75% inhibition of the enzyme (Table 1). Second, the phosphonic acids (**8a**–**n** and **16a**–**r**) and lipophilic esters (**7a**–**n**, **11**, **12**, **15a**–**r**, and **17**–**21**) were evaluated for growth inhibition activity against *E. coli*, Yp, and Mtb. The Mtb MIC values are shown in Table 2.

Figure 3 shows the inhibition of Mtb and Yp Dxr by both series of compounds. The percent residual enzyme activity following treatment at 100 μM of each compound is shown in Figure 3A. Overall, across the two series, the inhibition activities generally paralleled each other. That is, compounds that displayed activity against one homologue were generally active against the other, and compounds that did not inhibit one homologue generally did not inhibit the other. For example, **8b**, the *n*-hexyl *N*-acyl analog, inhibited Dxr from both species, while diphenyl **8n** was

DOI: 10.1021/acsinfecdis.6b00125
ACS Infect. Dis. 2016, 2, 923–935

Table 1. Inhibition of Mtb and Yp Dxr by Selected *N*-Acyl and *O*-Linked MEPicides

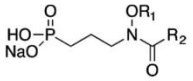

cmpd no.	R_1	R_2	Mtb Dxr IC_{50},[a] μM	Yp Dxr IC_{50},[a] μM
1 (Fos)	H	H	0.44	0.71
2 (FR)	H	CH_3	2.91	0.23
8b	H	hexyl	(43)	(27)
8e	H	Ph	(70)	4.45
8f	H	(4-CH_3)Ph	(74)	16.03
8h	H	$CH_2CH_2CH_2Ph$	17.8	(34)
16d	(4-ipr)Bn	CH_3	48.4	1.19
16e	$CH(CH_3)Ph$	CH_3	(38.1)	(19)
16g	CH_2CH_2(4-OH)Ph	CH_3	(59)	(22)
16i	CH_2-(1-naphthyl)	CH_3	(29)	22.35
16j	CH_2-(2-naphthyl)	CH_3	1.45	0.33
16k	CH_2-4-(1,1′-biphenyl)	CH_3	(36.8)	8.40
16r	CH_2-4-(4′-CF_3)-1,1′-biphenyl)	CH_3	(70)	(19)

[a]Values in parentheses are percent remaining enzyme activity at 100 μM.

ineffective against both enzymes. Similarly, in the *O*-linked series, **16d**, **16j**, and **16k** were potent inhibitors of both Dxr homologues, but **16b** and **16c** were not. This pattern of correlated activities was generally followed throughout the data set. Exceptions, however, did exist; *N*-acyl analogs **8e** and **8f**, the phenyl and toluyl analogs, respectively, were significantly more potent against Yp Dxr compared with the Mtb homologue. *O*-Linked compound **16g** showed the same trend.

Against Yp Dxr, the most active *N*-acyl analogs were **8b**, **8e**, **8f**, and **8h**, whereas the most active *O*-linked compounds were **16d**, **16e**, **16g**, **16i**, **16j**, **16k,** and **16r**. On the other hand, *N*-acyl analogs displaying the greatest inhibition of Mtb Dxr were **8a**, **8b**, and **8h**, although the level of inhibition was not as significant as that seen against Yp Dxr. *O*-Linked compounds displaying the greatest inhibition of Mtb Dxr were **16d**, **16e**, **16i**, **16j**, and **16k**.

Figure 3B is a comparative plot showing the overall ability of each chemical class to inhibit the enzymes. Activities of the *O*-linked compounds against the two enzymes were the best correlated (Pearson coefficient = 0.76). The activities of the *N*-acyl compounds were best correlated when **8e** and **8f** were left out (Pearson coefficient = 0.71).

Compounds showing at least 75% inhibition of enzyme activity were further evaluated to determine half-maximal inhibitory concentrations (IC_{50} values) (Table 1). The most potent compound was *O*-linked analog **16j**, with IC_{50} values of 1.45 and 0.33 μM against Mtb and Yp Dxr, respectively. Notably, against Yp Dxr, compound **16j** has an IC_{50} value approximately equal to half the enzyme concentration used in the assay (0.89 μM). This is comparable to the IC_{50} values of the tight-binding inhibitors fosmidomycin (**1**) and FR900098 (**2**); hence the IC_{50} could be even lower than the value reported. As seen for the primary screen (Figure 3), homologue inhibition across each series was roughly in parallel, with Yp Dxr generally being inhibited to a greater extent. Compounds **8e**, **16d**, **16i**, and **16k** show selectivity

Table 2. Antitubercular Activities of Saturated Acid and Ester MEPicides

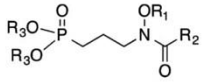

cmpd no.	R_1	R_2	R_3	*M. tuberculosis* MIC[a] (μg/mL)
INH	N/A	N/A	N/A	0.01
1 (Fos)	H	H	H/Na	>500
2 (FR900098)	H	CH_3	H/Na	>500
3	H	CH_3	$CH_2OCOtBu$	50−100 (62.5)
8e	H	Ph	H/Na	≥200
8h	H	$(CH_2)_3Ph$	H/Na	>200
7h	H	$(CH_2)_3Ph$	CH_2CH_3	200
12	H	$(CH_2)_3Ph$	$CH_2OCOtBu$	150
8d	H	$(CH_2)_2$cyclohexyl	H/Na	>200 (25)
7d	H	$(CH_2)_2$cyclohexyl	CH_2CH_3	>200 (37)
8l	H	CH_2O(4-Cl)Ph	H/Na	>200 (25)
16d	(4-ipr)Bn	CH_3	H/Na	200 (25)
17	(4-ipr)Bn	CH_3	$CH_2OCOtBu$	12.5 (6.25−12.5)
16k	CH_2−4-(1,1′-biphenyl)	CH_3	H/Na	25−50
15k	CH_2−4-(1,1′-biphenyl)	CH_3	CH_2CH_3	200 (100)
19	CH_2−4-(1,1′-biphenyl)	CH_3	$CH_2OCOtBu$	12.5 (3.13−6.25)
16p	CH_2−4-(4′-ipr)-1,1′-biphenyl	CH_3	H/Na	100 (6.25−12.5)
16h	$(CH_2)_4Ph$	CH_3	H/Na	≥200
15h	$(CH_2)_4Ph$	CH_3	CH_2CH_3	100−200
21	$(CH_2)_4Ph$	CH_3	CH_2OCOPh	25
18	$(CH_2)_4Ph$	CH_3	$CH_2OCOtBu$	12.5 (6.25−12.5)
16j	CH_2−(2-naphthyl)	CH_3	H/Na	≥200
15j	CH_2−(2-naphthyl)	CH_3	CH_2CH_3	200 (100)
20	CH_2−(2-naphthyl)	CH_3	$CH_2OCOtBu$	18.75 (4.7)

[a]Data using 7H9 media. When different, MIC in GAST-Fe media is given in parentheses.

DOI: 10.1021/acsinfecdis.6b00125
ACS Infect. Dis. 2016, 2, 923−935

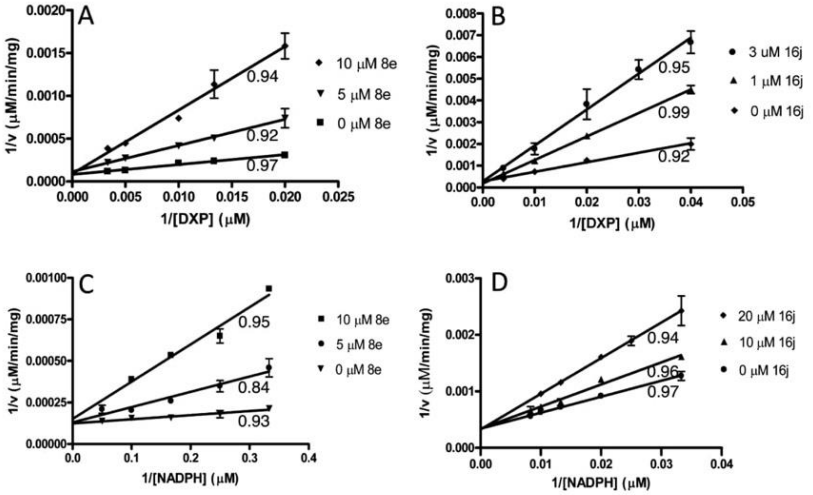

Figure 4. Lineweaver–Burk analysis. Shown against Yp Dxr, compound **8e** is competitive with respect to both DXP (A) and NADPH (C), as is compound **16j** (panels B and D, respectively) shown against Mtb Dxr. Each assay was performed in duplicate. Data was fit by linear regression, and R^2 values are indicated.

between homologues and are more potent against Yp Dxr. None of the analogs showed preferential specificity toward Mtb Dxr.

To determine whether the *N*-acyl and *O*-linked compounds act as bisubstrate inhibitors, we evaluated representative compounds **8e** and **16j** for binding modality. Using classical Lineweaver–Burk double reciprocal plots to determine inhibitor modality, both *N*-acyl compound **8e** and *O*-linked compound **16j** appear competitive with both NADPH and DXP (Figure 4), indicating bisubstrate binding behavior. Our prior work showed that *N*-acyl compound **8h** binds competitively with DXP but noncompetitively with NADPH.[8] Comparing these results leads us to believe that flexibility of the *N*-acyl/*O*-linked substituent influences the exact binding modality of the inhibitor to Dxr. In other words, the longer/more flexible phenpropyl substituent of **8h** may adopt an alternate binding pattern compared with the smaller CH_2-2-naphthyl (**16j**) and phenyl (**8e**) substituents, which are more constrained. By plotting the apparent K_m versus inhibitor concentration, the K_i values are calculated for **8e** with Yp Dxr as 1.8 μM with respect to NADPH and 7.9 μM relative to DXP. The calculated K_i values for **16j** with Mtb Dxr are 17.8 μM relative to NADPH and 1.0 μM with respect to DXP. Notably, these values resemble the relative differences in apparent Michaelis constants (K_m^{app}) between the homologous enzymes (Yp Dxr $K_m^{app,NADPH}$ = 12.7 μM, $K_m^{app,Dxp}$ = 221.5 μM; Mtb Dxr $K_m^{app,NADPH}$ = 29.7 μM, $K_m^{app,Dxp}$ = 47 μM),[9] suggesting that the enhanced potency of the inhibitors toward the Yp Dxr predominantly reflects an enhanced ability of the inhibitor to associate with its NADPH binding site.

The most potent inhibitors of Dxr were selected for evaluation in growth inhibition assays against Yp, Mtb, and *E. coli*. While compound **2** potently inhibits bacterial propagation in a dose-dependent manner, none of the newly synthesized MEPicide inhibitors demonstrated appreciable activity against Yp or *E. coli* MG1655 (data not shown). Interestingly, deletion of an outer membrane protein involved in the efflux of protein toxins and antibiotics (tolC)[43] in *E. coli* dramatically improved the antibacterial activities of *N*-acyl analog **15k** (IC_{50}(WT) = 169.7 μg/mL; IC_{50}(tolC) = 35.9 μg/mL) and *O*-linked compound **7l** (IC_{50}(WT) = 213.6 μg/mL; IC_{50}(tolC) = 54.6 μg/mL), leading to the likelihood that low MEPicide activity against *E. coli* (and other organisms) is due at least in part to efflux.

As a class, the MEPicides were more active against Mtb. The antitubercular activities are shown in Table 2. Two media were used to measure the minimum inhibitory concentration (MIC) values against *M. tuberculosis* H37Rv. Middlebrook 7H9 is a nutrient-rich media, while GAST-Fe is a minimal, low iron media. The low protein content in GAST-Fe helps evaluate lipophilic compounds that may suffer from high protein binding. The MIC values obtained from the *N*-acyl series are poor and likely reflect the low potency of the compounds against Mtb Dxr (Table 2). Better antitubercular MIC values were obtained using the *O*-linked series. Perhaps unsurprisingly, the most potent MIC values were obtained from the dipivaloyloxymethyl (POM) esters of compounds that displayed the highest level of enzyme inhibition. For example, **16k**, **16d**, and **16j** yielded the best IC_{50} values in the series. POM esters of these compounds (**17**–**20**) yielded MIC values of 12.5–18.75 μg/mL in 7H9 media and 3.13–12.5 μg/mL in GAST-Fe media. Similarly, methyl benzoate **21**, ester of **16h**, yielded an MIC of 25 μg/mL in 7H9. The lipophilic character of the esters likely facilitates penetration across the mycobacterial cell wall.

■ CONCLUSION

We present here two series of compounds designed to further explore inhibition of Dxr. Extended *N*-acyl and *O*-linked analogs of FR900098 inhibited the enzyme. While most compounds were moderate inhibitors, some analogs inhibited Dxr to the same extent as FR900098. These results agree with *N*-acyl analogs previously reported.[34] Of particular interest, however, is the inhibitory activity of the *O*-linked compounds, since these represent a new mode of binding to the enzyme, one that does not rely on an anionic interaction with the metal cation.

DOI: 10.1021/acsinfecdis.6b00125
ACS Infect. Dis. 2016, 2, 923–935

Catalysis by Dxr undergoes an ordered bi−bi reaction mechanism, wherein NADPH binds to the enzyme before DXP binds.[44] This mechanism is reflective of a conformational change that occurs in the protein upon NADPH binding, resulting in the formation of the DXP binding site. Compounds **1** and **2** are competitive inhibitors with respect to DXP and uncompetitive relative to NADPH.[8,44] That is, NADPH must bind to Dxr before either of these inhibitors can occupy the DXP binding site. Since we rationally designed the bisubstrate inhibitors to occupy both the DXP and NADPH binding sites, compounds **8e** and **16j** were further examined in terms of their mechanism-of-inhibition. *N*-Acyl compound **8e** and *O*-linked compound **16j** were both found to be competitive with respect to NADPH and DXP, suggesting both binding sites were blocked upon inhibitor binding. Hence, both inhibitors appear to function via a "flip-and-lock" mechanism. That is, a portion of the inhibitor binds to the NADPH site, causing a Dxr conformational change ("flip"), and then a second portion of the compound binds to the DXP binding site, holding the enzyme in an inhibited state ("lock"). Flexibility of the substituent (*N*-acyl or *O*-linked) appears to be highly influential in determining the specific binding mode at the enzyme. We are seeking protein crystal structures with the bound inhibitors, the results of which will further our mechanistic understanding of how these compounds inhibit the enzyme.

Overall, compounds tend to show greater inhibition of Yp Dxr compared with the Mtb homologue. It is not clear why this occurs but may reflect increased flexibility of the Yp Dxr active site and neighboring residues compared with those in the Mtb enzyme. In previous work, it was noted that Yp Dxr shows striking similarity in terms of sequence and proposed structure to *E. coli* Dxr,[9] which is known to have considerable conformational flexibility, especially in the loop region of residues 186−216.[45] This loop closes down in the active conformation to form part of the active site. As shown in Figure 5, while this loop region

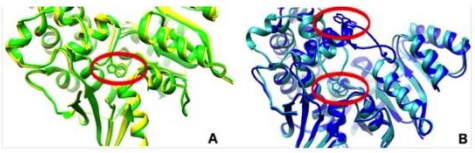

Figure 5. Dxr active site variation. (A) The Mtb Dxr apoenzyme (PDB 2JD2, yellow) is structurally similar in the active site loop region to the catalytically active conformation of the enzyme (PDB 4AIC, green), as followed by Trp203 (circled). (B) In contrast, the Ec Dxr active site conformation (PDB 2EGH, teal) has a dramatically different topology in the loop region relative to the apoenzyme (PDB 1KSH chain A, blue), as followed by Trp212 (circled).

(as followed using loop residue Trp203) is relatively stable in Mtb between an apo and active conformation,[46] it moves quite dramatically in *E. coli*. Due to this movement, we speculate that the Yp Dxr can accommodate a larger variety of structures compared with the relatively static Mtb homologue.

In contrast to the natural products fosmidomycin (**1**) and FR900098 (**2**), several of our synthesized MEPicides demonstrate significant growth inhibition of *M. tuberculosis*. Particularly due to the increased lipophilicity with loss of the retrohydroxamate, the antitubercular activity of the *O*-linked compounds is especially interesting. Our prior work indicated that using a POM ester to mask the phosphonate improved penetration across the Mtb cell wall.[6] The improved MIC values of POM esters **17**−**20** further corroborate this view. It is also noteworthy that the improvement in MIC parallels an increase in enzyme potency; the most striking example of this is found in the *O*-linked series with compounds **16k**/**19** and **16j**/**20**. Further exploration into the SAR of the *O*-linked MEPicides will lead to a deeper understanding of Dxr inhibition and support the development of novel antimicrobial drugs.

METHODS

Synthesis. All reagents were purchased from commercial suppliers and used without further purification. THF and dichloromethane were distilled under argon immediately before use from sodium/benzophenone and calcium hydride, respectively. All air sensitive reactions were carried out under a nitrogen atmosphere. ^{1}H and ^{13}C NMR spectra were recorded in acetone-d_6, $CDCl_3$, or D_2O on an Agilent spectrometer at 200 or 400 MHz (^{1}H) and 50 or 100 MHz (^{13}C). Chemical shifts are given in parts per million (ppm, δ) relative to the internal standard (TMS) or residual solvent peak. Spin multiplicities are given with the following abbreviations: s (singlet), bs (broad singlet), d (doublet), t (triplet), q (quadruplet), quin/qt (quintet), sex (sextet), and m (multiplet). Coupling constants *J* are given in hertz. Mass spectra were obtained in the ESI mode on an LC-MSD Agilent 1100 (HyperSil Gold aQ). High-resolution mass spectroscopy spectra (HRMS) were recorded in negative ESI mode on a JEOL HX110/HX100 four sector tandem mass spectrometer (UMBC Mass Spectrometry Facility) or on a VG Analytical VG70SE double focusing magnetic sector mass spectrometer (JHU Mass Spectrometry Facility). Thin layer chromatography (TLC) was performed on Merck 60 F254 silica gel plates. Automated flash column chromatography was carried out using a Biotage Isolera chromatography system and Merck silica gel 60 (35−70 μm). Purity of compounds (>95%) was determined by ^{1}H/^{13}C NMR, LC-DAD-MS, and HRMS.

General Method for Preparation of Compounds 8a−n. *N*,*O*-Bis(trimethylsilyl)trifluoroacetamide (3 equiv) was added under nitrogen to **7a**−**n** (1 equiv) in CH_2Cl_2 and stirred at room temperature for 20 min. The reaction mixture was cooled to 0 °C and bromotrimethylsilane (10 equiv) was added dropwise to the reaction. The reaction was warmed to room temperature and stirred overnight under nitrogen. Ethyl bromide and excess silylating agent were removed under reduced pressure, and the residue was dissolved in aqueous NaOH (1 equiv) and stirred for a second night. The reaction mixture was partitioned between H_2O and CH_2Cl_2 to remove any residual impurities or organics. The aqueous fractions were combined, and the solvent was removed by lyophilization to give the desired compound in 75−100% yields.

*Sodium Hydrogen-3-(N-hydroxypentanamido)propyl Phosphonate (**8a**).* ^{1}H NMR (200 MHz, acetone-d_6/D_2O) δ (ppm): 0.95 (t, *J* = 7.4 Hz, 3H), 1.39 (sex, *J* = 13.8, 7.1 Hz, 2H), 1.61 (quin, *J* = 8.3, 7.8 Hz, 4H), 1.77−2.07 (m, 2H), 2.55 (t, *J* = 7.7 Hz, 2H), 3.62−3.72 (m, 2H). ^{13}C NMR (50 MHz, acetone-d_6/D_2O) δ (ppm): 13.52, 21.09, 22.30, 24.11, 27.02, 32.01, 49.00 (d, *J* = 18.8 Hz), 176.33, 214.78. LCMS (ESI) *m*/*z* 240.1 [M + H]. HRMS (ESI) *m*/*z* calcd for $C_8H_{17}NO_5P$ (M − Na): 238.0838. Found: 238.0833.

*Sodium Hydrogen-3-(N-hydroxyheptanamido)propyl Phosphonate (**8b**).* ^{1}H NMR (200 MHz, acetone-d_6/D_2O) δ (ppm): 1.25 (t, *J* = 6.2 Hz, 3H), 1.58−1.82 (m, 6H), 1.82−2.08 (m, 4H), 2.12−2.39 (m, 2H), 2.86 (t, *J* = 7.6 Hz, 2H), 4.04 (t, *J* = 6.7 Hz, 2H). ^{13}C NMR (50 MHz, acetone-d_6/D_2O) δ (ppm): 13.86, 21.26, 22.46, 24.24, 24.85, 26.91, 31.47, 32.39,

DOI: 10.1021/acsinfecdis.6b00125
ACS Infect. Dis. 2016, 2, 923−935

49.03 (d, J = 20.4 Hz), 175.82, 213.84. LCMS (ESI) m/z 268.0 [M + H]. HRMS (ESI) m/z calcd for $C_{10}H_{21}NO_5P$ (M − Na): 266.1151. Found: 266.1147.

*Sodium Hydrogen-3-(N-hydroxypivalamido)propyl Phosphonate (**8c**).* ^{1}H NMR (200 MHz, acetone-d_6/D_2O) δ (ppm): (80/20 mixture of two conformers) 1.12−1.34 (m, 9H), 1.42−1.67 (m, 2H), 1.73−1.95 (m, 2H), 3.10 (t, J = 6.8 Hz, 20/100 of 2H), 3.68 (t, J = 6.8 Hz, 80/100 of 2H). ^{13}C NMR (50 MHz, acetone-d_6/D_2O) δ (ppm): 23.98, 26.62 (d, J = 8.4 Hz), 39.07, 50.90 (d, J = 18.7 Hz), 180.66 (d, J = 14.8 Hz). LCMS (ESI) m/z 240.1 [M + H]. HRMS (ESI) m/z calcd for $C_8H_{17}NO_5P$ (M − Na): 238.0838. Found: 238.0833.

*Sodium Hydrogen-3-(3-cyclohexyl-N-hydroxypropanamido)propyl Phosphonate (**8d**).* ^{1}H NMR (400 MHz, D_2O) δ (ppm): (80/20 mixture of two conformers) 0.91 (q, J = 13.6, 12.9 Hz, 2H), 1.10−1.29 (m, 4H), 1.49 (q, J = 7.0 Hz, 2H), 1.62−1.77 (m, 5H), 1.81−1.95 (m, 2H), 2.54 (t, J = 8.0 Hz, 2H), 3.39 (t, J = 6.0 Hz, 20/100 of 2H), 3.70 (t, J = 6.8 Hz, 80/100 of 2H). ^{13}C NMR (101 MHz, D_2O) δ (ppm): 19.95, 25.78, 26.10, 29.44, 31.97, 32.49, 36.85, 48.30, 162.54. LCMS (ESI) m/z 294.1 [M + H]. HRMS (ESI) m/z calcd for $C_{12}H_{23}NO_5P$ (M − Na): 292.1308. Found: 292.1303.

*Sodium Hydrogen-3-(N-hydroxybenzamido)propyl Phosphonate (**8e**).* ^{1}H NMR (200 MHz, deuterium oxide/acetone-d_6) δ (ppm): 1.44−1.87 (m, 2H), 1.87−2.15 (m, 2H), 3.59−3.99 (m, 2H), 7.55 (s, 4H). ^{13}C NMR (50 MHz, D_2O/acetone-d_6) δ (ppm): 20.74, 23.16, 25.92, 50.56, 127.51, 128.89, 131.14, 133.83, 171.84. LCMS (ESI) m/z 259.9 [M + H]. HRMS (ESI) m/z calcd for $C_{10}H_{13}NO_5P$ (M − Na): 258.0525. Found: 258.0520.

*Sodium Hydrogen-3-(N-hydroxy-4-methylbenzamido)-propyl Phosphonate (**8f**).* ^{1}H NMR ($CDCl_3$, 200 MHz), δ (ppm): 1.37−1.73 (m, 2H), 1.79−2.06 (m, 2H), 2.37 (s, 3H), 3.55−3.86 (m, 2H), 7.25−7.54 (m, 4H$_{arom}$). ^{13}C NMR (50 MHz, D_2O) δ (ppm): 20.93 (d, J = 16.7 Hz), 23.64, 26.34, 53.60, 127.51, 129.31, 130.63, 141.89, 171.60. LCMS (ESI) m/z 274.0 [M + H]. HRMS (ESI) m/z calcd for $C_{11}H_{15}NO_5P$ (M − Na): 272.0682. Found: 272.0684.

*Sodium Hydrogen-3-(N-hydroxy-3-phenylpropanamido)-propyl Phosphonate (**8g**).* ^{1}H NMR (200 MHz, D_2O) δ (ppm): 1.39−2.09 (m, 4H), 2.76−2.98 (m, 4H), 3.62 (t, J = 6.7 Hz, 2H), 7.19−7.41 (m, 5H). ^{13}C NMR (101 MHz, D_2O) δ (ppm): 20.19 (d, J = 3.8 Hz), 25.04, 30.31, 33.24, 48.52 (d, J = 19.2 Hz), 126.36, 128.36 (d, J = 7.5 Hz), 128.65, 140.88, 175.22. LCMS (ESI) m/z 288.1 [M + H]. HRMS (ESI) m/z calcd for $C_{12}H_{18}NNaO_5P$ (M + H): 310.0814. Found: 310.0813.

*Sodium Hydrogen-3-(N-hydroxy-4-phenylbutanamido)-propyl Phosphonate (**8h**).* ^{1}H NMR (200 MHz, D_2O) δ (ppm): (58:42 mixture of two conformers) 1.42−2.06 (m, 6H), 2.34 (t, 42/100 of 2H, J = 7.4 Hz), 2.48 (t, 58/100 of 2H, J = 7.4 Hz), 2.64 (t, 2H, J = 7.5 Hz), 3.34 (t, 42/100 of 2H, J = 7.3 Hz), 3.62 (t, 58/100 of 2H, J = 6.7 Hz), 7.18−7.42 (m, 5H). ^{13}C NMR (50 MHz, D_2O) δ (ppm): 21.0, 25.1 (d, J = 134.4 Hz), 26.7, 31.9, 35.2, 49.2 (d, J = 19.0 Hz), 126.8, 129.3, 142.8, 176.8. LCMS (ESI) m/z 302.0 [M + H]. HRMS (ESI) m/z calcd for $C_{13}H_{20}NNaO_5P$ (M + H): 324.0971. Found: 324.0970.

*Sodium Hydrogen-3-(N-hydroxy-3-(4-methoxyphenyl)-propanamido)propyl Phosphonate (**8i**).* ^{1}H NMR (200 MHz, D_2O/acetone-d_6) δ (ppm): 1.67−1.92 (m, 2H), 1.91−2.16 (m, 2H), 2.80−2.91 (m, 2H), 2.91−3.02 (m, 2H), 3.79 (t, J = 6.6 Hz, 2H), 3.88 (s, 3H), 6.98 (d, J = 8.7 Hz, 2H), 7.29 (d, J = 8.7 Hz, 2H). ^{13}C NMR (50 MHz, D_2O/acetone-d_6) δ (ppm): 20.34, 34.26, 48.68 (d, J = 17.9 Hz), 55.42 (d, J = 3.8 Hz), 114.27, 129.77, 133.79, 157.82, 174.83. LCMS (ESI) m/z 318.0 [M + H]. HRMS (ESI) m/z calcd for $C_{13}H_{19}NO_5P$ (M − Na): 316.0944. Found: 316.0946.

*Sodium Hydrogen-3-(N-hydroxy-3-(3-(trifluoromethyl)-phenyl)acrylamido)propyl Phosphonate (**8j**).* ^{1}H NMR (400 MHz, D_2O) δ (ppm): (80:20 mixture of two conformers) 1.60−1.65 (m, 2H), 1.87−1.92 (m, 2H), 1.09−3.19 (m, 20/100 of 2H), 3.76−3.81 (m, 80/100 of 2H), 7.33−7.38 (m, 1H), 7.57−7.63 (m, 2H), 7.70−7.75 (m, 1H), 7.83−7.88 (m, 1H), 7.95−8.00 (m, 1H). ^{13}C NMR (101 MHz, D_2O) δ (ppm): 16.28, 25.77, 45.69, 110.81, 117.62, 124.57, 126.44, 129.53, 131.56, 141.83, 144.93, 152.92, 163.34. LCMS (ESI) m/z 354.0 [M + H]. HRMS (ESI) m/z calcd for $C_{13}H_{14}F_3NO_5P$ (M − Na): 352.0556. Found: 352.0558.

*Sodium (E)-Hydrogen-3-(N-hydroxy-3-(4-nitrophenyl)-acrylamido)propyl Phosphonate (**8k**).* ^{1}H NMR (400 MHz, acetone-d_6/D_2O) δ (ppm): 1.73−1.91 (m, 2H), 1.96−2.27 (m, 2H), 3.85−4.10 (m, 2H), 7.58 (d, J = 16.1 Hz, 1H), 7.78 (d, J = 15.1 Hz, 1H), 7.98 (d, J = 6.3 Hz, 2H), 8.42 (d, J = 7.5 Hz, 2H). ^{13}C NMR (101 MHz, acetone-d_6/D_2O) δ (ppm): 20.63, 49.45, 120.35, 124.39, 129.22, 140.85, 148.19, 167.40. HRMS (ESI) m/z calcd for $C_{12}H_{14}N_2O_7P$ (M − Na): 329.0533. Found: 329.0532.

*Sodium Hydrogen-3-(2-(4-chlorophenoxy)-N-hydroxyacetamido)propyl Phosphonate (**8l**).* ^{1}H NMR (400 MHz, acetone-d_6/D2O) δ (ppm): (80:20 mixture of two conformers) 1.65−1.89 (m, 2H), 1.89−2.10 (m, 2H), 3.42 (t, J = 7.6 Hz, 20/100 of 2H), 3.77 (t, J = 6.8 Hz, 80/100 of 2H), 5.02 (s, 2H), 7.02 (d, J = 9.0 Hz, 2H), 7.36 (d, J = 9.4 Hz, 2H). ^{13}C NMR (101 MHz, D_2O/acetone-d_6) δ (ppm): 20.44, 23.31, 26.02, 49.01 (d, J = 21.1 Hz), 65.33, 116.60, 125.92, 129.66, 157.11, 169.68. LCMS (ESI) m/z 324.0 [M + H]. HRMS (ESI) m/z calcd for $C_{11}H_{14}ClNO_6P$ (M − Na): 322.0241. Found: 322.0244.

*Sodium Hydrogen-3-(N-hydroxybiphenyl-4-ylcarboxamido)propyl Phosphonate (**8m**).* ^{1}H NMR (200 MHz, CD_3OD) δ (ppm): 1.64−1.86 (m, 2H), 1.91−2.16 (m, 2H), 3.83 (t, J = 6.0 Hz, 2H), 7.28−7.51 (m, 3H), 7.60−7.78 (m, 6H). ^{13}C NMR (50 MHz, CD_3OD) δ (ppm): 21.89, 27.10, 127.52, 128.07, 128.93, 129.97, 134.52, 141.44, 144.56, 171.48. Peak at 50 ppm is masked by solvent. LCMS (ESI) m/z 336.0 [M + H]. HRMS (ESI) m/z calcd for $C_{16}H_{17}NO_5P$ (M − Na): 334.0838. Found: 334.0840.

*Sodium Hydrogen-3-(1-hydroxy-3,3-diphenylureido)-propyl Phosphonate (**8n**).* ^{1}H NMR (200 MHz, acetone-d_6/D_2O) δ (ppm): 1.92−2.15 (m, 2H), 2.17−2.39 (m, 2H), 3.99 (t, J = 6.1 Hz, 3H), 7.57 (dd, J = 17.7, 7.9 Hz, 6H), 7.77 (t, J = 7.5 Hz, 4H). ^{13}C NMR (50 MHz, acetone-d_6/D_2O) δ (ppm): 24.13, 26.83, 52.36 (d, J = 18.1 Hz), 125.72, 126.38, 129.60, 145.39, 161.44. LCMS (ESI) m/z 351.0 [M + H]. HRMS (ESI) m/z calcd for $C_{16}H_{18}N_2O_5P$ (M − Na): 349.0947. Found: 359.0951.

General Procedure for the Deprotection of *N*-Acyl and *O*-Linked Ligands To Give 8a−n and 16a−r. To a solution of **7a−n** or **15a−r** (1 equiv) in CH_2Cl_2 (1.7 mL/mmol of phosphonate) at 0 °C was added dropwise bromotrimethylsilane (8 equiv). The reaction mixture was stirred overnight at room temperature. Ethyl bromide and excess silylating agent were removed by rotary evaporation at room temperature. The concentrate was solubilized in dry CH_2Cl_2 and evaporated again (×2). Then H_2O was added to the residue, and the mixture was stirred overnight at room temperature. The solution was filtered over cotton to remove the yellow oil (except for products with a low solubility in water) and concentrated *in vacuo* at 50 °C. The crude acid was rapidly neutralized with aqueous NaOH, and

DOI: 10.1021/acsinfecdis.6b00125
ACS Infect. Dis. 2016, 2, 923−935

the mixture was stirred overnight at room temperature. The reaction mixture was concentrated *in vacuo* at 50 °C to give the products as light yellow or white solids in 61% to quantitative yields.

*Sodium Hydrogen-3-(N-(4-bromobenzyloxy)acetamido)-propyl Phosphonate (**16a**).* ^{1}H NMR (200 MHz, D_2O) δ (ppm): δ 1.55−1.97 (m, 4H), 2.09 (s, 3H), 3.65−3.85 (m, 2H), 4.95 (s, 2H), 7.36−7.47 (m, 2H), 7.59−7.71 (m, 2H). ^{13}C NMR (D_2O) δ (ppm): 19.7, 20.9, 23.6, 26.3, 50.5, 75.5, 123.2, 131.4, 131.9, 132.1, 132.3, 133.1, 174.8. HRMS (ESI) m/z calculated for $C_{12}H_{17}BrNO_5P$ [$(M - Na + H)^+$], 366.0106; found, 366.0110.

*Sodium Hydrogen-3-(N-((4-(trifluoromethoxy)benzyl)oxy)-acetamido)propyl Phosphonate (**16b**).* ^{1}H NMR (200 MHz, D_2O) δ (ppm): 1.54−1.73 (m, 2H), 1.78−2.02 (m, 2H), 2.08 (s, 3H), 3.78 (bs, 2H), 5.00 (s, 2H), 7.38 (d, J = 7.8 Hz, 2H), 7.58 (d, J = 8.6 Hz, 2H). ^{13}C NMR (50 MHz, D_2O) δ (ppm): 19.6, 21.0, 23.7, 26.4, 45.7, 46.1, 75.2, 113.0, 121.4, 123.0, 127.7, 131.7, 132.9, 149.7, 174.6. HRMS (ESI) m/z calculated for $C_{13}H_{17}F_3NNaO_6P$ [$(M + Na)^+$], 394.0643; found, 394.0702.

*Sodium Hydrogen-3-(N-((3,4-dichlorobenzyl)oxy)-acetamido)propyl Phosphonate (**16c**).* ^{1}H NMR (200 MHz, D_2O) δ (ppm): 1.43−1.72 (m, 2H), 1.72−2.01 (m, 2H), 2.09 (s, 3H), 3.74 (t, J = 6 Hz, 2H), 4.90 (s, 2H), 7.33−7.43 (m, 1H), 7.48−7.66 (m, 2H). ^{13}C NMR (50 MHz, D_2O) δ (ppm): 19.7, 21.2, 24.0, 26.6, 45.9, 46.2, 74.7, 129.5, 131.0, 131.6, 132.8, 134.5, 137.6, 174.6. LCMS (ESI^+): m/z = 356.0 [$M + H]^+$, 378.0 [$M + Na]^+$. HRMS (ESI) m/z calculated for $C_{12}H_{16}Cl_2NNaO_5P$ [$(M + Na)^+$], 378.0041; found, 378.0045.

*Sodium Hydrogen-3-(N-((4-isopropylbenzyl)oxy)-acetamido)propyl Phosphonate (**16d**).* ^{1}H NMR (200 MHz, D_2O) δ (ppm): 1.21 (d, 6H, J = 6.9 Hz, CH_3-CH × 2), 1.36−1.62 (m, 2H, CH_2-P), 1.72−1.97 (m, 2H, CH_2-CH_2P), 2.04 (s, 3H, CH_3-CO), 2.85−3.09 (m, 1H, C*H*-Ar), 3.57−3.83 (m, 2H, CH_2-N), 4.92 (s, 2H, CH_2−O-N), 7.36 (d, 2H, J = 8.2 Hz, H_{ar}), 7.43 (d, 2H, J = 8.2 Hz, H_{ar}). ^{13}C NMR (50 MHz, $CDCl_3$) δ (ppm): 16.4, 16.5, 20.3, 20.4, 20.6, 21.6, 24.4, 45.6, 46.1, 61.6, 61.7, 75.4, 117.9, 121.2, 123.0, 130.6, 133.2, 149.6, 172.4. LCMS (ESI^+): m/z = 330.2 [$M + H]^+$. HRMS (ESI) m/z calculated for $C_{15}H_{24}NNaO_5P$ [$(M + Na)^+$], 352.1290; found, 352.1285.

*Sodium Hydrogen-3-(N-(1-phenylethoxy)acetamido)-propyl Phosphonate (**16e**).* ^{1}H NMR (200 MHz, D_2O) δ (ppm): 1.59 (d, 3H, J = 6.4 Hz, CH_3-CH), 1.40−1.88 (m, 4H, CH_2-P and CH_2-CH_2P), 1.96 (s, 3H, CH_3-CO), 3.24−3.48 (m, 1H, CH_2-N), 3.55−3.81 (m, 1H, CH_2-N), 5.14 (q, 1H, J = 6.5 Hz, C*H*-O), 7.40−7.58 (m, 5H, H_{ar}). ^{13}C NMR (50 MHz, D_2O) δ (ppm): 19.0, 19.5, 20.4, 23.3, 26.0, 46.3, 46.6, 82.7, 128.0, 129.0, 129.5, 139.3, 175.4. LCMS (ESI^+): m/z = 302.1 [$M + H]^+$. HRMS (ESI) m/z calculated for $C_{13}H_{20}NNaO_5P$ [$(M + Na)^+$], 324.0977; found, 324.1225.

*Sodium Hydrogen-3-(N-(4-methoxyphenethoxy)-acetamido)propyl Phosphonate (**16f**).* ^{1}H NMR (200 MHz, D_2O) δ (ppm): 1.26−1.49 (m, 2H, CH_2-P), 1.64−1.86 (m, 2H, CH_2-CH_2P), 1.91 (s, 3H, CH_3-CO), 2.94 (t, 2H, J = 6.0 Hz, CH_2-Ar), 3.60 (t, 2H, J = 6.8 Hz, CH_2-N), 3.82 (s, 3H, CH_3-O), 4.20 (t, 2H, J = 6.0 Hz, CH_2−O-N), 6.98 (d, 2H, J = 8.6 Hz, H_{ar}), 7.30 (d, 2H, J = 8.6 Hz, H_{ar}). ^{13}C NMR (50 MHz, D_2O) δ (ppm): 19.2, 21.8, 24.8, 27.4, 33.0, 45.8, 46.2, 55.7, 75.3, 114.4, 130.4, 131.1, 157.7, 174.2. LCMS (ESI^+): m/z = 332.1 [$M + H]^+$. HRMS (ESI) m/z calculated for $C_{14}H_{22}NNaO_6P$ [$(M + Na)^+$], 354.1082; found, 354.1215.

*Sodium Hydrogen-3-(N-(4-hydroxyphenethoxy)-acetamido)propyl Phosphonate (**16g**).* ^{1}H NMR (200 MHz, D_2O) δ (ppm): 1.38−1.77 (m, 4H), 1.93 (s, 3H), 2.85 (t, J = 6.4, 6.2 Hz, 2H), 3.54 (t, J = 7, 6.2 Hz, 2H), 4.11 (t, J = 6.4, 5.8 Hz, 2H), 6.82−6.86 (m, 2H), 7.16−7.20 (m, 2H). ^{13}C NMR (50 MHz, D_2O) δ (ppm): 19.2, 20.8, 23.6, 26.3, 33.1, 45.4, 45.8, 75.3, 115.6, 130.4, 154.2, 174.2. LCMS (ESI^+): m/z = 318.1 [$M + H]^+$, 635.1 [$2M + H]^+$. HRMS (ESI) m/z calculated for $C_{13}H_{20}NNaO_6P$ [$(M + Na)^+$], 340.0926; found, 340.0978.

*Sodium Hydrogen-3-(N-(4-phenylbutoxy)acetamido)-propyl Phosphonate (**16h**).* ^{1}H NMR (200 MHz, D_2O) δ (ppm): 1.49-2.01 (m, 8H, CH_2-P and CH_2-CH_2P and CH_2-CH_2O and CH_2-CH_2Ph), 2.15 (s, 3H, CH_3-CO), 2.68 (t, 2H, J = 6.5 Hz, CH_2-Ph), 3.70 (t, 2H, J = 7.0 Hz, CH_2-N), 3.89−4.04 (m, 2H, CH_2-O-N), 7.24−7.53 (m, 5H, H_{ar}). ^{13}C NMR (50 MHz, D_2O) δ (ppm): 19.6, 20.8, 23.1, 25.8, 27.3, 27.5, 35.3, 45.6, 45.9, 74.2, 125.9, 128.6, 128.7, 142.5, 173.4. LCMS (ESI^+): m/z = 330.2 [$M + H]^+$. HRMS (ESI) m/z calculated for $C_{15}H_{24}NNaO_5P$ [$(M + Na)^+$], 352.1290; found, 352.1441.

*Sodium Hydrogen-3-(N-(naphthalen-1-ylmethoxy)-acetamido)propyl Phosphonate (**16i**).* ^{1}H NMR (400 MHz, D_2O) δ (ppm): 1.56 (bs, 2H), 1.89−2.18 (m, 5H), 3.83 (bs, 2H), 5.51 (s, 2H), 7.59−7.77 (m, 4H), 8.06−8.09 (m, 2H), 8.28−8.41 (m, 1H). ^{13}C NMR (100 MHz, D_2O) δ (ppm): 19.3, 21.0, 24.5, 25.8, 45.9, 46.0, 73.8, 123.3, 125.6, 126.4, 127.2, 128.7, 129.7, 130.2, 131.6, 133.4, 173.4. HRMS (ESI) m/z calculated for $C_{16}H_{20}NNaO_5P$ [$(M + Na)^+$], 360.0977; found, 360.0978.

*Sodium Hydrogen-3-(N-(naphthalen-2-ylmethoxy)-acetamido)propyl Phosphonate (**16j**).* ^{1}H NMR (200 MHz, D_2O) δ (ppm): 1.23−1.51 (m, 2H, CH_2-P), 1.68−1.93 (m, 2H, CH_2-CH_2P), 2.01 (s, 3H, CH_3-CO), 3.73 (t, 2H, J = 6.6 Hz, CH_2-N), 5.03 (s, 2H, CH_2-O-N), 7.48−7.65 (m, 3H, H_{ar}), 7.84−8.02 (m, 4H, H_{ar}). ^{13}C NMR (100 MHz, D_2O) δ (ppm): 19.4, 20.7, 24.2, 25.5, 45.6, 45.7, 76.1, 126.7, 127.0, 127.2, 127.7, 128.0, 128.6, 129.4, 132.8, 133.2, 134.1, 174.5. LCMS (ESI^+): m/z = 338.1 [$M + H]^+$. HRMS (ESI) m/z calculated for $C_{16}H_{20}NNaO_5P$ [$(M + Na)^+$], 360.0977; found, 360.0984.

*Sodium Hydrogen-3-(N-([1,1′-biphenyl]-4-ylmethoxy)-acetamido)propyl Phosphonate (**16k**).* ^{1}H NMR (200 MHz, DMSO) δ (ppm): 1.29−1.60 (m, 2H), 1.60−1.89 (m, 2H), 2.03 (s, 3H), 3.66 (bs, 2H), 4.90 (s, 2H), 7.25−7.88 (m, 9H). ^{13}C NMR (50 MHz, DMSO) δ (ppm): 20.4, 21.0, 26.4, 29.0, 45.0, 45.5, 74.9, 126.7, 127.6, 128.9, 130.0, 134.0, 139.6, 140.4, 170.9. LCMS (ESI^+): m/z = 364.1 [$M + H]^+$. HRMS (ESI) m/z calculated for $C_{18}H_{22}NNaO_5P$ [$(M + Na)^+$], 386.1133; found, 386.1088.

*Sodium Hydrogen-3-(N-([1,1′-biphenyl]-3-ylmethoxy)-acetamido)propyl Phosphonate (**16l**).* ^{1}H NMR (200 MHz, D_2O) δ (ppm): 1.15−2.03 (m, 7H), 3.43 (bs, 2H), 4.29 (s, 2H), 6.46−7.34 (m, 9H). ^{13}C NMR (50 MHz, D_2O) δ (ppm): 20.0, 21.7, 24.3, 27.0, 46.4, 46.7, 76.1, 127.4, 127.9, 129.0, 129.3, 129.8, 134.7, 135.4, 140.3, 160.6, 141.0, 173.9. LCMS (ESI^+): m/z = 364.1 [$M + H]^+$, 727.2 [$2M + H]^+$. HRMS (ESI) m/z calculated for $C_{18}H_{22}NNaO_5P$ [$(M + Na)^+$], 386.1133; found, 386.1103.

*Sodium Hydrogen-3-(N-([1,1′-biphenyl]-2-ylmethoxy)-acetamido)propyl Phosphonate (**16m**).* ^{1}H NMR (200 MHz, D_2O) δ (ppm): 1.28−1.45 (m, 2H), 1.54−1.80 (m, 5H), 3.22 (t, J = 6 Hz, 2H), 4.64 (s, 2H), 7.02−7.54 (m, 9H). ^{13}C NMR (50 MHz, D_2O) δ (ppm): 19.2, 21.2, 24.1, 26.8, 45.8, 46.2, 73.6, 127.9, 128.3, 128.7, 129.3, 129.8, 130.3, 130.8, 132.2, 140.0, 143.5, 174.0. LCMS (ESI^+): m/z = 364.1 [$M + H]^+$, 727.2 [$2M + H]^+$. HRMS (ESI) m/z calculated for $C_{18}H_{22}NNaO_5P$ [$(M + Na)^+$], 386.1133; found, 386.1123.

*Sodium Hydrogen-3-(N-((4′-methyl-[1,1′-biphenyl]-4-yl)-methoxy)acetamido)propyl phosphonate (**16n**).* ^{1}H NMR (200 MHz, D_2O) δ (ppm): 1.40−1.70 (m, 2H), 1.70−1.99 (m, 2H),

DOI: 10.1021/acsinfecdis.6b00125
ACS Infect. Dis. 2016, 2, 923−935

2.07 (s, 3H), 2.37 (s, 3H), 3.59−3.85 (m, 2H), 4.99 (s, 2H), 7.28−7.78 (m, 8H). ^{13}C NMR (50 MHz, D_2O) δ (ppm): 19.6, 20.8, 21.3, 23.9, 26.6, 46.2, 46.4, 75.6, 126.8, 129.6, 130.2, 131.8, 133.2, 136.8, 137.2, 140.6, 173.7. HRMS (ESI) m/z calculated for $C_{19}H_{24}NNaO_5P$ [$(M + Na)^+$], 400.1290; found, 400.1247.

*Sodium Hydrogen-3-(N-((4′-methoxy-[1,1′-biphenyl]-4-yl)-methoxy)acetamido)propyl Phosphonate (**16o**).* ^{1}H NMR (200 MHz, DMSO) δ (ppm): 1.31−1.56 (m, 2H), 1.65−1.86 (m, 2H), 2.03 (s, 3H), 3.66 (t, J = 6.6 Hz, 2H), 3.79 (s, 3H), 4.89 (s, 2H), 7.02 (d, J = 8.6 Hz, 2H), 7.36−7.71 (m, 6H). ^{13}C NMR (50 MHz, DMSO) δ (ppm): 20.4, 20.9, 23.9, 26.6, 45.1, 45.5, 55.2, 75.0, 114.4, 126.2, 127.8, 130.1, 132.0, 133.2, 140.2, 159.1, 171.0. HRMS (ESI) m/z calculated for $C_{19}H_{24}NNaO_6P$ [$(M + Na)^+$], 416.1239; found, 416.1015.

*Sodium Hydrogen-3-(N-((4′-isopropyl-[1,1′-biphenyl]-4-yl)methoxy)acetamido)propyl Phosphonate (**16p**).* ^{1}H NMR (200 MHz, D_2O) δ (ppm): 0.94 (d, J = 5.8 Hz, 6H), 1.16−2.00 (m, 7H), 2.37−2.66 (m, 1H), 3.25−3.76 (m, 2H), 4.48 (s, 2H), 6.73−7.29 (m, 8H). ^{13}C NMR (50 MHz, D_2O) δ (ppm): 19.8, 21.4, 23.8, 26.4, 30.1, 33.5, 46.1, 46.6, 75.6, 126.6, 126.8, 130.1, 133.4, 137.8, 140.3, 147.1, 173.3. HRMS (ESI) m/z calculated for $C_{21}H_{28}NNaO_5P$ [$(M + Na)^+$], 428.1603; found, 428.1354.

*Sodium Hydrogen-(3-(N-((4′-(hydroxymethyl)-[1,1′-biphenyl]-4-yl)methoxy)acetamido)propyl Phosphonate (**16q**).* ^{1}H NMR (400 MHz, D_2O) δ (ppm): 1.59−1.67 (m, 2H), 1.90−1.95 (m, 2H), 2.14 (s, 3H), 3.84 (bs, 2H), 4.74 (s, 2H), 5.06 (s, 2H), 7.55 (d, J = 8 Hz, 2H), 7.64 (d, J = 8.4 Hz, 2H), 7.79 (t, J = 8, 7.6 Hz, 4H). ^{13}C NMR (100 MHz, D_2O) δ (ppm): 19.38, 20.82, 24.36, 25.71, 45.51, 63.49, 75.64, 127.15, 127.19, 128.03, 130.55, 132.94, 139.26, 139.84, 141.10, 174.71. LCMS (ESI^+): m/z = 394.2 $[M + H]^+$, 787.2 $[2M + H]^+$. HRMS (ESI) m/z calculated for $C_{19}H_{23}NNaO_6P$ [$(M + H)^+$], 416.12390; found, 416.12281.

*Sodium Hydrogen-3-(N-((4′-(trifluoromethyl)-[1,1′-biphenyl]-4-yl)methoxy)acetamido)propyl Phosphonate (**16r**).* ^{1}H NMR (400 MHz, CD_3OD) δ (ppm): 1.43−1.52 (m, 2H), 1.84−1.90 (m, 2H), 2.00 (s, 3H), 3.68 (t, J = 7.2 Hz, 2H), 4.88 (s, 2H), 7.48−7.50 (m, 2H), 7.62−7.66 (m, 4H), 7.73−7.75 (m, 2H). ^{13}C NMR (100 MHz, D_2O) δ (ppm): 19.8, 21.7, 23.3, 24.7, 48.4, 48.8, 75.8, 120.4, 123.2, 125.8, 125.9, 127.4, 128.5, 129.1 130.5, 134.4, 138.8, 139.8, 174.2. LCMS (ESI^+): m/z = 432.0 $[M + H]^+$, 863.0 $[2M + H]^+$. HRMS (ESI) m/z calculated for $C_{19}H_{20}NNaO_5P$ [$(M + H)^+$], 454.10072; found, 454.10024.

[({[(2,2-Dimethylpropanoyl)oxy]methoxy}[3-(*N*-{[4-(propan-2-yl)phenyl]methoxy}acetamido)propyl]-phosphoryl)oxy]methyl 2,2-Dimethylpropanoate (17). The acid of **16d** (52 mg, 0.159 mmol, 1 equiv) was dissolved in DMF (1.6 mL). Triethylamine (0.05 mL, 0.359 mmol, 2 equiv) was added, and the mixture was stirred for 5 min at room temperature; then chloromethyl pivalate (0.23 mL, 1.6 mmol, 10 equiv) was added. The resulting solution was heated overnight at 60 °C and concentrated. The residue was dissolved in CH_2Cl_2 and washed with sat. $NaHCO_3$ and brine. The aqueous layers were extracted with CH_2Cl_2 three times, and the combined organic layers were dried over $MgSO_4$, filtered, and evaporated under vacuum. Chromatographic separation on silica gel (toluene/acetone, 5/1) gave the expected compound as a yellow oil (45.8 mg, 52%). ^{1}H NMR (400 MHz, $CDCl_3$) δ (ppm): 1.21 (s, 18H), 1.25 (d, J = 6.4 Hz, 6H), 1.80−1.98 (m, 4H), 2.08 (s, 3H), 2.89−2.96 (m, 1H), 3.70 (t, J = 6.8, 6.4 Hz, 2H), 4.77 (s, 2H), 5.64 (s, 2H), 5.67 (s, 2H), 7.24−7.30 (m, 4H). ^{13}C NMR (100 MHz, $CDCl_3$) δ (ppm): 19.9, 20.0, 20.4, 23.3, 23.9, 24.7, 26.8, 34.0, 38.7, 45.0, 45.3, 76.3, 81.4, 81.4, 126.8, 129.4, 131.5, 150.0, 172.3, 176.8. LCMS (ESI^+): m/z = 558.8 $[M + H]^+$.

[({[(2,2-Dimethylpropanoyl)oxy]methoxy}({3-[*N*-(4-phenylbutoxy)acetamido]propyl})phosphoryl)oxy]-methyl 2,2-Dimethylpropanoate (18). A mixture of **15h** (100 mg, 0.259 mmol) in CH_2Cl_2 (0.4 mL) was prepared at 0 °C. Bromotrimethylsilane (0.27 mL, 2.072 mmol, 8 equiv) was added dropwise, and the reaction mixture was stirred overnight at room temperature. Ethyl bromide and excess silylating agent were removed by rotary evaporation at room temperature. The concentrate was solubilized in dry CH_2Cl_2 and evaporated again (×2). H_2O was added to the residue, and the mixture was stirred overnight at room temperature. The solution was filtered over cotton and freeze-dried on lyophilizer overnight. The crude acid (58 mg, 0.176 mmol), a yellow oil, was dissolved in DMF (1.8 mL), and triethylamine (0.05 mL, 0.352 mmol, 2 equiv) was added. The mixture was stirred for 5 min at room temperature, and chloromethyl pivalate (0.25 mL, 1.760, 10 equiv) was added. The resulting solution was heated overnight at 60 °C. DMF was removed on the rotavapor at 60 °C, and the residue was dissolved in CH_2Cl_2. The solution was washed with aqueous $NaHCO_3$, and the aqueous phase was extracted three times with CH_2Cl_2. The combined organic layers were washed with brine, and the aqueous phase was extracted three times with CH_2Cl_2. The combined organic layers were dried over $MgSO_4$, filtered, and concentrated *in vacuo*. Flash chromatography (toluene/acetone, 5/1) gave **18** (32 mg, 33%) as a yellow oil. ^{1}H NMR (200 MHz, $CDCl_3$) δ (ppm): 1.22 (s, 18H, $C(CH_3)_3 \times 2$), 1.56−2.02 (m, 8H, CH_2-P and CH_2-CH_2P and CH_2-CH_2O and CH_2-CH_2Ph), 2.65 (t, 2H, J = 7.1 Hz, CH_2-Ph), 2.10 (s, 3H, CH_3-CO), 3.64 (t, 2H, J = 6.4 Hz, CH_2-N), 3.80 (t, 2H, J = 6.0 Hz, CH_2-O-N), 5.65 (d, 4H, J = 13.0 Hz, CH_2-O-P × 2), 7.13−7.36 (m, 5H, H_{ar}). ^{13}C NMR (50 MHz, $CDCl_3$) δ (ppm): 20.1, 20.3, 22.7, 25.5, 27.0, 27.8, 28.0, 35.8, 38.9, 44.8, 45.3, 74.2, 81.4, 81.6, 126.1, 128.5, 141.8, 172.0, 177.0. LCMS (ESI^+): m/z = 558.2 $[M + H]^+$.

[({[(2,2-Dimethylpropanoyl)oxy]methoxy}(3-{*N*-[(4-phenylphenyl)methoxy]acetamido}propyl)phosphoryl)-oxy]methyl 2,2-Dimethylpropanoate (19). The acid of **16k** (41 mg, 0.113 mmol, 1 equiv) in DMF (1.2 mL) was prepared. Triethylamine (0.03 mL, 0.215 mmol, 2 equiv) was added, and the mixture was stirred for 5 min at room temperature. Then chloromethyl pivalate (0.16 mL, 1.11 mmol, 10 equiv) was added, and the reaction was heated overnight at 60 °C then concentrated. The residue was dissolved in CH_2Cl_2 and washed with sat. $NaHCO_3$ and brine. The aqueous layers were extracted with CH_2Cl_2 three times, and the combined organic layers were dried over $MgSO_4$, filtered, and evaporated under vacuum. Chromatographic separation on silica gel (toluene/acetone, 5/1) gave the expected compound as a yellow oil (59.1 mg, 89%). ^{1}H NMR (200 MHz, $CDCl_3$) δ (ppm): 1.21 (s, 18H), 1.80−2.00 (m, 4H), 2.12 (s, 3H), 3.73 (t, J = 6.2, 6.0 Hz, 2H), 4.85 (s, 2H), 5.63 (s, 2H), 5.70 (s, 2H), 7.27−7.64 (m, 9H). ^{13}C NMR (50 MHz, $CDCl_3$) δ (ppm): 20.1, 20.7, 22.8, 25.6, 27.0, 38.9, 45.4, 45.6, 76.4, 81.5, 81.6, 127.3, 127.7, 127.8, 129.1, 129.9, 133.4, 140.6, 142.2, 171.2, 172.5. LCMS (ESI+): m/z = 592.8 $[M + H]^+$.

[({[(2,2-Dimethylpropanoyl)oxy]methoxy}({3-[*N*-(naphthalen-2-ylmethoxy)acetamido]propyl})-phosphoryl)oxy]methyl 2,2-Dimethylpropanoate (20). The acid of **16j** (71 mg, 0.211 mmol, 1 equiv), a light yellow oil, was solubilized in anhydrous DMF, and triethylamine (0.06 mL, 0.451 mmol, 2 equiv) was added at room temperature. After the reaction mixture was stirred at room temperature for

DOI: 10.1021/acsinfecdis.6b00125
ACS Infect. Dis. 2016, 2, 923−935

5 min, chloromethyl pivalate (0.3 mL, 2.08 mmol, 10 equiv) was added. The resulting solution was stirred at 60 °C overnight and concentrated under vacuum. The residue was solubilized in CH_2Cl_2 and washed with aqueous saturated $NaHCO_3$, and the aqueous phase was extracted with CH_2Cl_2 three times. The combined organic layers were dried with anhydrous $MgSO_4$, filtered, and concentrated. Chromatographic separation on silica gel (CH_2Cl_2/EtOAc, 5/1 to 3/2) gave the expected compound as a light yellow oil (46 mg, 0.081 mmol, 32%). ^{1}H NMR (400 MHz, $CDCl_3$) δ (ppm): 1.20 (s, 18H), 1.81−2.01 (m, 4H), 2.12 (s, 3H), 3.72 (t, J = 6.8 Hz, 2H), 4.98 (s, 2H), 5.64 (s, 2H), 5.67 (s, 2H), 7.47−7.54 (m, 3H), 7.83−7.88 (m, 4H). ^{13}C NMR (100 MHz, $CDCl_3$) δ (ppm): 20.04, 20.08, 20.65, 23.41, 24.82, 26.95, 38.82, 45.66, 76.83, 77.16, 77.48, 81.46, 81.52, 126.54, 126.64, 126.80, 127.87, 128.20, 128.74, 131.86, 133.25, 133.53, 172.56, 176.97. LCMS (ESI$^+$): m/z = 566.2 $[M + H]^+$.

[{{[(Benzoyl)oxy]methoxy}({3-[*N*-(4-phenylbutoxy)-acetamido]propyl})phosphoryl)oxy]methyl Benzoate (21). To a solution of **15h** (120 mg, 0.311 mmol) in CH_2Cl_2 (0.5 mL) at 0 °C was added dropwise bromotrimethylsilane (0.33 mL, 2.488 mmol, 8 equiv). The reaction mixture was stirred overnight at room temperature. Ethyl bromide and excess silylating agent were removed by rotary evaporation at room temperature. The concentrate was dissolved in dry CH_2Cl_2 and evaporated again (×2). H_2O was added to the residue, and the mixture was stirred overnight at room temperature. The solution was freeze-dried on lyophilizer overnight. The crude acid (73 mg, 0.220 mmol), a yellow oil, was solubilized in DMF (1.2 mL), and triethylamine (0.06 mL, 0.440 mmol, 2 equiv) was added. The mixture was stirred for 5 min at room temperature, and chloromethyl benzoate (376 mg, 2.200 mmol, 10 equiv) was added in solution in DMF (1.0 mL). The resulting solution was heated overnight at 60 °C. DMF was removed on the rotavapor at 60 °C, and the residue was dissolved in CH_2Cl_2. The solution was washed with aqueous $NaHCO_3$, and the aqueous phase was extracted three times with CH_2Cl_2. Then the combined organic layers were washed with brine, and the aqueous phase was extracted three times with CH_2Cl_2. The combined organic layers were dried over $MgSO_4$, filtered, and concentrated *in vacuo*. Flash chromatography (toluene/acetone, 5/1) gave **21** (48 mg, 37%) as a yellow oil. ^{1}H NMR (200 MHz, $CDCl_3$) δ (ppm): 1.49−2.01 (m, 8H, CH_2-P and CH_2-CH_2P and CH_2-CH_2O and CH_2-CH_2Ph), 2.04 (s, 3H, CH_3-CO), 2.61 (t, 2H, J = 7.1 Hz, CH_2-Ph), 3.61 (t, 2H, J = 6.2 Hz, CH_2-N), 3.73 (t, 2H, J = 6.0 Hz, CH_2-O-N), 5.84−6.00 (m, 4H, CH_2-O-P × 2), 7.12−7.67 (m, 11H, H_{ar}), 7.99−8.13 (m, 4H, H_{ar}). ^{13}C NMR ($CDCl_3$) δ (ppm): 20.0, 20.3, 23.3, 24.8, 27.7, 27.9. 29.8, 35.7, 44.8, 45.0, 74.2, 81.8, 81.9, 126.1, 128.4, 128.5, 128.5, 128.7, 128.8, 130.1, 134.0, 141.8, 165.0. LCMS (ESI$^+$): m/z = 598.2 $[M + H]^+$.

Dxr Inhibition Assays. Dxr activity was assayed at 37 °C by spectrophotometrically monitoring the enzyme-catalyzed oxidation of NADPH, as previously described.[47] To determine percent inhibition for each inhibitor, 120 μL of assay solutions were used, containing 100 mM Tris, pH 7.8, 25 mM $MgCl_2$, 150 μM NADPH, 0.89 μM Dxr, 100 μM inhibitor, and the appropriate K_M value of DXP (Echelon Biosciences, Salt Lake City, Utah), which is 252 μM for Yp Dxr[9] and 47 μM for Mtb Dxr.[48] The assays were performed by preincubating the mixture of Tris, $MgCl_2$, Dxr, and inhibitor for 10 min (37 °C) to facilitate binding of the inhibitor, followed by the addition of NADPH, a 5 min incubation (37 °C), and then the addition of DXP. The half-maximal inhibition (IC_{50}) values were determined by plotting enzyme fractional activity as a function of inhibitor concentration (1 nM to 100 μM) and using GraphPad Prism (La Jolla, CA) nonlinear curve fitting to a sigmoidal dose−response curve. Lineweaver−Burk plots were generated using 120 μL assay solutions containing 100 mM Tris, pH 7.8, 25 mM $MgCl_2$, 0.89 μM Dxr, and variable concentrations of inhibitor. Each assay solution was incubated for 10 min at 37 °C to facilitate inhibitor binding. NADPH was subsequently added, to a final concentration of 150 μM for the DXP-dependent plots and at variable concentrations for the NADPH-dependent plots (ranging from 30 to 120 μM for compound **16j** against Mtb Dxr,and 3−20 μM for compound **8e** against Yp Dxr). Assays were incubated for 10 min (37 °C) following the addition of NADPH. Enzymatic reactions were initiated with addition of 252 μM (for Yp) or 47 μM (for Mtb) DXP for the NADPH dependent plots and at variable DXP concentrations for the DXP-dependent plots (ranging from 25 to 200 μM for compound **16j** against Mtb Dxr and 50−300 μM for compound **8e** against Yp Dxr). The resulting Lineweaver−Burk plots were fit by linear regression using Graphpad prism. K_i values were calculated by linear regression using Graphpad Prism as the negative x-intercept of a plot of apparent K_m of the substrate versus inhibitor concentration.

■ ASSOCIATED CONTENT

Supporting Information

The Supporting Information is available free of charge on the ACS Publications website at DOI: 10.1021/acsinfecdis.6b00125.

Synthetic procedures and analytical information for all compounds and full Dxr and antibacterial inhibition methods and data (PDF)

■ AUTHOR INFORMATION

Corresponding Author

*Phone: 202-994-8405. Fax: 202-994-5873. E-mail: cdowd@gwu.edu.

Author Contributions

#G.S.J. and E.R.J. contributed equally to this work.

Notes

The authors declare no competing financial interest.

■ ACKNOWLEDGMENTS

We gratefully acknowledge technical assistance from Teresa Hawley (GWU Medical Center), Joshua Wilhide (UMBC), and Phil Mortimer (JHU) for assistance with HRMS analysis. Financial support was provided by George Washington University's Department of Chemistry and University Facilitating Fund, NIH (Grant AI086453 to C.S.D. and Grants AI103280 and AI123808 to A.R.O.), George Mason University's Department of Chemistry and Biochemistry, the U.S. Army Medical Research and Materiel Command (Grant W23RYX1291N601 to R.D.C.), and the Division of Intramural Research, NIAID, NIH.

■ REFERENCES

(1) WHO (2014) *Antimicrobial Resistance: Global Report on Surveillance*, WHO, Geneva.

(2) Hampton, T. (2013) Report reveals scope of US antibiotic resistance threat. *Jama 310*, 1661−1663.

(3) Shlaes, D. M., Sahm, D., Opiela, C., and Spellberg, B. (2013) The FDA reboot of antibiotic development. *Antimicrob. Agents Chemother. 57*, 4605−4607.

(4) Boucher, H. W., Talbot, G. H., Bradley, J. S., Edwards, J. E., Gilbert, D., Rice, L. B., Scheld, M., Spellberg, B., and Bartlett, J. (2009) Bad bugs,

no drugs: no ESKAPE! An update from the Infectious Diseases Society of America. *Clin. Infect. Dis. 48*, 1−12.
(5) Silver, L. L. (2011) Challenges of antibacterial discovery. *Clin Microbiol Rev. 24*, 71−109.
(6) Uh, E., Jackson, E. R., San Jose, G., Maddox, M., Lee, R. E., Lee, R. E., Boshoff, H. I., and Dowd, C. S. (2011) Antibacterial and antitubercular activity of fosmidomycin, FR900098, and their lipophilic analogs. *Bioorg. Med. Chem. Lett. 21*, 6973−6976.
(7) McKenney, E. S., Sargent, M., Khan, H., Uh, E., Jackson, E. R., San Jose, G., Couch, R. D., Dowd, C. S., and van Hoek, M. L. (2012) Lipophilic prodrugs of FR900098 are antimicrobial against Francisella novicida in vivo and in vitro and show GlpT independent efficacy. *PLoS One 7*, e38167.
(8) San Jose, G., Jackson, E. R., Uh, E., Johny, C., Haymond, A., Lundberg, L., Pinkham, C., Kehn-Hall, K., Boshoff, H. I., Couch, R. D., and Dowd, C. S. (2013) Design of Potential Bisubstrate Inhibitors against Mycobacterium tuberculosis (Mtb) 1-Deoxy-D-Xylulose 5-Phosphate Reductoisomerase (Dxr)-Evidence of a Novel Binding Mode. *MedChemComm 4*, 1099−1104.
(9) Haymond, A., Johny, C., Dowdy, T., Schweibenz, B., Villarroel, K., Young, R., Mantooth, C. J., Patel, T., Bases, J., San Jose, G., Jackson, E. R., Dowd, C. S., and Couch, R. D. (2014) Kinetic characterization and allosteric inhibition of the Yersinia pestis 1-deoxy-D-xylulose 5-phosphate reductoisomerase (MEP synthase). *PLoS One 9*, e106243.
(10) Jackson, E. R., San Jose, G., Brothers, R. C., Edelstein, E. K., Sheldon, Z., Haymond, A., Johny, C., Boshoff, H. I., Couch, R. D., and Dowd, C. S. (2014) The effect of chain length and unsaturation on Mtb Dxr inhibition and antitubercular killing activity of FR900098 analogs. *Bioorg. Med. Chem. Lett. 24*, 649−653.
(11) http://www.who.int/mediacentre/factsheets/fs104/en/index.html (accessed Oct 11, 2016).
(12) Dye, C., Glaziou, P., Floyd, K., and Raviglione, M. (2013) Prospects for tuberculosis elimination. *Annu. Rev. Public Health 34*, 271−286.
(13) Dye, C., Watt, C. J., Bleed, D. M., Hosseini, S. M., and Raviglione, M. C. (2005) Evolution of tuberculosis control and prospects for reducing tuberculosis incidence, prevalence, and deaths globally. *JAMA 293*, 2767−2775.
(14) Centers for Disease Control and Prevention. Plague Maps, http://www.cdc.gov/plague/maps/index.html (accessed Oct 11, 2016).
(15) Galimand, M., Carniel, E., and Courvalin, P. (2006) Resistance of Yersinia pestis to antimicrobial agents. *Antimicrob. Agents Chemother. 50*, 3233−3236.
(16) Rodriguez-Concepcion, M., and Albert, B. (2002) Elucidation of the methylerythritol phosphate pathway for isoprenoid biosynthesis in bacteria and plastids. A metabolic milestone achieved through genomics. *Plant Physiol. 130*, 1079−1089.
(17) Rohmer, M. (1999) The discovery of a mevalonate-independent pathway for isoprenoid biosynthesis in bacteria, algae and higher plants. *Nat. Prod. Rep. 16*, 565−574.
(18) Imlay, L., and Odom, A. R. (2014) Isoprenoid metabolism in apicomplexan parasites. *Curr. Clin Microbiol Rep 1*, 37−50.
(19) Jackson, E. R., and Dowd, C. S. (2012) Inhibition of 1-deoxy-D-xylulose-5-phosphate reductoisomerase (Dxr): a review of the synthesis and biological evaluation of recent inhibitors. *Curr. Top. Med. Chem. 12*, 706−728.
(20) Masini, T., Kroezen, B. S., and Hirsch, A. K. (2013) Druggability of the enzymes of the non-mevalonate-pathway. *Drug Discovery Today 18*, 1256−1262.
(21) Singh, N., Cheve, G., Avery, M. A., and McCurdy, C. R. (2007) Targeting the Methyl Erythritol Phosphate (MEP) Pathway for Novel Antimalarial, Antibacterial and Herbicidal Drug Discovery: Inhibition of 1-Deoxy-D-Xylulose-5-Phosphate Reductoisomerase (DXR) Enzyme. *Curr. Pharm. Des. 13*, 1161−1177.
(22) Brown, A. C., and Parish, T. (2008) Dxr is essential in Mycobacterium tuberculosis and fosmidomycin resistance is due to a lack of uptake. *BMC Microbiol. 8*, 78.
(23) Freiberg, C., Wieland, B., Spaltmann, F., Ehlert, K., Brotz, H., and Labischinski, H. (2001) Identification of novel essential Escherichia coli genes conserved among pathogenic bacteria. *J. Mol. Microbiol Biotechnol 3*, 483−489.
(24) Hunter, W. N. (2007) The non-mevalonate pathway of isoprenoid precursor biosynthesis. *J. Biol. Chem. 282*, 21573−21577.
(25) Nair, S. C., Brooks, C. F., Goodman, C. D., Strurm, A., McFadden, G. I., Sundriyal, S., Anglin, J. L., Song, Y., Moreno, S. N., and Striepen, B. (2011) Apicoplast isoprenoid precursor synthesis and the molecular basis of fosmidomycin resistance in Toxoplasma gondii. *J. Exp. Med. 208*, 1547−1559.
(26) Odom, A. R., and Van Voorhis, W. C. (2010) Functional genetic analysis of the Plasmodium falciparum deoxyxylulose 5-phosphate reductoisomerase gene. *Mol. Biochem. Parasitol. 170*, 108−111.
(27) Jomaa, H., Wiesner, J., Sanderbrand, S., Altincicek, B., Weidemeyer, C., Hintz, M., Turbachova, I., Eberl, M., Zeidler, J., Lichtenthaler, H. K., Soldati, D., and Beck, E. (1999) Inhibitors of the nonmevalonate pathway of isoprenoid biosynthesis as antimalarial drugs. *Science 285*, 1573−1576.
(28) Kojo, H., Shigi, Y., and Nishida, M. (1980) FR-31564, a new phosphonic acid antibiotic: bacterial resistance and membrane permeability. *J. Antibiot. 33*, 44−48.
(29) Kuzuyama, T., Shimizu, T., Takahashi, S., and Seto, H. (1998) Fosmidomycin, a specific inhibitor of 1-Deoxy-D-xylulose 5-phosphate reductoisomerase in the nonmevalonate pathway for terpenoid biosynthesis. *Tetrahedron Lett. 39*, 7913−7916.
(30) Okuhara, M., Kuroda, Y., Goto, T., Okamoto, M., Terano, H., Kohsaka, M., Aoki, H., and Imanaka, H. (1980) Studies on new phosphonic acid antibiotics. I. FR-900098, isolation and characterization. *J. Antibiot. 33*, 13−17.
(31) Schultz, C. (2003) Prodrugs of biologically active phosphate esters. *Bioorg. Med. Chem. 11*, 885−898.
(32) Andaloussi, M., Henriksson, L. M., Wieckowska, A., Lindh, M., Bjorkelid, C., Larsson, A. M., Suresh, S., Iyer, H., Srinivasa, B. R., Bergfors, T., Unge, T., Mowbray, S. L., Larhed, M., Jones, T. A., and Karlen, A. (2011) Design, synthesis, and X-ray crystallographic studies of alpha-aryl substituted fosmidomycin analogues as inhibitors of Mycobacterium tuberculosis 1-deoxy-D-xylulose 5-phosphate reductoisomerase. *J. Med. Chem. 54*, 4964−4976.
(33) Haemers, T., Wiesner, J., Van Poecke, S., Goeman, J., Henschker, D., Beck, E., Jomaa, H., and Van Calenbergh, S. (2006) Synthesis of alpha-substituted fosmidomycin analogues as highly potent Plasmodium falciparum growth inhibitors. *Bioorg. Med. Chem. Lett. 16*, 1888−1891.
(34) Jansson, A. M., Wieckowska, A., Bjorkelid, C., Yahiaoui, S., Sooriyaarachchi, S., Lindh, M., Bergfors, T., Dharavath, S., Desroses, M., Suresh, S., Andaloussi, M., Nikhil, R., Sreevalli, S., Srinivasa, B. R., Larhed, M., Jones, T. A., Karlen, A., and Mowbray, S. L. (2013) DXR inhibition by potent mono- and disubstituted fosmidomycin analogues. *J. Med. Chem. 56*, 6190−6199.
(35) Miller, M. J. (1989) Syntheses and Therapeutic Potential of Hydroxamic Acid Based Siderophores and Analogues. *Chem. Rev. 89*, 1563−1579.
(36) Blazewska, K., and Gajda, T. (2003) N-(diethylphosphoryl)-O-benzylhydroxylamine-a convenient substrate for the synthesis of N-substituted O-benzylhydroxylamines. *Tetrahedron 59*, 10249−10254.
(37) Devreux, V., Wiesner, J., Jomaa, H., Rozenski, J., Van der Eycken, J., and Van Calenbergh, S. (2007) Divergent strategy for the synthesis of alpha-aryl-substituted fosmidomycin analogues. *J. Org. Chem. 72*, 3783−3789.
(38) McKenna, C. E., Higa, M. T., Cheung, N. H., and McKenna, M.-C. (1977) The facile dealkylation of phosphonic acid dialkyl esters by bromotrimethylsilane. *Tetrahedron Lett. 18*, 155−158.
(39) Verbrugghen, T., Cos, P., Maes, L., and Van Calenbergh, S. (2010) Synthesis and evaluation of alpha-halogenated analogues of 3-(acetylhydroxyamino)propylphosphonic acid (FR900098) as antimalarials. *J. Med. Chem. 53*, 5342−5346.
(40) Haemers, T., Wiesner, J., Giessmann, D., Verbrugghen, T., Hillaert, U., Ortmann, R., Jomaa, H., Link, A., Schlitzer, M., and Van

DOI: 10.1021/acsinfecdis.6b00125
ACS Infect. Dis. 2016, 2, 923−935

Calenbergh, S. (2008) Synthesis of beta- and gamma-oxa isosteres of fosmidomycin and FR900098 as antimalarial candidates. *Bioorg. Med. Chem. 16*, 3361−3371.
(41) Reichenberg, A., Wiesner, J., Weidemeyer, C., Dreiseidler, E., Sanderbrand, S., Altincicek, B., Beck, E., Schlitzer, M., and Jomaa, H. (2001) Diaryl ester prodrugs of FR900098 with improved in vivo antimalarial activity. *Bioorg. Med. Chem. Lett. 11*, 833−835.
(42) Baudy, R. B., Butera, J. A., Abou-Gharbia, M. A., Chen, H., Harrison, B., Jain, U., Magolda, R., Sze, J. Y., Brandt, M. R., Cummons, T. A., Kowal, D., Pangalos, M. N., Zupan, B., Hoffmann, M., May, M., Mugford, C., Kennedy, J., and Childers, W. E., Jr. (2009) Prodrugs of perzinfotel with improved oral bioavailability. *J. Med. Chem. 52*, 771−778.
(43) Koronakis, V., Eswaran, J., and Hughes, C. (2004) Structure and function of TolC: the bacterial exit duct for proteins and drugs. *Annu. Rev. Biochem. 73*, 467−489.
(44) Koppisch, A. T., Fox, D. T., Blagg, B. S., and Poulter, C. D. (2002) E. coli MEP synthase: steady-state kinetic analysis and substrate binding. *Biochemistry 41*, 236−243.
(45) Reuter, K., Sanderbrand, S., Jomaa, H., Wiesner, J., Steinbrecher, I., Beck, E., Hintz, M., Klebe, G., and Stubbs, M. T. (2002) Crystal structure of 1-deoxy-D-xylulose-5-phosphate reductoisomerase, a crucial enzyme in the non-mevalonate pathway of isoprenoid biosynthesis. *J. Biol. Chem. 277*, 5378−5384.
(46) Bjorkelid, C., Bergfors, T., Unge, T., Mowbray, S. L., and Jones, T. A. (2012) Structural studies on Mycobacterium tuberculosis DXR in complex with the antibiotic FR-900098. *Acta Crystallogr., Sect. D: Biol. Crystallogr. 68*, 134−143.
(47) Takahashi, S., Kuzuyama, T., Watanabe, H., and Seto, H. (1998) A 1-deoxy-D-xylulose 5-phosphate reductoisomerase catalyzing the formation of 2-C-methyl-D-erythritol 4-phosphate in an alternative nonmevalonate pathway for terpenoid biosynthesis. *Proc. Natl. Acad. Sci. U. S. A. 95*, 9879−9884.
(48) Dhiman, R. K., Schaeffer, M. L., Bailey, A. M., Testa, C. A., Scherman, H., and Crick, D. C. (2005) 1-Deoxy-D-xylulose 5-phosphate reductoisomerase (IspC) from Mycobacterium tuberculosis: towards understanding mycobacterial resistance to fosmidomycin. *J. Bacteriol. 187*, 8395−8402.

DOI: 10.1021/acsinfecdis.6b00125
ACS Infect. Dis. 2016, 2, 923−935

APPENDIX 2 – SUPPLEMENTARY INFORMATION

Specific Aim 1, Part 1 — Rational Compound Screen with IspC

Paper I: Design of Potential Bisubstrate Inhibitors against Mycobacterium tuberculosis (Mtb) 1-Deoxy-D-Xylulose 5-Phosphate Reductoisomerase (Dxr)- Evidence of a Novel Binding Mode

The following supplementary figure is reproduced from Paper I[127].

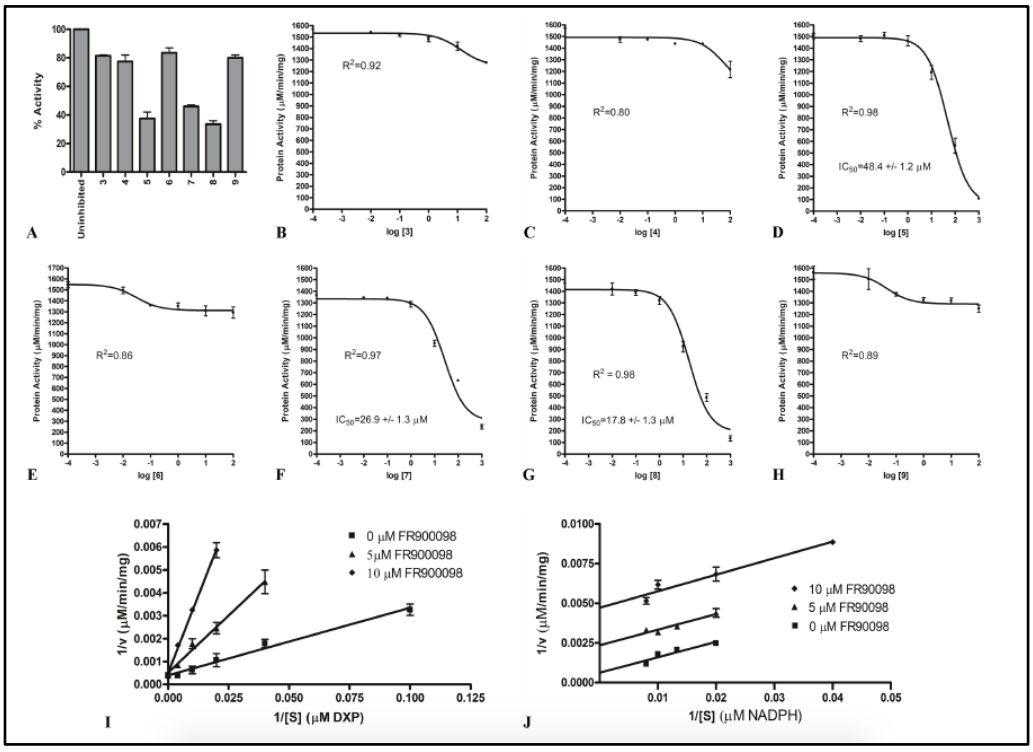

Figure 82. Kinetic characterization of inhibitor activity. A) Relative inhibition by compounds 3-9 at 100 μM concentration. B) through H) Dose-response plots obtained using the indicated inhibitors. The LineweaverBurk plots (I and J) reveal that FR900098 is a competitive inhibitor relative to DXP and an uncompetitive inhibitor with respect to NADPH, indicating that the inhibitor binds to the enzyme only after NADPH is bound.

Paper II: Kinetic Characterization and Allosteric Inhibition of the Yersinia pestis 1-Deoxy-D-Xylulose 5-Phosphate Reductoisomerase (MEP Synthase)

The following supplementary figures are reproduced from Paper II[141].

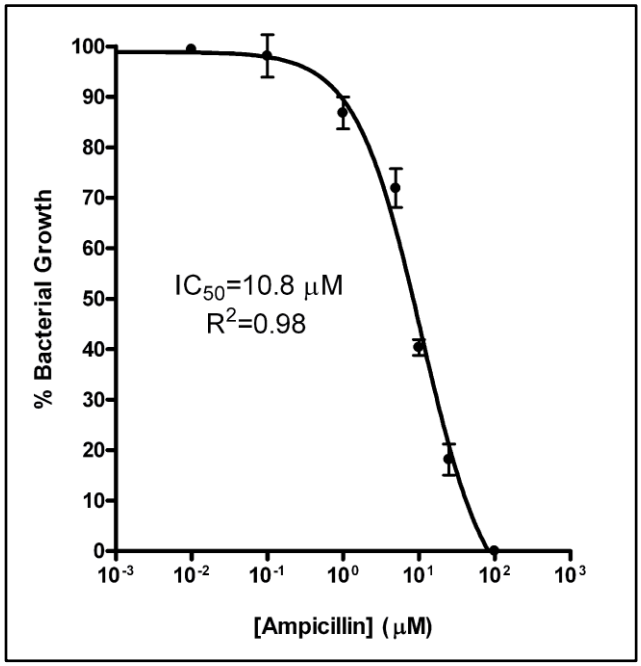

Figure 83. Dose-response plot of *Y. pestis* growth as a function of ampicillin concentration. Fractional growth is calculated as the ratio of cell density (OD_{600}) in the presence of inhibitor to cell density in the absence of inhibitor. Ampicillin is an FDA approved inhibitor of bacterial transpeptidase, resulting in the disruption of cell wall biosynthesis. Nonlinear regression fitting was performed, resulting in an IC_{50} of 10.8 µM (3.8 µg/mL). The goodness-of-fit (R^2) value is indicated.

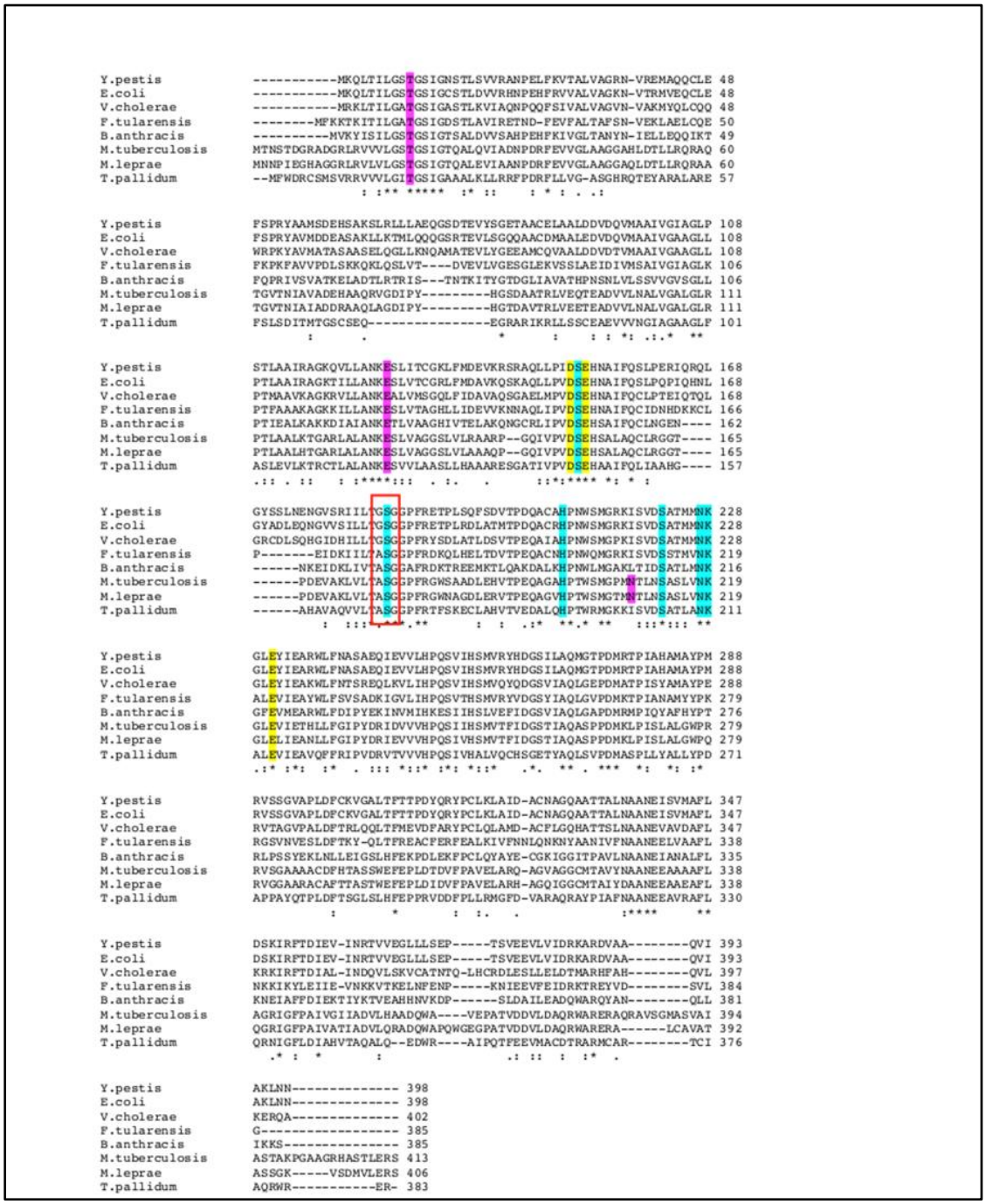

Figure 84. Sequence alignment of various IspC homologs using Clustal Omega, where identical residues are denoted by an asterisk (*) and chemically similar residues are denoted by a colon (:). Each residue involved in catalysis[113] is colored based on the substrate or cofactor with which it primarily interacts, with residues in pink associating with NADPH, residues in blue associating with DXP, and residues in yellow coordinating the divalent cation. The serine residue boxed in red was identified as a possible phosphorylation site used for regulation of the enzyme[189].

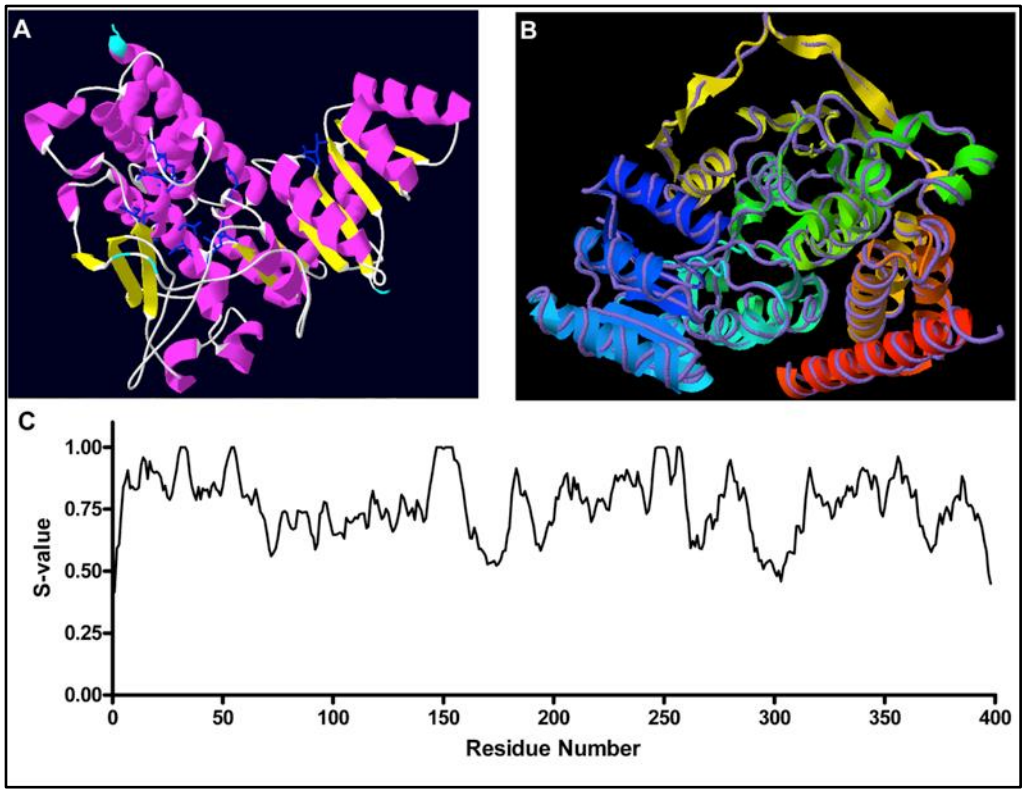

Figure 85. Structural features of the *Y. pestis* IspC. A) Predicted structure of the *Y. pestis* IspC, homology modeled using templates selected by I-TASSER's threading alignment algorithm. A cartoon representation of the tertiary structure is shown, with alpha helices colored pink, beta sheets colored yellow, and coiled regions colored white. Residues comprising the substrate binding site (colored dark blue with backbone and sidechain residues shown) were identified via primary sequence alignment and the resolved structure of *M. tuberculosis* IspC[113]. B) Overlay of the predicted *Y. pestis* IspC (shown as a cartoon representation) and the resolved crystal structure of the *E. coli* IspC (PBD 2EGH; shown as a purple ribbon). The two structures are highly similar, with a TM-score of 0.996 and a RMSD of 0.46. C) ProQ2 was used to evaluate the quality of the *Y. pestis* IspC model, providing scores ranging from 0 (unreliable) to 1 (reliable). Regions of the model scoring <0.5 are colored light blue in the structure shown in A), and are comprised of residues 1, 301, 303, 397, and 398.

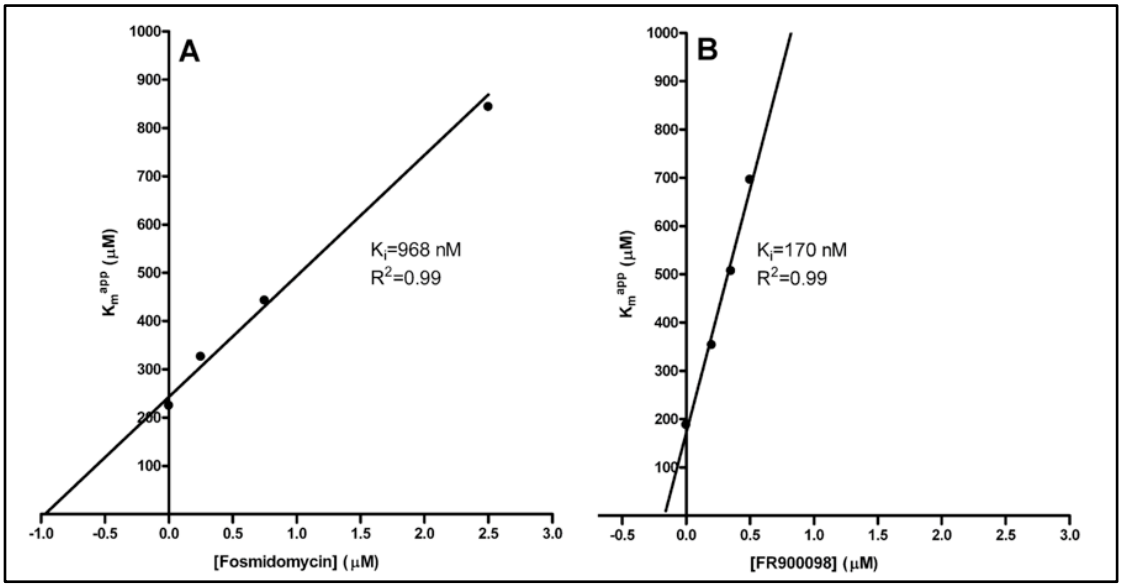

Figure 86. Graphical determination of the inhibition constant. Because fosmidomycin and FR900098 are slow, tight binding inhibitors, the *Y. pestis* IspC was preincubated with the inhibitor for 10 minutes prior to addition of substrate. The absolute value of the X intercept of the line produced from linear regression fitting the plot of $K_M^{app,DXP}$ as a function of inhibitor concentration defined the K_i as 968 nM and 170 nM for fosmidomycin and FR900098, respectively. The R^2 values are indicated.

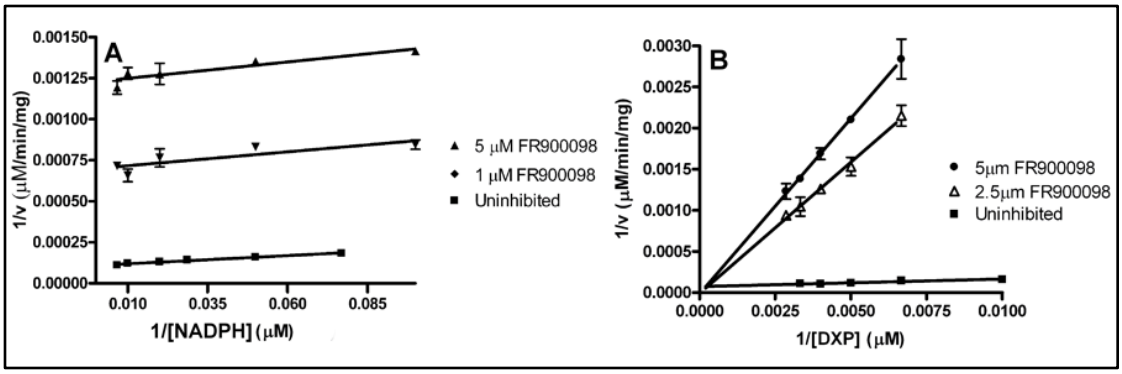

Figure 87. Mode of inhibition by FR900098. The Lineweaver–Burk plots indicate that FR900098 is uncompetitive with respect to NADPH (A), but competitive with respect to DXP (B). All assays were performed in duplicate using purified *Y. pestis* IspC.

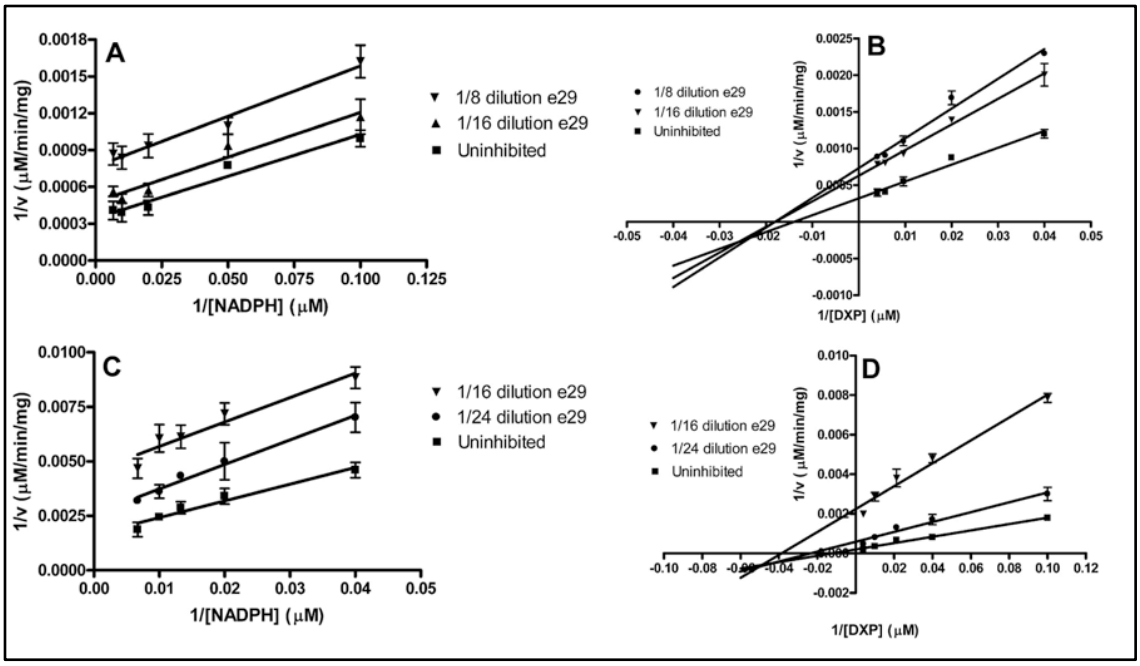

Figure 88. The Lineweaver–Burk plots generated from assays with purified *F. tularensis* IspC (A and B) or purified *M. tuberculosis* IspC (C and D) indicate that e29 is uncompetitive with respect to NADPH and noncompetitive with respect to DXP.

Paper IV: Synthesis and bioactivity of β-substituted fosmidomycin analogues targeting 1-deoxy-D-xylulose-5-phosphate reductoisomerase

The following supplementary figures are reproduced from Paper IV[128].

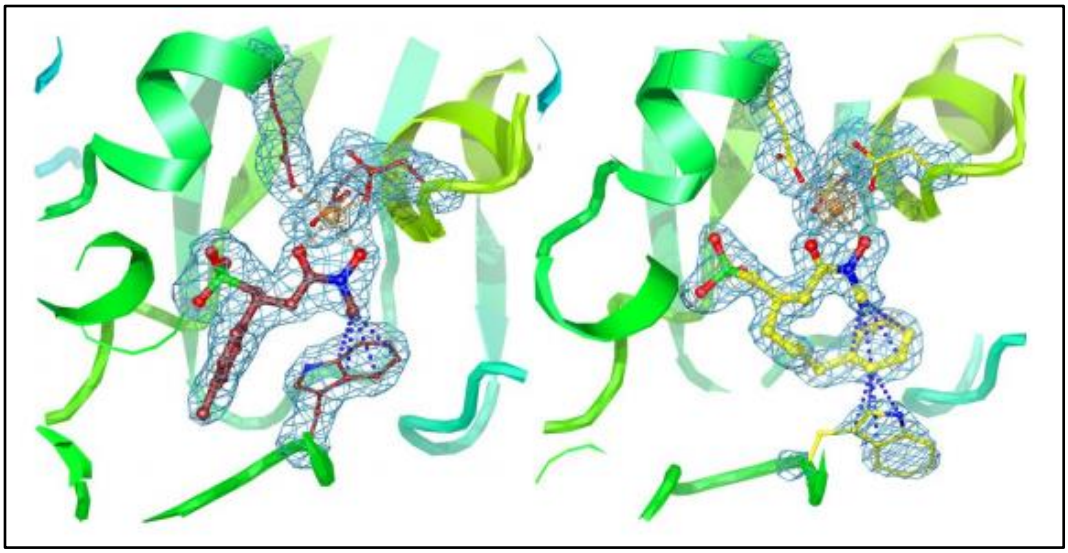

Figure 89. Electron density and aromatic interactions for compounds 7b and 8d.

Table 13. Crystallization conditions for the successful crystallographic experiments.

Ligand	Well[1]	Conditions
7a	F1	10% w/v PEG 20,000, 20% v/v PEG MME 550[2], 0.02M each of D-glucose,D- mannose, D-galactose, L-frucose, D-xylose, N-acetyl-D-glucosamine, 0.1 M MES/imidazole pH[3] 6.5
7b	H5	10% w/v PEG 20,000 20% v/v PEG MME 550, 0.02M each of sodium L-glutamate, DL-alanine, glycine, DL-lysine HCl, DL-serine, 0.1M MES/imidazole pH 6.5
8c	H2	10% w/v PEG 8000, 20% v/v ethylene glycol, 0.02M each of sodium Lglutamate, DL-alanine, glycine, DL-lysine HCl, DL-serine, 0.1M MES/imidazole pH 6.5
8d	A6	10% w/v PEG 8000, 20% v/v ethylene glycol, 0.03M MgCl2, 0.03M CaCl2, 0.1M MOPS/HEPES-Na pH 7.5

1 The letter-number code refers to the Morpheus numbering system in Table 1 of Gorrec (2009).
2 PEG MME is polyethylene glycol monomethyl ether 550.
3 pH refers to the buffer component only and not the pH of the complete formulation.

Table 14. Statistics for X-ray data and refinement

Complex with	**7a**	**7b**	**8c**	**8d**
PBD entry code	4Y6R	4Y6S	4Y67	4Y6P
Data collection				
Environment	ESRF - ID29	ESRF - ID29	ESRF - ID29	ESRF - ID29
Wavelength (Å)	0.97856	0.97856	0.97856	0.97856
Cell dimensions, angles (Å, °)	51.04, 54.85, 85.21 89.64, 105.40, 107.61	51.40, 54.96, 85.0 89.41, 105.42.6, 107.28	51.57, 56.47, 86.02 104.11, 103.25, 100.16	51.38, 55.76, 85.43 103.18, 102.83, 100.90
Space group	P1	P1	P1	P1
Resolution (Å) [1]	47.08 - 1.9 (2.0 - 1.9)	47.15 - 2.10 (2.21 - 2.10)	48.65 - 1.6 (1.69 - 1.6)	48.47 - 1.9 (2.0 - 1.9)
Unique reflections	64,132	46,811	110,454	65,358
Average multiplicity[1]	5.5 (5.7)	4.1 (4.1)	3.4 (3.4)	3.9 (4.0)
Completeness (%) [1]	95.5 (95.0)	93.9 (91.3)	94.2 (90.3)	95.2 (95.0)
Rmerge[1]	14.8 (79.8)	8.5 (33.5)	8.0 (47.8)	9.5 (54.2)
Rmeas[1]	0.163 (0.879)	0.097 (0.385)	0.094 (0.565)	0.110 (0.626)
Rp.i.m.[1]	0.069 (0.366)	0.047 (0.187)	0.050 (0.299)	0.055 (0.311)
$\langle I/\sigma(I)\rangle$[1]	9.2 (2.0)	10.7 (3.7)	8.2 (2.1)	9.8 (3.0)
Wilson plot B factor (Å^2)	17.5	19.3	13.8	17.0
Refinement				
No. of reflections (completeness, %)	60,876 (95.5)	44,433 (93.9)	104,856 (94.2)	62,042 (95.2)
Resolution range (Å)	47.08-1.90	47.15-2.10	48.65-1.60	48.47-1.90
R-factor/R-free (%)	18.7/21.8	21.7/25.2	17.7/20.6	16.5/19.6
Number of non-hydrogen atoms (mean B, Å^2)	7087 (29.6)	6843 (33.5)	7396 (22.6)	7205 (21.6)
Number solvent atoms	454	251	714	573
Average B-values (Å^2)				
Protein Atoms (A,B)	27.0, 32.0	31.0, 36.3	21.8, 22.7	22.2, 21.2
Solvent Atoms	35.9	33.6	31.5	31.7
Mn^{2+} ions	21.5	25.3	11.7	14.0
Inhibitor (A, B)	22.3, 22.8	28.3, 25.7	17.2, 15.8	20.3, 18.7
Other atoms	(Cl-, sulfate) 45.6	-	-	(Ca2+, sulfate) 53.5
Ramanchandran outliers (%)[2]	2.0, 2.5	2.5, 3.0	2.0, 2.0	3.0, 2.3
RMSD from ideal bond length (Å)[3]	0.008	0.008	0.011	0.009
RMSD from ideal bond angle (°)[3]	1.4	1.4	1.3	1.4

1 Values in parentheses refer to the outer resolution shell

2 Calculated using a strict-boundary Ramachandran plot definition [190]

3 Ideal values from Engh & Huber (1991) [191]

Table 15. Phosphonate interactions the four enzyme-inhibitor complexes. Each fosmidomycin analogue has a phosphonate group containing three oxygen atoms (1,2,3) that interact with conserved structural features. Oxygen 1 has three interacting groups in all complexes, oxygen 2 has two interacting groups, and oxygen 3 has either two or three interacting groups. Only oxygen 1 has the same interacting groups in all four complexes, and only five groups interact in the same site in all complexes; one group (K312 NZ) interacts in all complexes, but with two different oxygens.

	7a	**7b**	**8c**	**8d**
S270 OG	1	1	1	1
S306 OG	1	1	1	1
Water 1	1	1	1	1
Water 2	2	2	2	2
N311 ND2	2	2	2	
S270 N	3	3	3	3
K312 NZ	3	3	3	2
S269 OG	3	3		
Water 3				3

Paper V: Structure-Activity Relationships of the MEPicides: N-Acyl and O-linked Analogs of FR900098 as Inhibitors of Dxr from Mycobacterium tuberculosis and Yersinia pestis

The following supplementary figures are reproduced from Paper V[145].

Table 16. Percent Residual Activity Values from Yp and Mtb IspC Inhibition

Compound	Yp Trial 1	Yp Trial 2	Yp Average	(+/-) Yp 95% C. I.	Mtb Trial 1	Mtb Trial 2	Mtb Average	(+/-) Mtb 95% C.I.
DMSO (standardized)	100.00	100.00	100.00	0.00	100.00	100.00	100.00	0.00
Fosmidomycin (1)	4.67	1.99	3.33	2.62	5.14	4.29	4.71	0.83
FR900098 (2)	2.03	0.79	1.41	1.22	6.10	7.10	6.60	0.98
8a	36.14	37.18	36.66	1.02	43.67	50.61	47.14	6.80
8b	25.30	28.07	26.68	2.71	43.64	42.59	43.12	1.03
8c	84.91	82.62	83.77	2.25	80.15	73.17	76.66	6.85
8d	44.49	44.40	44.45	0.08	50.75	56.02	53.39	5.16
8e	1.77	2.08	1.93	0.31	72.69	67.38	70.04	5.20
8f	13.93	12.53	13.23	1.37	74.74	75.77	75.26	1.01
8g	89.25	82.12	85.69	6.98	49.57	47.64	48.61	1.89
8h	25.34	20.41	22.87	4.83	36.00	31.00	33.50	4.90
8i	73.34	72.34	72.84	0.98	58.49	56.10	57.30	2.35
8j	93.45	93.75	93.60	0.29	88.35	95.49	91.92	7.00
8k	69.06	71.31	70.18	2.20	79.33	62.27	70.80	16.72
8l	69.81	73.34	71.57	3.46	57.51	56.24	56.88	1.24
8m	49.41	49.44	49.43	0.03	58.06	63.15	60.60	4.99
8n	57.05	58.47	57.76	1.39	92.19	98.62	95.41	6.29
16a	88.88	88.77	88.82	0.11	98.26	108.99	103.62	10.52
16b	70.97	73.50	72.24	2.48	74.17	75.82	74.99	1.61
16c	89.54	84.11	86.83	5.32	76.47	77.93	77.20	1.43
16d	9.60	11.44	10.52	1.80	27.07	27.00	27.04	0.07
16e	20.32	17.72	19.02	2.54	36.21	39.97	38.09	3.68
16f	64.77	72.67	68.72	7.74	60.12	68.25	64.19	7.96
16g	23.05	21.01	22.03	2.00	57.85	61.96	59.91	4.03
16h	104.27	101.17	102.72	3.04	61.98	71.78	66.88	9.60
16i	15.60	14.42	15.01	1.16	30.47	27.20	28.83	3.20
16j	5.31	5.50	5.40	0.19	17.18	15.86	16.52	1.30
16k	13.99	11.91	12.95	2.04	35.22	38.34	36.78	3.06
16l	46.31	45.56	45.93	0.74	72.95	72.69	72.82	0.25

16m	40.29	39.73	40.01	0.54	65.60	66.42	66.01	0.81
16n	72.06	71.63	71.85	0.42	84.92	95.80	90.36	10.66
16o	47.53	52.32	49.93	4.69	78.13	83.52	80.83	5.28
16p	70.06	67.73	68.90	2.28	70.32	72.38	71.35	2.02
16q	31.88	38.39	35.14	6.38	40.38	42.81	41.59	2.38
16r	20.33	19.14	19.73	1.17	69.88	69.57	69.72	0.30

Table 17. MIC and IC_{50} values for N-acyl compounds against Mtb and E. coli

Compound	7H9 Mtb MIC (μg/mL)	GAST-Fe Mtb MIC (μg/mL)	E.coli IC50 (μg/Ml)
Isoniazid (INH)	0.01	0.02	N/A
Fosmidomycin (1)	>500	>500	
FR900098 (2)	>500	>500	
8a	>200	150	
7a	>200	150	
8b	>200	100	
7b	>200	50	
8c	>200	150	
7c	ND	ND	
8d	>200	25	>250
7d	200	37	>250
8e	>200	150	180.7
7e	>200	150	>250
8f	>200	150	
7f	>200	150	
8g	>200	150	
7g	400	≥400	
8h	>200	>200	>250
7h	200	200	
8i	>200	75	
7i	>200	150	
8j	>200	50	
7j	>200	37	
8k	>200	150	
7k	>200	150	
8l	>200	150	>250
7l	>200	25	213.6
8m	>200	50	
7m	>200	75	
8n	>200	150	
7n	>200	75	
11	200	50	
12	150	150	>250

Table 18. MIC and IC50 values for O-linked compounds against Mtb and E. coli

Compound	7H9 Mtb MIC (μg/mL)	GAST-Fe Mtb MIC (μg/mL)	E.coli IC50 (μg/mL)
Isoniazid (INH)	.01	.02	N/A
Fosmidomycin (1)	>500	>500	
FR900098 (2)	>500	>500	
14	>200	>200	
16b	>400	>400	
15b	400	200-400	
16c	>400	200-400	
15c	200	100	
16d	200	25	197.5
15d	400	200	
16e	>200	>200	>250
15e	200-400	N/A	>250
16f	>200	>200	
15f	200-400	N/A	
16g	>400	400	>250
15g	200-400	100	>250
16h	≥200	200	
15h	100-200	N/A	
16i	>400	200-400	
15i	400	100-200	
16j	≥200	≥200	191
15j	200	100	243.8
16k	25-50	25-50	>250
15k	200	100	169.7
16l	200-400	25-50	
15l	100	50	
16m	200-400	50	
15m	200-400	100	
16n	100-200	25-50	
15n	200-400	100-200	
16o	200-400	50-100	
15o	≥400	200-400	
16p	100	6.25-12.5	
15p	200-400	200	
16q	200	200	
15q	100	100	
16r	75	12.5	
15r	100	100	
17	12.5	6.25-12.5	119.1
18	12.5	6.25-12.5	
19	12.5	3.13-6.25	>250
20	18.75	4.7	
21	25	25	

Specific Aim 2

The Screening of the LOPAC^{1280} Library

Table 19. Primary Screen of the LOPAC^{1280} Library with YpIspC and FtIspD

Plate #	Compound (by Well #)	Compound Name	Compound #	Residual Activity YpIspC	Residual Activity FtIspD
1	A2	DL-alpha-Methyl-p-tyrosine	1	95.03891051	36.22677465
1	A3	6-Methoxy-1,2,3,4-tetrahydro-9H-pyrido[3,4b] indole	2	85.70038911	74.53072892
1	A4	Acetamide	3	81.3229572	59.00905193
1	A5	Amantadine hydrochloride	4	98.39494163	33.33968556
1	A6	GABA	5	91.09922179	60.26679371
1	A7	Gabaculine hydrochloride	6	89.49416342	42.68699381
1	A8	O-(Carboxymethyl)hydroxylamine hemihydrochloride	7	69.79571984	21.41972368
1	A9	(±)-2-Amino-7-phosphonoheptanoic acid	8	86.86770428	30.08099095
1	A10	N-Acetylprocainamide hydrochloride	9	75.77821012	74.64506908
1	A11	Actinonin	10	69.64980545	66.26965222
1	B2	N-Phenylanthranilic acid	11	-5.058365759	92.82515484
1	B3	S-(4-Nitrobenzyl)-6-thioguanosine	12	43.23929961	65.78370653
1	B4	N-(4-Aminobutyl)-5-chloro-2-naphthalenesulfonamide hydrochloride	13	89.20233463	17.9037637
1	B5	Aminophylline ethylenediamine	14	92.26653696	60.98141972
1	B6	3'-Azido-3'-deoxythymidine	15	94.16342412	52.72034302
1	B7	AC 915 oxalate	16	95.03891051	35.51214864
1	B8	5-(N,N-Dimethyl)amiloride hydrochloride	17	-36.72178988	39.62839447
1	B9	(±)-2-Amino-5-phosphonopentanoic acid	18	81.76070039	25.73606479
1	B10	Sodium Taurocholate	19	86.57587549	73.64459266
1	B11	Methotrexate	20	50.24319066	82.76322058
1	C2	S(-)-p-Bromotetramisole oxalate	21	84.97081712	59.35207242
1	C3	TMB-8 hydrochloride	22	102.0428016	42.94425917
1	C4	L-azetidine-2-carboxylic acid	23	85.40856031	35.45497856
1	C5	S-(p-Azidophenacyl)glutathione	24	91.39105058	91.33873273
1	C6	Acetyl-beta-methylcholine chloride	25	95.91439689	58.40876608
1	C7	AA-861	26	88.18093385	6.612672701
1	C8	Azathioprine	27	15.6614786	29.79514054
1	C9	L-732,138	28	65.41828794	87.93711291
1	C10	Amifostine	29	82.78210117	53.23487375
1	C11	Atropine methyl bromide	30	82.19844358	125.9552168

1	D2	5-Aminovaleric acid hydrochloride	31	90.6614786	59.66650786
1	D3	4-Aminopyridine	32	92.70428016	48.28966174
1	D4	p-Aminoclonidine hydrochloride	33	75.34046693	61.46736541
1	D5	Aminopterin	34	79.57198444	39.7141496
1	D6	5-azacytidine	35	-1.556420233	74.38780372
1	D7	9-Amino-1,2,3,4-tetrahydroacridine hydrochloride	36	90.07782101	38.97093854
1	D8	Acyclovir	37	78.25875486	50.40495474
1	D9	Acetylsalicylic acid	38	-59.3385214	73.3873273
1	D10	Acetazolamide	39	85.9922179	39.79990472
1	D11	Amperozide hydrochloride	40	82.19844358	186.7270129
1	E2	(±)-Nipecotic acid	41	124.5136187	60.26679371
1	E3	Atropine sulfate	42	119.6984436	51.49118628
1	E4	3-aminobenzamide	43	118.0933852	41.28632682
1	E5	N-Acetyl-5-hydroxytryptamine	44	117.8015564	27.96569795
1	E6	5-(N-Ethyl-N-isopropyl)amiloride	45	30.25291829	98.11338733
1	E7	Finasteride	46	117.8015564	171.0624107
1	E8	Amiprilose hydrochloride	47	120.8657588	13.70176274
1	E9	5-(N-Methyl-N-isobutyl)amiloride	48	-0.243190661	22.02000953
1	E10	Arecoline hydrobromide	49	116.4883268	68.55645545
1	E11	Aminoguanidine hemisulfate	50	112.4027237	72.58694616
1	F2	Azelaic acid	51	94.16342412	49.14721296
1	F3	Atropine methyl nitrate	52	98.83268482	66.44116246
1	F4	(±)-Norepinephrine (+)bitartrate	53	80.30155642	57.12243926
1	F5	Aurintricarboxylic acid	54	-26.6536965	8.470700333
1	F6	3-Aminopropionitrile fumarate	55	101.0214008	48.34683182
1	F7	1-Aminobenzotriazole	56	95.1848249	53.8351596
1	F8	Sandoz 58-035	57	97.37354086	38.7994283
1	F9	Acetylthiocholine chloride	58	88.03501946	51.291091
1	F10	A-315456	59	81.4688716	119.1519771
1	F11	Agmatine sulfate	60	83.36575875	157.884707
1	G2	Tryptamine hydrochloride	61	99.56225681	50.31919962
1	G3	Arcaine sulfate	62	93.14202335	64.09718914
1	G4	4-Amino-1,8-naphthalimide	63	79.13424125	33.48261077
1	G5	(±)-2-Amino-4-phosphonobutyric acid	64	98.97859922	44.68794664
1	G6	Apigenin	65	-143.2392996	61.21010005
1	G7	3-Amino-1-propanesulfonic acid sodium	66	54.47470817	42.14387804
1	G8	(±)-2-Amino-3-phosphonopropionic acid	67	89.05642023	29.68080038
1	G9	4-Androsten-4-ol-3,17-dione	68	93.72568093	60.58122916
1	G10	GR 4661	69	-129.0856031	29.10909957
1	G11	4-Aminobenzamidine dihydrochloride	70	59.28988327	63.81133873

1	H2	5-Fluoroindole-2-carboxylic acid	71	88.32684825	51.46260124
1	H3	1-Aminocyclopropanecarboxylic acid hydrochloride	72	108.1712062	65.44068604
1	H4	Reserpine	73	21.64396887	80.87660791
1	H5	N-arachidonylglycine	74	94.74708171	117.8656503
1	H6	W-7 hydrochloride	75	89.78599222	20.19056694
1	H7	Apomorphine hydrochloride hemihydrate	76	71.9844358	38.25631253
1	H8	L-Arginine	77	69.94163424	30.42401143
1	H9	2-(2-Aminoethyl)isothiourea dihydrobromide	78	89.78599222	54.92139114
1	H10	2-Hydroxysaclofen	79	91.24513619	58.2086708
1	H11	3-Aminopropylphosphonic acid	80	85.26264591	50.03334921
2	A2	N-Acetyl-L-Cysteine	81	58.84032114	98.63197425
2	A3	6-Aminohexanoic acid	82	91.59678858	59.20064378
2	A4	Altretamine	83	63.76449599	62.04399142
2	A5	Adenosine 3',5'-cyclic monophosphate	84	72.75646744	96.78111588
2	A6	(±)-AMT hydrochloride	85	85.17395183	45.35944206
2	A7	5'-N-Methyl carboxamidoadenosine	86	76.82426405	80.06974249
2	A8	1-Allyl-3,7-dimethyl-8-p-sulfophenylxanthine	87	37.64495986	79.21137339
2	A9	Acetohexamide	88	82.17662801	46.21781116
2	A10	cis-Azetidine-2,4-dicarboxylic acid	89	74.04103479	72.96137339
2	A11	2,3-Butanedione monoxime	90	33.79125781	89.61909871
2	B2	L-2-aminoadipic acid	91	83.46119536	48.49785408
2	B3	ATPO	92	80.24977698	74.59763948
2	B4	N-Acetyldopamine monohydrate	93	67.19000892	53.64806867
2	B5	L(-)-Norepinephrine bitartrate	94	93.95182872	54.5332618
2	B6	Paroxetine hydrochloride hemihydrate (MW = 374.83)	95	95.02230152	43.69635193
2	B7	PNU-37887A	96	60.12488849	72.93454936
2	B8	trans-(±)-ACPD	97	59.48260482	87.04399142
2	B9	SKF 97541 hydrochloride	98	48.34968778	36.05150215
2	B10	trans-Azetidine-2,4-dicarboxylic acid	99	79.60749331	39.64592275
2	B11	SB 222200	100	-138.1266726	42.06008584
2	C2	N-Acetyltryptamine	101	49.84834969	122.0761803
2	C3	Allopurinol	102	95.02230152	57.2693133
2	C4	Aminoguanidine hydrochloride	103	75.11150758	47.82725322
2	C5	5-(N,N-hexamethylene)amiloride	104	-158.4656557	30.92811159
2	C6	Antozoline hydrochloride	105	77.89473684	43.93776824
2	C7	(+)-N-Allylnormetazocine hydrochloride	106	65.90544157	74.78540773
2	C8	(±)-N-Allylnormetazocine hydrochloride	107	86.67261374	71.37875536
2	C9	cis-4-Aminocrotonic acid	108	71.47190009	28.46030043

2	C10	CBIQ	109	22.65834077	29.72103004
2	C11	1-benzoyl-5-methoxy-2-methylindole-3-acetic acid	110	-35.57537913	70.17167382
2	D2	Amiloride hydrochloride	111	-210.2765388	83.95922747
2	D3	Amitriptyline hydrochloride	112	89.88403211	53.94313305
2	D4	BW 284c51	113	71.25780553	59.73712446
2	D5	Aniracetam	114	85.8162355	71.24463519
2	D6	Amoxapine	115	65.26315789	47.88090129
2	D7	1-Amino-1-cyclohexanecarboxylic acid hydrochloride	116	7.457627119	51.26072961
2	D8	N6-2-(4-Aminophenyl)ethyladenosine	117	106.1552186	87.76824034
2	D9	AIDA	118	65.04906334	36.5611588
2	D10	p-Benzoquinone	119	59.48260482	49.81223176
2	D11	Amperozide hydrochloride	120	62.90811775	58.23497854
2	E2	(±)-Atenolol	121	84.53166815	87.68776824
2	E3	Amiodarone hydrochloride	122	-161.4629795	46.72746781
2	E4	Adenosine	123	71.90008921	72.45171674
2	E5	(±)-p-Aminoglutethimide	124	82.81891169	71.96888412
2	E6	1,3-Diethyl-8-phenylxanthine	125	4.032114184	55.472103
2	E7	Aminobenztropine	126	57.55575379	47.02253219
2	E8	Alaproclate hydrochloride	127	82.60481713	75.10729614
2	E9	Opipramol dihydrochloride	128	40.64228368	47.63948498
2	E10	A-77636 hydrochloride	129	24.58519179	20.06437768
2	E11	8-Bromo-cGMP sodium	130	62.26583408	72.3444206
2	F2	4-(2-Aminoethyl)benzenesulfonyl fluoride hydrochloride	131	75.75379126	120.7349785
2	F3	L-Aspartic acid	132	99.94647636	44.7693133
2	F4	(±)-HA-966	133	69.97323818	54.10407725
2	F5	8-(p-Sulfophenyl)theophylline	134	81.96253345	62.95600858
2	F6	Arecaidine propargyl ester hydrobromide	135	-293.9875112	61.21244635
2	F7	Psora-4	136	58.41213202	67.00643777
2	F8	gamma-Acetylinic GABA	137	-73.89830508	74.57081545
2	F9	ATPA	138	71.04371097	45.09120172
2	F10	H-89	139	79.82158787	68.64270386
2	F11	Agmatine sulfate	140	81.53434434	76.90450644
2	G2	L-allylglycine	141	104.2283675	120.5203863
2	G3	Ancitabine hydrochloride	142	100.1605709	67.99892704
2	G4	Astaxanthin	143	35.50401427	85.30042918
2	G5	Androsterone	144	90.95450491	71.16416309
2	G6	1,3-Dipropyl-8-p-sulfophenylxanthine	145	-231.6859946	69.39377682
2	G7	R(+)-Atenolol	146	52.41748439	67.83798283
2	G8	SB 200646 hydrochloride	147	68.90276539	65.47746781
2	G9	AB-MECA	148	71.25780553	52.6555794

2	G10	ARL 67156 trisodium salt	149	70.82961641	74.49034335
2	G11	Bromoenol lactone	150	15.16503122	262.6877682
2	H2	H-9 dihydrochloride	151	89.66993756	126.6899142
2	H3	Alprenolol hydrochloride	152	110.8652988	62.60729614
2	H4	N-(4-Amino-2-chlorophenyl)phthalimide	153	77.68064228	79.29184549
2	H5	Amsacrine hydrochloride	154	-1.534344335	55.55257511
2	H6	2-Methylthioadenosine triphosphate tetrasodium	155	63.76449599	114.1362661
2	H7	S(-)-Atenolol	156	68.90276539	82.45708155
2	H8	D(-)-2-Amino-7-phosphonoheptanoic acid	157	117.7163247	100.9388412
2	H9	Alloxazine	158	36.36039251	54.93562232
2	H10	Beclomethasone	159	70.18733274	72.53218884
2	H11	Benzamide	160	67.19000892	73.73927039
3	A2	3-Bromo-7-nitroindazole	161	-86.5221213	48.30023115
3	A3	Bumetanide	162	-24.99267507	57.31069919
3	A4	(±)-Baclofen	163	63.60972751	65.33472711
3	A5	Brefeldin A from Penicillium brefeldianum	164	71.87225315	46.96043933
3	A6	BP 897	165	62.02754175	67.61679009
3	A7	Bupropion hydrochloride	166	60.09375916	62.09566997
3	A8	BU224 hydrochloride	167	14.38617052	39.1867022
3	A9	Ciprofibrate	168	85.2329329	63.96548932
3	A10	CGP-7930	169	63.25813068	49.50751608
3	A11	Chlorprothixene hydrochloride	170	37.94315851	64.46607088
3	B2	(+)-Bromocriptine methanesulfonate	171	-117.9900381	76.90699489
3	B3	Betaine hydrochloride	172	59.03896865	48.49162998
3	B4	SB 202190	173	-86.69791972	170.0740566
3	B5	Budesonide	174	82.77175505	42.26380648
3	B6	(E)-5-(2-Bromovinyl)-2'-deoxyuridine	175	41.45912687	150.1833012
3	B7	(-)-Bicuculline methbromide, 1(S), 9(R)	176	-32.90360387	49.81669881
3	B8	B-HT 933 dihydrochloride	177	47.08467624	58.62104504
3	B9	6-Chloromelatonin	178	69.93847055	59.91666789
3	B10	CGP-13501	179	72.22384999	38.81862752
3	B11	Choline bromide	180	67.30149429	32.62025
3	C2	O6-benzylguanine	181	72.92704366	151.2139103
3	C3	Betaine aldehyde chloride	182	59.91796074	54.02747309
3	C4	Bay 11-7085	183	-1.611485497	60.32891153
3	C5	8-Bromo-cAMP sodium	184	70.64166423	35.47650947
3	C6	BRL 15572	185	12.45238793	38.42110687
3	C7	(±)-Bay K 8644	186	62.02754175	88.56760059
3	C8	(±)-Butaclamol hydrochloride	187	-3.72106651	52.37849855
3	C9	Carmustine	188	65.54351011	70.81167827

3	C10	CP55940	189	65.01611485	57.6493279
3	C11	Ceramide	190	66.24670378	49.16888738
3	D2	N-Bromoacetamide	191	69.58687372	73.07901827
3	D3	Benazoline oxalate	192	48.666862	25.0231887
3	D4	Betaxolol hydrochloride	193	76.44301201	44.89922115
3	D5	Benztropine mesylate	194	95.25344272	49.50751608
3	D6	Chloroethylclonidine dihydrochloride	195	81.54116613	34.60785324
3	D7	Bromoacetylcholine bromide	196	83.82654556	44.07473388
3	D8	BRL 37344 sodium	197	52.18283035	32.88526376
3	D9	PK 11195	198	78.02519777	48.13827829
3	D10	L-Cycloserine	199	87.51831234	40.541217
3	D11	CB 1954	200	-160.5332552	35.9034761
3	E2	(±)-Brompheniramine maleate	201	91.03428069	57.63460491
3	E3	BWB70C	202	82.94755347	36.84574727
3	E4	Benzamidine hydrochloride	203	67.12569587	46.28318193
3	E5	Ro 20-1724	204	90.68268386	124.1383372
3	E6	6-Fluoronorepinephrine hydrochloride	205	85.93612657	42.74966505
3	E7	BMY 7378 dihydrochloride	206	82.94755347	29.02784117
3	E8	BRL 54443 maleate	207	66.59830062	34.19560961
3	E9	Caffeic Acid	208	34.77878699	45.14951193
3	E10	ML-9	209	1.728684442	38.45055285
3	E11	Carcinine dihydrochloride	210	73.27864049	42.16074557
3	F2	Benzamil hydrochloride	211	-115.7046587	31.83993169
3	F3	5-Bromo-2'-deoxyuridine	212	92.79226487	34.87286701
3	F4	Betamethasone	213	63.60972751	52.12820777
3	F5	Bestatin hydrochloride	214	71.16905948	33.76864298
3	F6	Bromoacetyl alprenolol menthane	215	23.17609142	31.41296506
3	F7	R(+)-6-Bromo-APB hydrobromide	216	49.54585409	30.9123835
3	F8	BW 723C86	217	60.97275125	31.97243857
3	F9	Cilostazol	218	91.73747436	36.6985174
3	F10	(+)-Catechin Hydrate	219	92.26486962	36.22738181
3	F11	Corticosterone	220	79.60738353	47.93215648
3	G2	L-Buthionine-sulfoximine	221	102.8127747	54.48388569
3	G3	Bepridil hydrochloride	222	-168.0925872	29.69037558
3	G4	Buspirone hydrochloride	223	75.56401992	56.44204296
3	G5	Bretylium tosylate	224	60.97275125	50.24366543
3	G6	Benoxathian hydrochloride	225	89.97949018	50.83258491
3	G7	BTCP hydrochloride	226	91.91327278	49.19833336
3	G8	Chlorambucil	227	86.81511866	38.47999882
3	G9	Caffeine	228	90.85848227	35.35872558
3	G10	Chlorpropamide	229	84.1781424	37.90580233
3	G11	Carboplatin	230	74.68502783	52.15765374

3	H2	DL-Buthionine-[S,R]-sulfoximine	231	167.1549956	41.05652155
3	H3	(+)-Brompheniramine maleate	232	120.9200117	39.02474934
3	H4	Benserazide hydrochloride	233	5.420451216	52.6582353
3	H5	BRL 50481	234	93.49545854	41.23319739
3	H6	Phenoxybenzamine hydrochloride	235	73.80603575	45.075897
3	H7	DAPH	236	-141.1954292	12.71477157
3	H8	Citicoline sodium	237	88.92469968	35.7856922
3	H9	Cyclophosphamide monohydrate	238	101.9337826	36.03598298
3	H10	1-(4-Chlorobenzyl)-5-methoxy-2-methylindole-3-acetic acid	239	88.57310284	28.4241987
3	H11	Cortisone	240	78.55259303	37.46411272
4	A2	Chelerythrine chloride	241	-224.1875	-6.705183045
4	A3	Cyclosporin A	242	60.0625	145.4863619
4	A4	Carbachol	243	69.4375	70.02388756
4	A5	Cephalexin hydrate	244	57.8125	56.72462641
4	A6	1-(3-Chlorophenyl)piperazine dihydrochloride	245	83.5	36.89239487
4	A7	Cyproheptadine hydrochloride	246	71.3125	75.35692462
4	A8	CB34	247	34.9375	59.35781345
4	A9	Cantharidin	248	80.875	68.55730237
4	A10	Chlorpromazine hydrochloride	249	35.3125	54.29142825
4	A11	Centrophenoxine hydrochloride	250	43	53.29148381
4	B2	1-(2-Chlorophenyl)-1-(4-chlorophenyl)-2,2-dichloroethane	251	34	67.0573857
4	B3	D-Cycloserine	252	80.3125	48.12510416
4	B4	Chlorzoxazone	253	58.375	86.45630798
4	B5	Chlorothiazide	254	72.25	55.05805233
4	B6	SB 204741	255	62.875	48.75840231
4	B7	5'-(N-Cyclopropyl)carboxamidoadenosine	256	69.4375	84.35642464
4	B8	Cefaclor	257	19.1875	65.4241431
4	B9	Citalopram hydrobromide	258	81.4375	47.49180601
4	B10	Cefsulodin sodium salt hydrate	259	56.875	45.29192823
4	B11	Clemastine fumarate	260	75.4375	53.92478196
4	C2	(±)-Chlorpheniramine maleate	261	51.25	72.29042831
4	C3	8-(4-Chlorophenylthio)-cAMP sodium	262	78.8125	65.55746903
4	C4	L-Cysteinesulfinic Acid	263	52.1875	103.688684
4	C5	(+)-Chlorpheniramine maleate	264	80.875	42.82539859
4	C6	Ceftriaxone sodium	265	55.1875	55.49136159
4	C7	Cefmetazole sodium	266	81.8125	81.28992834
4	C8	DL-Cycloserine	267	16.75	58.25787456
4	C9	Clonidine hydrochloride	268	89.5	58.75784679
4	C10	Caffeic acid phenethyl ester	269	-293.5625	55.89133937
4	C11	beta-Chloro-L-alanine hydrochloride	270	67	69.69057275

4	D2	Cortisone 21-acetate	271	22.9375	62.62429865
4	D3	Calmidazolium chloride	272	-11.9375	-4.305316371
4	D4	9-cyclopentyladenine	273	85.1875	65.65746347
4	D5	Cefazolin sodium	274	61.75	42.2587634
4	D6	4-Chloromercuribenzoic acid	275	-22.4375	60.95772457
4	D7	Clozapine	276	22.1875	85.58968946
4	D8	McN-A-343	277	15.625	60.02444309
4	D9	Cefotaxime sodium	278	87.8125	62.72429309
4	D10	Cephapirin sodium	279	36.25	49.22504305
4	D11	Pyrocatechol	280	48.4375	63.05760791
4	E2	Cephalosporin C zinc salt	281	49.9375	79.55669129
4	E3	GR 113808	282	119.875	52.95816899
4	E4	Cephalothin sodium	283	83.3125	99.4555858
4	E5	Clemizole hydrochloride	284	42.0625	73.3903672
4	E6	(-)-Cotinine	285	64.1875	52.99150047
4	E7	(±)-p-Chlorophenylalanine	286	68.125	59.55780234
4	E8	N-(2-[4-(4-Chlorophenyl)piperazin-1-yl]ethyl)-3-methoxybenzamide	287	30.8125	57.12460419
4	E9	Cilostamide	288	95.6875	55.75801344
4	E10	Cephradine	289	29.125	44.82528748
4	E11	Z-L-Phe chloromethyl ketone	290	28.75	61.95766902
4	F2	CGP-74514A hydrochloride	291	65.5	52.05821899
4	F3	Carbamazepine	292	77.875	76.32353758
4	F4	Cimetidine	293	94.75	100.2555414
4	F5	2-Chloroadenosine	294	56.6875	42.2587634
4	F6	CL 316,243	295	65.125	61.55769124
4	F7	Chloroquine diphosphate	296	-45.125	261.0466085
4	F8	Cystamine dihydrochloride	297	63.0625	56.05799678
4	F9	Chelidamic acid	298	66.8125	80.18998945
4	F10	DSP-4 hydrochloride	299	73.375	44.69196156
4	F11	CPCCOEt	300	55.1875	52.3915338
4	G2	Cyproterone acetate	301	66.4375	97.88900617
4	G3	Captopril	302	179.3125	63.19093384
4	G4	Cyclobenzaprine hydrochloride	303	81.4375	90.48941725
4	G5	Bethanechol chloride	304	53.6875	44.62529859
4	G6	7-Chloro-4-hydroxy-2-phenyl-1,8-naphthyridine	305	32.3125	65.15749125
4	G7	Clofibrate	306	55.5625	82.6231876
4	G8	Clomipramine hydrochloride	307	21.625	46.62518749
4	G9	N6-Cyclopentyladenosine	308	47.6875	69.32392645
4	G10	Cinoxacin	309	-208.0625	52.02488751
4	G11	Colchicine	310	-151.0625	57.59124493
4	H2	DL-p-Chlorophenylalanine methyl ester	311	110.875	54.42475418

		hydrochloride			
4	H3	CNS-1102	312	101.875	47.6917949
4	H4	Carbetapentane citrate	313	131.3125	88.92283762
4	H5	Cinnarizine	314	56.6875	64.39086717
4	H6	Clotrimazole	315	51.0625	65.09082829
4	H7	Cytosine-1-beta-D-arabinofuranoside hydrochloride	316	110.5	72.39042275
4	H8	Calcimycin	317	70.75	79.22337648
4	H9	Cantharidic Acid	318	69.4375	68.55730237
4	H10	Carisoprodol	319	74.5	50.29165046
4	H11	L-Canavanine sulfate	320	76.1875	68.55730237
5	A2	Cyclothiazide	321	71.33272339	64.51290458
5	A3	(±)-CPP	322	91.46081122	51.97816917
5	A4	CGS-21680 hydrochloride	323	72.61360171	40.85284181
5	A5	CGS-15943	324	48.82586154	40.792867
5	A6	Chloro-IB-MECA	325	75.17535834	111.6830931
5	A7	Debrisoquin sulfate	326	77.92009759	50.50878631
5	A8	Diltiazem hydrochloride	327	74.99237572	52.6978669
5	A9	(S)-3,5-Dihydroxyphenylglycine	328	79.74992376	87.39329482
5	A10	Phenytoin sodium	329	86.52028057	27.29853462
5	A11	Daphnetin	330	-87.49618786	31.70668319
5	B2	N6-Cyclohexyladenosine	331	78.10308021	79.20673317
5	B3	CGS-12066A maleate	332	-213.5712107	88.02303033
5	B4	Y-27632 dihydrochloride	333	93.47362001	37.73415166
5	B5	2-Chloro-2-deoxy-D-glucose	334	90.54589814	31.01697287
5	B6	WB-4101 hydrochloride	335	91.27782861	43.46174607
5	B7	2',3'-didehydro-3'-deoxythymidine	336	87.43519366	68.89106575
5	B8	Dextromethorphan hydrobromide monohydrate	337	84.14150656	44.12146898
5	B9	Dequalinium dichloride	338	-80.1768832	18.54221227
5	B10	Doxepin hydrochloride	339	83.59255871	28.49803083
5	B11	DM 235	340	78.65202806	45.59085184
5	C2	(S)-(+)-Camptothecin	341	-14.3031412	51.22848404
5	C3	2-Cyclooctyl-2-hydroxyethylamine hydrochloride	342	90.36291552	41.15271586
5	C4	1-(m-Chlorophenyl)-biguanide hydrochloride	343	92.37572431	28.49803083
5	C5	4'-Chloro-3-alpha-(diphenylmethoxy)tropane hydrochloride	344	93.65660262	25.70920214
5	C6	DNQX	345	-153.7358951	47.00025989
5	C7	Droperidol	346	90.72888076	72.24965514
5	C8	SB 203186	347	85.60536749	26.0990384
5	C9	Doxylamine succinate	348	90.72888076	78.00723696
5	C10	S(-)-Pindolol	349	72.24763647	39.29349673

5	C11	5,5-Dimethyl-1-pyrroline-N-oxide	350	80.48185422	46.94028508
5	D2	CK2 Inhibitor 2	351	15.70600793	57.64578877
5	D3	5-Carboxamidotryptamine maleate	352	80.84781946	41.33264029
5	D4	2-Chloroadenosine triphosphate tetrasodium	353	83.77554132	114.3819596
5	D5	Cirazoline hydrochloride	354	90.54589814	35.42512145
5	D6	Dihydroouabain	355	86.33729796	83.13508327
5	D7	L-3,4-Dihydroxyphenylalanine methyl ester hydrochloride	356	83.40957609	69.58077607
5	D8	Dihydroergotamine methanesulfonate	357	76.82220189	39.71332041
5	D9	Desipramine hydrochloride	358	85.97133272	65.35255193
5	D10	(-)-alpha-Methylnorepinephrine	359	53.58340958	39.59337078
5	D11	2',3'-dideoxycytidine	360	68.40500152	42.5021491
5	E2	(+)-cis-Dioxolane iodide	361	76.27325404	71.14012115
5	E3	7-Chlorokynurenic acid	362	-146.0506252	56.23638072
5	E4	(+)-Cyclazocine	363	85.97133272	35.48509626
5	E5	CGP 20712A methanesulfonate	364	16.80390363	36.05485696
5	E6	Dobutamine hydrochloride	365	80.11588899	46.61042362
5	E7	1,4-Dideoxy-1,4-imino-D-arabinitol	366	74.80939311	78.7869095
5	E8	Diphenyleneiodonium chloride	367	90.91186337	18.51222487
5	E9	trans-Dehydroandrosterone	368	93.29063739	85.6240379
5	E10	Dilazep hydrochloride	369	83.40957609	52.48795506
5	E11	Diacylglycerol Kinase Inhibitor II	370	-119.3351632	12.90458008
5	F2	OXA-22 iodide	371	91.09484599	52.39799284
5	F3	(±)-CGP-12177A hydrochloride	372	85.23940226	30.98698547
5	F4	Capsazepine	373	75.72430619	30.56716179
5	F5	(2S,1'S,2'S)-2-(carboxycyclopropyl)glycine	374	92.19274169	17.94246417
5	F6	Dihydrokainic acid	375	78.46904544	58.51542352
5	F7	2,4-Dinitrophenyl 2-fluoro-2-deoxy-beta-D-glucopyranoside	376	48.45989631	56.89610364
5	F8	Diphenhydramine hydrochloride	377	84.87343702	29.93742628
5	F9	5,5-Diphenylhydantoin	378	85.97133272	82.26544851
5	F10	Dehydroisoandrosterone 3-sulfate sodium	379	66.94114059	43.88156974
5	F11	Dihydrexidine hydrochloride	380	68.22201891	40.28308111
5	G2	8-Cyclopentyl-1,3-dipropylxanthine	381	84.14150656	62.77363507
5	G3	S-(-)-Carbidopa	382	86.33729796	98.69854661
5	G4	Chlormezanone	383	96.76730711	82.59530997
5	G5	CNQX disodium	384	-80.1768832	26.48887467
5	G6	Decamethonium dibromide	385	6.007929247	56.02646888
5	G7	D-ribofuranosylbenzimidazole	386	93.47362001	49.78908858
5	G8	2,3-Butanedione	387	89.08203721	35.21520961
5	G9	N^G,N^G-Dimethylarginine hydrochloride	388	77.92009759	75.9680934

5	G10	1,7-Dimethylxanthine	389	69.50289722	37.9740509
5	G11	N-Methyldopamine hydrochloride	390	70.41781031	75.63823194
5	H2	8-Cyclopentyl-1,3-dimethylxanthine	391	77.18816712	72.30962996
5	H3	(±)-Chloro-APB hydrobromide	392	66.75815797	47.36010875
5	H4	8-(3-Chlorostyryl)caffeine	393	-30.7715767	78.27712361
5	H5	CX 546	394	98.04818542	28.8878671
5	H6	P1,P4-Di(adenosine-5')tetraphosphate triammonium	395	93.65660262	69.94062494
5	H7	Dequalinium analog, C-14 linker	396	-103.5986581	4.268207353
5	H8	N,N,N',N'-Tetramethylazodicarboxamide	397	57.79200976	26.27896284
5	H9	Clodronic acid	398	78.28606282	98.00883629
5	H10	2,3-Dimethoxy-1,4-naphthoquinone	399	17.16986886	32.39639351
5	H11	1,1-Dimethyl-4-phenyl-piperazinium iodide	400	80.29887161	33.62587713
6	A2	PD 169316	401	-124.3257821	33.67869774
6	A3	Disopyramide	402	92.50269687	53.30098848
6	A4	Dephostatin	403	5.798274002	47.0436202
6	A5	Diazoxide	404	87.2437972	47.92781355
6	A6	Doxycycline hydrochloride	405	-85.08629989	71.1208851
6	A7	R(-)-N-Allylnorapomorphine hydrobromide	406	55.82524272	64.04733835
6	A8	4-DAMP methiodide	407	70.65803668	74.86170309
6	A9	N,N-Dipropyl-5-carboxamidotryptamine maleate	408	95.73894283	108.6650948
6	A10	Dihydroergocristine methanesulfonate	409	20.76591154	99.85716877
6	A11	Enoximone	410	-194.0399137	81.08506393
6	B2	Disopyramide phosphate	411	85.35598706	599.8685046
6	B3	Daidzein	412	-4.449838188	72.27713793
6	B4	3',4'-Dichlorobenzamil	413	-58.52211435	30.27795411
6	B5	3,4-Dihydroxyphenylacetic acid	414	99.11003236	50.27432665
6	B6	6,7-ADTN hydrobromide	415	81.98489752	54.45724132
6	B7	JHW 007 hydrochloride	416	87.51348436	42.01051963
6	B8	1,3-Dipropyl-7-methylxanthine	417	75.91693635	101.7955926
6	B9	6,7-Dichloroquinoxaline-2,3-dione	418	-54.20711974	101.6595629
6	B10	2,6-Diamino-4-pyrimidinone	419	37.35167206	51.39657205
6	B11	Etoposide	420	79.15318231	91.21927995
6	C2	Demeclocycline hydrochloride	421	3.910463862	82.75142831
6	C3	Dubinidine	422	93.7162891	79.31667725
6	C4	3-deazaadenosine	423	78.61380798	47.7917838
6	C5	Dantrolene sodium	424	-63.2416397	64.99954657
6	C6	R(-)-Apocodeine hydrochloride	425	76.45631068	52.51881745
6	C7	Icilin	426	61.62351672	60.4425501
6	C8	Domperidone	427	68.50053937	54.59327106

6	C9	3,7-Dimethyl-I-propargylxanthine	428	85.08629989	95.81028385
6	C10	DL-alpha-Difluoromethylornithine hydrochloride	429	30.47464941	51.87267616
6	C11	ET-18-OCH3	430	93.0420712	199.3969348
6	D2	Diethylenetriaminepentaacetic acid	431	96.81769148	60.23850549
6	D3	Dicyclomine hydrochloride	432	105.4476807	86.62827605
6	D4	(Z)-Guggleste rone	433	91.69363538	91.59336175
6	D5	DCEBIO	434	96.81769148	45.88736737
6	D6	R(-)-Propylnorapomorphine hydrochloride	435	63.64617044	76.76611952
6	D7	(±)-SKF-38393 hydrochloride	436	84.14239482	97.1705813
6	D8	Propofol	437	82.92880259	111.7937789
6	D9	5,7-Dichlorokynurenic acid	438	-4.854368932	123.2882924
6	D10	SCH-28080	439	40.58791802	53.64106285
6	D11	Etazolate hydrochloride	440	27.37324703	184.2296182
6	E2	Diclofenac sodium	441	92.36785329	74.35159155
6	E3	3,4-Dichloroisocoumarin	442	36.27292341	110.0934071
6	E4	Danazol	443	71.46709817	64.31939784
6	E5	1-Deoxynojirimycin hydrochloride	444	100.4584682	48.23388048
6	E6	R(-)-2,10,11-Trihydroxyaporphine hybrobromide	445	60.00539374	46.97560533
6	E7	GBR-12909 dihydrochloride	446	83.19848975	65.44164324
6	E8	Dextrorphan D-tartrate	447	73.08522114	97.9187449
6	E9	4-Diphenylacetoxy-N-(2-chloroethyl)piperidine hydrochloride	448	91.5587918	152.0585835
6	E10	S(-)-DS 121 hydrochloride	449	47.46494067	70.33871407
6	E11	7-Cyclopentyl-5-(4-phenoxy)phenyl-7H-pyrrolo[2,3-d]pyrimidin-4-ylamine	450	-50.8360302	80.13285572
6	F2	DL-erythro-Dihydrosphingosine	451	92.77238403	61.12269883
6	F3	DBO-83	452	88.99676375	93.12369638
6	F4	N,N-Dihexyl-2-(4-fluorophenyl)indole-3-acetamide	453	-30.07011866	46.70354584
6	F5	L-3,4-Dihydroxyphenylalanine	454	82.52427184	41.80647502
6	F6	R(-)-2,10,11-Trihydroxy-N-propylnoraporphine hydrobromide	455	53.802589	51.83866872
6	F7	R(+)-SCH-23390 hydrochloride	456	97.22222222	47.85979868
6	F8	R(+)-Butylindazone	457	78.34412082	87.17239503
6	F9	1,10-Diaminodecane	458	90.48004315	107.0667453
6	F10	Vanillic acid diethylamide	459	51.91477886	64.11535322
6	F11	Emetine dihydrochloride hydrate	460	79.69255663	89.45089326
6	G2	R-(-)-Desmethyldeprenyl hydrochloride	461	103.5598706	70.91684048
6	G3	7,7-Dimethyl-(5Z,8Z)-eicosadienoic acid	462	100.3236246	131.9601886
6	G4	(R,R)-cis-Diethyl tetrahydro-2,8-chrysenediol	463	-193.3656958	30.5500136
6	G5	Dipyridamole	464	61.7583603	62.55101115
6	G6	Dipropyldopamine hydrobromide	465	93.58144552	65.64568786

6	G7	(±)-DOI hydrochloride	466	96.54800431	69.6245579
6	G8	Eliprodil	467	69.71413161	88.05658837
6	G9	Dihydro-beta-erythroidine hydrobromide	468	103.1553398	111.6577492
6	G10	Epibestatin hydrochloride	469	47.19525351	60.8166319
6	G11	5'-N-Ethylcarboxamidoadenosine	470	84.2772384	107.5088419
6	H2	2,2'-Bipyridyl	471	102.0765912	67.48208942
6	H3	(±) trans-U-50488 methanesulfonate	472	106.7961165	74.24956924
6	H4	SP600125	473	33.03667745	53.84510746
6	H5	Doxazosin mesylate	474	-73.08522114	78.53450621
6	H6	(+)-Butaclamol hydrochloride	475	76.72599784	71.76702639
6	H7	(±)-2,3-Dichloro-alpha-methylbenzylamine hydrochloride	476	100.5933118	74.52162873
6	H8	3,5-Dinitrocatechol	477	19.14778857	12.59408724
6	H9	(R)-(-)-DOI hydrochloride	478	15.10248112	102.5097488
6	H10	Etodolac	479	-0.539374326	102.7137934
6	H11	E-64	480	79.42286947	68.12823071
7	A2	SB 415286	481	51.83459522	44.55385913
7	A3	rac-2-Ethoxy-3-octadecanamido-1-propylphosphocholine	482	108.0372743	149.6521818
7	A4	(-)-Physostigmine	483	100.1747234	210.2719306
7	A5	S-(-)-Eticlopride hydrochloride	484	62.4635993	109.8111844
7	A6	R-(-)-Fluoxetine hydrochloride	485	103.960396	185.9698256
7	A7	Fenofibrate	486	97.11706465	270.5905381
7	A8	Forskolin	487	102.3587653	131.071762
7	A9	Fexofenadine hydrochloride	488	100.9027373	66.32637697
7	A10	N-(3,3-Diphenylpropyl)glycinamide	489	99.73791497	51.02839763
7	A11	L-Canavanine	490	97.11706465	66.74797482
7	B2	S-Ethylisothiourea hydrobromide	491	81.24635993	55.15403379
7	B3	N-Ethylmaleimide	492	98.86429819	100.9275153
7	B4	NBI 27914	493	90.85614444	232.7671876
7	B5	(S)-ENBA	494	92.74898078	139.8048604
7	B6	Fluvoxamine maleate	495	103.3779849	96.83199325
7	B7	Fenspiride hydrochloride	496	101.0483401	165.4621014
7	B8	Famotidine	497	99.73791497	114.268076
7	B9	Formoterol	498	98.86429819	55.42506098
7	B10	Glibenclamide	499	91.72976121	63.9473605
7	B11	GW1929	500	50.66977286	57.3824796
7	C2	(-)-Ephedrine hemisulfate	501	-62.17239371	100.5962598
7	C3	(-)-Epinephrine bitartrate	502	94.05940594	106.7997711
7	C4	beta-Estradiol	503	95.07862551	236.8928238
7	C5	erythro-9-(2-Hydroxy-3-nonyl)adenine hydrochloride	504	98.7186954	134.2939742
7	C6	1-(4-Fluorobenzyl)-5-methoxy-2-	505	93.04018637	38.62137501

		methylindole-3-acetic acid			
7	C7	Flumazenil	506	106.2900408	139.8952028
7	C8	FSCPX	507	100.1747234	112.2805433
7	C9	Felodipine	508	27.81013395	83.22040534
7	C10	GW2974	509	-205.2999418	53.2267293
7	C11	GW5074	510	-33.77984857	14.65052549
7	D2	Edrophonium chloride	511	90.56493885	73.82479598
7	D3	Ethylene glycol-bis(2-aminoethylether)-N,N,N',N'-tetraacetic acid	512	93.18578917	89.21311772
7	D4	Estrone	513	107.6004659	242.9156503
7	D5	Opipramol dihydrochloride	514	80.22714036	140.6480561
7	D6	Furegrelate sodium	515	90.41933605	63.13427892
7	D7	Foliosidine	516	92.89458358	104.3002981
7	D8	Farnesylthiosalicylic acid	517	71.34536983	42.20495679
7	D9	Fluspirilene	518	76.00465929	37.20601078
7	D10	Guanfacine hydrochloride	519	95.3698311	51.51022375
7	D11	Genistein	520	-46.44729179	76.05324179
7	E2	Efaroxan hydrochloride	521	70.32615026	67.8320836
7	E3	(±)-Epinephrine hydrochloride	522	97.40827024	248.6373355
7	E4	Methyl beta-carboline-3-carboxylate	523	25.91729761	219.0050291
7	E5	Felbamate	524	71.78217822	144.2918662
7	E6	Fiduxosin hydrochloride	525	-105.8532324	50.8175987
7	E7	Fusaric acid	526	103.3779849	86.86421538
7	E8	Flunarizine dihydrochloride	527	41.20559115	78.49248652
7	E9	cis-(Z)-Flupenthixol dihydrochloride	528	85.6144438	90.74893848
7	E10	L-Glutamic acid hydrochloride	529	101.1939429	87.73752522
7	E11	GW7647	530	91.43855562	64.79055621
7	F2	Ellipticine	531	-64.50203844	32.11672238
7	F3	Ethosuximide	532	103.8147932	268.5728913
7	F4	N-Methyl-beta-carboline-3-carboxamide	533	27.37332557	156.7290029
7	F5	Fusidic acid sodium	534	92.74898078	137.3957298
7	F6	Furosemide	535	36.98311008	81.05218779
7	F7	5-Fluorouracil	536	107.4548631	46.81241907
7	F8	5-fluoro-5'-deoxyuridine	537	103.6691904	75.75210046
7	F9	Furafylline	538	73.52941176	91.56202006
7	F10	Ganciclovir	539	99.44670938	65.03146927
7	F11	alpha-Guanidinoglutaric acid	540	98.13628422	52.17273466
7	G2	Ebselen	541	-54.16423995	78.07088867
7	G3	Endothall	542	96.53465347	252.4618303
7	G4	Methyl 6,7-dimethoxy-4-ethyl-beta-carboline-3-carboxylate	543	5.387303436	165.7331286
7	G5	Fenoterol hydrobromide	544	100.9027373	168.4132864

7	G6	p-Fluoro-L-phenylalanine	545	97.55387303	77.13735056
7	G7	Flecainide acetate	546	107.7460687	73.64411118
7	G8	Flupirtine maleate	547	30.72218987	80.6908182
7	G9	FPL 64176	548	61.44437973	94.63366158
7	G10	L-Glutamine	549	97.99068142	100.7167164
7	G11	Gallamine triethiodide	550	93.04018637	58.4063601
7	H2	rac-2-Ethoxy-3-hexadecanamido-1-propylphosphocholine	551	102.9411765	124.1153974
7	H3	Emodin	552	50.66977286	247.4026561
7	H4	(-)-Eseroline fumarate	553	41.20559115	142.6054747
7	H5	S-(+)-Fluoxetine hydrochloride	554	92.60337798	158.2347095
7	H6	Fluphenazine dihydrochloride	555	77.16948165	102.3428795
7	H7	Fenoldopam bromide	556	79.64472918	78.04077454
7	H8	Flutamide	557	35.81828771	72.25886108
7	H9	Fluoxetine hydrochloride	558	96.09784508	98.9098684
7	H10	Guanidinyl-naltrindole di-trifluoroacetate	559	86.05125218	56.35859909
7	H11	GBR-12935 dihydrochloride	560	16.16191031	41.03050562
8	A2	Isoguvacine hydrochloride	561	88.09119088	49.89848347
8	A3	GYKI 52895	562	-25.89741026	64.97058092
8	A4	MHPG piperazine	563	92.89071093	70.31573713
8	A5	DL-threo-beta-hydroxyaspartic acid	564	88.24117588	90.04930803
8	A6	17alpha-hydroxyprogesterone	565	88.24117588	57.69868236
8	A7	L-Histidine hydrochloride	566	88.09119088	87.4388829
8	A8	L-Hyoscyamine	567	81.79182082	70.00497224
8	A9	4-Hydroxybenzhydrazide	568	82.69173083	41.69429021
8	A10	R-(+)-7-Hydroxy-DPAT hydrobromide	569	77.44225577	63.29245048
8	A11	Iodoacetamide	570	73.69263074	72.24247949
8	B2	Guvacine hydrochloride	571	99.34006599	78.05378304
8	B3	GR-89696 fumarate	572	94.39056094	95.08369935
8	B4	Hypotaurine	573	93.64063594	71.68310268
8	B5	4-Methoxy-3-hydroxyphenethylamine hydrochloride	574	91.54084592	83.15032734
8	B6	1,3,5-tris(4-hydroxyphenyl)-4-propyl-1H-pyrazole	575	3.799620038	2.972984172
8	B7	(±)-8-Hydroxy-DPAT hydrobromide	576	85.39146085	65.25026933
8	B8	Hydroquinone	577	84.04159584	65.56103423
8	B9	Hemicholinium-3	578	34.69653035	55.21256319
8	B10	GR 125487 sulfamate salt	579	80.59194081	57.69868236
8	B11	HA-100	580	77.29227077	74.13814536
8	C2	(±)-AMPA hydrobromide	581	100.989901	85.20137565
8	C3	Gabapentin	582	90.64093591	91.19913815
8	C4	Haloperidol	583	88.69113089	80.44667274
8	C5	Hydroxytacrine maleate	584	-15.39846015	95.02154637

8	C6	1-(4-Hydroxybenzyl)imidazole-2-thiol	585		
8	C7	Dopamine hydrochloride	586	96.64033597	75.10151653
8	C8	BU99006	587	10.99890011	29.60553576
8	C9	HA-1004 hydrochloride	588	82.69173083	44.49117428
8	C10	IEM-1460	589	75.34246575	59.90511312
8	C11	Ipratropium bromide	590	75.94240576	66.27579349
8	D2	Muscimol hydrobromide	591	105.0394961	71.96279108
8	D3	DL-Homatropine hydrobromide	592	98.44015598	69.35236596
8	D4	Hydralazine hydrochloride	593	63.79362064	80.60205519
8	D5	Hydrocortisone	594	102.639736	75.75412281
8	D6	Histamine dihydrochloride	595	90.79092091	59.00389492
8	D7	Hydroxyurea	596	84.64153585	70.25358416
8	D8	3-Hydroxybenzylhydrazine dihydrochloride	597	51.34486551	51.76307284
8	D9	BRL 50481	598	69.6430357	75.13259302
8	D10	Ibudilast	599	16.54834517	72.55324439
8	D11	Idarubicin	600	49.24507549	110.6219441
8	E2	Guanabenz acetate	601	101.889811	82.34233861
8	E3	(±)-Vanillylmandelic acid	602	68.59314069	68.66868319
8	E4	4-Imidazolemethanol hydrochloride	603	100.089991	46.26253418
8	E5	Lithium Chloride	604	83.74162584	79.35899561
8	E6	Harmane	605	6.349365063	64.47335709
8	E7	(+)-Hydrastine	606	83.59164084	62.57769122
8	E8	Serotonin hydrochloride	607	86.74132587	83.98939256
8	E9	Hexahydro-sila-difenidol hydrochloride, p-fluoro analog	608	95.14048595	66.8351703
8	E10	Imidazole-4-acetic acid hydrochloride	609	70.69293071	61.67647303
8	E11	Metolazone	610	42.19578042	91.38559708
8	F2	gamma-D-Glutamylaminomethylsulfonic acid	611	103.089691	69.13483053
8	F3	6-Hydroxymelatonin	612	72.04279572	71.18587884
8	F4	Hexamethonium dichloride	613	94.54054595	59.90511312
8	F5	Hydrochlorothiazide	614	85.39146085	88.30902461
8	F6	NG-Hydroxy-L-arginine acetate	615	93.79062094	78.30239496
8	F7	(±)-7-Hydroxy-DPAT hydrobromide	616	91.39086091	72.61539736
8	F8	L-165,041	617	55.84441556	84.89061076
8	F9	Histamine, R(-)-alpha-methyl-, dihydrochloride	618	99.34006599	85.60537002
8	F10	Indirubin-3'-oxime	619	Not available	Not available
8	F11	SB 228357	620	51.79482052	57.79191183
8	G2	Glipizide	621	104.739526	60.71310185
8	G3	Hexamethonium bromide	622	98.14018598	81.84511478
8	G4	Hydrocortisone 21-hemisuccinate sodium	623	108.3391661	77.52548272

8	G5	SB 218795	624	25.54744526	68.17145935
8	G6	Retinoic acid p-hydroxyanilide	625	-226.1273873	41.35244883
8	G7	MHPG sulfate potassium	626	91.24087591	78.20916549
8	G8	5-Hydroxy-L-tryptophan	627	89.8910109	84.26908096
8	G9	5-hydroxydecanoic acid sodium	628	93.79062094	82.59095053
8	G10	NSC 95397	629	60.79392061	62.70199718
8	G11	IMID-4F hydrochloride	630	76.54234577	54.43565095
8	H2	GYKI 52466 hydrochloride	631	54.49455054	62.6398442
8	H3	4-Hydroxy-3-methoxyphenylacetic acid	632	92.89071093	81.87619127
8	H4	6-Hydroxy-DL-DOPA	633	-84.39156084	17.98292865
8	H5	Hispidin	634	-44.94550545	87.03488854
8	H6	HE-NECA	635	86.29137086	81.75188531
8	H7	5-Hydroxyindolacetic acid	636	96.94030597	83.49216872
8	H8	Hydroxylamine hydrochloride	637	91.54084592	82.0626502
8	H9	R-(+)-8-Hydroxy-DPAT hydrobromide	638	100.239976	67.33239413
8	H10	Imazodan	639	70.2429757	67.51885307
8	H11	R(-)-Isoproterenol (+)-bitartrate	640	75.49245075	72.89508577
9	A2	ML-7	641	97.01415966	126.7554412
9	A3	3-Isobutyl-1-methylxanthine	642	93.16642725	69.81200694
9	A4	Iproniazid phosphate	643	86.08659963	838.4434622
9	A5	m-Iodobenzylguanidine hemisulfate	644	81.93104864	57.13926034
9	A6	Imetit dihydrobromide	645	80.54586497	66.32909976
9	A7	JL-18	646	45.45454545	190.9584289
9	A8	Kenpaullone	647	28.21670429	119.4539249
9	A9	LY-367,265	648	-18.26390314	37.45873664
9	A10	Leflunomide	649	88.24132978	61.25160857
9	A11	LFM-A13	650	71.4652165	48.28512281
9	B2	(±)-Ibotenic acid	651	99.3227991	75.22520002
9	B3	Idazoxan hydrochloride	652	100.5540735	82.61064175
9	B4	S(+)-Isoproterenol (+)-bitartrate	653	100.8618921	110.4738992
9	B5	S(+)-Ibuprofen	654	107.9417197	75.89660382
9	B6	1,5-Isoquinolinediol	655	16.98132567	65.44788228
9	B7	Kainic acid	656	111.3277242	87.35243104
9	B8	Karakoline	657	102.2470757	61.71319868
9	B9	LY-310,762 hydrochloride	658	98.24543402	53.65635316
9	B10	VER-3323 hemifumarate salt	659	93.93597373	29.86348123
9	B11	NNC 55-0396	660	51.457008	46.6905388
9	C2	Ifenprodil tartrate	661	105.9408988	71.74229284
9	C3	1-(5-Isoquinolinylsulfonyl)-3-methylpiperazine dihydrochloride	662	95.3211574	105.7740726
9	C4	L-N6-(1-Iminoethyl)lysine hydrochloride	663	102.5548943	134.0989202
9	C5	p-Iodoclonidine hydrochloride	664	105.1713523	56.3000056

9	C6	Molindone hydrochloride	665	82.54668582	92.47188497
9	C7	Ketoconazole	666	102.400985	151.8071952
9	C8	L-701,324	667	54.53519393	124.867118
9	C9	L-368,899	668	94.70552021	109.8444581
9	C10	Lidocaine hydrochloride	669	94.85942951	56.04822917
9	C11	Ro 90-7501	670	-405.1918736	47.73960723
9	D2	Isotharine mesylate	671	105.7869895	135.5256532
9	D3	(-)-Isoproterenol hydrochloride	672	104.8635338	88.40149947
9	D4	3-Iodo-L-tyrosine	673	103.4783501	91.12907738
9	D5	R(+)-IAA-94	674	74.38949313	73.96631791
9	D6	IB-MECA	675	100.4001642	91.21300285
9	D7	Ketorolac tris salt	676	-77.21116355	106.6133274
9	D8	loxoprofen	677	91.01169711	74.51183349
9	D9	Lomefloxacin hydrochloride	678	-90.75518161	89.28271695
9	D10	Lidocaine N-ethyl bromide quaternary salt	679	82.23886723	57.22318581
9	D11	Loratadine	680	37.14344346	58.94365803
9	E2	Isoliquiritigenin	681	-167.2481018	111.3131539
9	E3	1-(5-Isoquinolinylsulfonyl)-2-methylpiperazine dihydrochloride	682	98.39934332	68.34331114
9	E4	L-N5-(1-Iminoethyl)ornithine hydrochloride	683	99.63061769	95.19946288
9	E5	Indatraline hydrochloride	684	81.16150215	58.35617971
9	E6	Indomethacin morpholinylamide	685	92.85860866	-32.74492251
9	E7	Ketoprofen	686		
9	E8	Labetalol hydrochloride	687	77.77549764	60.74805573
9	E9	Lamotrigine	688	66.07839113	75.85464108
9	E10	L-Leucinethiol, oxidized dihydrochloride	689	72.38867228	84.20522576
9	E11	(-)-Tetramisole hydrochloride	690	71.00348861	63.30778269
9	F2	(±)-Ibuprofen	691	101.9392571	109.382868
9	F3	Indomethacin	692	-16.41699159	103.4241593
9	F4	Ivermectin	693	75.3129489	118.6566329
9	F5	Iofetamine hydrochloride	694	105.0174431	122.1815028
9	F6	3-(1H-Imidazol-4-yl)propyl di(p-fluorophenyl)methyl ether hydrochloride	695	95.01333881	80.55446763
9	F7	K 185	696	77.92940694	164.9415319
9	F8	L-162,313	697	-23.49681921	37.7524758
9	F9	alpha-Lobeline hydrochloride	698	91.01169711	67.62994461
9	F10	LE 300	699	92.08906218	45.26380574
9	F11	L-655,708	700	78.08331623	67.08442903
9	G2	IIK7	701	67.77139339	153.1500028
9	G3	Imipramine hydrochloride	702	101.4775292	52.43943378
9	G4	Imiloxan hydrochloride	703	102.400985	80.5125049

9	G5	ICI 204,448 hydrochloride	704	100.7079828	106.9070665
9	G6	Isonipecotic acid	705	83.00841371	82.90438091
9	G7	Ketotifen fumarate	706	76.23640468	48.9565266
9	G8	Lidocaine N-methyl hydrochloride	707	106.2487174	72.79136127
9	G9	Loperamide hydrochloride	708	91.62733429	59.15347172
9	G10	Lansoprazole	709	88.39523907	106.1517373
9	G11	LY-294,002 hydrochloride	710	18.21260004	73.08510043
9	H2	(±)-Isoproterenol hydrochloride	711	103.940078	135.8613551
9	H3	Isoxanthopterin	712	66.23230043	74.21809433
9	H4	CR 2945	713	91.62733429	103.3402339
9	H5	ICI 118,551 hydrochloride	714	90.08824133	53.99205506
9	H6	JWH-015	715	63.76975169	79.79913837
9	H7	Kynurenic acid	716	-33.19310486	126.0840374
9	H8	beta-Lapachone	717	71.92694439	75.81267834
9	H9	Lonidamine	718	89.01087626	69.93789515
9	H10	L-687,384 hydrochloride	719	79.62240919	43.96296089
9	H11	Loxapine succinate	720	43.14590601	89.82823253
10	A2	LY-53,857 maleate	721	102.1549513	111.640875
10	A3	L-750,667 trihydrochloride	722	57.67060031	64.8695021
10	A4	4-Methylpyrazole hydrochloride	723	87.83991791	87.01785066
10	A5	5-Methoxy DMT oxalate	724	86.30066701	61.60293002
10	A6	Molsidomine	725	42.89379169	54.748078
10	A7	Metergoline	726	90.76449461	69.59613291
10	A8	Meclofenamic acid sodium	727	67.67573114	74.54548454
10	A9	(±)-Metoprolol (+)-tartrate	728	95.22832222	167.2220939
10	A10	MRS 1754	729	50.59004618	92.38789719
10	A11	MDL 28170	730	64.90507953	83.2068499
10	B2	Lorglumide sodium	731	114.0071832	140.7925562
10	B3	Linopirdine	732	97.22934838	60.76154024
10	B4	Nocodazole	733	-34.68445357	108.8939849
10	B5	Metaproterenol hemisulfate	734	97.84504874	69.74461346
10	B6	3-Methyl-6-(3-[trifluoromethyl]phenyl)-1,2,4-triazolo[4,3-b]pyridazine	735	87.37814264	89.7152473
10	B7	(-)-cis-(1S,2R)-U-50488 tartrate	736	100.7696254	70.16530834
10	B8	Milrinone	737	-55.46434069	76.77269278
10	B9	6-Methyl-2-(phenylethynyl)pyridine hydrochloride	738	96.76757311	167.2468407
10	B10	2-methoxyestradiol	739	87.37814264	95.77820306
10	B11	Myricetin	740	-153.668548	37.89553568
10	C2	LY-278,584 maleate	741	104.1559774	70.70973702
10	C3	L-741,626	742	98.4607491	36.78193157
10	C4	N-omega-Methyl-5-hydroxytryptamine oxalate salt	743	106.0030785	89.54202

10	C5	Mianserin hydrochloride	744	110.0051308	72.76371795
10	C6	Mizoribine	745	106.772704	81.17761573
10	C7	Clorgyline hydrochloride	746	102.7706516	70.80872406
10	C8	(±)-alpha-Methyl-4-carboxyphenylglycine	747	102.9245767	82.04375227
10	C9	Mibefradil dihydrochloride	748	88.76346845	155.4921305
10	C10	Cysteamine hydrochloride	749	81.8368394	101.6679315
10	C11	NG-Monomethyl-L-arginine acetate	750	69.21498204	96.00092388
10	D2	cis(+/-)-8-OH-PBZI hydrobromide	751	103.8481272	78.28224503
10	D3	L-733,060 hydrochloride	752	98.15289892	61.62767677
10	D4	Moxonidine hydrochloride	753	102.6167265	80.06401161
10	D5	Mevastatin	754	101.0774756	92.56112449
10	D6	S-Methylisothiourea hemisulfate	755	105.2334531	88.27993533
10	D7	MRS 2179	756	118.3170857	65.01798264
10	D8	1-Methylhistamine dihydrochloride	757	92.76552078	69.22493153
10	D9	N6-Methyladenosine	758	94.15084659	176.1061801
10	D10	alpha,beta-Methylene adenosine 5'-triphosphate dilithium	759	94.30477168	157.7440855
10	D11	MK-912	760	66.59825552	87.16633121
10	E2	L-703,606 oxalate	761	110.9286814	-15.92866335
10	E3	Metoclopramide hydrochloride	762	87.993843	-24.81274953
10	E4	MRS 1845	763	-2.975885069	86.47342198
10	E5	8-Methoxymethyl-3-isobutyl-1-methylxanthine	764	103.5402771	91.94245554
10	E6	MG 624	765	23.34530528	62.04837166
10	E7	Meloxicam sodium	766	-151.2057465	56.62883162
10	E8	Moxisylyte hydrochloride	767	101.2314007	69.07645098
10	E9	(S)-MAP4 hydrochloride	768	97.38327347	176.1556736
10	E10	Methoxamine hydrochloride	769	85.83889174	94.63985218
10	E11	(±)-3-(3,4-dihydroxyphenyl)-2-methyl-DL-alanine	770	70.44638276	78.9504075
10	F2	Levallorphan tartrate	771	115.2385839	66.97297654
10	F3	R(-)-Me5	772	98.4607491	75.28788729
10	F4	BIO	773	-48.99948692	59.67268288
10	F5	MK-886	774	-6.977937404	42.86963408
10	F6	N-Methyl-D-aspartic acid	775	106.3109287	56.05965619
10	F7	Morin	776	-84.71010775	27.22968291
10	F8	S-Methyl-L-thiocitrulline acetate	777	102.1549513	78.25749827
10	F9	(±)-Methoxyverapamil hydrochloride	778	105.6952283	225.7976705
10	F10	Mitoxantrone	779	27.19343253	137.1052892
10	F11	MRS 2159	780	-36.83940482	177.8879467
10	G2	AFMK	781	72.60133402	71.92232818
10	G3	Dihydrocapsaicin	782	105.3873781	75.53535487
10	G4	MRS 1523	783	101.2314007	83.2068499

10	G5	Mexiletene hydrochloride	784	108.9276552	101.9401458
10	G6	alpha-Methyl-DL-tyrosine methyl ester hydrochloride	785	114.6228835	78.10901772
10	G7	Minoxidil	786	100.4617753	80.80641436
10	G8	Melatonin	787	96.9214982	83.60279803
10	G9	Metrazoline oxalate	788	56.59312468	169.3750619
10	G10	O-Methylserotonin hydrochloride	789	92.61159569	86.42392847
10	G11	GR 127935 hydrochloride	790	-20.21549513	79.54432969
10	H2	L-745,870 hydrochloride	791	90.14879425	81.10337546
10	H3	(-)-Naproxen sodium	792	98.15289892	82.63767446
10	H4	Melphalan	793	101.2314007	79.74230376
10	H5	Methylergonovine maleate	794	61.05695228	86.9931039
10	H6	ML 10302	795	101.0774756	88.47790939
10	H7	3-Methoxy-4-hydroxyphenethylamine hydrochloride	796	105.5413032	69.59613291
10	H8	L-Methionine sulfoximine	797	102.1549513	83.62754479
10	H9	GW9662	798	84.29964084	171.8249909
10	H10	Se-(methyl)selenocysteine hydrochloride	799	91.84197024	96.07516415
10	H11	2,6-Difluoro-4-[2-(phenylsulfonylamino)ethylthio]phenoxyacetamide	800	76.29553617	54.2778896
11	A2	Mifepristone	801	-54.76003147	62.24944738
11	A3	Minocycline hydrochloride	802	-112.5098348	101.8133453
11	A4	(-)-MK-801 hydrogen maleate	803	84.18568057	42.16777191
11	A5	Methiothepin mesylate	804	89.37844217	88.66284515
11	A6	MDL 105,519	805	23.60346184	95.29429396
11	A7	nor-Binaltorphimine dihydrochloride	806	57.90715972	66.37068675
11	A8	NCS-356	807	83.71361133	67.15746881
11	A9	(-)-Nicotine hydrogen tartrate salt	808	81.35326515	45.42729759
11	A10	Nicardipine hydrochloride	809	-21.71518489	44.67798134
11	A11	NF 023	810	-189.6144768	67.04507137
11	B2	L-alpha-Methyl-p-tyrosine	811	92.21085759	97.80450339
11	B3	Maprotiline hydrochloride	812	95.83005507	67.719456
11	B4	2-Methyl-5-hydroxytryptamine maleate	813	88.11959087	34.00022479
11	B5	2-Methylthioadenosine diphosphate trisodium	814	93.15499607	143.5877262
11	B6	Metrifudil	815	91.26671912	83.00550747
11	B7	Neostigmine bromide	816	90.63729347	74.3509048
11	B8	S-Nitrosoglutathione	817	79.62234461	60.26375932
11	B9	NG-Nitro-L-arginine	818	81.66797797	65.20924656
11	B10	Nifedipine	819	18.56805665	90.12401184
11	B11	Nimustine hydrochloride	820	75.05900865	42.35510097
11	C2	SB-215505	821	26.12116444	81.73166985
11	C3	H-8 dihydrochloride	822	83.24154209	37.67187441

11	C4	alpha-Methyl-5-hydroxytryptamine maleate	823	78.52084972	45.87688734
11	C5	Mesulergine hydrochloride	824	83.87096774	61.38773369
11	C6	p-MPPF dihydrochloride	825	95.20062943	92.74661871
11	C7	CR 2249	826	81.82533438	51.42182758
11	C8	NCS-382	827	83.87096774	73.60158855
11	C9	Naphazoline hydrochloride	828	83.08418568	39.95728897
11	C10	Naloxone hydrochloride	829	82.45476003	50.22292158
11	C11	Norcantharidin	830	78.36349331	63.63568244
11	D2	1-Methylimidazole	831	105.1140834	77.23577236
11	D3	Proglumide	832	70.81038552	81.5818066
11	D4	Metolazone	833	24.07553108	58.0907422
11	D5	MDL 26,630 trihydrochloride	834	95.04327301	43.62893859
11	D6	(-)-3-Methoxynaltrexone hydrochloride	835	93.15499607	56.44224645
11	D7	S-(4-Nitrobenzyl)-6-thioinosine	836	76.31785995	65.54643887
11	D8	Nalidixic acid sodium	837	-67.03383163	66.74534487
11	D9	3-Nitropropionic acid	838		
11	D10	7-Nitroindazole	839	-24.54760031	53.70724214
11	D11	Noscapine hydrchloride	840	60.58221873	65.13431494
11	E2	Mecamylamine hydrochloride	841	96.61683714	81.24461429
11	E3	R-(-)-Deprenyl hydrochloride	842	115.9716758	70.34206287
11	E4	DFB	843	64.98819827	41.00633172
11	E5	ZM 39923 hydrochloride	844	-39.65381589	60.07643026
11	E6	Niflumic acid	845	18.25334382	81.76913566
11	E7	Naltrexone hydrochloride	846	81.82533438	54.1942977
11	E8	Nalbuphine hydrochloride	847	94.8859166	54.23176352
11	E9	NG-Nitro-L-arginine methyl ester hydrochloride	848	96.61683714	47.93750702
11	E10	NS 521 oxalate	849	88.27694729	91.84743921
11	E11	(+)-Nicotine (+)-di-p-toluoyl tartrate	850	58.53658537	69.33048593
11	F2	Methapyrilene hydrochloride	851	105.4287962	90.57360159
11	F3	(±)-Muscarine chloride	852	91.73878836	65.80869956
11	F4	L-alpha-Methyl DOPA	853	95.04327301	40.81900266
11	F5	3-Morpholinosydnonimine hydrochloride	854	90.47993706	34.71207523
11	F6	Nimesulide	855	-39.65381589	67.64452437
11	F7	S-Nitroso-N-acetylpenicillamine	856	83.87096774	47.71271215
11	F8	5-Nitro-2-(3-phenylpropylamino)benzoic acid	857	-35.24783635	67.45719531
11	F9	(±)-Normetanephrine hydrochloride	858	88.11959087	65.54643887
11	F10	2-(alpha-Naphthoyl)ethyltrimethylammonium iodide	859	-32.73013375	90.64853321
11	F11	Naltrindole hydrochloride	860	69.55153423	42.99201978
11	G2	Memantine hydrochloride	861	113.1392604	68.35637481

11	G3	Methoctramine tetrahydrochloride	862	93.6270653	10.39676295
11	G4	Methysergide maleate	863	-2.675059009	42.50496422
11	G5	3-Methoxy-morphanin hydrochloride	864	98.03304485	43.32921209
11	G6	Nialamide	865	95.83005507	62.84890038
11	G7	Niclosamide	866	-33.3595594	106.9086958
11	G8	NF449 octasodium salt	867	47.36428009	204.0200817
11	G9	Nortriptyline hydrochloride	868	100.0786782	40.48181035
11	G10	6-Nitroso-1,2-benzopyrone	869	58.53658537	62.21198157
11	G11	Sertraline hydrochloride	870	77.10464201	60.75081488
11	H2	Me-3,4-dephostatin	871	-94.41384736	36.77269492
11	H3	(+)-MK-801 hydrogen maleate	872	91.26671912	46.3639429
11	H4	Methylcarbamylcholine chloride	873	99.44925256	42.35510097
11	H5	S15535	874	96.1447679	69.03075943
11	H6	Nomifensine maleate	875	89.22108576	79.10906298
11	H7	NAN-190 hydrobromide	876	87.49016522	67.98171668
11	H8	Nordihydroguaiaretic acid from Larrea divaricata (creosote bush)	877	36.82140047	39.76995991
11	H9	NADPH tetrasodium	878	95.98741149	74.53823386
11	H10	Nilutamide	879	72.22659323	105.1103368
11	H11	NO-711 hydrochloride	880	73.32808812	85.55318272
12	A2	Nitrendipine	881	22.33196399	73.94202606
12	A3	Naloxone benzoylhydrazone	882	85.00131107	89.5970104
12	A4	Olomoucine	883	85.7879556	70.96252904
12	A5	Orphenadrine hydrochloride	884	91.03225243	114.8974851
12	A6	(±)-Octoclothepin maleate	885	88.67231885	102.019998
12	A7	O-Phospho-L-serine	886	77.5281881	102.4239976
12	A8	Pancuronium bromide	887	67.4329167	49.65155035
12	A9	Pentolinium di[L(+)-tartrate]	888	81.59251814	52.73204727
12	A10	Valproic acid sodium	889	85.13241849	79.6990203
12	A11	Pyrilamine maleate	890	75.29936194	96.66700333
12	B2	Nimodipine	891	12.2366926	80.35551964
12	B3	NS-1619	892	100.6030941	96.31350369
12	B4	Oleic Acid	893	96.27654925	-48.87385113
12	B5	TG003	894	-121.4928765	122.1189779
12	B6	Progesterone	895	89.32785596	97.72750227
12	B7	(±)-Propranolol hydrochloride	896	85.39463334	57.78204222
12	B8	3-alpha,21-Dihydroxy-5-alpha-pregnan-20-one	897	85.91906302	26.21957378
12	B9	1-Phenyl-3-(2-thiazolyl)-2-thiourea	898	-25.91556682	69.2960307
12	B10	Promethazine hydrochloride	899	76.08600647	71.51802848
12	B11	Piroxicam	900	-119.5262652	105.7569942
12	C2	Nisoxetine hydrochloride	901	97.58762346	48.43955156
12	C3	Naloxonazine dihydrochloride	902	82.51027008	113.988486

12	C4	Oxymetazoline hydrochloride	903	94.96547505	55.004545
12	C5	Ofloxacin	904	27.31404598	96.06100394
12	C6	Palmitoylethanolamide	905	97.58762346	95.45500454
12	C7	SKF-525A hydrochloride	906	84.21466655	58.43854156
12	C8	Pirfenidone	907	71.10392448	81.71901828
12	C9	Thiolactomycin	908	65.33519797	56.67104333
12	C10	Praziquantel	909	85.91906302	79.9010201
12	C11	3-n-Propylxanthine	910	83.55912945	27.48207252
12	D2	Nylidrin hydrochloride	911	94.57215278	66.16503383
12	D3	NBQX disodium	912	3.714710253	117.018483
12	D4	Sodium Oxamate	913	96.53876409	72.07352793
12	D5	Oxotremorine sesquifumarate salt	914	84.87020365	110.9079891
12	D6	Piceatannol	915	-215.4968971	72.57852742
12	D7	Picrotoxin	916	83.82134429	73.28552671
12	D8	1,3-Dimethyl-8-phenylxanthine	917	78.70815488	86.01151399
12	D9	Cisplatin	918	17.21877458	57.12554287
12	D10	Propafenone hydrochloride	919		
12	D11	Phenylephrine hydrochloride	920	87.09902981	98.18200182
12	E2	N6-Cyclopentyl-9-methyladenine	921	83.82134429	126.4114736
12	E3	NS 2028	922	97.58762346	124.3409757
12	E4	Oxybutynin Chloride	923	88.27899659	116.4124836
12	E5	Oxatomide	924	89.85228564	133.1784668
12	E6	Pentamidine isethionate	925	91.55668211	56.36804363
12	E7	4-Phenyl-3-furoxancarbonitrile	926	80.80587361	88.48601151
12	E8	PRE-084	927	73.46385805	88.89001111
12	E9	Podophyllotoxin	928	93.65440084	65.76103424
12	E10	5alpha-Pregnan-3alpha-ol-11,20-dione	929	50.65116686	87.07201293
12	E11	Perphenazine	930	75.43046936	170.1444299
12	F2	Naltriben methanesulfonate	931	81.59251814	80.35551964
12	F3	(±)-Octopamine hydrochloride	932	96.66987151	125.7044743
12	F4	Oxiracetam	933	79.88812167	88.28401172
12	F5	SB 216763	934	-8.216065029	36.52156348
12	F6	TBB	935	86.96792238	86.01151399
12	F7	Pentoxifylline	936	90.2456079	75.86102414
12	F8	PPNDS tetrasodium	937	-70.62319727	266.7508332
12	F9	SU 9516	938	-158.727384	80.65851934
12	F10	Pempidine tartrate	939	95.62101215	59.8020402
12	F11	Pentylenetetrazole	940	83.16580718	111.4129886
12	G2	Naftopidil dihydrochloride	941	98.37426798	86.66801333
12	G3	N-Oleoylethanolamine	942	102.0452758	291.5463085
12	G4	Ouabain	943	96.80097894	90.2030098
12	G5	Oxaprozin	944	96.14544183	105.1509948

12	G6	Parthenolide	945	85.26352592	114.038986
12	G7	Pimozide	946	35.18049122	41.92505807
12	G8	PD 404,182	947	-13.06703959	84.64801535
12	G9	Palmitoyl-DL-Carnitine chloride	948	96.01433441	113.028987
12	G10	Piracetam	949	89.32785596	64.7005353
12	G11	(+)-Pilocarpine hydrochloride	950	90.63893016	117.8769821
12	H2	Bisoprolol hemifumarate salt	951	90.63893016	94.6975053
12	H3	Oxolinic acid	952	51.43781138	132.4714675
12	H4	ODQ	953	28.36290534	76.61852338
12	H5	Oxotremorine methiodide	954	92.86775632	104.3429957
12	H6	Pindolol	955	90.2456079	119.5939804
12	H7	L-Glutamic acid, N-phthaloyl-	956	85.52574076	130.3504696
12	H8	Papaverine hydrochloride	957	80.41255135	93.08150692
12	H9	R(-)-N6-(2-Phenylisopropyl)adenosine	958	88.67231885	117.5234825
12	H10	Phosphomycin disodium	959	70.71060222	74.04302596
12	H11	Pilocarpine nitrate	960	88.41010401	124.037976
13	A2	Promazine hydrochloride	961	77.89634146	56.43905432
13	A3	Pirenzepine dihydrochloride	962	98.93292683	38.84903969
13	A4	1,3-PBIT dihydrobromide	963	105.0304878	58.52720495
13	A5	(±)-cis-Piperidine-2,3-dicarboxylic acid	964	86.2804878	84.46982209
13	A6	Piribedil maleate	965	87.19512195	87.54895946
13	A7	Procaine hydrochloride	966	97.86585366	86.09787174
13	A8	Phaclofen	967	91.76829268	111.4388184
13	A9	Pregnenolone sulfate sodium	968	69.81707317	77.53291492
13	A10	PD 168,077 maleate	969	75.30487805	98.73295267
13	A11	Quinacrine dihydrochloride	970	23.32317073	50.52852626
13	B2	Phenelzine sulfate	971	98.62804878	59.87211552
13	B3	Putrescine dihydrochloride	972	112.195122	33.36322024
13	B4	Protoporphyrin IX disodium	973	41.15853659	79.7272427
13	B5	Protriptyline hydrochloride	974	105.1829268	53.71384078
13	B6	Paromomycin sulfate	975	99.23780488	73.60436034
13	B7	2-Phenylaminoadenosine	976	96.49390244	96.75097919
13	B8	BF-170 hydrochloride	977	-222.2560976	99.37001557
13	B9	PPADS	978	-12.04268293	78.38233212
13	B10	SU 6656	979	-7.774390244	46.42300977
13	B11	Quazinone	980	61.2804878	80.68283705
13	C2	Pheniramine maleate	981	93.29268293	59.30583738
13	C3	Phentolamine mesylate	982	113.2621951	39.80463404
13	C4	1,4-PBIT dihydrobromide	983	98.7804878	47.34321174
13	C5	Pergolide methanesulfonate	984	53.65853659	36.93785097
13	C6	1,10-Phenanthroline monohydrate	985	88.41463415	64.50851777
13	C7	R(+)-3PPP hydrochloride	986	93.75	76.54192818

13	C8	1-Phenylbiguanide	987	90.70121951	89.99103393
13	C9	S(+)-PD 128,907 hydrochloride	988	67.5304878	53.74923317
13	C10	Quinolinic acid	989	92.98780488	69.14492001
13	C11	(-)-Quinpirole hydrochloride	990	77.43902439	89.46014818
13	D2	Phosphonoacetic acid	991	86.12804878	77.07281393
13	D3	Propionylpromazine hydrochloride	992	90.24390244	57.92553442
13	D4	Phenylbutazone	993	102.7439024	71.58699448
13	D5	6(5H)-Phenanthridinone	994	17.5304878	73.71053749
13	D6	Procainamide hydrochloride	995	104.2682927	73.71053749
13	D7	S(-)-3PPP hydrochloride	996	93.59756098	86.84111179
13	D8	SKF 94836	997	71.64634146	127.2238214
13	D9	Phenamil methanesulfonate	998	-155.3353659	69.74659053
13	D10	Quercetin dihydrate	999	-132.4695122	54.06776462
13	D11	Quipazine, N-methyl-, dimaleate	1000	-7.774390244	86.02708697
13	E2	(-)-Perillic acid	1001	107.3170732	84.04511349
13	E3	Prazosin hydrochloride	1002	-11.12804878	47.06007267
13	E4	Picotamide	1003	107.1646341	98.30824407
13	E5	5alpha-Pregnan-3alpha-ol-20-one	1004	83.07926829	130.6214903
13	E6	Prilocaine hydrochloride	1005	97.86585366	72.22405738
13	E7	(±)-PPHT hydrochloride	1006	86.2804878	65.67646642
13	E8	Pirenperone	1007	-306.25	125.6311642
13	E9	Phenylbenzene-omega-phosphono-alpha-amino acid	1008	89.32926829	65.46411212
13	E10	Quinidine sulfate	1009	-31.55487805	65.46411212
13	E11	Quipazine, 6-nitro-, maleate	1010	-119.054878	90.84045113
13	F2	Pyrazinecarboxamide	1011	98.47560976	77.49752253
13	F3	Phloretin	1012	-53.35365854	44.47642867
13	F4	Tranylcypromine hydrochloride	1013	106.7073171	55.66042188
13	F5	Propantheline bromide	1014	105.7926829	90.02642631
13	F6	Propentofylline	1015	96.79878049	90.55731207
13	F7	3-Phenylpropargylamine hydrochloride	1016	107.7743902	83.01873437
13	F8	IC 261	1017	-10.97560976	133.2405266
13	F9	Phthalamoyl-L-glutamic acid trisodium	1018	83.99390244	75.1970176
13	F10	Quipazine dimaleate	1019	-98.62804878	72.22405738
13	F11	Quinelorane dihydrochloride	1020	85.21341463	76.01104242
13	G2	Primidone	1021	101.3719512	56.12052286
13	G3	Pargyline hydrochloride	1022	107.9268293	69.8173753
13	G4	(S)-Propranolol hydrochloride	1023	117.0731707	50.70548818
13	G5	Piperidine-4-sulphonic acid	1024	104.5731707	82.77098768
13	G6	(S)-(-)-propafenone hydrochloride	1025	93.29268293	72.68415837
13	G7	N6-2-Phenylethyladenosine	1026	98.01829268	102.4137606
13	G8	A3 hydrochloride	1027	86.43292683	111.7219574

13	G9	PD 98,059	1028	-11.12804878	216.5895899
13	G10	Quinine sulfate	1029	40.09146341	68.29550281
13	G11	(±)-Quinpirole dihydrochloride	1030	83.53658537	70.98532396
13	H2	(±)-threo-1-Phenyl-2-decanoylamino-3-morpholino-1-propanol hydrochloride	1031	111.7378049	104.2895569
13	H3	Phorbol 12-myristate 13-acetate	1032	97.86585366	-32.82053702
13	H4	Ammonium pyrrolidinedithiocarbamate	1033	107.9268293	60.15525459
13	H5	Prochlorperazine dimaleate	1034	80.94512195	134.7623991
13	H6	Pyridostigmine bromide	1035	100.152439	89.70789486
13	H7	N6-Phenyladenosine	1036	98.7804878	132.072578
13	H8	Pinacidil	1037	86.2804878	109.1029211
13	H9	(±)-PD 128,907 hydrochloride	1038	73.01829268	72.36562692
13	H10	(+)-Quisqualic acid	1039	88.56707317	83.93893634
13	H11	Cortexolone	1040	83.53658537	105.8114294
14	A2	Ritodrine hydrochloride	1041	101.5684566	64.80995129
14	A3	REV 5901	1042	28.86395817	66.92293
14	A4	Ro 8-4304	1043	83.759939	80.49613217
14	A5	Ro 41-0960	1044	-181.8973968	65.09645688
14	A6	Ro 04-6790 dihydrochloride	1045	92.74588825	52.99159584
14	A7	Cortexolone maleate	1046	-11.81788476	134.2875561
14	A8	Spermidine trihydrochloride	1047	68.23875395	75.44647121
14	A9	SB 204070 hydrochloride	1048	81.96274916	59.86772992
14	A10	Sphingosine	1049	63.66408888	65.09645688
14	A11	(±)-Sulpiride	1050	79.18527394	44.32480183
14	B2	Raloxifene hydrochloride	1051	-259.9934648	32.39900678
14	B3	Rottlerin	1052	-338.0895327	52.56183746
14	B4	RX 821002 hydrochloride	1053	75.75427513	111.1880432
14	B5	Reactive Blue 2	1054	-120.9563228	94.28421354
14	B6	(±)-Sotalol hydrochloride	1055	87.3543187	53.8869258
14	B7	SKF 86466	1056	96.99379153	90.12988253
14	B8	SNC80	1057	78.04160767	66.8513036
14	B9	N-Oleoyldopamine	1058	64.64437425	66.63642441
14	B10	SB 269970 hydrochloride	1059	69.54580111	33.65246872
14	B11	CV-3988	1060	79.34865483	74.19300926
14	C2	Retinoic acid	1061	-230.7482845	105.0997994
14	C3	Ranolazine dihydrochloride	1062	88.33460407	98.61761054
14	C4	Ribavirin	1063	87.5176996	81.89284691
14	C5	Riluzole	1064	102.8755038	54.71062936
14	C6	SB-366791	1065	9.09486984	25.3438067
14	C7	SR 57227A	1066	70.85284827	76.55668036
14	C8	SKF 83959 hydrobromide	1067	67.74861126	57.21755324
14	C9	Spironolactone	1068	82.12613005	89.84337695

14	C10	Spiperone hydrochloride	1069	69.38242022	49.4819024
14	C11	Sulindac	1070	-93.67171332	63.66392895
14	D2	Ruthenium red	1071	50.43023636	17.93047464
14	D3	Rolipram	1072	94.86983989	108.4304269
14	D4	Ranitidine hydrochloride	1073	-5.60941074	94.10514755
14	D5	Risperidone	1074	98.79098137	63.84299494
14	D6	Sodium nitroprusside dihydrate	1075	98.62760048	51.02186993
14	D7	(-)-Scopolamine hydrobromide	1076	101.8952184	86.4769363
14	D8	Spermine tetrahydrochloride	1077	76.8979414	51.20093592
14	D9	SCH-202676 hydrobromide	1078	-51.68282322	56.78779486
14	D10	SR 2640	1079	-41.55320771	76.19854837
14	D11	Succinylcholine chloride	1080	63.66408888	57.39661923
14	E2	13-cis-retinoic acid	1081	48.9598083	144.9957024
14	E3	Ro 25-6981 hydrochloride	1082	90.62193661	79.56498902
14	E4	Ritanserin	1083	-60.01524888	126.3370261
14	E5	S(+)-Raclopride L-tartrate	1084	75.26413245	75.33903161
14	E6	(±)-Synephrine	1085	91.60222198	47.97774807
14	E7	SC-560	1086	23.96253131	98.15203896
14	E8	SKF 75670 hydrobromide	1087	66.93170679	56.82360806
14	E9	D-Serine	1088	81.14584468	35.94451342
14	E10	(-)-Sulpiride	1089	74.44722797	59.65285073
14	E11	Salbutamol	1090	84.41346259	48.33588005
14	F2	Rutaecarpine	1091	5.663871038	12.55849489
14	F3	Phosphoramidon disodium	1092	95.85012526	102.0198644
14	F4	Rauwolscine hydrochloride	1093	97.64731511	106.4965142
14	F5	Sobuzoxane	1094	103.3656464	124.2240474
14	F6	Sulfaphenazole	1095	103.2022655	79.35010983
14	F7	Semicarbazide hydrochloride	1096	100.914933	108.0722949
14	F8	SC 19220	1097	85.55712885	67.88988635
14	F9	Albuterol hemisulfate	1098	80.00217841	53.27810142
14	F10	SKF 96365	1099	86.86417602	98.68923694
14	F11	Salmeterol xinafoate	1100	-12.96155103	48.51494604
14	G2	Ropinirole hydrochloride	1101	118.7234506	76.66411995
14	G3	Roscovitine	1102	102.8755038	104.8491071
14	G4	Ro 16-6491 hydrochloride	1103	91.11207929	90.02244294
14	G5	Rilmenidine hemifumarate	1104	84.57684348	120.4994747
14	G6	Seglitide	1105	68.07537305	82.68073727
14	G7	(-)-Scopolamine methyl nitrate	1106	98.30083869	81.42727533
14	G8	SKF 89626	1107	68.23875395	57.71893802
14	G9	Sanguinarine chloride	1108	-105.4351378	27.6000382
14	G10	(-)-Scopolamine,n-Butyl-, bromide	1109	87.02755691	41.60299876
14	G11	SU 5416	1110	-13.45169372	33.00783115

14	H2	Resveratrol	1111	-64.91667574	85.08022156
14	H3	Rotenone	1112	34.41890862	65.16808328
14	H4	Ro 41-1049 hydrochloride	1113	97.64731511	104.5626015
14	H5	R(-)-Denopamine	1114	86.37403333	159.9656193
14	H6	Sulindac sulfone	1115	-71.12514977	76.41342756
14	H7	DL-Stearoylcarnitine chloride	1116	100.914933	69.71635947
14	H8	SKF 83565 hydrobromide	1117	72.32327633	161.720466
14	H9	N-Succinyl-L-proline	1118	80.3289402	54.49575017
14	H10	SB 205384	1119	51.57390262	45.64989017
14	H11	(-)-Scopolamine methyl bromide	1120	72.81341902	61.94489543
15	A2	SU 4312	1121	35.01604902	57.96963041
15	A3	1-(2-Methoxyphenyl)piperazine hydrochloride	1122	87.68602276	91.02009899
15	A4	Sepiapterin	1123	38.51765392	70.80356793
15	A5	Tiapride hydrochloride	1124	83.01721622	84.4379726
15	A6	Trihexyphenidyl hydrochloride	1125	79.95331193	67.08153217
15	A7	Terbutaline hemisulfate	1126	92.5007295	110.8448368
15	A8	Tyrphostin AG 1478	1127	-32.38984535	180.3489572
15	A9	Tyrphostin AG 528	1128	-93.95973154	48.27545677
15	A10	(±)-alpha-Lipoic Acid	1129	93.37613073	58.50126027
15	A11	Triprolidine hydrochloride	1130	85.93522031	53.56466547
15	B2	SR 59230A oxalate	1131	104.9022469	65.39682125
15	B3	PAPP	1132	94.98103297	130.4344987
15	B4	R(-)-SCH-12679 maleate	1133	87.10242194	97.71976336
15	B5	Taurine	1134	95.27283338	108.689974
15	B6	Theophylline	1135	93.08433032	135.2143762
15	B7	4-Hydroxyphenethylamine hydrochloride	1136	97.31543624	103.479124
15	B8	Tetrahydrozoline hydrochloride	1137	91.47942807	76.60210785
15	B9	Terazosin hydrochloride	1138	-21.73913043	74.01627248
15	B10	DL-Thiorphan	1139	93.81383134	57.67849447
15	B11	Tyrphostin AG 112	1140	-87.10242194	61.98822008
15	C2	BRL 52537 hydrochloride	1141	83.16311643	68.92296039
15	C3	Spiroxatrine	1142	93.81383134	104.6545037
15	C4	(±)-SKF 38393, N-allyl-, hydrobromide	1143	85.05981908	74.29052775
15	C5	Thiothixene hydrochloride	1144	56.75517946	192.1419336
15	C6	(E)-4-amino-2-butenoic acid	1145	82.87131602	98.85596375
15	C7	Triflupromazine hydrochloride	1146	73.82550336	114.2142587
15	C8	Tyrphostin AG 494	1147	-90.74992705	82.98833762
15	C9	Tyrphostin AG 537	1148	-263.6416691	89.29620875
15	C10	Tulobuterol hydrochloride	1149	91.91712868	53.76056209
15	C11	Tyrphostin 1	1150	-122.847972	105.0854762
15	D2	SKF 89976A hydrochloride	1151	88.9991246	104.1059931

15	D3	SR-95531	1152	38.37175372	87.53313918
15	D4	SDZ-205,557 hydrochloride	1153	85.35161949	107.2795184
15	D5	Tolbutamide	1154	89.72862562	106.5351112
15	D6	Tetradecylthioacetic acid	1155	75.72220601	-39.64294576
15	D7	Trimipramine maleate	1156	98.77443828	92.97906518
15	D8	N-p-Tosyl-L-phenylalanine chloromethyl ketone	1157	24.21943391	136.1938593
15	D9	Tyrphostin AG 555	1158	-98.92033849	102.9306134
15	D10	Trazodone hydrochloride	1159	41.87335862	84.47715192
15	D11	Tyrphostin 23	1160	-63.75838926	35.1503833
15	E2	SIB 1757	1161	-29.90954187	83.30177221
15	E3	(±)-6-Chloro-PB hydrobromide	1162	97.60723665	76.99390109
15	E4	SB 206553 hydrochloride	1163	74.26320397	91.09845764
15	E5	Tetraethylthiuram disulfide	1164	-7.149110009	113.9791827
15	E6	Trequinsin hydrochloride	1165	-167.9311351	142.1882958
15	E7	Tyrphostin AG 490	1166	-100.0875401	101.2459025
15	E8	(6R)-5,6,7,8-Tetrahydro-L-biopterin hydrochloride	1167	42.60285964	78.24763945
15	E9	Tyrphostin AG 698	1168	-107.6743507	108.4940774
15	E10	Tyrphostin AG 34	1169	22.90633207	76.32785258
15	E11	TFPI hydrochloride	1170	92.06302889	-10.37599091
15	F2	SIB 1893	1171	-30.34724249	76.87636311
15	F3	SKF 91488 dihydrochloride	1172	103.2973446	105.0071176
15	F4	SB 224289 hydrochloride	1173	3.209804494	28.56825691
15	F5	TCPOBOP	1174	96.87773563	95.72161784
15	F6	Tyrphostin AG 879	1175	17.0703239	81.26444738
15	F7	TTNPB	1176	69.01079662	91.05927832
15	F8	Tyrphostin AG 527	1177	-15.90312226	116.800094
15	F9	Tyrphostin AG 808	1178	-26.69973738	966.2078333
15	F10	Triamcinolone	1179	96.87773563	84.67304854
15	F11	Na-p-Tosyl-L-lysine chloromethyl ketone hydrochloride	1180	84.76801868	60.0292539
15	G2	1-(1-Naphthyl)piperazine hydrochloride	1181	105.9235483	83.41931018
15	G3	Suramin hexasodium	1182	-86.22702072	62.92852385
15	G4	L-Tryptophan	1183	93.81383134	100.8541093
15	G5	Tetraisopropyl pyrophosphoramide	1184	101.5465422	134.587507
15	G6	Tetraethylammonium chloride	1185	86.95652174	94.27198287
15	G7	L-765,314	1186	-54.56667639	133.9998172
15	G8	Theobromine	1187	102.7137438	115.703073
15	G9	Thio-NADP sodium	1188	44.79136271	99.32611563
15	G10	S(-)-Timolol maleate	1189	81.85001459	74.64314166
15	G11	Tyrphostin 25	1190	26.99153779	74.25134842
15	H2	Ketanserin tartrate	1191	108.2579516	93.60593436

15	H3	SQ 22536	1192	112.6349577	95.72161784
15	H4	Tranilast	1193	-424.5695944	146.4980214
15	H5	Tetramisole hydrochloride	1194	104.318646	117.5053219
15	H6	Tolazamide	1195	67.40589437	-41.09258074
15	H7	Triamterene	1196	-70.61569886	86.59283541
15	H8	(±)-Taxifolin	1197	-144.5871024	117.1527079
15	H9	Tyrphostin AG 835	1198	5.544207762	101.911951
15	H10	N,N,N-trimethyl-1-(4-trans-stilbenoxy)-2-propylammonium iodide	1199	-12.40151736	82.20475115
15	H11	1-[2-(Trifluoromethyl)phenyl]imidazole	1200	83.01721622	75.07411422
16	A2	Taxol	1201	28.0511811	77.96442784
16	A3	Tomoxetine	1202	86.66338583	72.24433124
16	A4	Tamoxifen citrate	1203	4.724409449	39.30244155
16	A5	Telenzepine dihydrochloride	1204	78.39566929	80.3698018
16	A6	Uridine 5'-diphosphate sodium	1205	81.05314961	67.52158481
16	A7	U-69593	1206	71.7519685	104.4235414
16	A8	U-99194A maleate	1207	91.68307087	62.06549266
16	A9	Vincristine sulfate	1208	69.68503937	85.79656012
16	A10	WIN 62,577	1209	-7.82480315	33.87568323
16	A11	Yohimbine hydrochloride	1210	68.06102362	79.57778842
16	B2	Tetracaine hydrochloride	1211	36.46653543	77.2017483
16	B3	T-0156	1212	-125.9350394	97.88209756
16	B4	Terfenadine	1213	80.46259843	-1.559581895
16	B5	Thioperamide maleate	1214	81.3484252	72.97767696
16	B6	U-74389G maleate	1215	-26.27952756	8.325918393
16	B7	UK 14,304	1216	-34.99015748	93.59935857
16	B8	U0126	1217	-50.49212598	29.41694126
16	B9	N-Vanillylnonanamide	1218	98.91732283	85.15121589
16	B10	S(-)-Willardiine	1219	71.8996063	57.66541835
16	B11	YS-035 hydrochloride	1220	74.40944882	71.71632232
16	C2	Tyrphostin 47	1221	-49.01574803	37.57174566
16	C3	3-Tropanyl-3,5-dichlorobenzoate	1222	98.17913386	89.46328871
16	C4	Tropicamide	1223	85.92519685	36.98506908
16	C5	(±)-Thalidomide	1224	83.85826772	98.9381154
16	C6	U-83836 dihydrochloride	1225	10.92519685	25.13420227
16	C7	U-62066	1226	88.43503937	97.4127563
16	C8	Vinblastine sulfate salt	1227	92.42125984	87.43925453
16	C9	(±)-Vesamicol hydrochloride	1228	93.30708661	54.79070313
16	C10	WAY-100635 maleate	1229	73.37598425	56.697402
16	C11	YC-1	1230	-85.62992126	78.08176316
16	D2	Tyrphostin 51	1231	-62.4507874	74.38570074
16	D3	Trifluoperazine dihydrochloride	1232	80.46259843	136.1920779

16	D4	THIP hydrochloride	1233	100.5413386	81.98316238
16	D5	R(+)-Terguride	1234	99.9507874	105.6555622
16	D6	U-73122	1235	76.18110236	46.98790468
16	D7	S(-)-UH-301 hydrochloride	1236	78.39566929	85.53255566
16	D8	(±)-Verapamil hydrochloride	1237	91.68307087	58.75077001
16	D9	XK469	1238	-10.18700787	64.08952685
16	D10	S-5-Iodowillardiine	1239	85.33464567	52.73733512
16	D11	Zaprinast	1240	85.33464567	64.73487108
16	E2	T-1032	1241	-60.67913386	144.6695544
16	E3	D-609 potassium	1242	78.2480315	109.4102923
16	E4	Trifluperidol hydrochloride	1243	96.11220472	50.39062882
16	E5	Thiocitrulline	1244	106.5944882	98.46877414
16	E6	SKF 95282 dimaleate	1245	111.761811	37.60107948
16	E7	R(+)-UH-301 hydrochloride	1246	95.66929134	91.57532438
16	E8	VUF 5574	1247	85.48228346	63.18017815
16	E9	Wortmannin from Penicillium funiculosum	1248	47.39173228	55.81738714
16	E10	Xylazine hydrochloride	1249	91.68307087	71.51098552
16	E11	Zonisamide sodium	1250	85.62992126	65.79088891
16	F2	I-OMe-Tyrphostin AG 538	1251	-144.8326772	37.7184148
16	F3	Thioridazine hydrochloride	1252	76.18110236	78.46310293
16	F4	3-Tropanyl-indole-3-carboxylate hydrochloride	1253	96.70275591	71.21764723
16	F5	Tyrphostin A9	1254	31.88976378	110.2316395
16	F6	4-Imidazoleacrylic acid	1255	99.21259843	58.28142875
16	F7	(+)-trans-(1R,2R)-U-50488 hydrochloride	1256	83.56299213	86.06056458
16	F8	Vinpocetine	1257	100.8366142	73.41768439
16	F9	1400W dihydrochloride	1258	104.0846457	68.72427179
16	F10	Xamoterol hemifumarate	1259	100.246063	11.17129978
16	F11	Zardaverine	1260	68.94685039	76.23373195
16	G2	Tyrphostin AG 538	1261	-101.5748031	26.63022753
16	G3	Thapsigargin	1262	81.05314961	139.1841284
16	G4	Tracazolate	1263	98.17913386	85.62055715
16	G5	TPMPA	1264	100.5413386	105.6555622
16	G6	Urapidil hydrochloride	1265	91.24015748	68.0202599
16	G7	(-)-trans-(1S,2S)-U-50488 hydrochloride	1266	83.12007874	89.81529466
16	G8	Vancomycin hydrochloride from Streptomyces orientalis	1267	109.6948819	51.24130985
16	G9	WB 64	1268	-208.6122047	26.36622307
16	G10	Xylometazoline hydrochloride	1269	88.58267717	63.47351644
16	G11	Olprinone hydrochloride	1270	-102.3129921	47.42791212
16	H2	Trimethoprim	1271	94.04527559	70.27896471

16	H3	Tyrphostin AG 126	1272	86.51574803	108.6182789
16	H4	3-Tropanylindole-3-carboxylate methiodide	1273	104.2322835	114.8077168
16	H5	U-75302	1274	102.6082677	83.21518319
16	H6	Urapidil, 5-Methyl-	1275	94.63582677	134.5200497
16	H7	U-101958 maleate	1276	89.61614173	117.0957554
16	H8	(±)-gamma-Vinyl GABA	1277	111.3188976	86.08989841
16	H9	(R)-(+)-WIN 55,212-2 mesylate	1278	-132.726378	80.34046797
16	H10	Xanthine amine congener	1279	17.86417323	85.62055715
16	H11	Zimelidine dihydrochloride	1280	82.82480315	74.41503457

Table 20. Secondary Screen of MtbIspC with lead compounds from the primary screen of LOPAC[1280]

Plate #	Compound (by Well #)	Compound Name	Compound #	Residual Activity MtbIspC
1	B2	N-Phenylanthranilic acid	1	75.30
1	H4	Reserpine	2	67.98
1	D6	5-azacytidine	3	96.80
1	C8	Acyclovir	4	88.44
1	E9	5-(N-Methyl-N-isobutyl)amiloride	5	74.65
1	F5	Aurintricarboxylic acid	6	17.98
1	G6	Apigenin	7	44.88
1	B8	5-(N,N-Dimethyl)amiloride hydrochloride	8	79.35
1	D9	Acetylsalicylic acid	9	76.96
1	G10	GR 4661	10	99.20
2	H5	Amsacrine hydrochloride	11	66.41
2	E6	1,3-Diethyl-8-phenylxanthine	12	68.62
2	D7	1-Amino-1-cyclohexanecarboxylic acid hydrochloride	13	79.03
2	G11	Bromoenol lactone	14	64.68
2	D2	Amiloride hydrochloride	15	74.81
2	E3	Amiodarone hydrochloride	16	40.80
2	C5	5-(N,N-hexamethylene)amiloride	17	68.21
2	F6	Arecaidine propargyl ester hydrobromide	18	74.80
2	G6	1,3-Dipropyl-8-p-sulfophenylxanthine	19	24.92
2	F8	gamma-Acetylinic GABA	20	82.25
2	B11	SB 222200	21	76.49
2	C11	1-benzoyl-5-methoxy-2-methylindole-3-acetic acid	22	88.50
3	C4	Bay 11-7085	23	16.35
3	H4	Benserazide hydrochloride	24	38.10
3	C6	BRL 15572	25	66.64
3	F6	Bromoacetyl alprenolol menthane	26	95.28
3	A8	BU224 hydrochloride	27	61.70
3	C8	(±)-Butaclamol hydrochloride	28	45.09
3	E10	ML-9	29	111.41
3	A2	3-Bromo-7-nitroindazole	30	67.32
3	B2	(+)-Bromocriptine methanesulfonate	31	27.88
3	F2	Benzamil hydrochloride	32	46.70
3	A3	Bumetanide	33	54.04
3	G3	Bepridil hydrochloride	34	34.41
3	B4	SB 202190	35	78.85
3	B7	(-)-Bicuculline methbromide, 1(S), 9(R)	36	57.65
3	H7	DAPH	37	82.04
3	D11	CB 1954	38	88.33

4	A2	Chelerythrine chloride	39	27.82
4	D2	Cortisone 21-acetate	40	76.82
4	D3	Calmidazolium chloride	41	13.51
4	D6	4-Chloromercuribenzoic acid	42	51.55
4	D7	Clozapine	43	77.53
4	F7	Chloroquine diphosphate	44	69.76
4	B8	Cefaclor	45	67.48
4	C8	DL-Cycloserine	46	69.89
4	D8	McN-A-343	47	69.50
4	G8	Clomipramine hydrochloride	48	63.84
4	C10	Caffeic acid phenethyl ester	49	73.88
4	G10	Cinoxacin	50	63.90
4	G11	Colchicine	51	33.48
5	C2	(S)-(+)-Camptothecin	52	91.15
5	D2	CK2 Inhibitor 2	53	79.23
5	B3	CGS-12066A maleate	54	116.78
5	E3	7-Chlorokynurenic acid	55	70.96
5	H4	8-(3-Chlorostyryl)caffeine	56	87.12
5	E5	CGP 20712A methanesulfonate	57	102.23
5	G5	CNQX disodium	58	72.58
5	C6	DNQX	59	75.53
5	G6	Decamethonium dibromide	60	81.11
5	H7	Dequalinium analog, C-14 linker	61	19.01
5	B9	Dequalinium dichloride	62	37.63
5	H10	2,3-Dimethoxy-1,4-naphthoquinone	63	71.16
5	A11	Daphnetin	64	63.71
5	E11	Diacylglycerol Kinase Inhibitor II	65	42.69
6	C2	Demeclocycline hydrochloride	66	93.36
6	B3	Daidzein	67	120.00
6	A4	Dephostatin	68	91.64
6	H8	3,5-Dinitrocatechol	69	90.56
6	D9	5,7-Dichlorokynurenic acid	70	74.07
6	H9	(R)-(-)-DOI hydrochloride	71	79.56
6	A10	Dihydroergocristine methanesulfonate	72	74.40
6	H10	Etodolac	73	80.22
6	A2	PD 169316	74	76.20
6	B4	3',4'-Dichlorobenzamil	75	56.22
6	F4	N,N-Dihexyl-2-(4-fluorophenyl)indole-3-acetamide	76	65.99
6	G4	(R,R)-cis-Diethyl tetrahydro-2,8-chrysenediol	77	48.30
6	C5	Dantrolene sodium	78	63.20
6	H5	Doxazosin mesylate	79	75.02

6	A6	Doxycycline hydrochloride	80	61.53
6	B9	6,7-Dichloroquinoxaline-2,3-dione	81	57.55
6	A11	Enoximone	82	36.76
6	E11	7-Cyclopentyl-5-(4-phenoxy)phenyl-7H-pyrrolo[2,3-d]pyrimidin-4-ylamine	83	64.46
7	C2	(-)-Ephedrine hemisulfate	84	108.23
7	F2	Ellipticine	85	82.11
7	G2	Ebselen	86	84.61
7	G4	Methyl 6,7-dimethoxy-4-ethyl-beta-carboline-3-carboxylate	87	111.50
7	E6	Fiduxosin hydrochloride	88	68.46
7	C10	GW2974	89	83.29
7	C11	GW5074	90	8.24
7	D11	Genistein	91	106.44
7	H11	GBR-12935 dihydrochloride	92	115.50
8	A3	GYKI 52895	93	61.28
8	H4	6-Hydroxy-DL-DOPA	94	19.12
8	C5	Hydroxytacrine maleate	95	63.53
8	H5	Hispidin	96	37.59
8	B6	1,3,5-tris(4-hydroxyphenyl)-4-propyl-1H-pyrazole	97	14.70
8	E6	Harmane	98	69.92
8	G6	Retinoic acid p-hydroxyanilide	99	45.75
8	C8	BU99006	100	63.91
8	D10	Ibudilast	101	74.40
9	E2	Isoliquiritigenin	102	50.88
9	F3	Indomethacin	103	104.44
9	B6	1,5-Isoquinolinediol	104	95.82
9	D7	Ketorolac tris salt	105	71.69
9	H7	Kynurenic acid	106	63.30
9	F8	L-162,313	107	122.06
9	A9	LY-367,265	108	102.83
9	D9	Lomefloxacin hydrochloride	109	66.13
9	C11	Ro 90-7501	110	0.00
9	G11	LY-294,002 hydrochloride	111	97.20
10	B4	Nocodazole	112	61.70
10	E4	MRS 1845	113	63.11
10	F4	BIO	114	48.09
10	F5	MK-886	115	43.10
10	E6	MG 624	116	60.62
10	E7	Meloxicam sodium	117	42.69
10	F7	Morin	118	36.54
10	B8	Milrinone	119	52.98

10	B11	Myricetin	120	38.60
10	F11	MRS 2159	121	39.59
10	G11	GR 127935 hydrochloride	122	136.73
11	A2	Mifepristone	123	73.74
11	H2	Me-3,4-dephostatin	124	75.50
11	A3	Minocycline hydrochloride	125	108.70
11	D4	Metolazone	126	88.45
11	G4	Methysergide maleate	127	95.21
11	E5	ZM 39923 hydrochloride	128	61.70
11	A6	MDL 105,519	129	93.73
11	E6	Niflumic acid	130	80.08
11	F6	Nimesulide	131	87.07
11	G7	Niclosamide	132	92.47
11	D8	Nalidixic acid sodium	133	56.38
11	F8	5-Nitro-2-(3-phenylpropylamino)benzoic acid	134	91.00
11	A10	Nicardipine hydrochloride	135	84.43
11	B10	Nifedipine	136	80.76
11	D10	7-Nitroindazole	137	71.97
11	F10	2-(alpha-Naphthoyl)ethyltrimethylammonium iodide	138	50.22
11	A11	NF 023	139	19.70
12	A2	Nitrendipine	140	110.97
12	B2	Nimodipine	141	91.19
12	D3	NBQX disodium	142	68.91
12	B5	TG003	143	22.38
12	F5	SB 216763	144	79.13
12	D6	Piceatannol	145	26.38
12	F8	PPNDS tetrasodium	146	51.53
12	G8	PD 404,182	147	8.01
12	B9	1-Phenyl-3-(2-thiazolyl)-2-thiourea	148	66.90
12	D9	Cisplatin	149	71.81
12	F9	SU 9516	150	33.68
12	B11	Piroxicam	151	31.23
13	D5	6(5H)-Phenanthridinone	152	89.71
13	A11	Quinacrine dihydrochloride	153	79.91
13	E3	Prazosin hydrochloride	154	76.51
13	D3	Propionylpromazine hydrochloride	155	85.94
13	B8	BF-170 hydrochloride	156	54.04
13	F8	IC 261	157	84.80
13	E8	Pirenperone	158	26.45
13	B9	PPADS	159	84.90

13	D9	Phenamil methanesulfonate	160	78.05
13	G9	PD 98,059	161	79.75
13	B10	SU 6656	162	71.24
13	D10	Quercetin dihydrate	163	47.51
13	E10	Quinidine sulfate	164	60.97
13	F10	Quipazine dimaleate	165	48.75
13	D11	Quipazine, N-methyl-, dimaleate	166	65.13
13	E11	Quipazine, 6-nitro-, maleate	167	56.66
14	F2	Rutaecarpine	168	73.48
14	D4	Ranitidine hydrochloride	169	69.09
14	A7	Cortexolone maleate	170	131.12
14	E7	SC-560	171	63.47
14	F11	Salmeterol xinafoate	172	87.19
14	G11	SU 5416	173	76.07
14	B2	Raloxifene hydrochloride	174	43.46
14	C2	Retinoic acid	175	81.26
14	H2	Resveratrol	176	61.52
14	B3	Rottlerin	177	9.95
14	E4	Ritanserin	178	91.94
14	A5	Ro 41-0960	179	38.13
14	B5	Reactive Blue 2	180	8.62
14	H6	Sulindac sulfone	181	65.75
14	D9	SCH-202676 hydrobromide	182	6.22
14	G9	Sanguinarine chloride	183	8.06
14	D10	SR 2640	184	78.79
14	C11	Sulindac	185	49.60
14	C6	SB-366791	186	12.27
15	E2	SIB 1757	187	52.39
15	F2	SIB 1893	188	73.07
15	G3	Suramin hexasodium	189	14.54
15	F4	SB 224289 hydrochloride	190	98.26
15	H4	Tranilast	191	0.00
15	E5	Tetraethylthiuram disulfide	192	52.18
15	E6	Trequinsin hydrochloride	193	62.41
15	F6	Tyrphostin AG 879	194	87.08
15	E7	Tyrphostin AG 490	195	50.62
15	G7	L-765,314	196	107.78
15	H7	Triamterene	197	80.16
15	A8	Tyrphostin AG 1478	198	102.71
15	C8	Tyrphostin AG 494	199	51.47
15	D8	N-p-Tosyl-L-phenylalanine chloromethyl ketone	200	117.43

15	F8	Tyrphostin AG 527	201	48.85
15	H8	(±)-Taxifolin	202	54.50
15	A9	Tyrphostin AG 528	203	65.10
15	B9	Terazosin hydrochloride	204	70.72
15	C9	Tyrphostin AG 537	205	41.01
15	D9	Tyrphostin AG 555	206	40.62
15	E9	Tyrphostin AG 698	207	46.54
15	F9	Tyrphostin AG 808	208	68.50
15	H9	Tyrphostin AG 835	209	52.73
15	E10	Tyrphostin AG 34	210	70.10
15	H10	N,N,N-trimethyl-1-(4-trans-stilbenoxy)-2-propylammonium iodide	211	67.13
15	B11	Tyrphostin AG 112	212	34.27
15	C11	Tyrphostin 1	213	40.60
15	D11	Tyrphostin 23	214	74.31
16	A4	Tamoxifen citrate	215	87.63
16	C6	U-83836 dihydrochloride	216	46.52
16	H10	Xanthine amine congener	217	100.69
16	C2	Tyrphostin 47	218	59.36
16	D2	Tyrphostin 51	219	60.26
16	E2	T-1032	220	60.26
16	F2	I-OMe-Tyrphostin AG 538	221	16.10
16	G2	Tyrphostin AG 538	222	24.30
16	B3	T-0156	223	60.85
16	B6	U-74389G maleate	224	36.76
16	B7	UK 14,304	225	60.95
16	B8	U0126	226	49.89
16	D9	XK469	227	58.05
16	G9	WB 64	228	21.43
16	H9	(R)-(+)-WIN 55,212-2 mesylate	229	68.05
16	A10	WIN 62,577	230	57.24
16	C11	YC-1	231	82.21
16	G11	Olprinone hydrochloride	232	56.62

Table 21. Secondary Screen of EcIspD with lead compounds from the primary screen of LOPAC[1280]

Plate #	Compound (by Well #)	Compound Name	Compound #	Residual Activity EcIspC
1	A8	O-(Carboxymethyl)hydroxylamine hemihydrochloride	1	80.10883737
1	B4	N-(4-Aminobutyl)-5-chloro-2-naphthalenesulfonamide hydrochloride	2	96.59996599
1	C7	AA-861	3	49.29765886
1	E8	Amiprilose hydrochloride	4	64.0371861
1	E9	5-(N-Methyl-N-isobutyl)amiloride	5	78.54543393
1	F5	Aurintricarboxylic acid	6	9.962020294
1	H6	W-7 hydrochloride	7	95.11478941
2	E10	A-77636 hydrochloride	8	56.24170965
3	H7	DAPH	9	44.74122782
4	A2	Chelerythrine chloride	10	3.444475937
4	D3	Calmidazolium chloride	11	5.433932317
5	B9	Dequalinium dichloride	12	11.95510459
5	E11	Diacylglycerol Kinase Inhibitor II	13	36.80516977
5	F5	(2S,1'S,2'S)-2-(carboxycyclopropyl)glycine	14	43.66010714
5	H7	Dequalinium analog, C-14 linker	15	3.837877671
6	H8	3,5-Dinitrocatechol	16	81.1246528
7	C11	GW5074	17	47.26942917
8	B6	1,3,5-tris(4-hydroxyphenyl)-4-propyl-1H-pyrazole	18	55.32566181
8	H4	6-Hydroxy-DL-DOPA	19	7.650359957
9	E6	Indomethacin morpholinylamide	20	81.57360694
10	E2	L-703,606 oxalate	21	74.53318973
10	E3	Metoclopramide hydrochloride	22	101.6302931
11	G3	Methoctramine tetrahydrochloride	23	32.57298339
12	B4	Oleic Acid	24	104.9577688
13	H3	Phorbol 12-myristate 13-acetate	25	99.33563857
14	D2	Ruthenium red	26	34.43909075
14	F2	Rutaecarpine	27	55.95714529
15	D6	Tetradecylthioacetic acid	28	86.41800351
15	E11	TFPI hydrochloride	29	103.9215464
15	H6	Tolazamide	30	101.9352644
16	B4	Terfenadine	31	68.5063205
16	B6	U-74389G maleate	32	5.284734425
16	F10	Xamoterol hemifumarate	33	95.762145

REFERENCES

1. Lederberg, J. Infectious history. *Science* **288,** 287–293 (2000).
2. Kau, A. L., Ahern, P. P., Griffin, N. W., Goodman, A. L. & Gordon, J. I. Human nutrition, the gut microbiome, and immune system: envisioning the future. *Nature* **474,** 327–336 (2011).
3. Cantarel, B. L., Lombard, V. & Henrissat, B. Complex Carbohydrate Utilization by the Healthy Human Microbiome. *PLOS ONE* **7,** e28742 (2012).
4. Thaiss, C. A., Zmora, N., Levy, M. & Elinav, E. The microbiome and innate immunity. *Nature* **535,** 65–74 (2016).
5. Ziebuhr, W., Ohlsen, K., Karch, H., Korhonen, T. & Hacker, J. Evolution of bacterial pathogenesis. *Cell. Mol. Life Sci. CMLS* **56,** 719–728 (1999).
6. WHO | Tuberculosis. *WHO* Available at: http://www.who.int/mediacentre/factsheets/fs104/en/. (Accessed: 13th September 2016)
7. Raoult, D. *et al.* Molecular identification by ‘suicide PCR’ of Yersinia pestis as the agent of Medieval Black Death. *Proc. Natl. Acad. Sci.* **97,** 12800–12803 (2000).
8. Ali, M. *et al.* The global burden of cholera. *Bull. World Health Organ.* **90,** 209–218 (2012).

9. WHO | Typhoid. *WHO* Available at: http://www.who.int/immunization/diseases/typhoid/en/. (Accessed: 13th September 2016)
10. Center for Disease Control. Achievements in Public Health, 1900-1990: Control of Infectious Diseases. Available at: http://www.cdc.gov/mmwr/preview/mmwrhtml/mm4829a1.htm. (Accessed: 25th November 2015)
11. Sykes, R. Penicillin: from discovery to product. *Bull. World Health Organ.* **79,** 778–779 (2001).
12. de Lima Procópio, R. E., da Silva, I. R., Martins, M. K., de Azevedo, J. L. & de Araújo, J. M. Antibiotics produced by Streptomyces. *Braz. J. Infect. Dis.* **16,** 466–471 (2012).
13. Davies, J. Where have All the Antibiotics Gone? *Can. J. Infect. Dis. Med. Microbiol.* **17,** 287–290 (2006).
14. Lewis, K. Platforms for antibiotic discovery. *Nat. Rev. Drug Discov.* **12,** 371–387 (2013).
15. Powers, J. H. Antimicrobial drug development – the past, the present, and the future. *Clin. Microbiol. Infect.* **10,** 23–31 (2004).
16. Falagas, M. E., Kasiakou, S. K. & Saravolatz, L. D. Colistin: The Revival of Polymyxins for the Management of Multidrug-Resistant Gram-Negative Bacterial Infections. *Clin. Infect. Dis.* **40,** 1333–1341 (2005).

17. Pinho, M. G., Kjos, M. & Veening, J.-W. How to get (a)round: mechanisms controlling growth and division of coccoid bacteria. *Nat. Rev. Microbiol.* **11,** 601–614 (2013).

18. Goffin, C. & Ghuysen, J. M. Multimodular penicillin-binding proteins: an enigmatic family of orthologs and paralogs. *Microbiol. Mol. Biol. Rev. MMBR* **62,** 1079–1093 (1998).

19. Ghuysen, J. M. Serine beta-lactamases and penicillin-binding proteins. *Annu. Rev. Microbiol.* **45,** 37–67 (1991).

20. Curtis, N. A. C., Hayes, M. V., Wyke, A. W. & Ward, J. B. A mutant of Staphylococcus aureus H lacking penicillin-binding protein 4 and transpeptidase activity in vitro. *FEMS Microbiol. Lett.* **9,** 263–266 (1980).

21. Sauvage, E. & Terrak, M. Glycosyltransferases and Transpeptidases/Penicillin-Binding Proteins: Valuable Targets for New Antibacterials. *Antibiotics* **5,** (2016).

22. Tipper, D. J. & Strominger, J. L. Biosynthesis of the Peptidoglycan of Bacterial Cell Walls XII. Inhibition of Cross-linking by Penicillins and Cephalosporins: Studies in Staphylococcus aureus in vivo. *J. Biol. Chem.* **243,** 3169–3179 (1968).

23. Reynolds, P. E. Structure, biochemistry and mechanism of action of glycopeptide antibiotics. *Eur. J. Clin. Microbiol. Infect. Dis. Off. Publ. Eur. Soc. Clin. Microbiol.* **8,** 943–950 (1989).

24. Wright, G. D. Molecular mechanisms of antibiotic resistance. *Chem. Commun.* **47,** 4055–4061 (2011).

25. Laursen, B. S., Sørensen, H. P., Mortensen, K. K. & Sperling-Petersen, H. U. Initiation of Protein Synthesis in Bacteria. *Microbiol. Mol. Biol. Rev.* **69,** 101–123 (2005).

26. Wilson, D. N. Ribosome-targeting antibiotics and mechanisms of bacterial resistance. *Nat. Rev. Microbiol.* **12,** 35–48 (2014).

27. Kotra, L. P., Haddad, J. & Mobashery, S. Aminoglycosides: Perspectives on Mechanisms of Action and Resistance and Strategies to Counter Resistance. *Antimicrob. Agents Chemother.* **44,** 3249–3256 (2000).

28. Chopra, I. & Roberts, M. Tetracycline Antibiotics: Mode of Action, Applications, Molecular Biology, and Epidemiology of Bacterial Resistance. *Microbiol. Mol. Biol. Rev.* **65,** 232–260 (2001).

29. Jenner, L. *et al.* Structural basis for potent inhibitory activity of the antibiotic tigecycline during protein synthesis. *Proc. Natl. Acad. Sci. U. S. A.* **110,** 3812–3816 (2013).

30. Borovinskaya, M. A., Shoji, S., Holton, J. M., Fredrick, K. & Cate, J. H. D. A steric block in translation caused by the antibiotic spectinomycin. *ACS Chem. Biol.* **2,** 545–552 (2007).

31. Schluenzen, F. *et al.* The antibiotic kasugamycin mimics mRNA nucleotides to destabilize tRNA binding and inhibit canonical translation initiation. *Nat. Struct. Mol. Biol.* **13,** 871–878 (2006).

32. Brodersen, D. E. *et al.* The structural basis for the action of the antibiotics tetracycline, pactamycin, and hygromycin B on the 30S ribosomal subunit. *Cell* **103,** 1143–1154 (2000).

33. Pioletti, M. *et al.* Crystal structures of complexes of the small ribosomal subunit with tetracycline, edeine and IF3. *EMBO J.* **20,** 1829–1839 (2001).

34. Borovinskaya, M. A., Shoji, S., Fredrick, K. & Cate, J. H. D. Structural basis for hygromycin B inhibition of protein biosynthesis. *RNA N. Y. N* **14,** 1590–1599 (2008).

35. Wang, L. *et al.* Allosteric control of the ribosome by small-molecule antibiotics. *Nat. Struct. Mol. Biol.* **19,** 957–963 (2012).

36. Carter, A. P. *et al.* Functional insights from the structure of the 30S ribosomal subunit and its interactions with antibiotics. *Nature* **407,** 340–348 (2000).

37. Bulkley, D., Johnson, F. & Steitz, T. A. The antibiotic thermorubin inhibits protein synthesis by binding to inter-subunit bridge B2a of the ribosome. *J. Mol. Biol.* **416,** 571–578 (2012).

38. Stanley, R. E., Blaha, G., Grodzicki, R. L., Strickler, M. D. & Steitz, T. A. The structures of the anti-tuberculosis antibiotics viomycin and capreomycin bound to the 70S ribosome. *Nat. Struct. Mol. Biol.* **17,** 289–293 (2010).

39. Belova, L., Tenson, T., Xiong, L., McNicholas, P. M. & Mankin, A. S. A novel site of antibiotic action in the ribosome: interaction of evernimicin with the large ribosomal subunit. *Proc. Natl. Acad. Sci. U. S. A.* **98,** 3726–3731 (2001).

40. Harms, J. M. *et al.* Translational regulation via L11: molecular switches on the ribosome turned on and off by thiostrepton and micrococcin. *Mol. Cell* **30,** 26–38 (2008).

41. Hansen, J. L., Moore, P. B. & Steitz, T. A. Structures of five antibiotics bound at the peptidyl transferase center of the large ribosomal subunit. *J. Mol. Biol.* **330,** 1061–1075 (2003).

42. Hansen, J. L., Schmeing, T. M., Moore, P. B. & Steitz, T. A. Structural insights into peptide bond formation. *Proc. Natl. Acad. Sci. U. S. A.* **99,** 11670–11675 (2002).

43. Dunkle, J. A., Xiong, L., Mankin, A. S. & Cate, J. H. D. Structures of the Escherichia coli ribosome with antibiotics bound near the peptidyl transferase center explain spectra of drug action. *Proc. Natl. Acad. Sci. U. S. A.* **107,** 17152–17157 (2010).

44. Wilson, D. N. *et al.* The oxazolidinone antibiotics perturb the ribosomal peptidyl-transferase center and effect tRNA positioning. *Proc. Natl. Acad. Sci. U. S. A.* **105,** 13339–13344 (2008).

45. Hansen, J. L. *et al.* The structures of four macrolide antibiotics bound to the large ribosomal subunit. *Mol. Cell* **10,** 117–128 (2002).

46. Schlünzen, F., Pyetan, E., Fucini, P., Yonath, A. & Harms, J. M. Inhibition of peptide bond formation by pleuromutilins: the structure of the 50S ribosomal subunit from Deinococcus radiodurans in complex with tiamulin. *Mol. Microbiol.* **54,** 1287–1294 (2004).

47. Harms, J. M., Schlünzen, F., Fucini, P., Bartels, H. & Yonath, A. Alterations at the peptidyl transferase centre of the ribosome induced by the synergistic action of the streptogramins dalfopristin and quinupristin. *BMC Biol.* **2,** 4 (2004).

48. Gene M. Brown. The Biosynthsis of Folic Acid II. Inhibition by Sulfonamides. *J. Biol. Chem.* **237,** 536–540 (1962).

49. Gleckman, R., Blagg, N. & Joubert, D. W. Trimethoprim: mechanisms of action, antimicrobial activity, bacterial resistance, pharmacokinetics, adverse reactions, and therapeutic indications. *Pharmacotherapy* **1,** 14–20 (1981).

50. Campbell, E. A. *et al.* Structural Mechanism for Rifampicin Inhibition of Bacterial RNA Polymerase. *Cell* **104,** 901–912 (2001).

51. Floss, H. G. & Yu, T.-W. RifamycinMode of Action, Resistance, and Biosynthesis. *Chem. Rev.* **105,** 621–632 (2005).

52. Aldred, K. J., Kerns, R. J. & Osheroff, N. Mechanism of Quinolone Action and Resistance. *Biochemistry (Mosc.)* **53,** 1565–1574 (2014).

53. Polymyxins - Infectious Disease and Antimicrobial Agents. Available at: http://www.antimicrobe.org/d05.asp. (Accessed: 29th October 2016)

54. Robbel, L. & Marahiel, M. A. Daptomycin, a Bacterial Lipopeptide Synthesized by a Nonribosomal Machinery. *J. Biol. Chem.* **285,** 27501–27508 (2010).

55. WHO Fact sheet| Antimicrobial resistance. *WHO* Available at: http://www.who.int/mediacentre/factsheets/fs194/en/. (Accessed: 12th July 2015)

56. Center for Disease Control. *Antibiotic Resistance Threats in the United States, 2013*. (U.S. Department for Health and Human Services, 2013).

57. WHO global report| Antimicrobial resistance. *WHO* Available at: http://www.who.int/drugresistance/en/. (Accessed: 15th November 2014)

58. Dever, L. A. & Dermody, T. S. Mechanisms of bacterial resistance to antibiotics. *Arch. Intern. Med.* **151,** 886–895 (1991).

59. Sköld, O. Sulfonamide resistance: mechanisms and trends. *Drug Resist. Updat. Rev. Comment. Antimicrob. Anticancer Chemother.* **3,** 155–160 (2000).

60. Kong, K.-F., Schneper, L. & Mathee, K. Beta-lactam Antibiotics: From Antibiosis to Resistance and Bacteriology. *APMIS Acta Pathol. Microbiol. Immunol. Scand.* **118,** 1–36 (2010).

61. Olaitan, A. O., Morand, S. & Rolain, J.-M. Mechanisms of polymyxin resistance: acquired and intrinsic resistance in bacteria. *Front. Microbiol.* **5,** 643 (2014).

62. Schwarz, S., Kehrenberg, C., Doublet, B. & Cloeckaert, A. Molecular basis of bacterial resistance to chloramphenicol and florfenicol. *FEMS Microbiol. Rev.* **28,** 519–542 (2004).

63. Leclercq, R. Mechanisms of Resistance to Macrolides and Lincosamides: Nature of the Resistance Elements and Their Clinical Implications. *Clin. Infect. Dis.* **34,** 482–492 (2002).

64. Rice, L. B. Mechanisms of Resistance and Clinical Relevance of Resistance to β-Lactams, Glycopeptides, and Fluoroquinolones. *Mayo Clin. Proc.* **87,** 198–208 (2012).

65. Bozdogan, B. & Appelbaum, P. C. Oxazolidinones: activity, mode of action, and mechanism of resistance. *Int. J. Antimicrob. Agents* **23,** 113–119 (2004).

66. Tran, T. T., Munita, J. M. & Arias, C. A. Mechanisms of drug resistance: daptomycin resistance. *Ann. N. Y. Acad. Sci.* **1354,** 32–53 (2015).

67. Lambert, P. A. Bacterial resistance to antibiotics: Modified target sites. *Adv. Drug Deliv. Rev.* **57,** 1471–1485 (2005).

68. Golemi-Kotra, D. *et al.* The importance of a critical protonation state and the fate of the catalytic steps in class A beta-lactamases and penicillin-binding proteins. *J. Biol. Chem.* **279,** 34665–34673 (2004).

69. Wright, G. D. Bacterial resistance to antibiotics: Enzymatic degradation and modification. *Adv. Drug Deliv. Rev.* **57,** 1451–1470 (2005).

70. Drawz, S. M. & Bonomo, R. A. Three Decades of β-Lactamase Inhibitors. *Clin. Microbiol. Rev.* **23,** 160–201 (2010).

71. Sun, J., Deng, Z. & Yan, A. Bacterial multidrug efflux pumps: Mechanisms, physiology and pharmacological exploitations. *Biochem. Biophys. Res. Commun.* **453,** 254–267 (2014).

72. Poole, K. Efflux-mediated antimicrobial resistance. *J. Antimicrob. Chemother.* **56,** 20–51 (2005).

73. Coates, A. R., Halls, G. & Hu, Y. Novel classes of antibiotics or more of the same? *Br. J. Pharmacol.* **163,** 184–194 (2011).

74. Center for Disease Control. *About Antimicrobial Resistance,*.

75. FACT SHEET: Obama Administration Releases National Action Plan to Combat Antibiotic-Resistant Bacteria. *whitehouse.gov* Available at: https://www.whitehouse.gov/the-press-office/2015/03/27/fact-sheet-obama-

administration-releases-national-action-plan-combat-ant. (Accessed: 13th July 2015)

76. Odom, A. R. Five Questions about Non-Mevalonate Isoprenoid Biosynthesis. *PLoS Pathog* **7,** e1002323 (2011).

77. Gershenzon, J. & Dudareva, N. The function of terpene natural products in the natural world. *Nat. Chem. Biol.* **3,** 408–414 (2007).

78. Nowicka, B. & Kruk, J. Occurrence, biosynthesis and function of isoprenoid quinones. *Biochim. Biophys. Acta BBA - Bioenerg.* **1797,** 1587–1605 (2010).

79. Sáenz, J. P. *et al.* Hopanoids as functional analogues of cholesterol in bacterial membranes. *Proc. Natl. Acad. Sci. U. S. A.* **112,** 11971–11976 (2015).

80. Brown, A. C. & Parish, T. Dxr is essential in Mycobacterium tuberculosis and fosmidomycin resistance is due to a lack of uptake. *BMC Microbiol.* **8,** 78 (2008).

81. Gallagher, L. A. *et al.* A comprehensive transposon mutant library of Francisella novicida, a bioweapon surrogate. *Proc. Natl. Acad. Sci.* **104,** 1009–1014 (2007).

82. Baba, T. *et al.* Construction of Escherichia coli K-12 in-frame, single-gene knockout mutants: the Keio collection. *Mol. Syst. Biol.* **2,** 2006.0008 (2006).

83. Cameron, D. E., Urbach, J. M. & Mekalanos, J. J. A defined transposon mutant library and its use in identifying motility genes in Vibrio cholerae. *Proc. Natl. Acad. Sci.* **105,** 8736–8741 (2008).

84. Lange, B. M., Wildung, M. R., McCaskill, D. & Croteau, R. A family of transketolases that directs isoprenoid biosynthesis via a mevalonate-independent pathway. *Proc. Natl. Acad. Sci. U. S. A.* **95,** 2100–2104 (1998).

85. Julliard, J. H. & Douce, R. Biosynthesis of the thiazole moiety of thiamin (vitamin B1) in higher plant chloroplasts. *Proc. Natl. Acad. Sci.* **88,** 2042–2045 (1991).

86. Julliard, J.-H. Biosynthesis of the pyridoxal ring (vitamin B6) in higher plant chloroplasts and its relationship with the biosynthesis of the thiazole ring (vitamin B1). *Comptes Rendus Académie Sci. Sér. 3 Sci. Vie* **314,** 285–290 (1992).

87. Hill, R. E., Sayer, B. G. & Spenser, I. D. Biosynthesis of vitamin B6: incorporation of D-1-deoxyxylulose. *J. Am. Chem. Soc.* **111,** 1916–1917 (1989).

88. Hill, R. E. *et al.* The Biogenetic Anatomy of Vitamin B6 A 13CC NMR Investigation of the Biosynthesis of Pyridoxol in Escherichia coil. *J. Biol. Chem.* **271,** 30426–30435 (1996).

89. Andrew T Koppisch, D. T. F. E. coli MEP synthase: steady-state kinetic analysis and substrate binding. *Biochemistry (Mosc.)* **41,** 236–43 (2002).

90. Rohdich, F. *et al.* Cytidine 5'-triphosphate-dependent biosynthesis of isoprenoids: YgbP protein of Escherichia coli catalyzes the formation of 4-diphosphocytidyl-2-C-methylerythritol. *Proc. Natl. Acad. Sci. U. S. A.* **96,** 11758–11763 (1999).

91. Kuzuyama, T., Takagi, M., Kaneda, K., Dairi, T. & Seto, H. Formation of 4-(cytidine 5′-diphospho)-2-C-methyl-d-erythritol from 2-C-methyl-d-erythritol 4-phosphate by 2-C-methyl-d-erythritol 4-phosphate cytidylyltransferase, a new enzyme in the nonmevalonate pathway. *Tetrahedron Lett.* **41,** 703–706 (2000).

92. Kuzuyama, T. *et al.* Studies on the nonmevalonate pathway: conversion of 4-(cytidine 5′-diphospho)-2-C-methyl-d-erythritol to its 2-phospho derivative by 4-

(cytidine 5′-diphospho)-2-C-methyl-d-erythritol kinase. *Tetrahedron Lett.* **41,** 2925–2928 (2000).

93. Lüttgen, H. *et al.* Biosynthesis of terpenoids: YchB protein of Escherichia coli phosphorylates the 2-hydroxy group of 4-diphosphocytidyl-2C-methyl-d-erythritol. *Proc. Natl. Acad. Sci.* **97,** 1062–1067 (2000).
94. Herz, S. *et al.* Biosynthesis of terpenoids: YgbB protein converts 4-diphosphocytidyl-2C-methyl-d-erythritol 2-phosphate to 2C-methyl-d-erythritol 2,4-cyclodiphosphate. *Proc. Natl. Acad. Sci.* **97,** 2486–2490 (2000).
95. Altincicek, B. *et al.* LytB, a novel gene of the 2-C-methyl-D-erythritol 4-phosphate pathway of isoprenoid biosynthesis in Escherichia coli. *FEBS Lett.* **499,** 37–40 (2001).
96. Campos, N., Rodríguez-Concepción, M., Seemann, M., Rohmer, M. & Boronat, A. Identification of gcpE as a novel gene of the 2-C-methyl-D-erythritol 4-phosphate pathway for isoprenoid biosynthesis in Escherichia coli. *FEBS Lett.* **488,** 170–173 (2001).
97. Hecht, S. *et al.* Studies on the nonmevalonate pathway to terpenes: The role of the GcpE (IspG) protein. *Proc. Natl. Acad. Sci.* **98,** 14837–14842 (2001).
98. Kollas, A.-K. *et al.* Functional characterization of GcpE, an essential enzyme of the non-mevalonate pathway of isoprenoid biosynthesis. *FEBS Lett.* **532,** 432–436 (2002).

99. Rohdich, F. *et al.* The deoxyxylulose phosphate pathway of isoprenoid biosynthesis: Studies on the mechanisms of the reactions catalyzed by IspG and IspH protein. *Proc. Natl. Acad. Sci.* **100,** 1586–1591 (2003).

100. Rohdich, F., Bacher, A. & Eisenreich, W. Isoprenoid biosynthetic pathways as anti-infective drug targets. *Biochem. Soc. Trans.* **33,** 785 (2005).

101. Altincicek, B. *et al.* GcpE Is Involved in the 2-C-Methyl-d-Erythritol 4-Phosphate Pathway of Isoprenoid Biosynthesis in Escherichia coli. *J. Bacteriol.* **183,** 2411–2416 (2001).

102. Cunningham, F. X., Lafond, T. P. & Gantt, E. Evidence of a Role for LytB in the Nonmevalonate Pathway of Isoprenoid Biosynthesis. *J. Bacteriol.* **182,** 5841–5848 (2000).

103. Altincicek, B. *et al.* LytB protein catalyzes the terminal step of the 2-C-methyl-D-erythritol-4-phosphate pathway of isoprenoid biosynthesis. *FEBS Lett.* **532,** 437–440 (2002).

104. McAteer, S., Coulson, A., McLennan, N. & Masters, M. The lytB Gene of Escherichia coli Is Essential and Specifies a Product Needed for Isoprenoid Biosynthesis. *J. Bacteriol.* **183,** 7403–7407 (2001).

105. Rohdich, F. *et al.* Studies on the nonmevalonate terpene biosynthetic pathway: Metabolic role of IspH (LytB) protein. *Proc. Natl. Acad. Sci.* **99,** 1158–1163 (2002).

106. Adam, P. *et al.* Biosynthesis of terpenes: Studies on 1-hydroxy-2-methyl-2-(E)-butenyl 4-diphosphate reductase. *Proc. Natl. Acad. Sci.* **99,** 12108–12113 (2002).

107. Seemann, M., Tse Sum Bui, B., Wolff, M., Miginiac-Maslow, M. & Rohmer, M. Isoprenoid biosynthesis in plant chloroplasts via the MEP pathway: Direct thylakoid/ferredoxin-dependent photoreduction of GcpE/IspG. *FEBS Lett.* **580,** 1547–1552 (2006).

108. Cassera, M. B. *et al.* The methylerythritol phosphate pathway is functionally active in all intraerythrocytic stages of Plasmodium falciparum. *J. Biol. Chem.* **279,** 51749–51759 (2004).

109. Koppisch, A. T., Fox, D. T., Blagg, B. S. J. & Poulter, C. D. E. coli MEP synthase: steady-state kinetic analysis and substrate binding. *Biochemistry (Mosc.)* **41,** 236–243 (2002).

110. Lauw, S., Illarionova, V., Bacher, A., Rohdich, F. & Eisenreich, W. Biosynthesis of isoprenoids: studies on the mechanism of 2C-methyl-D-erythritol-4-phosphate synthase. *FEBS J.* **275,** 4060–4073 (2008).

111. Munos, J. W., Pu, X., Mansoorabadi, S. O., Kim, H. J. & Liu, H. A secondary kinetic isotope effect study of the 1-deoxy-D-xylulose-5-phosphate reductoisomerase-catalyzed reaction: evidence for a retroaldol-aldol rearrangement. *J. Am. Chem. Soc.* **131,** 2048–2049 (2009).

112. Li, H., Tian, J., Sun, W., Qin, W. & Gao, W.-Y. Mechanistic insights into 1-deoxy-D-xylulose 5-phosphate reductoisomerase, a key enzyme of the MEP terpenoid biosynthetic pathway. *FEBS J.* **280,** 5896–5905 (2013).

113. Henriksson, L. M. *et al.* Structures of Mycobacterium tuberculosis 1-deoxy-D-xylulose-5-phosphate reductoisomerase provide new insights into catalysis. *J. Biol. Chem.* **282,** 19905–19916 (2007).

114. Andaloussi, M. *et al.* Design, synthesis, and X-ray crystallographic studies of α-aryl substituted fosmidomycin analogues as inhibitors of Mycobacterium tuberculosis 1-deoxy-D-xylulose 5-phosphate reductoisomerase. *J. Med. Chem.* **54,** 4964–4976 (2011).

115. Björkelid, C., Bergfors, T., Unge, T., Mowbray, S. L. & Jones, T. A. Structural studies on Mycobacterium tuberculosis DXR in complex with the antibiotic FR-900098. *Acta Crystallogr. Sect. D* **68,** 134–143 (2012).

116. Mac Sweeney, A. *et al.* The crystal structure of E.coli 1-deoxy-D-xylulose-5-phosphate reductoisomerase in a ternary complex with the antimalarial compound fosmidomycin and NADPH reveals a tight-binding closed enzyme conformation. *J. Mol. Biol.* **345,** 115–127 (2005).

117. Reuter, K. *et al.* Crystal structure of 1-deoxy-D-xylulose-5-phosphate reductoisomerase, a crucial enzyme in the non-mevalonate pathway of isoprenoid biosynthesis. *J. Biol. Chem.* **277,** 5378–5384 (2002).

118. Kholodar, S. A. *et al.* Alteration of the Flexible Loop in 1-Deoxy-d-xylulose-5-phosphate Reductoisomerase Boosts Enthalpy-Driven Inhibition by Fosmidomycin. *Biochemistry (Mosc.)* **53,** 3423–3431 (2014).

119. Kuzuyama, T., Shimizu, T., Takahashi, S. & Seto, H. Fosmidomycin, a specific inhibitor of 1-deoxy-d-xylulose 5-phosphate reductoisomerase in the

nonmevalonate pathway for terpenoid biosynthesis. *Tetrahedron Lett.* **39,** 7913–7916 (1998).

120. Okuhara, M. *et al.* Studies on new phosphonic acid antibiotics. I. FR-900098, isolation and characterization. *J. Antibiot. (Tokyo)* **33,** 13–17 (1980).
121. Yajima, S. *et al.* Structure of 1-deoxy-D-xylulose 5-phosphate reductoisomerase in a quaternary complex with a magnesium ion, NADPH and the antimalarial drug fosmidomycin. *Acta Crystallograph. Sect. F Struct. Biol. Cryst. Commun.* **63,** 466–470 (2007).
122. Na-Bangchang, K., Ruengweerayut, R., Karbwang, J., Chauemung, A. & Hutchinson, D. Pharmacokinetics and pharmacodynamics of fosmidomycin monotherapy and combination therapy with clindamycin in the treatment of multidrug resistant falciparum malaria. *Malar. J.* **6,** 70 (2007).
123. Lell, B. *et al.* Fosmidomycin, a Novel Chemotherapeutic Agent for Malaria. *Antimicrob. Agents Chemother.* **47,** 735–738 (2003).
124. Oyakhirome, S. *et al.* Randomized Controlled Trial of Fosmidomycin-Clindamycin versus Sulfadoxine-Pyrimethamine in the Treatment of Plasmodium falciparum Malaria. *Antimicrob. Agents Chemother.* **51,** 1869–1871 (2007).
125. Ruangweerayut, R. *et al.* Assessment of the pharmacokinetics and dynamics of two combination regimens of fosmidomycin-clindamycin in patients with acute uncomplicated falciparum malaria. *Malar. J.* **7,** 225 (2008).
126. Bergan, T. Pharmacokinetic comparison between fosfomycin and other phosphonic acid derivatives. *Chemotherapy* **36 Suppl 1,** 10–18 (1990).

127. San Jose, G. *et al.* Design of Potential Bisubstrate Inhibitors against Mycobacterium tuberculosis (Mtb) 1-Deoxy-D-Xylulose 5-Phosphate Reductoisomerase (Dxr)-Evidence of a Novel Binding Mode. *MedChemComm* **4,** 1099–1104 (2013).

128. Chofor, R. *et al.* Synthesis and bioactivity of β-substituted fosmidomycin analogues targeting 1-deoxy-D-xylulose-5-phosphate reductoisomerase. *J. Med. Chem.* **58,** 2988–3001 (2015).

129. Richard, S. B. *et al.* Structure of 4-diphosphocytidyl-2-C- methylerythritol synthetase involved in mevalonate- independent isoprenoid biosynthesis. *Nat.Struct.Biol.* **8,** 641–648 (2001).

130. Richard, S. B. *et al.* Kinetic analysis of Escherichia coli 2-C-methyl-D-erythritol-4-phosphate cytidyltransferase, wild type and mutants, reveals roles of active site amino acids. *Biochemistry (Mosc.)* **43,** 12189–12197 (2004).

131. Bjorkelid, C. *et al.* Structural and Functional Studies on Mycobacterial Ispd Enzymes. *Acta CrystallogrSectD* **67,** 403–null (2010).

132. Gabrielsen, M. *et al.* Biosynthesis of isoprenoids: a bifunctional IspDF enzyme from Campylobacter jejuni. *Eur. J. Biochem. FEBS* **271,** 3028–3035 (2004).

133. Gabrielsen, M. *et al.* Hexameric assembly of the bifunctional methylerythritol 2,4-cyclodiphosphate synthase and protein-protein associations in the deoxy-xylulose-dependent pathway of isoprenoid precursor biosynthesis. *J. Biol. Chem.* **279,** 52753–52761 (2004).

134. Masini, T., Kroezen, B. S. & Hirsch, A. K. H. Druggability of the enzymes of the non-mevalonate-pathway. *Drug Discov. Today* **18,** 1256–1262 (2013).

135. Witschel, M. C. *et al.* Inhibitors of the herbicidal target IspD: allosteric site binding. *Angew. Chem. Int. Ed Engl.* **50,** 7931–7935 (2011).

136. Kunfermann, A. *et al.* Pseudilins: halogenated, allosteric inhibitors of the non-mevalonate pathway enzyme IspD. *Angew. Chem. Int. Ed Engl.* **53,** 2235–2239 (2014).

137. Spangenberg, T. *et al.* The Open Access Malaria Box: A Drug Discovery Catalyst for Neglected Diseases. *PLoS ONE* **8,** e62906 (2013).

138. Imlay, L. S. *et al.* Plasmodium IspD (2-C-Methyl-D-erythritol 4-Phosphate Cytidyltransferase), an Essential and Druggable Antimalarial Target. *ACS Infect. Dis.* **1,** 157–167 (2015).

139. Price, K. E. *et al.* Molecular Mechanism of Action of Antimalarial Benzoisothiazolones: Species-Selective Inhibitors of the Plasmodium spp. MEP Pathway enzyme, IspD. *Sci. Rep.* **6,** (2016).

140. Jackson, E. R. & Dowd, C. S. Inhibition of 1-deoxy-D-xylulose-5-phosphate reductoisomerase (Dxr): a review of the synthesis and biological evaluation of recent inhibitors. *Curr. Top. Med. Chem.* **12,** 706–728 (2012).

141. Haymond, A. *et al.* Kinetic Characterization and Allosteric Inhibition of the Yersinia pestis 1-Deoxy-D-Xylulose 5-Phosphate Reductoisomerase (MEP Synthase). *PLoS ONE* **9,** e106243 (2014).

142. Tsang, A. *et al.* Francisella tularensis 2-C-Methyl-D-Erythritol 4-Phosphate Cytidylyltransferase: Kinetic Characterization and Phosphoregulation. *PLoS ONE* **6,** e20884 (2011).

143. Dove, A. Drug screening—beyond the bottleneck. *Nat. Biotechnol.* **17,** 859–863 (1999).

144. Jackson, E. R. *et al.* The effect of chain length and unsaturation on Mtb Dxr inhibition and antitubercular killing activity of FR900098 analogs. *Bioorg. Med. Chem. Lett.* **24,** 649–653 (2014).

145. San Jose, G. *et al.* Structure-Activity Relationships of the MEPicides: N-Acyl and O-linked Analogs of FR900098 as Inhibitors of Dxr from Mycobacterium tuberculosis and Yersinia pestis. *ACS Infect. Dis.* (2016). doi:10.1021/acsinfecdis.6b00125

146. Databases & Tools | DTP. Available at: https://dtp.cancer.gov/dtpstandard/dwindex/index.jsp. (Accessed: 18th January 2017)

147. Mitosch, K. & Bollenbach, T. Bacterial responses to antibiotics and their combinations. *Environ. Microbiol. Rep.* **6,** 545–557 (2014).

148. Strelow, J. *et al.* in *Assay Guidance Manual* (eds. Sittampalam, G. S. et al.) (Eli Lilly & Company and the National Center for Advancing Translational Sciences, 2004).

149. Bernal, C., Palacin, C., Boronat, A. & Imperial, S. A colorimetric assay for the determination of 4-diphosphocytidyl-2-C-methyl-D-erythritol 4-phosphate synthase activity. *Anal. Biochem.* **337,** 55–61 (2005).

150. Curly Dock (Rumex crispus). Available at: http://www.illinoiswildflowers.info/weeds/plants/curly_dock.htm. (Accessed: 5th April 2017)

151. McKenney, E. S. *et al.* Lipophilic prodrugs of FR900098 are antimicrobial against Francisella novicida in vivo and in vitro and show GlpT independent efficacy. *PloS One* **7,** e38167 (2012).

152. Shoichet, B. K. Interpreting Steep Dose-Response Curves in Early Inhibitor Discovery. *J. Med. Chem.* **49,** 7274–7277 (2006).

153. Shoichet, B. K. Screening in a spirit haunted world. *Drug Discov. Today* **11,** 607–615 (2006).

154. McGovern, S. L. & Shoichet, B. K. Kinase Inhibitors: Not Just for Kinases Anymore. *J. Med. Chem.* **46,** 1478–1483 (2003).

155. Owen, S. C. *et al.* Colloidal Drug Formulations Can Explain 'Bell-Shaped' Concentration–Response Curves. *ACS Chem. Biol.* **9,** 777–784 (2014).

156. McGovern, S. L., Helfand, B. T., Feng, B. & Shoichet, B. K. A Specific Mechanism of Nonspecific Inhibition. *J. Med. Chem.* **46,** 4265–4272 (2003).

157. Feng, B. Y., Shelat, A., Doman, T. N., Guy, R. K. & Shoichet, B. K. High-throughput assays for promiscuous inhibitors. *Nat. Chem. Biol.* **1,** 146–148 (2005).

158. Feng, B. Y. & Shoichet, B. K. A Detergent-Based Assay for the Detection of Promiscuous Inhibitors. *Nat. Protoc.* **1,** 550–553 (2006).

159. Coan, K. E. D., Maltby, D. A., Burlingame, A. L. & Shoichet, B. K. Promiscuous Aggregate-Based Inhibitors Promote Enzyme Unfolding. *J. Med. Chem.* **52,** 2067–2075 (2009).

160. Tritsch, D., Zinglé, C., Rohmer, M. & Grosdemange-Billiard, C. Flavonoids: True or promiscuous inhibitors of enzyme? The case of deoxyxylulose phosphate reductoisomerase. *Bioorganic Chem.* **59,** 140–144 (2015).

161. Weissig, V. *et al.* DQAsomes: a novel potential drug and gene delivery system made from Dequalinium. *Pharm. Res.* **15,** 334–337 (1998).

162. Haberland, M. E. & Reynolds, J. A. Self-association of Cholesterol in Aqueous Solution. *Proc. Natl. Acad. Sci.* **70,** 2313–2316 (1973).

163. Seidler, J., McGovern, S. L., Doman, T. N. & Shoichet, B. K. Identification and Prediction of Promiscuous Aggregating Inhibitors among Known Drugs. *J. Med. Chem.* **46,** 4477–4486 (2003).

164. pmhdev. Suramin (Injection route). *PubMed Health* (2017).

165. Zhang, Y.-L., Keng, Y.-F., Zhao, Y., Wu, L. & Zhang, Z.-Y. Suramin Is an Active Site-directed, Reversible, and Tight-binding Inhibitor of Protein-tyrosine Phosphatases. *J. Biol. Chem.* **273,** 12281–12287 (1998).

166. De Clercq, E. Suramin in the treatment of AIDS: Mechanism of action. *Antiviral Res.* **7,** 1–10 (1987).

167. Zhou, W., Wang, Y., Xie, J. & Geraghty, R. J. A fluorescence-based high-throughput assay to identify inhibitors of tyrosylprotein sulfotransferase activity. *Biochem. Biophys. Res. Commun.* **482,** 1207–1212 (2017).

168. Krüger, E. A. & Figg, W. D. Protein Binding Alters the Activity of Suramin, Carboxyamidotriazole, and UCN-01 in an ex Vivo Rat Aortic Ring Angiogenesis Assay. *Clin. Cancer Res.* **7,** 1867–1872 (2001).

169. Bruijn, E. A. D. *et al.* Therapeutic Drug Monitoring of Suramin and Protein Binding. *J. Liq. Chromatogr.* **14,** 3719–3733 (1991).

170. Cha, J. H., Dure LS, I. V., Sakurai, S. Y., Penney, J. B. & Young, A. B. 2,4,5-Trihydroxyphenylalanine (6-hydroxy-dopa) displaces [3H]AMPA binding in rat striatum. *Neurosci. Lett.* **132,** 55–58 (1991).

171. Rosenberg, P. A., Loring, R., Xie, Y., Zaleskas, V. & Aizenman, E. 2,4,5-trihydroxyphenylalanine in solution forms a non-N-methyl-D-aspartate glutamatergic agonist and neurotoxin. *Proc. Natl. Acad. Sci. U. S. A.* **88,** 4865–4869 (1991).

172. Feng, B. Y. *et al.* A high-throughput screen for aggregation-based inhibition in a large compound library. *J. Med. Chem.* **50,** 2385–2390 (2007).

173. Gonzalez, R. G., Haxo, R. S. & Schleich, T. Mechanism of action of polymeric aurintricarboxylic acid, a potent inhibitor of protein-nucleic acid interactions. *Biochemistry (Mosc.)* **19,** 4299–4303 (1980).

174. Garman, E. F. & Mitchell, E. P. Glycerol concentrations required for cryoprotection of 50 typical protein crystallization solutions. *J. Appl. Crystallogr.* **29,** 584–587 (1996).
175. hr006660_binder1.pdf.
176. hr007379_index_documents.pdf.
177. hr008114_binder1.pdf.
178. hr008115_binder1.pdf.
179. 1054309_ps_xtal_phclear-suite.pdf.
180. 1054308_ps_xtal_phclear-ii-suite.pdf.
181. Anand David, A. V., Arulmoli, R. & Parasuraman, S. Overviews of Biological Importance of Quercetin: A Bioactive Flavonoid. *Pharmacogn. Rev.* **10,** 84–89 (2016).
182. Al-Bakri, A. G., Othman, G. & Bustanji, Y. The assessment of the antibacterial and antifungal activities of aspirin, EDTA and aspirin-EDTA combination and their effectiveness as antibiofilm agents. *J. Appl. Microbiol.* **107,** 280–286 (2009).
183. Downer, M. K. *et al.* Regular Aspirin Use and the Risk of Lethal Prostate Cancer in the Physicians' Health Study. *Eur. Urol.* (2017). doi:10.1016/j.eururo.2017.01.044
184. Takahashi, S., Kuzuyama, T., Watanabe, H. & Seto, H. A 1-deoxy-d-xylulose 5-phosphate reductoisomerase catalyzing the formation of 2-C-methyl-d-erythritol 4-phosphate in an alternative nonmevalonate pathway for terpenoid biosynthesis. *Proc. Natl. Acad. Sci.* **95,** 9879–9884 (1998).

185. LOPAC1280 – Library of Pharmacologically Active Compounds. *Sigma-Aldrich* Available at: http://www.sigmaaldrich.com/life-science/cell-biology/bioactive-small-molecules/lopac1280-navigator.html. (Accessed: 12th December 2015)

186. Dhiman, R. K. *et al.* 1-Deoxy-d-Xylulose 5-Phosphate Reductoisomerase (IspC) from Mycobacterium tuberculosis: towards Understanding Mycobacterial Resistance to Fosmidomycin. *J. Bacteriol.* **187,** 8395–8402 (2005).

187. Scripps Center For Metabolomics and Mass Spectrometry - METLIN. Available at: https://metlin.scripps.edu/index.php. (Accessed: 9th October 2016)

188. ExPASy ProtParam tool. Available at: http://web.expasy.org/cgi-bin/protparam/protparam. (Accessed: 29th January 2017)

189. Jawaid, S. *et al.* Kinetic characterization and phosphoregulation of the Francisella tularensis 1-deoxy-D-xylulose 5-phosphate reductoisomerase (MEP synthase). *PloS One* **4,** e8288 (2009).

190. Kleywegt, G. J. & Jones, T. A. Phi/psi-chology: Ramachandran revisited. *Struct. Lond. Engl. 1993* **4,** 1395–1400 (1996).

191. Engh, R. A. & Huber, R. Accurate bond and angle parameters for X-ray protein structure refinement. *Acta Crystallogr. A* **47,** 392–400 (1991).

BIOGRAPHY

Amanda Haymond graduated from Fauquier High School, Warrenton, Virginia, in 2008. She received her Bachelor of Science in Chemistry from George Mason University in 2013. She was employed as a Graduate Research Assistant or a Graduate Teaching Assistant at George Mason University during her tenure as a doctoral student in the Chemistry and Biochemistry Department.